Elucidating the molecular determinants of vector tropism of Uukuniemi virus

Alexandra Wilson, MBiochem

Submitted in fulfilment of the requirements for the Degree of
Doctor of Philosophy in Molecular Virology

School of Infection and Immunity
College of Medical, Veterinary and Life Sciences
University of Glasgow

Abstract

Ticks are vectors capable of transmitting viruses, such as those within the order *Bunyavirales*. These interactions between virus and vector are severely understudied, despite ticks and the viruses they transmit posing an ever-increasing risk to human and animal health. Once exposed, ticks can be persistently infected, capable of transmitting the virus to other hosts for the duration of their lifespan and in some cases can pass on the virus to any offspring through vertical transmission. Additionally, as the impact of climate change increases, the abundance, activity window and geographical reach of ticks is expanding, further increasing the risk of exposure to the viruses they carry.

Over the last 80 years, the emergence and re-emergence of tick-borne bunyaviruses has led to several epidemics, with the mortality of some of these virus species exceeding 30%. However, as it stands, little information is known about the factors which dictate the vector specificity of these viruses, and the intracellular interactions within the tick that allow for persistent infection to be established. The work carried out within this thesis aims to begin tackling both gaps within our understanding. By using Uukuniemi virus (UUKV) as a model bunyavirus, the vector specificity of UUKV for ticks is confirmed and the stage at which viral replication is unable to proceed in non-vector arthropod cells has been identified. This work highlights the interactions within vector and non-vector arthropod cells in order to determine the requirements needed for UUKV to overcome this transmission barrier and demonstrates UUKV is unable to infect and replicate in cell lines derived from mosquitoes but readily infects human and tick cell cultures. In tandem with these findings, this work also presents the first tick cell line-derived RNA binding proteome (RBPome), achieved by using a cell line from the tick species *Ixodes scapularis*. The work also elucidates RNA binding proteins that are significantly differentially expressed during UUKV infection. As this methodology employs the use of RNA interactome capture through UV crosslinking and oligo(dT) capture beads to isolate samples for mass-spectrometry, the proteins highlighted in these findings reflect changes of activity within the cell as opposed to changes in overall protein abundance, as is seen with classical whole cell proteomics. Further biochemical analysis and downstream validation through dsRNA transfections to achieve gene knockdowns gives insights into both the makeup of the ISE6 cell line derived RBPome and preliminary insights into the importance of these proteins in viral replication kinetics. In summary, this work lays the foundations to elucidating the molecular determinants of Uukuniemi virus tropism within vector cells, alongside providing novel data on the

intracellular landscape of the ISE6 cell line RBPome in naïve and rUUKV-infected conditions.

Author's Declaration

I, Alexandra L. Wilson, declare that, except where reference is made to the contribution of others, that this thesis is the result of my own work and has not been submitted for any other degree at the University of Glasgow or any other institution.

Printed Name: ALEXANDRA L. WILSON

Signature:

Acknowledgements

I have encountered the most amazing people throughout my time in Glasgow, who helped shape who I am as both a person and a researcher. I would like to extend my gratitude to the many people who have aided me throughout my journey, though the list is far too extensive to mention everyone, my appreciation to each of you is immeasurable.

Firstly, I want to thank my PI Dr Benjamin Brennan for welcoming me into his lab and helping me discover my love (although sometimes love-hate) for tick-borne viruses. As the first of what I'm sure in future will be a long line of Brennan lab PhD students, your mentorship provided me with the freedom and encouragement to continue developing as an independent researcher and pursue my scientific curiosity, alongside the gentle nudges I needed to get this thesis over the finish line. It has been a privilege, and I will carry the lessons you have taught me through the rest of my scientific career.

I was lucky enough to have two amazing secondary supervisors during my time at the CVR. Professor Alain Kohl, I cannot thank you enough for all your support and patience in making me feel understood, and for reminding me that I am capable of much more than I sometimes think I am. I'm sad that our time was cut short, but am grateful that even as you move on to the next stages of your career you still check in and give me support. Professor Alfredo Castello, although it's a bit strange how small the world can be, it was wonderful to collaborate with your lab again during my research, alongside having you take over as my secondary supervisor. My internship with your lab during the second summer of my undergrad was my first official taste of research, and helped set me on course to pursue my PhD. Your help has been an integral part of my development into making me the scientist I am today, and I'm so happy to have been able to show you how much I've grown and developed as a researcher.

I owe a massive thank you to Mazi, Andy, Kelsey, Igor, Alma, Marine, Mel, Colin, James, Anna, Marko, Wael, Zaydah, Rozeena, Natasha, Gav, Ingeborg, Hollie, Daniel, Lea, Lois, Lauren, Eilidh, Liam, Harris, Stephen, Kristyn, Zack, Rebecca, Doug, Victoria, Sam, Rob, Sergi, Diogo, Emma, Jordan, Mickey, Gavin, Jake, Anna, and Nick. Mazi, you taught me the ropes when I first joined the CVR, thank you for your patience and for always getting things down from the high shelves for me. Andy, Kelsey, and Igor, my lab siblings, thank you for listening to every sleep-deprived rant I've ever had and putting up with me before I'd had a sufficient amount of caffeine, you made going into the lab a much more fun experience. Alma, Mel and Marine, I cannot express my gratitude to you all enough, you took care of

me and were a fundamental part of my support system within the lab, I hope in future I can be like you for whoever next steps into my shoes. Colin, you sharing your expertise and forbidden knowledge of the confocal microscope helped form a whole chapter of this work, and without it I definitely would have broken something, thank you for your patience in teaching me and your infectious enthusiasm. To the members of the Castello lab, particularly Marko and Wael, thank you for guiding me, for your support and friendship, and for always providing an excuse to take a break and have coffee. I hope this will not be the last time we collaborate together. To the games gang, DnD groups, and crafternoon girlies, hanging out with you all are some of my favourite memories of Glasgow and I adore you all so much. Finally, to Nick, I hope you knew how much you helped me when I moved to Glasgow, as without you I don't know if I would have made it past the first year.

To my PhD Pals, Spyros, Anna, Kasim, and Innes, I could not have done this without you all. We struggled through the hardships together and I'm so proud of us. Spyros, your boundless enthusiasm and positive outlook is a ray of sunshine, even in the middle of a lockdown, and I know you will take Japan by storm. Kasim, you're one of the kindest and calmest people I know, and I will always fondly recall our memories of failed baking attempts and walks through the botanics. Innes, your wit and humour make even the most miserable times better, I know I can trust you with anything, and I already miss our bi-weekly brunches at Beefcake. Anna, you are a beautiful daffodil inside and out, you are a soul sister, and I will forever be in awe of your sense of style and funky vibes. Although I know we are all off to different corners of the globe, I have no doubt we're stuck with each other for life, and I can't wait to see what happens next.

I am also blessed to know many incredible people from before my time in Glasgow, but in particular I would like to thank Olivia, Emma and Daria. You three are my oldest friends, have stuck by me through thick and thin, have believed in me and supported me throughout my PhD, and I don't think there are enough words to express my love and gratitude. Olivia, your frank advice and determination always keeps me grounded and helps me tackle anything. Emma, your kindness and positivity has helped me weather the stressful times and see the brighter side of things. Daria, although we may not be doing a PhD in the same field, you have been invaluable to bounce ideas off of and to commiserate with, and I know you'll be right behind me in completing your thesis.

Finally, this thesis is dedicated to my family, whose unconditional love and unwavering support has made all of this possible. Mum, Dad, and Sarah, I have lost track the number of times I've called you thinking the world is ending, and every time you have listened and advised without judgment, no matter the time or day. Your belief in me helped push me

forward when I wasn't sure I'd be able to manage, and I will forever be grateful to you. Mum and Dad, you worked so hard throughout my life to make sure Sarah and I had every opportunity we could want, and supported us in whatever made us happy without ever making demands or expectations for us. You inspire me to work hard and persevere, and I owe my determination and success to you both. Sarah, you are simply the best sister anyone could ask for. You have always been there to humour my terrible ideas, I know I can rely on you for anything, and now you have it in writing that I would donate one of my kidneys to you (should you ever need one). I could not have done this without you guys, and of course without the fluffy therapy and demands for affection from Kodak and Disco. If awards were given for invading personal space and sitting on peoples laps during writing, I would probably have to make Disco a co-author.

I love you all, and I hope I continue to do you proud.

Table of Contents

List of Tables

List of Figures

Definitions/Abbreviations

Abbreviation	Definition
AAG2	Aedes aegypti 2
ACN	Acetonitrile
ADJ.P.VAL	Adjusted P-value
AF647	Alexa Fluor 647 succinimidyl ester dye
AGO	Argonaute
AGO2	Argonaute RISC Catalytic Component 2
AMP	Antimicrobial peptides
AP-2	Adaptor protein complex 2
ARBONET	National Arbovirus Surveillance System
BHAV	Bhanja virus
BLAST	Basic local alignment search tool
BUNV	Bunyamwera virus
CACL2	Calcium chloride
CCHF	Crimean Congo haemorrhagic fever
CDC	Centre for disease control
CEPI	Coalition for Epidemic Preparedness Innovations
CPE	Cytopathic effect
CPSF2	Cleavage And Polyadenylation Specific Factor 2
CRNA	Complementary RNA
CUL1	Cullin 1
C-IAA	Indole-3-acetic acid
DCR	Dicer
DC-SIGN	Dendritic cell-specific ICAM-3 grabbing non-integrin
DDA	Data dependant analysis
DENV	Dengue virus
DIA	Data independent analysis
DMEM	Dulbecco’s modified Eagle’s medium
DMSO	Dimethyl sulfoxide
DS	Double stranded
DTT	Dithiothreitol
ECACC	European Collection of Authenticated Cell Cultures
ECDC	European Centre for Disease Prevention and Control
EDTA	Ethylenediaminetetraacetic acid

EGFP	Enhanced GFP
EIF	Eukaryotic Translation Initiation Factor
EJC	Exon junction complex
EMSA	Electrophoretic mobility shift assay
ENDO-SIRNA	Endogenous small interfering RNA
EXO-SIRNA	Exogenous small interfering RNA
FAK	Active focal adhesion kinase
FC	Fold change
FCS	Foetal Calf Serum
FDR	False discovery rate
FFU	Foci forming units
FMRP	Fragile X mental retardation protein
G418	Geneticin
GC	Glycoprotein C
GLCCER	Glycolipid glucosylceramide
GMEM	Glasgow modified Eagle's medium
GN	Glycoprotein N
GO	Gene ontology
HAZV	Hazara virus
HELA	Henrietta Lack
HEPES	4-(2-hydroxyethyl)-1-piperazineethanesulfonic acid
HI	Hydrophobicity
HCL	Hydrochloric acid
HNRNP	Heterogeneous nuclear ribonucleoproteins
HRTV	Heartland virus
ICN	Bovine lipoprotein
ICTV	International Committee on Taxonomy of Viruses
IDT	Integrated DNA technologies
IFN	Interferon
IGPAL	Octylphenoxypolyethoxyethanol
IMD	Immune Deficiency
IRF-3	Interferon regulatory factor 3
IRPS	Iron regulatory proteins
JAK/STAT	Janus kinase/signalling transducer and activator of transcription
JNK	Jun-N-terminal kinase
KH	K homology
LACV	LaCrosse virus
LAMP1	Lysosomal-associated membrane protein 1

LC-MS/MS	Liquid chromatography–mass spectrometry
LDH	Lactate dehydrogenase
LDL	Low-density lipoprotein
LFQ	Liquid -free quantification
LGTV	Langat virus
LICL	Lithium chloride
LIDS	Lithium dodecyl sulphate
MAGOH	Mago homolog
MAPK	Mitogen activated protein kinase
MAVS	Mitochondrial antiviral-signalling protein
MDH	Malate dehydrogenase
MIRNA	Micro RNA
MLN51	Metastatic lymph node 51
MOI	Multiplicity of infection
MRNA	Messenger RNA
NACL	Sodium chloride
NAOH	Sodium hydroxide
N/NCAP	Nucleocapsid
NCBI	National Centre for Biotechnology Information
NCRNA	Non-coding RNA
NMD	Nonsense mediated decay
NS	Non-structural
NSM	Non-structural M protein
NSS	Non-structural S protein
OPTI-MEM	Opti-minimum essential media
ORF	Open reading frame
OROV	Oropouche virus
P.I	Post infection
P.VAL	P-value
PABP1	Polyadenylate-binding protein 1
PAGE	Polyacrylamide gel electrophoresis
PAMP	Pathogen-associated molecular pattern
PCA	Principal component analysis
PCR	Polymerase chain reaction
PI	Isoelectric point
PIRNA	Piwi-interacting RNA
PKR	Protein kinase RNA-activated
POLY(A)	Polyadenylated

POWV	Powassan virus
PPIL2	Peptidylprolyl Isomerase Like 2
PRKRA	Protein kinase EIF2AK2
PRR	Pattern recognition receptor
RAFRI	Rendered average far-red intensity
RBD	RNA-binding domain
RBM8A	RNA-binding protein 8A
RBP	RNA binding protein
RBPOME	RNA binding proteome
RDRP	RNA-dependant RNA-polymerase
RIC	RNA interactome capture
RIG-I	Retinoic acid-inducible gene I
RISC	RNA-induced silencing complex
RNP	Ribonucleoprotein complex
RRM	RNA recognition motif
RRNA	Ribosomal RNA
RT QPCR	Real-time quantitative PCR
RVFV	Rift Valley fever virus
SAP30	Sin3A associated protein 30
SBV	Sindbis virus
SCF	SKP1-CUL1/CDC53-F box protein
SDS	Sodium dodecyl sulfate
SFRNA	Sub-genomic flavivirus RNA
SFTSV	Severe Fever with Thrombocytopenia Syndrome Virus/ Dabie Bandavirus
SFV	Semliki Forest virus
SIRNA	Small interfering RNA
SMRNA	Small RNA
SNAP-25	Synaptosomal-Associated Protein, 25kDa
SND1	Staphylococcal nuclease and tudor domain-containing protein 1
SNRNA	Small nuclear RNA
SNRPE	Small nuclear ribonucleoprotein E
SP3	Bead-based single-pot, solid-phase-enhanced sample-preparation
SS	Single stranded
SSHV	Snowshoe hare virus
STAT	Signal transducer and activator of transcription
TBEV	Tick-borne encephalitis virus
TBK-1	TANK-binding kinase 1
TBP	Tryptose Phosphate Buffer

TCEP	Tris(2-carboxyethyl)phosphine
TFIIH	Transcription factor II H
TOP3B	Topoisomerase 3 beta
TOSV	Toscana virus
TRIM25	Tripartite motif-containing protein 25
TRNA	Transfer RNA
U SNRNPS	U-rich small nuclear ribonucleoproteins
UNKL	Unk-like zinc finger
UTR	Untranslated region
UUKV	Uukuniemi virus
UV	Ultraviolet
VA-1	Venom allergen-1
VAMP3	Vesicle-associated membrane protein 3
VIRNA	Viral interfering RNA
VLP	Virus-like particle
VRNA	Viral RNA
WHO	World Health Organisation
WNV	West Nile virus
XRN1	5’-3’ exoribonuclease 1
YY1	Yin Yang 1
ZIKV	Zika virus

Chapter 1 Introduction

This chapter will discuss ticks, in the context as both vectors of pathogens and cell lines derived from tick embryos as a laboratory tool. Following this, an overview of the order *Bunyavirales*, including classification, structure, disease prevalence and vector transmission, is given. Examples from both tick-borne and mosquito-borne species within are described, before concluding with a more detailed review of the species *Uukuniemi uukuniemiense*, herein referred to by the isolate used, Uukuniemi virus (UUKV), as a model tick-borne bunyavirus. With the exception of hantaviruses, which use small mammals as vectors and are transmitted through the aerosolised excreta, all bunyaviruses are arthropod-borne (Albornoz, Hoffmann, Lozach, & Tischler, 2016; Boshra, 2022; Burrell, Howard, & Murphy, 2017). For the purposes of this research, the *Hantaviridae* will not be discussed in this thesis.

1.1 Ticks

It is estimated that fewer than 10% of known tick species are competent vectors of viruses. Despite this, these organisms pose a substantial and increasing risk to animal and human health (Kazimirova et al., 2017; Mazelier et al., 2016; Romano, Stefanini, Canale, & Benelli, 2018). There are large gaps in knowledge surrounding ticks, partially due to their difficulty to maintain within a laboratory setting. This was particularly true before the establishment of artificial blood feeding, as rearing is time consuming, expensive, and requires specialist resources (Elhachimi et al., 2021). Although artificial blood-feeding has now lightened these burdens, there are very few facilities globally which contain tick-colonies, and as a result these species are still highly understudied (Fogaça et al., 2021; Romano et al., 2018). Cell lines derived from various tick species offer a compromise to these drawbacks, allowing for infection studies to be performed and the intracellular mechanisms to be investigated. However, more work is required to characterize these cell lines. Many gaps within our understanding of tick biology have begun to be tackled within the past 60 years through the use of these tools, alongside experiments using whole organisms (both laboratory-reared and from the wild), clinical data, and disease and vector surveillance (Bell-Sakyi, Zweygarth, Blouin, Gould, & Jongejan, 2007). All species of ticks are grouped into three families: *Argasidae* (soft-shell), *Ixodidae* (hard-shell), and *Nuttalliellidae* (monotypic). The focus of this work, in relation to bunyaviruses, is limited to the study of the hard-shelled *Ixodidae* family and therefore all further references to tick species will be from the *Ixodidae* family unless specified otherwise (Nava, 2009).

At an organismal level there is little published within the literature on the genomes of ticks. Despite being arguably one of the most important vectors for the transmission of tick-borne

diseases, only relatively recently has the genome sequence for *I. ricinus* been published, with the most recent draft covering approximately 67% of the non-repetitive sequences within the genome. The group also used BLAST to compare the protein scaffolds to the annotated proteins of *Ixodes scapularis (I. scapularis)* to enhance this mapping (Cramaro, Hunewald, Bell-Sakyi, & Muller, 2017; Cramaro et al., 2015). The first tick genome to be sequenced was that of *I. scapularis* in 2016, covering around 57% of the total genetic material (Gulia-Nuss et al., 2016). Following this, a higher-quality *I. scapularis* genome with an improved, continuous genome and over 10,000 extra defined protein-coding genes has been published. In addition, this work used nano- liquid chromatography–mass spectrometry (LC-MS/MS) to identify 4927 proteins from *I. scapularis* across different life stages of the tick (De et al., 2023). This is currently the most detailed genomic report for any tick species, although more work is required to ascertain the protein products for many of the transcripts, and their function within the organism (Fogaça et al., 2021).

1.1.1 Organism

1.1.1.1 Lifecycle

Although timings and exact environmental conditions may differ between species, most ticks follow a very similar lifecycle. This begins with the egg stage followed by hatching and three life stages: larva, nymph, and adult. To move from one life stage to the next a blood meal is required (James H. Oliver, 1993; Kahl & Gray, 2023). Depending on the life stage of the tick, the length of time spent taking a blood meal can vary from two days at the larval stage, to up to ten days as an adult female (Süss, Klaus, Gerstengarbe, & Werner, 2008). Completing this life cycle may take anywhere between 2-6 years, dependent on environmental conditions. Once a bloodmeal is taken, the tick will detach from the host and shelter, usually within undergrowth or leaf litter to preserve energy and resources. During this time, the tick will wait until the weather is warmer (typically June-October) to moult, meaning depending on when the blood meal is taken the tick may remain sheltered for several months in an engorged state (H. G. Koch & Tuck, 1986). The process of moulting, triggered by the apolysis (separating the layer to be shed from the underlying epithelium) takes several weeks to complete. The ectodermal tissue degenerates and allows for the formation of new tissues, with old tissue being digested and new tissue forming simultaneously. In the last two weeks of this process, the tick sheds any remaining waste leftover from the process, and is then considered to have begun the next stage of its life cycle (James H. Oliver, 1993; Kahl & Gray, 2023). If the tick is an adult female at the time of taking the bloodmeal, and is mated during or before the bloodmeal, once engorged the

female will detach and immediately lay eggs as long as the temperature remains above 4 °C (if the temperature drops the laying will pause until it is increased above the threshold), and once laying is complete the female dies (J. S. Gray, Kahl, Lane, Levin, & Tsao, 2016; Kahl & Gray, 2023). To take a blood meal (at any life stage), the mouth parts pierce the skin, causing the blood to pool due to damage to the blood vessels and skin tissue. The mouthparts contain a barbed structure that acts as an anchor and a straw to imbibe the blood meal. Following penetration of the mouth parts, saliva secretions act to further anchor the tick in place during feeding. The saliva additionally acts to counter the hosts blood-clotting abilities and reduce detection of the bite by the host, with acquisition of blood alternating with the secretion of saliva during feeding (Richter, Matuschka, Spielman, & Mahadevan, 2013; Vancova et al., 2020). The compounds released by tick saliva vary depending on the species, life stage, and sex of the tick, and many of the compounds isolated require further experimental testing to confirm their function. Briefly, compounds have been identified that target vasodilation/vasoconstriction, wound healing/angiogenesis, platelet aggregation, blood coagulation, innate immune response, the compliment system, and acquired immune response (Diaz-Martin et al., 2013; P. A. Nuttall, 2023; Ribeiro et al., 2006; Simo, Kazimirova, Richardson, & Bonnet, 2017).

1.1.1.2 Immune System

Most of the knowledge on arthropod immune responses has been gained from studies on species from the *Aedes* and *Anopheles* genera of mosquito or the fruit fly genus *Drosophila* (Blair, 2011; Fogaça et al., 2021; Y. Li et al., 2017). The arthropod immune system incorporates only an innate immune response, which can be divided into two main factions: cellular and humoral. The cellular response is predominantly carried out by dedicated immune cells, named haemocytes, responding to microbes such as bacteria, yeast and spirochetes. Within the humoral response, a variety of pattern-recognition proteins trigger four major immune signalling pathways: Toll, immune deficiency (IMD), Jun-N-terminal kinase (JNK), and Janus kinase/signalling transducer and activator of transcription (JAK/STAT). Through additional experiments on the species previously mentioned and other works on mites, lice and others, it is widely agreed that arthropod immune systems display a wide diversification within these pathways (Baxter, Contet, & Krueger, 2017; Fogaça et al., 2021; W. J. Palmer & Jiggins, 2015; Rosa et al., 2016; Sheehan, Garvey, Croke, & Kavanagh, 2018). For example, through microbial challenge experiments in BME6 cells (derived from the *Rhipicephalus microplus* tick species) it was revealed that, unlike mosquitoes, ticks may lack central components of both the Toll and JAK/STAT signalling pathways (W. J. Palmer & Jiggins, 2015). Despite this, when *I. scapularis* were exposed to

Anaplasma phagocytophilum bacteria, silencing of STAT or JAK components, but not components of the Toll or IMD pathways, resulted in an increase in bacterial output, indicating the JAK/STAT pathway is involved in controlling bacterial infection though regulating the production of antimicrobial peptides (AMPs) (L. Liu et al., 2012). It has also been determined that some immune-signalling genes within arthropods are constitutively transcribed, with microbial challenge causing differences in transcriptional patterns rather than an 'on-off' system (Rosa et al., 2016). Triggering of these pathways can have a variety of outcomes, including producing effector molecules such as AMPs. When the mosquito *Aedes aegypti* is infected by viruses the Toll pathway is triggered, culminating in specific AMP expression (Baxter et al., 2017; Xi, Ramirez, & Dimopoulos, 2008). When using basic local alignment search tool (BLAST) for immune pathway components, 234 genes were found which were associated across nine families involved in humoral or cellular immune response, including 55 genes relating to Toll, IMD and JAK-STAT in *I. scapularis* (A. A. Smith & Pal, 2014).

Several studies have been carried out at both the proteomic and transcriptomic levels to explore the response of ticks (both cell lines and organism) to various microorganismal infections. In ISE6 cells, infection with *Anaplasma phagocytophilum* resulted in the upregulation of ~300 miRNAs associated with infection response and cellular metabolic processes, and downregulation of ~33 miRNAs associated with gene expression and development (Artigas-Jeronimo et al., 2019). By comparing the transcriptional response of *A. phagocytophilum* infection in ISE6 and IRE/CTVM20, the ISE6 response resembled that of the tick haemocyte immune cells, whereas the IRE20 cell line behaviour to infection more closely resembled the response of an infected midgut. In the ISE6 cells, of the 174 differentially expressed, 45 were upregulated with the other 129 genes were downregulated during infection. Both upregulated and downregulated transcripts were involved with cellular and metabolic processes, alongside homeostasis functions. This pathogen also causes the downregulation of proteins associated with apoptosis to inhibit cell death (P. Alberdi et al., 2015; P. Alberdi et al., 2016).

In the context of viral infection, the RNA interference (RNAi) pathways are the primary antiviral defence mechanism employed in arthropods. Within these pathways, viral dsRNA is cleaved into single-stranded siRNAs, roughly 21 nucleotides in length in mosquitoes and 22 nucleotides in length in ticks, by a Dicer (Dcr) protein. These are known as viral interfering RNAs (viRNAs) and are then loaded into Argonaute (Ago) proteins, which use the viRNA as guides to degrade any RNA the guide associates with. This complex will further couple to other related proteins, such as RNA dependant RNA polymerases (e.g.

EGO-1), to form a RNA induced silencing complex (RISC) (Aliyari & Ding, 2009; Asgari, 2014; Blair, 2011; Grubaugh et al., 2016; Obbard, Gordon, Buck, & Jiggins, 2009; W. J. Palmer & Jiggins, 2015; Schnettler et al., 2014). It is important to note that, as bunyaviruses have negative-sense RNA genomes, the path to RNAi production is unclear. This is because it has been widely demonstrated that dsRNA is not usually detectable during the replication cycle of negative-strand RNA viruses during host infection, meaning the production of the viRNAs may be reliant on ssRNA secondary structures (Blair, 2011). Beyond this, the Dcr and Ago proteins are very interesting proteins. Not only do they act as PRRs to activate the pathways mentioned upon detection of vRNA or transposable elements, but additionally through the formation of the RISC complexes, they are able to carry out their own anti-viral functions (Aliyari & Ding, 2009; Blair, 2011; Jaronczyk, Carmichael, & Hobman, 2005; Obbard et al., 2009; Paradkar, Duchemin, Voysey, & Walker, 2014). When mapping viRNAs from the antiviral response to a flavivirus and bunyavirus infection, the viRNAs mapping to the viral genome were found at the highest frequency around the 5' and 3' UTRs, although the ORF was also seen to be targeted (Asgari, 2014; Brackney, Beane, & Ebel, 2009; Brackney et al., 2010; Dietrich, Shi, et al., 2017; Grubaugh et al., 2016).

As it stands, there are four known RNAi pathways arthropods employ. Three where the source of the RNA is endogenous; piRNA (piwi-interacting RNA), endo-siRNA (endogenous small interfering RNA), and miRNA (microRNA). The main difference in these pathways is that the former pathway is Dicer-independent and involves the PIWI family of Ago proteins, whereas the latter two require both Ago or Ago-like and Dcr proteins. The fourth pathway is exo-siRNA (exogenous small interfering RNA) which is often considered the most important mosquito antiviral innate immune response (Blair, 2011). Of these pathways, it is the siRNAi pathways which shows the highest diversification across arthropod species and a high evolution, which may be due to this pathway being the most dominant antiviral defence (Aliyari & Ding, 2009; Fogaça et al., 2021; Obbard et al., 2009; W. J. Palmer & Jiggins, 2015). miRNAs, on the other hand, show less diversification and are also able to regulate mRNA translation and stability through binding to 5'-UTR recognition sites to alter cellular function (Asgari, 2014; Fabian, Sonenberg, & Filipowicz, 2010). The production and differential transcription of endogenous miRNAs in *Aedes aegypti* is triggered by blood feeding, and these transcripts are important for development and producing a 'pre-emptive' immune response (Hussain, Walker, O'Neill, & Asgari, 2013). A similar reaction occurs upon blood feeding in ticks, for example the acquisition of a blood meal over 3-days in *I. scapularis* nymphs is accompanied by transcription levels in salivary glands. Although many of these transcripts were undefined within the study,

differential regulated transcripts involved with producing putative secreted proteins, lipocalins, Kunitz domain-containing proteins, and anti-microbial peptides were detected (McNally et al., 2012). The specific mechanisms by which these genes are induced in either case are unclear, as taking a blood-meal not only produces an influx of nutrients but thermal stress due to the heat of the blood meal (Rosche, Sidak-Loftis, Hurtado, Fisk, & Shaw, 2020).

RNAi responses can be detected at all stages of a ticks lifecycle (Grubaugh et al., 2016), and *I. scapularis* has shown significant gene expansion of RNAi elements. For example, their genome contains five Ago homologous genes: Ago-78, Ago-96, Ago-68, Ago-16, and Ago-30, and two Dcr genes: Dcr-89 and Dcr-90. Of these genes, Ago-78 is homologous to insect Ago-1, whilst the rest are homologous to insect Ago-2, and the Dcr genes were homologous to *Drosophila* Dcr-2 and Dcr-1, respectively (Baxter et al., 2017; Fogaça et al., 2021). Approximately 31 key RNAi-related proteins and 23 homologous proteins related to dsRNA up-taking and processing have been identified through genomic analysis, including Ago-2, FMRp, and EGO-1, with loss-of-function studies also supporting these genes for tick-specific RNAi pathways (Kurscheid et al., 2009; A. A. Smith & Pal, 2014). Despite evidence of RNAi, Toll, IMD, and JAK/STAT components being present in the genome, limited experimentation has been conducted leading to a paucity of information as to whether all these components are transcribed and involved in the tick antiviral response. The piRNA response to infection has not been touched on within the literature, although this may be due to *I. scapularis* lacking an Ago3 homolog which is integral to ping-pong amplification needed in this process and the biogenesis of piRNA varying between germline and somatic cells. The piRNA pathway appears to be triggered by ssRNA (Asgari, 2014; Blair, 2011; Fogaça et al., 2021; Grubaugh et al., 2016; Perveen et al., 2023; Schnettler et al., 2014). The RNAi response does not just affect the vector. In the salivary glands of *I. scapularis*, Powassan virus (POWV) infection causes differential expression of miRNAs, 35 upregulated and 17 downregulated, which are secreted with the saliva and can affect the host response to POWV (Hermance, Widen, Wood, & Thangamani, 2019).

When challenged with viral infection, sub-genomic flavivirus (sf)RNAs are expressed in cells infected with many different *Flaviviridae* members, such as POWV, Langat virus (LGTV) and TBEV, which act to counter the tick RNAi system and can be required for transmission (Fogaça et al., 2021; Schnettler et al., 2014; Slonchak et al., 2020; Weisheit et al., 2015). Endogenous miRNA expression also appears to be able to be modulated by viruses as a method of controlling replication within the vector (Asgari, 2014; Fogaça et al., 2021). This antiviral RNAi responses promotes viral evolution by creating positive selection pressure, and this pressure causes escape mutations depending on the target of the RNAi.

RNAi that targets the 3' and 5' end is more likely to produce escape mutations, compared to RNAi that targets the structural regions of the vRNA which is less likely to produce mutations and is hypothesised to be a method of controlling virus replication within the tick (Grubaugh et al., 2016). When the RNAi system is activated against one virus segment in a recombinant virus system, RNA silencing can work against subsequent infection for the wild-type virus. For example, when recombinant SFV containing the Hazara virus (HAZV) nucleoprotein is used to induce the RNAi response in ISE6 cells prior to super-infection, upon challenge with the wild-type HAZV, replication of the virus was inhibited. However, this was sequence specific, as infection with a recombinant SFV containing the CCHFV nucleocapsid sequence did not illicit silencing of HAZV upon challenge (Garcia et al., 2005). This does indicate that once a better understanding of the intracellular workings of the tick vector is achieved, we can establish pathogen-derived resistance via exploiting the RNAi pathway (Garcia et al., 2005; Garcia et al., 2006).

There is evidence that the RNAi pathways and immune signalling pathways interact and display crosstalk (Fogaça et al., 2021; Paradkar et al., 2014). In *Culex* species mosquitoes, when Dcr-2 recognises West Nile Virus (WNV) dsRNA the signalling cascade causes increased Vago expression, which is in turn secreted from the infected cells. This compound then interacts with cellular receptors in surrounding uninfected cells, triggering the JAK/STAT pathway and inducing an anti-viral state through upregulation of anti-viral genes such as *vir-1* (Fogaça et al., 2021; Paradkar et al., 2014; Paradkar, Trinidad, Voysey, Duchemin, & Walker, 2012). In both *Ae. aegypti* derived cell lines (Aag2) and in whole *Drosophila* flies, crosstalk has been seen between the RNAi and Toll pathway. In the former species, endogenous miRNA inhibited activation of NF-κB, reducing AMP synthesis and enhancing dengue virus (DENV) infection. In the latter, endogenous miRNA regulates a Toll-derived anti-microbial peptides. miRNAs co-targeting the same transcripts is also an example of the tight regulation within the arthropod cells to allow for a balanced immune response (Baxter et al., 2017; Fogaça et al., 2021; Xi et al., 2008). Currently however, there is only one study reporting crosstalk in immune signalling where the authors knocked down the transcription factors Dorsal, Relish, or STAT in organism *R. microplus* and challenged these knockdowns with *A. marginale*, indicating the crosstalk of the immune pathways in ticks may enhance the immune response, although these studies need further investigation. Additionally, there is an indication that apoptosis (programmed cell death) plays a role the immune response of ticks, and pathogens may try to inhibit this apoptotic response (P. Alberdi et al., 2016; Capelli-Peixoto et al., 2017; Fogaça et al., 2021).

1.1.1.3 Geographical distribution and Climate Change

To date there are over 700 known species within the *Ixodidae* family, spread worldwide over 226 countries and territories (Guglielmone, Nava, & Robbins, 2023; Nava, 2009). For example, *I. scapularis* is established in the eastern United States and Canada, *I. pacificus* in the western United States, *I. ricinus* in Europe and Asia, and *I. persulcatus* in Asia. *I. ricinus* alone is estimated to account for up to 95% of all human tick bite incidences in Europe (Rahlenbeck, Fingerle, & Doggett, 2016; Schotthoefer & Frost, 2015; Süss et al., 2008). Species within the *Ixodes* genus are vectors of several pathogens that can have a severe impact on human health (including Lyme borreliosis and tick-borne encephalitis virus (TBEV)).

The main factors to determine if an environment is suitable for tick survival are high humidity, warm temperatures, vegetation for questing (host finding behaviour)/shelter, and the presence of hosts. Hard ticks only take on water by absorption and during blood meals, meaning the tick may regurgitate the water back into the host to prevent an excess influx of water into its system. In addition to the secretion of saliva, this is an additional means by which pathogens may be transmitted during feeding. High humidity and vegetation to provide shelter from direct sunlight prevent ticks from desiccation, and warmer temperatures allow ticks to be active (ticks are known to become dormant when the temperature decreases below 4-6°C on average) (Bertrand & Wilson, 1996; Fielden & Lighton, 1996; Leger, Vourc'h, Vial, Chevillon, & McCoy, 2013; Süss et al., 2008). As climate change causes an increase in average precipitation/humidity and global temperature, more favourable environmental conditions are being created for ticks. Additionally, increased human activities such as travel, livestock transport, and environmental modifications are providing more opportunities to expand their geographical reach (Dantas-Torres, 2015; Lauterbach, Wells, O'Hara, Kalko, & Renner, 2013; Leger et al., 2013; Süss et al., 2008). There are many studies within the literature which directly tie climate change to the expansion of tick populations geographically, the increased number of ticks within populations, and an increase in the activity timeframe of ticks throughout the year (Leger et al., 2013; van Oort, Hovelsrud, Risvoll, Mohr, & Jore, 2020). One study noted that, in central Germany, during the winter period (September to March) of 2006/2007 tick activity could be seen throughout the timeframe as opposed to the expected winter dormancy period (Süss et al., 2008). More recently, according the European Centre for Disease Prevention and Control (ECDC), as of November 2023 *I. ricinus* has become established within new areas of Croatia, France and Spain (https://www.ecdc.europa.eu/en/disease-vectors/surveillance-and-disease-data/tick-maps [accessed January 2024]).

When looking at the impact of tick populations on instances of tick-borne viruses, the increased distribution of these vector species is reflected within the increased incidence of disease in areas where the pathogen is already established, and as the vector expands into new territories the risk of transmission in these naive territories increases (Rochlin & Toledo, 2020; Süss et al., 2008; van Oort et al., 2020). Using mathematical modelling to analyse the impact of different types of transmission on the average number of cases of an infectious disease (R_0) of TBEV, it is theorized that the co-aggregation of ticks is more impactful on the R_0 than the number of systemically infected hosts, meaning any increase in tick numbers or geographical distribution will substantially increase the risk of virus transmission and outbreaks (Johnstone-Robertson, Diuk-Wasser, & Davis, 2020). Modelling has also been applied to try to calculate the impact of variables such as climate change on the movement of ticks and tickborne diseases. However, this is only able to predict the likelihood of outcomes and should be used as a guide rather than a certainty. For example, in a study published in 2015, climate change models did not predict the incursion of TBEV in the UK, however as of 2019 TBEV seropositive samples, and ticks containing TBEV RNA, was detected within the UK for the first time. Since then, several cases of TBEV infection have been confirmed within humans in the UK ((Holding et al., 2020; Medlock & Leach, 2015) https://www.gov.uk/guidance/tick-borne-encephalitis-epidemiology-diagnosis-and-prevention [accessed January 2024]). This is particularly alarming as other, more highly pathogenic viruses such as Crimean Congo haemorrhagic fever virus (CCHFV), have also begun to move into more highly populated areas of countries such as Spain where the virus had not previously been considered endemic before 2010 (Carrera-Faja et al., 2022).

1.1.2 Tick- derived cell culture systems

In the past 60 years, over 40 cell lines have been developed from 13 *Ixodidae* and one *Argasidae* tick species (Bell-Sakyi et al., 2007), and have been crucial for elucidating the biology of ticks, particularly concerning their immune responses (Bell-Sakyi et al., 2007; Sidak-Loftis et al., 2022; Simser, Macaluso, Mulenga, & Azad, 2004). However, despite the development of these pivotal reagents, there are still large gaps in knowledge regarding these resources, with only one cell line (ISE6) having a published genome (Miller et al., 2018).

The ISE6 cell culture, derived from *I. scapularis* embryos, is one of the most widely used tick-derived cell lines for examining tick-pathogen interactions (Mateos-Hernandez et al., 2021). This cell line was produced in 1994, and although several tick cell lines had been produced before this date, most cell lines were unable to be maintained past 6 months in culture. Munderloh, alongside developing the ISE6 cell line, developed a reliable method

for the freezing and regeneration of the tick cell lines which allowed them to have a greater application in research (Bell-Sakyi et al., 2007; Munderloh, Liu, Wang, Chen, & Kurtti, 1994). One of the main factors to note for tick cell line production is that due to their establishment from embryonic cells and the immortalisation methodology used, no selective efforts were made to differentiate the cells into a specific tissue type. The cells contained within these cultures show a variety of morphologies and cell types, which can decline as passage number increases. However, analysis of the several isozymes including phosphogluconate dehydrogenase, acid phosphatase, lactate dehydrogenase (LDH), malate dehydrogenase (MDH), and esterases remained consistent even after a year of cell line propagation. The presence and banding patterns of these isozymes were also consistent with enzyme activity data from *Ixodes* tick tissue extracts. It is therefore unclear what causes these morphological changes, or the extent at which the intracellular landscape of the cells differs over time (Munderloh et al., 1994). Interestingly, cells within these homogenous mixes can gain or lose chromosomes without affecting survival, but attempts to isolate singular cells for cloning and cell culture growth have proved unsuccessful, implying that this co-culturing of different cell types is required for cell line survival (Bell-Sakyi et al., 2007; Kotsarenko et al., 2020). In a laboratory setting, unlike most tick cell cultures which are not strongly adherent, ISE6 cell cultures are able to be cultured on various tissue culture surfaces. Tick cell lines have a replication time of 5 to 6 days, and do not exhibit monolayer contact inhibition (Bell-Sakyi et al., 2007; Thorpe, Wang, Munderloh, & Kurtti, 2021).

In terms of cell line sequences, as mentioned previously, only ISE6 has a published genome, as many ‘omic’ analyses employing the use of tick cell lines have focussed on the changes in the genome under different conditions. The draft genome sequence of ISE6 cell cultures was first published in 2018 by Miller and colleagues and was produced using single-molecule, long read sequencing technology (Miller et al., 2018). This lack of genomic data is due, in part, to the large size and the high percentage of repetitive sequences within the tick cell genome, which can range from ~50% to ~70% making sequencing and construction of the genome difficult. In addition, as mentioned the genetic characteristics of the cell line can change over passaging, and the genetic diversity within the same species of tick in nature is currently unknown (Cramaro et al., 2017; De et al., 2023; Fogaça et al., 2021; Jia et al., 2020; Meyer, Kurtti, Van Zee, & Hill, 2010; M. J. Palmer, Bantle, Guo, & Fargo, 1994; Ullmann, Lima, Guerrero, Piesman, & Black, 2005). The ISE6 cell line currently has ~19000 identified protein coding messenger RNA (mRNA) transcripts for which protein FASTA files are accessible, and 4408 non-coding RNA gene transcripts (Miller et al., 2018). By using protein BLAST analysis of known sequences for both tick and other species homologs

and orthologs (respectively), in addition to further proteomic and functional analysis, many of the mRNA gene transcript products have been identified and characterised. For example, BLAST analysis of known *H. longicornis* and *I. ricinus* iron storage proteins (ferritins) and iron regulatory proteins (IRPs), important in iron homeostasis, allowed for sequence prediction and primer design to these transcripts within ISE6 cells. Further exposure of the cell lines to different concentrations of ferrous sulphate to induce gene expression, and gene silencing assays, confirmed the identity of these genes within ISE6 cell cultures and the mechanism of action was elucidated (Hernandez et al., 2018). Prior proteomic analysis indicated that the ISE6 cells contained neuronal and immune-response protein markers. In the study of 'An Ixodes scapularis cell line with a predominantly neuron-like phenotype', 322 proteins were identified in the ISE6 cell line, compared to 200 from native *I. scapularis* synganglia and 355 in IDE/CTVM12 samples, these markers were in significantly larger quantities when compared to IDE/CTVM12, but synganglia possessed more unique neuronal proteins. To support these data, modified ISE6 cells expressing mCherry were injected into unfed *I. scapularis* larva and nymphs incubated for 6 weeks. When ticks injected with these were allowed to feed and moult, the fluorescent ISE6 cells further differentiated into elongated neuron-like cells within the organism (Oliver, Chavez, Felsheim, Kurtti, & Munderloh, 2015). Much of the characterisation of the ISE6 cell line investigated the cellular response resulting from exposure to different pathogens compared to other tick-derived cell lines. When exposed to the bacterium *Anaplasma phagocytophilium*, the ISE6 cell line transcriptional response resembled that of haemocytes (P. Alberdi et al., 2016), which are cells that circulate through the haemolymph (circulating fluid) and can be considered the arthropod equivalent of mammalian immune cells (Simser et al., 2004).

Finally, many pathogens that were previously unable to be grown efficiently in mammalian culture have been propagated and studied in the ISE6 cell line, including *Anaplasma phagocytophilum* (Massung et al., 2007), *Borrelia burgdorferi* (Bugrysheva, Dobrikova, Godfrey, Sartakova, & Cabello, 2002), TBEV (Kevely et al., 2022), louping ill virus, Powassan virus (POWV) and West Nile virus (WNV) (Lawrie, Uzcategui, Armesto, Bell-Sakyi, & Gould, 2004).

1.2 The *Bunyavirales* order

1.2.1 Classification

Upon establishment in 2017 by the International Committee on Taxonomy of Viruses (ICTV), the order *Bunyavirales* (commonly referred to as Bunyaviruses) contained nine families. Prior to this, the *Bunyavirales* was first recognised as a family, in 1975. This order was further developed through subsequent taxonomic updates, and currently contains 14 families and over 400 named virus species in total. (Abudurexiti et al., 2019; Blitvich et al., 2018; Kuhn et al., 2022; Maes et al., 2019; Maes et al., 2018; Plyusnin, 2012).

Most known bunyaviruses show vector specificity, for example a bunyavirus vectored by mosquitoes will not be isolated in ticks (Psylvia Léger & Lozach, 2015; Anna Papa, Zelená, Papadopoulou, & Mrázek, 2018). There is limited evidence to show there has been isolation of a small number of bunyaviruses in non-vector arthropod species. To date there are no conclusive studies to show in these cases the infected arthropods are able to transmit the isolated bunyavirus. It is hypothesised that non-vector arthropods may take blood meals from infected hosts, and although not infected themselves, if the arthropod is then probed for the presence of virus the infected blood meal present within the gut causes a false positive (Fontenille et al., 1998; Linthicum, Davies, Kairo, & Bailey, 1985; Pepin, Bouloy, Bird, Kemp, & Paweska, 2010). Therefore, when discussing vector tropism of these viruses within this thesis, where appropriate these viruses can be broadly categorized into ‘mosquito-borne’ (vectored by mosquitoes) and ‘tick-borne’ (vectored by ticks).

1.2.2 Structure

Most bunyaviruses have tri-segmented, linear, single-stranded, negative- or ambisense-RNA genomes, packaged within virions of 80-120 nm in diameter (Blitvich et al., 2018; Plyusnin, 2012). An exception to this is the *Arenaviridae* family, as species within this family have been found to have bi-segmented negative or ambisense genomes. The *Arenaviridae* family was first established in 1976 and reclassified to be within the order Bunyavirales in 2018. Similar to Hantaviridae, many of the species within this family are transmitted via rodents. Due to the genome structure and vector species, *Arenaviridae* will not be discussed within this thesis (Maes et al., 2018). These viruses A schematic representation of a bunyavirus particle is shown in Figure 1.1. Bunyaviruses express four structural proteins; glycoprotein n (Gn) and glycoprotein c (Gc) which are produced as a polyprotein from the medium (M) segment before being cleaved by host cell enzymes post-translationally, the nucleocapsid (N) protein encoded in the small (S) segment, and an RNA-

dependent RNA polymerase encoded by the large (L) segment. Non-structural (NS) proteins, termed NSs (encoded for on the S segment) and NSm (encoded for on the M segment) are produced in some bunyavirus species. The presence of these proteins is not mutually exclusive, and to date NSm has only been found in one of the tick-borne bunyaviruses, the highly pathogenic CCHFV. Use of reverse genetic systems to knockout this NSm protein from CCHFV indicated the protein is involved in promoting virion assembly and secretion, but is not required to complete the replication cycle or cause lethality (Burrell et al., 2017; Fares & Brennan, 2022; Freitas et al., 2020; A. Papa, Kontana, Tsioka, Chaligiannis, & Sotiraki, 2016; M. G. a. R. Rossmann, V.B, 2012; Welch et al., 2020). There is evidence to suggest that NSm is involved in vector-competence, while NSs is often associated with evasion of the mammalian hosts immune system, although further research is needed to fully elucidate the roles and mechanisms of these proteins (Kading, 2014). Additionally, no research has been published within the literature to determine if host factors are present within the viral particle, from either the host or the vector depending on the origin of the virus. This incorporation of host or vector cellular factors is likely to occur, as demonstrated in plant infecting RNA viruses, where packaging of host RNA and protein has been demonstrated, and these packaged factors influence the course of viral infection (Pena et al., 2022; Ranjan et al., 2023; Slater et al., 2022)

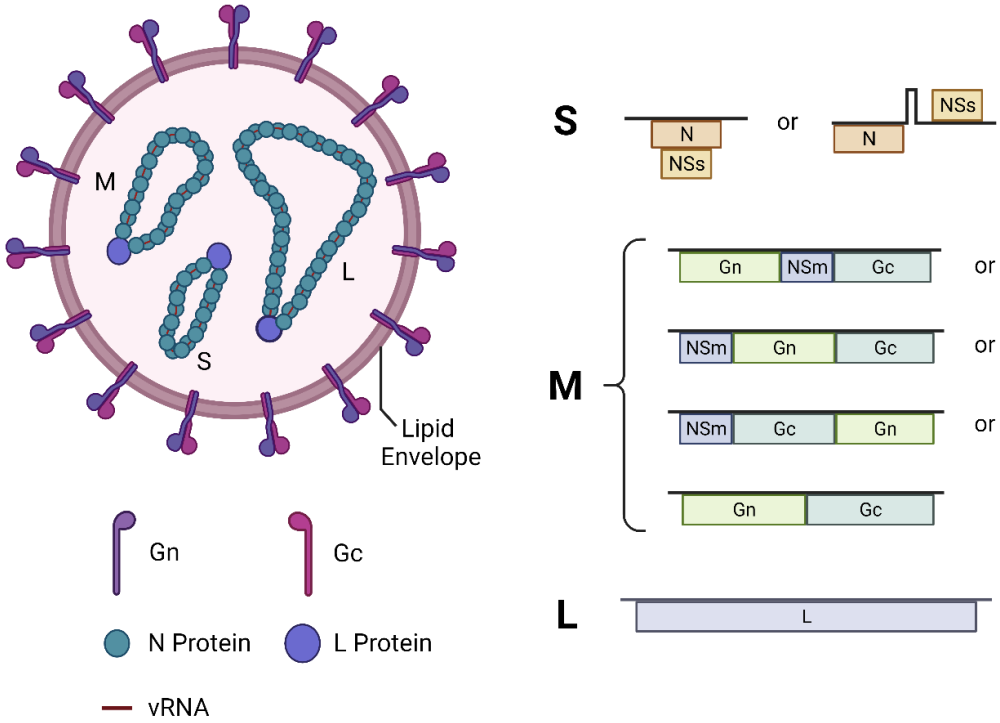

Figure 1.1: Schematic representation of a Bunyavirus particle and genome. Diagram of a bunyavirus particle with labelled structural proteins and viral RNA (left) and known genome structures (right), based on work by Léger and Lozach (Psylvia Léger & Lozach, 2015).

The production of bunyavirus proteins is regulated through the genus conserved 5' and 3' untranslated regions (UTRs), which are associated with regulation of transcription and replication of sub genomic messenger RNAs from which the viral proteins are translated. Previous work in a severe fever with thrombocytopenia syndrome virus (SFTSV) reverse-genetics system highlighted the importance of these sequences. A deletion in the 5' UTR and 3' UTR of the S segment abolished the minigenome/S segment activity, which was fully restored when both single nucleotide deletions were corrected (and half restored when only one was corrected) (Brennan et al., 2015; Gauliard, Billecocq, Flick, & Bouloy, 2006). Although this virus was renamed in 2023, for the writing within this thesis the species *Dabie bandavirus* will be referred to by the virus isolate name (SFTSV or HB29), as the acronym for *Dabie bandavirus* has not been confirmed within the literature.

1.2.3 Replication within the mammalian host

Infection of a mammalian host with a bunyavirus usually occurs via the bite of an infected arthropod, meaning the first cells to encounter the virus are likely Langerhans cells (a type of dendritic cells found in the skin), and dermal macrophages. These provide a pathway through the lymphatic system for the virus to spread throughout the host (Heath & Carbone, 2013; Le May & Bouloy, 2012; Psylvia Léger & Lozach, 2015). The virus particles bind to host cells via the viral glycoproteins, which are 'spike-like' projections spaced in an icosahedral lattice on the surface of the viral particle (Albornoz et al., 2016; Överby, Pettersson, & Neve, 2007). The binding specificity and efficiency of the viral particle varies between each viral species. UUKV binds to specific receptors, but this binding is inefficient. The UUKV virus particles are endocytosed in a mostly clathrin-coat independent manner, while opposite seems to occur with Rift Valley fever virus (RVFV), which mainly undergoes endocytosis in a clathrin-dependent manner (Psylvia Léger & Lozach, 2015; Lozach et al., 2010). Binding triggers endocytosis and internalisation of the receptor protein, carrying the virus with it, before the two dissociate within the early endosome. At this point, the receptor proteins are most likely recycled to the cell surface, whilst the endosome carrying the viral particles progresses through the endocytic pathway. Co-receptor or additional receptors may also be utilized in this process, but further investigation of these is needed for each viral species and vector/host cell combinations (Hofmann & Pohlmann, 2011). For example, there is evidence to suggest that in the case of RVFV infection, heparin sulphate is an attachment factor for the virus (Ganaie, Leung, Hartman, & Amarasinghe, 2023).

Bunyaviruses are late-penetrating, requiring being transported to late-stage endosomes where the pH is below 5.8. This allows the virus to gain access to the cell cytoplasm through

an acid-triggered membrane fusion activity mediated via Gc (a class II membrane fusion protein) (Garry & Garry, 2004; Plassmeyer, Soldan, Stachelek, Martin-Garcia, & Gonzalez-Scarano, 2005). Host or vector cell factors also play a key role in this stage, although the potential arthropod factors have not been explored in detail. In UUKV infection, mammalian host cell factors such as VAMP3, LAMP1, and BMP are important in trafficking the virus to late-endosomes and supporting fusion (J. Koch, Xin, Tischler, & Lozach, 2021; Meier et al., 2014). In comparison, RVFV used low-density lipoprotein (LDL) to increase infection and CCHFV depends on the presence of adaptor protein complex 2 (AP-2) to gain entry to the cells during endocytosis (Ganaie et al., 2023; Shtanko, Nikitina, Altuntas, Chepurnov, & Davey, 2014) Once fused, the ribonucleoprotein (RNP) is released into the cytosol and the replication lifecycle (as defined in Figure 1.2) can begin (Psylvia Léger & Lozach, 2015).

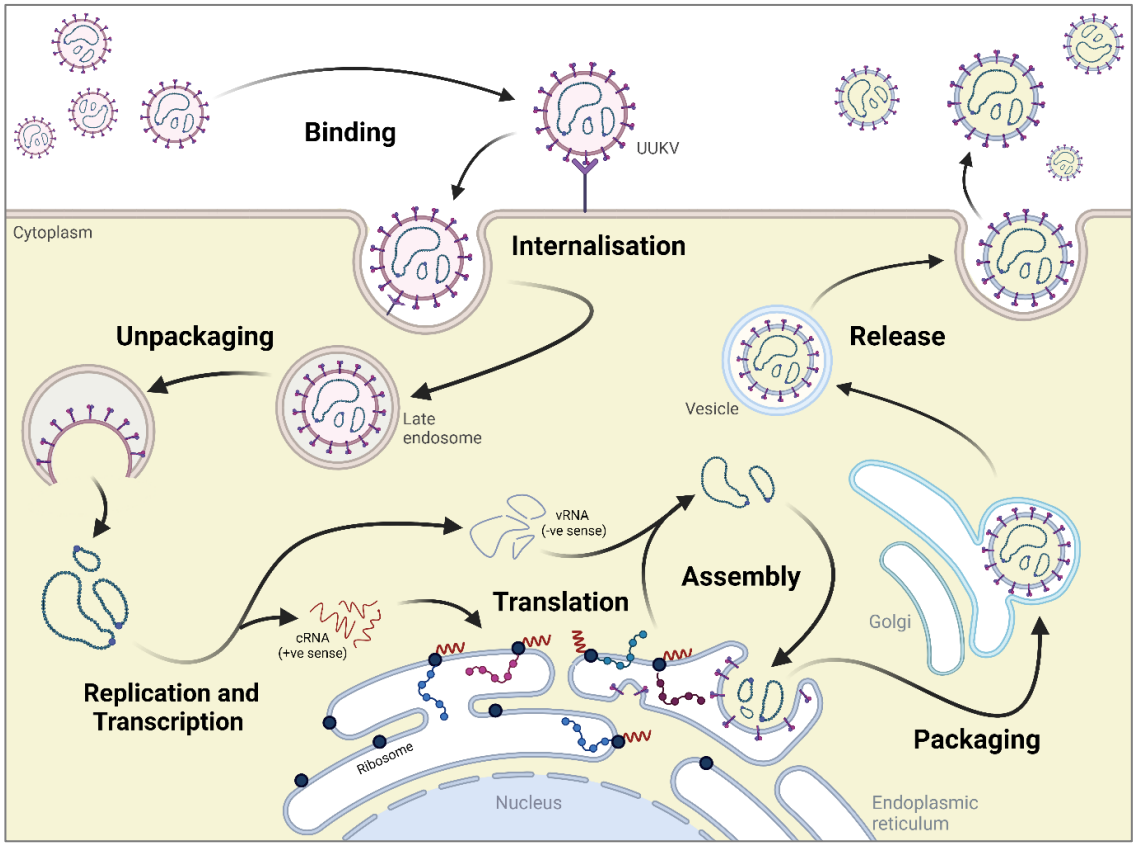

Figure 1.2: Schematic of Bunyavirus replication cycle within a host cell. Diagram showing a simplified Bunyavirus replication cycle within a host cell. Arrows indicate the movement through the stages of the viral lifecycle. Viral particles with pink membranes, such as those on the top left corner, represent infecting particles. Viral particles with blue membranes, such as those in the top right corner, represent viral progeny produced through the replication cycle. Negative sense viral genomic RNA (vRNA) is represented by blue lines. Positive sense complementary viral RNA (cRNA) is represented by red lines. Ribosomes are defined as solid blue circles on the membrane of the endoplasmic reticulum, and attached chained circles represent proteins being produced through translation.

As the RNP is released into the cytosol, the viral RNA (vRNA) of the bunyavirus must first undergo a round of replication in a primer-dependent manner to produce complementary RNA (cRNA) to act as a template, from which copies of viral RNA (vRNA) can be produced and translated into viral proteins (M. G. Rossmann & Rao, 2012; Walter & Barr, 2011). However, during the first attempts of the virus to transcribe its genome, the process undergoes premature termination to produce sub-genomic vRNAs. Transcription termination is believed to be caused through the action of termination sequences in the intergenic regions or UTRs, however RNA secondary structure may also play a role. Through this, the shorter sub-genomic vRNAs are transcribed through the action of the RdRp, allowing for the translation of viral proteins from the virally encoded ORF, which in turn increases the quantity of viral proteins within the cell. Translation occurs simultaneously alongside transcription to prevent the recognition of spurious termination signals that would otherwise form within the secondary structure. Once large enough quantities of N proteins have amassed within the cell, the interaction between the cRNA and N protein prevent premature transcription termination. This allows the production of full length antigenomic segments to be packaged into new virions (Barr, 2007; Boshra, 2022; Leger et al., 2013; Malet, Williams, Cusack, & Rosenthal, 2023; M. G. Rossmann & Rao, 2012; Spiegel, Plegge, & Pohlmann, 2016; Walter & Barr, 2011).

When cRNA and vRNA is made through the action of the viral RNA-dependant RNA-polymerase (RdRp), the RdRp ‘cap snatches’ via an endonuclease activity (similar to influenza A) the 5’ sequence from a host RNA to use as a primer to begin transcription. During these processes, the newly produced viral proteins and cRNA assemble in ‘tube-like’ replication factories produced through the modulation of the Golgi complex to produce vRNA. This is advantageous as it allows maximal packaging of new virion RNPs and additionally adds a level of ‘shielding’ to minimise interaction with host ‘immunity surveillance’ proteins (M. G. Rossmann & Rao, 2012; Walter & Barr, 2011). The mechanisms behind the formation of replication factories have only been investigated with a few species of bunyaviruses, primarily RVFV and BUNV. For species which produce NSm, studies using NSm deletant BUNV have demonstrated that this protein plays a role in forming tubules (alongside host proteins such as actin) that support the structure of the replication factories and therefore viral assembly (Fontana, Lopez-Montero, Elliott, Fernandez, & Risco, 2008).

The following rounds of replication/transcription produce copies of both vRNA and cRNA (and therefore viral proteins). Further study needs to be done to elucidate what host factors interact with the replication, transcription, and translation of the virus in a pro-viral manner.

However, it is known that several cellular proteins are involved in the correct folding and maturation of Gn and Gc, including golgi-specific brefeldin A-resistance guanine nucleotide exchange factor 1 (GBF1), BiP, calnexin, and calreticulin (Boshra, 2022; Malet et al., 2023; R. Persson & Pettersson, 1991; Uckeley et al., 2019; Veijola & Pettersson, 1999). The glycoproteins dimerize and are trafficked to the Golgi apparatus where, when critical viral protein concentration is reached, viral particle assembly and budding occurs (Gahmberg, Kuismanen, Keranen, & Pettersson, 1986; Överby, Pettersson, et al., 2007). This translocation and protein accumulation also allows for the association of the nucleocapsid proteins of newly formed RNPs with the processed glycoproteins, triggering budding of new viral particles into the Golgi lumen and release through the exocytic pathway (Andersson, Melin, Bean, & Pettersson, 1997; Gahmberg et al., 1986; Överby, Pettersson, et al., 2007; Överby, Popov, Pettersson, & Neve, 2007; Ronnholm, 1992).

This association between the RNP and glycoproteins to induce packaging of the genomic segments of bunyaviruses prior to release appears to not be a highly selective process, relying more on each of the viral RNA segments stochastic, non-specific interactions with Gn. One, two, and four segmented viral replicons have been visualised when investigating RVFV replication in mammalian cells, alongside some virions which were engineered to contain packaged cRNA. Most virions lack one or more genomic segments, however these virions are still able to infect cell cultures, as the lack of segments is compensated through having many virions binding the same cell in a trans complementation mechanism. In addition, during studies using RVFV infection of mammalian Vero E6 cells, 50% of the particles produced contained no viral genomic segments at all. Further work needs to be carried out to determine if these ‘empty’ particles carry host proteins or mRNA that may affect infection of RVFV within subsequent cells (Bermudez-Mendez et al., 2022; Bermudez-Mendez, Katrukha, Spruit, Kortekaas, & Wichgers Schreur, 2021; Wichgers Schreur & Kortekaas, 2016; Wichgers Schreur, Oreshkova, Moormann, & Kortekaas, 2014).

1.2.4 Mammalian host immune interactions

Despite the replication factories, the products of RNA virus infection, such as 5’triphosphorylated uncapped single-stranded (ss)RNA and dsRNA – collectively known as pathogen-associated molecular patterns (PAMPs), are sensed by the pattern recognition receptors (PRRs) in the host cell. When activated, these PRRs go on to signal downstream pathways that produce an antiviral immune response through establishing an antiviral intracellular environment and activating the innate and following adaptive immune responses. Unlike arthropods, which as mentioned rely on the RNAi system during viral

infection, the mammalian immune response relies more heavily on interferon-mediated responses, and there is evidence to suggest that cross-talk occurs between the interferon and RNAi pathways (Backes et al., 2014; Rezelj et al., 2017; Watson, Knol, Witteveldt, & Macias, 2019). Bunyaviruses have evolved different methods to suppress the immune response in hosts, varying by viral species due in part to the variability in amino acid sequence of the NSs protein (Rezelj et al., 2017). For example, despite the NSs amino acid sequences of RVFV and UUKV having 70% sequence similarity, RVFV NSs localizes to the nucleus (although is also present within the cytoplasm), whereas the NSs of SFTSV and UUKV localize within the cytoplasm (Giorgi et al., 1991; Ly & Ikegami, 2016).

Many of the more highly pathogenic bunyaviruses demonstrate some overlap in their mechanisms of action. The NSs proteins of SFTSV and HRTV contain 63% homogeneity, and can both effectively prevent activation of IRF-3 as they inhibit signalling proteins further downstream within the IFN induction pathway. These proteins interact and block IFN type I and III signalling and production by inhibition of the phosphorylation and therefore activation of TANK-binding kinase 1 (TBK-1), and signal transducer and activator of transcription (STAT)-2 (Billecocq et al., 2004; McMullan et al., 2012; Rezelj et al., 2017). Both NSs proteins are incapable of effectively blocking the action of IFN type II signalling due to their lack of direct interaction with STAT-1 (Feng, Deng, Hu, Wang, & Ning, 2019; Kitagawa et al., 2018; Rezelj et al., 2017). However, beyond the previously mentioned mechanisms of action, SFTSV can further impair the IFN signalling pathway due to the differences in distribution within the cytoplasm compared to HRTV (J. K. Lee & Shin, 2021; Rezelj et al., 2017). Whilst NSs appears to usually have a generalized cytoplasmic distribution when localised to this compartment of the cell, SFTSV NSs proteins form aggregates in the cytoplasm when examined by immunofluorescent staining, termed inclusion bodies, capable of isolating the factors mentioned previously and preventing them from interacting with the IFN signalling pathway. These allow for association and isolation of proteins involved in downstream immune signalling; tripartite motif-containing protein 25 (TRIM25), retinoic acid-inducible gene I (RIG-I), TBK1, IRF-3, STAT1 and STAT2 (Brennan et al., 2015; Feng et al., 2023; J. K. Lee & Shin, 2021; Min, Ning, Wang, & Deng, 2020; Ning et al., 2015; Rezelj et al., 2017). RVFV NSs achieves this block in IFN by interacting with sin3A associated protein 30 (SAP30), which is part of a repressor complex that interacts with the Yin Yang 1 (YY1) transcription factor, forming a complex on the IFN-β promoter that inhibits recruitment of the necessary proteins to carry out IFN-β transcription. RVFV NSs also interacts with other promoters and cellular factors in order to modulate activities such as increased degradation of protein kinase RNA-activated (PKR).

The formation of filamentous NSs structures co-localize with p44, disrupting its assembly with transcription factor II H (TFIIH) and inhibiting cellular transcription of host genes (Eifan, Schnettler, Dietrich, Kohl, & Blomstrom, 2013; Ikegami et al., 2009; Kalveram, Lihoradova, & Ikegami, 2011; Le May & Bouloy, 2012; Le May et al., 2008). Unlike the other species mentioned in this paragraph, this species also codes for a non-structural protein in the viral M segment, NSm. When deleting NSm using a reverse genetic systems the virus maintained some virulence in animal models, however the deletion of both RVFV NSm and NSs prevented the virus from causing illness and allowed an immunological response to be built in the models (Kading, 2014; Kreher et al., 2014). Work carried out by Won and colleagues also demonstrated that RVFV NSm has anti-apoptotic properties through suppressing caspase-3 activation and inhibiting the staurosporine-induced activation of caspase-8 and caspase-9, enhancing infection through preventing the death of infected cells (Won, Ikegami, Peters, & Makino, 2007). The NSm of RVFV also has the ability to interact with cleavage and polyadenylation specific factor 2 (CPSF2), peptidylprolyl isomerase like 2 (PPIL2), and synaptosomal-associated protein, 25kDa (SNAP-25), which indicate that this protein also has roles in neuro-invasion, protein trafficking, and mRNA nuclear transport (Engdahl, Näslund, Lindgren, Ahlm, & Bucht, 2012; Kreher et al., 2014). RVFV is not the only bunyavirus to inhibit cellular apoptosis. Bunyamwera virus (BUNV) also acts on the interferon signalling pathway by inhibiting the activation of IRF-3 by suppressing its promoter. This is achieved through the NSs protein in BUNV, meaning although BUNV also produces NSm protein, individual bunyaviruses will employ the NSm and NSs proteins (where applicable) in species specific ways when interacting with the host (Blakqori et al., 2007; Burrell et al., 2017; Engdahl et al., 2012; Kohl et al., 2003; Weber et al., 2002).

1.2.5 Virus transmission cycles

Many Bunyaviruses are spread by hematophagous ectoparasitic arthropods that feed externally on the blood of their host, namely mosquitoes and ticks. Non-hematophagous arthropods, such as thrips, are also capable of transmitting Bunyaviruses such as species within the *Tospoviridae* family, however these organisms transmit between plant species and do not affect mammals (Riley, Joseph, Srinivasan, & Diffie, 2011). When discussing vector transmission this work focuses on hematophagous arthropods. Depending on the organism, the arthropods will either actively search for (e.g. mosquitoes) or passively seek by living close to (e.g. most species of tick) the hosts. The hosts can be sensed through a variety of means including visual, odour, increased CO_2, and temperature. Studies have been undertaken to discern what factors are most influential in the likelihood of arthropod biting,

and there is some evidence to suggest that infection within a host may increase the attraction of arthropods to the host (Coutinho-Abreu, Riffell, & Akbari, 2022; Cozzarolo, Glaizot, Christe, & Pigeault, 2020; Poldy, 2020; Verhulst, Boulanger, & Spitzen, 2018).

The presence of bunyaviruses within the population is believed to be maintained through a cycle of horizontal transmission between vectors and hosts as shown in Figure 1.3, and all vector species appear to be asymptomatic upon infection, although some argue that virus infection can affect behaviour (Horne & Vanlandingham, 2014; Moutailler et al., 2011; Sim, Jupatanakul, & Dimopoulos, 2014). Direct transmission from an infected arthropod to a naive arthropod via taking a blood meal can be broken down into two routes, systemic or via co-feeding. Systemic transmission occurs when an infected arthropod causes a systemic infection in the host it feeds from through taking a blood meal, following which a naïve arthropod will take a blood meal containing the virus causing an infection within the naïve arthropod (the bottom two dark blue arrows in Figure 1.3). Transmission via co-feeding can theoretically occur in an infected host, although this is less likely to occur or be detectable due to systemic transmission. It is more likely to occur when a naïve arthropod feeds in close proximity to an infected feeding arthropod, thereby taking up some of the virus released by the infected arthropod during feeding (top two dark blue arrows in Figure 1.3). This can also then lead to a systemic infection of the host (Johnstone-Robertson et al., 2020). As previously highlighted, tick saliva contains many compounds, of which many are capable of impacting virus transmission. In the case of tick-borne viruses for example, saliva-activated transmission occurred when mice were exposed to low doses of virus of POWV (Hermance & Thangamani, 2015). In mosquitoes, the saliva can have a variety of impacts on infection. *Aedes aegypti* saliva contains sialokinin, a compound that increases vascular permeability in the host and therefore enhancement of arbovirus infection (Lefteri et al., 2022). This saliva also contains venom allergen-1 (VA-1) which promoted *Flavivirus* infection by inducing autophagy in the hosts immune cells (Sun et al., 2020). While the modulation of the hosts physiology and immune system may have evolved for the mosquitoes benefit, it appears that this has been coopted by arboviruses to aid in transmission from the vector to the host (Visser, Koenraadt, Koopmans, & Rockx, 2023).

It has been shown that a singular bite is enough to expose the host to pathogens carried by the vector, and vice versa. This arguably has different implications for pathogens, including viruses, transmitted by mosquitoes and ticks. In nature, mosquitoes can feed almost daily, and take multiple blood meals, which may be on different hosts across larger distances, increasing the likelihood they will encounter an infected host (Brackney, LaReau, & Smith, 2021; Scott & Takken, 2012). In comparison, as previously mentioned, ticks feed far less,

often requiring only one meal per life stage (except for adult females in order to lay eggs), where feeding can take 4-10 days when uninterrupted. Additionally, ticks will often stay close to where they've hatched, meaning many will feed on the same host at the same time (alongside other ticks from the surrounding area), which is an important factor for increasing the likelihood of transmission via co-feeding (Brackney et al., 2021; Johnstone-Robertson et al., 2020; Kahl & Gray, 2023; Migne et al., 2022; Scott et al., 2000). Once a bloodmeal is taken, the virus is able to infect the arthropod, resulting in infection of the salivary glands which allows for vector to then further transmit the virus upon its next blood meal (Franz, Kantor, Passarelli, & Clem, 2015; Sanchez-Vargas, Olson, & Black, 2021; Simo et al., 2017). This process has not been well examined within ticks, due to the difficulties in rearing tick colonies and lack of dissection optimization, with the focus of the current work to date being on the dissemination of bacteria such as *Borrelia burgdorferi* and what occurs within mosquitoes (Dunham-Ems et al., 2009; J. Gray, Kahl, & Zintl, 2021; Hadi & Adventini, 2015; Kahl & Gray, 2023; Kocan, de la Fuente, & Coburn, 2015). Briefly, the midgut cells become infected, and following this the virus is able to traverse the basal lamina of the midgut (a dense network of proteoglycans which protect the internal tissue), as blood feeding degrades the integrity of this barrier. Once this is breached, the virus can disseminate through the circulatory system within the vector, infecting secondary tissues including the salivary glands (Armstrong et al., 2020; Brackney et al., 2021; Franz et al., 2015). As ticks undergo moulting post-blood meal to move onto the next life stage, the virus must ensure infection of cells within the tick which are not affected by the moulting histolysis, with different viruses appear to target different tissues in order to establish a persistent infection (P. A. Nuttall, Jones, Labuda, & Kaufman, 1994).

As shown in Figure 1.3, transmission can also be carried out transovarially in the absence of taking a blood meal. This occurs when the female adult is infected prior to laying eggs, and so the virus is present within the ovaries and passed on to the offspring. Many studies have provided evidence to show this occurs both within a laboratory setting and within nature. For example, in mosquitoes, it has been demonstrated that Zika virus (ZIKV) and chikungunya virus (CHIKV) was passed on to the offspring of infected *Aedes aegypti* in the Brazilian Amazon (da Costa et al., 2018). However, there is also evidence to suggest that CHIKV infection negatively impacts mosquitoes' fertility (Resck et al., 2020). Within ticks, research carried out within the bunyavirus field has shown that SFTSV is able to infect the ovaries of *Haemaphysalis longicornis*, with no mention of impact on the fertility or survival rate of the offspring (Hu et al., 2020; Zhuang et al., 2018). On the other hand, when looking at Heartland virus (HRTV), infection of *A. americanum* caused the females to lay eggs at a

later timepoint than uninfected females and caused the production of fewer eggs, thereby suggesting that HRTV infection negatively affects tick fertility (Godsey, Savage, Burkhalter, Bosco-Lauth, & Delorey, 2016). Despite tick eggs often requiring an incubation period of several weeks or months before hatching, it is unknown what occurs intracellularly during infection of the eggs in order to allow the virus to be maintained *in ovo*. (Hadi & Adventini, 2015). Given the presence or existence of reservoir species for many bunyaviruses (outside of the vectors) is unknown, transovarial transmission is considered a key part of maintaining the presence of virus in nature (Hartman & Myler, 2023).

The strategy of switching between vector and host constrains bunyavirus evolution and prevents genomic instability and natural attenuation. Evidence for this includes that when RVFV was passaged through either arthropod or mammalian cells as opposed to alternating between the two, significant mutations occur – particularly within the NSs coding region (Elliott, 2009; Horne & Vanlandingham, 2014; Moutailler et al., 2011). The replication of the virus within the vector or host also affords the viral particles different molecular compositions, which may yield advantages when carrying out the next transmission to a new host or vector (Psylvia Léger & Lozach, 2015; Anna Papa et al., 2018). Due to the segmented nature of bunyaviruses and the potential for co-infection with other species, it is also believed that reassortment can occur, leading to the emergence of new viruses (Hartman & Myler, 2023). This has been seen in within a laboratory setting, where mosquitoes were infected with both wild-type LACV and snowshoe hare virus (SSHV), following which 2-3% of genomes produced showed reassortment (Borucki, Chandler, Parker, Blair, & Beaty, 1999). Interestingly, when investigating the reassortment potential of *Batai* and *Bunyamwera orthobunyavirus* (BATV and BUNV, respectively), Heitmann and colleagues found reassortment occurred within mammalian (host) cell lines to produce Ngari-like and novel reassortment viruses, but no reassortment was observed within arthropod cells. Therefore, the potential for reassortment may depend on the infected organism alongside the species of virus involved (Heitmann et al., 2021). Within nature, Ngari virus itself is evidence that bunyavirus reassortment occurs. Ngari virus a reassortant virus first isolated in East Africa in 1997, and is made up of the BUNV L and S segments combined with the M segment of a Batai virus (Briese, Calisher, & Higgs, 2013; Gerrard, Li, Barrett, & Nichol, 2004).

.

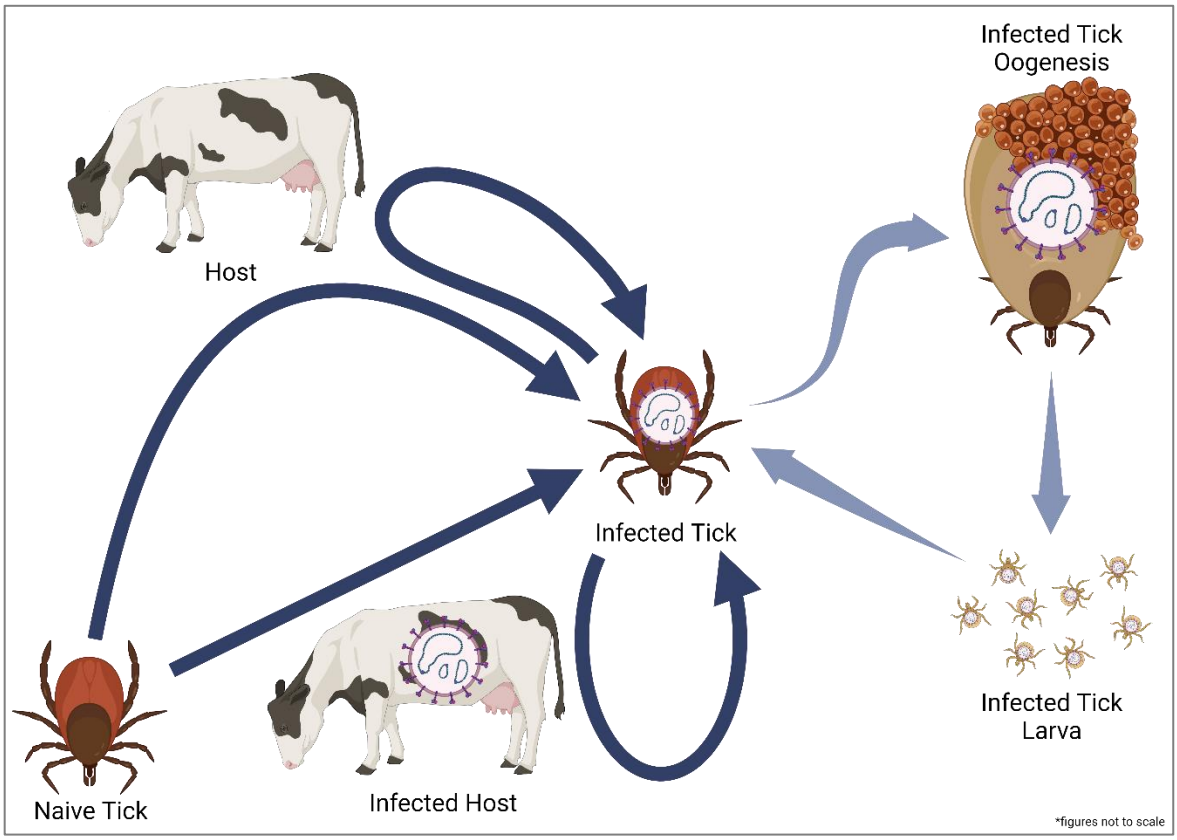

Figure 1.3: Schematic demonstrating generalized horizontal and vertical transmission of arboviruses in arthropods. Using ticks to represent arthropods, and cows to represent host species, the schematic shows a simplified representation of the transmission cycle that occurs in nature. The dark blue arrows (*square end arrows*) dictate direct transmission via taking a blood meal blood meal from an infected host to a naïve tick (left to right) and vice versa (right to left). The light blue arrows (*pointed end arrows*) represent vertical transmission; However, this is often arthropod and virus species dependent (Crispin et al., 2014; Le May & Bouloy, 2012).

1.2.6 Replication within the vector

In the context of virology, arthropods as vectors are severely understudied both within the areas of susceptibility to infection and the replication cycle that occurs once vectors are infected. This is particularly worrying as upon exposure to bunyaviruses, most arthropods become persistently infected for life (Ballinger & Taylor, 2019). When Chen and colleagues undertook a review of all mosquito-arbovirus competence experiments reported within the literature, they concluded that over 90% of potential mosquito-virus interactions had not been tested in experimental settings, despite many having potential clinical and public health relevance. This study also noted that the combinations published in literature tended to centre more on flavi- and alphaviruses, with less focus on bunyaviruses (B. Chen et al., 2023). Although bunyaviruses show vector specificity as previously described, this level of specificity can vary, i.e. although RVFV is transmitted selectively by mosquitoes it has been

shown that over 40 different species of mosquitoes can transmit the virus. It remains unclear what factors determine whether a mosquito species can spread the virus, and from mutational studies different factors seem to impact different species (Horne & Vanlandingham, 2014). As ticks are even less well studied than mosquitoes, the gaps in knowledge that are present when investigating virus-vector interactions are even greater. The knowledge and gaps therein are expanded on in Chapter 1.3.1, however an overview of virus-arthropod interactions is described below.

Unlike mammalian hosts, the exact factors and mechanisms by which bunyaviruses bind and infect arthropod cells (either mosquito or tick) are unknown, although the main steps of the cycle (such as replicating within the cytoplasm) remain consistent (Bermudez-Mendez et al., 2021; Horne & Vanlandingham, 2014). As mentioned in Section 1.2.3, mammalian infections with bunyaviruses often yield viral progeny which do not contain all three genomic segments, but it has been demonstrated that these viruses can efficiently complement each other to produce a persistent infection that results in the mosquito being able to achieve viral transmission (Bermudez-Mendez et al., 2022). When comparing infections of RVFV and Sindbis virus (SINV) in mosquito cells to the equivalent within mammalian cultures, the copy numbers of each genomic RNA segment were seen to be higher in mammalian cell culture, however this did not always correspond to higher infectious viral titres. When analysing infected cells individually, it was seen that lower levels of genomic material within the mosquito cells yielded higher titres. Both of these results suggest that packaging of bunyavirus segments is more efficient within insect cells. Additionally, unlike mammalian cells where the S segment is packaged more often than the M and L segments, the opposite is seen within the mosquito, and the percentage of empty virions drops from 50% to 30% (Bermudez-Mendez et al., 2021). When the RVFV genome is edited using recombinant systems to produce viruses with four segments; such as separating the NSm-G_n and G_c open reading frames (ORFs) within two separate segments, the virus is able to replicate (although at a reduced rate) within the mammalian cells but has a highly limited spread in the mosquito cells, further indicating that replication within the arthropod is, although more specific, also more efficient and requires the virus segments to be intact (Wichgers Schreur et al., 2014).

When focusing on the persistence of infection, it has been shown in infection of mosquitoes by bunyaviruses (e.g. BUNV and LACV) that the virus carries out replication limiting steps, which may contribute to establishing a persistent infection (Hacker, Raju, & Kolakofsky, 1989). For example, the progeny virus produced from persistent BUNV infection had a higher proportion defective-interfering particles, and within the cells higher ratios of S

segment compared to the other genomic segments and detectable sub genomic RNAs derived from the L segment were present. It is still to be confirmed what the exact mechanisms are by which these factors support persistent infection (Scallan & Elliott, 1992). In the case of LACV, over time the genome replication is downregulated as the S segment becomes encapsidated and is therefore unable to be accessed by the host machinery, although as seen in BUNV it is unclear how significant this process is when establishing persistence (Hacker et al., 1989).

As mentioned in host immune interactions (Section 1.2.4), NSs antagonizes the hosts immune response in order to promote infection. Arthropods lack an adaptive immune system, but do possess an innate immune system primarily (in the context of viral infection) relying on the use of RNAi pathways via machinery including dicers, argonauts, dsRNA binding proteins, exonucleases and RdRps (P. Léger et al., 2013). This immune system has been shown to be competent in silencing viral genomic segments in sequence specific manners. When using the Semliki Forest virus (SFV) replicon system to express the gene corresponding to the Hazara virus (HAZV) nucleoprotein, the tick RNAi pathway was able to silence the expression of this gene, however this system was also unable to silence the gene corresponding to CCHFV nucleoprotein (Garcia et al., 2005). Due to the specificity of the response, different viruses have evolved different methods to counteract the intracellular immune pathways of the vector. Both the NSs and NSm proteins have been implicated in the response to the intracellular immune system of the vector and the establishment of persistent infection, alongside replication and vector tropism, although no NSm protein has been found to be produced by the majority of tickborne bunyaviruses. As much of the research surrounding the non-structural proteins is concerned with the impact on the mammalian host, there are still large gaps in the current understanding of these proteins within the vector.

NSs is required for the establishment of BUNV infection in *Aedes albopictus* U4.4 or *Aedes aegypti* cell cultures, and caused lower infection rates in *Aedes albopictus* C6/36 and C7-10 cell lines when deleted (Szemiel, Failloux, & Elliott, 2012). In comparison to this, in RVFV-infected arthropod cells, the mosquito RNAi pathway suppresses the formation of NSs filaments seen in mammalian host infection, restricting viral replication (Horne & Vanlandingham, 2014). This seems to be enough to control but not clear viral infection, allowing the infected vector to go on to infect new hosts (Kading, 2014). Deleting the RVFV NSs protein had no impact upon the virus being able to infect the mosquito vector, although it did lower the virus dissemination rate within the arthropod, supporting the role of NSs in causing a persistent infection. Instead, in RVFV the deletion of the NSm protein abolished

the ability of the virus to replicate in the vector (Crabtree et al., 2012; Kading, 2014; Moutailler, Krida G Fau - Madec, Madec Y Fau - Bouloy, Bouloy M Fau - Failloux, & Failloux). As mentioned previously, NSm is not as extensively studied in relation to the *Phenuiviridae* family (of which UUKV is a member), as SFTSV, HRTV, and UUKV do not express an NSm protein (Leventhal, Wilson, Feldmann, & Hawman, 2021). For mosquito-borne viruses that do express the protein, such as RVFV, NSm is produced by the cleavage of the M segment polyprotein precursor using either host or vector cellular protease, alongside a 78-kDa protein NSm-G_n. The NSm, an additional protein of RVFV, is arguably the most well studied of the bunyaviral NSm proteins (Eifan et al., 2013; Won et al., 2007). The deletion of the NSm protein for RVFV appears to prevent the virus breaching and escaping the epithelial barrier within an infected mosquito, although it is unclear by what mechanism NSm allows the virus to overcome this barrier (Kading, 2014).

1.2.7 Prevalence and disease

Bunyaviruses are present in almost all corners of the globe, with many re-emergences and spread since individual viruses were first isolated (Ferron, Weber, de la Torre, & Reguera, 2017; MacLachlan & Dubovi, 2017). Some of the notable examples of bunyaviruses previously mentioned within this introduction, which cause disease in both humans and animals, are described briefly below. The first example being a mosquito borne bunyavirus, with the latter three being tick borne.

One of the earliest isolated bunyaviruses was RVFV, a member of the *Phlebovirus* genus within the *Phenuiviridae* family. Although reports of high mortality rates in sheep across farms in the Rift Valley of East Africa were recorded as early as 1912, RVFV was first isolated in 1930 during investigations into these high mortality rates (Daubney, Hudson, & Garnham, 1931; Nicoletti, 2014; Swanepoel & Paweska, 2011). For the first 20 years after isolation, outbreaks were confined to areas of Rift Valley corresponding to areas where livestock were maintained and flooding occurring, after this point outbreaks began occurring further afield at an average of one outbreak per 3.6 years (Murithi et al., 2011). RVFV has spread from Kenya to not only throughout Africa but into the Arabian Peninsula. (Grossi-Soyster & LaBeaud, 2020; Rolin, Berrang-Ford, & Kulkarni, 2013; Tong et al., 2019). In smaller, younger animals, such as kids and lambs, RVFV mortality rate is above 70%. In humans, and other older animals such as cattle, goats, and buffalo, the mortality on average reaches up to 10-20% (Bird, Ksiazek, Nichol, & Maclachlan, 2009; Chevalier, Pépin, Plée, & Lancelot, 2010). In addition to this, acute RVFV infection is associated with an increased chance of miscarriage for both humans and animals, partially through targeting the maternal-

foetal interface (Baudin et al., 2016; Budasha, Gonzalez, Sebhatu, & Arnold, 2018; Oymans, Wichgers Schreur, van Keulen, Kant, & Kortekaas, 2020). In humans, after an incubation period of 1 to 6 days, RVFV infection produces milder, self-limiting clinical manifestations including fever, nausea, vomiting, abdominal pain, jaundice. In 1-2% of cases, these symptoms can develop further to include thrombocytopenia, renal failure encephalitis, blindness, and haemorrhagic syndrome (Anywaine, Lule, Hansen, Warimwe, & Elliott, 2022; Kahlon et al., 2010; Madani et al., 2003). There are currently no antiviral treatments specifically targeting RVFV, no licensed vaccines against RVFV in humans, and only live attenuated or inactivated commercially available vaccines for ruminants (however these are unsuitable to be used in non-endemic countries) (Kitandwe, McKay, Kaleebu, & Shattock, 2022). Advances are being made within this area, with several new vaccines based on a variety of techniques including DNA, virus-like particles (VLPs), and genetically attenuated viruses currently undergoing clinical trials. One of the most prominent candidates from this work is the ChAdOX1 RVF vaccine, which appears able to provide immunity in both animals and humans with minimal side effects (Jenkin et al., 2023; Kitandwe et al., 2022).

The first tickborne bunyavirus to be isolated, based on the published literature, Bhanja virus (BHAV) was originally isolated in 1954 in India from a paralyzed goat. This virus is currently classified as a member of the *Bandavirus* genus within the *Phenuiviridae* family (Shah Kv Fau - Work & Work, 1969). BHAV has been found across Asia, Africa, and Europe within several tick species within the *Ixodidae* family (Hubalek, 1987; Hubalek, Mittermayer, Halouzka, & Cerny, 1988; D. K. Lvov, Shchelkanov, Alkhovsky, & Deryabin, 2015; Pavlov et al., 1978; Verani, Balducci, Lopes, & Sacca, 1970; J. Vesenjak-Hirjan et al., 1977; Vilibic-Cavlek et al., 2023). To date no large outbreaks have been noted within the literature, despite BHAV appearing to have the ability to cause disease and mortality when able to access the CNS/brain, particularly in younger animals (Hubálek, 1987; Oluwayelu, Adebiyi, & Tomori, 2018; Sikutova et al., 2009). In humans, most infections of BHAV appear to be asymptomatic. The clinical manifestations of BHAV are fever, muscle and joint pain, headache and photophobia which lasts on average 48 hours, however infections can progress to more severe symptoms including meningoencephalitis (Calisher & Goodpasture, 1975; D. K. Lvov et al., 2015). The first case of disease caused by BHAV was in 1974, where a laboratory worker accidentally infected himself with the virus. Following this, two additional accidental laboratory infections and one retrospective diagnosis of BHAV from a ‘natural’ infection have been recorded (Calisher & Goodpasture, 1975; D. K. Lvov et al., 2015; Punda, Beus, Calisher, & Vesenjak-Hirjan, 1980; J Vesenjak-Hirjan, Calisher, Beus, & Marton, 1980; Vilibic-Cavlek et al., 2023). As these symptoms are quite generic, as there

are few reported cases, it is likely the number of infections is underreported. At the time of writing there are still large gaps in the knowledge surrounding BHAV, and no treatments or vaccines in development or available for either humans or animals.

Although BHAV was the first tickborne Bunyavirus to be isolated, it is not the first tickborne Bunyavirus to be identified. Crimean Congo haemorrhagic fever was first identified in 1944 in the Crimean Peninsula by Dr A. P. Gutfraind, but the virus was not isolated or characterized until 1967. CCHFV is now categorised as a member of the *Orthonairovirus* genus in the *Nairoviridae* family. (Gligić, Stamatović, Stojanović, Obradović, & Bosković, 1977). CCHFV is now considered to be endemic in all of Africa, the Balkans, the Middle East and Asia, and there is evidence to show that that due to the expansion of the vector *Hyalomma marginatum* the virus is spreading further into Europe. When assessing the seroprevalence in Hungary (where *H. marginatum* were first found to have migrated to in 2011) by analysing the serum samples of 2700 healthy volunteers, 0.37% of those tested were positive for CCHFV, which is the first concrete evidence of CCHFV presence within the Hungarian population (Hawman & Feldmann, 2023; Magyar et al., 2021; Messina et al., 2015). Currently, the risk estimates for the establishment of CCHFV has increased from low to medium for both France and Italy (Bernard et al., 2022; Fanelli & Buonavoglia, 2021). CCHFV has demonstrated the ability to infect a variety of different species of animals, both wild and domesticated. Although many of these animal infections produces viremia, currently only humans exhibit a severe illness, allowing CCHFV to establish a variety of asymptomatic reservoir hosts that can result in zoonotic spillover (Atim et al., 2023; Fanelli & Buonavoglia, 2021; Fanelli, Tizzani, & Buonavoglia, 2022; Hawman & Feldmann, 2023; Shepherd, Leman, & Swanepoel, 1989; Sorvillo et al., 2020; Spengler, Bergeron, & Rollin, 2016; Zeller, Cornet, & Camicas, 1994). The fatality rate of CCHFV in humans is estimated to be 30% at a minimum, but this can reach up to 80%. After an incubation period of 1 to 9 days, patients begin to experience symptoms such as fever, nausea, headache, and myalgia. By day 6, more severe symptoms present such as epistaxis and thrombocytopenia, with most deaths occurring 5-14 days after the onset of symptoms if the patient doesn't recover (Aslam et al., 2016; Cevik et al., 2008; Hawman & Feldmann, 2023; Swanepoel et al., 1989). As there was an increase in human cases and isolation in ticks of CCHFV in non-endemic areas around 2019-2020, a renewed One Health push for both surveillance and therapeutic/vaccine development began (Charrel et al., 2004; Kuehnert, Stefan, Badger, & Ricks, 2021; A. A. Patel, Dalal, Parikh, Gandhi, & Shah, 2023). Although currently there are no licensed treatments or vaccines available for CCHFV, several antiviral and vaccine candidates currently in development have shown promise with high efficacy in preclinical models (de

la Calle-Prieto et al., 2018; Hawman & Feldmann, 2023). Similar to RVFV, a vaccine against CCHFV based on the COVID-19 ChAdOx2 system launched safety trials of the 4th of August 2023 after ChAdOx2 CCHF completed preclinical trials (Saunders et al., 2023)

Although the above viruses were isolated over 50 years ago, many more bunyaviruses have been discovered since this time. Severe fever with thrombocytopenia syndrome virus (SFTSV), being proposed for renaming by the type species *Dabie bandavirus* in July 2022 and this change was ratified in March 2023 by the ITCV (https://ictv.global/taxonomy/taxondetails?taxnode_id=202000166 [accessed January 2024]) and will be referred to by the acronym SFTSV in this text. This virus is a member of the genus *Bandavirus* in the family *Phenuiviridae*. SFTSV was first isolated in China in 2009 after an increased number of cases of acute febrile illness within several provinces (Yu et al., 2011). This disease has since become endemic in China and spread to other East Asian countries such as Korea and Japan, which both reported cases in 2012-2013. This spread is believed to be a combination of the migratory pattern of bird present within the country, and the geographical expansion of the tick vectors (the principle vector being *H. longicornis*) (K. H. Kim et al., 2013; Takahashi et al., 2014; S. Wang et al., 2015). Similar to CCHFV, many animals are able to be infected with SFTSV, most of which do not show symptoms. One of the exceptions to this is domestic cats, where the estimated mortality rate is around 62% of those infected (Mekata, Umeki, Yamada, Umekita, & Okabayashi, 2023). The detection of vRNA and antibodies has occurred in many domestic animals, including sheep, cattle, dogs, pigs and chickens, which play an important role in being reservoir species for the virus and the potential for zoonotic spillover (Mekata et al., 2023; Niu et al., 2013). The mortality rate of SFTSV is up to 30%, although after the development of a more efficient luciferase immunoprecipitation system assay in the early 2020's many patients which were not previously diagnosed due to mild or subclinical symptoms tested positive for serological evidence of SFTSV infection (S. Chen et al., 2022; Xiong et al., 2016; Yu et al., 2011). The incubation period of SFTSV is 5 to 14 days, with common symptoms being fever, nausea, vomiting, abdominal pain, diarrhoea, and neurological symptoms. These symptoms can progress in severity to thrombocytopenia, leukopenia acute kidney injury, myocarditis, arrhythmia, and meningoencephalitis, with an average of 9 days from symptom onset occurring to death (J. C. Li, Zhao, Li, Fang, & Liu, 2022; Q. Liu, He, Huang, Wei, & Zhu, 2014; S. Miyamoto et al., 2019; Park et al., 2018; Seo, Kim, Yun, & Kim, 2021; Yu et al., 2011). In terms of treatment, several therapeutic treatments are currently being evaluated, such as Favipiravir, Quinoline analogues, and corticosteroids (Bang, Kim, Kim, & Yun, 2022; J. C. Li et al., 2022; Y. Zhang, Huang, & Xu, 2022). Similarly to the antiviral

treatment, at present there is no approved SFTSV vaccine, although live-attenuated virus-based, viral vector-based, mRNA-based, or DNA-based vaccine candidates are in development, with efficacy being confirmed in animal models (Brennan et al., 2015; Bryden et al., 2022; J. Y. Kim, Jeon, Hong, et al., 2023; J. Y. Kim, Jeon, Park, et al., 2023; Yoshikawa, 2021).

The recent emergence of several tick-borne bunyaviruses, likelihood of further disease-causing bunyaviruses being discovered, and the lack of available treatments or vaccines has highlighted the need for further study into this area, as these viruses are an increasing threat to human and animal health (Albornoz et al., 2016; Elliott & Brennan, 2014; B. Hoffmann et al., 2012; McMullan et al., 2012; J. Wang et al., 2014; Yu et al., 2011). There are large gaps in our knowledge not only about the mechanisms of entry, replication and interaction with host cell factors employed by these viruses, but also their global geographical distribution, meaning future outbreaks of known and novel bunyaviruses are likely (Psylvia Léger & Lozach, 2015; Matsuno et al., 2015). As mentioned previously, the potential for segment reassortment between members of the same species and even members of the same genera further complicate the matter, not just by making identification of the virus more difficult, but by increasing the likelihood of vector or host expansion or increase in virulence (Horne & Vanlandingham, 2014). Beyond this, the ever-expanding population and urbanization of the globe, increased travel, and climate change means that contact with arthropod vectors is becoming more likely and frequent, and so too is the likelihood in contracting one of the diseases they carry (Elliott, 2009; Léger and Lozach, 2015). Organizations such as World Health Organisation (WHO) and Coalition for Epidemic Preparedness Innovations (CEPI) list several bunyaviruses such as CCHFV, RVFV, Lassa fever and other arboviruses like CHIKV on their vaccine development priority list. Due to the severity of the disease these viruses cause, they are more difficult and time-consuming to study, requiring specialist facilities given the statuses of these viruses as Hazard Group 3 or 4 microorganisms requiring their use in specialist containment facilities. Therefore, model bunyaviruses such as UUKV have been fundamental in expanding our knowledge and are used to lay the groundwork in studying these more highly pathogenic viruses (Mazelier et al., 2016).

1.3 Uukuniemi virus

UUKV has yet, to date, been associated with disease, despite evidence of seropositivity in both human and animal populations alongside its ability to infect several species (Matsuno et al., 2015). This makes it an ideal candidate to study more pathogenic related bunyaviruses

as the lower risk allows it to be handled at containment level 2 within the UK and much of Europe (Mazelier et al., 2016; A. Papa et al., 2016). However, it is important to note that UUKV is not the perfect model for several reasons, such as the huge genetic divergence between bunyavirus species even between species within a genus. Additionally, deep sequencing analysis of suspected bunyavirus samples on a large scale is not currently feasible (Matsuno et al., 2015), and so our current knowledge is based on a comparatively small number of isolates (Albornoz et al., 2016).

1.3.1 Discovery, prevalence, and disease

UUKV was first isolated in Finland in 1959 in *Ixodes ricinus* ticks (Kreher et al., 2014; Saikku & Brummer-Korvenkontio, 1973; Wróblewska-Mularczykowa, Sadowski, & Żukowski, 1970). Various isolates have been found in other locations including Scandinavia, Central and Eastern Europe, (CDC Arbovirus catalogue [wwwn.cdc.gov/arbocat/], (Charles et al., 2021), England (Eley & Nuttall, 1984) and Scotland (Mazelier et al., 2016; P A Nuttall, Carey, Reid, & Harrap, 1981; Anna Papa et al., 2018). Currently, UUKV is one of 23 species assigned to the Uukuvirus group, a genus within the *Phenuiviridae* family (https://ictv.global/report/chapter/phenuiviridae/phenuiviridae/uukuvirus [accesses January 2024]) The known geographical distribution corresponds to the geographical range of its primary vector *Ixodes ricinus*, which have been expanding into new territories over the last 30 years (Jaenson, Jaenson, Eisen, Petersson, & Lindgren, 2012) (https://www.ecdc.europa.eu/en/publications-data/ixodes-ricinus-current-known-distribution-march-2022 [accessed January 2024]). Other closely related *Ixodes spp*. ticks, such as *Ixodes scapularis* and *Ixodes pacificus*, which may also be able to vector UUKV are found further afield. *Ixodes scapularis*, for example, was originally localized across the Eastern Seaboard and in the upper Midwest of the USA. However, since 1975 the population has expanded West and further inland within the USA, into Canada and into Mexico (L. Eisen & Eisen, 2023). In 1979, UUKV was also isolated from *Ixodes persulcatus* in the Belozersky District in Russia (D. Lvov, 1979).

1.3.2 Genome and structure

Characterization of UUKV was achieved through investigating the UUKV S23 prototype strain in the early 1970's. This work revealed a virus with a novel structure, made up of four structural proteins and a segmented, ssRNA genome (R. Pettersson & Kaariainen, 1973; R. Pettersson, Kaariainen, von Bonsdorff, & Oker-Blom, 1971; R. F. Pettersson & von Bonsdorff, 1975). A schematic of the structure and genome of UUKV, adapted from the

previous generic bunyavirus in Figure 1.1, is shown in Figure 1.4. UUKV has a tri-segmented genome, where each segments contains a unique primary sequence that does not contain a significant amount of overlap between the segments. These segments have negative or ambisense polarity and are the; L segment, M segment, and S segment (Elliott, Dunn, Simons, & Pettersson, 1992; R. F. Pettersson, Hewlett, Baltimore, & Coffin, 1977). The L segment contains a single ORF which produces the RdRp, with the isolation of this activity being the first instance an RNA polymerase was shown to be contained within a bunyavirus (Elliott et al., 1992; Ranki & Pettersson, 1975). Although the M segment also consists of a single ORF, this is a precursor for the glycoproteins G_n and G_c (originally named G_1 an G_2), which are produced through cleavage of the polyprotein by the host post-translation (Mazelier et al., 2016; Ronnholm & Pettersson, 1987). These proteins also undergo further post-translational modifications (primarily glycosylation), although the nature of these modifications is dependent on the species from which the infected cell is derived from. For example, when virus progeny was produced in tick cells, the Gc protein was highly mannosylated, with the Gn protein containing N-glycans (Mazelier et al., 2016). Unlike the L and M segments, the S segment has an ambisense coding strategy, where the N and NSs proteins are encoded in separate ORFs transcribed with opposite polarities from wither the genomic or antigenomic sense RNAs. When Simons and colleagues probed for the viral negative sense RNA and complementary positive sense RNA, they found that despite no positive M segment RNA was packaged in virions, a ratio of 1:10 positive to negative S genomic segments were packaged (Simons, Hellman, & Pettersson, 1990). Interestingly, although UUKV is a ss negative sense RNA virus, reverse genetic systems based on the positive sense or negative sense sequences have shown no significant difference in rescuing both minigenome RNAs and recombinant virus, indicating that the cRNA can aid in the establishment of infection (R. Flick & Pettersson, 2001; Överby, Popov, Neve, & Pettersson, 2006; F. Ren et al., 2021; Rezelj, Overby, & Elliott, 2015). Each segment is flanked by a 3' and 5' untranslated region (UTR) that mediate replication and transcription, the promoter strength of which (in decreasing order) is M>L>S in mammalian reverse genetic systems (K. Flick et al., 2004). When virions are visualised utilising electron microscopy, the genomic segments appear to be circularized. However, it was found the UTR sequences for each segment showed that this circularization is not covalently closed. When the genomes were subjected to denaturing conditions these circular forms were linearized, with recirculation occurring when annealing conditions were introduced. This circularization is maintained through the complementary sequences within the terminal nucleotides of the viral UTRs to form a 'panhandle' secondary structure and increases the efficiency of

replication and transcription (K. Flick et al., 2004; Hewlett, Pettersson, & Baltimore, 1977; Överby, Pettersson, Grunewald, & Huiskonen, 2008; R. F. Pettersson et al., 1977).

UUKV virions, like most bunyaviruses, are roughly spherical with a ~100nm diameter (Burrell et al., 2017). The membrane of these virions, taken from the cell the virus was produced from, are covered in glycoproteins. There is experimental data to suggest that infection of UUKV upregulates the production of the glycolipid glucosylceramide (GlcCer) within the infected cell, and that not only is this lipid enriched within the viral progeny, but is important for virus attachment to host cells (Uckeley et al., 2022). The external structure of UUKV shows pleomorphism, and on examination using electron cryotomography two distinct 'spike' (glycoprotein protrusions) conformations were observed, extruding from the membrane at 5-10nm. The shape of the particles is due to the interactions of the two membrane glycoproteins, with the most regular particles showing an icosahedral lattice (with a triangulation of T = 12) arrangement. This was also the first time this structural arrangement had been confirmed within a virus (Överby et al., 2008). The two different conformational states occurred depending on the pH, as G_c is a class II membrane protein fusion protein that undergoes a conformational change to allow fusion in acidic conditions (Garry & Garry, 2004; Halldorsson et al., 2018; Överby et al., 2008). Through comparative work with the G_n protein of RVFV it is believed that UUKV G_n functions to prevent premature fusion of UUKV by shielding the hydrophobic fusion loops of the G_c protein, alongside its role in attaching to cells for infection through its glycosylation (Halldorsson et al., 2018; Lozach et al., 2010). The C-terminus of these glycoproteins was also visualized to interact with the RNPs during electron microscopy within the viral particle. Överby and colleagues determined, through mutational analysis and minigenome systems to generate VLPs, that four amino acids within the Gn cytoplasmic tail were key to packaging RNPs through interaction with RNPs regardless of the segment (Överby, Pettersson, et al., 2007). UUKV N protein oligomerizes through the α-helices on both termini of the protein, with the core region for the stability of this polymerization being within the N-terminal. Due to sequence similarities, it is likely this fold is used throughout the *Phlebovirus* genus. The current mechanistic model is that the N protein associates with the vRNA, causing a conformational change and allowing the recruitment and oligomerization of further N proteins onto the RNA (Hornak, Lanchy, & Lodmell, 2016; Katz et al., 2010). This association of N and vRNA is also required for transcription to occur, alongside aiding shielding and transporting the RNA within the cell (Hornak et al., 2016; Katz et al., 2010; Lopez, Muller, Prehaud, & Bouloy, 1995; Överby et al., 2006; F. Ren et al., 2021). Finally, NSs is the only non-structural protein produced by UUKV. UUKV is unable to fully prevent

interferon regulatory factor 3 (IRF-3) activation, subsequent interferon (IFN) production and does not suppress IFN signalling. The NSs protein directly interacts with mitochondrial antiviral-signalling protein MAVS, but this interaction is weak and does not inhibit where other signalling pathways converge to stimulate IFN production. This is likely the reason UUKV does not cause disease. This protein may also have a role in vector competence, although further investigations need to be carried out in order to confirm this, and it is also unclear if this protein is packaged within viral progeny during infection (Rezelj et al., 2017; Rezelj et al., 2015).

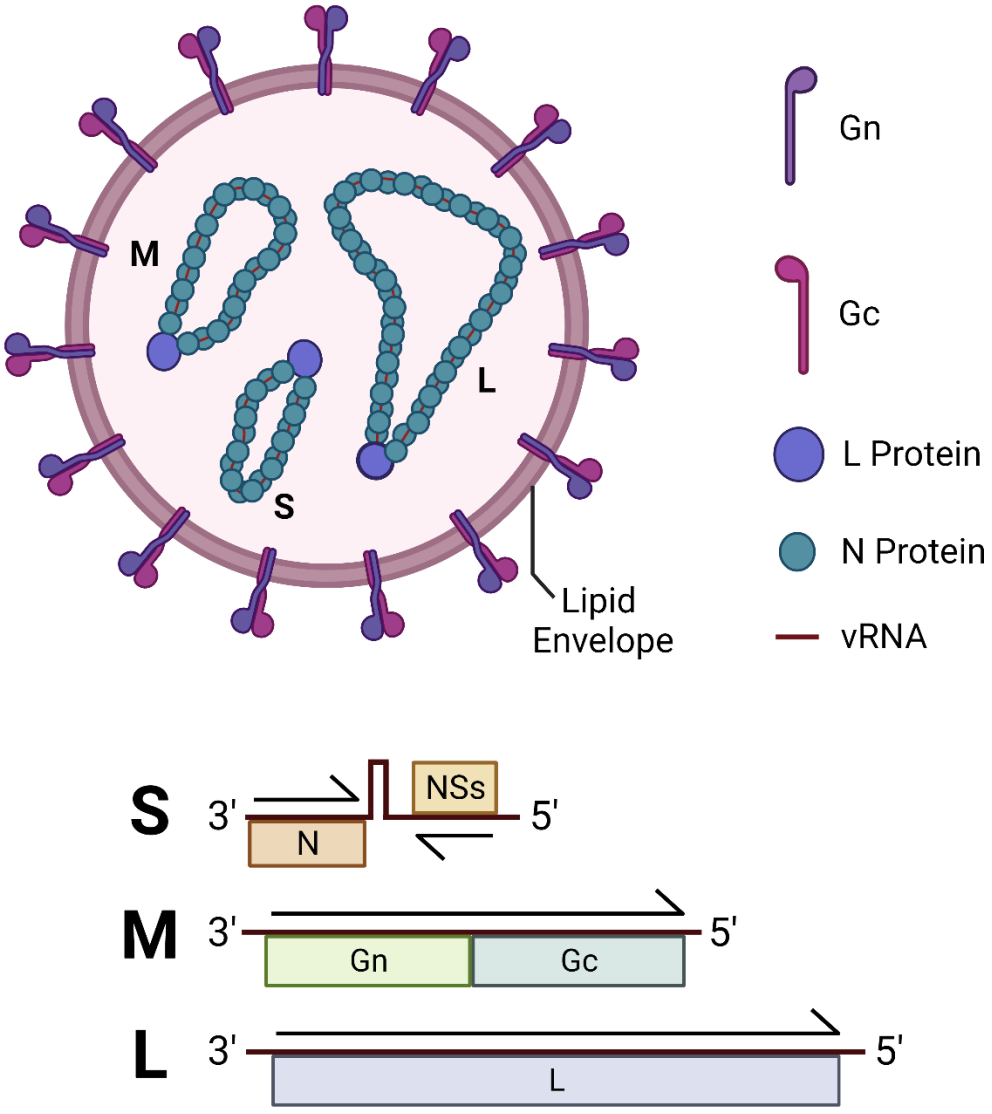

Figure 1.4: Schematic of *Uukuniemi Uukuvirus*. Diagram of a bunyavirus particle with labelled structural proteins (top) and genome structure (bottom) with direction of protein translation (*black arrows*), based on work by (Burrell et al., 2017; Hewlett et al., 1977; R. F. Pettersson et al., 1977)

Chapter 2 Aims

Chapter 2

Ticks and tickborne diseases are an ever-increasing threat to human and animal health. In particular, emergence and re-emergence of several species within the *Bunyavirales* order have led to outbreaks across the globe over the last 80 years. These viruses cause disease with mortality rates reaching 30% or higher in some cases. Despite this, factors which dictate the vector specificity of these viruses and the mechanisms by which the vectors are able to be persistently infected remain elusive.

The overarching aim of this work was two-fold. Firstly, using a model bunyavirus Uukuniemi virus (UUKV), determine the stage at which viral replication was blocked during UUKV replication in non-vector (mosquito) cells. Secondly, utilizing UV crosslinking and oligo(dT) capture, to determine the intracellular factors within tick cells that impact UUKV kinetics to begin elucidating the mechanisms by which a persistent infection is established in arthropod cells.

Specifically, I aimed to:

- Confirm the replication kinetics of UUKV in vector and non-vector arthropod cells, using mammalian cells as a control baseline for replication.
- Visualize, using fluorescent glycoprotein dye and confocal microscopy, if UUKV was able to bind and be internalized by non-vector arthropod cells to begin elucidating the factors preventing UUKV replication in non-vector cells.
- Optimize RNA interactome capture (RIC) through the use of UV crosslinking and oligo(dT) capture beads in tick cell culture (ISE6), as this technique has previous not been carried out on any tick cell line.
- Establish the first tick cell line RNA binding proteome (RBPome) through isolating ISE6 RNA binding proteins (RBPs) using RIC for mass-spectrometry analysis.
- Establish the first UUKV infected tick cell line RBPome using RIC and mass-spectrometry analysis.
- Compare the naïve, non-infected ISE6 RBPome to the RBPome of UUKV infected ISE6 cells to elucidate the differentially expressed RBPs during infection and identify proteins which are significantly upregulated within UUKV-infected ISE6 cells.
- Optimize a magnetofectamine dsRNA knockdown protocol within ISE6 cells and design dsRNA against the proteins that are significantly upregulated within the infected ISE6.

- Transfect dsRNA into ISE6 cells to degrade the target protein in question and visualize the effects on UUKV viral replication within the vector cell line in order to begin elucidating the vector factors important to establishment of UUKV infection.

Chapter 3 Materials

3.1 Cell Culture

3.1.1 Mammalian cell lines

The mammalian cell lines used in this project are as follows:

- **A549**: Obtained from the European Collection of Authenticated Cell Cultures (ECACC), derived from human lung adenocarcinoma basal epithelial cells. This cell line is maintained in Dulbecco's modified Eagle's medium (DMEM) (Thermo Fisher Scientific) supplemented with 10% (v/v) Foetal Bovine Serum (FBS). Incubation conditions are 37°C, 5% CO2. Cell line was passaged when confluency was reached, on average 3 times per week, with a 1:10 split.
- **BHK-21 clone 13**: Referred to as BHK cells, obtained from the University of Glasgow MRC Experimental virus research unit, derived from baby hamster kidney fibroblast cells (Macpherson & Stoker, 1962). This cell line is maintained in Glasgow modified Eagle's medium (GMEM) (Gibco) supplemented with 10% (v/v) FBS and 10% (v/v) Tryptose Phosphate Buffer (TBP) (Gibco). Incubation conditions are 37°C, 5% CO_2. Cell line was passaged when confluency was reached, on average 3 times per week, with a 1:10 split.
- **BSR**: Kindly provided by Dr Karkl-Klaus from the Ludwig-Maximilians-Universität München, this cell line is a clone of BHK-21 (Sato, Maeda, Yoshida, Urade, & Saito, 1977). This cell line is maintained in DMEM (Thermo Fisher Scientific) supplemented with 10% (v/v) FBS. Incubation conditions are 37°C, 5% CO_2. Cell line was passaged when confluency was reached, on average 3 times per week, with a 1:10 split.
- **BSR-T7/5-CL21**: Referred to as BSR-T7 cells. Kindly provided by Dr Karl-Klaus from the Ludwig-Maximilians-Universität München, this cell line is a modified BSR cell line stably transfected with the bacteriophage T7 RNA polymerase (Buchholz, Finke, & Conzelmann, 1999). This cell line is maintained in DMEM (Thermo Fisher Scientific) supplemented with 10% (v/v) FBS, 10% (v/v) TBP, and 1mg/ml of the selection agent Geneticin (G418). Incubation conditions are 37°C, 5% CO_2. Cell line was passaged when confluency was reached, on average 3 times per week, with a 1:10 split.

Incubation temperatures are the optimal growth temperatures for the respective cell line and are used for the respective cell lines unless stated otherwise.

3.1.2 Arthropod cell lines

All tick cell lines for this research were provided by Lesley Bell-Sakyi from the University of Liverpool Tick Cell Biobank. Cell lines were grown in flat-sided tubes (Nunc) for maintenance and transferred to sealed T25 or T80 non-vented flasks (Nunc). Cell lines required passaging when confluency was sufficient for cells to begin detachment from the surface of the tube, on average once per two weeks with a 1:2 split. L-15 (Leibovitz) basal medium is required for all tick cell culture, composition of the media required are listed in the table below.

L15B Basal Media	
MilliQ Water (Autoclaved)	1 Litre
L- 15 Powder (Thermo Fisher #41300-021)	1 Packet
L- Aspartic Acid (Thermo Fisher #A13520.30)	299mg
L-Glutamic Acid (Thermo Fisher #156212500)	500mg
L-Proline (Thermo Fisher #157620250)	300mg
A-Ketoglutaric Acid (Thermo Fisher #439351000)	299mg
D-Glucose (Thermo Fisher #A16828.36)	2239mg
Mineral Stock*	1ml
Vitamin Stock**	1ml

Table 3.1.A: Composition of L15 B Basal Media

***Mineral stock**	
Reduced glutathione (Thermo Fisher #78259)	1000mg
Ascorbic acid (Thermo Fisher #A15613.36)	1000mg
Ferrous sulphate (Merck # 7782-63-0)	50mg
Stock solution A***	1ml
Sodium molybdate dihydrate (Merck #10102-40-6)	1ml of 20mg/100ml H_2O solution
Sodium selenite (Merck #10102-18-8)	1ml of 20mg/100ml H_2O solution

Table 3.1.B: Composition of Mineral Stock required for L15B Basal Media

***Stock solution A	
MilliQ water (autoclaved)	100ml
Cobalt(II) chloride hexahydrate (Merck #7791-13-1)	20mg
Copper(II) sulphate pentahydrate (Merck #7758-99-8)	20mg
Manganese(II) sulphate monohydrate (Merck #10034-96-05)	160mg
Zinc sulphate heptahydrate (Merck #7446-20-0)	200mg

Table 3.1.C: Composition of Stock Solution A required for Mineral Stock

** Vitamin stock	
MilliQ water (autoclaved)	100ml
p-aminobenzoic acid (Merck #150-12-0)	100mg
Cyanocobalamin (B12) (Merck #68-19-9)	50mg
d-biotin (Merck #58-85-5)	10mg

Table 3.1.D: Composition of Vitamin Stock required for L15B Basal Media

All mosquito cell lines were obtained from the ECACC.

All arthropod cell lines were maintained in dry incubators with 0% CO_2. All tick media were adjusted using sterile 1M sodium hydroxide to achieve a deep orange colour before adding to the cell monolayers. The arthropod cell lines used in this project are as follows:

- **BME/CTVM6:** Referred to as BME6 cells, this cell line is derived from embryonic stem cells from the tick species *Rhipicephalus microplus* (Bell-Sakyi, 2004). This cell line is maintained in L-15 complete media (by volume); 70% L-15 (Leibovitz) basal medium (described above), 10% TBP, 20% FBS, and 1% 200mM L-glutamine (Thermo Fischer). Incubation temperature for this cell line is 28°C.
- **BME/CTV23:** Referred to as BME23 cells, this cell line is derived from embryonic stem cells from the tick species *Rhipicephalus microplus* (M. P. Alberdi, Nijhof, Jongejan, & Bell-Sakyi, 2012). This cell line is maintained in L-15 complete media (see above). Incubation temperature for this cell line is 32°C.
- **IRE/CTV20:** Referred to as IRE20, this cell line is derived from embryonic stem cells from the tick species *Ixodes ricinus* (Bell-Sakyi et al., 2007). This cell line is maintained in L-15 complete media (see above). Incubation temperature for this cell line is 28°C.
- **ISE6:** This cell line is derived from embryonic stem cells from the tick species *Ixodes scapularis* (Kurtti, Munderloh, Andreadis, Magnarelli, & Mather, 1996). This cell line is maintained in L-15B300 media (by volume); L-15 basal medium (65ml),

sterile MilliQ water (20ml), TBP (10ml), FBS (5ml), bovine lipoprotein (ICN) 10% solution in L-15 basal medium (1ml), and L-glutamine 200mM (1ml). Incubation temperature for this cell line is 32°C.

- **AF5.** This cell line is a single cell clone derived from the Aag2 (*Aedes aegypti 2* cell line). Aag2-AF5 is immunocompetent for RNAi (siRNA and piRNA pathways) and NF-kB signalling (Varjak et al., 2017). This cell line is maintained L-15 Media (Thermo Fisher #31415) supplemented with 10% TBP and 10% FBS. Incubation temperature for this cell line is 28°C.
- **AF319.** This cell line is a clonal homozygous cell line derived from the Aag2-AF5 clonal derivative of the Aag2 cell line that is deficient in siRNA pathway activity due to a Dicer2 knockout mutation, (Varjak et al., 2017). This cell line is maintained L-15 Media (Thermo Fisher #31415) supplemented with 10% TBP and 10% FBS. Incubation temperature for this cell line is 28°C.

3.1.3 Competent bacterial strains

Plasmid stocks for recombinant virus production (rUUKV and rUUKVdelNSseGFP) were generated using the bacterial *E. coli* strain JM109 (Promega #P9751) genotype *end*A1, *rec*A1, *gyr*A96, *thi*, *hsd*R17 (r_k^-, m_k^+), *rel*A1, *sup*E44, Δ(*lac-pro*AB), [F´ *tra*D36, *pro*AB, *lac*I^qZΔM15]. The bacteria were made competent using the Mix & Go *E. col*i transformation kit and buffer set (Zymo research # T3001). The bacteria were grown at room temperature, either in Luria-Bertani (LB) broth or on LB agar plates which have been supplemented with 100 µg/ml of ampicillin as the selection agent.

3.2 Virus strains and sequence accession numbers

3.2.1 Virus strains

The wild-type UUKV used in this project was a recombinant UUKV based on the prototype tick isolate S-23, whose plasmids were designed by Dr Veronica Rezelj (Rezelj et al., 2015). This research also produced the rUUKVdelNSseGFP virus. Dr Rezelj kindly provided both the recombinant virus and the plasmids used to rescue both rUUKV and rUUKVdelNSseGFP for use within this research. Further working stocks of both viruses were generated through recombinant virus rescue.

The recombinant BUNV used within this study was kindly provided by the Dr E. Pondeville at the University of Glasgow MRC - Centre for Virus Research. Viral stocks were amplified

in the same manner as described for rUUKV (Hart, Kohl, & Elliott, 2009; Pingen et al., 2016).

3.2.2 Virus sequence accession numbers

The accession numbers of the nucleotide sequences used for the generation of the previously mentioned virus rescue plasmids and for the design of sequencing, RT quantitative (q)PCR, and dsUUKV N RNA primers are listed in Table 3.2:

Virus	Segment	GenBank accession number
UUKV	S	M33551.1
	M	M17417.1
	L	D10759.1

Table 3.2: Accession numbers corresponding to Uukuniemi viral genomic segments.

3.3 Oligonucleotides

All primers used in this project and a description of their purpose are listed in Table 3.3. Primers were designed using the National Center for Biotechnology Information (NCBI) primer production tools or Benchling using the appropriate species as a background (Ye et al., 2012). Primers are standard desalted synthetic 25 nM scale oligonucleotides purchased from Integrated DNA technologies (IDT) and reconstituted sterile H_2O to a stock solution of 100 nM.

Primers				
Overall research purpose	Primer name	Primer sequence	Description of primer use	Where primers were acquired from
Rescue plasmid and viral cDNA sequencing	UUK L Forward 1	ACACAAAGTCCGCCAAGATGGAAG	Sequencing the L segment of UUKV and the rescue plasmid pT7UUKL	Made by Dr Veronica Rezelj (Rezelj et al., 2017; Rezelj et al., 2015)
	UUK L Forward 2	CTCTGCTGAGACCATCCAGCATC		
	UUK L Forward 3	GAAGGACGCTTTTGAGAATCTC		
	UUK L Forward 4	CAGAATGCCTGCTGCTTCAATTC		

	UUK L Forward 5	CAGCTGTGCCGGAGTCAACCTGG		
	UUK L Forward 6	GTACTTGAATCCTGATAGACCAG		
	UUK L Forward 7	CTGAGCTCTGCAAGACATCCAC		
	UUK L Forward 8	GAATGGCCAGTTTTTGCTTTGG		
	UUK L Forward 9	CATCACTAGGAGGGTCCCCAAG		
	UUK L Forward 10	CTCATTCCCAGCCCAGAAGGGTAC		
	UUK L Forward 11	GTGCTCATTGTTGAACATCAAGTC		
	UUK L Forward 12	CCTTAACCATGTTCAAGCTCTCC		
	UUK L Forward 13	GAGATTGTTCCTGGTCTGACCGG		
	UUK L Reverse 1	ACACAAAGACGCCAAGATGCTTTTA		
	UUK M Forward 1	ACACAAAGACACGGCTACATGGAACAAC	Sequencing the M segment of UUKV and the rescue plasmid pT7UUKM	
	UUK M Forward 2	GACTTTTCAAGCGTGTTCTTCAC		
	UUK M Forward 3	GAAACTTTGTGCCGTGTAGATCC		
	UUK M Forward 4	GATCCTAATAGAGTCCACTGCTG		
	UUK M Forward 5	GACCTCACTGCAACTAGTATTAG		
	UUK M Forward 6	GCATGTGAATTCTGTGCAAAAC		
	UUK M Forward 7	GTGATTGACACTGACTTCATCAATG		

	UUK M Reverse 1	ACACAAAGACGG CTACCATGGTAAG		
	UUK S Forward 1	ACACAAAGACCCT TCCAACATTAAGC	Sequencing the S segment of UUKV and the rescue plasmids; pT7UUKS, pT7UUKSdelN SseGFP, and pT7UUKSNSse GFP	
	UUK S Forward 2	ATAAGGAGAATGA AGCTCACTG		
	UUK S Forward 3	GCTCAGCAGGTAA GCTCTCTTCTG		
	UUK S Forward 4	ATGTCCCTCAGCA TCTGGTCCC		
	UUK S Reverse 1	ACACAAAGACCTC CAACTTAGC		
	UUK S Reverse 2	CCAGCAGGCTGCA ACTGTCCTC		
	UUK S Reverse 3	CCCTTGTGACTAG TCTTTTCTGG		
UUKV M RT qPCR	UUKM Standard Forward	ACTTGGCATCTGC CACCATGTTAATC	Producing the DNA standards from reverse transcribed UUKV M RNA for UUKV M RNA detection using RT qPCR	Designed during this research
	UUKM Standard Reverse	GCCGACCCACACA AAGACA		
	UUKM qPCR Forward	TGCTACTTTCGGT GCCCTAA	Performing RT qPCR to detect UUKV M	
	UUKM qPCR Reverse	CAGGAGGCTTTGA ACCAACC		

18s RT qPCR	18s Standard Forward	CGTAGTTCCGACCATAAACGA	Producing the DNA standards from reverse transcribed 18s isolated from BSR whole cell lysate for UUKV 18s detection using RT qPCR	Designed during this research using Homo sapiens 18S ribosomal RNA (LOC100008588), non-coding RNA - Nucleotide – NCBI as a reference
	18s Standard Reverse	CATCTAAGGGCATCACAGACC		
	18s qPCR Forward	GACTCAACACGGGAAACCTC	Performing RT qPCR to detect 18s	
	18s qPCR Reverse	TAACCAGACAAATCGCTCCAC		
Production of negative control eGFP dsRNA	eGFP dsRNA Forward	GTAATACGACTCACTATAGGGATGGTGAGCAAGGGCGAGGAGCTGTTC	Producing cDNA from PCR of pT7UUKSdelNSseGFP for making eGFP dsRNA	Designed during this research using Genbank accession number M17417.1 (UUKM) as a reference
	eGFP dsRNA Reverse	GTAATACGACTCACTATAGGGCTGGGTGCTCAGGTAGTGGTTGTCGGGC		
Production of positive control eGFP dsRNA	UUKV N dsRNA Forward	GTAATACGACTCACTATAGGGATGAGACCCTCCCTGAGGAC	Producing cDNA from PCR of pT7UUKS for making UUKV N dsRNA	Designed during this research
	UUKV N dsRNA Reverse	GTAATACGACTCACTATAGGGATCTGAGGACAGTTGCAGCC		
Production of ISE6 gene dsRNA	AGO2 dsRNA Forward	GTAATACGACTCACTATAGGGACGTGAACAAGACGTCTCCC	Producing the corresponding ISE6 gene cDNA from	Designed during this research using FASTA files acquired

	AGO2 dsRNA Reverse	GTAATACGACTCACTATAGGGGGAGCTCCTTCACCATCGAG	PCR of whole ISE6 cell lysate RT for making specific gene dsRNA	from ISE6 genome (Miller et al., 2018) as reference
	PABP1 dsRNA Forward	GTAATACGACTCACTATAGGGGGCTGTTCCCCCTCATCCAC		
	PABP1 dsRNA Reverse	GTAATACGACTCACTATAGGGTCACTCCTTCTTGAGCGAG		
	XRN1 dsRNA Forward	GTAATACGACTCACTATAGGGCAACTGCCGGAAAGGTGTTG		
	XRN1 dsRNA Reverse	GTAATACGACTCACTATAGGGCTGCTTGTTGGGTGGCTTTC		
	TOP3B dsRNA Forward	GTAATACGACTCACTATAGGGCCGTCTACGAGTACATGGGC		
	TOP3B dsRNA Reverse	GTAATACGACTCACTATAGGGGGTAGTCACAGCCTTGACCC		
	SND1 dsRNA Forward	GTAATACGACTCACTATAGGGTTGACTACGGCAATCGGGAC		
	SND1 dsRNA Reverse	GTAATACGACTCACTATAGGGGACCA		

		GCAGGGTCACAAAGT		
	RBM8A dsRNA Forward	GTAATACGACTCACTATAGGGGGAAGGCTGGATCCTGTACG		
	RBM8A dsRNA Reverse	GTAATACGACTCACTATAGGGTGCGGCGATGACTTCTTTTC		
	EIF3A dsRNA Forward	GTAATACGACTCACTATAGGGTGCCACACCGTTCTATCTCG		
	EIF3A dsRNA Reverse	GTAATACGACTCACTATAGGGATTCCTTGATCTCGTCCGGC		
	UNKL dsRNA Forward	GTAATACGACTCACTATAGGGCCTGTACGAGTACCAGGGGG		
	UNKL dsRNA Reverse	GTAATACGACTCACTATAGGGTCCAGGTCCTGTGGCCTAA		
	RUXE dsRNA Forward	GTAATACGACTCACTATAGGGGGACCAGGCCAAAAAGTTCAG		
	RUXE dsRNA Reverse	GTAATACGACTCACTATAGGGCCAAACCTGAATCCGAGCCC		

	CUL1 dsRNA Forward	GTAATACGACTCACTATAGGGATGTGCTGCGGTTCTACACA		
	CUL1 dsRNA Reverse	GTAATACGACTCACTATAGGGATCTCGTAGATGCCCTTGCG		
	PRKRA dsRNA Forward	GTAATACGACTCACTATAGGGCTACATGGGGCTGAAGGAGC		
	PRKRA dsRNA Reverse	GTAATACGACTCACTATAGGGGTGCTGAGCTCGTCTATGGG		
ISE6 gene RT qPCR	AGO2 qPCR Forward	CGAGAGCGGGAGATCAACAA	Performing RT qPCR to detect the corresponding ISE6 gene mRNA	Designed during this research using FASTA files acquired from ISE6 genome (Miller et al., 2018) as reference
	AGO2 qPCR Reverse	GAATGCGACCTCGTACCTCC		
	PABP1 qPCR Forward	ACATGATCACTCGCCGATCC		
	PABP1 qPCR Reverse	TCGGCTTGTTCTTGATGGCA		
	XRN1 qPCR Forward	GCTCCGAATCTCTGGACGAG		
	XRN1 qPCR Reverse	CGCCCGAAAAAGTGACTTGG		
	TOP3B qPCR Forward	GCGTGGAGGCTGTACGATTA		
	TOP3B qPCR Reverse	CCCGGATTGATGACGCTCTT		

	SND1 qPCR Forward	GACAACGGTCACTGGAGGTT		
	SND1 qPCR Reverse	GCGGAGTAGTCCTTCCACAG		
	RBM8A qPCR Forward	CTGAAGGAACGAGCTCGGAA		
	RBM8A qPCR Reverse	TTCATCCGTGTCCATGGCTT		
	EIF3A qPCR Forward	ACCCCCTGGAAGAGAGGTG		
	EIF3A qPCR Reverse	ATGTCCCTCGAACGGTCCAT		
	UNKL qPCR Forward	TACGACGAGACGACGGGTAT		
	UNKL qPCR Reverse	GCCCGTCTTGTAGTAACGCA		
	RUXE qPCR Forward	CTACAGAACAGGGCTCGGATT		
	RUXE qPCR Reverse	GCTTCCGCTGCTTAGTCTTTG		
	CUL1 qPCR Forward	GAGGCCAGCATGATCTCCAA		
	CUL1 qPCR Reverse	AAGGGCCTCTTCGGAGTTTG		
	PRKRA qPCR Forward	TTTGGCATCTCTTGCCTCGT		
	PRKRA qPCR Reverse	ATCATCTTGTAGGCAGCCTGG		

Table 3.3: Table of primers used in this research including primer name, sequence and description of use.

3.4 Enzymes

PCR – Either GoTaq® G2 Flexi DNA polymerase (Promega), or KOD Hot Start DNA polymerase (Novagen, Sigma) were used for PCR.

RT qPCR - Reverse transcription reactions were carried out using GoScript reverse transcriptase (Promega) and random hexamers (50 µM) (Promega). Real-time quantitative PCR (RT qPCR) was carried out using SYBR™ Green PCR Master Mix (Thermo Fisher).

Nucleic acid digestion – Benzonase® nuclease (Sigma) was used to remove all DNA and RNA from protein samples, for example during cell lysis for western blot. DNase I, RNase-free (1 U/µL) (Thermo Fisher) was used to remove template DNA for PCR and reverse transcription outputs. RNase A (Promega) was used to remove RNA from oligo(DT) capture and cDNA samples.

dsRNA production – MEGAscript™ RNAi kit enzymes (T7 enzyme mix, RNase, and DNase I) were used to produce dsRNA.

Cloning – In-Fusion enzyme (Takara) was used for restriction-free cloning.

Protein digestion – Proteinase K (Qiagen) was dissolved in proteinase K buffer (1µg/1µl); 50mM Tris-HCl (pH 7.5), 750mM NaCl, 1% (wt/vol) SDS, 50mM EDTA, 2.5mM DTT, and 25mM $CaCl_2$.

3.5 Plasmids

The plasmids used in this project are listed below in Table 3.4, and all contained an ampicillin resistance gene (amp^R).

Plasmid	Description	Source
pT7UUKS(+)	Whole antigenomic sense UUKV S segment subcloned into the pTVT7 plasmid (Johnson, Zeddam, & Ball, 2000). The segments are flanked by a bacteriophage T7 promoter at the 5' end, and a hepatitis Δ ribozyme at the 3' end, followed by a T7 terminator. Rezelj et al 2015 introduced a silent mutation resulting in an XhoI restriction site at 963.	Made by Dr Veronica Rezelj (Rezelj et al., 2017; Rezelj et al., 2015)
pT7UUKM(+)	Whole antigenomic sense UUKV M segment subcloned into the pTVT7 plasmid (Johnson et al., 2000). The segments are flanked by a bacteriophage T7 promoter at the 5' end, and a hepatitis Δ ribozyme at the 3' end, followed by a T7 terminator.	Made by Dr Veronica Rezelj (Rezelj et al., 2017; Rezelj et al., 2015)
pT7UUKL(+)	Whole antigenomic sense UUKV L segment subcloned into the pTVT7 plasmid (Johnson et al., 2000). The segments are flanked by a bacteriophage T7 promoter at the 5' end, and a hepatitis Δ ribozyme at the 3' end, followed by a T7 terminator.	Made by Dr Veronica Rezelj (Rezelj et al., 2017; Rezelj et al., 2015)
pT7UUKdelNSsGFP(+)	Modified pT7UUKS(+) plasmid. The UUKV NSs 874-1696 nucleotide ORF was excised and replaced by enhanced GFP (eGFP) in the same negative-sense orientation.	Made by Dr Veronica Rezelj (Rezelj et al., 2017; Rezelj et al., 2015)

Table 3.4: Table of Plasmids used within this research, including plasmid description and plasmids source.

3.6 Antibodies

The antibodies used in this project are listed in Table 3.5 below:

Antibody	Company and Catalogue Number	Target	Western Blot Dilution	Immuno-fluorescence Dilution
Mouse anti-UUKV (generated from hybridoma 8B11A3, kindly provided by Dr Anna Overby)	N/A	UUKV N	1:1000	1:500
Mouse anti-α tubulin	Sigma - T6199	Mouse, Human and Tick α-tubulin	1:1000	-
Rabbit anti-DDX1	Atlas Antibodies - HPA034502	Human DDX1	1:1000	-
Rabbit anti-FUS/TLS	Cell Signalling - 4885S	Human FUS/TLS	1:500	-
Rabbit anti-HNRNPA1	Cusabio - CSB-PA010600HA01HU	Human HNRNPA1	1:1000	-
Mouse anti-PTBP1	Sigma - WH0005725M1	Human PTBP1	1:1000	-
Rabbit anti-MOV10	Cusabio - CSB-PA862068LA01HU	Human MOV10	1:1000	-
Rabbit anti-DDX41	ProSci - 7349	Human DDX41	1:1000	-
Rabbit anti-PA2G4	Cusabio - CSB-PA891987LA01HU	Human PA2G4	1:1000	-
Rabbit anti-HMGB1	ProSci - 7715	Human HMGB1	1:1000	-
Rabbit anti-Hsp90α/β	AbClonal - A5027	Human Hsp90α/β	1:1000	-

Anti-mouse IgG (H&L) Secondary	Invitrogen - T6199	Mouse primary antibodies	1:5000	1:1000
Anti-rabbit IgG (H&L) Secondary	Invitrogen - SA535521	Rabbit primary antibodies	1:5000	1:1000
Anti-mouse IgG & IgM HRP conjugate	Sigma - A11011	Mouse primary antibodies	-	1:1000

Table 3.5: List of antibodies used within this research, their source, their targets, and dilutions used for each technique.

3.7 Reagents and chemicals

3.7.1 Bacterial culture

- Ampicillin sodium: used at a concentration of 100 µg/mL in LB agar and LB broth was purchased from Formedium.
- LB agar: 4% (w/v) LB Agar Miller (Formedium) dissolved in MilliQ H_2O and sterilized via autoclaving.
- LB broth: 2.5% (w/v) LB Broth Agar Miller (Formedium) dissolved in MilliQ H2O and sterilized via autoclaving.

3.7.2 Eukaryotic and arthropod cell culture

- PBS: Cell culture grade DPBS; no calcium, no magnesium, pH 7.4 was purchased from Gibco.
- FBS; foetal bovine serum (FBS) was purchased from Gibco.
- Mammalian cell base medias: both DMEM and GMEM were purchased from Gibco.
- Arthropod cell base medias: L15 was purchased from (Sigma-Aldrich), tryptose phosphate buffer (TBP) was purchased from Gibco.
- Formaldehyde fixative solution: 8% (v/v) formaldehyde (Fisher Scientific) was diluted in pre-autoclaved MilliQ H_2O.
- Opti-MEM; Opti-minimum essential media (Opti-MEM) was purchased for Gibco and used in all transfections.
- Mammalian transfection: TransIT-LT1 transfection reagent was purchased from MirusBio.

- Arthropod transfection: magnet, CombiMag, and MTX reagent (Magnetofectamine O2 transfection kit) was purchased from Oz Biosciences.
- Viability assay: CellTiter-Glo® 2.0 Cell Viability Assay was purchased from Promega.
- Luminescence reader: GloMax® Navigator Microplate Luminometer (Promega) was used to measure luminescence.
- Laemmli buffer: 100mM Tris-HCl, 4% (v/v) SDS, 20% (v/v) glycerol, 200mM DTT, 0.2% bromophenol blue (v/v), and 3µl/ml endonuclease.

3.7.3 Foci-forming and plaque-forming assays

- 1X PBS: 10X PBS was purchased from Gibco and diluted to 1X in MilliQ H_2O.
- PBST; 0.1% (v/v) tween (Sigma) in PBS.
- Permeabilization solution: 0.5% (v/v) Triton X-100 (Roth) in PBS.
- 2X MEM: Media was made up prior to plaque/foci forming assays and stored for up to 3 months. 20% (v/v) 10x Modified Eagle's Medium (MEM) was purchased from Gibco, diluted in H_2O and supplemented with 2% (v/v) L-glutamine and 0.453% (v/v) sodium bicarbonate (Gibco).
- Avicel overlay: Purchased from FMC, 1.2% Avicell (w/v in MilliQ H_2O), after sterilization via autoclaving, was diluted in a 1:1 ratio with 2X MEM and supplemented with 2% (v/v) FBS directly prior to use.
- Plaque assay stain: Toluidine blue stain was purchased from Sigma-Aldrich and diluted to 1% (v/v) in MilliQ H_2O.
- Blocking buffer: 4% (w/v) semi-skimmed milk powder in PBST.
- Immunodetection substrate: TrueBlue Peroxidase Substrate was purchased from KPL.

3.7.4 DNA and RNA analysis

- Plasmid isolation from bacterial cultures: For small volumes of bacteria (<50ml of LB broth) the QIAprep Spin Miniprep kit (Qiagen) was used. For larger volumes, the QIAprep Spin Maxiprep kit (Qiagen) was used following the instructions for midi-prep.
- 1X TAE buffer: 50X TAE buffer was purchased from Thermo Fisher and diluted 1:50 with MilliQ H_2O.

- Agarose gel: 1-2% (w/v) molecular grade agarose (Bioline) was dissolved in 1X TAE buffer before being supplemented with ethidium bromide (3µl per 100µl of agarose gel) (Promega) and allowed to solidify.
- DNA ladder: 1 Kb Plus DNA ladder from Thermo Fisher Scientific.
- Nucleotide loading buffer: DNA Gel Loading Dye (6X) was purchased from Thermo Fisher Scientific.
- Nucleotide product isolation from gels: purification and extraction of nucleotide products from agarose gels was done using the Wizard® SV Gel and PCR Clean-up System purchased from Promega. Nucleotide products were eluted in nuclease-free water (Qiagen).
- Measuring nucleotide product purity and concentration: Eluted nucleotide products were measured using a Nanodrop One (Thermo Scientific).
- DNA sequencing: All DNA sequencing was done through Eurofins and Source Bioscience using the primers listed in Table 3.2 unless otherwise stated.

3.7.5 Total cellular RNA extraction

- Cell lysis: TRIzol® was purchased from Thermo Fisher Scientific.
- Phase separation: Chloroform was purchased from Sigma-Aldrich.
- RNA precipitation: GlycoBlue™ Coprecipitant (15 mg/mL) was purchased from Invitrogen. Propan-2-ol was purchased from VWR Chemicals.
- RNA wash: 75% (v/v) ethanol was purchased from VWR chemicals and diluted in MilliQ H_2O.
- Resuspending RNA: RNA was dissolved in nuclease-free water purchased from Qiagen and measured using a Nanodrop One (Thermo Fisher Scientific) at 260mn.

3.7.6 Reverse Transcription

- Reverse transcription (RT): RT was carried out using the SuperScript™ Reverse Transcriptase kit purchased from Thermo Fisher Scientific, following the manufacturer's instructions.
- Non-specific primer amplification: Random hexamers (50µM) were purchased from Thermo Fisher Scientific.
- RNase inhibition: RNaseOUT™ Recombinant RNase Inhibitor was purchased from Thermo Fisher Scientific.

3.7.7 Real-time Quantitative PCR

- Thermocycler: All RT qPCR reactions were carried out using a QuantStudio™ Real-Time PCR System (Thermo Fisher), using consumables (e.g. 384 well plates) compatible with this machine which were purchased from Thermo Fisher Scientific.
- SYBR Green: SYBR™ Green PCR Master Mix was purchased from Fisher Scientific.
- Primers: The primers specified in Table 3.2 were diluted to a concentration of 10μM in nuclease-free H_2O.

3.7.8 dsRNA Production

- MEGAscript™ RNAi Kit with Manual was purchased from Thermo Fisher Scientific.

3.7.9 Dying viral particles

- Coomassie blue staining solution was purchased from Abcam.
- UltraPure™ BSA (50 mg/mL) was purchased from Thermo Fisher Scientific.
- 10X HNE buffer: 100mM HEPES (Sigma), 1.5M NaCl (VWR Chemicals), 10mM EDTA (Sigma) were prepared in MilliQ H2O and filtered through a 0.2μm filtration membrane (Starlab).
- Sucrose density gradient: Sucrose was purchased from Sigma-Aldrich and dissolved in filtered 1X HNE buffer (10X HNE supplemented in sterile MilliQ) to produce 10%, 20%, 25%, 30%, 35%, and 50% (w/v) sucrose solutions.
- Density gradient ultracentrifugation: Virus ultracentrifugation was carried out using the Sorvall™ WX+ Ultracentrifuge (Thermo) with a drum compatible 5ml open-top thinwall polypropylene tubes purchased from Beckman Coulter.
- Extracting density separated virus: 5ml syringes (HENKE-JECT) with 27G gauge needle (Sterican) were used to extract banded dyed virus.
- Negative stain electron microscopy preparation was carried out through the CVR microscopy facilities and imaging done on a JEOL JEM 1400 (JEOL, Japan) electron microscope.
- AF647: Alexa Fluor 647 succinimidyl ester dye (AF647) was purchased from Thermo Fisher Scientific.
- Confocal microscopy was carried out using a Carl Zeiss LSM 880 confocal microscope equipped with a 64x objective.

3.7.10 Immunofluorescence

- DAPI: DAPI was purchased from Thermo Fisher Scientific.
- Membrane Dye: CellMask™ Green Plasma Membrane Stain was purchased from Invitrogen.
- Hoechst Stain: Hoechst 33342 nuclear counterstain solution (20mM) was purchased from Thermo Fisher Scientific.

3.7.11 Protein analysis and western blotting

- Gels: NuPAGE Novex (4-12%) Bis-Tris protein gels and NuPAGE™ MES SDS Running Buffer (20X) were purchased from Thermo Fisher Scientific. Running buffer was diluted 1:20 in MilliQ H_2O.
- Electrophoresis: Gels were subjected to electrophoresis using the Invitrogen ™ XCell SureLock™ Mini-Cell.
- Protein loading buffer: NuPAGE™ LDS Sample Buffer (4X) was purchased from Thermo Fisher Scientific.
- Protein ladder: PageRuler™ Plus Prestained Protein Ladder, 10 to 250 kDa was purchased from Thermo Fisher Scientific.
- Gel Fixative: 10% (v/v) glacial acetic acid and 30% (v/v) ethanol were purchased from VWR Chemicals and diluted in MilliQ H_2O.
- Gel Wash: 10% (v/v) ethanol was purchased from VWR Chemicals and diluted in MilliQ H_2O.
- Silver stain: Pierce™ Silver Stain Kit was purchased from Thermo Fisher Scientific.
- Silver stain stop solution: 5% (v/v) Glacial Acetic Acid was purchased from VWR Chemicals and diluted in MilliQ H_2O
- Western blotting: NuPAGE™ Transfer Buffer (20X) was purchased from Thermo Fisher Scientific and diluted in a 1:20 ratio in MilliQ H_2O. Amersham Hybond ECL nitrocellulose membrane was purchased from GE Healthcare Life Sciences and blotting pads purchased from VWR Chemicals.
- Protein transfer: Semi-dry western blotting was carried out using the Trans-Blot® Turbo™ Transfer System (Biorad).

3.7.12 UV crosslinking and oligo(dT) capture

All Oligo(dT) buffers components were dissolved in nuclease-free water (Qiagen) and filtered through a 0.2µm filtration membrane (StarLab) before use.

- UV exposure: Cells were exposed to 254nm UV using a CL-508 Crosslinker (UVITEC Cambridge).
- Oligo(dT) capture beads: Dynabeads™ Oligo$(dT)_{25}$ and DynaMag-2 magnetic rack were purchased from Invitrogen.
- Oligo(dT) lysis buffer: 20mM Tris-HCl (pH 7.5), 500mM LiCl, 0.5% (w/v) LiDS, 1mM EDTA, 0.1% (v/v) IGPAL, and 5mM DTT.
- Lysis homogenization: Lysis was homogenized through 5ml syringes (HENKE-JECT) with 27G gauge needle (Sterican).
- Oligo(dT) buffer 1: 20mM Tris-HCl (pH 7.5), 500mM LiCl, 1mM EDTA, 0.01% (v/v) IGEPAL, and 5mM DTT.
- Oligo(dT) buffer 2: 20mM Tris-HCl (pH 7.5), 500mM LiCl, 1mM EDTA, 0.01% (v/v) IGPAL, and 5mM DTT.
- Oligo(dT) buffer 3: 20mM Tris0HCl (pH 7.5), 200mM LiCl, 1mM EDTA, and 5mM DTT.
- Oligo(dT) elution buffer: 20mM Tris-HCl (pH 7.5) and 1mM EDTA.

3.7.13 SP3 and mass spectrometry

SP3: Bead-based single-pot, solid-phase-enhanced sample-preparation (SP3) was performed by our collaborator Dr Wael Kamel following (Hughes et al., 2019).

- Reduction and alkylation buffer: 10mM TCEP, 50mM C-IAA.
- Carboxylated beads: Speed Bead Magnetic Carboxylate Modified Particles (Sigma-Aldrich)
- 100% acetonitrile (ACN)
- 70% ethanol
- Trypsin: Trypsin Gold (MS grade; Promega)
- DMSO
- Formic Acid

Mass spectrometry: ISE6 RIC prepared samples were sent to Prof. Shabaz Mohammed at the Rosalind Franklin Institute, who provided the raw data files upon completion. All other samples were sent to the Dundee proteomics facility, where SP3 preparation was performed in house before being subject to mass spectrometry analysis. For immunoprecipitation samples, SP3 was not performed, and instead in-gel digestion carried out after separating the samples via gel electrophoresis. Nano-liquid chromatography tandem mass spectrometry with data-dependent analysis (DDA) (for ISE6) or data-independent analysis (DIA) (in

A549) label-free quantification (nLC-MS/MS (DDA/DIA-LFQ)) was used to analyse the mass spectrometry samples.

3.8 Software Packages

3.8.1 Bioinformatics and qPCR analysis

- Primers were designed using Benchling or NIH Primer-BLAST online tools.
- RT qPCR data was measured and analysed using QuantStudio (Thermo Fisher Scientific).
- Mass spectrometry data analysis was carried out using MaxQuant (Cox & Mann, 2008), Perseus (Tyanova et al., 2016), and R Studio (R version 4.3.1).
- Downstream analysis of proteins produced from mass spectrometry analysis was carried out by the tools available in VectorBase, InParanoiDB (version 9), InterproScan (version 97.0), MobiDB Lite (version 5.0).

3.8.2 Graphing, statistical analysis and figures

- Graphing and statistical analysis was carried out using R studio (R version 4.3.1) and GraphPad Prism version 10.
- Diagrams and schematic figures were produced using BioRender.
- For mass spectrometry data statistical analysis was carried out in R using the empirical Bayesian method moderated t test, where p values were adjusted for multiple-testing using the Benjamin-Hochberg method.

3.8.3 Imaging

Imaris for cell biologists (Oxford Instruments), ZEN (Zeiss) software, and ImageJ (Schneider, Rasband, & Eliceiri, 2012) were used for processing of confocal and EVOS images.

Chapter 4 Methods

4.1 Cell Culture

4.1.1 Eukaryotic cell line maintenance

Cells were grown in T-75 cm^2 or T-175 cm^2 vented flasks and split 1:10 when monolayers reached 90% confluency. To split, the cell media was removed, and the monolayer washed with PBS before being incubated with trypsin for 5 minutes at 37°C. Trypsin treated cells were resuspended in appropriate fresh media upon detachment. Cells were incubated in the conditions outlined in Materials.

4.1.2 Arthropod cell line maintenance

All arthropod cells were maintained in enriched media.

Mosquito cells were grown in T-80 cm^2 non-vented flasks (Nunc) and split 1:5 when cells reached 100% confluency. All mosquito cells were mechanically detached using a cell scraper before being separated into single-cell suspension via pipetting. Resuspended cells were supplemented with fresh media and incubated in the conditions outlined in Materials.

Tick cells were grown in flat-sided tubes (Nunc), T-25 and T-80 non-vented flasks (Nunc) and split 1:2 when cell monolayers began to detach from the cell culture surface. Additionally, once a week, half the volumes of all tick cell media were removed and replaced with the appropriate fresh media. To split the tick cells, monolayers were mechanically detached and separated into single cell-suspension via pipetting. Resuspended cells were supplemented with fresh media and incubated in the conditions outlined in Materials.

4.2 Virus rescue

Virus rescues were carried out using the UUKV reverse genetic system. Transfection of the three-plasmid T7 RNA polymerase-driven rescue system were carried out in BSR-T7 cells as previously described (Rezelj et al., 2017; Rezelj et al., 2015).

Transfection mixes were prepared prior to cells being passaged. 1µg of the rescue plasmids; pT7UUKL(+), pT7UUKM(+), and either pT7UUKS(+), pT7UUKdelNSseGFP(+), or pT7NSseGFP(+) (Table 3.4) were incubated with 7.5µl TransIT-LT1 (MirusBio) and 250µl OptiMEM (Gibco) for 30 minutes at room temperature (RT) to produce the transfection mixes for producing recombinant UUKV (rUUKV) or rUUKVdelNSseGFP, respectively. During this incubation, cells were split and resuspended in media which did not contain the selection reagent G418. Approximately $2x10^5$ cells per well were seeded in a 6-well plate,

and immediately following this the plasmid transfection mix was added to the well drop wise.

Transfected cells were incubated at 37°C for 7 days, with the cell monolayers being monitored for cytopathic effect (CPE). The supernatant was then collected and clarified by centrifugation at 5,000 xg for 5-10 minutes and stored at -80°C. Titre was then determined by focus-forming assays on rescued virus supernatant. The sequences of all recombinant rUUKV viruses ORFs were also confirmed to be correct through RNA extraction and reverse transcription, the cDNA of which was then sequenced through Eurofins or Source Bioscience.

4.3 Virus infections

Cells were seeded at the indicated cell densities in Table 4.1 below.

Cell Type	Experiment Type					
	FBS Assay	Growth Curve	Binding and Internalisation	RIC	dsRNA Knockdowns	Immuno-precipitation
BSR	6 well plate – $2x10^5$ cells per well	12 well plate – $1x10^5$ cells per well	96 well plate – $1x10^4$ cells per well	N/A	N/A	N/A
BHK	6 well plate – $2x10^5$ cells per well	N/A	N/A	N/A	N/A	N/A
A549	N/A	12 well plate – $1x10^5$ cells per well	N/A	3 x 10cm dishes – $2.2x10^6$ cells per plate	N/A	N/A
AF5	N/A	12 well plate – 2.5x105 cells per well	96 well plate – $7.5x10^4$ cells per well	N/A	N/A	N/A
AF319	N/A	12 well plate – 2.5x105 cells per well	N/A	N/A	N/A	N/A
ISE6	N/A	12 well plate – 2.5x105 cells per well	96 well plate – $7.5x10^4$ cells per well	3 x 10cm dishes – $1.5x10^7$ cells per plate	24 well plates – $4.45x10^5$ cells per well or 6 well plates – $2.25x10^6$ cells per well	3 x 10cm dishes – $1.5x10^7$ cells per plate

Table 4.1: Tissue culture plate or well size and the corresponding seeding densities for each cell type dependent upon experimentation method.

Cells were seeded 24 hours before infection, except for during knockdown experiments where cells were seeded 24 hours before transfection and subsequently incubated for another 20 hours before infection. To infect, appropriate virus dilutions were made in 2% FBS (v/v) PBS unless specified otherwise. Cell culture medium was removed, replaced with virus

inoculum, and cells were incubated at the appropriate temperature for each cell line (as defined by their incubation temperature in materials) for one hour. Following incubation, the inoculum was removed. Mammalian cell cultures were washed once with PBS before the appropriate fresh media were added. This wash step was not applied to arthropod cell cultures due to lack of adherence in these cells. Replacement of the appropriate fresh cell culture medium was defined as 0 hours post-infection (p.i.). The inocula and media volumes for each cell culture vessel are described below in Table 4.2:

Plate Size	Virus inoculum volume per monolayer (ml)	Media volume per monolayer (ml)
T-225 flasks	20	60
T-175 flask	15	40
T-75/80 flask	5	15
10mm Plate	5	15
6 well plate	1	3
12 well plate	0.5	0.5
96 well plate	0.1	0.2

Table 4.2: Inoculation and Cell media volumes used, depending on tissue culture vessel size.

4.4 Virus stock production

Stocks of the recombinant viruses were generated through infection of BSR cells at a low multiplicity of infection (MOI) of 0.01 focus forming units (FFU)/cell, before the virus progenies were concentrated via ultra-centrifugation. All media used in virus production were FBS-free and used phenol-red free DMEM (Gibco) to prevent potential artifacts when dying the virus. BSR cells were seeded at a confluency between 40%-50% in T-175 flasks ($1x10^7$ cells per flask) and T-225 flasks ($1.5x10^7$ cells per flask) and infected in FBS-free inoculum as described in virus infections. Flasks were incubated in fresh FBS-free media at 33°C and harvested between 7-10 days p.i. once signs of cell monolayer detachment and CPE were seen. The cell monolayer supernatants were pooled and clarified by centrifugation at 5,000 xg for 10 minutes at 4°C.

The virus within the pooled, clarified supernatant was then concentrated using ultracentrifugation. Virus ultracentrifugation was carried out using the Sorvall™ WX+ Ultracentrifuge (Thermo Fisher Scientific) in a SureSpin 632 rotor and 38.5ml open-top thinwall polypropylene tubes purchased from Beckman Coulter. 10X HNE buffer 100mM HEPES (Sigma), 1.5M NaCl (VWR Chemicals), 10mM EDTA (Sigma) was dissolved in

MilliQ H2O and filtered through a 0.2µm filtration membrane (Starlab). Virus was resuspended in 1X HNE buffer diluted in Milli H_2O sterilized via autoclaving. Sucrose was purchased from Sigma and dissolved in filtered 1X HNE buffer to produce a 27% (w/v) sucrose solution. The 27% sucrose cushion was overlayed with the clarified supernatant before being centrifuged at a speed of 25,000xg for 2.5 hours at 4°C. Post-ultracentrifugation, supernatant was discarded, and the virus pellet resuspended in 150µl of 1X HNE buffer per tube by rocking overnight on ice. Parafilm was used to seal the ultracentrifuge tubes to prevent evaporation. Resuspended virus was pooled, aliquoted and stored at -80°C. Virus titre was measured through focus-forming assay for all UUKV rescue viruses, and plaque-forming assay for BUNV viral titre assay.

BSR cells were seeded in a 24 well plate at a density of $5x10^5$ cells per well. The virus was sequentially diluted in 2% FBS PBS to a final volume of 100µl per well before being used to inoculate the cell monolayers. Following the 1 hour infection with the virus inoculum at 37°C, the cells were overlayed with 2ml of Avicel overlay. The assays were incubated for either 4 days (rBUNV), 5 days (rUUKV), or 6 days (rUUKVdelNSseGFP). After incubation, the cell monolayers were fixed by adding 1.5ml of formaldehyde fixative solution per well for 1 hour.

For rUUKV viruses, after fixation, the monolayer was washed with MilliQ H_2O two times before being treated with permeabilization buffer for 30 minutes. Following this treatment and between all buffer changes cell monolayers were washed three times with PBS. During this process, mouse anti-UUKV N antibody 8B11A3 was diluted in blocking buffer to produce primary antibody buffer at the concentration described in Table 3.5. Once cells were permeabilised, the monolayers were incubated for either 1.5 hours at room temperature or overnight at 4°C with 150µl of primary antibody buffer. Secondary antibody buffer was made by diluting the appropriate amount of anti-mouse HRP-linked antibody, as indicated by Table 3.5, in blocking buffer. Next, the cell monolayers were incubated with 150µl of secondary antibody buffer for 1 hour at room temperature. After washing the wells three times with PBS, the cells were washed once with MilliQ H_2O before foci were detected using TrueBlue peroxidase substrate. Wells were incubated with 125µl of TrueBlue peroxidase substrate for 20 minutes or until foci were clearly visible, before wells are washed with MilliQ H_2O and foci counted.

For rBUNV, after fixation, the monolayer was washed with MilliQ H_2O two times before being incubated with the toluidine blue plaque assay stain. Wells were incubated with 1ml

of plaque assay stain per well for 20 minutes at room temperature, before being washed with MilliQ H_2O and plaques counted.

Virus titres were calculated using the equation:

$$Virus\ titre\ \left(\frac{PFU\ or\ FFU}{mL}\right) = \frac{Number\ of\ plaques\ (p.f.u.) or\ foci\ (f.f.u.)}{dilution\ factor\ x\ volume\ (mL)}$$

In this equation, the dilution factor is the dilution for the well from which the number of plaques was counted. For example, if the foci were counted from the well corresponding to the 10^{-2} sequential dilution, the dilution factor would be $1x10^2$. Volume is the multiplication factor required to cause the inoculation volume to equal 1mL. For plaque assays in this research the inoculation volume was 100µl, and therefore the volume is 10. PFU = plaque-forming unit and FFU = focus-forming unit.

4.5 Immunofluorescence

For immunofluorescence analysis, cells were seeded at the densities indicated in Table 3.6 and undergo knockdown and/or infection as described in the further methods, viral infection and kinetics, viral binding and internalisation, and whole cell western blot. When the cell monolayers reached the condition or timepoint to be fixed, the cell supernatant was removed, and monolayers washed with PBS once unless stated otherwise. Next, the cells were fixed in 8% formaldehyde fixative solution for 1 hour and permeabilised in permeabilization buffer for 30 minutes. For both primary and secondary antibody buffers, the corresponding antibodies were diluted in blocking buffer at the concentration described in Table 3.5. The cell monolayers were then washed three times with PBS before being probed with primary antibody buffer. Primary antibody incubation was carried out for 1.5 hours at room temperature or overnight at 4°C. Next, fixed cells were washed three times with PBS before being probed for 1 hour at room temperature with secondary antibody buffer. Cells were washed once with PBS before being incubated with DAPI diluted (unless the cell nuclei were already stained using Hoechst 33342) in PBS at a concentration of 3µl:10mL for ten minutes at room temperature. Finally, cell monolayers were washed three times with PBS. Cells were kept at 4°C in PBS until imaging via EVOS or confocal microscopy.

4.6 Molecular Techniques

4.6.1 PCR

To amplify DNA, PCR was performed. For high-fidelity reactions, KOD HotStart DNA polymerase (Merck) was used, and for low-fidelity GoTaq® G2 Flexi DNA polymerase (Promega) was used. For 50µl reactions, the following conditions indicated in Table 4.6.1 were used according to the manufacturer's specifications, and these volumes could be scaled to suit the needs of the experiment.

KOD HotStart DNA polymerase				
Reaction components		PCR conditions		Cycle Number
10X KOD polymerase buffer	5µl	Initial denaturation – 95°C	5 min	1
dNTP mix (2mM each)	5µl	Denaturation - 95°C	30 sec	30
$MgSO_4$ (25mM)	3µl	Annealing – 52 to 56°C	30 sec	
Forward 5' primer (10µM)	1.5µl	Extension – 70°C	25 sec/kb	
Reverse 3' primer (10µM)	1.5µl	Final extension – 70°C	10 min	1
Template DNA (1-10ng)	1µl	Indefinite hold – 4°C	∞	1
KOD polymerase (1 U)	1µl			
Sterile ddH_2O	32µl			
GoTaq® G2 Flexi DNA polymerase				
Reaction components		PCR conditions		Cycle Number
5X Q5 reaction buffer	10µl	Initial denaturation – 98°C	5 min	1
dNTP mix (10mM)	1µl	Denaturation - 98°C	10 sec	30
Forward 5' primer (10µM)	2.5µl	Annealing – 52 to 56°C	30 sec	
Reverse 3' primer (10µM)	2.5µl	Extension – 72°C	25 sec/kb	
Template DNA (1-10ng)	1µl	Final extension – 72°C	5 min	1
Q5 HF DNA polymerase (1 U)	1µl	Indefinite hold – 4°C	∞	1
Sterile ddH_2O	32.5µl			

Table 4.3: PCR component volumes and thermocycler conditions.

The primer annealing temperature was determined using the tools available in Benchling and IDT. As described in the table, the extension time was dictated by the length of the DNA to be amplified as outlined in the manufacturer's guide.

4.6.2 Agarose gel electrophoresis and gel extraction

PCR products and dsRNA were separated based on nucleotide length using agarose gel electrophoresis. For products 300 nucleotides in length or less, 1% agarose was dissolved in 1X TAE buffer with 3µl/100ml of ethidium bromide (Sigma-Aldrich). For PCR products over 300 nucleotides in length, 2% agarose were prepared. Once solidified, the gel was submerged in 1X TAE buffer. Nucleotide samples were mixed in a ratio of 5:1 (v/v) with DNA Gel Loading Dye (6X) (Thermo Fisher Scientific). The prepared samples were loaded into the submerged gel alongside the 1 Kb Plus DNA ladder (Thermo Fisher Scientific). Electrophoresis was performed at 100V for smaller products and 125V for larger products for at least 20 minutes, until clear separation of the ladder and products was achieved.

Separated products were visualized using a UV transilluminator. Bands were then excised from the gel using a sterile scalpel and stored in a 1.5ml microcentrifuge tube (Eppendorf). Nucleotide products were then extracted from these excised bands using the Wizard® SV Gel and PCR Clean-up System (Promega), following the manufacturer's instructions. Nucleotide products were eluted in nuclease-free H_2O, with concentration and purity measured using a NanodropOne (Thermo Fisher Scientific). Purity was measured through monitoring the ratio of absorbance at 260nm and 280nm for DNA and RNA, respectively. As mentioned in methods, all eluted DNA products were sequenced through Eurofins and Source Bioscience using the primers listed in Table 3.3 unless otherwise stated. DNA samples were stored at -20°C.

4.6.3 Plasmid production through bacterial transformation

Using the Z-competent Transformation kit (Zymo Research), following manufacturer's instructions, the E. coli stain JM109 were made chemically competent, aliquoted, and stored at -80°C until used. To transform the bacteria, 100µl of competent bacteria were thawed on ice before incubation with 2-10µl plasmid DNA for a final plasmid quantity of 1-50ng for 5 minutes on ice. Glass beads were used to spread transformed bacterial cells on LB agar plates supplemented with ampicillin (100µg/ml) and incubated at room temperature until bacterial colonies could be seen. Glass beads were sterilised for future use by autoclaving.

Once colonies reached a suitable size for selection and amplification, single colonies were picked using a P200 pipette tip. All further growth steps were carried out at room

temperature. Tips were incubated by circular rotation at 180 rpm (xg) in 5ml LB broth containing ampicillin (100µg/ml). Cultures were incubated until the media appeared cloudy. For preparation of maxi preps and larger bacterial samples, the 5ml bacterial broth was transferred to larger volumes of LB broth containing ampicillin (100-300ml) and incubated by circular rotation at 180 rpm until the media appeared cloudy. Once bacterial broth reached the desired cloudiness, the bacterial broth was centrifuged at 5,000xg for 5 minutes to pellet the bacteria. Bacterial pellets produced from 5ml LB broth were subjected to minipreps, whereas larger pellets were subjected to Maxiprep, using the QIAprep Spin Miniprep kit (Qiagen) or QIAprep Spin Maxiprep kit (Qiagen) following the manufacturer's instructions, respectively. Isolated plasmids were eluted in nuclease-free H_2O, the plasmid concentration was measured using the Nanodrop One (Thermo fisher Scientific) and sequenced by Eurofins and Source Bioscience using the primers listed in Table 3.3 unless otherwise stated.

4.6.4 RNA Extraction

To extract total cellular RNA, cells were washed with PBS before being incubated with 1ml of TRIzol reagent (Thermo Fisher Scientific) for 10 minutes at room temperature. When carrying out RNA extraction of stock virus, 20ul of virus stock was incubated with 1ml of TRIzol, and for extracting RNA from clarified cell supernatant, 200µl of supernatant was incubated with 1ml of TRIzol before the 10-minute incubation at room temperature. Following this incubation, the TRIzol cell lysis was transferred to a 1.5ml microcentrifuge tube (Eppendorf) and 200µl of chloroform added before manually inverting the microcentrifuge tube 10 times. The cell lysis solution was then incubated for 5 minutes at room temperature before centrifuging at 12,000xg for 15 minutes to allow for phase separation of the RNA. During this process, fresh 1.5ml microcentrifuge tubes were prepared and 3µl of GlycoBlue were added to each tube. After phase separation, the aqueous phase was removed, transferred to the GlycoBlue containing microcentrifuge tube and 500µl of propan-2-ol added before inverting to mix 10 times. The propan-2-ol mix was then incubated at room temperature for 10 minutes before the RNA was pelleted by centrifugation at a speed of 16,000xg for 15 minutes at 4°C. The supernatant was removed, and the RNA pellet washed with chilled 500µl 75% (v/v) ethanol before centrifugation at 12,000xg for 10 minutes at 4°C. After centrifugation, the supernatant was removed, and the pellet air-dried before the RNA was resuspended in 30µl nuclease-free water. The quantity and quality of the RNA was measured using the NanodropOne (Thermo Fisher Scientific). RNA was stored at -80°C.

4.6.5 cDNA Synthesis

Reverse-transcription was used to generate cDNA from extracted RNA for RT qPCR analysis and sequencing of recombinant rUUKV viruses. cDNA was produced using the SuperScript™ III Reverse Transcriptase kit (Thermo Fisher Scientific) as defined in Table 4.4 below for a 20µl output. Volumes were scaled as needed:

<table>
<tr><th colspan="3">SuperScript™ III Reverse Transcriptase</th></tr>
<tr><th colspan="2">Reaction components</th><td>RT conditions</td></tr>
<tr><td>Specific primers (2pmol) (see appendices) or random hexamers (50µM)</td><td>1µl</td><td rowspan="4">65°C for 5 minutes</td></tr>
<tr><td>10pg - 5µg total RNA</td><td>1µl</td></tr>
<tr><td>dNTP mix (10mM)</td><td>1µl</td></tr>
<tr><td>Nuclease-free H_2O</td><td>10µl</td></tr>
<tr><td colspan="3">Incubate above on ice for 1 minute before adding the below and continuing</td></tr>
<tr><td>5X First-strand buffer</td><td>4µl</td><td rowspan="4">Mix by gentle pipetting.
If using random primers, incubate samples at 25°C for 5 minutes.
50°C for 60 minutes.
70°C for 15 minutes.</td></tr>
<tr><td>DTT (0.1M)</td><td>1µl</td></tr>
<tr><td>RNaseOUT™ Recombinant RNase Inhibitor</td><td>1µl</td></tr>
<tr><td>SuperScript III RT (200 units/µl)</td><td>1µl</td></tr>
</table>

Table 4.4: Components and conditions for RNA reverse transcription.

Once cDNA was generated, template RNA was degraded by incubating cDNA samples with RNase A for 20 minutes at 37°C, before samples were stored at -20°C.

4.6.6 Real-time qPCR

All real-time quantitative PCR (RT qPCR) samples were analysed in technical triplicates and used to measure cellular mRNA levels or levels of vRNA. The cDNA produced from RT, as previously described, was combined with the components as described in Table 4.5 below to produce a 20µl reaction mix:

RT qPCR	
cDNA	2µl
SYBR™ Green PCR Master Mix	10µl
Forward Primer (10µM)	1µl
Reverse Primer (10µM)	1µl
Nuclease-free H2O	6µl

Table 4.5: Component volumes for real-time quantitative PCR (qPCR).

The reaction mix was vortexed before transferring 5µl per well to a 384 well plate. To provide a positive control during RT qPCR, the cDNA from whole cell random hexamer RT was used when using primers against cell-specific genes, and cDNA generated from virus stock random hexamer RT was used for UUKV M RNA detection. For negative controls, cDNA was replaced with nuclease-free H_2O. The RT qPCR reactions were performed and analysed using the QuantStudio™ Real-Time PCR System and associated software, following the cycle conditions listed below in Table 3.11.

qPCR Cycle Conditions			
Initial denaturation	95°C	30 seconds	1 cycle
Denaturation	95°C	5 seconds	40 cycles
Annealing and extension	60°C	30 seconds	
Melt curve	95°C 60°C 95°C	15 seconds 1 minute 15 seconds	1 cycle, 0.1°C increase per second

Table 4.6: Quantitative PCR reaction conditions.

If the cycle threshold (Ct) values were too low, the cDNA was diluted 1:10 in nuclease-free water before the process was repeated.

The delta delta Ct (ΔΔCt) analysis method was used to calculate the normalised expression of the RNA per sample. For cellular genes this is the expression of mRNA, whereas for viral genes as UUKV is an RNA virus with no DNA intermediate, this is the expression of vRNA. To calculate the normalised expression, the mean Ct of the technical triplicates of the control samples (XA, XB, and XC representing the biological triplicates generated) and the sample

of interest's (YA, YB, and YC) for both the housekeeping/normalising (Hk) gene (X_{Hk} and Y_{Hk}, respectively) and the gene of interest (GOI) (X_{GOI} and Y_{GOI}, respectively).

This analysis process is demonstrated below in Table 4.7.

ΔΔCt										
Target Gene	**Sample**	**Ct1**	**Ct2**	**Ct3**	**Mean Ct**	**Control Average Ct**	**ΔCt per sample per target**	**Relative quantity ($2^{\Delta Ct}$)**	**Normalisation Factor (geomean RQ controls)**	**Normalised expression per sample (ΔΔCt)**
Hk	XA	XA_{Hk1}	XA_{Hk2}	XA_{Hk3}	$XA_{HkMean} = \frac{Sum(XA_{Hk1-3})}{3}$	X_{HkMean}	$XA_{HkCt} = \frac{XA_{HkMean}}{X_{HkMean}}$	$2^{XA_{HkCt}}$	N/A	N/A
	XB	XB_{Hk1}	XB_{Hk2}	XB_{Hk3}	$XB_{HkMean} = \frac{Sum(XB_{Hk1-3})}{3}$		$XB_{HkCt} = \frac{XB_{HkMean}}{X_{HkMean}}$	$2^{XB_{HkCt}}$		
	XC	XC_{Hk1}	XC_{Hk2}	XC_{Hk3}	$XC_{HkMean} = \frac{Sum(XC_{Hk1-3})}{3}$		$XC_{HkCt} = \frac{XC_{HkMean}}{X_{HkMean}}$	$2^{XC_{HkCt}}$		
	YA	YA_{Hk1}	YA_{Hk2}	YA_{Hk3}	$YA_{HkMean} = \frac{Sum(YA_{Hk1-3})}{3}$	N/A	$YA_{HkCt} = \frac{YA_{HkMean}}{X_{HkMean}}$	$2^{YA_{HkCt}}$		
	YB	YB_{Hk1}	YB_{Hk2}	YB_{Hk3}	$YB_{HkMean} = \frac{Sum(YB_{Hk1-3})}{3}$		$YB_{HkCt} = \frac{YB_{HkMean}}{X_{HkMean}}$	$2^{YB_{HkCt}}$		
	YC	YC_{Hk1}	YC_{Hk2}	YC_{Hk3}	$YC_{HkMean} = \frac{Sum(YC_{Hk1-3})}{3}$		$YC_{HkCt} = \frac{YC_{HkMean}}{X_{HkMean}}$	$2^{YC_{HkCt}}$		
Goi	XA	XA_{Goi1}	XA_{Goi2}	XA_{Goi3}	$XA_{GoiMean} = \frac{Sum(XA_{Goi1-3})}{3}$	$X_{GoiMean}$	$XA_{GoiCt} = \frac{XA_{GoiMean}}{X_{GoiMean}}$	$2^{XA_{GoiCt}}$	$XA_{NF} = GEOMEAN(2^{XA_{HkCt}})$	$XA_{GoiEXP} = \frac{2^{XA_{GoiCt}}}{XA_{NF}}$
	XB	XB_{Goi1}	XB_{Goi2}	XB_{Goi3}	$XB_{GoiMean} = \frac{Sum(XB_{Goi1-3})}{3}$		$XB_{GoiCt} = \frac{XB_{GoiMean}}{X_{GoiMean}}$	$2^{XB_{GoiCt}}$	$XB_{NF} = GEOMEAN(2^{XB_{HkCt}})$	$XB_{GoiEXP} = \frac{2^{XB_{GoiCt}}}{XB_{NF}}$
	XC	XC_{Goi1}	XC_{Goi2}	XC_{Goi3}	$XC_{GoiMean} = \frac{Sum(XC_{Goi1-3})}{3}$		$XC_{GoiCt} = \frac{XC_{GoiMean}}{X_{GoiMean}}$	$2^{XC_{GoiCt}}$	$XC_{NF} = GEOMEAN(2^{XC_{HkCt}})$	$XC_{GoiEXP} = \frac{2^{XC_{GoiCt}}}{XC_{NF}}$
	YA	YA_{Goi1}	YA_{Goi2}	YA_{Goi3}	$YA_{GoiMean} = \frac{Sum(YA_{Goi1-3})}{3}$	N/A	$YA_{GoiCt} = \frac{YA_{GoiMean}}{X_{GoiMean}}$	$2^{YA_{GoiCt}}$	$YA_{NF} = GEOMEAN(2^{YA_{HkCt}})$	$YA_{GoiEXP} = \frac{2^{YA_{GoiCt}}}{YA_{NF}}$
	YB	YB_{Goi1}	YB_{Goi2}	YB_{Goi3}	$YB_{GoiMean} = \frac{Sum(YB_{Goi1-3})}{3}$		$YB_{GoiCt} = \frac{YB}{X_{GoiMean}}$	$2^{XB_{GoiCt}}$	$YB_{NF} = GEOMEAN(2^{YB_{HkCt}})$	$YB_{GoiEXP} = \frac{2^{YB_{GoiCt}}}{YB_{NF}}$
	YC	YC_{Goi1}	YC_{Goi2}	YC_{Goi3}	$YC_{GoiMean} = \frac{Sum(YC_{Goi1-3})}{3}$		$YC_{GoiCt} = \frac{YC_{GoiMean}}{X_{GoiMean}}$	$2^{XC_{GoiCt}}$	$YC_{NF} = GEOMEAN(2^{XAYC_{HkCt}})$	$YC_{GoiEXP} = \frac{2^{YC_{GoiCt}}}{YC_{NF}}$

Table 4.7: Schematic representation of the ΔΔCt calculations.

For experiments where there was no housekeeping gene present to allow for the ΔΔCt calculation, such as when isolating UUKV M RNA from supernatant, Ct values were normalised, or a standard curve was produced to allow for the calculation of copy number. To normalise the Ct values, the following calculation was used:

$$Normalised\ Ct\ Value = 40\ - Ct$$

The maximum detection limit for the thermocycler was defined as a Ct of 40, and therefore any Ct < 40 is within the detection limit. The normalised Ct was calculated by subtracting the samples Ct from the maximum detection limit. Negative controls produced a Ct of 30 or above, producing a normalised Ct ≤ 10. Any samples which produced a normalised Ct ≤ 10 was therefore classified as a negative result. For calculating copy number, a standard curve was prepared by sequentially diluting the standard curve fragment produced by PCR (using the primers described in Table 3.3). By comparing the Ct value of the sample against this standard curve, the concentration of DNA in g/µl can be determined. The molecular weight of the dsDNA was calculated by multiplying the length of the product produced from PCR. The concentration of DNA was then divided by this molecular weight and multiplied by Avogadro's constant to give the DNA copy number per µl.

4.6.7 Preparation of cell lysates for protein analysis

Cell monolayers were washed with PBS before being lysed in Laemmli buffer, unless otherwise specified. The corresponding volumes of Laemmli lysis buffer are described below in Table 4.8.

Cell Lysis for Protein Analysis	
Plate Size	Lysis Volume per Well
24-well plate	50µl
12-well plate	100µl
6-well plate	200µl
10cm^2 plate	3ml

Table 4.8: The volumes of cell lysis buffer required depending on the well or flask size used.

Cell lysates were then collected in 1.5ml microcentrifuge tubes (Eppendorf) tubes for volumes smaller than 1ml, and 5ml tubes (Sigma Aldrich) for volumes larger than 1ml. For protein samples harvested in Laemmli buffer, samples were mixed in a 3:1 ratio (v/v) with 4X LDS loading buffer and boiled at 95°C for 10 minutes. Samples were stored at -20° until processing.

4.6.8 Protein SDS PAGE gel electrophoresis

Polyacrylamide gel electrophoresis (PAGE) was carried out using 15-well 1.5mm precast NuPAGE Novex 4-12% Bis-Tris gels submerged in 1X MES SDS running buffer in denaturing conditions. For silver staining, 10µl of sample was loaded per well alongside 5µl of PageRuler™ Plus Prestained Protein Ladder (Thermo Fisher Scientific) diluted 1:10 in lysis buffer. For western blotting, 20µl of sample was loaded per well with 5µl of PageRuler™ Plus Prestained Protein Ladder (Thermo Fisher Scientific). Protein separation was achieved by subjecting the gel to 150V for 40+ minutes, until the desired separation, determined by the ladder position, was achieved.

4.6.9 Silver stain

Silver staining was carried out using the Pierce™ Silver Stain Kit (Thermo Fisher Scientific), following the manufacturer's instructions. Briefly, gels were washed twice for 5 minutes in MilliQ H_2O before being fixed. Gels were fixed through incubating with fixative buffer (30% (v/v) ethanol and 10% (v/v) acetic acid in MilliQ H_2O) for 15 minutes, before fixative buffer was replaced with fresh fixative buffer and incubated for another 15 minutes. Fixed gels were then washed in 10% (v/v) ethanol twice for 5 minutes and MilliQ H_2O twice for five minutes. Gels were sensitized by being submerged in sensitizer solution (50µl sensitizer in 25ml H_2O) before being washed in MilliQ H_2O twice for 1 minute. Sensitized gels were stained by incubating the gel in staining solution (0.5ml stain enhancer in 25ml stain solution) for 30 minutes. Stained gels were washed twice in MilliQ H_2O for 20 seconds to remove any remaining stain solution before the gels were developed by incubating with developing buffer (0.5ml stain enhancer in 25ml developer solution) until bands were visualized. To stop development once the stain was at an optimal level, gels were incubated with 5% (v/v) acetic acid in MilliQ H_2O for ten minutes and stored in MilliQ H_2O until imaging.

4.6.10 Western blot assay

To transfer the proteins which have undergone protein SDS PAGE gel electrophoresis onto a nitrocellulose membrane (0.45µm pore size, Amersham), semi-dry transfer was done using a Trans-Blot Turbo Blotting system (BioRad). All components (the gel, membrane, and blotting pads) of the transfer were soaked in 1X NuPage transfer buffer. Transfer was performed at a constant voltage of 10V for 50 minutes.

Upon completion of transfer, the membrane was blocked at room temperature for one hour in blocking buffer. When transferring the membrane between buffers, the membranes were

washed 3 times with PBST. Primary antibodies were diluted in blocking buffer as described in Table 3.5 and the membrane incubated in 50ml tubes (Sigma Aldrich) with constant rotation for one hour at room temperature or overnight at 4°C. Once probed with primary antibody, membranes were incubated with secondary antibody diluted in standard blocking buffer as described in the Table 3.5. Incubation was carried out for 1 hour at room temperature under constant rotation in fresh 50ml tubes. For light-sensitive secondary antibodies, 50ml black-plastic tubes (Sigma Aldrich) were used to prevent photo-bleaching.

After final washing, membranes were imaged using an Odyssey® CLx Imaging System (Li-Cor) and analysed using the associated software.

4.7 Viral infection and kinetics

4.7.1 FBS assay

BSR or BHK cells were seeded in 6 well plates and infected with either mock inoculum or rUUKV as previously described in methods. Briefly, a low MOI of 0.1 FFU/cell was used to infect BSR or BHK-21 cell monolayers. After adsorption, cell monolayers were supplemented with media containing varying percentages of FBS (v/v) and incubated at either 33°C or 37°C. At 3- or 6-days post-infection, viral load in the supernatant was titred via focus forming assays.

4.7.2 Virus growth curves

A549, BSR, AF5, AF319, and ISE6 cell monolayers seeded at the density described in Table 3.6 were infected with rUUKV at a MOI of 0.1 FFU/cell. In addition, BSR cell monolayers that were seeded at a density of $5x10^4$ cells/ml were infected with rUUKVdelNSseGFP or rBUNV at a MOI of 0.1 FFU/cell. Following the 1 h virus adsorption period, cell monolayers were supplemented with media containing 10% FBS (v/v) and incubated at 37°C. Starting at 0 h, cell supernatant was harvested every 24 hours and the virus titre determined by focus-forming or plaque assay (for rUUKV/delNSseGFP and rBUNV, respectively) in BSR cells. In parallel, cell monolayers were lysed at each timepoint, and extracts prepared for western blot detecting α-tubulin and the respective viral nucleocapsid protein.

4.8 Viral binding and internalisation

4.8.1 Dying UUKV virus particles

To dye the viral stock, the quantity of viral glycoproteins (G_n and G_c) was first determined. To do this 5µl, 10µl, and 15µl of virus were made up to 20µl each with 5µl of 4X LDS

loading buffer and (if required) nuclease-free water to produce a final volume of 20µl. In addition to the viral samples, a BSA standard curve was produced by diluting UltraPure BSA (Thermo Fisher Scientific) to give 20µl final volumes for BSA quantities of 0.1-1µg at 0.1µg intervals. The virus dilutions and BSA standard curve samples were prepared by boiling and then subjected to gel electrophoresis as described previously.

The gels were then washed in MilliQ H_2O before band visualisation was done through incubating the gel with Coomassie Blue stain for 20 minutes. The gels were then washed again and stored in MilliQ H_2O until being imaged on a Gel Imaging system (Thermo Fisher Scientific). An example of this band visualisation is shown in Appendices [Figure 4.1]. The background and intensity of the BSA bands (at 66 kDa) were determined using ImageJ and plotted against the BSA concentration to produce a BSA standard curve. The intensity of the G_n (75 kDa) and G_c (65 kDa) bands in the three viral concentrations were also measured to allow for the estimation of the amount of G_n and G_c within the viral stock per ml. Using this concentration, the number of moles can be calculated by dividing the concentration of glycoproteins by the average molecular weight of the glycoproteins (55246.39g).

A working stock of AF647 (Thermo Fisher Scientific) was made by diluting the dye in DMSO to produce a final concentration of 1µg/µl. To dye the virus, the working stock of dye was added to the viral stock to produce a glycoprotein to dye ratio of 1:5 (mol:mol). The virus-dye mix was vortexed before unbound dye removed via sucrose density gradient ultracentrifugation. To do this, 600µl of 10%, 20%, 25%, 30%, 35%, and 50% (m/v) sucrose in 1X HNE buffer were carefully pipetted on top of each other in 5ml open-top thinwall polypropylene tubes (Beckman Coulter), starting with the highest concentration and moving to the lowest. The dye-virus mix was then overlayed on this sucrose density gradient and spun at 100,000xg using a Sorvall™ WX+ Ultracentrifuge (Thermo), with acceleration and deceleration set to maximum and minimum. This ultracentrifugation causes the dyed viral particles to band between the 25% to 35% densities, while unbound dye remains at the top of the gradient.

The dyed virus band was then extracted from the tube via syringe and aliquoted into 1.5ml microcentrifuge tubes (Eppendorf). Virus stocks were stored at -80°C. Virus titre was measured via focus-forming assay and the morphology of the dyed virus particles was compared to that of undyed virus particles by negative stain electron microscopy on a JEOL JEM 1400 (JEOL, Japan) electron microscope. Negative staining and cryo-EM were carried out by Dr Swetha Vijayakrishnan at the MRC – Centre for Virus Research Scottish Centre for Macromolecular Imaging.

4.8.2 UUKV binding assay

BSR, AF5, and ISE6 cells were seeded at the densities indicated in Table 4.1. Prior to virus infection, cell monolayers were washed and incubated with the appropriate cell media supplemented with 1µl per 10ml media Hoechst 33342 solution for ten minutes before the cells were washed again with PBS three times. Following this, a 1X working stock of CellMask Green plasma membrane stain was made, and cell monolayers were incubated for one hour with the relevant cell media supplemented with 10µl of working stain solution per 10ml of media. Both incubations were carried out at the relevant temperature for the cell type. Cell monolayers were washed 3 times and infected with pre-chilled PBS or inoculum for 1 hour on ice. For inactivation experiments, the dyed virus in its final volume was boiled at 95°C for 5 minutes before being cooled on ice and used as inoculum.

Once the incubation was complete, the inoculum was removed, and cell monolayers were either incubated with trypsin before washing three times or washed with PBS the required number of times before being fixed in 8% formaldehyde. After fixation, cell monolayers were washed three times with PBS and stored at 4°C until imaging. Where possible, the cell monolayers were shielded from light at all steps of this process, to prevent photo-bleaching. Imaging was carried out on a Carl Zeiss LSM 880 confocal microscope equipped with a 64x objective, using tile scan and Z-stack imaging.

For RT qPCR binding experiments, instead of fixing after washing the cell monolayers were lysed with 1ml TRIzol. RNA extraction, cDNA synthesis and qPCR were performed to calculate the expression of intracellular UUKV M RNA using the samples washed once with PBS as the baseline for comparison.

4.8.3 UUKV internalisation assay

Cells were prepped and infected as described in the UUKV binding assay above. Once incubation was complete, the inoculum removed and cell monolayer washed, the corresponding media for each cell line (pre-warmed to the appropriate temperature) was added to the cell-monolayers. This was considered the 0 h timepoint. The cell monolayers were then incubated in media for the relevant time period before media were removed and cell monolayers washed in PBS, followed by fixation to determine fluorescence through confocal imaging or were lysed in TRIzol and subject to RT qPCR as described in the UUKV binding assay section.

4.9 UV crosslinking and oligo(dT) capture

4.9.1 UV crosslinking

For BSR and ISE6, 5x and 3x 10cm^2 plates (respectively) were seeded and infected following the methods described in virus infections. After incubation and washing, cell monolayers were incubated for 24 hours (for A549) or 9 days (for ISE6) in the appropriate conditions. Once the cell monolayers were incubated for the appropriate amount of time, the cell media were removed, and the cell monolayers were washed with PBS 3 times. After the final wash, the PBS was removed, and cell monolayers exposed to 150mJ/cm^2 on ice or mock-exposed. Following ultraviolet (UV) exposure, 3ml of lysis buffer was used to harvest the cell monolayers and the extracts stored on ice. Lysed monolayers were then mechanically homogenised by passing the sample through a 0.4 mm diameter needle using a 5ml syringe on ice. 100µl input sample from each supernatant was stored at -80°C until processing.

4.9.2 Oligo(dT) capture

To capture polyadenylated (poly(A)) RNAs 300µl or 450µl of bead slurry was used for 3x 10cm^2 plates and 5x 10cm^2 plates, respectively. Bead slurry was vortexed before the desired volume was aliquoted. For every buffer change during this process, beads were secured by placing the sample containing 1.5ml microcentrifuge tubes (Eppendorf) within the magnetic tube rack for 30-60 seconds before buffer was removed by pipetting and the next buffer added using a fresh pipette tip. Beads were washed three times in 1ml of lysis buffer to equilibrate the beads. The equilibrated beads were then added to the appropriate homogenised supernatant, which was then subjected to gentle rotation for 1 hour at 4°C.The supernatant was removed from the beads on ice. For multiple rounds of oligo(dT) capture, the supernatant was kept on ice, otherwise the supernatant was discarded. The beads were then washed with lysis buffer, wash buffer 1, wash buffer 2 on ice, followed by wash buffer 3 at room temperature. To wash, 1ml of the appropriate buffer was added to the beads. The beads were inverted 10 times per minute, for five minutes, whilst being stored on ice or at room temperature as specified. Following this incubation, the wash buffer was removed, and the process repeated twice more, meaning the beads were washed 3 times with lysis buffer before being washed with wash buffer 1, and so on. Once all wash steps were complete, captured mRNA was eluted by incubating the beads with 125µl of elution buffer for 3 minutes at 55°C, inverting the tubes 10 times per minute. The eluate was transferred to a fresh microcentrifuge tube and used beads were incubated with 400µl of NaOH at 55°C for 5 minutes. If performing more than one round of capture, the beads were then washed with

lysis buffer and added back to the corresponding homogenised supernatant set aside from the beginning of the process, and the capture was repeated. The eluted RNA quantity was measured using the Nanodrop One and after measurement the eluate was stored at -80°C until protein analysis, with 20µl of eluate being stored in a separate microcentrifuge tube for RNA analysis.

4.9.3 RNA isolation in RIC

For RNA analysis, the proteins in the eluate and an aliquot of the input were degraded by incubating with 5µl of proteinase K solution for 1 hour at 50°C before 1ml of TRIzol was added. RNA was extracted and analysed as described previously by RNA extraction, cDNA synthesis and RT qPCR.

4.9.4 Protein isolation in RIC

For protein analysis, the RNA in the eluate and an aliquot of the input sample were degraded by incubating with 3µl RNase A/100µl of lysate for 1.5 hours at 37°C before incubating for 15 minutes at 50°C. For silver stain analysis, 10µl of the samples were removed and incubated with 4µl of LDS loading buffer before being subjected to gel electrophoresis and silver staining as described previously. The remainder of the proteins isolated from RIC were stored at -80°C until being sent for mass spectrometry analysis.

4.10 Mass spectrometry

4.10.1 Sample preparation through SP3

SP3 sample preparation was carried out by Dr Wael Kamel. Briefly, eluate samples from oligo(dT) capture were incubated in the dark, at room temperature, for 30 minutes with 10mM TCEP and 50mM C-IAA to reduce and alkylate the proteins within the sample. The samples were then split into two in order to maximise protein retention during processing and 100µg per 300µl of sample of carboxylated beads were added alongside 80% (v/v) ACN. Samples were incubated at room temperature for 30 minutes before being placed on a magnetic rack for 10+ minutes to allow for the supernatant to be removed and discarded. Beads were then put through a washing procedure; first beads were washed twice with 70% ethanol and then once with 100% ACN. This wash procedure was repeated until no detergent was detected within the supernatant. Following washing, the samples were supplemented with 250ng of trypsin and incubated overnight at 37°C to cleave proteins from the beads and to digest the proteins into peptide fragments. The fragments were then collected by placing

the tubes on the magnetic rack and transferring the supernatant to a 1.5ml microcentrifuge tube (Eppendorf). Corresponding samples which have previously been split were combined and acidified with neat formic acid (FA) prior to loading onto the mass spectrometer.

4.10.2 Mass spectrometry

ISE6 RIC prepared samples were sent to the Advanced Proteomics Facility at the Biochemistry department of University of Oxford for mass-spectrometry analysis, who provided the raw data files upon completion. All other samples were sent to the Dundee FingerPrints Proteomics facility, where SP3 preparation was performed in house before being subjected to mass spectrometry analysis. For immunoprecipitation samples, SP3 was not performed. Nano-liquid chromatography tandem mass spectrometry with data-dependent analysis (ISE6) or data-independent analysis (A549) label-free quantification (nLC-MS/MS (DDA/DIA-LFQ)) was used to analyse the mass spectrometry samples.

The FingerPrints Proteomics facility (Dundee) carry out mass spectrometry using an Ultimate 3000 RSLC nano-system (Thermo Fisher Scientific) coupled to a LTQ OrbiTrap Velos Pro (Thermo Fisher Scientific) for DDA or an Orbitrap Exploris 480 Mass Spectrometer (Thermo Fishe Scientific). Progenesis LC-MS software was used to identify peptides and MaxQuant v2.4.11.0 was used to obtain label free quantification intensity values.

At the Rosalind Franklin Institute, liquid chromatography was performed using Ultimate 3000 ultra-HPLC system (Thermo Fisher Scientific), where peptides were trapped in C18 300µm inner diameter x 5mm 100A PepMap 100 pre-columns (Thermo Fisher Scientific) incubated with 0.1% (v/v) formic acid and 5µM medronic acid. Peptide separation was carried out on the 75µm inner diameter x 50cm packed with ReproSil-Pur 120 (C18-AQ) in a 60 min 15-35% (v/v) acetonitrile gradient with constant 200nl/min flow rate. Mass spectra were required in a LTQ OrbiTrap Velos Pro (Thermo Fisher Scientific) in data-dependent mode. Protein identification and quantification were obtained using Andromeda search engine implemented in MaxQuant, and searched against the ISE6 reference proteome (Miller et al., 2018). MaxQuant searches were performed with ‘match between run’ activated and false discovery rate set to 10% and 1%. PCA analysis was carried out whereby each samples data was treated as individual and unlabelled, and samples clustered based on their similarity in order to summarise the variability between the samples, allowing the visualisation of the large protein sets whilst still factoring in the types of proteins and intensities within the samples.

Downstream analysis of proteins produced from mass spectrometry analysis was carried out by the tools available in VectorBase, InParanoiDB (version 9), InterproScan (version 97.0), MobiDB Lite (version 5.0) as mentioned in Materials. Gene ontology (GO) analysis was carried out using VectorBase, where the proteins within the 10% false discovery rate (FDR) and 1% FDR protein groups for each condition were compared against the ISE6 background to determine enriched terms for molecular domain functions and intracellular pathway involvement. InterproScan was used to scan the FASTA files of the proteins to determine the domain types present within the proteins and the percentage intrinsic disorder. Finally, MobiDB was used to predict the hydrophobicity of the protein using the FASTA file.

4.11 Knockdowns

4.11.1 dsRNA production

DNA for each dsRNA target was produced by PCR using the corresponding primers listed in Table 3.3 and whole cell RNA random hexamer produced cDNA (for ISE6 genes), random hexamer cDNA of vRNA (for UUKV N knockdown), or pTVUUKS plasmid were used as the template. PCR products were analysed by agarose gel electrophoresis and purified by gel extraction. The primers added the appropriate T7 minimal promoter sequence overhangs to the PCR products. The MEGAscript® RNAi Kit (Thermo Fisher Scientific) was used to produce the dsRNA, following the manufacturer's instructions. Briefly, all components were vortexed before use and all buffers except from the 10X reaction buffer were kept on ice. The transcription reaction was assembled at room temperature to produce a single 20µl reaction as described in Table 4.9 below.

dsRNA Production	
Nuclease-free water	Make up to 20µl
Linear template DNA	2µg
10X T7 reaction buffer	2µl
ATP solution	2µl
CTP solution	2µl
GTP solution	2µl
UTP solution	2µl
T7 enzyme mix	2µl

Table 4.9: Components for dsRNA production.

The mixture was gently flicked to mix before brief centrifugation. The reaction was then incubated at 37°C for 4 hours. To ensure complementary strand annealing, the reaction mix

was heated to 75°C for 5 minutes before being left to cool on the benchtop until the mix returned to room temperature. DNase and RNase treatments were then carried out to remove and template DNA and unannealed ssRNA by assembling the following mixture indicated in Table 4.10 on ice.

dsRNA Nuclease Digestion	
dsRNA mix (see above)	20µl
Nuclease-free water	20µl
10X Digestion buffer	5µl
DNase I	2µl
RNase	2µl

Table 4.10: Components for dsRNA nuclease digestion.

The above reaction mix was then incubated at 37°C for 1 hour.

Finally, the dsRNA was column purified. The dsRNA was mixed with binding mix to be prepared for filter cartridge isolation by preparing the mixture shown in Table 4.11.

dsRNA Purification	
dsRNA (see above)	50µl
10X Binding buffer	50µl
Nuclease-free water	150µl
100% Ethanol	250µl

Table 4.11: Components for dsRNA purification mixture.

The mixture was gently mixed by pipetting before being added to the filter cartridge. The cartridge was centrifuged at 15,000 rpm for 2 minutes using a 5430 benchtop centrifuge (Eppendorf), before flow-through was discarded. The cartridge was washed twice by adding 500µl of wash solution and centrifuging as before. After the second wash, once the flow through was discarded, the cartridge was spun for an additional 30 seconds. dsRNA was eluted from the cartridge by adding 50µl of elution solution, preheated to 95°C, and centrifuged at 15,000 rpm for 2 minutes. To determine the quality of the dsRNA, the concentration was determined using the Nanodrop One, and size of dsRNA confirmed by agarose gel electrophoresis.

4.11.2 ISE6 cell gene knockdowns

ISE6 cells were seeded as described in Table 3.6. 1ug of dsRNA was used per 1 million cells, alongside a ratio of 1:1, 1:2, or 1:3 (m/v) dsRNA to transfection reagent as required. 2µl of magnetofectamine beads were used per well. the dsRNA, transfection reagent, and magnetofectamine beads were incubated in 250µl OptiMEM (Gibco) per well. The transfection mix was incubated for 30 minutes at room temperature before cell monolayers were placed on top of the cell culture magnet and transfection mix pipetted dropwise onto the cell monolayers. The cell monolayers were then incubated for 30 minutes at the appropriate cell culture temperature whilst remaining on the magnet. Once incubation was complete, the media were removed carefully from the cells and fresh media applied before the cell monolayers were removed from the magnet. The cells were incubated at the appropriate cell culture conditions for 20 hours before infection or further processing.

4.11.3 Whole cell western blot

dsRNA transfected and infected cells were washed once with PBS before being fixed and stained as described in the immunofluorescence section. Cell monolayers were imaged using an Odyssey® CLx Imaging System (Li-Cor) and analysed using the associated software to determine the total UUKV N fluorescence compared to an empty well as a blank.

4.11.4 Cell viability assay

CellTiter-Glo® 2.0 Cell Viability Assay was used to determine the viability of transfected cell monolayers. At the appropriate timepoint, the cell monolayers were washed before being resuspended in 150µl of fresh PBS. To produce technical triplicates of each biological sample, 50µl of the cell resuspension was pipetted into opaque-walled 94 well plates. 50µl of PBS was used as a blank. The cell resuspension was then mixed with 50µl of viability reagent and incubated in the dark for 10 minutes at room temperature. Well luminescence was measured using the GloMax® Navigator Microplate Luminometer (Promega).

4.11.5 Knockdown supernatant analysis

To determine the UUKV M RNA copy number within the supernatant, total RNA was extracted from 100µl of clarified supernatant by adding 1ml of TRIZol as described in RNA extraction and cDNA synthesis. RT qPCR was then performed as described in real-time quantitative PCR (Chapter 3.7.7).

4.12 Statistical analysis

For each condition, biological triplicates were produced, where each biological sample was tested (for example by RT qPCR) in triplicate, and an average of the technical replicates was then used for plotting and statistical analysis. Testing for statistical significance was carried out by either unpaired t-test, one-way ANOVA, or two-way ANOVA with Tukey's multiple comparison. Unpaired t-testing was used to determine statistical significance of two groups at a singular condition/timepoint, for example comparing normalised results of trypsinised vs untrypsinised virus on one cell line. One-way ANOVA with Tukey's multiple comparison was used to compare more than two sample groups at a singular condition/timepoint, for example comparing the results of mock-infected, trypsinised or untrypsinised dyed virus on a singular cell line. Two-way ANOVA with Tukey's multiple comparison was used to compare more than two sample groups at multiple conditions/timepoints, for example comparing the dyed, undyed or mock infected samples in treated and untreated conditions. The cut-off for significance was set at $p<0.05$. Where analysis was employed, unless stated otherwise both "ns" and a lack of notation indicated no significance.

Mass spectrometry - MaxQuant outputs (proteinGroups) were used for downstream analysis. Using the R-package ‘DEP’, potential contaminants were removed (X. Zhang et al., 2018). Protein raw intensities were then normalized and transformed, correlation analysis between replicates was carried out and for samples where proteins were missing values in all

replicates from that experimental condition, missing value imputation were performed. Principal component analysis (PCA) was performed to assess the variability of the samples by visualising the clustering patterns when analysis was carried out in absence of sample labels.

Protein sequence analysis – The amino acid sequences (FASTA files) of the proteins identified were analysed using Interpro scan to identify the domains contained in each protein, as defined by their protein family (pfam) ID. From these results, each protein was analysed to determine if they contained 'classical' and/or 'nonclassical' RNA binding domains (RBDs) . Odds ratio analysis was then carried out on the protein groups , both on the quantity of classical and nonclassical domains, and the number of specific types of domain, to determine if there was a difference in enrichment of these domains in comparison to the whole cell proteome. Gene ontology analysis was carried out using the tools available in vectorbase to determine pathways/terms which are enriched within the sample group when compared to the whole cell background.

Chapter 5 Defining Uukuniemi virus replication kinetics and binding tropism using mammalian and arthropod cell lines

5.1 Introduction

The first stage of any virus replication cycle is the binding and internalization of the virion to the host or vector cell. Previous studies have found that UUKV binds to specific surface receptors on mammalian cells, for example DC-SIGN acts as an attachment factor for dendritic cells, to facilitate entry. However, the process of internalisation is inefficient, with only roughly 25% of virus bound to cells being endocytosed within the first 10 minutes of incubation and acid-activated penetration beginning 20-40 mins later (Lozach et al., 2010). In addition, despite UUKV being able to infect mammalian cells, the virus is unable to overcome the mammalian intracellular immune pathways and is cleared from the system. In comparison, UUKV is capable of persistently infecting IRE/CTVM19 and IRE/CTVM20 cell lines derived from *Ixodes ricinus* ticks, the vector species of UUKV (Mazelier et al., 2016; Rezelj et al., 2017; Xu et al., 2022). Despite this persistence, the immune system of ticks and therefore the kinetics and mechanism of the viral replication cycle within the vector are poorly understood or defined, including the receptors responsible for the entry of UUKV in to ISE6 cells (Fogaça et al., 2021; Mazelier et al., 2016).

Just as the cellular factors that allow for vector infection are undefined, so are the factors that determine which organisms can transmit UUKV. Despite the potential for mosquitoes to be exposed to mammalian hosts infected with UUKV, and many other species of virus being transmitted through mosquitoes, to date there is no evidence to suggest UUKV can complete its replication cycle within mosquito cell culture or whole mosquitoes. The opposite of this is true for mosquito-vectored bunyaviruses, hence why many bunyaviruses are often referred to as 'vector-specific' (Horne & Vanlandingham, 2014; Lawrie et al., 2004; Matsuno et al., 2018). It is unknown where the perceived block in UUKV replication occurs when the virus is introduced to mosquito cell culture, and the factors that are responsible for this vector tropism are yet to be determined.

For this study, the cell line ISE6 was used, which was derived from the species *Ixodes scapularis*, although this is not the primary vector for UUKV (Kurtti et al., 1996). This was primarily due to the growth rate of the cell lines and ability to form monolayers on different cell culture surfaces making them suitable for routine experiments, alongside having a well-defined and annotated genome, and additional evidence of UUKV being able to be vectored by multiple species of tick as described in Chapter 1.

5.2 Aims

The aims of the research presented in this chapter were to:

- **Examine the viral replication kinetics of UUKV in mammalian (BSR or A549), tick (ISE6), and mosquito (AF5 and AF319) cell lines.** UUKV replication within mammalian host cells has been investigated by prior studies. In contrast to UUKV infection in mammalian cell cultures, which manifests as a short duration productive infection, resulting in minimal disease in infected host species, tick cell lines are capable of being persistently infected (Mazelier et al., 2016). This research aims to define the viral replication kinetics of UUKV in mammalian (BSR) cells and tick (ISE6) cells, representing a comparison between the mammalian host and tick vector. In addition, as it is reported that many bunyaviruses are vector specific, we aim to demonstrate that UUKV also shows this vector specificity by investigating its replication kinetics in mosquito cell lines.
- **Investigate the barrier to replication for UUKV in mosquito cell lines.** As described in the introduction, there are several areas within the viral replication cycle where host cell proteins are necessary to perpetuate the virus life cycle. Evidence has shown that UUKV replication is unable to be completed within mosquito cell lines, despite many other species within the *Bunyavirales* order being transmitted by mosquitoes. This research aims to elucidate where the block in the UUKV replication cycle occurs during infection of mosquito cell cultures.

5.3 Results

5.3.1 Defining the optimal conditions for UUKV stock propagation

In order to determine the optimal temperature and serum conditions for UUKV growth to produce virus stocks, BSR or BHK-21 clone 13 cells were infected with rUUKV and maintained in various culture conditions and virus replication monitored by focus forming assay. rUUKV titred at $1x10^6$ FFU/ml was kindly provided by Dr Veronica Rezelj (Rezelj et al., 2015).

At 3 days p.i., the titre of UUKV recovered in BHK cell cultures incubated at 33°C and supplemented with 1% FBS was significantly lower than those recorded for the other FBS concentrations across both temperatures. This significant decrease at 1% FBS was not observed at 6 days p.i. Virus yields from cell cultures supplemented with 10% FBS recorded significantly increased titres over those grown in other FBS concentrations. This result is perhaps unsurprising as 10% FBS is the normal growth conditions for virus assays within BSR/BHK cell types. Surprisingly, virus titres recorded in cell monolayers grown at 37°C were lower than the corresponding 33°C samples at both 3- and 6-days p.i., with no significant effect of FBS concentration observed (Figure 6.1.A).

UUKV-infected BSR cell cultures incubated at 37°C post-infection showed rapid cell death and complete detachment by day 6 p.i., and therefore did not produce high enough titres to be readable. As such these results were excluded. At 3 days post-infection, there was no significant difference in the viral titres recorded for virus cultures in monolayers supplemented with the different FBS percentages. At 6 days post-infection only virus culture media containing 2% FBS showed a significant increase in titre compared to other samples (Figure 6.1.B).

Thus, using the BSR cell line, we have identified 33°C and 2% FBS as the optimal conditions for production of UUKV stocks.

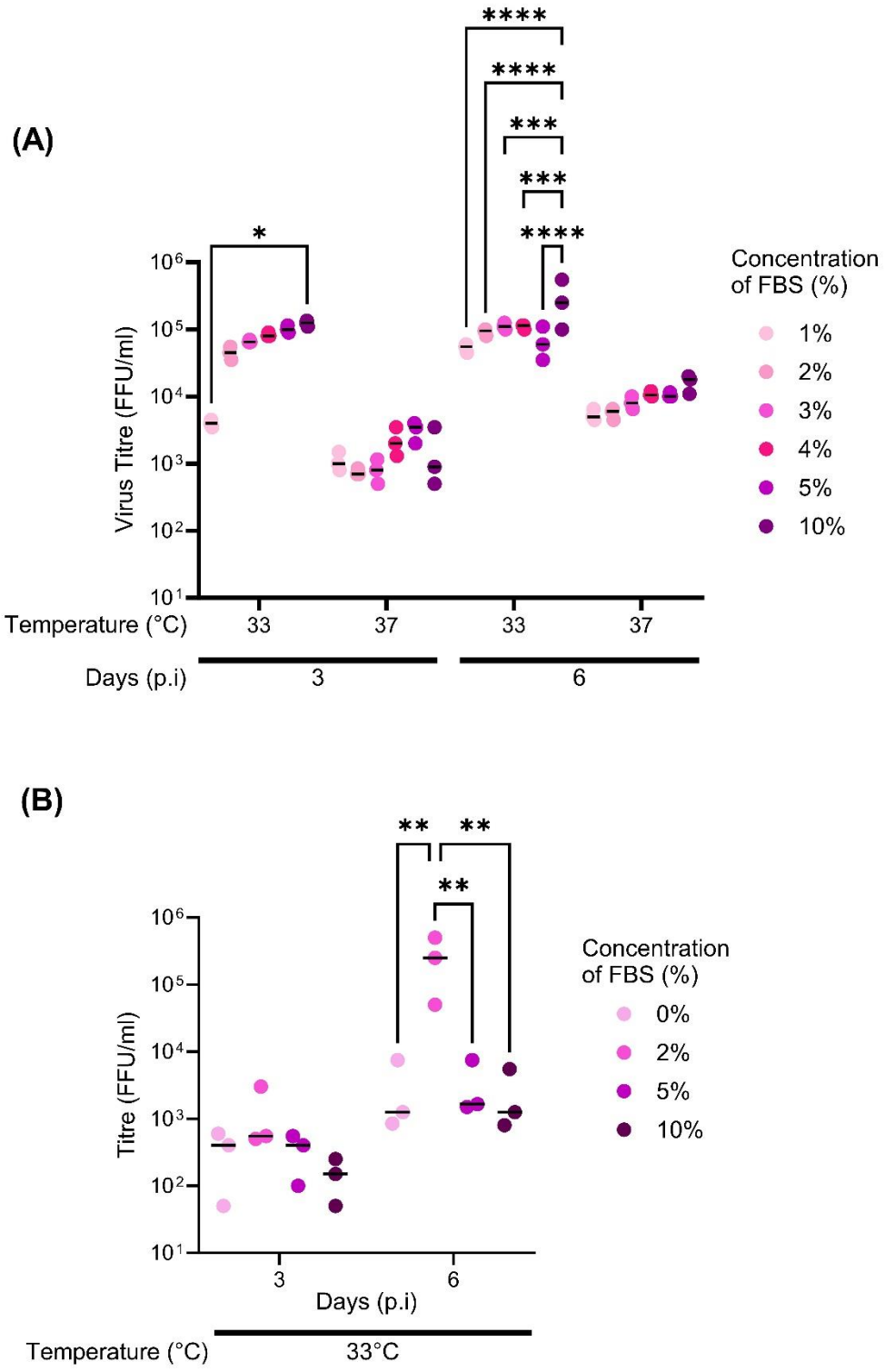

Figure 5.1: Optimisation of growth conditions for Uukuniemi virus (UUKV). BHK-21 clone 13 at 33°C and 37°C (A) or BSR at 33°C (B) cell monolayers were grown in culture media supplemented with the percentage of foetal bovine serum (FBS) and at the temperatures indicated. Cell monolayers were inoculated with rUUKV at a MOI of 0.1 FFU/cell. At 3 or 6 days p.i., culture media were collected and clarified via centrifugation for titration by immunofocus assay. Asterisks indicate

significance **** = $p < 0.0001$, *** = $p \leq 0.001$, ** = $p \leq 0.01$, * = $p \leq 0.05$, ns = not significant, as measured by ordinary two-way ANOVA with Tukey's multiple comparison test.

5.3.2 UUKV Growth kinetics in mammalian, tick, and mosquito cell lines

To determine UUKV growth kinetics within mammalian (A549 and BSR), tick (ISE6), or mosquito (AF5 and AF319) cell lines, cell monolayers were infected with tick-borne rUUKV, and growth curves performed. At each timepoint, samples were assayed to determine supernatant titre and cell monolayers were lysed and subjected to probing for the UUKV nucleocapsid protein. Mosquito-borne rBUNV infections were carried out in tandem for comparison between differently vectored viruses. No bands were seen for A549 cell lysate preparations when probed for UUKV N and so data for A549 are not shown.

In BSR cells, rUUKV reached titres of 10^6 FFU/ml by 72 h p.i., whereas rUUKVdelNSseGFP only reached titres of 10^3 FFU/ml (Figure 5.2.A). This is in line with prior work which indicates that although UUKV NSs protein is not essential for replication, the presence of NSs during infection may allow more efficient replication of virus through aiding in recruitment of cellular factors required for replication, transcription, and translation (Rezelj et al., 2015). Compared to BSR, rUUKV only reached a titre of 10^3 FFU/ml in A549 cells peaking at 48 h p.i., which is expected as A549 have a functional interferon response, unlike BSR, capable of overcoming and clearing an UUKV infection (Sutejo et al., 2012). Similar trends in levels of virus titre produced when comparing BSR and A549 cells have been observed in other virus species, such as Nipah virus and Hendra virus infections (Aljofan et al., 2009). In contrast to this, rBUNV infection in BSR cell monolayers reached titres of 10^7 PFU/ml by 48 h p.i. before plateauing. BUNV is more efficient at infecting BSR cells and appears to have a faster rate of replication, as the virus plateaus (indicating a maximum titre has been reached and all naïve cells have been infected) faster than UUKV (Figure 5.2.A). Analysis of UUKV viral nucleocapsid protein expression in BSR cells, showed that the N protein was first detected at 24 h p.i., whereafter the quantity of N protein increased over time. During rUUKVdelNSseGFP infection, the N protein was only able to be detected faintly at 72 h p.i (Figure 5.2.B), which corresponds to the reduced titres seen in Figure 6.2.A. No nucleocapsid was detected in A549 cells at any timepoint for any the UUK viruses (data not shown). Although no N protein signal was detected at 24 hours post-infection, a strong BUNV nucleocapsid signal was detected at 48 h post-infection, which then increased at 72 h post-infection (Figure. 5.2.C). In all recombinant virus infections, the intensity of the band corresponding to tubulin increases over time, which is exemplified most when comparing the 0 and 24 hours p.i. timepoints in rBUNV infection.

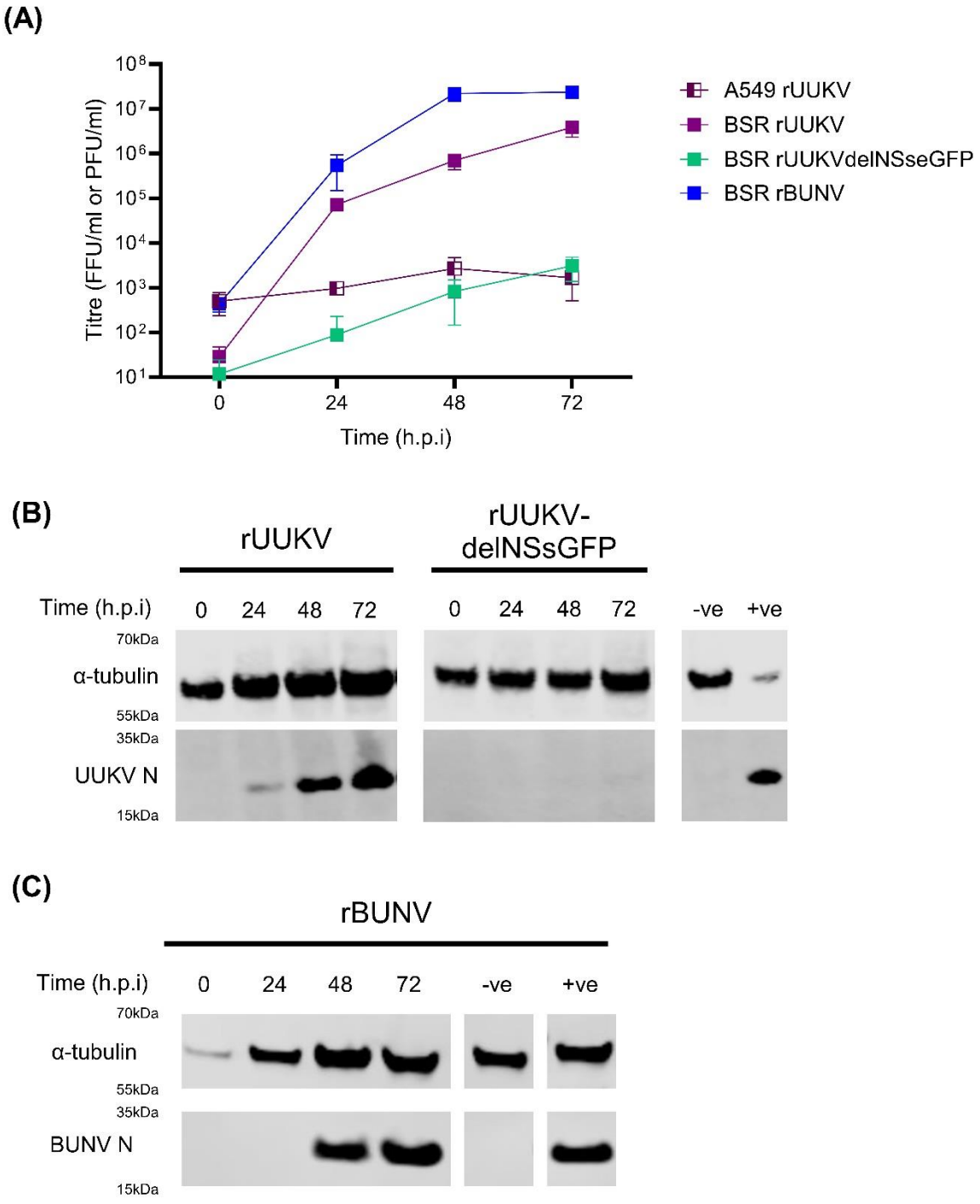

Figure 5.2: Growth properties of recombinant viruses in mammalian cell lines. Human (A549) or hamster (BSR) cell monolayers were infected with rUUKV, rUUKVdelNSseGFP or rBUNV at a MOI of 0.1 FFU/cell. At the indicated time p.i., culture supernatants were collected for virus titration by immunofocus or plaque assay on BSR cells, as appropriate (A). Data are plotted as the mean virus titre (FFU/ml) ± SD of n=3 biological replicates. (B) Cell extracts from infected BSR cell monolayers were also prepared to analyse virus protein expression. Western blots were probed with anti-α tubulin or anti-UUKV N antibodies as indicated in the representative image. '-ve': mock-infected cell lysate; '+ve': sample known to be infected with rUUKV. (C) Cell extracts from infected cell monolayers were also prepared to analyse virus protein expression. Western blots were probed with anti-tubulin,

or anti-BUNV N antibodies as indicated in the representative image. No bands were seen when probing for UUKV N in A549 lysate and so data is not shown. '-ve': mock-infected cell lysate; '+ve': sample known to be infected with rBUNV.

Parallel studies were also conducted in the tick cell line, ISE6. As before, at each timepoint cell monolayers were lysed and prepared for western blot detecting α-tubulin and the respective viral nucleocapsid protein (Figure 5.3).

As shown in Figure 5.3.A, even when infected at disparate MOIs, rUUKV replicated to titres of roughly 10^7 FFU/ml by 12 days p.i., which is in line with data from UUKV infection of other tick cell lines (IRE/CTVM19 and IRE/CTVM20). Mazelier *et al* (2016), demonstrated that infected tick cells produce a maximum titre between 10^7 and 10^8 FFU/ml after 12 days of incubation (Mazelier et al., 2016).

When ISE6 cell cultures were infected with rUUKVdelNSseGFP, the recorded viral titre dropped by day 6 post-infection before remaining at approximately 10^2 FFU/ml, indicating that internalisation may have been occurring, but no active replication was taking place within the infected cell monolayers. This is consistent with unpublished work in our lab showing that, unlike in mammalian cell cultures where the viral NSs protein is not required for replication and suppresses the innate immune response. In tick cell lines, UUKV NSs may have a more crucial role in facilitating replication within the infected arthropod cell. BUNV is a mosquito-borne bunyavirus, and as such was not expected to replicate within ISE6 cells, which was reflected in the rBUNV growth curve (Figure 5.3.A). rBUNV titres decreased gradually over the 12-day time course, indicating potential degradation of the viral particles in the cell culture media as opposed to the internalisation observed with rUUKVdelNSseGFP infection (Figure 5.3.A and 5.3.D).

Analysis of rUUKV viral nucleocapsid protein expression in ISE6 cell monolayers demonstrated that N protein was first detected at 9 days p.i. and increased by 12 days p.i. when initially infected at a MOI of 5 FFU/cell. Whereas for cells infected with rUUKV at an MOI of 1 FFU/cell, N protein was only detected at 12 days p.i. and not at any timepoint at the lowest MOI (Figure 5.3). Although infectious virus was detected in the supernatant of rUUKV-infected ISE6 cells from 3 days post-infection, N protein was not detectable in infected cell monolaters by Western blotting. In mammalian cells, increasing N protein expression is correlated with increasing viral titres in the supernatant. In tick cells, N protein concentration may require longer times to accumulate in infected cells at detectable levels or for enough cells to be infected to generate a detectable signal (Figure 5.3.B). Fitting with the viral titres, no UUKV N protein was detected in lysates from rUUKVdelNSseGFP- (Figure 5.3.C) or rBUNV-infected ISE6 cell monolayers (Figure 5.3.D). Although there is a slight increase in the intensity of tubulin across the timeframe, overall no significant differences were observed.

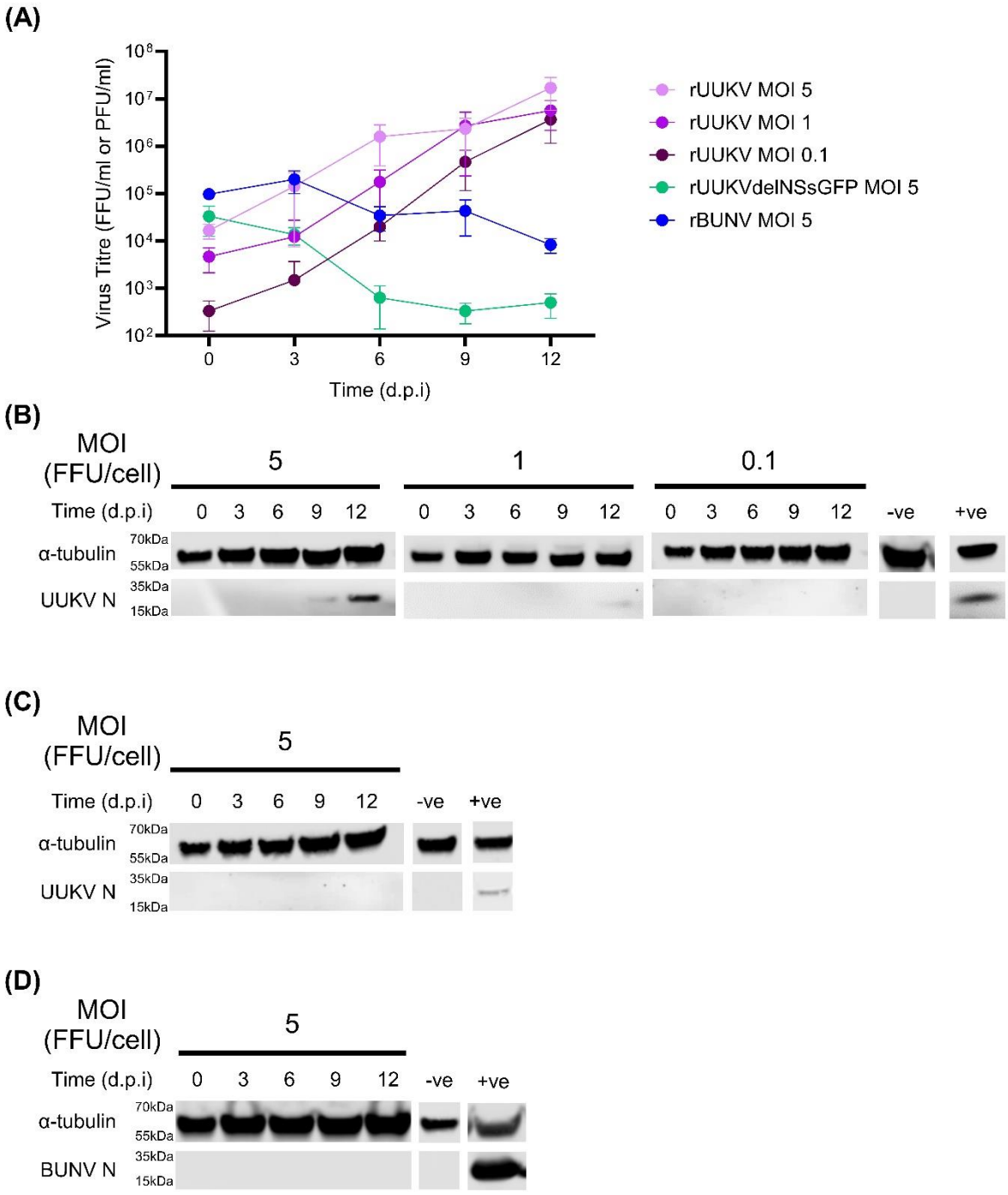

Figure 5.3: Growth properties of recombinant viruses in a tick cell line. Cell cultures derived from the tick *Ixodes scapularis* (ISE6) were infected with rUUKV at varying MOI or with rUUKVdelNSseGFP at a MOI of 0.1 FFU/cell. At the indicated time p.i., culture supernatants were collected for virus titration by immunofocus assay on BSR cells. Data are plotted as the mean virus titre (FFU/ml) ± SD of n=3 biological replicates (A). Cell extracts from rUUKV- (B), rUUKVdelNSseGFP (C) or rBUNV-infected (D) cell monolayers were prepared to analyse virus protein expression. Western blots were probed with anti-α tubulin, anti-UUKV N or anti-BUNV N

antibodies as indicated in the representative image. ‘-ve’: mock-infected cell lysate; ‘+ve’: sample known to be infected with rUUKV or rBUNV respectively.

As it was demonstrated that the mosquito-borne rBUNV was not able to infect tick cell cultures, the reciprocal experiments were conducted to see if the recombinant UUKV and UUKVdelNSseGFP could infect mosquito cell lines. Two different mosquito cell lines were used that had a functional or dysregulated RNAi response (AF5 or AF319 cell lines, respectively). As previously described, viral growth kinetics were measured by viral plaque/focus assay and western blotting of lysates prepared from infected monolayers at the indicated timepoints (Figure 5.4).

No increase in titre was observed following rUUKV or rUUKVdelNSseGFP infection in either AF5 or AF319 cell lines (Figure 5.4.A). This result follows previous literature as UUKV is a tick-borne bunyavirus, and therefore, similar to other tick-borne bunyaviruses, does not show evidence of completing the replication cycle in mosquito cell culture (Lawrie et al., 2004; Matsuno et al., 2018). In comparison, the titres of rBUNV increased after 24 hours in both infected AF5 and AF319 cell lines, with titres reaching 10^4 or 10^5 PFU/ml, respectively. This difference in titre is likely due to AF319 being RNAi incompetent, allowing the virus to replicate faster due to fewer intracellular immune barriers (Figure 5.4.A).

In line with the viral titre results, analysis of UUKV nucleocapsid protein accumulation showed no detectable N protein at any timepoint for either rUUKV- or rUUKVdelNSseGFP-infection in AF5 (Figure 5.4.B) or AF319 (Figure 5.4.C) cell monolayers. rBUNV nucleocapsid was only detectable in rBUNV-infected AF319 cells at 72 h p.i. and was undetected in rBUNV-infected AF5 cells. This result reflected in the plaque assay data as rBUNV growth curves reached 10-fold higher titre in rBUNV-infected AF319 cells at 72 h p.i. compared to that seen in AF5 cell monolayers (Figure 5.4.D). Similarly to the results seen in the BSR recombinant virus western blots (Figure 5.2), the intensity of the band corresponding to tubulin increased over time.

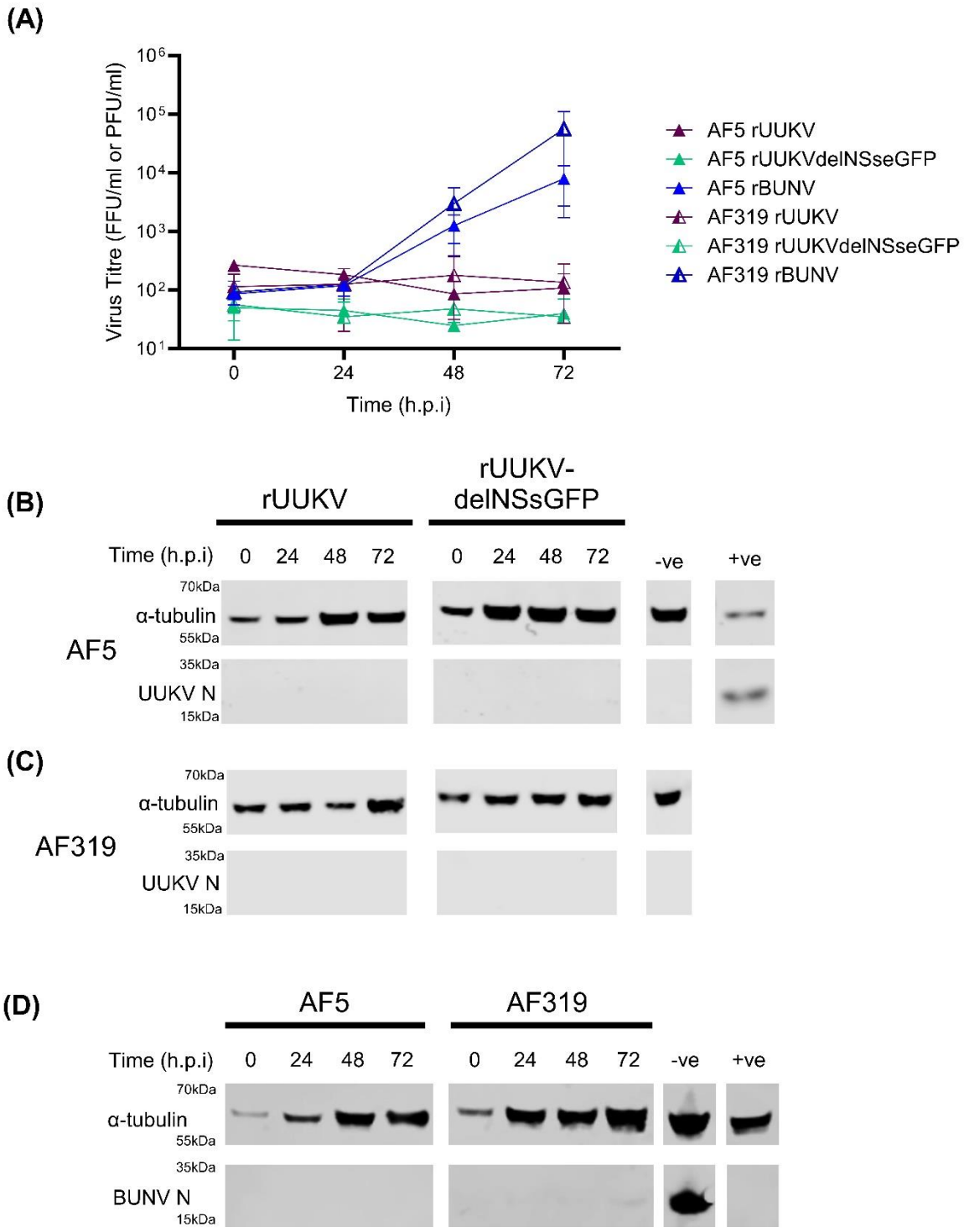

Figure 5.4: Growth properties of recombinant viruses in mosquito cell lines. Cell cultures derived from the mosquito *Aedes aegypti* that possess either competent (AF5) or deficient (AF319) RNAi innate immune pathways were infected with rUUKV, rUUKVdelNSseGFP or rBUNV at a MOI of 0.1 FFU/cell. At the indicated time p.i., culture supernatants were collected for virus titration by immunofocus assay on BSR cells (A). Data are plotted as the mean virus titre (FFU/ml) ± SD of n=3 biological replicates. Cell extracts from rUUKV infected AF5 (B) or AF319 (C) cell monolayers were prepared to analyse virus protein expression. Western blots were probed with anti-tubulin or anti-UUKV N antibodies as indicated in the representative image. '+ve': sample known to be infected

with rUUKV. Cell extracts from rBUNV infected AF5 or AF319 cell monolayers were also prepared to analyse virus protein expression (D). Western blots were probed with anti-tubulin or anti-BUNV N antibodies as indicated in the representative image. '+ve': sample known to be infected with rBUNV.

5.3.3 Generation and use of dyed UUKV for use in analysing viral entry in mammalian, tick and mosquito cell lines

We aimed to adapt a method developed by Hoffmann and colleagues (A. B. Hoffmann, Mazelier, Leger, & Lozach, 2018) utilising fluorescent glycoprotein dye UUKV glycoproteins, view and quantify rUUKV binding to cell types of interest; ISE6 (tick) and AF5 (mosquito). BSR cells would be used as a positive control as UUKV binds to and enters mammalian cell lines (BHK and A549) (A. B. Hoffmann et al., 2018). However, before this methodology could be implemented, we needed to 1) confirm if it could be applied to the cell types of interest, and 2) determine if any potential signal visualised was indeed dyed UUKV (rUUKVAF647) and not non-specific background (such as cellular debris). AF647 was used to dye rUUKV at a dye to glycoprotein molar ratio of 1:5. AF647 targets the viral envelope glycoproteins by reacting with primary amine groups. The fluorophore has an excitation peak at 650nm and an emission peak at 665nm. Growth curves of dyed rUUKV (rUUKVAF647) or rUUKV were performed at a MOI of 0.1 FFU/cell to confirm that there was no reduction in replication by dying the viral glycoproteins (Figure 5.5.A). At every timepoint sampled, there was no statistical difference between the viral titres from the dyed or undyed UUKV infected monolayers, therefore no difference in replication kinetics of rUUKVAF647 compared to rUUKV (Figure 5.5.A).

To examine the effect of the dye on virus morphology, rUUKV and rUUKVAF647 samples were prepared for negative stain electron microscopy and imaged on a JEOL JEM 1400 (JEOL, Japan) electron microscope. UUKV particles have been shown to display variable degrees of pleiomorphism, with particle size ranging from 105 to 145nm in diameter and some viral particle aggregation observed (Överby et al., 2008). In rUUKV samples, what is assumed to be cellular debris was present within the sample (Figure 5.5.B). However, viral particles were seen which displayed the characteristics expected of UUKV as indicated by black arrows (Figure 5.5.C). In rUUKVAF647 samples less debris was seen, however fewer viral particles were also seen within the sample, which may be a consequence of the purification process (Figure 5.5.D). Despite fewer viral particles being present within the sample, the dyed virus particles showed no noticeable differences in morphology when compared to rUUKV (Figure 5.5.E).

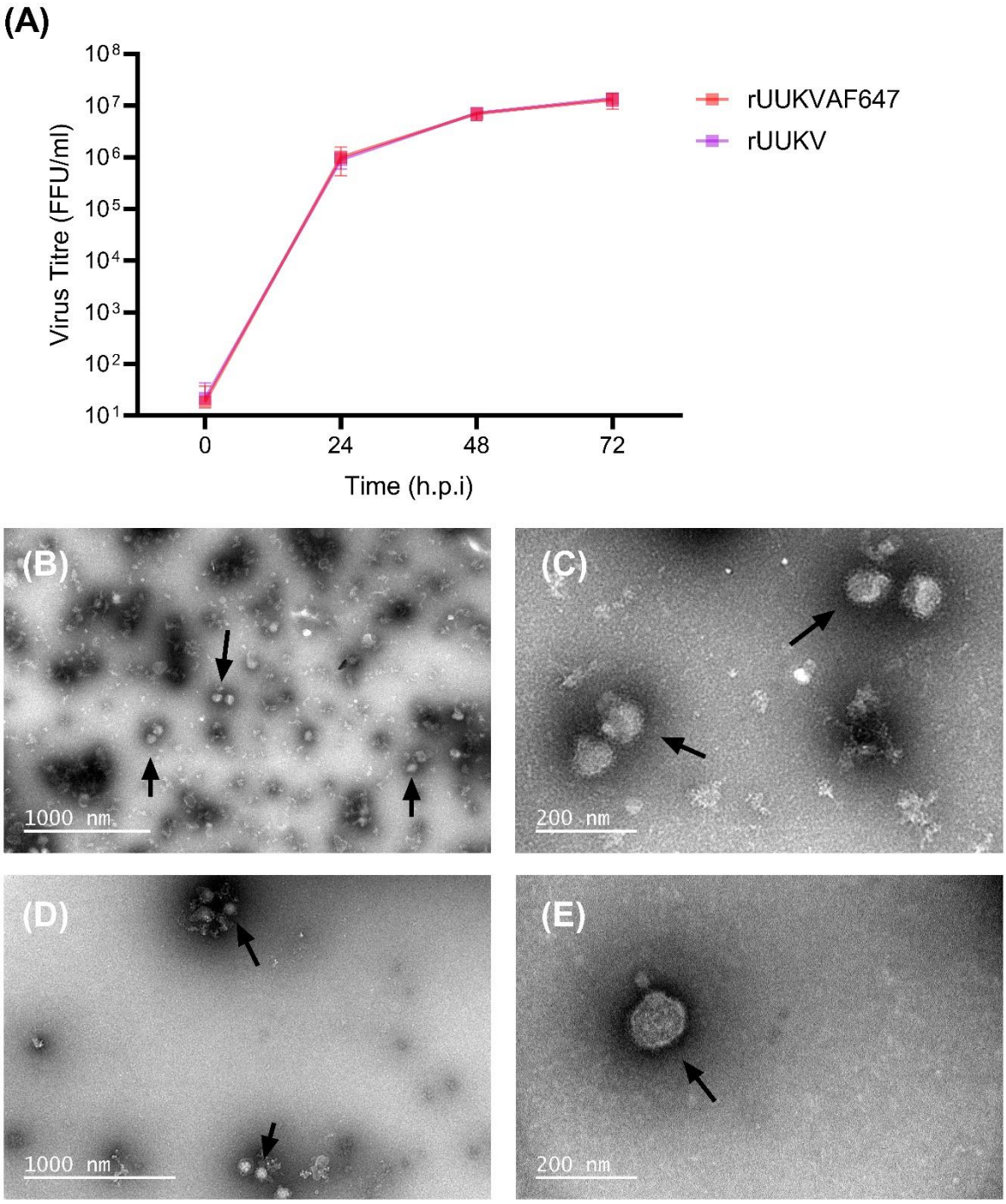

Figure 5.5: Growth properties of Uukuniemi virus dyed with Alexa-Fluor 647 (rUUKVAF647). Preparations of purified UUKV virions dyed with AF647 or were left undyed. To assess the replication kinetics of the wild-type and dyed viruses in mammalian cell cultures, monolayers of BSR cells were infected with rUUKV (undyed) or rUUKVAF647 (dyed) at a MOI of 0.1 FFU/cell. At the indicated time p.i., culture supernatants were collected for virus titration by immunofocus assay on BSR cells. Data are plotted as the mean virus titre (FFU/ml) ± SD of n=3 biological replicates. Two-way ANOVA statistical analysis with Tukey's multiple comparison was applied, and the data showed no significant difference between rUUKV and rUUKVAF647 at each timepoint (A). (B-E) To assess the integrity of the dyed virions in greater detail, samples were prepared for negative stain electron microscopy and imaged on a JEOL JEM 1400 (JEOL, Japan) electron. Images

presented show the undyed rUUKV (B & C) and the dyed rUUKVAF647 (D & E). Arrows indicate viral particles and scale bars indicate size. Images taken by Dr Swetha Vijayakrishnan.

Next, heat-inactivation assays were used to determine if the far-right dye signal visualised on the surface of rUUKVAF647-infected cell cultures corresponded to dyed virions and not cellular debris. rUUKVAF647 was heat-inactivated at 95°C for 10 minutes, denaturing the viral proteins and disrupting the specific structures necessary to bind to cell receptors. This method has previously been used to successfully inactivate highly pathogenic viruses (Elveborg, Monteil, & Mirazimi, 2022). After infection with rUUKVAF647 or wt rUUKV, cell monolayers were stained with Hoechst 33342 nuclear stain and CellMask cell membrane stain. Hoechst stain allows for the easy counting of cell numbers by staining the individual nuclei, and CellMask stains the cell membrane allowing for the visualisation of the cell surface. Untreated or heat-inactivated (H-I) virus preparations containing a MOI of 5 FFU/cell, or mock-infection preparations, were prepared and incubated with mammalian (BSR), tick (ISE6) or mosquito (AF5) cell cultures at 4°C (and on ice) for 1 hour to allow for virus binding whilst preventing internalisation occurring, as has been done in previous studies (Burkard et al., 2014; A. B. Hoffmann et al., 2018). Cell monolayers were then washed to remove unbound virus and fixed in 4% (v/v) formaldehyde. Confocal microscopy was used to take four z-stack images of three biological replicates, which were then examined for AF647 fluorescence, indicating viral binding. Z-stacking was used to allow for the building of 3D for rendering and analysis.

As seen in Figure 6.6, for every cell line, punctate dots of signal associated with the far-red channel, corresponding to AF647 can be seen in the untreated channel (indicated by white arrows). These punctate dots are associated with the cell membrane and may be dyed virions bound to the cell. During image analysis, it was observed that the number of dots was higher in BSR cells, and when comparing the diameter of the dots using the scale bar and measuring tools in ZenBlack software reached larger diameters (Figure 5.6.A), than in those of ISE6 (Figure 5.6.B) and AF5 (Figure 5.6.C). This is also supported as the volume of each individual 'dot' has a larger volume on average when rendered. In all cell lines, heat-inactivation diminished or removed the signal from the far-red channel, indicating no AF647 was present in these samples and that the signal seen was derived from intact dyed virus particles. When punctate dots of signal were seen in the heat-inactivated far-red channels, the diameter of the dots were larger and less smooth/regular, indicating these are aggregations of denatured viral proteins as opposed to intact viruses. Overall, incubation of cell lines with rUUKVAF647 causes far red signal to be associated with cell membranes, whereas heat-inactivation removes notable signal from the far-red channel and therefore little rUUKVAF647 is associated with the cell membranes. To quantitatively measure the

effect of heat-inactivation on rUUKVAF647 across all three cell lines, both raw fluorescence intensity (Figure 5.7) and rendered fluorescence intensity (Figure 5.8) were analysed.

The raw fluorescence intensity is defined as the sum of the far-red signal (AU) normalised to the number of cells, as determined by the number of nuclei visualised with the Hoechst 33342 stain, to give the average far-red intensity (AFRI) per cell in each image using IMARIS software. In BSR cells, only untreated rUUKVAF647 produced a significantly higher level of average far-red intensity when compared to either rUUKV or mock-infected samples. For heat-inactivated samples, there was no significance in the average far-red intensity between the rUUKV and rUUKVAF647 samples, although there was a slight increase in the intensity of rUUKV in comparison to mock-infected samples.

When comparing cells incubated with either heat-inactivated or untreated virus preparations, the fluorescence of rUUKAF647 was significantly decreased in heat-inactivated conditions (Figure 5.7.A). To remove background signal in BSR cells, rUUKVAF647 and rUUKV AFRI were normalised against mock-infected controls (Figure 5.7.B). The AFRI recorded following incubation with rUUKVAF647 was significantly higher when compared with untreated wt rUUKV or heat-inactivated rUUKVAF647. However, no significance difference was found between the AFRI of rUUKVAF647 or rUUKV from samples incubated with heat-inactivated virions. Overall, both raw analyses indicated that the fluorescence seen in the far-red channel from rUUKVAF647 corresponded to dyed viral particles, and heat-inactivation removed the ability of these viral particles to associate with the cell membrane (Rezelj et al., 2015). The results seen in BSR cells were also mirrored in ISE6 cells (Figure 5.7.A-5.7.C). When removing background signal, the AFRI score for cells incubated with rUUKVAF647 was significantly higher when compared with untreated rUUKV and heat-inactivated rUUKVAF647, and no significant difference was found between rUUKVAF647 and rUUKV in heat-inactivated conditions (Figure 5.7.D). As seen in BSR cells, both raw analyses indicated that the fluorescence seen in the far-red channel corresponded to dyed viral particles, although the intensity of AFRI per cell was lower (approximately 50% less) in ISE6 than in BSR cells. This may be due to the size differences between the two cell lines, as BSR cells are larger than ISE6. In addition, the binding receptors of ISE6 for UUKV are unknown and therefore the capacity of ISE6 cells to bind UUKV is yet to be evaluated.

Finally, AF5 cells incubated with untreated rUUKVAF647 produced a significantly higher level of AFRI when compared to both undyed rUUKV or mock-infected cells. However, the

increase in fluorescence intensity is not significant as observed with the previous two cell lines.

It was noted that the far-red intensity was higher across all mosquito cell experiments and more variability in AFRI was recorded. In cell cultures treated with heat-inactivated virions, both rUUKVAF647 and rUUKV infected monolayers had significantly higher fluorescence intensity than mock-infected samples (Figure 5.7.E). In heat-inactivated samples, there was no significant difference in AFRI between rUUKVAF647 and rUUKV infected cell monolayers, however compared to infection in other cell lines, the intensity of far-red signal was much higher in heat-inactivated samples (Figure 5.7.F). When examining the z stack images of AF5 cells incubated with heat-inactivated virions, intracellular far-red signal could be seen, indicating that this result may be due to a cellular response to the presence of denatured and aggregated protein (data not shown).

The rendered fluorescence intensity is defined as the sum of the far-red signal (AU) associated to the cellular membrane normalised to the number of cells, as determined by the number of nuclei visualised via the Hoechst 33342 stain, to give the rendered average far-red intensity (RAFRI) per cell in each image. To isolate the far-red signal associated with the cellular membranes, z stack images were rendered using IMARIS software. Once all boundaries were defined, only far-red fluorescence intensity 0.001nm either side of the cell membrane were included in the analysis.

When analysing the data using RAFRI and comparing it to the AFRI score in BSR or ISE6 cells, only dyed virion-infected cells (rUUKVAF647) produced a significantly higher level of far-red intensity when compared to either rUUKV, mock-infected or those samples that had been heat inactivated. The RAFRI recorded for rUUKV- or mock-infected cells were almost undetectable (Figure 5.8.A) and no far-red signal was detected in data from heat-inactivated samples (Figure 5.8.B). Overall, both rendered analyses support the raw analysis data showing that the fluorescence seen in the far-red channel from rUUKVAF647-infected samples corresponds to dyed viral particles, and heat-inactivation removed the ability of these viral particles to associate with the cell membrane. In ISE6 cells, the average fluorescence intensity in the samples was approximately one tenth of that recorded in the BSR cell line (Figure 5.8.C & 5.8.D).

Finally, for infected AF5 cell monolayers, only samples infected with untreated rUUKVAF647 produced a significant and detectable level of far-red intensity (Figure 5.8.E). In addition, unlike in comparison of raw intensities, heat-inactivated samples showed little

to no far-red intensity, supporting the conclusion that the signal seen in the raw intensity analysis was intracellular in origin (Figure 5.8.F).

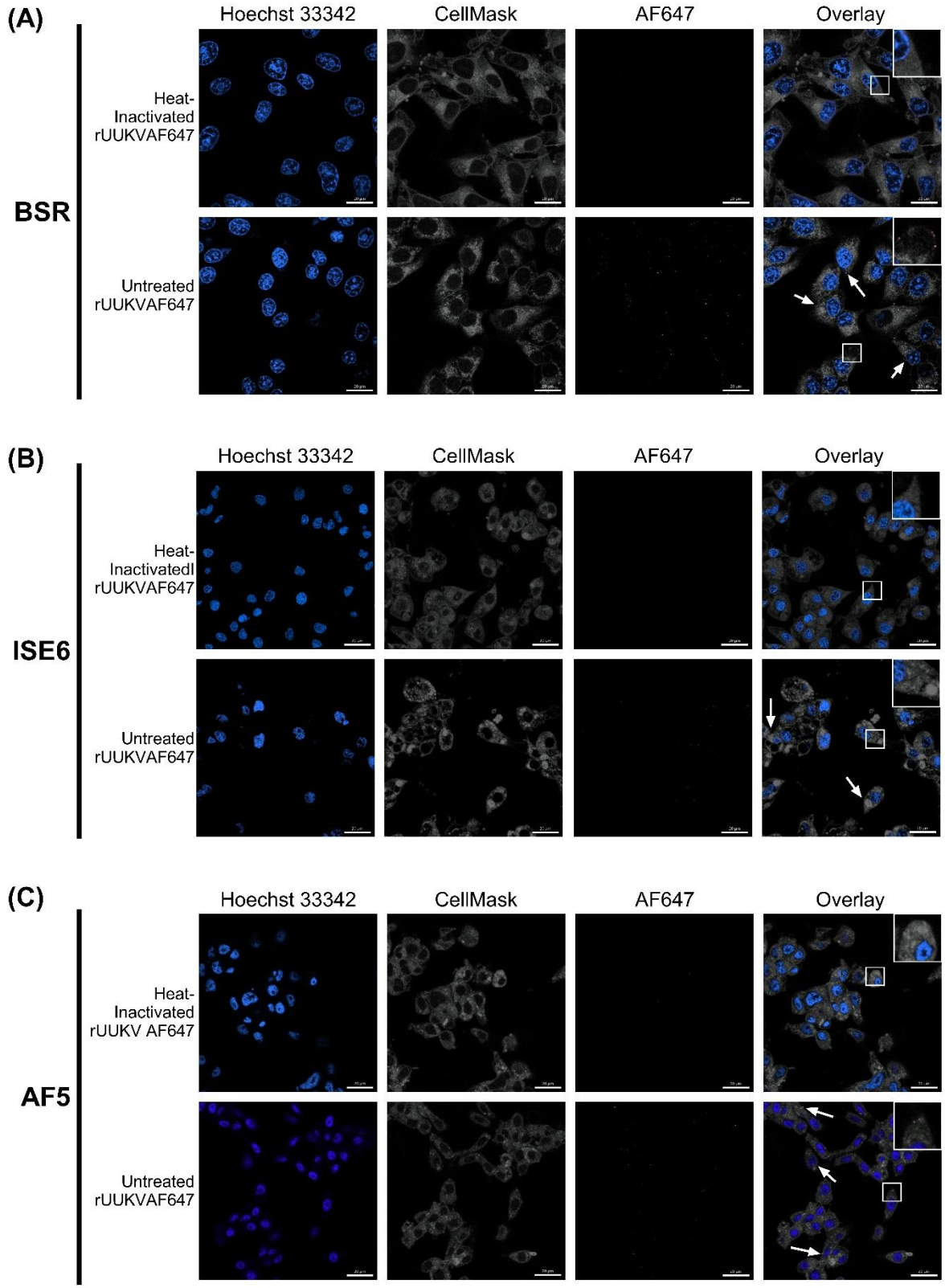

Figure: 5.6: Heat inactivation prevents rUUKVAF647 binding to cell monolayers in culture. Preparations of rUUKVAF647 virions were heat-inactivated by subjecting the samples to 95°C heat for 10 min (H-I) or mock-inactivated (untreated). Virus preparations containing a MOI of 5 FFU/cell were incubated with mammalian (BSR; A), tick (ISE6; B) or mosquito (AF5; C) cell cultures at

4°C/ice for 1 h. Cell monolayers were then fixed in 4% (v/v) formaldehyde. Infected cell monolayers were counter stained with the nuclear stain, Hoechst 33342 (blue); cell membranes were visualized with CellMask (grey) while AF647 fluorescence (pink) and virus binding were analysed by confocal microscopy. Data presented are representative images of n=3 biological replicates, each containing n=4 z-stacked images per well. Arrows highlight membrane associated AF647 signal. Scale bar indicates 20 µm.

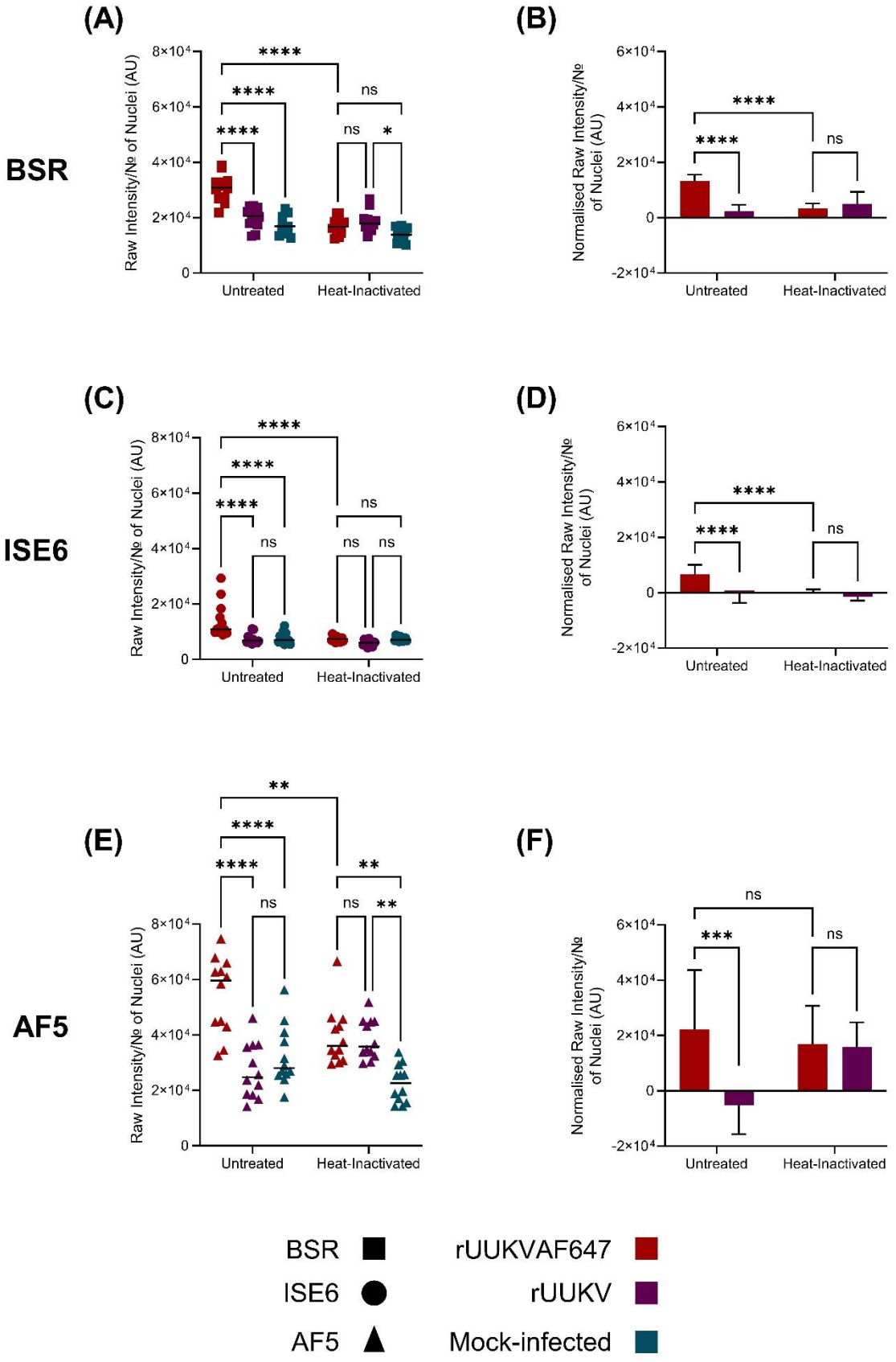

Figure 5.7: Quantitative analysis of raw fluorescence intensity from heat inactivation experiments. Fluorescence data from 12 images generated in Figure 5.6 were analysed and quantified using IMARIS software. Data was calculated by dividing the sum of the raw far-red intensity by the number of nuclei recorded in each z-stack and the mean arbitrary units plotted for

rUUKVAF647-infected BSR (A), ISE6 (C) or AF5 (E) cell lines. The data for each cell line was normalized to the respective mock-infected control to eliminate background signal for rUUKVAF647-infected BSR (B), ISE6 (D) or AF5 (F). Asterisks indicates significance **** = $p < 0.0001$, *** = $p \leq 0.001$, ** = $p \leq 0.01$, * = $p \leq 0.05$, ns = not significant, as measured by ordinary two-way ANOVA with Tukey's multiple comparison test.

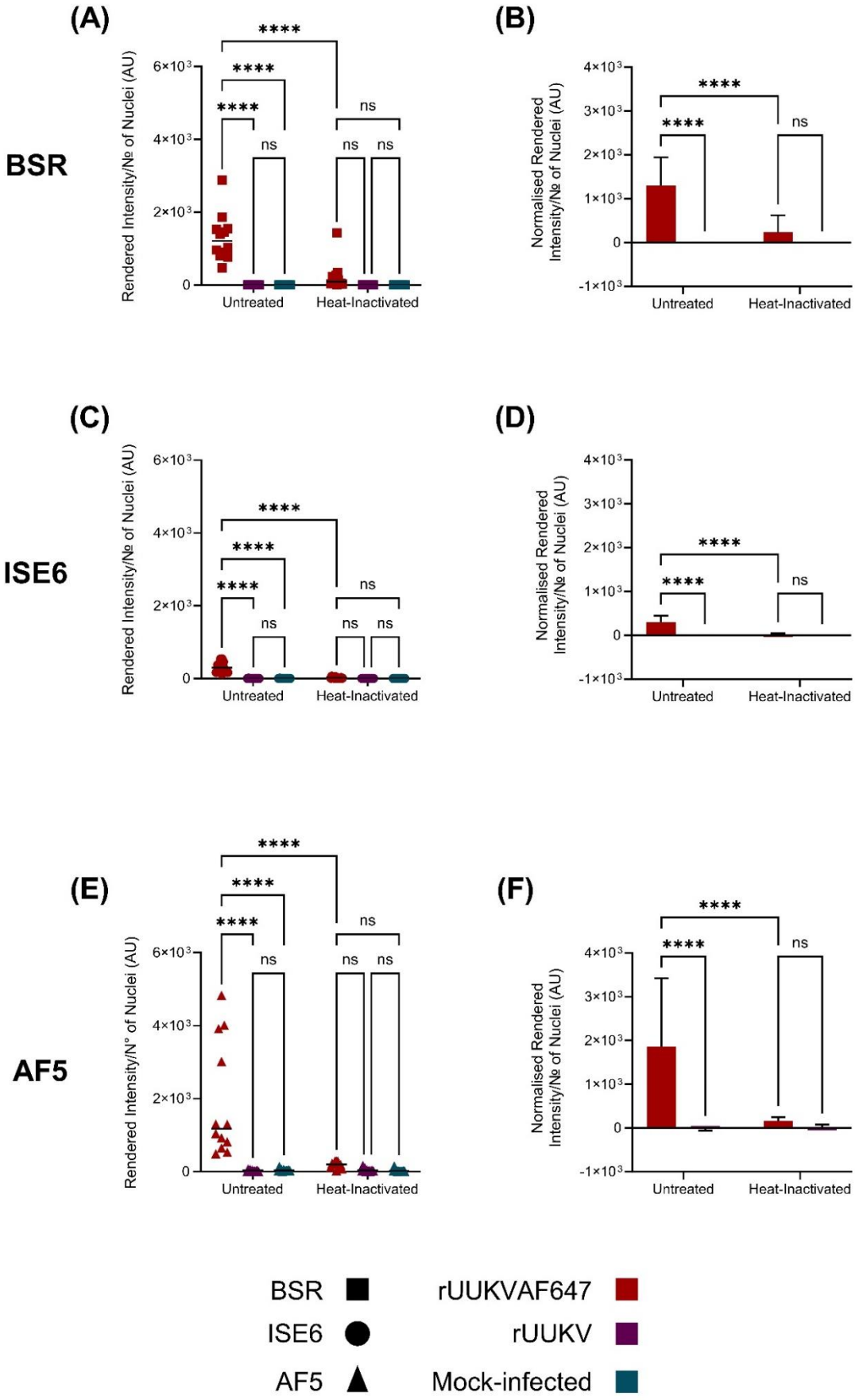

Figure 5.8: Quantitative analysis of rendered fluorescence intensity from heat inactivation experiments. Fluorescence data from 12 images generated in Figure 5.6 were analysed. Z-stacks

were rendered using IMARIS software to define the nuclei, cell membrane and far-red surfaces. Virus bound to rendered membrane was determined by excluding rendered far-red intensity at a distance greater than 0.01 µm either side of the rendered membrane. Data was calculated by dividing the sum of the rendered far-red intensity by the number of nuclei recorded in each z-stack and the mean arbitrary units plotted for rUUKVAF647-infected BSR (A), ISE6 (B) or AF5 (C) cell lines. The data for each cell line was normalized to the respective mock-infected control to eliminate background signal for rUUKVAF647-infected BSR (D), ISE6 (E) or AF5 (F) Asterisks indicates significance **** = $p < 0.0001$, *** = $p \leq 0.001$, ** = $p \leq 0.01$, * = $p \leq 0.05$, ns = not significant, as measured by ordinary two-way ANOVA with Tukey's multiple comparison test.

To determine if the dyed virus association with the cell surfaces was protein mediated and not due to the dye causing increased non-specific binding to the cells, trypsin assays were used. Trypsin exposure after virion binding causes the removal of virus bound through protein-protein interactions. Briefly, cell monolayers [mammalian (BSR), tick (ISE6) or mosquito (AF5)] were stained with Hoechst 33342 nuclear stain and CellMask cell membrane stain after which time they were infected with rUUKVAF647 at a MOI of 5 FFU/ml or mock-infected at 4°C (and on ice) for 1 hour. Virus incubated cell monolayers were then washed to remove unbound virus and incubated with either trypsin or 2% FBS in PBS at the respective cell culture temperature for 5 minutes. Mock-infected cell monolayers were incubated with 2% FBS in PBS for 5 minutes. Trypsin has previously been shown to block binding by cleaving proteins responsible for virion/cell interaction. It can also be used to demonstrate if binding is reliant on protein-protein interactions (Wild & Brown, 1967). Cell monolayers were then washed to remove any cleaved viral particles before being fixed in 4% (v/v) formaldehyde. Confocal microscopy was used to take 4 z-stack images of 3 biological replicates, which were then examined for AF647 fluorescence, indicating viral binding.

As seen in Figure 6.9, a punctate staining pattern can be observed in mock treated samples in the far-red channel, corresponding to the AF647 virions. As indicated by the white arrows shown in the overlay images, these punctate dots were associated with the cell membrane. For all cell lines, trypsin incubation removed nearly all of the visible signal from the far-red channel, indicating trypsin incubation removed the AF647-labelled proteins from the cell membranes (Figure 5.9). To quantitatively measure the effect of trypsinization on AFRI across all three cell lines, both raw fluorescence intensity (Figure 5.10) and rendered fluorescence intensity (Figure 5.11) were analysed.

In BSR cells, following incubation at 4°C, exposure of rUUKVAF647 to trypsin caused a significant decrease in far-red intensity to levels comparable to mock-infected samples. However, the signal was not completely reduced to the level of the mock-infected control, indicating not all virus was removed from the cell surface (Figure 5.10.A). This observation was also seen when samples were normalised to the mock-infected results (Figure 5.10.B). Similar results were observed in parallel experiments with rUUKVAF647-infected ISE6 cells. However, the difference in fluorescence intensity between non-trypsinised and trypsinised rUUKVAF647-infected samples was less significant. A small increase in far-red intensity was observed in trypsinised rUUKVAF647-infected samples compared to mock-infected controls (Figure 5.10.C). When the data were normalised to mock-infected controls, there was a small, yet significant difference between trypsinised and non-trypsinised

rUUKVAF647-infected samples, indicating that proportionally the reduction in AFRI was smaller through the incubation of trypsin (Figure 5.10.D).

In experiments using AF5 cells, trypsinisation caused a significant decrease in far-red intensity of rUUKVAF647-infected samples, and there was no significant difference in fluorescence intensity between trypsinised rUUKVAF647- or mock-infected samples (Figure 5.10.E). When normalised to mock-infected controls there was no significant difference between +/- trypsinisation conditions. However, in similar observations to the heat-inactivation results, following incubation AF5 cells display a tendency to show intracellular far-red signal which may be triggered through extracellular stressors such as aggregated protein, presence of virus or trypsin (Figure 5.10.F).

When the rendered fluorescence intensity was analysed, BSR cell lines displayed no far-red signal associated with mock-infected cell membranes. In rUUKVAF647-infected samples, incubation with trypsin caused a significant decrease in far-red intensity, although trypsinisation did not fully remove the far-red signal in either the raw or normalised data (Figure 5.11.A & 5.11.B). Although the overall level of fluorescence intensity observed was lower in ISE6 cells than in BSR cells; trypsinisation of rUUKVAF647-infected samples again caused a significant decrease in far-red signal, but this incubation did not fully remove all AF647 from the cell surface (Figure 5.11.C & 5.11.D).

Finally, in AF5 cells, fluorescent intensities observed in non-trypsinised rUUKVAF647-infected samples was comparable to that observed in ISE6 samples. The fluorescence intensity was reduced in the presence of trypsin in both the raw data and that normalised to mock-infected controls (Figure 6.11.E & 5.11.F). It was also noted that the fluorescent intensity values decreased in mock-infected samples treated with trypsin, supporting the conclusion that the signal from the raw intensity in these samples was generated by intracellular components.

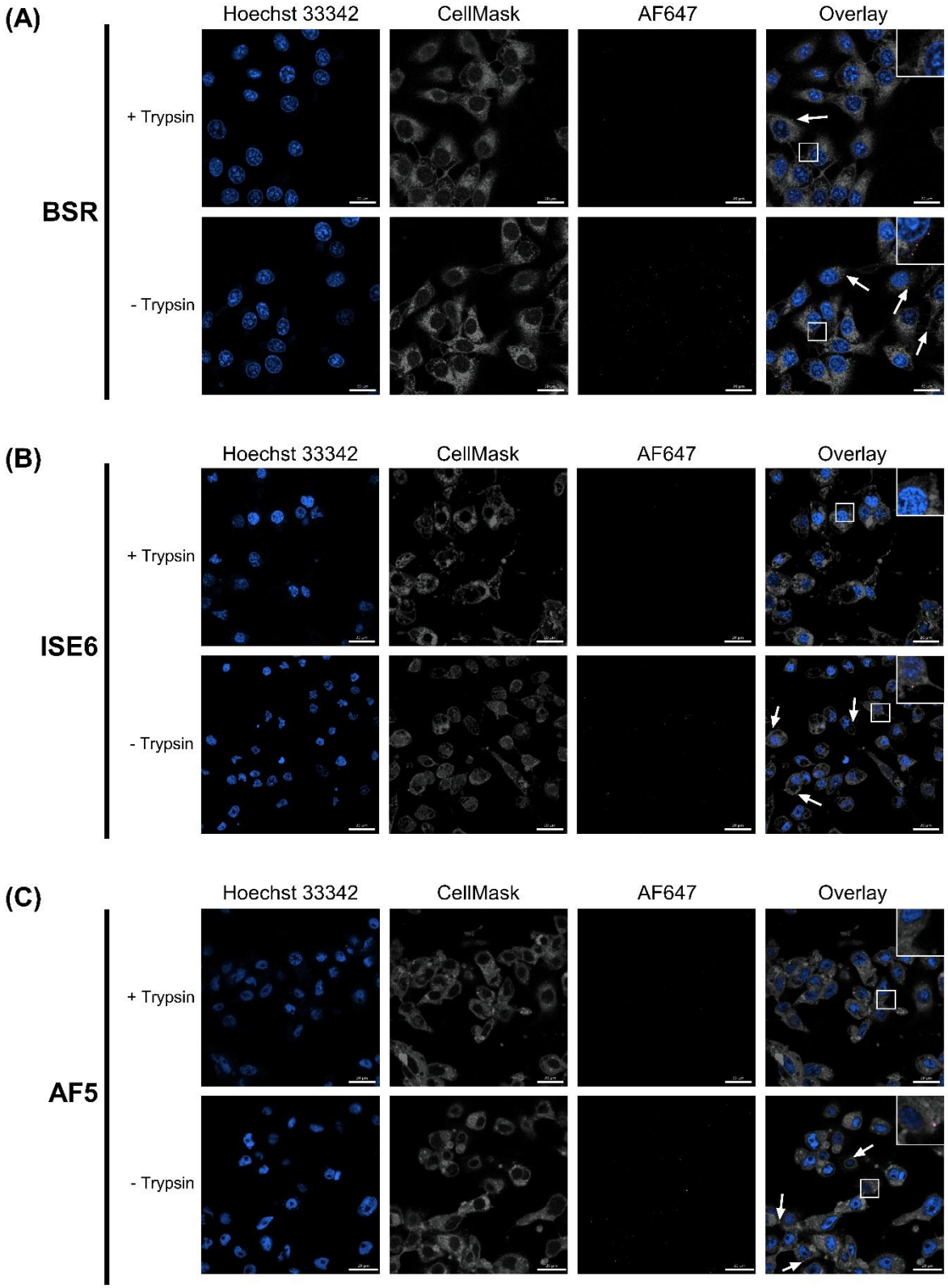

Figure 5.9: Trypsin disrupts rUUKVAF647 binding to cell monolayers in culture. Virus preparations containing rUUKVAF647 at a MOI of 5 FFU/cell were incubated with mammalian (BSR; A), tick (ISE6; B) or mosquito (AF5; C) cell cultures at 4°C/ice for 1 h. Following the binding period, cell monolayers were washed with PBS and then incubated in the presence (+trypsin) or absence (-trypsin; 2% FBS PBS only) of trypsin for 5 min. After a further washing step in PBS, cell monolayers were fixed in 4% (v/v) formaldehyde. Infected cell monolayers were counter stained

with the nuclear stain, Hoechst 33342 (blue); cell membranes were visualized with CellMask (grey) as well as examined for AF647 fluorescence (pink) and virus binding was analysed by confocal microscopy. Data presented are representative images of n=3 biological replicates, each containing n=4 z-stacked images per well. Arrows highlight membrane associated AF647 signal. Scale bar indicates 20 μm.

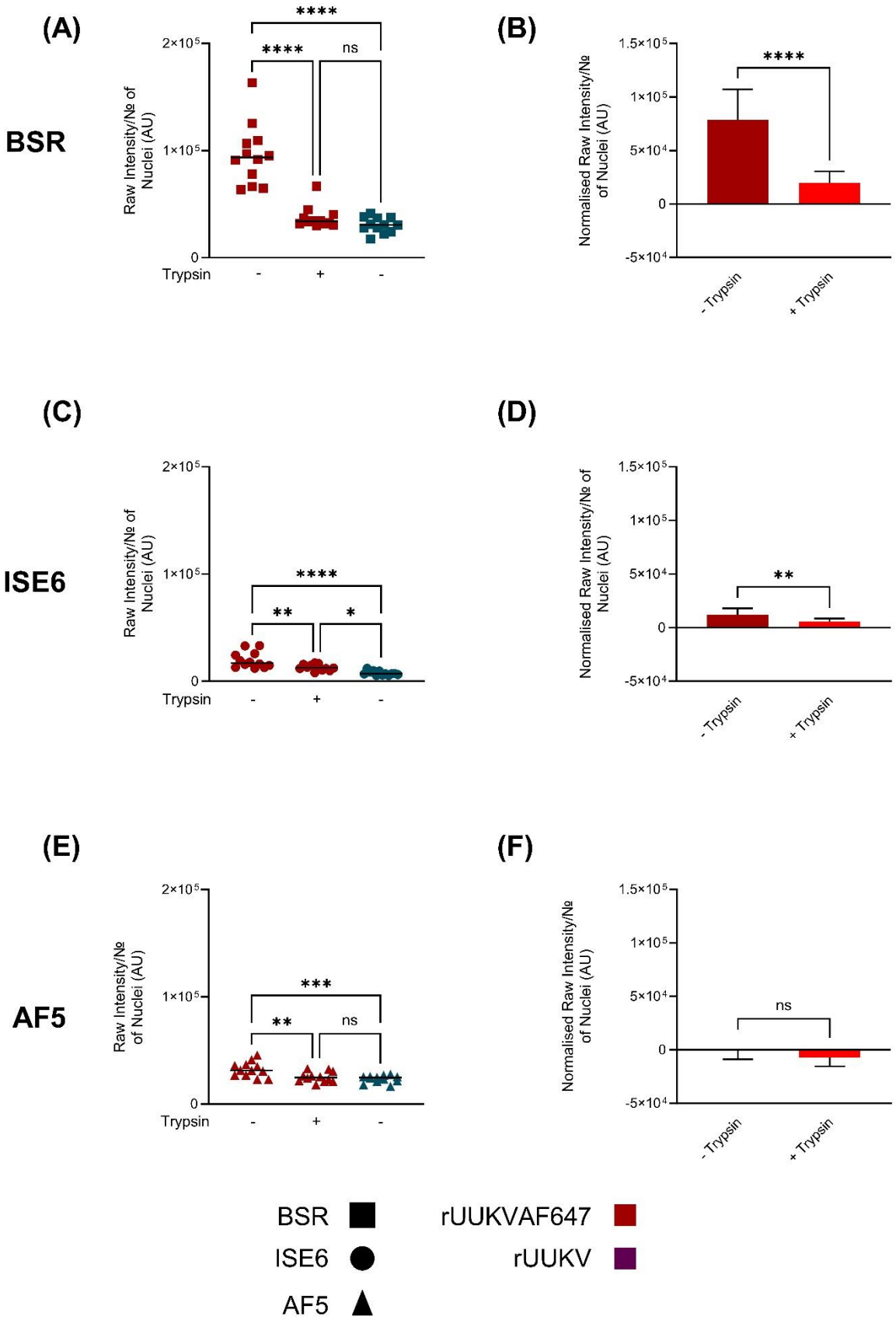

Figure 5.10: Quantitative analysis of raw fluorescence intensity from trypsinisation experiments. Fluorescence data from 12 images generated in Figure 5.9 were analysed and quantified using IMARIS software. Data was calculated by dividing the sum of the raw far-red

intensity by the number of nuclei recorded in each z-stack and the mean arbitrary units plotted for rUUKVAF647-infected BSR (A), ISE6 (B) or AF5 (C) cell lines. The data for each cell line was normalized to the respective mock-infected control to eliminate background signal. Normalised data for rUUKVAF647-infected BSR (D), ISE6 (E) or AF5 (F) cell lines are also shown. Statistical significance was measured by ordinary one-way ANOVA with Tukey's multiple comparison test (A, B, C) and an unpaired t-test (D, E, F). Asterisks indicates significance **** = $p < 0.0001$, *** = $p \leq 0.001$, ** = $p \leq 0.01$, * = $p \leq 0.05$, ns = not significant.

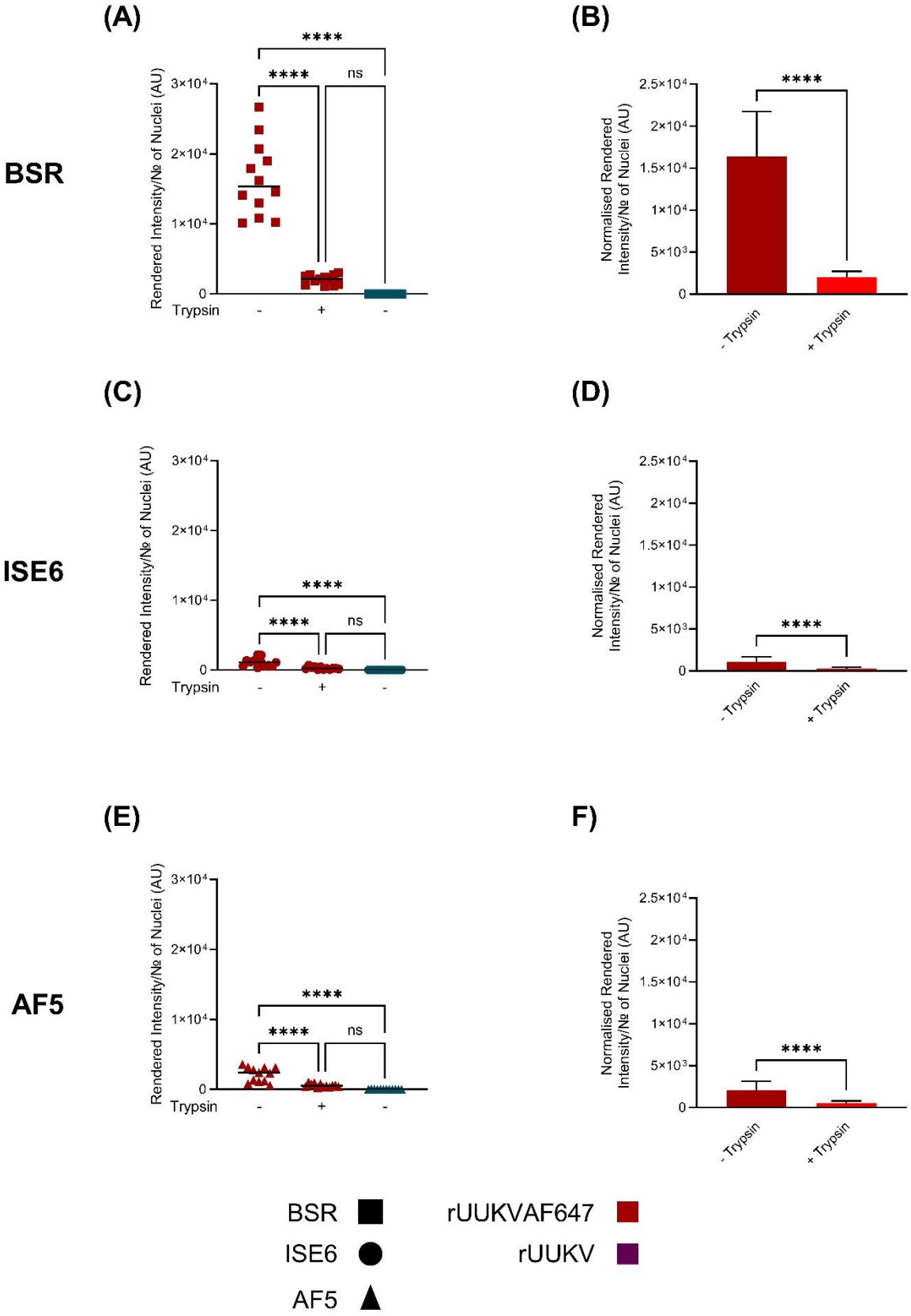

Figure 5.11: Quantitative analysis of rendered fluorescence intensity from trypsinisation experiments. Fluorescence data from 12 images generated in Figure 5.6 were analysed. Z-stacks were rendered using IMARIS software to define the nuclei, cell membrane and far-red surfaces. Virus bound to rendered membrane was determined by excluding rendered far-red intensity at a

distance greater than 0.01 µm either side of the rendered membrane. Data were calculated by dividing the sum of the rendered far-red intensity by the number of nuclei recorded in each z-stack and the mean arbitrary units plotted for rUUKVAF647-infected BSR (A), ISE6 (B) or AF5 (C) cell lines. The data for each cell line was normalized to the respective mock-infected control to eliminate background signal. Normalised data for rUUKVAF647-infected BSR (D), ISE6 (E) or AF5 (F) cell lines are also shown. Statistical significance was measured by ordinary one-way ANOVA with Tukey's multiple comparison test (A, B, C) and an unpaired t-test (D, E, F). Asterisks indicates significance **** = $p < 0.0001$, *** = $p \leq 0.001$, ** = $p \leq 0.01$, * = $p \leq 0.05$, ns = not significant.

5.3.4 Quantification of binding and internalisation of recombinant UUK viruses in mammalian, tick and mosquito cell lines

Next a mechanical washing protocol was then used to investigate the strength of rUUKVAF647 binding to the various cell lines in this study, using rUUKV (undyed) and mock-infected preparations as controls. Briefly, cell cultures were infected at a MOI of 5 FFU/ml or mock-infected at 4°C on ice for 1 hour. Cell monolayers were then washed one, three or five times with PBS 1X and fixed in 4% (v/v) formaldehyde. Confocal microscopy was used to take 4 z-stack images of 3 biological replicates, which were then examined for far-red fluorescence, corresponding to rUUKVAF647 localisation.

As seen in Figure 5.12 to 5.14, punctate dots of far-red signal were observed and found associated with the cell membrane for each washing condition. The number of punctate dots appeared to decrease slightly as the number of washes increased and in all rUUKV- or mock-infected samples no punctate signal was observed.

To quantitatively measure the effect of mechanical washing on rUUKVAF647 binding across all three cell lines, both raw fluorescence intensity (Figure 5.15 & 5.17) and rendered fluorescence intensity (Figure 5.16 & 5.18) were analysed. In all samples analysed there was a significant increase in fluorescence intensity in rUUKVAF647-infected samples compared to either rUUKV- or mock-infected samples at each wash number (Figure 5.15B, 5.15D & 5.15F). Overall, BSR cells showed higher levels of far-red intensity than ISE6 and AF5, and this level appeared to drop as the number of washes increased. ISE6 and AF5 cells both started with similar levels of far-red intensity; However, the level of intensity appeared to decrease in ISE6 cells whereas in AF5 cells it remained consistent as the number of washes increased (Figure 5.16.A). When analysing the raw intensity values, the titres of rUUKVAF647 did not decrease significantly in either the AF5 or the ISE6 cell lines upon washing. However, there was a small but statistically significant decrease in fluorescence between wash 1 and wash 3 or 5 recorded in the BSR cell line (Fig 5.16.B).

When examining the rendered fluorescent intensity, rUUKVAF647-infected BSR cell monolayers displayed a significant decrease in intensity between wash 1 and wash 3 or 5 (Figure 5.17 & 5.18), similar to that observed for the raw intensity values described above. A decrease in rendered fluorescent intensity was also observed on the rUUKVAF647-infected ISE6 cell line but was not statistically significant and no decrease was observed in the mosquito cell line (Figure 5.18).

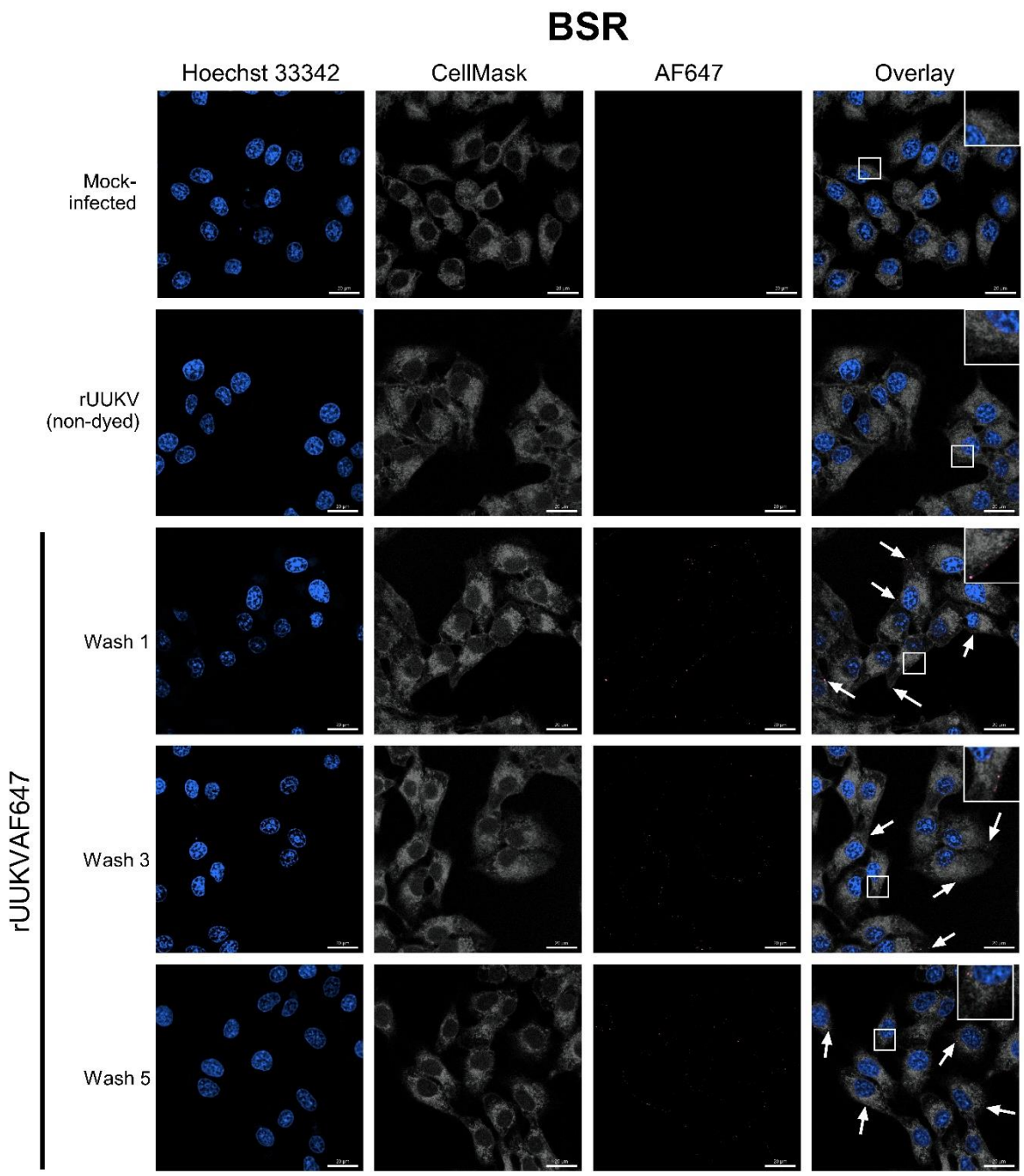

Figure 5.12: Mechanical washing to assess rUUKVAF647 binding to BSR cell cultures. Monolayers of BSR cells were incubated with rUUKV (undyed), rUUKVAF647 (dyed) at an MOI of 5 FFU/ml, or mock-infected virus preparations at 4°C for 1 h. Following the binding period, cell monolayers were washed in PBS for the indicated number of times. Following washing, cell monolayers were fixed in 4% (v/v) formaldehyde. Cell monolayers were counter stained with the nuclear stain, Hoechst 33342 (blue); cell membranes were visualized with CellMask (grey) as well as examined for AF647 fluorescence (pink) and virus binding was analysed by confocal microscopy. Data presented are representative images of n=3 biological replicates, each containing n=4 z-stacked images per well. Arrows highlight membrane associated AF647 signal. Scale bar indicates 20 µm.

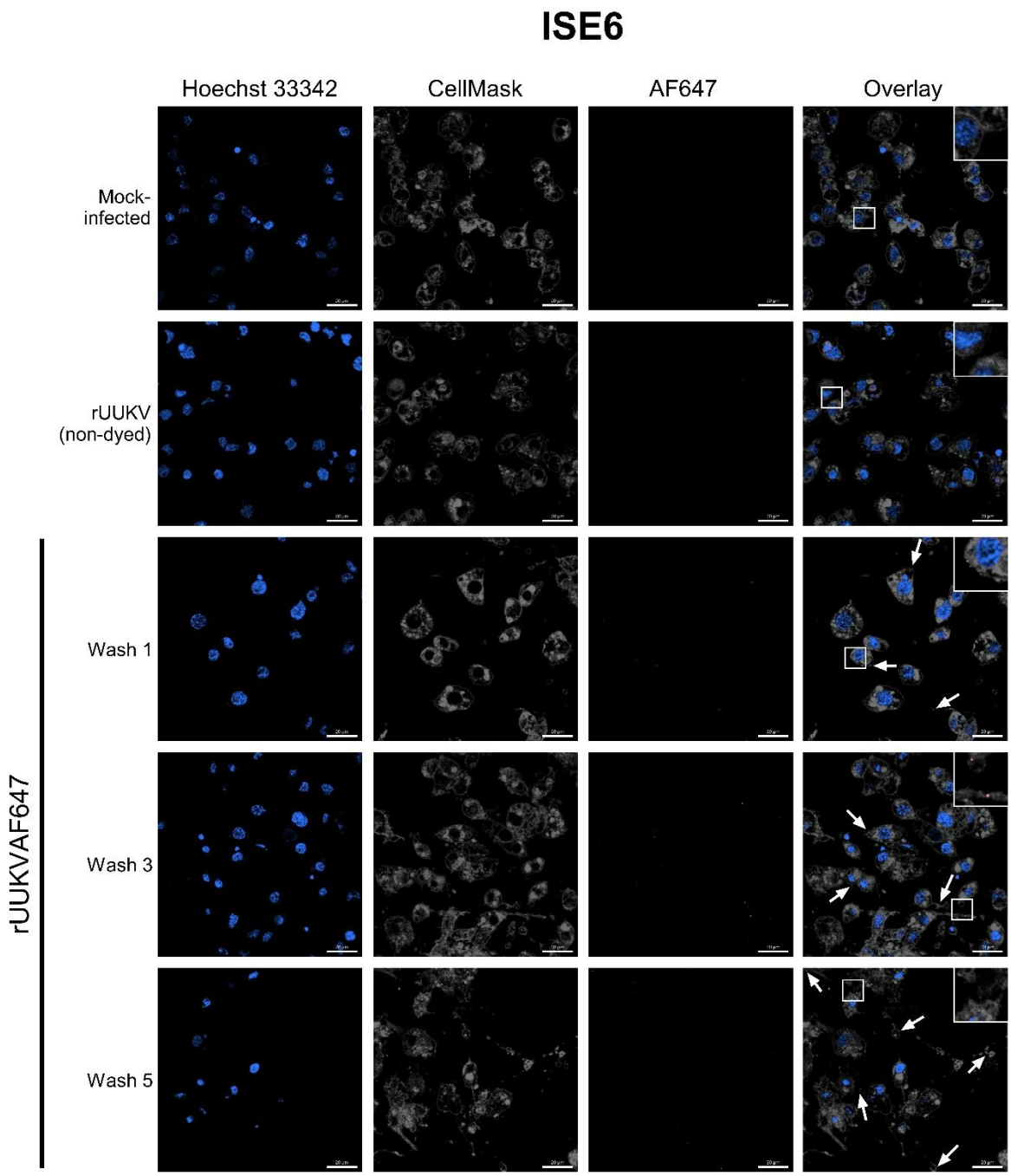

Figure 5.13: Mechanical washing to assess rUUKVAF647 binding to ISE6 cell cultures. Monolayers of ISE6 cells were incubated with rUUKV (undyed), rUUKVAF647 (dyed) at an MOI of 5 FFU/ml, or mock-infected virus preparations at 4°C for 1 h. Following the binding period, cell monolayers were washed in PBS for the indicated number of times. Following washing, cell monolayers were fixed in 4% (v/v) formaldehyde. Cell monolayers were counter stained with the nuclear stain, Hoechst 33342 (blue); cell membranes were visualized with CellMask (grey) as well as examined for AF647 fluorescence (pink) and virus binding was analysed by confocal microscopy. Data presented are representative images of n=3 biological replicates, each containing n=4 z-stacked images per well. Arrows highlight membrane associated AF647 signal. Scale bar indicates 20 µm.

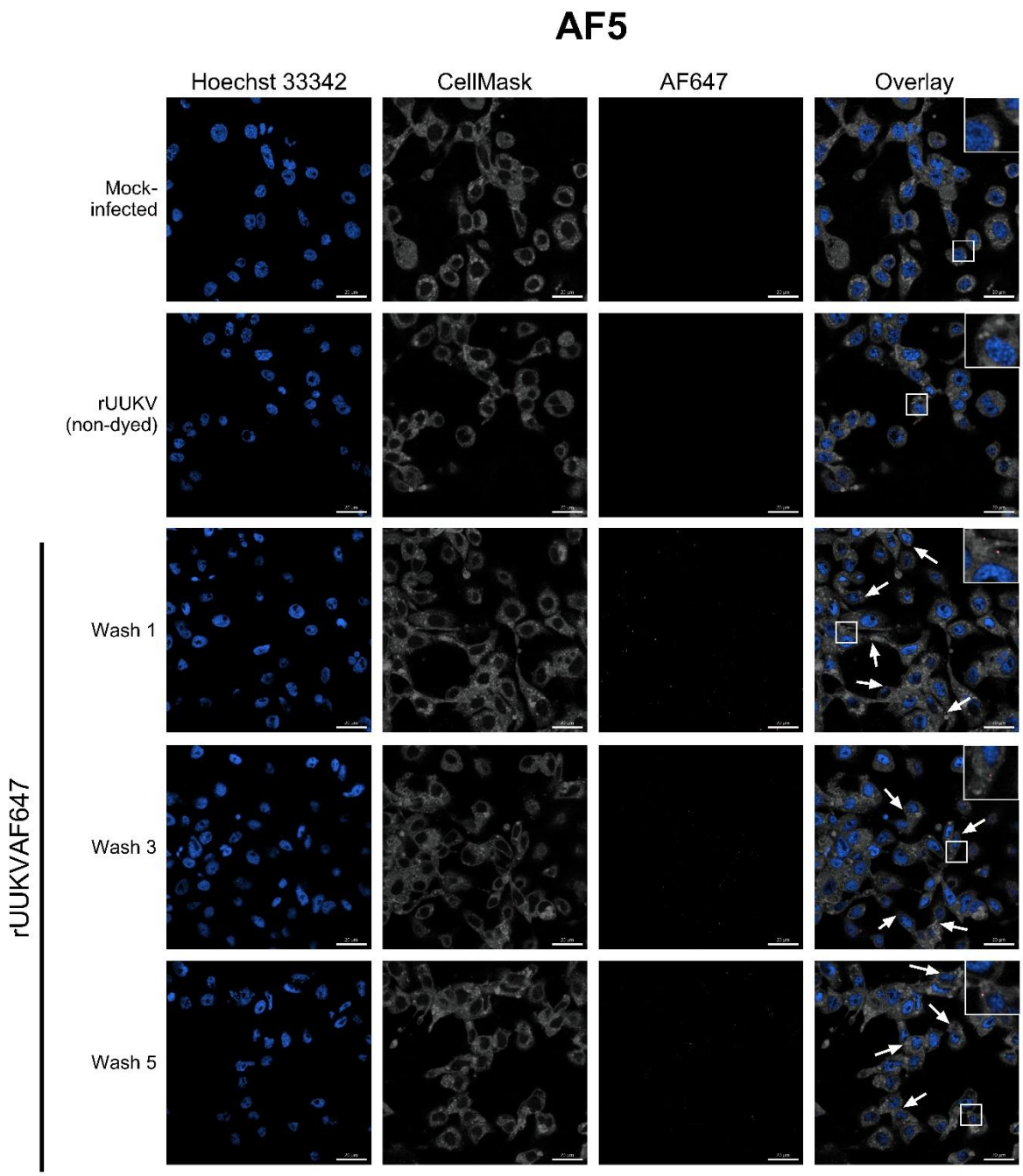

Figure 5.14: Mechanical washing to assess rUUKVAF647 binding to AF5 cell cultures. Monolayers of AF5 cells were incubated with rUUKV (undyed), rUUKVAF647 (dyed) at an MOI of 5 FFU/ml, or mock-infected virus preparations at 4°C for 1 h. Following the binding period, cell monolayers were washed in PBS for the indicated number of times. Following washing, cell monolayers were fixed in 4% (v/v) formaldehyde. Cell monolayers were counter stained with the nuclear stain, Hoechst 33342 (blue); cell membranes were visualized with CellMask (grey) as well as examined for AF647 fluorescence (pink) and virus binding was analysed by confocal microscopy. Data presented are representative images of n=3 biological replicates, each containing n=4 z-stacked images per well. Arrows highlight membrane associated AF647 signal. Scale bar indicates 20 µm.

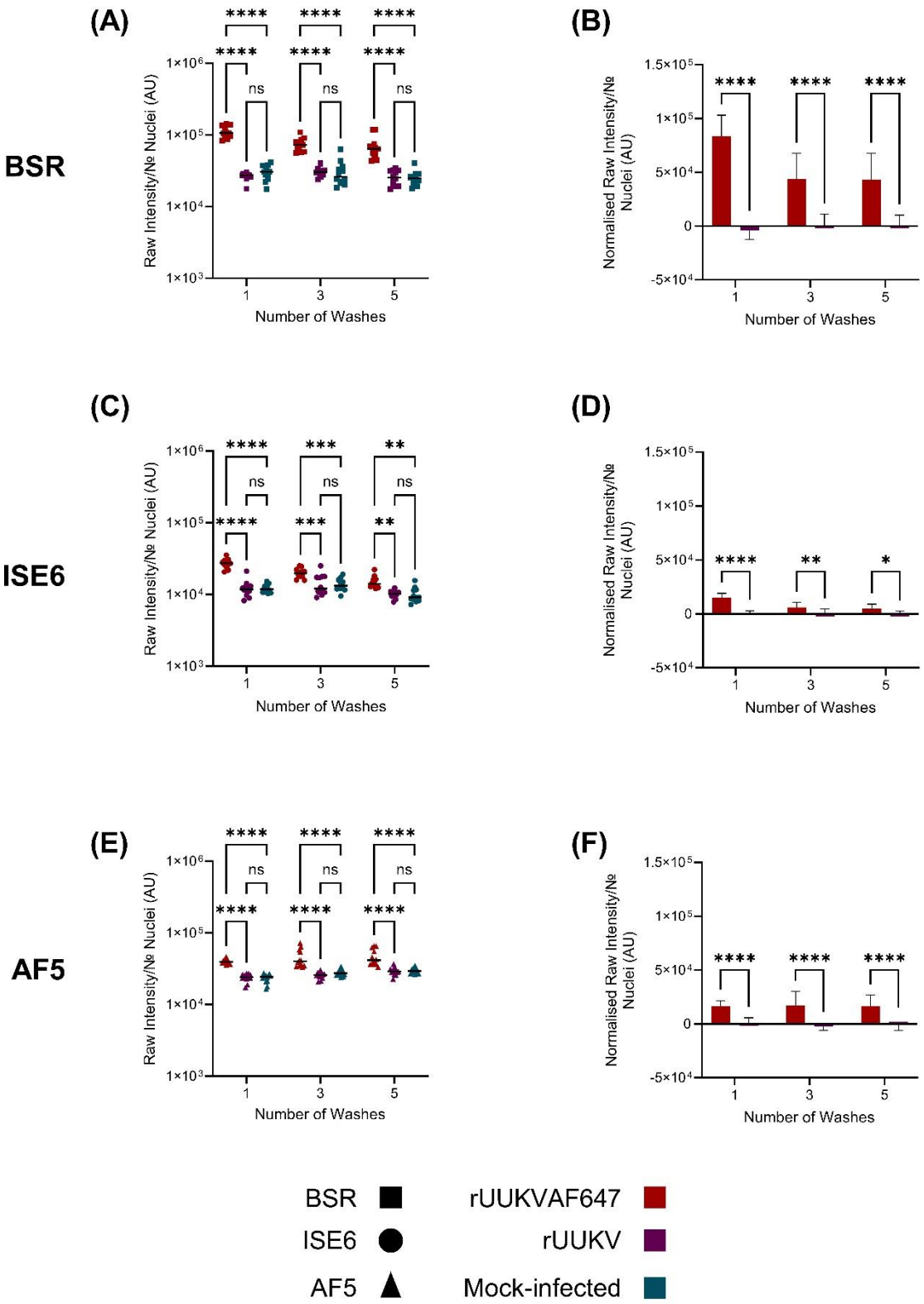

Figure 5.15: Quantitative analysis of raw fluorescence intensity from washing experiments. Fluorescence data from 12 images generated in each of Figure 5.12 to Figure 5.14 were analysed and quantified using IMARIS software. Data were calculated by dividing the sum of the raw far-red intensity by the number of nuclei recorded in each z-stack and the mean arbitrary units plotted for rUUKVAF647-infected BSR (A), ISE6 (C) or AF5 (E) cell lines. The data for each cell line were normalized to the respective mock-infected control to eliminate background signal. Normalised data

for rUUKVAF647-infected BSR (B), ISE6 (D) or AF5 (F) cell lines are also shown. Statistical significance was measured by ordinary two-way ANOVA with Tukey's multiple comparison test. Asterisks indicates significance **** = $p < 0.0001$, *** = $p \leq 0.001$, ** = $p \leq 0.01$, * = $p \leq 0.05$, ns = not significant.

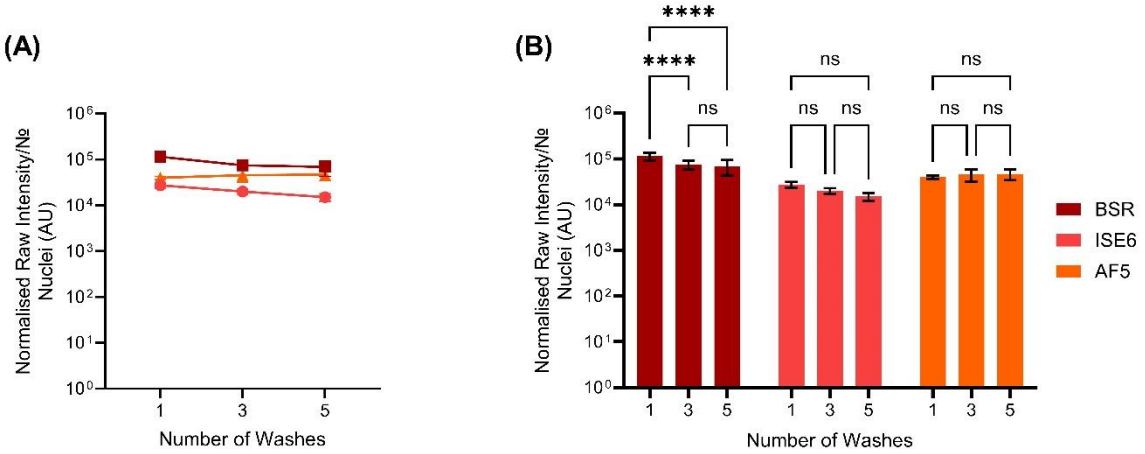

Figure 5.16: Comparison of quantitative analysis of raw fluorescence intensity from washing experiments. Fluorescence data from Figure 5.15 were analysed and plotted against each other (A) alongside being displayed as a bar chart to show statistical significance, which was measured by ordinary two-way ANOVA with Tukey's multiple comparison test. Asterisks indicates significance **** = $p < 0.0001$, *** = $p \leq 0.001$, ** = $p \leq 0.01$, * = $p \leq 0.05$, ns = not significant.

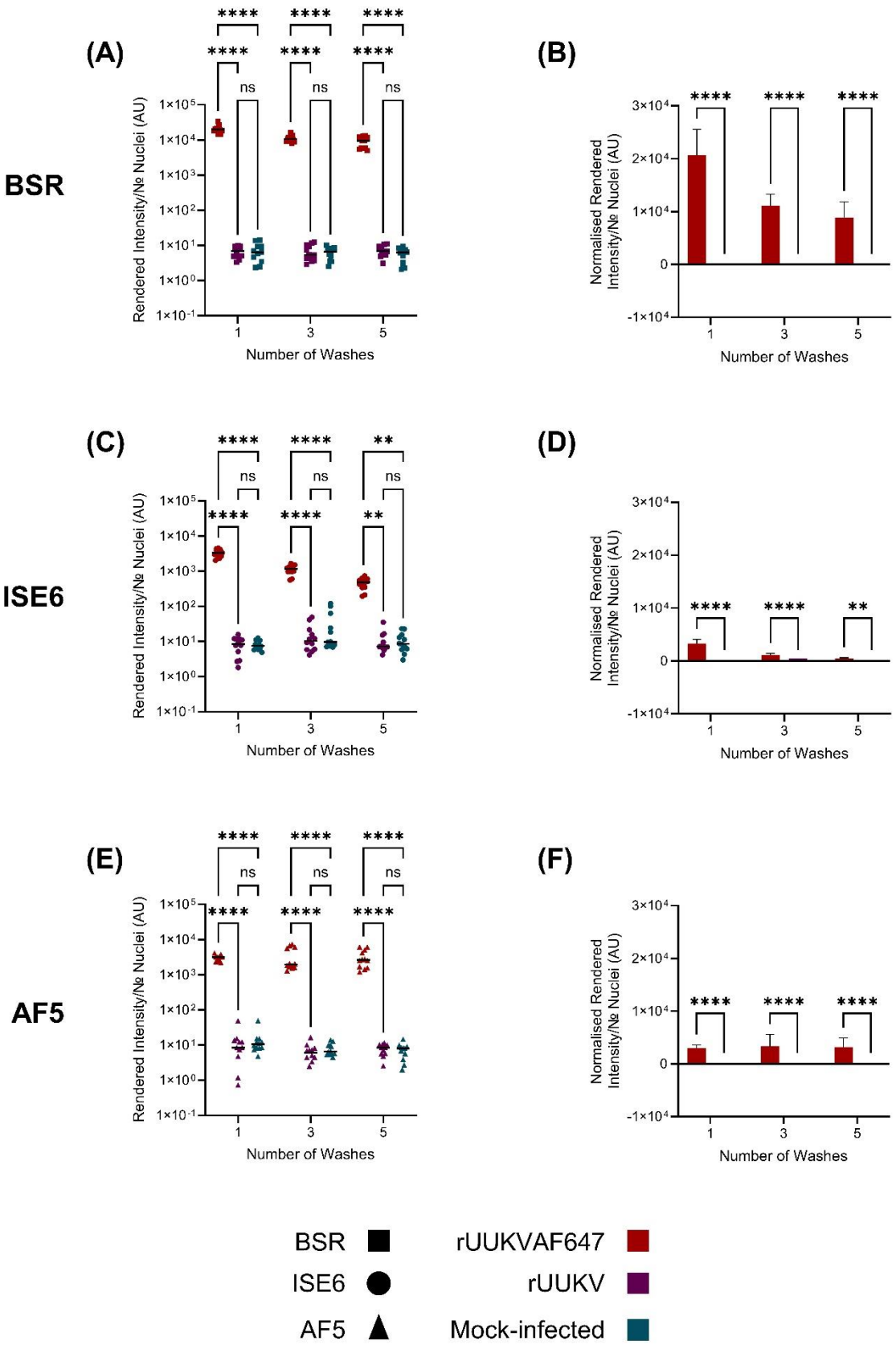

Figure 5.17: Quantitative analysis of rendered fluorescence intensity from washing experiments. Fluorescence data from 12 images generated in each of Figure 5.12 to Figure 5.14 were analysed. Z-stacks were rendered using IMARIS software to define the nuclei, cell membrane and far-red surfaces. Virus bound to rendered membrane was determined by excluding rendered far-

red intensity at a distance greater than 0.01 µm either side of the rendered membrane. Data were calculated by dividing the sum of the rendered far-red intensity by the number of nuclei recorded in each z-stack and the mean arbitrary units plotted for rUUKVAF647-infected BSR (A), ISE6 (C) or AF5 (E) cell lines. Statistical significance was measured by ordinary two-way ANOVA with Tukey's multiple comparison test. Asterisks indicates significance **** = $p < 0.0001$, *** = $p \leq 0.001$, ** = $p \leq 0.01$, * = $p \leq 0.05$, ns = not significant.

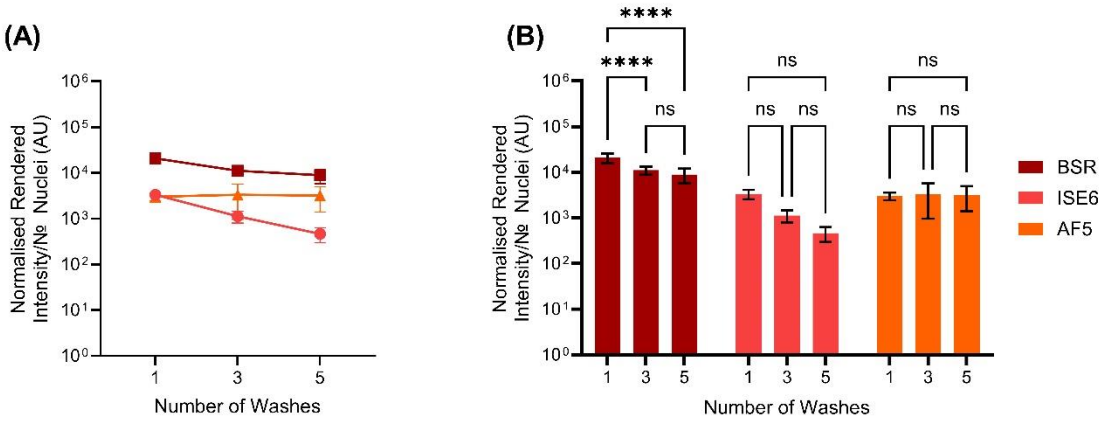

Figure 5.18: Comparison of quantitative analysis of rendered fluorescence intensity from washing experiments. Fluorescence data from Figure 5.16 were analysed and plotted against each other (A) alongside being displayed as a bar chart to show statistical significance, which was measured by ordinary two-way ANOVA with Tukey's multiple comparison test. Asterisks indicates significance **** = $p < 0.0001$, *** = $p \leq 0.001$, ** = $p \leq 0.01$, * = $p \leq 0.05$, ns = not significant.

To further confirm that the observed rUUKVAF647 far-red signal corresponds to viral particles following the mechanical washing process, two assays were conducted to assess virus binding and subsequent internalisation to the cell. This was achieved using RT qPCR analyses of UUKV M segment on cell monolayer lysates. Briefly, cell cultures were mock- or rUUKVAF647-infected for at 4°C (and on ice) for 1 hour. For binding RT qPCR analysis, cell monolayers were then washed one, three or five times as indicated. For internalisation RT qPCR analysis, inoculum was removed and cells incubated in media at the relevant temperature before being exposed to trypsin (as performed in Figure 5.9), washing and harvesting at the indicated time points. Cell monolayers were lysed in TRIzol and total cellular RNA was isolated. Extracted RNA was then reverse transcribed and RT qPCR performed to quantify levels of UUKV M RNA and the ribosomal 18S subunit as a housekeeping control. Results were analysed by $2^{-\Delta\Delta CT}$ method using the wash 1 or 0 h samples as the baseline (Figure 5.19).

RT qPCR quantification of the total UUKV M RNA showed little detectable change in the RNA levels of the BSR cells with each subsequent wash step. In rUUKVAF647-infected ISE6 or AF5 cell monolayers, UUKV M RNA levels decreased with each wash step employed. However, this decrease only achieved statistical significance in the AF5 samples (Figure 6.19.A). This observed decrease could be achieved through the virions being removed/washed off with each subsequent wash. However, this loss may not account for the total decrease of AFRI within each cell line, as it is plausible internalisation occurs during the washing stages. It has previously been shown that in mammalian cell lines 25% of UUKV bound was internalised within 10 minutes (Lozach et al., 2010). Therefore next, the discrepancy between observed fluorescence and UUKV M RNA level was investigated to determine if it was due to virus internalisation. The quantity of vRNA present within the cell was measured by RT qPCR over a time course spanning the first 60 minutes after the 1 h adsorption period at 4°C (Figure 5.19.B). In infected BSR cell monolayers, the levels of intracellular viral M RNA increased until 60 minutes where levels plateaued. This may be due to viral RNP entry and degradation though intracellular antiviral mechanisms, as acid-penetration is thought to occur within 20-40 minutes of internalisation (Lozach et al., 2010). In rUUKV-infected ISE6 cells, internalisation appeared to begin after 15 minutes, with the level of vRNA significantly increasing by 60 min p.i. Finally, there was a decrease in UUKV M RNA present in rUUKV-infected AF5 cell cultures over the 60-minute time course. The presence of vRNA may be due to inefficient trypsin digestion as observed with the fluorescence data during the trypsin assays (Figure 5.10 & 5.11). These data suggest that

while rUUK virions may bind to AF5 cell lines, the virus does not appear to be internalised and replicate in cultures derived from the mosquito vector.

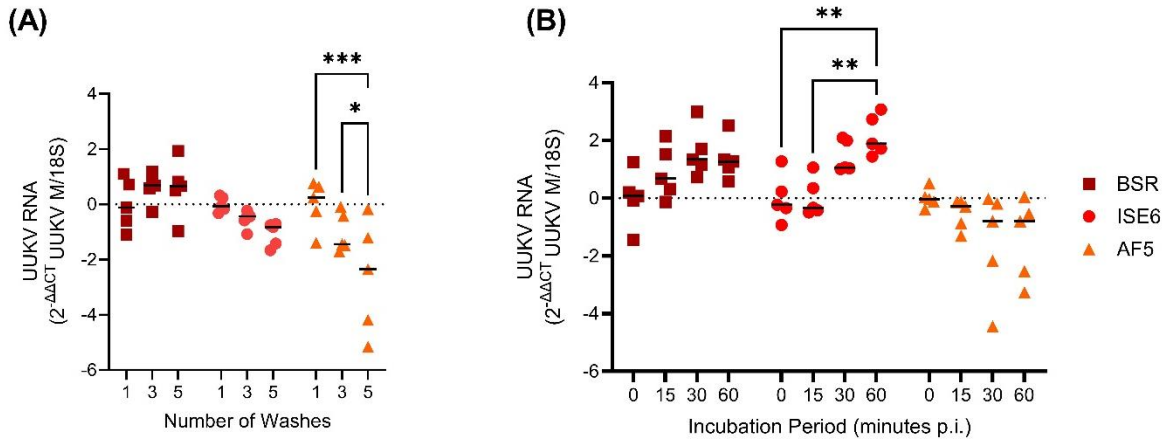

Figure 5.19: Comparison of viral RNA quantity during mechanical washing or incubation. Monolayers of BSR, ISE6 or AF5 cells were incubated with rUUKV virus preparations at a MOI of 5FFU/cell at 4°C for 1 h. Following the binding period, cell monolayers were washed in PBS for the indicated number of times (A) or incubated at the corresponding temperature for each cell line for the indicated time period before being washed and incubated with trypsin (B). Cells were lysed and total cellular RNA was isolated. Extracted RNA was then reverse transcribed and RT qPCR performed to quantify levels of UUKV M RNA and the ribosomal 18S subunit as a housekeeping control. 2-ΔΔCT was calculated using the wash 1 (A) or 0 h (B) samples as the control. Each sample condition contains an n = 5. Statistical significance was measured by ordinary two-way ANOVA with Tukey's multiple comparison test. Asterisks indicates significance **** = $p < 0.0001$, *** = $p \leq 0.001$, ** = $p \leq 0.01$, * = $p \leq 0.05$, no label = not significant.

5.4 Discussion

5.4.1 Optimal conditions for viral propagation

The recombinant virus stock used for this study was kindly provided by Dr Veronica Rezelj, and was initially grown in BHK-21 cells before working stocks were propagated in BSR cells, both cell lines were grown in DMEM supplemented with 2% FBS at and incubated at 37°C during virus propagation (Rezelj et al., 2015). Studies involving the use of UUKV grow stock virus in either BSR or BHK-21 cell lines and vary in the percentage of FBS supplemented within the media. However, in general, all seem to fall within 2%, 5% and 10% FBS (v/v) in BSR or 1-10% FBS (v/v) in BHK cell lines, and are incubated at temperatures of 33°C or 37°C (Bitto, Halldorsson, Caputo, & Huiskonen, 2016; Mazelier et al., 2016; Överby et al., 2008; Rezelj et al., 2015). As the research carried out within this thesis required a high MOI, FBS assays were carried out in both BHK-21 and BSR cell cultures to investigate the optimal conditions for virus stock production to achieve high titres compatible with our experimental setup. In BHK cells, incubation temperature was the most critical factor for achieving high virus titres. Aside from 0% and 10% FBS (v/v), the titres recorded between 3 and 6 days p.i. for each FBS concentration did not appear to increase, indicating that the exponential phase of virus growth had been completed. The apparent delay in completing the exponential phase of virus growth at 1% FBS (v/v) could be due to the cells being deprived of required growth nutrients. FBS starvation is a well-known method of restricting cell growth in order to synchronise cell cycling within a culture, as this lack of FBS slows the processes throughout the cell leading to a restriction point at the G0/G1 phase, likely slowing viral replication intracellularly (Cooper, 2003). In addition, FBS is known to stimulate the mitogen activated protein kinase (MAPK) signalling pathway, which is a major cell signalling pathway involved in a wide range of intracellular functions such as the immune response, gene expression and cell survival (Kumar et al., 2018). Many viruses are known to activate or manipulate this pathway during viral replication. Varying the level of FBS therefore may impact MAPK activation, which in turn may impact virus production, although at this time it is unclear if this pathway activation would have a positive or negative effect on viral kinetics (E. Vibeke Thrane, 2009; Kumar et al., 2018). When looking at higher FBS concentrations, although 10% FBS (v/v) appears to produce a higher titre of virus, BHK-21 cell culture application manuals by Thermo Fisher Scientific (https://assets.thermofisher.com/TFS-Assets/LSG/manuals/bhk_man.pdf) recommend not using 10% FBS (v/v) media for viral production as this accelerates cell division and therefore confluency is achieved too rapidly, leading to the production of a higher number of defective

particles. During the FBS assays, BHK-21 cell monolayers achieved confluency before the end of the 6-day experiment (data not shown), which may have inhibited the production of a higher titre viral stock (Figure 5.1.A). In BSR cells incubated at 37°C, cell monolayers were completely detached before the 6-day timepoint, indicating that cells became over-confluent, resulting in detachment and cell death. At an incubation temperature of 33°C, only 2% (v/v) FBS produced a significantly higher titre. The slower increase in titre in 0% FBS is most likely again due to the cell cycle restriction, but as mentioned previously could also be due in part to the lack of MAPK activation. At 6 days both 5% and 10% (v/v) FBS concentrations showed cell monolayer confluency, indicating the lower titre may have been due to confluency being achieved (data not shown). The increase in titre from 3 to 6 days at 2% (v/v) FBS also indicates that the virus replication was still in the exponential phase between these two timepoints (Figure 5.1.B).

For bunyavirus viral rescue and stock production, cell monolayers are seeded at low densities (Rezelj et al., 2015), and the results from Figure 5.1 indicate that this sub-confluency aids in extending the exponential phase of viral replication. When cell monolayers become confluent, contact inhibition occurs, leading to the (usually reversible) arrest of the cell cycle and prevention of cell growth which may impede the cell's ability to propagate. This also impacts many biological pathways within the cell and leads to detectable changes in the levels of certain proteins such as lysosomal-associated membrane protein 1 (LAMP1) and active focal adhesion kinase (FAK). As mentioned in the introduction, LAMP1 is used as a marker for endolysosomes as UUKV undergoes late-stage penetration. It is not unreasonable to hypothesise that contact inhibition may reduce levels of the host-cell proteins involved in the processes required for internalisation or viral replication, in turn reducing or limiting viral titres (J. Koch et al., 2021; Leontieva & Blagosklonny, 2014; Trajkovic, Valdez, Ysselstein, & Krainc, 2019). It is important to note however that this hypothesis must be tested further. For the purposes of this research, all viral stocks were grown in BSR cells at a temperature of 33°C, in either 0% (v/v) FBS supplemented media for assays involving dying of viral particles (as this is required for accurate calculations of dye quantities) or 2% (v/v) FBS supplemented media for all other experiments described in this study. These conditions were chosen to ensure that maximum time for exponential virus replication could occur in non-confluent cell monolayers, to not only achieve high viral yield but to try and minimise the potential for production of non-infectious or defective viral particles.

In future, it may benefit further studies to explore in more detail the impact of cell cycle and cell monolayer confluency upon the replication kinetics of UUKV. Many tick cell lines (including ISE6) show a much slower doubling rate, between 4 to 5 days, than the rate seen

in mammalian cell cultures (Thorpe et al., 2021). As the mammalian cell culture data suggest cell confluency impacts viral replication, most likely due to changes to the cell cycle, it is possible that this difference in cell cycle speed may impact virus replication and therefore potential long-term sustainability of virus production in different cell types. Given that ticks as vectors can maintain UUKV infection over the course of their lifetime this slower replication may be an important factor in viral persistence.

5.4.2 UUKV Growth kinetics in mammalian, tick and mosquito cell lines

A549 cell cultures have been used for growth curve studies of several recombinant bunyaviruses including Toscana virus (TOSV), BUNV and Oropouche viruses (OROV), where titres reached ~10^7 FFU/ml after 48 hours (Elliott et al., 2013; Tilston-Lunel, Acrani, Randall, & Elliott, 2015; van Knippenberg, Fragkoudis, & Elliott, 2013). Prior studies have found that when A549 cells were infected with UUKV at a MOI of 2 FFU/cell, recombinant viral titres can reach ~10^6 FFU/ml after 72 hours, and higher titres were achieved when infecting A549/PIV5-V cells, which have a diminished interferon response (Rezelj et al., 2015). The titres found in the growth curves of this study align with previous observations. UUKV encodes a very weak interferon antagonist (NSs) and is unable to prevent cells mounting an antiviral response, A549 cells demonstrate the potential to clear UUKV infection, particularly at lower MOI infections (Le May & Bouloy, 2012; Xu et al., 2022). It was observed that titres achieved in UUKV-infected A549 cells, which can produce an interferon response, were lower than in BSRs, which have a endogenous defect in IRF3 activation and therefore cannot mount an interferon response (Rieder et al., 2011; Sato, Tanaka, Yamada, & Yamamoto, 1977). The low level of UUKV replication in A549 cell lines is also evidenced by the inability to detect viral N protein expression across the time period of these experiments (Figure 5.2). A549 cells, therefore, serve as a better model for examining intracellular host responses to infection in a more biologically relevant setting.

BSR cells, for factors mentioned previously, allow an examination of viral kinetics as replication is not dampened by the mounting of an effective innate antiviral response. Infection of BSR cell lines with rBUNV yielded similar titres to those seen in BHK cells carried out in previous studies (van Knippenberg et al., 2013). Comparing viral titres of rBUNV to rUUKV following infection of BSR cell cultures displayed varying replication kinetics, which may be due to the ability of the virus to commandeer the intracellular machinery and produce new viral particles at a faster speed, meaning all cells within the culture become infected faster leading to the peak titre being achieved in a shorter timeframe

than UUKV. In addition, the N protein expression varies between the two viruses, with N protein being detectable in cell lysates at 24 h p.i. from UUKV but not in BUNV infected samples. This may be due to the export of new virions being faster during infection with BUNV opposed to UUKV, thereby preventing the accumulation of BUNV N protein within the cells until 48 h p.i. or more UUKV N protein being produced during an UUKV infection despite fewer virions being released. In all literature, UUKV and BUNV are described as tick- and mosquito- borne, respectively, although both are known to infect mammalian hosts (Burrell et al., 2017; Dutuze, Nzayirambaho, Mores, & Christofferson, 2018; Mazelier et al., 2016). The reflection of this in BSR cell culture makes this cell line useful as a baseline for expanding analysis of UUKV into other cell types, and for methodologies such as viral stock production and plaque assays.

As seen in previous work (Rezelj et al., 2015), rUUKVdelNSseGFP generates a lower titre at 72 h p.i. compared to wt rUUKV, which is reflected in the inability to detect the N protein by western blotting efficiently (Figure 5.2.A and B). In addition, plaque sizes produced by rUUKVdelNSseGFP are smaller than those of wt rUUKV, indicating viral kinetics have been impacted in some way and that the NSs protein (although not required for replication) has other functions which play a role in completing the replication cycle outside of antiviral response antagonism (Rezelj et al., 2015). The data from ISE6 cells shows this may also be true for vector species. As mentioned previously, BUNV is known to be mosquito-borne and there is no present evidence in the literature to suggest it is capable of replicating within ticks or tick cell lines (Dutuze et al., 2018). This is confirmed by the growth curve time course. The gradual decrease in rBUNV titre during ISE6 cell infection suggests a degradation of the viral particles in the medium that may have not been washed away after the inoculum was removed, as opposed to active internalisation and replication (Figure 5.3.A). In addition, BUNV N protein was not detected within rBUNV-infected ISE6 cell lysates at any time point. Both factors indicate that no active replication of BUNV occurred within the ISE6 cell line. In comparison, although there was no detectable increase in rUUKVdelNSseGFP over the time course, the over ten-fold drop in titre by 6 days indicates active uptake of virus occurs, but replication was unable to be completed (Figure 5.3.A). Similar results have been observed in our laboratory, where severe fever with thrombocytopenia syndrome virus (SFTSV) NSs protein has been shown to be required for productive infection of tick cell cultures, and the block in replication appears to be due to the specific degradation of the viral mRNA encoding the SFTSV NSs protein (Fares et al in preparation). When UUKV NSs was encoded and expressed during infection, increasing the MOI increased the viral titre until day 9 where the titres appeared to plateau (Figure 5.3.A). There was a delay in the detection

of UUKV N protein, with N protein being visible by western blotting several days after titres reach ~10^6 FFU/ml (Figure 5.3.B). Tick cell lines IRE/CTM19 and IRE/CTM20 have shown the ability to sustain UUKV infection and produce viable virus particles over the course of 100 days, plateauing after 10-20 days at a titre of approx. ~10^6 to ~10^7 FFU/ml (Mazelier et al., 2016). Overall, the results from the growth curves in ISE6 cells show the cell line can sustain a UUKV infection over an extended period, even though this is not a cell line established from *I. ricinus* the natural vector of the virus. Several tick-borne pathogens can be transmitted by both *I. ricinus* and *I. scapularis*, including TBEV. However, there are differences within the viral replication kinetics and intracellular responses between the two species (pathogen dependent) and so more investigation needs to be done to clarify the ability of *I. scapularis* to vector UUKV in nature (R. J. Eisen & Eisen, 2018; Gondard et al., 2018; Shi, Hu, Deng, & Shen, 2018; Weisheit et al., 2015).

Like BUNVs inability to replicate in tick cells, rUUKV does not appear to infect and replicate in AF5 and AF319 mosquito cell lines. As seen in the growth curves, infection of these cells with rBUNV produced titres of ~10^4 FFU/ml in AF5 cells and ~10^5 FFU/ml in AF319 cells (Figure 5.4.A). The difference in these titres is most likely due to AF319 cells harbouring a Dicer2 knockout mutation, hence lacking an RNAi response that would target the viral RNA for degradation, allowing for the increased production of viral progeny (Varjak et al., 2017). Therefore, once the BUNV is internalised into the cell and begins replicating, it is subjected to a weaker intracellular antiviral response. BUNV nucleocapsid protein was only faintly detectable at 72 h p.i. again demonstrating that it may take longer for viral proteins to accumulate within arthropod cells, after virus release begins. The ability to detect infectious virus output from these insect-derived cultures demonstrates that AF5 and AF319 cell lines are permissive to mosquito-borne bunyaviruses. An interesting observation when probing for the viral and cellular proteins was the increase in tubulin over time. This was partially expected, as the western blots were carried out using equivalent volumes of lysate rather than normalising the protein content of the samples, and therefore the increase most likely corresponds to an increase in cell number over time. However, this increase in tubulin was more apparent in rBUNV infections from the 0 to 24-hour p.i timepoints in both mosquito and mammalian cell cultures (Figures 5.2.C and 5.4.C). As this increase was not observed in ISE6 cells (Figure 5.3.C), where rBUNV replication was not achieved, it could be hypothesised that the initial infection of mosquito and mammalian cell cultures with rBUNV reduced cell adherence. By impacting adherence, an increased number of cells would detach during washing before the monolayer was lysed, causing a reduction in the quantity of tubulin within the sample. This hypothesis needs to be further investigated,

and at the time of writing there is no mention within the literature of the impact of BUNV on cell adherence during infection.

Finally, as previous literature has also shown, wt rUUKV was not able to complete replication cycles within mosquito cells (Lawrie et al., 2004; Matsuno et al., 2018). Our results support this model as for both rUUKV and rUUKVdelNSseGFP our results showed no increase in viral titre over 72 hours (Figure 5.4.A) and no UUKV nucleocapsid protein was detected (Figure 5.4.B). Despite the clear vector tropism of UUKV, little investigation has been carried out to investigate why this tropism happens or where the block in UUKV replication occurs in mosquito cells. From the lack of increase in titre and inability to detect UUKV N protein in the corresponding western blots, this block (or at least the first block in replication) occurred before translation was initiated.

5.4.3 Optimisation and use of dyed UUKV to analyse bunyavirus entry in mammalian, tick and mosquito cell lines

Given the viral kinetics data from each of the cell lines, our initial hypothesis was that UUKV was incapable of completing replication within mosquito cells as the virus was unable to bind and be internalised, potentially due to the mosquito cells lacking the necessary surface receptors. To further examine if the first block in UUKV replication in mosquito cells was indeed binding, the methodology developed by Hoffman et.al 2018 was adapted to examine the binding and internalisation of UUKV in BSR, ISE6 and AF5 cell lines (A. B. Hoffmann et al., 2018). AF647 far-red glycoprotein dye at a ratio of 1:5 viral glycoproteins to dye molecules was used to dye UUKV virions. Hoffmann et al described a ratio of 1:10 glycoproteins to dye molecules and above potentially interfered with the ability of the UUKV viral particles to bind and replicate. To ensure the dying of virions within this study did not interfere with the ability of the virus to complete replication, growth curves were carried out to compare the viral growth kinetics of dyed and undyed UUKV particles (Figure 5.5.A). In addition to this, the morphology of the dyed viruses was examined in comparison to the undyed wt rUUKV using electron microscopy (Figure 5.5.B-E). Although the edge of the dyed viral particle is darker, this may be due to experimental set up or the bound dye affecting the density of the virion surface, and overall due to the pleomorphic nature of UUKV there were no apparent differences in morphology between dyed and undyed viruses. This lack of difference was also seen in the growth curves, which fell in line with the previous optimisation assays by Hoffman et al, who also demonstrated that the AF647 glycoprotein dye binds effectively to the Gn and Gc viral proteins. There were fewer viral particles in the dyed virus sample, which may be due to some loss of material during a second

ultracentrifugation process in the protocol, but overall titres produced through this method were suitable for further experimentation.

It was important to determine whether UUKVAF647 viral particles were infectious and suitable for binding and internalisation assays, particularly that upon analysis by confocal microscopy any far-red signal detected corresponded to dyed virus, as opposed to debris/background/unbound dye. Although Hoffmann *et al.*, used an MOI 1 FFU/ml, previous studies have employed MOIs from 0.1-10 FFU/ml (Albornoz et al., 2016; Lozach et al., 2010). In line with the growth curve data and preliminary confocal analysis, a MOI of 5 FFU/cell was chosen for all experiments involving rUUKVAF647 to allow for the highest likelihood of observing dyed UUKV associated to the cell membranes, whilst still maintaining the ability to complete replication. These assays were carried out in BSR cell culture, as this cell line had been used to carry out previous UUKV experiments, and the mammalian binding and internalisation mechanisms had been well studied (Bitto et al., 2016; A. B. Hoffmann et al., 2018; Hofmann & Pohlmann, 2011; Lozach et al., 2011; Lozach et al., 2010). As little is known about binding and internalisation of viral particles in ISE6 cells and given that viral replication has been shown to occur within this cell line, implying viral entry must occur, carrying out these assays in ISE6 cells sheds further light on the mechanisms of binding and internalisation. To date, most research revolving around pathogen-tick cell interactions has involved investigations between the tick cells and bacteria, and therefore more investigation needs to be carried out to elucidate what cell surface factors interact with virions. Carrying out these assays in both BSR and ISE6 cells allow us to build a baseline of binding and internalisation kinetics, and confirm any far-red signal seen is from true virus binding. By performing these assays in AF5 cell lines in parallel we are also able to ascertain if this methodology is useful for defining where the first block to replication occurs.

In preliminary work, far-red punctate dots of signal were seen to be associated with BSR cells. These were also seen in non-treated and un-trypsinised rUUKVAF647 samples in Figures 5.6 and 5.9 in all three cell lines. To determine if this signal was 'true' dyed virus, samples of rUUKVAF647 were heat inactivated to remove the binding capabilities of the virus. Heat-inactivation is a common method for inactivating virus and works by denaturing the proteins and causing conformational changes preventing effective binding to the cell receptors. When looking across all three cell lines, both visually and through fluorescence intensity, this was reflected in the data. The lack of punctate dots in heat-inactivated rUUKVAF647, in comparison to the untreated samples where far-red signal was associated with the cell membrane as defined by the presence of cell mask membrane stain, indicated

that the heat-treatment removed the ability of the dyed virus to bind. If this far-red signal was caused through debris, unbound dye or by alternative means this shift in far-red intensity would not be expected to a comparable level, as debris may be capable of binding non-specifically to the cells and unbound dyes binding capability would be unaffected by denaturation conditions. Raw fluorescence intensity from the z-stack images taken from the samples was initially analysed. This showed that only untreated rUUKVAF647 produced a significantly increased far-red signal when compared to the mock infected sample. There was no significant difference between the low levels of far-red intensity between the rUUKV- and mock- infected samples derived from BSR and ISE6 cell lines. It is worth noting there was still some variability and signal seen in heat-inactivated rUUKVAF647 for both cell lines. However, from examination of the z-stack images, it is reasonable to assume this was generated from denatured dyed viral protein aggregates non-specifically 'sticking' to the cell surface. This conclusion is supported as when comparing normalized intensities in mock-infected samples, the difference between rUUKV and rUUKVAF647 in heat-inactivated samples was not significant. However, in AF5 cells, heat-inactivated rUUKV and rUUKVAF647 showed significantly higher far-red intensity compared to mock-infected samples, although still lower than untreated rUUKVAF647. Given untreated and heat-inactivated rUUKV and rUUKVAF647 were indistinguishable from each other, this indicates heat-inactivation of the virus preparations may be causing the mosquito cells to produce a far-red signal (Figure 5.6). Many arthropods, including mosquitoes, are known to have auto-fluorescent properties, which may vary depending on tissue and cellular function (Croce & Scolari, 2022; Scolari, Girella, & Croce, 2022). We therefore believe that the increase in far-red intensity is due to the AF5 cells producing intracellular components which auto-fluoresce within this frequency in response to the detection of aggregated proteins within the inoculum. This is supported when analysing the z-stack images, as far-red fluorescence within the AF5 cells can be seen within the intracellular compartments as defined by the presence of the cell mask membrane stain (data not shown). To ensure this did not impact the analysis of the results and only rUUKVAF647 far-red signal associated with the cell membranes was quantified, for all optimisation and binding experiments both raw fluorescence and rendered fluorescence were analysed. Rendered fluorescence only measured the far-red signal associated with the cell membrane (as defined by the cell mask membrane and modelled in IMARIS software). Due to the morphology of the different cell lines, each species required individual membrane boundary settings, which were then applied consistently across all z-stack images for that cell line. To allow for far-red intensity to be comparable across the cell lines, the far-red channel maintained the same settings (as

described in methods) and was subjected to the same boundary and limitation modelling rules across all z-stack image capture, minimising rendering bias. When these limitations are imposed on the heat-inactivation z-stack images, the overall trends of the data remain the same. In both BSR and ISE6 cell lines far-red signal in rUUKV and mock-infected samples in both untreated and heat-inactivated conditions was negligible, with a significant far-red signal only seen in untreated rUUKVAF647-infected samples. In AF5 cells, there was no significant difference between rUUKV and mock-infected samples in heat-treated conditions, and rUUKV and mock-infected samples for both conditions had negligible far-red signal. When looking at the normalised values the only conditions producing significant far-red signal was again untreated rUUKVAF647-infected samples, as seen in BSR and ISE6 cells. This supports the previous assumption that the variable and increased far red signal from heat inactivated rUUKVAF647 and rUUKV occurred due to an increase in intracellular autofluorescence, and that rendering allows for a more accurate analysis of virus bound to the cell membranes (Figure 5.7).

Previous studies have shown that UUKV binding to A549 cells is mediated through protein-protein interaction (Albornoz et al., 2016; A. B. Hoffmann et al., 2018; Hofmann & Pohlmann, 2011), and UUKV could use a similar mechanism to bind to ISE6 cells. To ensure the far-red signal produced from rUUKVAF647 was the result of virus actively binding to the cells, and that the dying process had not altered the ability of the virus to bind, e.g. causing the virus to become 'sticky' and bind non-specifically to the cell surface. The dye may also block the labelled protein's ability to bind allowing for only transient association. Trypsin incubation was therefore used to determine if binding was indeed protein mediated. Trypsin is a serine protease, and although some viruses such as SARS-CoV-2 and Influenza A have enhanced cell entry upon exposure to trypsin, there is evidence to show that class II membrane fusion protein tetramers (such as UUKVs glycoprotein) are resistant and unresponsive to trypsin treatment (Kielian, 2006; Y. Kim et al., 2022; Klenk, Rott, Orlich, & Blodorn, 1975; W. Ma, Tang, & Lai, 2005). As such we can assume that, if trypsin treatment impacts far-red fluorescence intensity once binding has occurred, rUUKVAF647 attachment to the cell surface is protein-mediated and specific, in line with the current UUKV model. This can be observed in the confocal images (Figure 5.10). A small number of red punctate dots can be seen in the trypsin treated cells across all cell lines. However, these are most likely due to the trypsin not fully being able to cleave every bound virus particle, potentially due to the incubation time being relatively short to prevent the cell monolayers from detaching or due to possible steric hinderance. When looking first at raw fluorescence, trypsinisation significantly reduced the levels of far-red intensity of

rUUKVAF647-infected samples to levels comparable with mock-infection in both BSR and ISE6 cell cultures. This was also seen when the trypsinisation results were normalised to mock-infected samples, however the signal from the trypsinised rUUKVAF647 samples was not fully depleted. In comparison, when looking at the raw fluorescence intensity of rUUKVAF647-infected AF5 cell cultures, trypsinised rUUKVAF647 levels were significantly lower than non-trypsinised levels and were not significantly different to mock-infected samples. Interestingly, when results were normalised to mock-infected samples the significant difference between the trypsinised and non-trypsinised rUUKVAF647 samples was lost. This is most likely due to the trypsin triggering increased levels of autofluorescence, as seen in the previous assay (Figure 5.10). This is supported by looking at the rendered data, where all three cell lines show trypsinisation significantly reduces the far-red intensity and therefore reduces the quantity of bound viruses to levels comparable with mock infected samples. This observation was maintained in all three cell lines when data was normalised to the respective mock-infected cells. It is worth highlighting that even though the levels of far-red signal were similar to those seen in mock-infected cells, when looking at the normalised data, some far-red signal was still present in trypsinised samples, showing that most of the binding was protein-protein mediated (Figure 5.11). The small quantity not removed via trypsinisation was either inaccessible to the trypsin, or the virions were binding/associating with the cell through alternative means (such as transient binding or lipid interaction). As co-factors have been suggested to be associated with mammalian cell binding (Lozach et al., 2011; Lozach et al., 2010; Mazelier et al., 2016), and the factors responsible for binding in arthropod cells have yet to be elucidated, it would be interesting to further investigate the factors required for binding to arthropod cells.

In conclusion the far-red signal seen in the rUUKVAF647-infected samples is likely to be 'true' signal derived from bound rUUKVAF647, and this methodology may be suitable for analysing binding kinetics in the cell lines studied. When analysing the fluorescence intensity per cell, there was a higher level observed in BSR cells when compared to arthropod cells, which may be primarily due to mammalian cells being larger in size than arthropod cells and therefore contain more receptors with which the virus was able to bind. As can be seen in these optimisation measures, rather unexpectedly, AF5 untreated and non-trypsinised samples show dyed virus associated with the membrane of the cells. Prior to this study the ability of UUKV to bind mosquito cells was unknown. In addition, results from the trypsinisation assay show it is likely that this binding was protein-protein mediated, indicating UUKV was binding to cell-surface proteins/receptors in cell cultures of mosquito origin.

5.4.4 Analysis of binding and internalisation of UUKV in mammalian, tick, and mosquito cell lines

To explore whether UUK virions could be internalised by BSR, ISE6 and AF5 cell lines, binding and internalisation assays were performed. Manual washing was used to determine the strength of the virus-receptor interaction. Following virus adsorption at 4°C to facilitate virus binding, one, three or five mechanical washes were carried out using PBS. If the binding was non-specific or weak, a significant decrease in the far-red fluorescence intensity would be expected with each wash, indicating viral particle were associated with the membrane but were not being internalised. This method has previously been employed to study the binding and internalisation of adeno-associated virus (Berry & Tse, 2017). Before analysing the binding affinity of the virus to the cell lines in the study, comparison of rUUKVAF647- to rUUKV-infection and mock-infected samples were carried out as previously described in the optimisation steps. In both BSR or ISE6 cell lines, dyed virions associated with the cell membranes as expected, and during analysis it was seen the number of AF647 dots did not decrease drastically as the number of mechanical washed increased, exemplified in the confocal microscopy images (Figure 5.12 and 13). In both the raw and rendered fluorescent analysis the difference between wt rUUKV (undyed) and mock-infected samples was negligible. While rUUKVAF647 infection produces a significant far-red signal which decreases slightly as the number of mechanical washes increases. This decrease was more apparent in ISE6 cells, indicating a greater loss of virus particles from the surface (Figure 5.15). In AF5 cells there appeared to be no significant decrease in the number of dyed viral particles across mechanical washes (Figure 5.14), and this was also reflected in the raw and rendered data analysis (Figure 5.15.C and 5.16.C). The individual cell line results, particularly when comparing the results of rUUKVAF647 with rUUKV and mock infected samples, indicate mechanical washing has no impact upon the far-red fluorescence, and therefore the results suggest the virus is bound to the cell surface. We then compared the binding at each mechanical wash stage between the cell lines (Figure 5.16 and 5.18). In the raw fluorescent analysis, only BSR cells showed a significant decrease in the far-red signal intensity (and therefore number of viral particles) as the number of mechanical washes increased. Although, this may in part be due to BSR cells having a higher quantity of virus particles initially bound due to the cell size difference as previously discussed. The decrease in BSR and ISE6 cell-membrane associated virus was more prominent in the rendered fluorescence analysis (Figure 5.18), and although variability of far-red intensity increased over the number of mechanical washes, no significant signal decrease was seen indicating UUKV binding was specific and strong for AF5 cells. To confirm this result, we

analysed the quantity of bound virus at the different mechanical wash stages using RT qPCR (Figure 5.19.A). Interestingly, BSR cells appeared to have a slight increase in vRNA over the number of mechanical washes, however, this was highly variable and not statistically significant. This indicates that the loss of fluorescence in BSR cells during mechanical washing may be due to internalisation occurring during the washing procedure, as opposed to virus being lost due to detachment. vRNA from infected ISE6 cells followed the more expected pattern of loss of vRNA across the mechanical wash conditions. However, this loss was not significant which could again indicate some level of internalisation of the bound virions during the washing process. In the AF5 cell cultures, although no significant loss of fluorescence was seen, there was a significant drop in vRNA across the mechanical washes. The more prominent decrease in fluorescence intensity in BSR and ISE6 cells compared to AF5 cells may have been due to these cells potentially internalising some of the bound rUUKVAF647 during mechanical washes. In addition, UUKV is known to 'clump' together when infecting or binding, and so some of this loss may be due to any aggregated or clustered virus detection, which may be more easily detectable when analysing vRNA compared to fluorescence intensity.

To determine whether the binding of UUKV to AF5 cells led to internalisation, and to confirm if any of the loss of fluorescence in ISE6 and BSR cells was likely due to internalisation beginning to occur over the course of the washes, internalisation assays were performed (Figure 5.19.B). As expected, the level of UUKV M RNA increased over the 1-hour adsorption period in the BSR cell cultures. However, this level plateaued between 30-60 minutes. Previous studies have found internalisation can occur within the first 10 minutes of adsorption to mammalian cells, with acid-penetration occurring by 20-40 minutes after internalisation (Lozach et al., 2010). Therefore, this plateau may have been due to the intracellular components accessing the RNPs and degrading some of the vRNA. This increase was also seen within infected ISE6 cell cultures, although this increase only began after the first 15 minutes, becoming significant by 60 minutes. This was in line with what is known about the growth rate of tick cells, as the slower rate of growth most likely carries over into a slower rate of internalisation and intracellular reactions. Surprisingly, in the infected AF5 cell cultures, no increase in UUKV RNA was seen over time, indicating that no internalisation was occurring. It should be noted that UUKV RNA was most likely still detected in these samples as previous assays have demonstrated, trypsin is not fully effective in cleaving all surface bound virus. However, given that a clear increase in UUKV M RNA was seen in BSR and ISE6 cells, we can be confident that the lack of any evidence for internalisation of UUKV is biologically significant.

In conclusion, BSR and ISE6 cells showed similar binding affinities for wt rUUKV, although the speed of internalisation may have been slower in infected ISE6 cell cultures. It will be interesting to determine how these affinities and internalisation kinetics relate to the mechanism for infection of UUKV in vector cells, but for that to occur the receptors responsible for allowing UUKV infection in ISE6 cells must be elucidated. It was first hypothesised that if UUKV was capable of binding AF5 cells, this binding would be passive and transient. Unexpectedly, the results showing UUKV can not only bind to AF5 cells, but this binding seemed to be minimally affected by mechanical washing, indicating specific and strong attachment (Figure 5.18 and 5.19). Additionally, the fluorescence data obtained for infected-AF5 cell cultures indicated a similar amount of bound viral particles per cell to that seen in the ISE6 samples. The data suggests that although UUKV is capable of effectively binding to AF5 cells, the virus is unable to trigger internalisation into the mosquito cells. I hypothesise this may be through the mosquito cells lacking key cellular receptors, or UUKV being unable to bind these receptors in a manner which would lead to the conformational changes needed to trigger internalisation.

Future work in this area would benefit from not just the elucidation of the tick receptors responsible for internalisation, but also a more detailed examination of the binding of UUKV to mosquito cells through the application of electron microscopy or similar techniques to identify the structures involved in this binding. In addition, the use of reverse genetic systems to produce either virus-like particles or virions with 'mix and match' properties, for example the RNP of UUKV packaged with the glycoproteins of a mosquito-borne bunyavirus, would allow for investigation into whether this barrier to infection can be overcome and if any further blockages occur once the viral genetic material is internalised.

The aim of this research chapter was to define the viral growth kinetics of UUKV across BSR, ISE6 and AF5 cell lines, comparing against the mosquito-borne virus BUNV, to confirm that UUKV was 'tick-borne' and incapable of replicating within mosquito cell culture. UUKV and other tick-borne viruses are highly understudied in their vector cell lines due to the difficulties of working with tick cells and the lack of genetic tools and knowledge available. There are clear differences in the growth kinetics of UUKV in tick and mammalian cell lines, which may be due in part to the speed of cell cycle replication between the two cultures, and to substantiate this hypothesis it would be useful to further investigate the effect of cell cycle on the growth kinetics of UUKV.

We also aimed to determine where the first block in replication occurs during UUKV infection of mosquito cells. The previous hypothesis was that UUKV lacked the ability to

bind to mosquito cell surface receptors, therefore preventing infection. This work has shown that not only does UUKV have the ability to bind mosquito cells, but that this binding appears to be strong and able to be disrupted through trypsin incubation. However, despite this binding, after allowing for incubation of the virus with mosquito cells before removing surface-associated virus through trypsin incubation no increase in internalised UUKV M RNA was detected. Additionally, a decrease in both the fluorescence intensity and total cellular UUKV M RNA was observed during increasing wash numbers. Therefore, the data suggests the first block in infection of the mosquito cells appears to be at the step of internalisation, with UUKV failing to trigger internalisation into mosquito cells over the one-hour adsorption period. To further strengthen this model, and to better clarify the mechanisms involved in tick cell binding and internalisation, future studies should include determining the structures involved in UUKV binding to various arthropod cell lines and identification of the cell surface receptors responsible.

Chapter 6 Defining the first tick cell line derived RBPome

6.1 Introduction

RNA binding proteins (RBPs) are crucial for cell biology, interacting with both protein coding mRNAs and non-coding RNAs (ncRNAs) to mediate or regulate their lifecycle and functions, including synthesis, processing, stability, transport, storage, translation, decay and antiviral immunity. Within arthropods, particularly ticks, the scope of RBPs remains largely unknown, despite cellular RNA-binding proteins (RBPs) having emerged as key regulators of virus infection in mammals and vectors (e.g. DICER2). Previous investigations into whole cell and immunoprecipitation proteomics, transcriptomic and genomic analysis of tick-derived cell lines have already been undertaken by several groups. However, no work has been conducted into understanding what interactions occur between the tick cell RNAs and proteins that maintain intracellular homeostasis and respond to environmental and pathological cues. My goal was to investigate the landscape of RBPs, the RNA-binding proteome (RBPome), using a state-of-the-art proteome-wide technique in order to begin mapping the function of these proteins. Following this, I would then use the establishment of this tick-derived cell line RBPome as the foundation to explore the impact of RBPs during infection (Glisovic, Bachorik, Yong, & Dreyfuss, 2008; Matera, Terns, & Terns, 2007). The importance of RBPs in the context of infection will be expanded upon in the following chapter, but in brief, the limited coding capacity of viral genomes enable the production of only a handful of proteins able to interact with RNA. However, RNA metabolic processes often involve large complexes (e.g. ribosome and spliceosome can consist of complexes containing over 100 proteins) and a plethora of molecular functions, making viruses reliant of host cell RBPs to replicate, express their proteins and package their genomes, while making viral transcripts stable in the hostile intracellular environment (Fatica & Tollervey, 2002; Wahl, Will, & Luhrmann, 2009).

Here, I will focus on the RBPs that interact with cellular mRNAs and other poly(A) RNA, however, many of these mRNA-binding proteins have been shown to play critical roles in infection of human cells. RBPs are capable of binding RNA through interactions with specific protein modules, termed RNA binding domains (RBDs). Globally speaking, RBPs are biochemically distinct from other proteins groups, having predominantly a higher isoelectric point (pI) due to the presence of positively charged residues that interact with the phosphate backbone of the RNA, and a low hydrophobicity (HI), compared to the average of the proteome (Castello et al., 2012). In addition, RBPs are often enriched in intrinsic disorder when compared to the whole proteome, and these regions may serve multiple purposes including allowing for putative interactions with DNA, acting as linker regions to coordinate multiple domains, and undergoing disordered-to-ordered transitions upon

interaction with other cellular factors in order to promote specific RNA binding (Calabretta & Richard, 2015; Ottoz & Berchowitz, 2020; Zhao et al., 2021). Through combining multiple RBD types and linker regions, RBPs increase their versatility of RBPs in terms of affinity and specificity, creating architectures that range from low to high selectivity and binding avidity. (Lunde, Moore, & Varani, 2007).

There are two overarching categories of RBDs: conventional and non-conventional. Conventional RBPs bind to RNA through specific, structurally well-defined RBDs such as the RNA recognition motif (RRM), DEAD box helicase, hnRNP, K homology (KH), and zinc finger domains, amongst others. Many RBPs contain multiple RBDs resulting in a modular protein architecture often leading to increased affinity and specificity (Y. Chen & Varani, 2005; Cléry & Allain, 2013; Hentze, Castello, Schwarzl, & Preiss, 2018). Initially, *in vitro* methods were used to discover RNA-RBP interactions, focusing on singular RBPs and target RNAs in an electrophoretic mobility shift assay (EMSA), or through using *in vitro* transcribed RNA as 'bait' in RNA capture-based enrichment. These methods, although informative, were insufficient to provide a more complete and physiologically relevant RBPome. They lacked spatial resolution due to cell lysis, and were prone to false positives because of RNA probe misfolding and the inability to distinguish between direct and indirect protein binding or nonphysiologically relevant binding. To overcome this bias, Castello and colleagues developed a novel method for capturing RBPs using UV crosslinking and oligo(dT) capture (Baltz et al., 2012; Castello et al., 2012; Castello et al., 2016; Castello et al., 2017; Castello et al., 2013; Iselin et al., 2022; Perez-Perri et al., 2021). This method, termed RNA interactome capture (RIC), “rediscovered” the compendium of classic RBPs known to interact with RNA, while discovering hundreds of novel non-conventional RBPs that do not rely on the commonly known RBDs to interact with RNA (Castello et al., 2012; Castello et al., 2013).

RIC uses UV light at a wavelength of 254 nm to immobilise RNA-protein interactions within cells by inducing covalent bonds between the RNA and proteins within a distance of <2 Å. Exposure to this UV radiation does not cause detectable protein-protein crosslinking or break phosphodiester bonds (Brimacombe, Stiege, Kyriatsoulis, & Maly, 1988; Castello et al., 2012; Castello et al., 2013; Greenberg, 1979; Perez-Perri et al., 2021). Once the RNA-protein interactions are 'frozen', cells can be lysed under denaturing conditions and poly(A) RNA (and any RBP crosslinked to it) is isolated using oligo(dT) magnetic beads. These beads have poly-deoxythymine tails attached to them that base pair with the poly-A tails that are present in nearly all cellular mRNAs. After denaturing washes, elution of protein-RNA complexes is performed, combining heat and either proteinase K (to isolate RNA) or RNase treatment

(to isolate RBPs) (Castello et al., 2012; Castello et al., 2013; Perez-Perri et al., 2021). The downstream steps employ quantitative proteomic analysis to identify comprehensively and systematically RBPs bound to poly(A) RNA. This method has several advantages, the use of oligo(dT) magnetic beads allows for stringent washing and depletion of highly abundant non-poly(A) RNAs (e.g., ribosomal RNA (rRNA) and transfer RNA (tRNA)) as well as proteins that do not interact with RNA, allowing for the stringent detection of RBPs. This protocol is adaptable to different experimental conditions, including both a variety of cell culture types or whole organisms, and viruses. In the context of this research, this technique is used on both naïve (Chapter 6) and UUKV-infected ISE6 cell cultures (Chapter 7). However, it is important to note that there are also drawbacks to this method. RBPs which are important to intracellular homeostasis or infection but bind to non- poly(A) RNA, or RBPs which undergo stochastic short-lived binding cycles with mRNA will not be identified due to low isolation or crosslinking (Castello et al., 2013; Perez-Perri et al., 2021).

The efforts within the RBPome field have allowed the production of an RBPome database 'RBP2GO' (Caudron-Herger, Jansen, Wassmer, & Diederichs, 2021), which collates all RIC data sets together alongside datasets generated through other approaches, for species such as *Homo sapiens* (Castello et al., 2012; Caudron-Herger et al., 2019), *Mus musculus* (Boucas et al., 2015; Kwon et al., 2013), and *Danio rerio* (Du et al., 2020). At the time of writing, the RBP2GO database contains 22,552 RBP candidates with different degrees of evidence across 13 species, although it is important to note that due to these candidates being detected through various techniques the level of filtering and validation is not consistent. The species are listed in the table below (Table 6.1), and 12 out of 13 of these species contain RBPomes using RIC, with the only species lacking RIC datasets being *Salmonella typhimurium* as there have been no studies where the RBPs have been identified under poly(A) enrichment (Caudron-Herger et al., 2021). However, despite these advances, the RBPome of ticks still remains unexplored.

To begin elucidating the RBPome of ticks and functionally mapping the RBPs, the ISE6 cell line was chosen to carry out all RIC experimentation within this thesis. This cell line was chosen due to the level of detail that is known about the cell line and *I. scapularis* organism (from which this cell line is derived), and the ease with which ISE6 cell cultures can be manipulated. The ISE6 cell line is used for both investigations into the biology of ticks and host-pathogen-vector interactions, alongside having a mapped and annotated genome to allow for interpretation of experimental RIC data. This genome, importantly, also facilitates the ability to do host subtraction, and homology analysis (Bell-Sakyi, Kohl, Bente, & Fazakerley, 2012; Cramaro et al., 2017; Miller et al., 2018). In addition, this cell line has

been shown to be permissive for both transfection and genetic manipulation (Kurtti et al., 2008).

Species	Common Name	Number of RBP Candidates	Number of RBP candidates via poly(A) enrichment
Homo sapiens	Human	6100	861
Mus Musculus	Mouse	2897	840
Danio rerio	Zebra fish	311	227
Drosophila melanogaster	Common fruit fly	2982	152
Caenorhabditis elegans	Roundworm	1873	1347
Saccharomyces cerevisiae	Brewer's yeast	2155	213
Arabidopsis thaliana	Thale cress	2352	1808
Trypanosoma brucei	Sleeping sickness parasite	169	155
Leishmania donovani	Black fever parasite	79	79
Leishmania mexicana	Braziliensis parasite	1162	1162
Plasmodium falciparum	Malaria parasite	1030	20
Salmonella typhimurium	*Salmonella sp.* bacteria	226	N/A
Escherichia coli	*E. coli* bacteria	1216	1182

Table 6.1: A summary of the number of RBP candidates for each species available in RBP2GO. The table displays the number of each species, alongside the common name for the species, number of RBP candidates and the number of candidates associated with poly(A) enrichment (Caudron-Herger et al., 2021).

6.2 Aims

The aims of the research presented in this chapter were to:

- **Optimise RIC protocol for use in cell lines derived from *Ixodes scapularis* (ISE6).** The RBPomes of several species have been investigated and defined through prior studies, most recently through methodology utilising UV crosslinking and oligo(dT) capture established by the Castello lab (Castello et al., 2012; Castello et al., 2013; Perez-Perri et al., 2021). In contrast, no work has been done to define the RBPome within any tick species or tick cell line. This research aims to optimise the RIC methodology for further investigations into the ISE6 RBPome.
- **Elucidate the RBPome of ISE6 cell cultures.** Upon establishment of an optimised RIC methodology, I aim to use this technique to define the RBPome of ISE6 cells as a foundation for UUKV infection studies. This will be the first time the RBPome of a naive tick cell culture will be established.

6.3 Results

6.3.1 Adaptation of UV crosslinking and oligo(dT) capture in ISE6 cell culture.

In order to determine the optimal UV dosage (mJ/cm^2) for crosslinking of ISE6 cellular RNA and proteins, cell monolayers of ISE6 cells were exposed to varying levels of UV radiation. The minimum dose being 150 mJ/cm^2 (the dose typically used in human cells), increasing in increments of 50 mJ/cm^2 to 400 mJ/cm^2, with an additional monolayer being mock-irradiated as a control. Following UV exposure, cell monolayers were immediately lysed with denaturing buffer and prepared for RIC. The input and eluate samples were resolved and visualised using polyacrylamide gel electrophoresis, followed by silver staining. No differences in banding patterns were detected between the input samples from each biological replicate. Conversely, no protein was detected in the mock-irradiated (0 mJ/cm^2) samples after elution indicating no proteins were present within these samples to a level detectable by silver staining. The banding pattern of the irradiated eluates was specific and distinctive from the respective inputs, implying this protocol had effectively and specifically enriched a protein subpopulation, whose banding pattern composition was compatible with RBPs (Beckmann et al., 2015; Castello et al., 2012; Kwon et al., 2013). Further, no difference in banding pattern was seen among the UV exposed eluates, although the bands appeared darker at the lower dosages, indicating that higher UV dosage may trigger RNA/protein degradation or cell membrane damage in ISE6 cells, reducing the RIC output (Figure 6.1.A).

Irradiated input and eluate samples were also prepared for western blot and probed for α-tubulin – an abundant intracellular protein that forms dynamic microtubules within cells and plays a key role in cell structure, intracellular transport, and cell division. As such, α-tubulin has been shown not to interact with RNA and be extracted during RIC (Binarova & Tuszynski, 2019; Castello et al., 2012). Therefore, α-tubulin can be considered a negative control. α-tubulin was present within all irradiated input samples as expected as these samples correspond to the whole cell lysate, although the band appeared to become less intense as the UV dosage increased suggesting potential protein damage or, as mentioned previously, a cellular response to the UV. No α-tubulin was detected in any of the crosslinked eluate samples, supporting the specificity of RIC (Figure 6.1.B). As a result of these optimisation experiments, 150mJ/cm^2 was chosen as the dosage for all further UV-crosslinking in ISE6 cell cultures. This dosage was chosen as it had previously been applied successfully to the RIC of mammalian cell cultures, and as the silver stain and western blot

results (Figure 6.1) indicated that this dosage allowed for the strongest enrichment of ISE6 RBPs with the minimal level of protein degradation or cellular distress before cellular lysis.

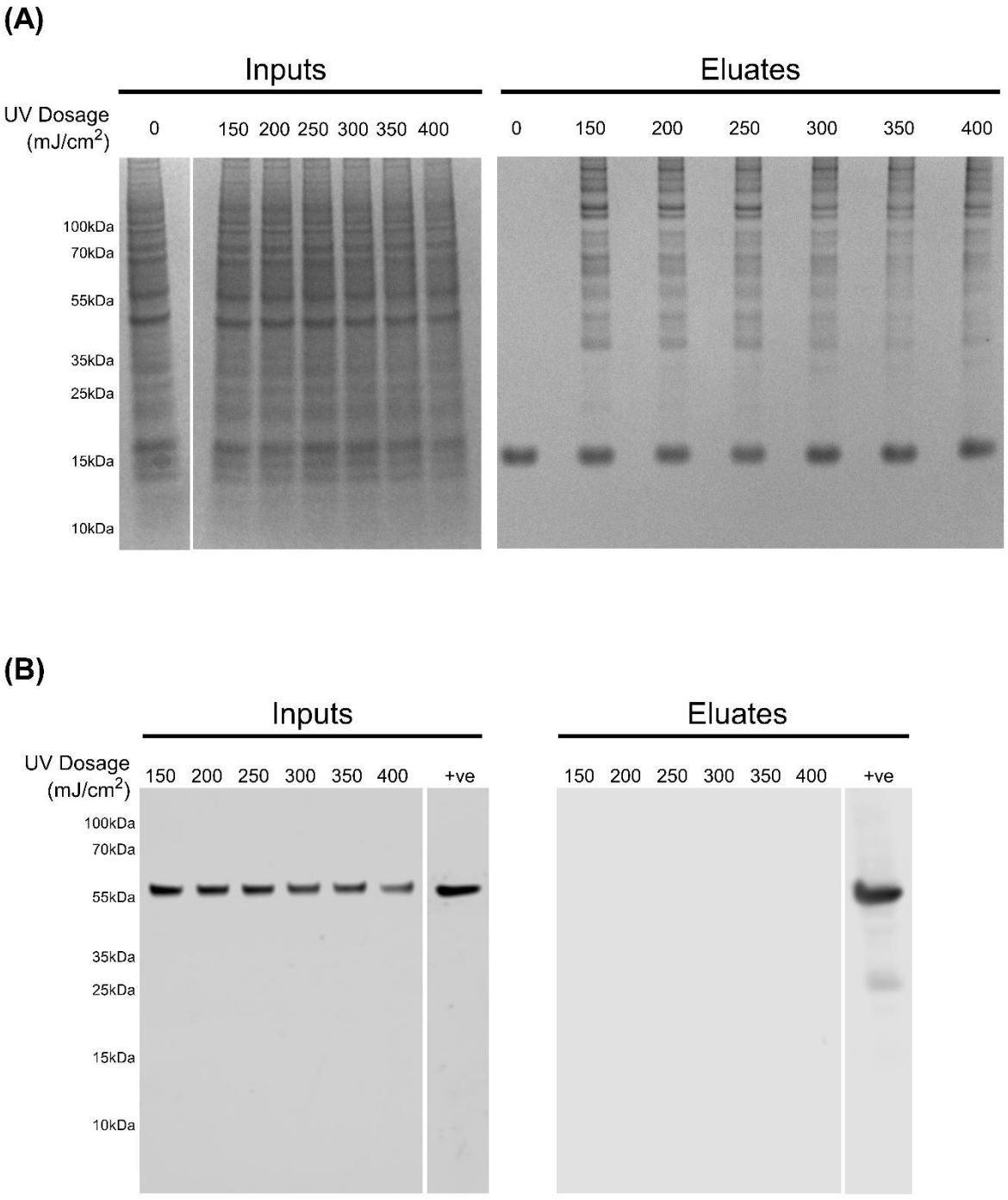

Figure 6.1: Optimising UV dosage for preliminary RNA interactome capture (RIC) in the ISE6 cell line. ISE6 cell monolayers were exposed to the indicated dosage of UV radiation (mJ/cm^2) or mock-irradiated, before lysis. (A) Input samples were extracted, and cell lysates prepared for RIC using oligo(dT) capture beads. Whole cell lysates from either before (input) or after (eluate) RNA capture were separated by SDS PAGE and resolved proteins were visualised using silver staining. (B) To ensure only RNA-binding proteins were captured, input and eluate samples were also prepared for western blotting and reacted with an anti-tubulin antibody. ISE6 whole cell lysate was used as a positive control (+ve).

Prototype RIC samples for UV-crosslinked and mock-irradiated ISE6 cell monolayers were generated for mass-spectrometry. ISE6 cell monolayers were exposed to 150mJ/cm^2 UV irradiation or mock-exposed. After UV exposure, cell monolayers were immediately lysed and prepared using the established RIC protocol. Two consecutive rounds of RIC were performed on the same input sample using the oligo(dT) capture beads to ensure maximal depletion of poly(A) RNA. The input and eluate samples were then resolved and visualised using PAGE and silver staining. No differences in banding patterns were detected between the crosslinked and non-crosslinked input samples, which was observed previously in the UV dosage optimisation experiment. Additionally, no protein was observed in the mock-exposed (0 mJ/cm^2) eluates, reinforcing the UV dependence of RIC. Again, a specific banding pattern was detected when UV was applied to the cultures. However, these bands were only visible in the first RIC cycle, suggesting that one cycle was sufficient to fully deplete the poly(A) RNA from the input lysates. For all further RIC experiments, only one cycle was carried out as no contribution to the proteomics results was expected from the second cycle (Figure 6.2.A).

These samples were processed for proteomics using the bead-based single-pot, solid-phase-enhanced sample-preparation (SP3) method (Hughes et al., 2019), which is more sensitive that standard approaches, and mass-spectrometry was carried out at the Rosalind Franklin Institute in collaboration with Prof. Shabaz Mohammed. The mass-spectrometry outputs were processed through MaxQuant software using FASTA files derived from the ISE6 cell line genome as a background. This enabled identifying peptides, assigning intensities and compile the qualitative and quantitative information to the protein level (Figure 6.2.B). Known contaminants identified by MaxQuant analysis were filtered from the data set. In total, 934 proteins were identified, with 54 proteins being exclusively found in non-irradiated samples and 680 proteins being enriched in UV-crosslinked samples (Figure 6.2.C). The results from this pilot experiment showed that UV-crosslinking strongly increased protein recovery upon oligo(dT) capture, making RIC suitable for establishing the RBPome of ISE6 cell cultures.

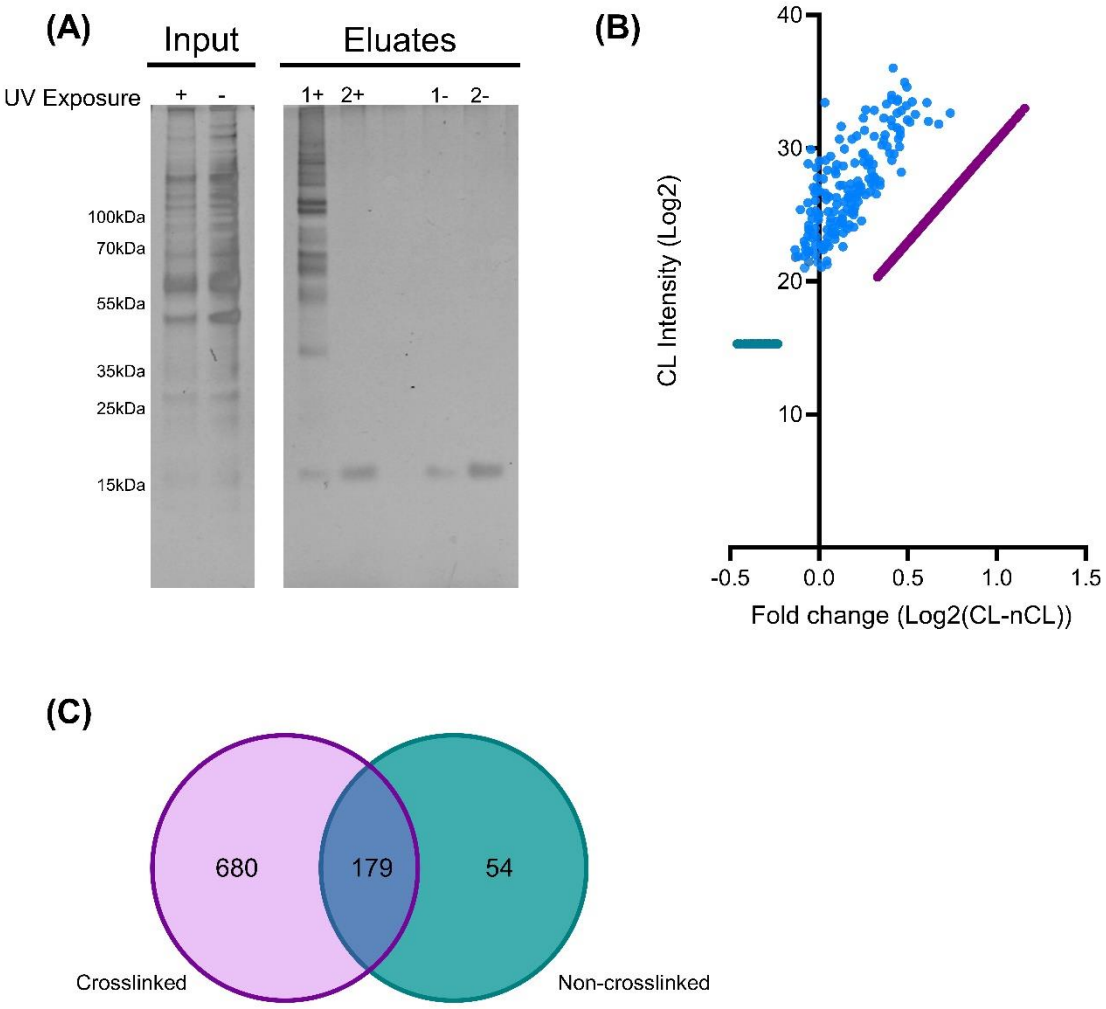

Figure 6.2: Analysis of preliminary RIC experiment conducted in the ISE6 cell line. ISE6 cell monolayers were exposed to 150mJ/cm^2 or mock irradiated before lysis. Input samples were extracted and cell lysates were prepared for RNA interactome capture (RIC) using oligo(dT) capture beads. Two rounds of RIC were conducted, therefore producing two eluate samples per crosslinking condition as indicated by the 1 and 2 in the eluate channels. (A) Whole cell lysates from either before (input) or after (eluate) RNA capture were separated by SDS PAGE and resolved proteins were visualised using silver staining. (B) The first round of UV-exposed and mock exposed eluates were prepared by utilising a SP3 protocol in preparation for liquid-chromatography mass spectrometry (LC-MS). The mass-spectrometry outputs were processed through MaxQuant. The Log2 intensity of the UV-exposed crosslinked (CL) sample was plotted against the intensity fold change of the Log2 intensity values of the UV-exposed crosslinked (CL) and non-crosslinked (NCL) samples. (C) Venn diagram comparing the number of proteins identified in the CL vs NCL experiment.

6.3.2 Sample preparation and quality assessment of mass-spectrometry for UV crosslinking and oligo(dT) capture in ISE6 cell monolayers.

To generate samples for mass spectrometry and for the establishment of the ISE6 RBPome, non-crosslinked and UV-crosslinked ISE6 samples were prepared in triplicate following the same protocol used to prepare the prototype. Small fractions of all inputs and eluates were taken and stored for protein and RNA analysis. As this work was done in tandem with a UUKV infection study, which will be expanded upon in the next chapter, ISE6 cell cultures were seeded and incubated for 9 days before UV exposure. All samples pertaining to the work described in this chapter are labelled 'Mock' to allow for differentiation between naïve and infected cell cultures in later chapters.

When analysing the triplicate samples, no differences in protein banding patterns were detected between the UV-crosslinked replicates, showing high reproducibility. Non-irradiated samples were depleted of proteins, and irradiated samples displayed a protein pattern that matched the previous experiments (Figure 6.3.A). For RNA analysis, the proteins present in the samples were degraded using proteinase K to release the RNA, which was subsequently analysed by RT qPCR using primers designed to target the tick cell 18S ribosomal RNA (rRNA) and ELF1A, and thus calculate, using the ΔΔCT method, the expression of 18S per sample normalised to ELF1A. The 18S is a highly abundant non-polyadenylated rRNA and so should be removed during the RIC procedure to enable the identification of proteins associated with less abundant RNAs such as mRNAs. ELF1A is a cellular poly(A) mRNA and should not be depleted substantially upon RIC oligo(dT) enrichment. As the aim of this method was to deplete abundant non-polyadenylated RNA, a minimum fold enrichment of >6 was required for samples to be suitable for mass spectrometry. All sample preparations met the minimum fold enrichment requirements, with NCL2 being the lowest recorded enrichment at 6.484 (Figure 6.3.B). Samples additionally showed some loss of total RNA between the inputs and eluates. However, this is most likely due to the loss of non-poly(A) transcripts (Figure 6.3.B). Samples were then prepared for proteomics by SP3 as described in Methods.

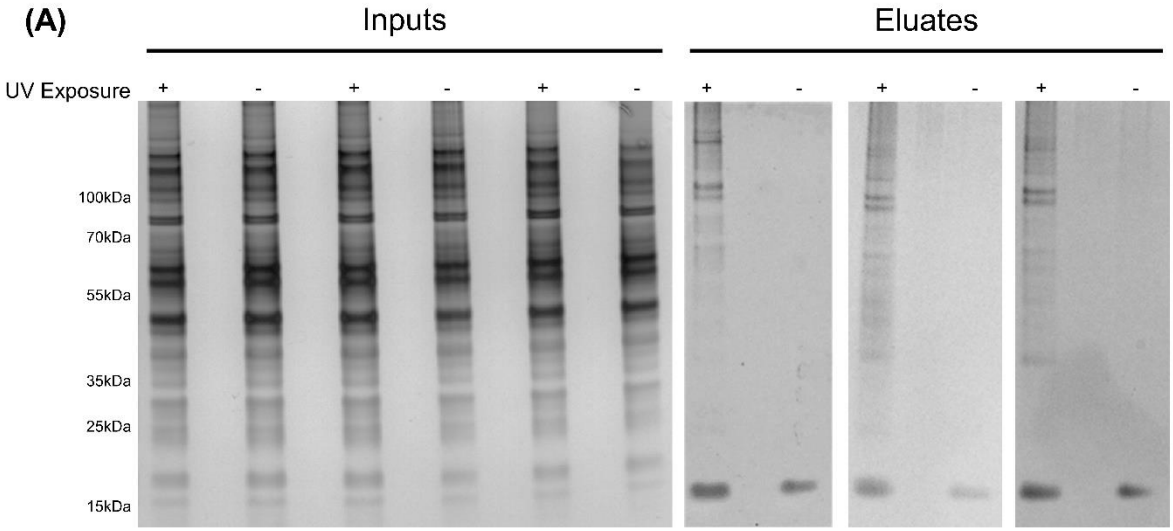

(B)

Sample	mRNA fold enrichment	Starting RNA quantity (ng/µl)	Eluted RNA quantity (ng/µl)
CL1	≥ 10	200.4	85
CL2	≥ 10	162.8	61.7
CL3	≥ 10	156.4	69.9
NCL 1	9.585	218.1	198.5
NCL 2	6.484	216.4	164.4
NCL 3	≥ 10	215.4	186.9

Figure 6.3: Preparation of triplicate RNA interactome capture (RIC) samples in the ISE6 cell line and validation for further mass spectrometry analysis. Preparations of ISE6 cell monolayers (in triplicate) were exposed to 150mJ/cm2 or mock irradiated before lysis. Input samples were extracted, and cell lysates were prepared for RNA interactome capture (RIC) using oligo(dT) capture beads. (A) Whole cell lysates from either before (input) or after (eluate) RNA capture were separated by SDS PAGE and resolved proteins were visualised using silver staining. (B) Prior to samples being prepared for gel electrophoresis, fractions of the input and eluate samples were processed through protein degradation to isolate the RNA in the three crosslinked (CL) and non-crosslinked (NCL) samples. RNA quantities in these samples were measured via a nanodrop spectrophotometer. RT qPCR was performed against tick cell 18S ribosomal RNA and eukaryotic elongation factor 1-alpha (ELF1A; mRNA used as a housekeeping gene). The ΔΔCT method was used to measure the quantity of 18S RNA normalised to ELF1A RNA levels, and the mRNA fold enrichment in the eluate compared to the input sample were calculated for each biological sample.

Before defining the ISE6 RBPome, the mass-spectrometry results were evaluated to determine the quality of the replicates for each condition. This evaluation involved i) plotting the protein intensities for each sample to compare the overall correlation across replicates and samples (Figure 6.4.A); ii) determining the incidence of missing values across samples (Figure 6.4.B); and iii) sample clustering by principal component analysis (PCA) (Figure 6.4.C). Firstly, the distribution of the Log2 intensity values of the proteins within each sample was plotted, as these intensity values allow for the examination of the relative abundance of proteins between the samples to test for consistency. The distribution of intensities for each of the replicates within each condition (i.e. crosslinked and non-crosslinked) showed no significant inter-replicate variation, supporting the robustness of the approach (Figure 6.4.A).The number of proteins where no intensity values were returned across each sample was used to determine the number of missing values. Overall, the non-irradiated samples contained ~3 times more missing values than the irradiated samples (Figure 6.4.B). Finally, PCA was used to examine the variability between the samples as described in Methods. Replicates for each condition grouped together in the PCA plot, and clear separation was observed between crosslinked and non-irradiated replicates. According to the analysis, ~85% of the variability was related to whether the sample was subjected to UV irradiation or not. This shows that one can use UV-dependent isolated proteins to determine the ISE6 RBPome (Figure 6.4.C).

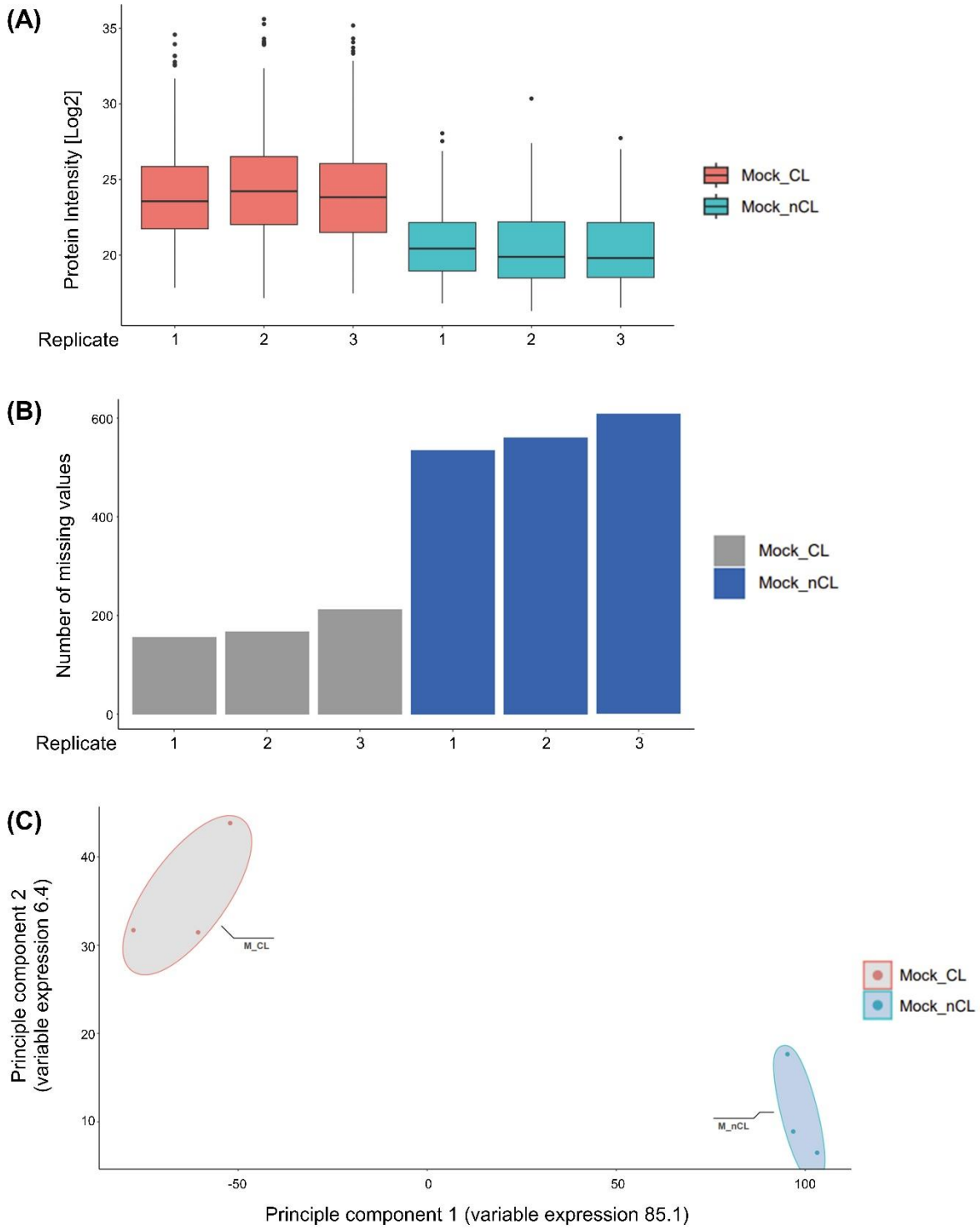

Figure 6.4: Diagnostics of mass spectrometry results from ISE6 RIC biological triplicates. Triplicate ISE6 cell monolayers were exposed to 150mJ/cm^2 UV-irradiation or mock irradiated prior to lysis. Input samples were extracted, and cell lysates were prepared for RNA interactome capture (RIC) using oligo(dT) capture beads. UV-exposed and mock exposed eluates were prepared by utilising a SP3 protocol in preparation for liquid-chromatography mass spectrometry (LC-MS). The mass spectrometry for this experiment was done alongside mass spectrometry of UUKV-infected ISE6 cell cultures also used for RIC assays (further described in chapter X). Therefore, for this current analysis the samples will be referred to as Mock (M). The mass-spectrometry outputs were

processed through MaxQuant to produce identified peptides with corresponding intensities for each sample, with potential contaminants subsequently removed. (A) The log2 intensity values for all proteins within the mock crosslinked (Mock_CL) and mock non-crosslinked (Mock_nCL) samples were plotted. (B) The number of unidentified proteins and missing values were plotted for the mock crosslinked (Mock_CL) and mock non-crosslinked (Mock_nCL) samples. (C) Principal component analysis (PCA) was carried out and plotted for the mock crosslinked (Mock_CL) and mock non-crosslinked (Mock_nCL) samples.

6.3.3 Defining the RBPome of ISE6 cells

Once quality control analysis of the proteomics output was completed, samples were deemed suitable to use in defining the ISE6 cell line RBPome. To do this, the CL/NCL fold change (FC) for each protein as well as its derived adjusted p-value (adj.P.val) were calculated. Proteins enriched with a false discovery rate (FDR) ≤ 10% and a FC ≤ 1 (where the adj.P.val of each protein within the grouping was ≤0.1 and ≤0.01, respectively) were classified as putative tick RBPs. Proteins which did not meet these criteria were discarded from further analysis. In total, 540 proteins were identified in the crosslinked samples, of which 495 proteins were significant to a FDR of 10% (coloured orange). For an additional stringency measure, proteins within the 1% FDR were also examined. A total of 450 proteins were within the 1% FDR (coloured red) and were considered "high confidence" RBPs (Figure 6.5.A). All subsequent analyses were performed using the 495 proteins from the 10% or below FDR group. The UUKV N protein was detected within the samples, labelled as NCAP (Figure 6.5.A). However, these peptides were only detected within one of the non-crosslinked and two of the crosslinked triplicates, and the intensity within these replicates was reduced ~10^6 compared to the infected samples. Therefore, this peptide assignment may have been due to an issue in matching between runs, where a peak signal was observed in the same ms/z position as NCAP causing this signal to be incorrectly assigned as NCAP. Additionally, through further testing of the silver stains and RT qPCR work when infected samples were analysed (Figures 6.3.A, 7.2.A, and 7.2.B), no N protein was visualised, and no viral RNA was detected within the non-infected cell lysates.

As the tick reference genome contains minimal information regarding protein names and functions, InParanoid analysis (E. Persson & Sonnhammer, 2022) was used to identify human orthologs to the RBP candidates through comparison of FASTA files containing the amino acid sequences of the proteins. Of the 495 proteins identified, approximately 66% were able to be matched to a human ortholog (Figure 6.5.B). Accordingly, when discussing individual genes and proteins, the human ortholog name will be used where possible.

As mentioned in the introduction, RBPs often display certain biochemical properties. Using the FASTA files for the putative tick RBPome, the hydrophobicity (HI) isoelectric point (pI) and percentage intrinsic disorder were calculated for each protein and plotted against the ISE6 whole cell proteome (Figure 6.5.C, 6.5.D and 6.5.E, respectively). The HI of the tick RBPome was slightly more negative than that of the whole RBPome, while the pI was overall higher. In addition, the proteome had multiple peaks within the pI plot, whereas the RBPome had a smoother curve and singular broader peak at the higher pI, indicating a more

homogeneous protein population regarding this biochemical feature. Finally, the proportion of intrinsic disorder regions was similar in magnitude in both mock RBPome and the whole proteome. Altogether, these results revealed that the tick RBPome was enriched in the known biochemical features of RBPs with the exception of intrinsic protein disorder (Calabretta & Richard, 2015; Ottoz & Berchowitz, 2020; Zhao et al., 2021). Protein disorder in RBPs expanded across evolution, being minimal in *Saccharomyces cerevisiae* and representing near 40% of the RBP length in humans (Beckmann et al., Nat Coms 2015). The lack of enrichment of protein disorder in tick RBPs may represent an early stage of protein evolution and diversification.

Once the biochemical properties of the 10% FDR RBP group were analysed, the next stage was to characterise the domains present within them, which will be referred to in all further writing as the “mock RBPome”.

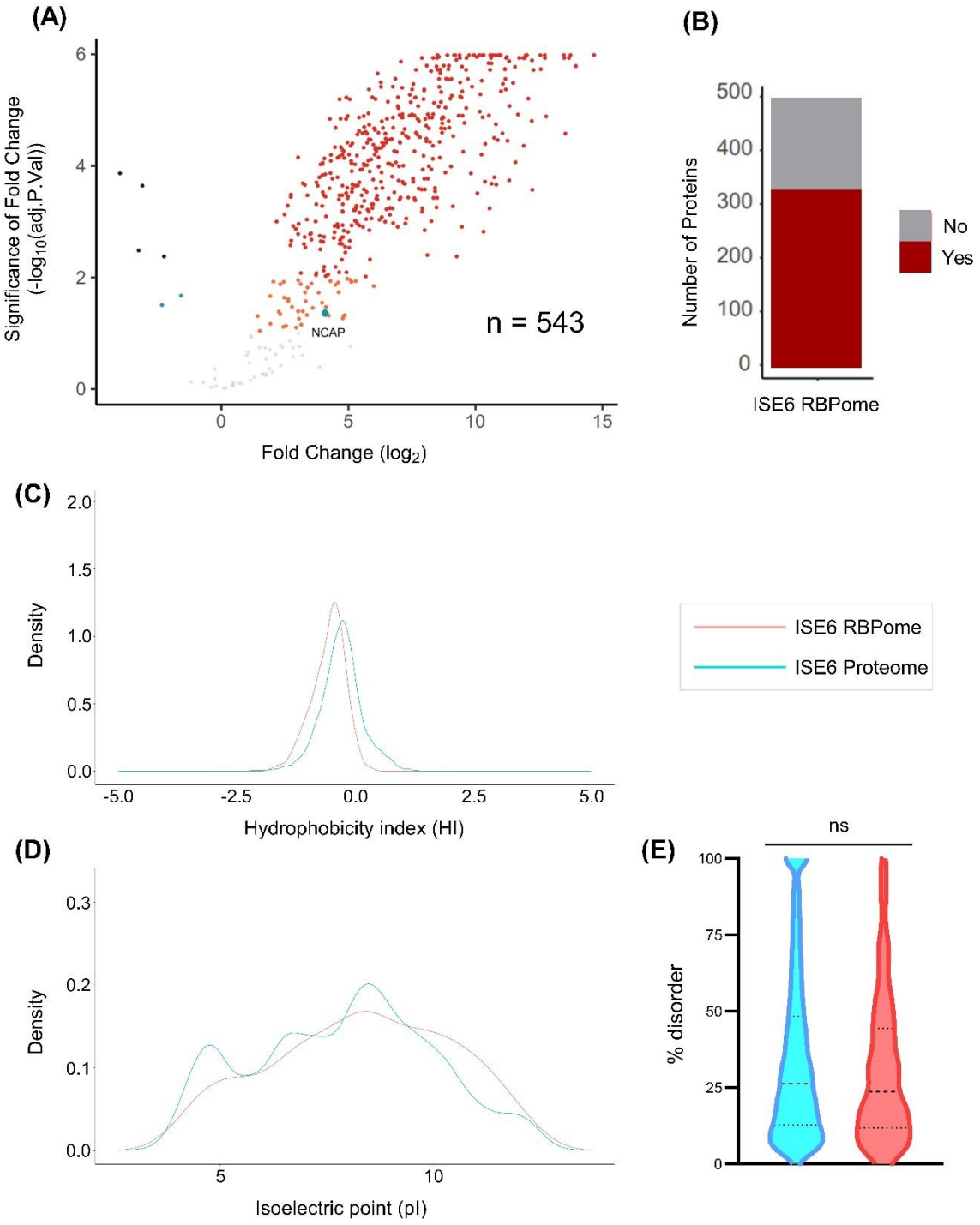

Figure 6.5: Analysis of ISE6 cell derived RNA Binding Proteome (RBPome). Analysis of samples prepared for mass spectrometry as described in Figure 6.4. Mass spectrometry of these samples was carried out alongside the mass spectrometry of UUKV-infected ISE6 cell cultures also used for RIC assays (further described in chapter 7). (A) The fold change of the proteins found in the mock crosslinked samples compared to the mock non-crosslinked (x axis) were plotted against the significance of this fold change (-log10(p value), y axis). Proteins with a FC >0 within the 1-10% false discovery rate group ($0.0001 > p > 0.001$) are labelled orange. Proteins within the 1% false discovery rate group ($p < 0.0001$) are labelled red. Proteins with a FC < 0 at a 1-10% false discovery rate - $0.0001 > p > 0.001$ (light blue), and proteins at a 1% false discovery rate - $p < 0.0001$ (dark

blue). Proteins within the 10% FDR group with a FC > 0 were used in further analysis (ISE6 RBPome). (B) InParanoid analysis was used to determine if the 10% FDR proteins had corresponding human orthologs (red) or no corresponding human orthologs (grey). The FASTA files for the 10% FDR proteins were then used to calculate the (C) hydrophobicity (D) isoelectric points of the proteins, and (E) % intrinsic disorder of the ISE6 RBPome (red), which were plotted using R and compared against the whole proteome (blue) derived from ISE6 cell cultures (whole proteome FASTA files were downloaded from VectorBase). This analysis was done through InterproScan MobiDB, and all proteins where 0% intrinsic disorder or those whose disorder were unable to be calculated were removed. Statistical significance in percentage disorder distribution was analysed using the non-parametric Kolmogorov-Smirnov test.

Analysis of the domains within the mock RBPome was carried out through Interpro scan. The FASTA files were scanned for any known protein domains, of which 81 proteins showed no identifiable domains within their sequence and were removed from further analysis. Of the proteins with identifiable domains, 229 (~55%) contained at least one domain that is a known RBD (Figure 6.6.A). It is important to note that even though the unknown protein group contains no recognised RBDs, this does not mean it contains no domains capable of interacting with and binding to RNA, as there is a growing list of non-canonical RNA-binding surfaces being discovered and characterised (Castello et al., 2016).

Protein RBDs are grouped into two broad classifications: classical RBDs and non-classical RBDs. The mock RBPome contained both classical and non-classical RBDs. The odds ratio of both domain types was substantially increased in the mock RBPome when compared to the whole cell proteome, and this difference was statistically significant (Figure 6.6.B). To further examine the different types of RBDs within these groups, the classical and non-classical RBDs can be grouped into overarching functional groups based on their protein family (pfam) IDs, which classify the protein sequences into families and domains. Only two of the functional groups in the classical RBD cohort, RNA binding motif and RNA recognition motif, displayed a significant increase in odds ratio, although zinc-finger containing family and RNA recognition motif 2 classical domain types and other known RBDs displayed a positive odd ratio. The lack of significance for these classical RBDs can be associated with the small group size and the poor annotation of the tick proteome (Figure 6.6.C). There are many more functional groups for non-classical RBDs with fewer pfam groups within each, due to their more recent classifications and less conserved functional domains. Due to this, there were many groups which had a significantly increased odds ratio when compared to the ISE6 background, and therefore for graphical plotting only functional groups with a statistically significant ($p<0.01$) odds ratio were plotted (Figure 6.6.D).

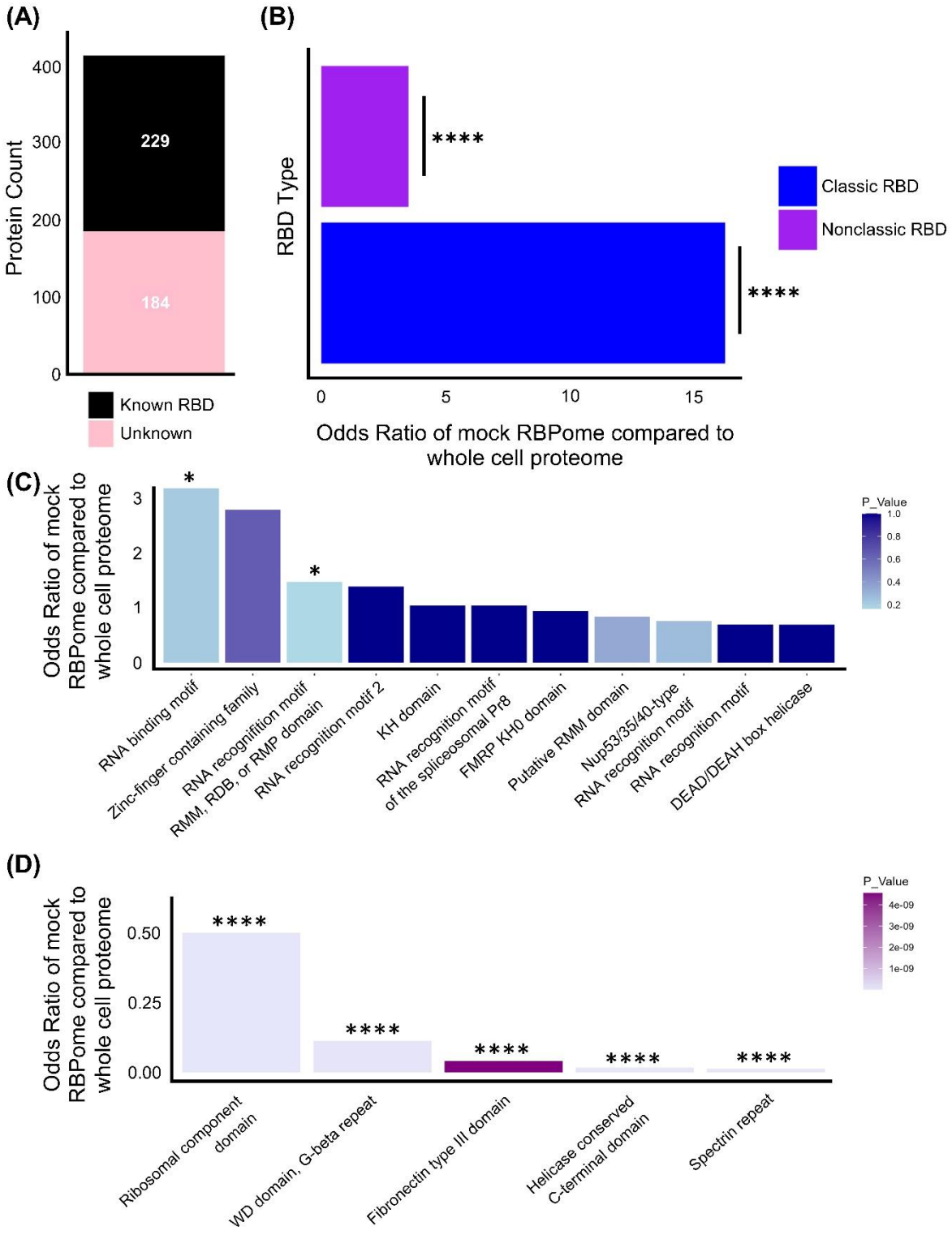

Figure 6.6: Analysis of ISE6 cell derived RNA Binding Proteome (RBPome) known RNA binding domains. The FASTA files of the proteins defined in the 10% FDR mock RBPome were analysed using Interpro scan to determine the protein domains present within the cells. Of which, 82 proteins from this group displayed no identifiable domains and were therefore removed from further analysis. (A) Using the established list of known RBDs, which includes both classical and nonclassical RBDs, the proteins were grouped based on whether they contained at least one known RBD (known RBD) or contained no known RBDs (unknown). (B) For the Known RBD group from

(A), the odds ratio and significance for a protein containing a classical or non-classical domain compared to the whole proteome proteins containing RBDs were calculated using Fisher's exact test. For proteins containing classical (C) and non-classical (D) domains, odds ratio and significance were calculated using Fisher's exact tests against the whole proteome proteins containing these respective domains. Results with an odds ratio < 0.01 were excluded for plotting. Statistical analysis was carried out using R. Asterisks indicates significance **** = $p < 0.01$, * = $p \leq 0.25$.

The subset group of proteins within the mock RBPome containing no known RBDs (Figure 6.5.A) were analysed to compare their biochemical properties against the whole proteome. Compared to the whole mock RBPome, the pI plot did not exhibit as higher an pI when the non-RBD containing group is isolated (Figure 6.7.A). In comparison, the HI curve shows the same trends as the whole mock RBPome, in that the proteins containing unknown domains have an overall more negative HI compared to the whole proteome. (Figure 6.7.B). Finally, the percentage of the intrinsic disorder of the proteins in the whole proteome, the mock RBPome, and the subset of the mock RBPome which contain unknown domains were plotted showing no difference as previously discussed (Figure 6.7.D).

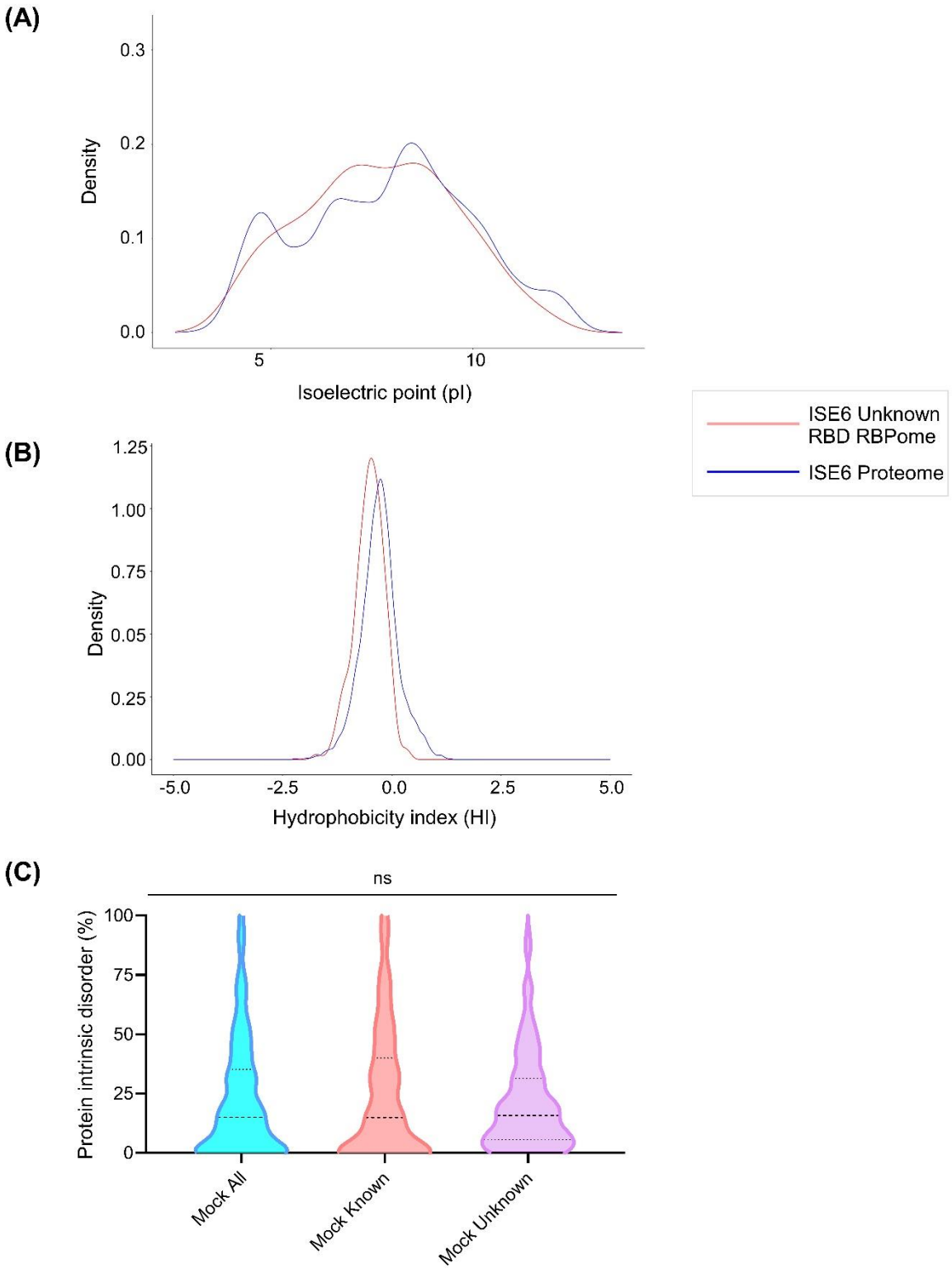

Figure 6.7: Analysis of ISE6 cell derived RNA Binding Proteome (RBPome) against proteins containing 'non-known' RNA binding domains. Proteins containing no known RBD domains from Figure 6.6.A were analysed to determine their (A) hydrophobicity and (B) isoelectric points. These were plotted using R and compared against the whole proteome derived from ISE6 cell cultures. (C) Protein intrinsic disorder was also calculated using MobiDB, comparing the whole

mock RBPome (blue), the mock RBPs with known RBDs (red), and the mock RBPs with no known RBDs (pink). From the data, 151 out of the 223 proteins with known RBDs and 154 out of 184 proteins with no known RBDs returned % intrinsic disorder scores, and therefore all results where no intrinsic order was returned were given a value of 0. A one-way ANOVA was used to determine statistical significance.

The analysis of the mock RBPome was then expanded to include gene ontology (GO) analysis using the tools available in VectorBase. This allows for exanimation of enrichment against the ISE6 genome and proteome background, with both computed and curated evidence inputted and a p-value cut-off of 0.05 (Amos et al., 2022). Overall, 241 biological processes were found to be enriched within the RBPome, with the most enriched expression being gene expression as seen in the word cloud (Figure 6.8.A). When focusing on the most enriched GO terms (Figure 6.8.A), I found that most of the processes were linked to mRNA, such as cleavage for processing or polyadenylation, processing, and splicing. To better visualise this, the fold enrichment of each GO term was plotted against its -Log2 p-value (from Figure 6.8.A), and 10 most significant pathways highlighted. These were: gene expression, translation, peptide biosynthesis, cellular nitrogen compound metabolism, peptide metabolism, cellular amide metabolism, cellular nitrogen compound biosynthesis, cellular macromolecule biosynthesis, and macromolecule biosynthesis, all of which refer to protein synthesis.

In conclusion, through this analysis, the mock RBPome of the ISE6 cells has been established. This is important for the vector community as we provide functional information to hundreds of cellular proteins that now can be annotated in VectorBase as RBPs. Moreover, the dataset provides a baseline for comparisons both within the ISE6 under different conditions, such as infection, but also for comparing with other species.

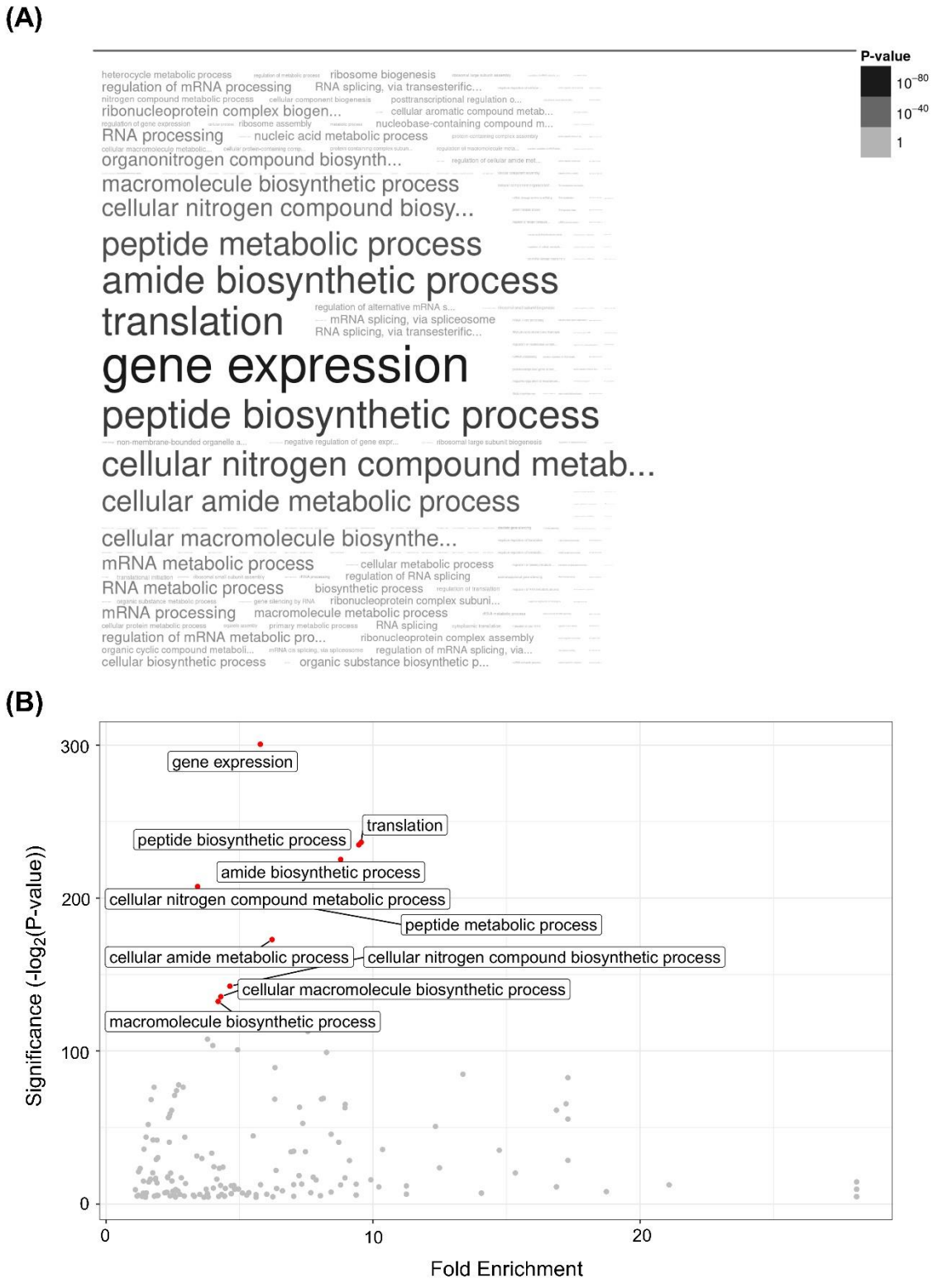

Figure 6.8: Analysis of biological processes enriched in the RBPome of ISE6 cell culture. The proteins from Figure 5 were analysed using the gene ontology (GO) enrichment analysis tools in VectorBase. (A) An analysis of the biological processes that the RBPome proteins are associated with. The word cloud demonstrates the most enriched processes compared to the background ISE6 proteome based on the associated p-value**.** (B) The biological processes that the identified proteins

from (A) are involved in were plotted against the fold enrichment of these processes. RIC samples compared to the background ISE6 proteome are shown on the x- axis and the significance plotted on the y-axis. The top ten most significant pathways are highlighted on the graph.

6.3.4 Comparison of ISE6 RBPome to other species and validation of potential antibodies for further analysis

Previous studies have established the RBPomes of several species (both eukaryotes and prokaryotes), including the human cell lines (mammalian), as shown in Table 6.1.A. By comparing the biochemical properties of the ISE6 mock RBPome to other species, it is possible to begin determining whether there are similarities between ISE6 and other organisms, allowing for further defining of the ISE6 RBPome. As more is elucidated about the mechanisms of RNPs within the ISE6 cell culture, it would also be useful to compare these with those of the other species and determine if there is any relationship between the biochemical properties and RBP mechanisms in future. Human orthologs were identified from the ISE6 proteins, and mouse anti-human α-tubulin antibody binds ISE6 α-tubulin. Hence, through analysis of sequences identified between orthologues, I can contribute to expanding the molecular toolkits available for ticks.

Next, the ISE6 RBPome and ISE6 whole proteome HI distribution were compared against that of poly(A) RBPomes and whole proteomes of relevant taxonomic species as shown in Figure 6.9 and described in Table 6.1. These data were obtained through RBP2GO (Caudron-Herger et al., 2021), which is an online repository that contains all published RBPome datasets generated by different methods. RBP2GO allows for the selection of proteins that interact with poly(A) RNA, therefore these datasets are more comparable to the ISE6 RBPome generated here. Most RBPomes exhibited lower HI profile than their respective proteome, reflecting the low incidence of membrane-associated proteins, with a few exceptions when this difference was subtle or non-existent such us for *E. coli* (Figure 6.9).

When comparing the pI profiles, I observed a general trend for RBPomes to be shifted to more basic values than the whole cell proteome, except for a few examples such as *D. melanogaster*, *A. thaliana* and, particularly, E. coli (Figure 6.9), E.coli exhibit a noticeable shift to acidic pIs for the RBPome that could be technical (adaptation of RIC to non-poly(A) RNAs required important modifications in the protocol) or biological as bacterial RBPs are expected to be an ancestor of or evolutionarily diverged from eukaryotic RBPs. The other datasets exhibiting unusual trends could be affected by technical or biological issues, as for example *D. melanogaster and A. thaliana* datasets include full embryo and leaves, respectively, while most of the other datasets focused on cell lines.

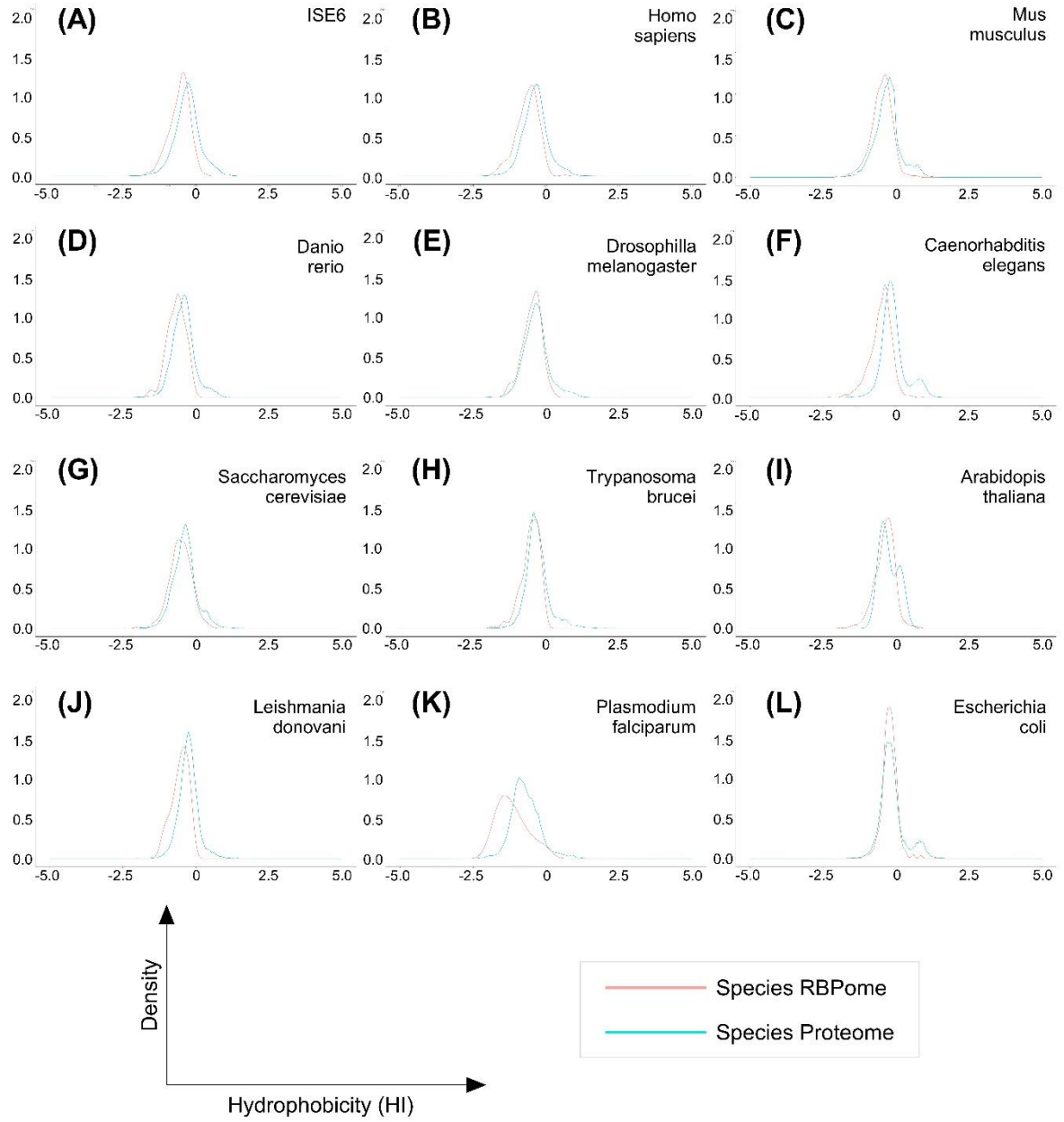

Figure 6.9: Comparison of the hydrophobicity points of the ISE6 RBPome alongside the background proteome with those of several other species. The FASTA files for the 10% FDR proteins were used to calculate the hydrophobicity (HI) value of the proteins, which were plotted in R against the whole ISE6 proteome (A). The RBPome of (B) *Homo sapiens*, (C) *Mus musculus*, (D) *Danio rerio*, (E) *Drosophila melanogaster*, (F) *Caenorhabditis elegans*, (G) *Saccharomyces cerevisiae*, (H) *Trypanosoma brucei*, (I) *Arabidopis thaliana*, (J) *Leishmania donovani*, (K) *Plasmodium falciparum*, and (L) *Escherichia coli* were also plotted for comparison. The Uniprot IDs for these species were obtained from the online database RBP2go, and RBPomes were selected for poly-A enrichment. ID mapping in Uniprot was used to acquire the species whole proteome and RBPome FASTS files.

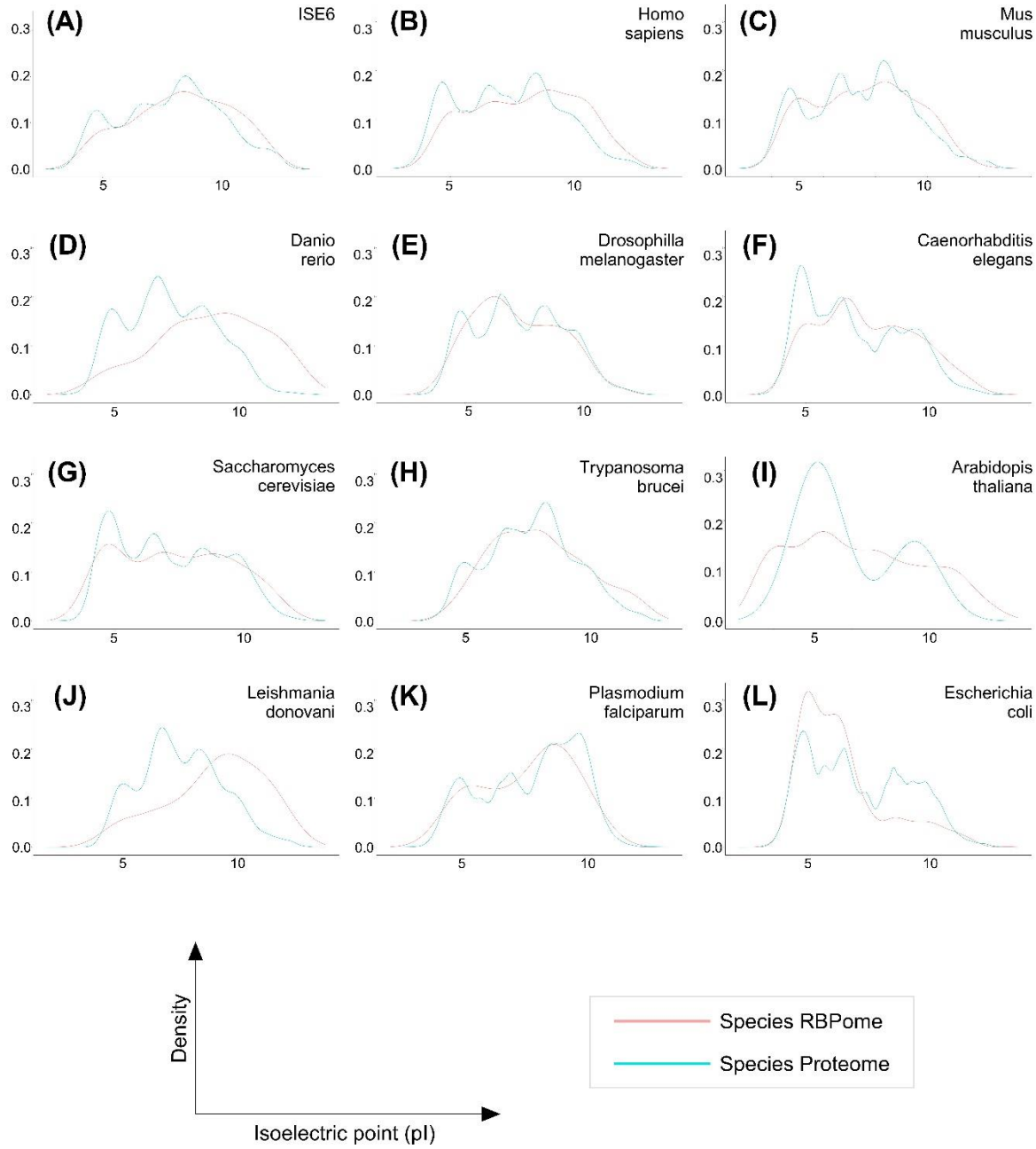

Figure 6.10: Comparison of the isoelectric points of the ISE6 RBPome alongside the background proteome with those of several other species. The FASTA files for the 10% FDR proteins were used to calculate the isoelectric point (pI) values of the proteins, which were plotted in R against the whole ISE6 proteome (A). The RBPome of (B) *Homo sapiens*, (C) *Mus musculus*, (D) *Danio rerio*, (E) *Drosophila melanogaster*, (F) *Caenorhabditis elegans*, (G) *Saccharomyces cerevisiae*, (H) *Trypanosoma brucei*, (I) *Arabidopis thaliana*, (J) *Leishmania donovani*, (K) *Plasmodium falciparum*, and (L) *Escherichia coli* were also plotted for comparison. The Uniprot IDs for these species were obtained from the online database RBP2go, and RBPomes were selected for poly-A enrichment. ID mapping in Uniprot was used to acquire the species whole proteome and RBPome FASTS files.

Finally, to begin expanding the potential downstream analysis for the tick RBPome through western blot validation, cell lysates were prepared from several tick cell lines: ISE6, BME/CTVM6, BME/CTVM 23 and IRE20, with the human derived A549 cell lysates acting as a positive control. As no tick-specific antibodies exist for these cell lines, or indeed any RBP, our collaborators in the Castello group kindly provided a selection of human anti-RBP antibodies, used in their studies, to probe the tick cell lysates (Figure 6.11). These were antibodies against the following proteins and their predicted kDa; DDX41 – 70 kDa (D), HMGB1 – 25 kDa (E), FUS – 70 kDa (F), A5027 – 109 kDa (G), PA2G4 – 44 kDa (H), DDX1 – 95 kDa (I), HNRNP1 – 40 kDa (J), MOV10 – 114 kDa (K), and PTBP1 – 65 kDa (L). Proteins within the cell lysates were visualised by staining with Coomassie (A). Western blots of the lysates were probed with anti-tubulin (positive control) (M), followed by anti-mouse secondary antibody or anti-rabbit secondary antibody (negative control) to show no non-specific binding occurred with the fluorescent probes.

Due to the presence of proteins with identifiable human orthologs within the ISE6 RBPome, it was theorised that the potential sequence similarity may allow for antibodies raised against human or mouse RBPs to bind tick RBPs. Unfortunately, no bands were seen at the predicted size for any of the anti-human RBP in any of the tick lysates. Additionally, due to the lack of labelling and mapping of proteins within the ISE6 genome we were unable to confirm the expected size of several of these proteins within the tick, and when an expected size was predicted no bands were observed at this size.

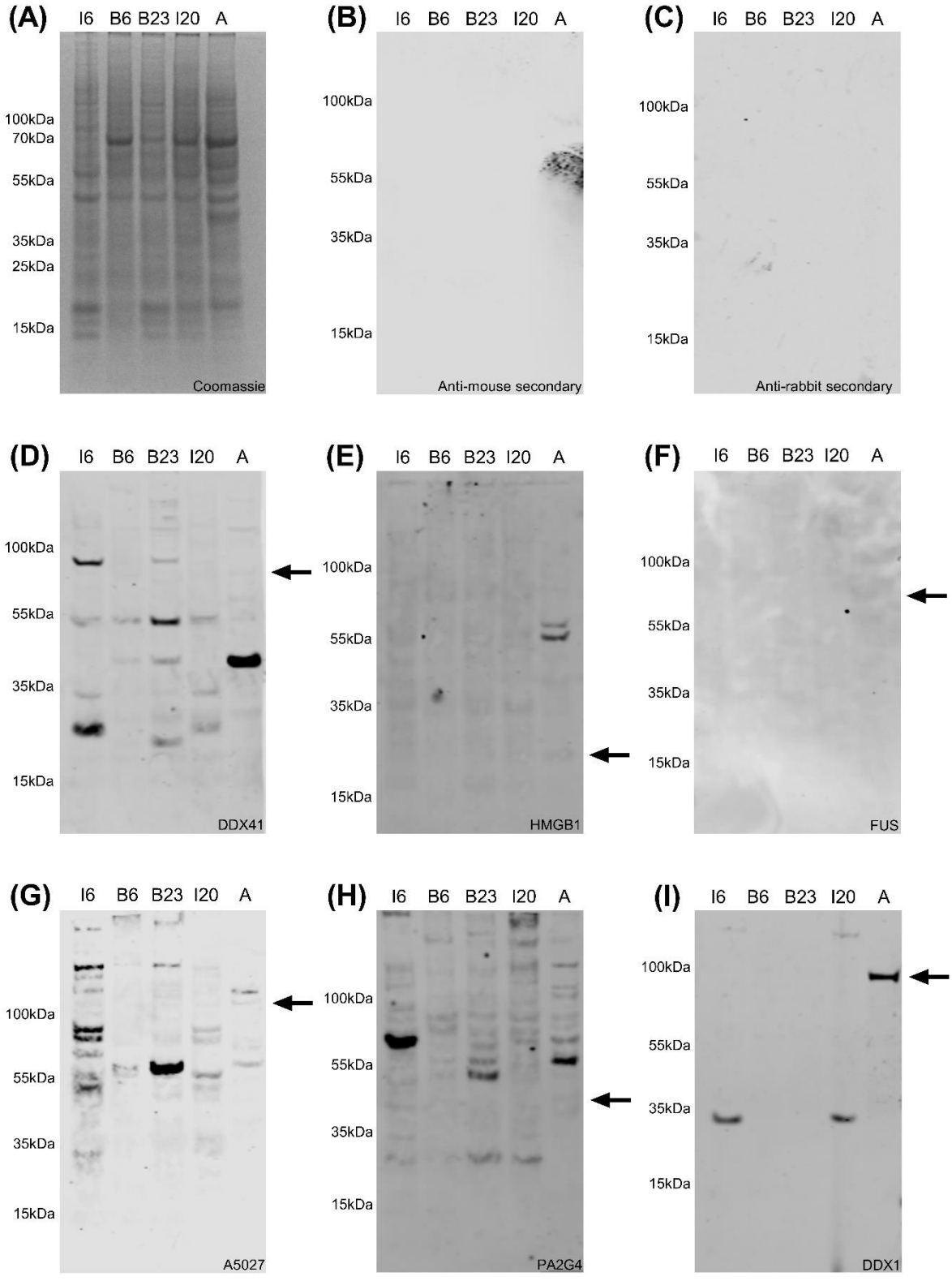
(A)
I6 B6 B23 I20 A
100kDa
70kDa
55kDa
35kDa
25kDa
15kDa
Coomassie
(B)
I6 B6 B23 I20 A
100kDa
55kDa
35kDa
15kDa
Anti-mouse secondary
(C)
I6 B6 B23 I20 A
100kDa
55kDa
35kDa
15kDa
Anti-rabbit secondary
(D)
I6 B6 B23 I20 A
100kDa
55kDa
35kDa
15kDa
DDX41
(E)
I6 B6 B23 I20 A
100kDa
55kDa
35kDa
15kDa
HMGB1
(F)
I6 B6 B23 I20 A
100kDa
55kDa
35kDa
15kDa
FUS
(G)
I6 B6 B23 I20 A
100kDa
55kDa
35kDa
15kDa
A5027
(H)
I6 B6 B23 I20 A
100kDa
55kDa
35kDa
15kDa
PA2G4
(I)
I6 B6 B23 I20 A
100kDa
55kDa
35kDa
15kDa
DDX1

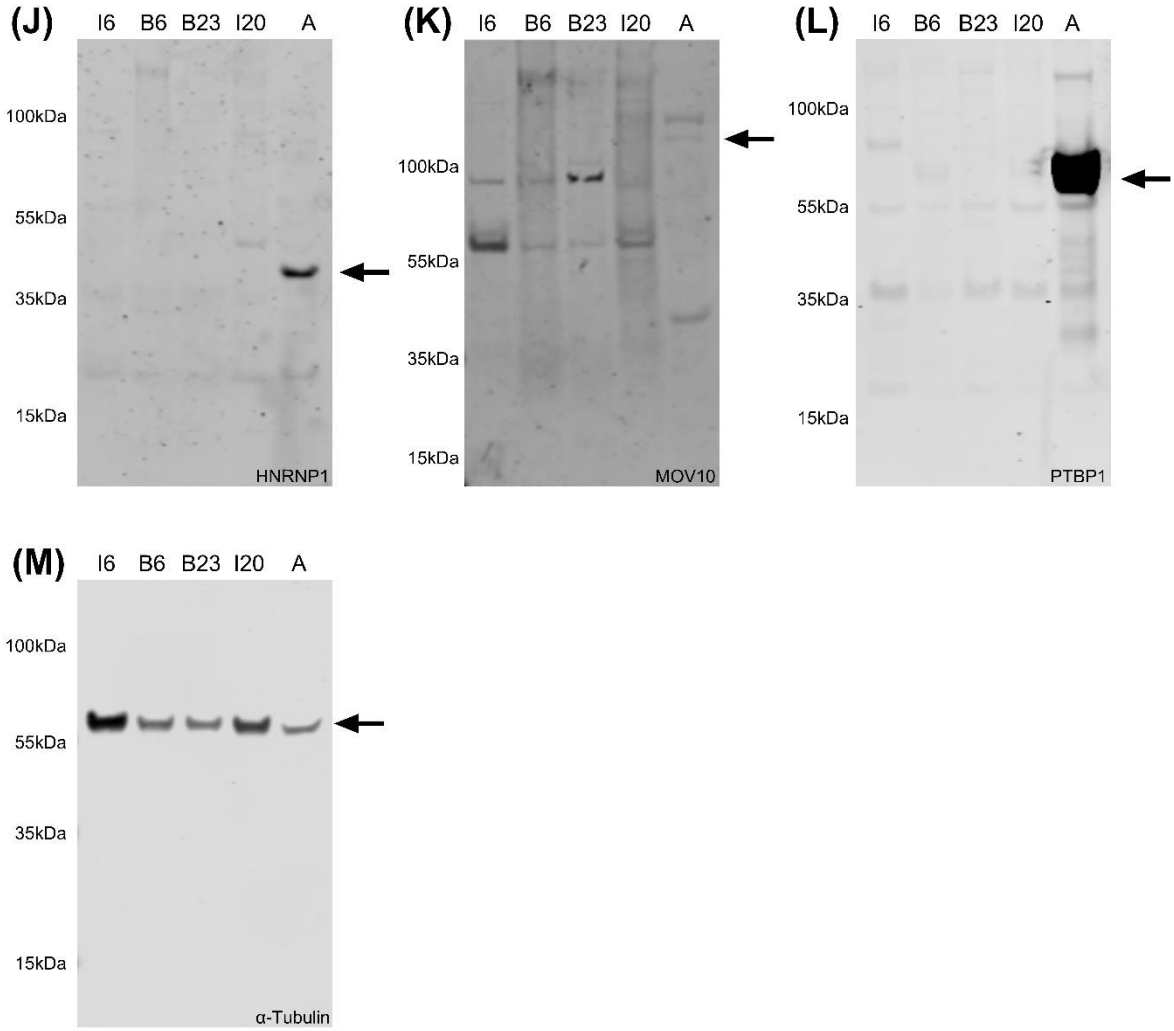

Figure 6.11: Testing anti-human RNA-binding protein antibodies against several tick cell derived whole cell lysates. Uninfected ISE6 [I6], BME6 [B6], BME23 [B23], and IRE20 [I20] tick cell line extracts were prepared for western blot analysis. A549 [A] cell extract was used as a positive control. (A) Whole cell lysates were separated by SDS PAGE and resolved proteins were visualised using Coomassie staining. Western blotting was conducted, and membranes were reacted with either fluorescent anti-mouse (B) or anti-rabbit (C) secondary antibodies as a negative control. Membranes were then probed with antibodies against DDX41 – 70 kDa (D), HMGB1 – 25 kDa (E), FUS – 70 kDa (F), A5027 – 109 kDa (G), PA2G4 – 44 kDa (H), DDX1 – 95 kDa (I), HNRNP1 – 40 kDa (J), MOV10 – 114 kDa (K), and PTBP1 – 65 kDa (L). Finally, cell lysates were probed with anti-tubulin antibodies as a positive control (M). Black arrows indicate the human protein size (kDa) as indicated in Uniprot.

6.4 Discussion

This work was carried out in close collaboration with the laboratory of Professor A. Castello at the University of Glasgow MRC - Centre for Virus Research, who developed RIC and have adapted it to different purposes and biological models. This method has been employed to investigate the RBPome of a variety of target cells and tissues from the species listed in table 6.1. These include: human cervical cancer (HeLa), hepatocytes, and myeloid leukaemia cells (Beckmann et al., 2015; Castello et al., 2012; Castello et al., 2016; Conrad et al., 2016), mouse macrophages, testes and embryonic stem cells (Du et al., 2020; Kwon et al., 2013; Liepelt et al., 2016), budding and fission yeast (Kilchert et al., 2020; Matia-Gonzalez, Jabre, & Gerber, 2021), drosophila embryos (Sysoev et al., 2016; Wessels et al., 2016), *E.coli* (Stenum et al., 2023), and plant leaves, sidling and protoplasts (Marondedze, Thomas, Serrano, Lilley, & Gehring, 2016; Reichel et al., 2016; Z. Zhang et al., 2016). To date however, neither this approach, nor any other RIC technique, has been applied to ticks at either a cell line or organism level. Due to this, we first chose to ensure the RIC protocol would be suitable to elucidate the ISE6 RBPome.

When carrying out irradiation previously, it was found that 150 mJ/cm^2 was the optimal dosage for UV crosslinking in mammalian cell lines, this maintaining the balance between protein and RNA recovery (Castello et al., 2013). *D. melanogaster* embryos, budding yeast and *A. thaliana* leaves required substantially higher doses of UV (~1000 mJ/cm^2) (Sysoev et al., 2016), due to poorer UV penetration of the cell wall, tissue, etc and/or absorption by pigments such as chlorophyl. Most studies have employed 150 mJ/cm2. We therefore decided to test a range of UV dosages starting with 150mJ/cm^2 and increasing in 50 mJ/cm^2 increments up to 400 mJ/cm^2, to confirm which dosage provided the optimal RIC output. When developing the silver stains for Figure 6.1.A, a band can be seen in both the input and eluates in all channels at ~15kDa. This corresponds to the RNaseOUT enzyme used to degrade the RNA from the RIC and can be disregarded. Beyond this, no bands were seen in the non-crosslinked channel of the eluates (Figure 6.1.A), so we can confirm that there is no significant carryover of non-specific proteins. This was as expected as I used denaturing conditions for lyses and washes. The banding pattern of the eluates of UV-irradiated samples for each dosage were consistent and distinct from the irradiated inputs, indicating the specific subpopulation of RBPs were isolated through the RIC. In addition, the eluate bands appeared to become lighter as the UV dosage was increased, indicating less protein material was present in each lane. As mentioned in the results, this may be due to higher UV dosage causing RNA or protein degradation within the cells, or causing the cells to become stressed and initiate degradation/apoptosis before they were able to be lysed. Accordingly, the lower

dosage was chosen to ensure this material loss in the elutes was minimised. To validate that this method isolated RBPs from the ISE6 cell culture, the aim would be to probe the eluates for known RBPs using a western blot. However, as there are no known antibodies against tick RBPs at this time, the irradiated input and eluate samples were probed for α-tubulin. This protein is highly abundant in all cells and has been shown to not interact with RNA, and therefore should not be pulled down during RIC (Castello et al., 2012). This was confirmed within the western blots, showing that the proteins that do not bind to RNA are not extracted during RIC (Figure 6.1.B). In agreement with the silver staining results, there was a stronger intensity of α-tubulin at the lower doses, meaning it is more likely that the loss of material was due to protein or/and RNA damage by UV irradiation, or the cellular stress response to UV exposure . Because the cells were kept at 4°C during irradiation and quickly lysed after, the possibility of intrinsic protein or RNA damage is more plausible. To maximise the protein recovery as well as minimise adverse effects on the cells, a UV dosage of 150 mJ/cm^2 was used for all RIC in ISE6 cells.

Once the UV dosage was confirmed and the analysed outputs indicated the ISE6 RBPs had been successfully isolated, the next step was to confirm these samples would be suitable for proteomics using mass spectrometry. Two rounds of RIC were carried out on the prototype lysates, however as the resulting silver stained gel indicated that one cycle was sufficient to deplete the proteins bound to the captured RNA from the lysates and to prevent dilution or increased likelihood of capturing non-specific material, only the eluates from the first round of capture were prepared via SP3 for proteomic analysis.

The aim of the pilot analysis was to analyse the number of identifiable proteins within the irradiated and non-irradiated prototype samples, without investigating the characteristics or types of proteins identified, to determine if the number of proteins identified would fall within a similar range to previous studies (Table 6.1). MaxQuant was used to process the mass spectrometry data and once potential contaminants, such as keratins present in the environment from skin and hair debris and residual reagents from upstream processes such as trypsin (Hodge, Have, Hutton, & Lamond, 2013), were removed, the crosslinked samples contained 859 proteins and the non-crosslinked contained 233 proteins, 179 of which were found in both crosslinked and non-crosslinked conditions (Figure 6.2.C). By plotting the log2 intensity fold change against the log2 crosslinked intensity we can see that most of the ‘shared’ proteins (proteins found in each sample) were more abundant in the crosslinked samples (Figure 6.2.B). In the previous studies mentioned, RIC of human, mouse and yeast produced from 400 to 1000 proteins, and drosophila and plant RIC produced lower amounts (Bach-Pages et al., 2020; Hentze et al., 2018), and therefore 859 proteins found within the

crosslinked samples was considered a successful experiment given the substantially worse annotation of tick proteins when compared to other species. These experiments also confirmed that $7.5x10^7$ cells was enough starting material for the RIC protocol.

As mentioned within the Methods (Chapter 4) and Defining the RBPome of ISE6 cells Results (Chapter 6.3), production and subsequent mass spectrometry to elucidate the ISE6 cell line RBPome (crosslinked and non-crosslinked triplicates samples) was carried out in tandem with rUUKV-infected ISE6 RIC to elucidate the differential expression of RBPs during UUKV infection. This will be expanded upon in the following Chapter (Chapter 7). This chapter focuses on defining the ISE6 steady-state RBPome through analysing UV-irradiated uninfected cells and the non-irradiated controls.

Analysis of the proteins within the crosslinked and non-crosslinked triplicates via silver staining showed that both the input and eluate samples displayed similar banding patterns to previous RIC, which indicated the methodology was reproducible and able to isolate the specific RBPs. Additionally, as seen within the pilot RIC, no protein bands were seen within the non-crosslinked eluates, which was expected. If bands are present within the non-crosslinked eluates this indicates that the RIC wash steps are not sufficient to remove non-specific, non-crosslinked proteins, and further wash steps or increasing the salt concentrations within the wash buffers may be required to interrupt these non-specific interactions and remove background protein (Figure 6.3.A). To ensure the samples were enriched for mRNA and no other types of cellular RNA such as the over-abundant rRNA or small nuclear RNA (snRNA) (and the associated bound proteins), RT qPCR was performed to measure the enrichment of mRNAs in the eluates when compared to the corresponding inputs. Non-polyadenylated RNAs can be captured via internal A-rich sequences or through strong RNA-RNA interactions. However, oligo(dT) selection is expected to deplete non-poly(A) RNAs to some extent, with >6-fold reduction of rRNA being recommended for RIC experiments. Indeed, RNAseq of olio(dT) selected RIC samples showed that mRNA comprises 70% of all the reads (Castello et al., 2012; Iselin et al., 2022), suggesting that they are the main contributors (although not the sole) to the proteomic results. If the eluates do not show sufficient enrichment for mRNA, this indicated the wash steps are not stringent enough and may need to be extended or altered (such as increasing the temperature for the last washes or the lysis volume and homogenisation process) to reduce non-mRNA interactions and remove these from the samples. With a fold-enrichment value of 6 or higher of mRNA over rRNA, I expect that over 95% of non-mRNA is removed from the samples. From results of the RT qPCR, all samples had over 6X fold enrichment in mRNA when comparing the eluates to the inputs, showing the wash steps were sufficient to remove most

non-mRNAs and ensuring the proteins within the eluates reflect the ISE6 RBPome (Figure 6.3.B). The triplicates for crosslinked and non-crosslinked ISE6 cells were prepared via single-pot, solid-phase-enhanced sample preparation (SP3) and analysed by mass-spectrometry. SP3 is considered a non-standard protocol within mass-spectrometry sample preparation and was chosen as RIC has not previously been carried out in tick cell culture meaning it was vital to maximise the protein retention (Hughes et al., 2019).

The mass spectrometry-based proteomics output was analysed as follows: plotting the log2 of the protein intensities for each sample to compare the overall distribution of intensities between the samples (Figure 6.4.A), determining the number of missing values when comparing the samples (Figure 6.4.B), and performing a PCA with every sample (Figure 6.4.C). These diagnostic analyses were undertaken to evaluate the variability between both the biological triplicates for each condition, and between the two conditions, to determine if the samples showed reproducibility and would be representative of the ISE6 RBPome. Some variability is expected between biological triplicates, as these samples were produced at different times using individual ISE6 cell monolayers. However, significant differences within the biological triplicates in either protein intensity distribution or number of missing values highlights a technical issue with the samples that can increase biological variance. If one sample showed significant variability, this sample would need to be excluded from further analysis, and if all samples showed significant differences the methodology would need to be re-evaluated to determine why reproducibility was not achieved. As no significant technical variability was seen between the biological triplicates for each condition, no samples were omitted from further analysis. The biological triplicates from each condition were then compared to each other. It is expected that crosslinking would produce eluates with both a higher quantity (higher protein intensities) and a higher number of proteins (fewer missing values), which would be reflective of the ISE6 RBPome, compared to the non-crosslinked samples which should include lower quantities (lower protein intensities) of non-specific ‘background proteins’(more missing values). If the crosslinked and non-crosslinked samples contained similar levels of protein intensity and no/few missing values, it would indicate there was no difference between the samples, and therefore the proteins in the crosslinked eluates would not be reflective of the ISE6 RBPome as these proteins would be unable to be differentiated from the background. This outcome may have occurred if too few cells were exposed sufficiently to UV crosslinking, and so binding the proteins to mRNA was not achieved to a level where RIC would allow RBPome enrichment, or if during the washing steps either mRNA was not enriched, or all RNA was stripped from the beads. Overall, the diagnostic analysis returned the expected results from samples, given that the

previous silver stains show specific banding of only the crosslinked eluates (Figure 6.3.A), the mRNA enrichment was achieved to above the required threshold and RNA was still detected within the eluates (Figure 6.3.B), the intensities of the proteins in the crosslinked samples were higher than that of the non-crosslinked (Figure 6.4.A), and the number of missing values was far larger in non-crosslinked eluates compared to crosslinked (Figure 6.4.B). However, these diagnostic analyses only account for the overall trends, and do not factor in the proteins identified through the mass spectrometry. To evaluate the variability of the samples, including the types of proteins isolated, a PCA was performed. As this analysis does not include the data labels for the origins or sources (crosslinked or non-crosslinked) of the data sets, grouping is carried out through comparing the types and quantities of proteins within each sample group, whereby the closer the data sets, the lower variations between them. The sample groups from each condition, crosslinked and non-crosslinked, would be expected to group together, as these should have similar outputs reflective of the ISE6 RBPome and non-specific cellular protein background, respectively. This is seen within the results of the PCA when visualised in a plot (Figure 6.4.C), as UV treatment accounts for ~85% of the variance. These results provide further confidence that the crosslinked samples contain proteins of the ISE6 RBPome. The additional variability may be due to a variety of biological factors, such as differing proportions of cell types within the heterogenous cell monolayer. Overall, I can conclude from the quality assessment of the mass spectrometry results that the RIC and sample preparation techniques applied to the ISE6 cell culture were effective in isolating reproducible samples which can be used to define the proteins involved in the ISE6 RBPome.

To determine which proteins were specific to the crosslinked sample, and therefore components of the ISE6 RBPome, the FC in each protein and its associated adj.P.val was calculated by comparing the crosslinked to non-crosslinked samples. When setting the FDR cut-off point, the number of proteins encompassed by both 10% and 1% FDR criteria were examined. Proteins which did not fall within these criteria are considered background, most likely abundant or highly ‘sticky’ non-specific proteins that were not removed during the wash procedure. In total, 540 proteins were identified from the crosslinked and non-crosslinked triplicates, of which 495 proteins were significant to an FDR of 10% or lower (coloured orange in Figure 6.5.A) and of 450 proteins were found at 1% FDR (coloured red in Figure 6.5.A). As the difference in proteins between the 10% and 1% FDR accounted for less than 10% of the ISE6 RBPome proteins, the 10% FDR group was considered the mock RBPome going forward to prevent loss of information through disqualifying potential RBPs. As this is the first time the RBPome is being explored within tick cell culture, the number of

proteins which would be isolated during RIC was unknown. The pilot experiment indicated a maximum number of 859 proteins could be enriched with this protocol and experimental settings (Figure 6.2.C), and the final number of 495 putative RBPs falls in line with the results of the pilot experiment. However, this number is lower than the RBPomes defined in human cells, such as the isolation of the 861 RBPs in HeLa cells (Castello et al., 2012; Castello et al., 2016). My result was therefore considered positive, but I acknowledge might be affected by poor annotation of tick proteins as well as limited starting material (Castello et al 2012 used $1x10^8$ cells and separation into 12 fractions), but future work can build on my results to generate a more comprehensive RBPome of *I. scapularis*.

The next step was to determine if any of the putative tick-derived RBPs had identifiable human orthologs using InParanoid analysis (E. Persson & Sonnhammer, 2022). Roughly 2/3rd of proteins were mapped to human orthologs (Figure 6.5.B). This was a larger than expected, as previous studies into drosophila and mouse systems showed between 50-60% of the RBPome mapping to human orthologs. For example, early fly embryo RBPome returned approximately 56% of RBPs mapped human orthologs, and studies into embryonic mouse RBPs returned approximately 59% of RBPs mapped to human orthologs (Kwon et al., 2013; Wessels et al., 2016). The increase in percent mapping may be in part due to the fact that annotation in ticks might be favoured by conservation in other species (Perez-Perri et al., 2021). Ortholog analysis is necessary due to the current lack of annotated tick genomes and will be crucial if studies are expanded to less-studied tick species. By analysing the human orthologs of the unidentified proteins found in the tick RBPome, one can hypothesise the function of these proteins. However, such inferred functionality based on human orthologs should be interpreted careful as the pairing of the human ortholog to the tick protein does not guarantee that these proteins have the same intracellular function or location due to the existence of divergent evolutionary mechanisms.

Next, further biochemical, molecular, and functional analysis were conducted on the putative ISE6 RBPome compared to the proteome of the background organism, in this case *Ixodes scapularis*. This was to determine if the attributes of the identified proteins, such as their HI, pI and intrinsic disorder aligned with properties expected for RBPs. HI was analysed as RBPs are enriched in positively charged and polar amino acids and normally lack transmembrane domains, making them less hydrophobic that the average protein in the cellular proteome and allowing them to interact with the negatively charged RNA (Castello et al., 2012; Corley, Burns, & Yeo, 2020; Lunde et al., 2007). The tick RBPome follows these rules, as when plotted the HI distribution of the RBPome proteins is lower than that of the ISE6 whole cell proteome. For pI, RBPs also often have a high pI as the phosphate

backbone of the RNA is negatively charged (Jacobson & Saleh, 2017), and positively charged residues such as Lysine and Arginine are key and abundant in RNA-protein interfaces (Castello et al., 2012; Perea & Greenbaum, 2020). The pI distribution of the ISE6 RBPome is overall more positive than the whole cell proteome as is expected from RBPs. In addition, unlike the whole cell proteome which contains several peaks, the ISE6 RBPome distribution had a smooth, broad peak, which is in line with previous RBPome analysis in mammalian HeLa cells (Figure 6.5.C) (Castello et al., 2012; Castello et al., 2016). Finally, the overall distribution of percentage (%) intrinsic protein disorder was analysed. Within proteins, intrinsically disordered regions (IDR) can form more flexible structures that can coordinate RBDs and add RNA-binding properties to the RBP, such as increasing affinity and specificity (Ottoz & Berchowitz, 2020). The overall distribution of percent intrinsic disorder within the proteins in the ISE6 RBPome compared to the whole proteome was calculated. It was expected that many of the mock RBPome proteins would feature disordered regions, as these have been found to be common within human RBPs (Castello et al., 2012). Although these results showed no significance between the RBPome and proteome, this does not imply that the disordered regions within RBPs are not biologically relevant to RNA interaction, and indeed, a previous report highlighted that intrinsically disorder regions in RBPs expanded across evolution and warrant further modelling and mechanistic investigation. Overall, as the biochemical properties of the ISE6 RBPome match what is expected of current or known RBPs, an in-depth domain analysis was performed on the dataset.

With InterproScan we identified the proteins which were annotated with RNA-binding related pfam IDs. I acknowledge, this annotation is likely to be incomplete and the proportion of classic RBP might be underestimated. Within the mock RBPome, 82 proteins showed no identifiable domains. However, this may be due to the quality of the proteome, rather than the proteins lack known domains. Due to poor annotation, these proteins may have incomplete or incorrect sequences, or yet unidentified domains, and as such were removed from further analysis. Overall, this accounts for ~17% of the ISE6 mock RBPome proteins. Although not having these inputs may affect the overall results of further domain enrichment analysis, this does not detract from the results obtained through analysis of the proteins which contained identifiable domains. As more work is done to elucidate the ISE6 proteome, redoing this analysis using the updated FASTA files for the 82 proteins would be beneficial to determine if this gap in information impacts the overall domain analysis. Using the list of known RBDs as defined by previous work (Castello et al., 2012; Castello et al., 2013; Hentze et al., 2018) it was determined if the mock RBPome and whole proteome

proteins contained RDBs. Upon analysis, 229 proteins (55%) in the mock RBPome contain RBDs, which aligns well with the human RBPome in which this is approximately 50% as determined in the 2016 work by Castello *et al* (Castello et al., 2016). This may indicate that there is a conserved mode of RNA binding across species, with organisms relying on both domain-specific RNA interactions and other means, such as using disordered regions of domains with non-canonical RNA-binding activity. When breaking down the types of RBDs present within the mock RBPome against the whole proteome as background using odds ratio analysis, both classical and non-classical RBDs are enriched when compared to the whole proteome. Rather than analyse enrichment of each individual domain when compared to the whole proteome, the classical and non-classical domains were assigned into overall architype groups, e.g. RNA recognition motifs are grouped by their class to allow for gaining statistic power. Although proteins containing classical domains have a higher odds ratio within the mock RBPome and therefore are enriched within the mock RBPome, when looking at the breakdown of the classical domains present, no binding domains showed a p-value smaller than 0.25 when analysed by fishers' exact tests, and therefore this enrichment was not statistically significant. This may be due to the number of proteins containing classical RBDs being high in the whole RBPome, and the mock RBPome only containing a subsection of the pfam domains present in the overall group classifications thereby, making the differences in the odds ratio smaller and harder to determine significance (Figure 6.6.C). As an alternative explanation also relates to poor annotation, as statistical power relies on the size of each domain class. From the odds ratio, it seems that the most enriched domains involve RNA-binding motif domains, Zinc-fingers, and RNA recognition motifs (RRMs). This is similar to data found in the literature examining RBPs in humans, and in addition these binding domains display the previously described biochemical properties typical of RBDs and then to be the larger classes amongst cellular RBPs (Castello et al., 2012). This supports the functional conservation of these domains across species. As non-classical RBDs are less characterised, and are more versatile within architype groups Therefore, when comparing to classical domain groups, there are more unique groups of non-classical RBDs with fewer RBDs per group. This could be due to the nature of non-classical RBDs being more varied and divergent in function. For example, only a small population of WD40-containing domains bind to RNA in human cells and this binding relies on the amino acid composition of each individual WD40 ring. Improving the coverage of the tick RBPome in the future will help to define the scope of non-canonical RBDs and approaches such as RBDmap (Castello 2016) can be employed to identify them experimentally.

For the proteins which did not contain a known RBD, one can hypothesise that either these proteins contain RBDs which have not yet been defined, or that they bind to RNA in a non-domain specific manner. Although there may be some domains that have yet to be defined, particularly given that tick cells are highly understudied, it can be hypothesised that the latter is more likely, whereby binding occurs through a less sequence/structure specific manner such as disordered sections of protein directly interacting with RNA, or allowing for multiple protein conformations dependant on additional protein/RNA interactions or post-translational modifications (Ottoz & Berchowitz, 2020). While no enrichment was found in disordered regions for no RBD containing proteins (Figure 6.7.C), it is known that RNA-binding disordered motifs are relatively short (20-30 amino acids) and contain specific signatures that are conserved from yeast to human (Beckmann et al, 2015) and are expected to be found here. Scanning of tick RBPs to identify compatible RNA-binding disordered motifs should be done in the future. As the HI of the proteins that contained no known RBDs within the mock RBPome showed no difference to the whole mock RBPome, the unknown mock proteins still retain some biochemical properties of RBPs. Structural analysis to identify regions within these proteins which demonstrate RNA-interaction potential, and domain-specific pI analysis, should be carried out to further characterise these unorthodox RBDs.

To conduct functional analysis, GO analysis tools available in VectorBase were utilised. This allowed for the direct comparison of the ISE6 RBPome against the ISE6 proteome background. When the RBPome was analysed for terms involving biological processes, 252 biological processes were found to be enriched. When analysing the most significant GO terms, the terms described pertain to transcription and translation alongside other metabolic processes (Figure 6.8). These results may be due to the number of proteins varying between the different processes, particularly as terms such as ‘gene expression’ are broader than ‘RNA splicing, via transesterification reactions with bulged adenosine as nucleophile’. Proteins may also be involved within many related pathways, such as ‘pre-mRNA cleavage required for polyadenylation’ and ‘mRNA cleavage involved in mRNA processing’, reflecting a prominent presence of proteins from the spliceosome and 3’ processing machinery. However, some level of overlapping between these GO terms is expected. Despite this, analysis using GO terms provides a good overall view of the data, particularly given the novel nature of this ISE6 RBPome, and provides a good basis for expanding ISE6 RBPome experiments into virus infection studies. However before moving on to infection studies, it was prudent to explore how our results describing the ISE6 RBPome compared to

the RBPomes defined for other species given the similarities seen between these results and the analysis of the mammalian RBPome from HeLa cell culture (Castello et al., 2012).

By expanding the comparison of the ISE6 RBPome to include other species, it is hoped that a better understanding can be gained of how the ISE6 mock RBPome proteins function and the intracellular pathways they are involved in using the information already available. This comparison will also allow further confirmation that the ISE6 mock RBPome follows the overall biochemical trends seen across different species RBPomes. The protein IDs corresponding to RBPs isolated through poly(A) RIC were accessed from RBP2GO, and IDs and all FASTA files corresponding to the protein IDs for these species were accessed from Uniprot. By selecting RBPs that were previously highlighted through poly(A) enrichment the species RBPome is comparable to the results produced through this research. When comparing the HI of the ISE6 RBPome against the background proteome to that of other species (Figure 6. 9), the ISE6 RBPome appears to be most like that of *Homo sapiens*, *Mus musculus*, *Danio rerio*, *Caenorhabditis elegans*, *Saccharomyces cerevisiae*, and *Leishmania donovani* as for these species the RBPome HI curve is shifted negatively when compared to the whole cell proteome. This is interesting, but somewhat expected, as these species include eukaryotes from several families, and so the ISE6 mock RBPome adds to the hypothesis that all eukaryotic RBPomes are more negatively hydrophobic than the whole proteome (Castello et al., 2012). This is not of the case for the ISE6 RBPome pI curve (Figure 6.10). Although the ISE6 proteome has a similar pI curve to *Homo sapiens*, *Mus musculus*, and *Drosophila melanogaster* which all have pI curves with three peaks below a pI of 10, the RBPome of ISE6 has a more similar shaped pI curve to *Danio rerio*. Both these species have broad curves peaking at just under a pI of 10 and which do not reflect the shape of the whole proteome curve, unlike the RBPome *Homo sapiens* for example. However, although it will be interesting to analyse the enrichment of RBDs within *D. rerio* and compare the results with the ISE6 mock RBPome to see if there is evidence of conserved domains and functions which could be biologically important, currently within the literature the work around the *D. rerio* RBPome is focused on embryonic development. In addition, this data set is relatively small and therefore may have only captured the most prominent, and therefore most likely to be conserved, RBPs and so it is unclear how comparable this data is to the ISE6 RBPome (Despic et al., 2017).

As mentioned previously, there is a lack of molecular tools available for ISE6 cell culture or for working with tick organisms as a whole. Given that 2/3rds of the tick RBPome had identifiable human orthologs, from the data previously described parallels can be drawn between the ISE6 and *Homo sapiens* RBPome data (for example when examining the % of

proteins with known RBDs and no known RBDs), and previous anti-human antibodies (predominantly α-tubulin) are able to probe for the equivalent tick proteins with specificity given the proteins conserved sequences. To see if it would be possible to repurpose the anti-human RNA binding protein antibodies available to detect the tick cell orthologs. If found, an antibody against a tick RBP would allow for the further validation of the mass spectrometry data, and to expand the RBPome research by using methods such as immunoprecipitation and validating gene knockdown or knock out experiments. Unfortunately, none of the antibodies tested were shown to specifically bind tick RBPome proteins (Figure 6.11), although now that the RBPome of ISE6 cells has been established it would be beneficial to broaden the scope of the search for repurposing antibodies to include the other species mentioned in Figures 9 and 10, particularly those which showed more similar biochemical properties to the conserved RBPs present within the ISE6 mock RBPome. As more tick genomes are sequenced in future, the genes corresponding to the RBPs identified in this research can be searched for within these genomes, allowing the assessment of sequence specificity and conservation, alongside functional annotation, of genes across different tick species. This can also be expanded to the analysis of other species, as the sequences of the identified RBPs within the ISE6 RBPome can be compared to the previously mentioned data sets in order to establish which proteins are highly conserved across species and broader taxonomic groups.

To conclude, the aim of this research was to optimise the UV crosslinking and oligo(dT) capture methodology to carry out RIC on ISE6 cell cultures derived from *Ixodes scapularis* and to determine if this methodology would be appropriate to establish the RBPome within ISE6 cell lines. This method has been successfully employed to establish the RBPome of many species. However, this technique has not yet been carried out on arthropod cells despite the paucity of information regarding the intracellular landscape of ISE6 cell lines. Through dosage optimisation and prototype mass spectrometry experiments, it was shown that 7.5 x 10^7 cells irradiated at a UV dosage of 150 mJ/cm^2 was sufficient to produce reproducible data to establish the RBPome of the ISE6 cell line. Triplicates of crosslinked and non-crosslinked ISE6 cells were prepared via the SP3 methodology and analysed via mass spectrometry and MaxQuant.

In this chapter, the first RBPome of any tick cell line has been elucidated. By establishing the ISE6 RBPome, this can be used as a starting point for not only investigating the structures and functions of these proteins (alongside improving the mapping of the proteome to the genome), but additionally this provides a baseline for exploring any differential RBPome expression observed during subsequent infection studies.

Chapter 7 Uncovering the tick RBPome response to UUKV infection

7.1 Introduction

There ars limited data describing the intracellular changes occurring in ticks during viral infection, and prior research has focused on changes in the overall transcriptome and/or proteome. One study found that when IDE8 (derived from *I. scapularis*) cell cultures were infected with TBEV and analysed over 6 days, ~8 identifiable transcripts and ~20 proteins were up regulated, and ~14 transcripts and between 10-32 proteins were downregulated. Within the biological processes these transcripts and proteins are involved in, the most abundant subcategories for transcripts included nucleic acid processing, metabolism, and cell stress, while the most abundant subcategories for proteins included immunity, transport, and cell stress (Weisheit et al., 2015). Similarly, when nymphs were infected with LGTV and given a blood-meal, transcripts related to immunity and host-defence were found to be upregulated, although several transcripts relating to AMPs were downregulated, indicating the interplay between the virus and the differentially expressed vector products is more complex than first anticipated (McNally et al., 2012). However, from searching through the literature, no research has been carried out to determine the proteins important to bunyavirus replication within tick cells that specifically interact with viral RNA, despite bunyaviruses posing a significant threat to human health and work within other species highlighting the importance of RBPs during infection.

RNA is a central molecule in virus infection, particularly for RNA viruses, where it does not only function as blueprint for the synthesis of proteins (mRNA) but also as storage of information (genome). Examples of the little that is known about viral RNA-cellular RBP interactions have previously been mentioned in Sections 1.2.4 and 1.1.1.2, when describing the replication cycle and immune response respectively (Girardi, Pfeffer, Baumert, & Majzoub, 2021; Iselin et al., 2022; Mazelier et al., 2016). When focusing on the proviral aspects of these interactions, viral genomes cannot encode all the proteins required for the metabolism of viral RNA, with a typical RNA virus encoding for a handful of RBPs. To contextualize, the spliceosome and ribosome are complex machineries that comprise over one hundred proteins each. Therefore, virus will inevitably rely on host resources to replicate, translate, stabilise, transport and package their RNAs. This is particularly relevant within the vectors, where replication is sustained at a level where the organism remains infectious. Through the virus mimicking host features, such as performing cap-snatching to allow transcription of viral cRNA, and interacting with these complex cellular machineries, they are capable of forming RNP complexes. These complexes are more difficult to distinguish from those native to the host, less easily detected by the intracellular antiviral response and can modulate the intracellular environment to promote the translation of viral

RNA over host RNA within viral replication factories (Bermudez, Hatfield, & Muller, 2023; Garcia-Moreno, Jarvelin, & Castello, 2018; Olschewski, Cusack, & Rosenthal, 2020; Singh, Pratt, Yeo, & Moore, 2015). For example, in the case of DENV infection, the host RBPs Vigilin and SERBP1 bind the viral genome and recruit additional host proteins to promote translation and replication. One of the proteins recruited is RACK1, a scaffold protein that binds the 40S ribosomal subunit. When Vigilin and SERBP1 are mutated and rendered incapable of binding RACK1, translation of the viral transcripts is severely impacted and DENV infection incapable of being established (Brugier et al., 2022). In the case of the mosquito vector during DENV infection, Shivaprasad and colleagues found the membrane associated Loquacious protein (Loqs) was able to interact and colocalise with both the viral NS3 protein and both the full length and sub-genomic vRNA. When this protein was depleted inhibition of DENV occurred, and this effect was also seen during YFV and ZIKV infection, indicating this protein may be an important pro-viral factor across several arbovirus species. Although the exact mechanism of action is still unclear, the group did demonstrate that the modulation of viral replication was independent of the RNAi pathway, despite Loqs being able to interact with both Dcr and Ago (Fukunaga & Zamore, 2012; Shivaprasad et al., 2022).

The proteins mentioned above are focused examples of a larger shift in the cellular RBPome activity during infection. Recent reports using RIC have shown that the landscape of cellular RBPs are extensively remodelled upon virus infection. These changes are intimately linked with virus infection, including RBPs playing proviral and antiviral roles that accumulate at the viral replication factories (Garcia-Moreno et al., 2019; Iselin et al., 2022; Kamel et al., 2021). Garcia-Moreno and colleagues have demonstrated that over 200 RBPs within mammalian cells undergo a shift in interaction during SINV infection. Within this group several upregulated RBPs, including both well-known and non-conventional, were identified and shown to be proviral through further research. The RBPs RTCB, DDX1, FAM98A, PPIA, HSP90AB1, PA2G4, and SRPK1, which play various important roles in the cell, were found to be recruited to SINV viral replication factories during infection and complexing with viral RNA. Although depletion of these proteins within the cell impacts SINV infection, demonstrating their importance to viral replication, it is unknown if these proteins enhance viral replication, act in a regulatory manner, or if viral protein interaction occurs with these proteins and further modulates function (Garcia-Moreno et al., 2019). Similarly, Kamel and colleagues demonstrated through this methodology that infection of human Calu-3 cells with SARS-CoV-2 causes 335 RBPs to be significantly altered by 24 hours post-infection without significantly altering the overall quantities of cellular proteins. When comparing these

results to those of the SINV induced RBPome, 40% of the changes in RBP activity were consistent between the data sets, indicating a level of conservation of the RBPome in responding to viral infection. Although several of the notable RBP examples that were consistent between the two data sets were anti-viral, which will be expanded on below, proviral proteins including RTCB, DDX1, and FAM98A were upregulated within SARS-CoV-2 infection. These RBPs directly interact with the viral RNA, and like the results with SINV, depletion of these proteins reduced the quantity of intracellular SARS-CoV-2 RNA (Garcia-Moreno et al., 2019; Kamel et al., 2021).

Outside of forming these RNP complexes within replication factories, RBPs may also play a pro-viral role through preventing the build-up of viral genetic material within the cell, minimizing the exposure of this material to the intracellular immune system whilst still allowing the progression of viral replication. For example, in mammalian systems XRN1 targets viral dsRNA to prevent accumulation within the cells. In the case of measles virus and IAV infection, this degradation of dsRNA aids in suppressing the innate immune response through prevention of detection of the RNA through PRRs. This was also found in the study by Garcia-Moreno and colleagues, where XRN1 was visualised adjacent to the SINV viral replication factories, likely to prevent viral RNA 'escaping' from these factories and being detected by the intracellular immune system, and that XRN1 is essential for SINV infection (BenDavid, Pfaller, Pan, Samuel, & Ma, 2022; Garcia-Moreno et al., 2019; Y. C. Liu et al., 2021).

Regarding antiviral activity, viral RNA is the "Achilles heel" of viruses as it often contains signatures (pathogen-associated molecular patterns, PAMPs) that make them different from cellular mRNAs and can be recognised by a specialised set of cellular RBPs with antiviral roles as sensors and effectors (Backes et al., 2014; Lerolle, Freitas, Cosset, & Legros, 2021; Rezelj et al., 2017; Sheehan et al., 2018; Watson et al., 2019). As previously mentioned, these molecular patterns include double stranded (ds)RNA, undermethylated cap structure, tri-phosphate ends, uncommon codon usage and CpG sequences. The host antiviral arsenal includes a wide variety of RBPs with unique capacities to recognise viral sequences, including RIGI (tri-phosphate ends), MDA5, ADAR and PKR (dsRNA) and IFIT1 (cap0) (Blair & Olson, 2015; Brennan et al., 2015; Feng et al., 2023; J. K. Lee & Shin, 2021; Min et al., 2020; Ning et al., 2015; Rezelj et al., 2017). However, the antiviral factors present in vector cells remain largely unknown. As described in Chapter 1, the best studied pathway is the RNAi pathway. If other antiviral systems operate in vector cells, at present they remain obscure.

Many of the antiviral factors play important ‘primary’ roles within the cells, where the antiviral functions can be considered additional or secondary functions, rather than the protein being solely dedicated to immune functions. By redirecting the function of these proteins, antiviral activity can be achieved without needing to drastically increase the quantity of protein present within the cell. This is illustrated well within the SINV infection research by Garcia-Moreno and colleagues, as several of the upregulated RBPs showed anti-viral functions alongside their ‘standard’ functions within uninfected cells. For example, the cellular general control non-derepressible-2 (GNC2) protein, a kinase that functions to regulate protein synthesis in a similar manner to PKR, binds the viral RNA. Through binding two nonadjacent regions of the virus RNA this protein acts in an anti-viral manner to block early viral translation (Berlanga et al., 2006; Garcia-Moreno et al., 2019). Additional RBPs identified within the SINV study have also been identified as anti-viral in infections with multiple viral species. In both SINV and SARS-CoV-2 infection, the anti-viral RBPs TRIM25, TRIM56, ZC3HAV1, DHX36, and GEMIN5 were upregulated. Again, alongside their ‘standard’ roles, these proteins are redirected to perform a range of anti-viral functions, such as GEMIN5. This protein is involved in the formation of the spliceosomes as part of the SMN complexes that, in infected cells, moonlight as an antiviral factor. Upon infection with SINV and SARS-CoV-2, GEMIN5 is massively upregulated in RNA-binding activity without changes in protein abundance. The protein then binds to the 5’ viral cap and through interaction with the large subunit of the ribosome blocks translation (Choudhury et al., 2017; Garcia-Moreno et al., 2019; Kamel et al., 2021).

There is also evidence to show that some anti-viral RBPs are conserved across host and vector species. DEAD-box helicase 17 (DDX17) is a type of DEAD box protein whose helicase activity that utilises ATP to bind and unwind RNA duplexes (Linder & Jankowsky, 2011). When this protein is depleted in human cells RVFV replication is increased. This protein acts in an antiviral manner through accessing the RVFV replication complexes and binding the viral RNA directly to restrict replication, alongside playing a role in antiviral surveillance and production of miRNA (Moy et al., 2014; Nelson et al., 2020). The impact of DDX17 on RVFV infection was first found to be an antiviral factor for bunyavirus infection in an RNAi screen using drosophila cells as the vector model. In this screen and subsequent experiments, the DDX17 ortholog Rm62 was shown to be antiviral against LACV and RVFV, but not SINV or Indiana vesiculovirus (VSV), indicating regardless of the organism being infected the impact of this protein is virus species specific (Moy et al., 2014). When looking further into RBP interactions with viral RNA in vector cells, decapping 2 (Dcp2) was also highlighted in a Drosophila RNAi screen. This protein removes the

mRNA ‘cap’, exposing the mRNA to degradation and preventing its translation, and therefore when depleted from the cells RVFV transcription is enhanced (Hopkins et al., 2013). Further to this, several other RBPs have also found to be important for DENV infection in mosquitoes. The study carried out by Yeh et al. referenced when discussing proviral RBPs found in mosquito vectors during DENV2s infection also identified several antiviral RBPS capable of binding the DENV2 3’ UTR, including AeGTPase, AeAtu, and AePur (Yeh et al., 2022). It would be beneficial in future, once the RBPs involved within the vectors are better understood, to further investigate the level of conservation between hosts and vectors and their roles in infection outcomes, and to determine if this is the case for pro-viral RBPs in addition to anti-viral RBPs.

Finally, many proteins can act in a pro- or anti-viral manner depending on virus species. This is exemplified by Ras GTPase-activating (SH3 domain) protein-binding protein (G3BP1), a highly conserved protein that has been shown to be target by a variety of viruses in mammalian systems. G3BP1 can act in a pro-viral and anti-viral manner, through promoting the viral lifecycle or amplifying innate immune signalling (respectively) (Jayabalan, Griffin, & Leung, 2023). There is some evidence to suggest that the post-translational modifications present on G3BP1 determines whether the protein acts in a pro-viral or antiviral manner. When examining the impact on CHIKV infection, the virus acts to reduce the level of G3BP1 ADP-ribosylation, to disrupt formation of anti-viral stress granules, and through an undefined mechanism plays a key role in the formation of CHIKV replication complexes (Jayabalan et al., 2021; Jayabalan et al., 2023; Scholte et al., 2015). In DENV infection, the virus is incapable of modulating the post-translational modifications of G3BP1, and therefore during infection this protein is recruited into stress granules, degrading viral RNA and significantly impairing viral protein synthesis (Jayabalan et al., 2023; Xia et al., 2015).

These examples represent the tip of the iceberg, and it is likely that hundreds of virus-regulatory proteins remain to be discovered, particularly in vectors. Furthermore, over the last four years many different studies have attempted to identify the RBPs that interact with viral RNA using antisense probe-based capture or specific labelling of viral RNA with the nucleotide analogue 4-thiouridine (Iselin et al., 2022). These discovered hundreds of cellular RBPs that engage with viral RNAs, most of which remain to be characterised.

Identifying the pro- and antiviral factors underpinning viral infection opens new avenues of investigation that are currently severely underrepresented within the literature. From the current data available it is clear certain factors are key components of infection for multiple species of virus and/or a variety of different organisms. However, as many of these examples

also demonstrate, whether a host RBP functions in a pro- or anti-viral manner depends on the species of virus. Therefore, further experiment is required once key RBPs are identified to provide more detailed mechanistic insight into the impact on viral replication and kinetics. This work is vital in the continued efforts to understand viral infection and highlight potential novel targets for future therapeutic measures. RIC has significantly advanced our capabilities to achieve these goals by allowing a broad analysis of RBPome activity during infection, from which individual protein targets can be selected for further investigation.

7.2 Aims

The aims of the research presented in this chapter were to:

- **Elucidate the RBPome of ISE6 cell culture upon infection with UUKV.** Work described in Chapter 5 demonstrated ISE6 cells are susceptible to rUUKV infection. We therefore aim to use the optimised RIC methodology to establish the RBPome produced in ISE6 cell cultures in response to rUUKV infection.
- **Investigate the differential expression of the ISE6 cell derived RBPome during infection.** Once the RBPome of rUUKV infected ISE6 cell cultures is established, we can compare this to the naïve RBPome to determine if the landscape of RBPs changes during infection. This will also allow us to select targets for further downstream analysis using dsRNA knockdown studies.

7.3 Results

7.3.1 Sample preparation and diagnostics of mass-spectrometry for UV crosslinking and oligo(dT) capture in UUKV infected ISE6 cell monolayers.

As mentioned in Chapter 6, mass spectrometry of non-infected and infected samples was carried out in tandem to reduce run-to-run mass spectrometry derived variability. This will be expanded later in this Chapter. However, before RIC, the cell-monolayer infection conditions needed to be confirmed to produce the maximum amount of cellular material for RIC.

From the pilot study in Chapter 6 (Figures 6.1 and 6.2) the UV dosage and seeding concentrations were optimised. For infecting the monolayers, data from Chapter 5 (Figure 5.3) indicated that the UV-crosslinking and oligo(dT) capture would need to be carried out at 9 d p.i. with an MOI rUUKV of 5 FFU/cell. These conditions were chosen as the virus is still expected to be within the exponential phase of replication (Figure 5.3.A), and this is the first point at which UUKV N protein can be visualised by western blot in infected cell monolayers (Figure 5.3.B). To improve RIC sensitivity, it is important to obtain a homogeneous infection across the culture to reduce the noise derived from non-infected cells. At a minimum it is recommended that 60% of the cells within the monolayer are in the desired state to be analysed (Castello et al., 2017; Castello et al., 2013).

To qualitatively investigate the level of infection within the cell monolayers, ISE6 cell monolayers seeded at the same density as used for RIC (Table 3.6) were mock-infected or infected with rUUKV at an MOI of 5 FFU/cell. After infection, the cell monolayers were fixed, DAPI stained and probed for UUKV N protein which were visualised using the EVOS microscope (Figure 7.1). No UUKV N staining could be seen within the mock-infected cell monolayer. When visualising the infected cell monolayers, most of the cell monolayer showed the presence of UUKV N, indicating a majority of the ISE6 cells at 9 days p.i. were infected with UUKV. These infection conditions were therefore suitable for investigating the RBPome of ISE6 cells using UV-crosslinking and oligo(dT) capture.

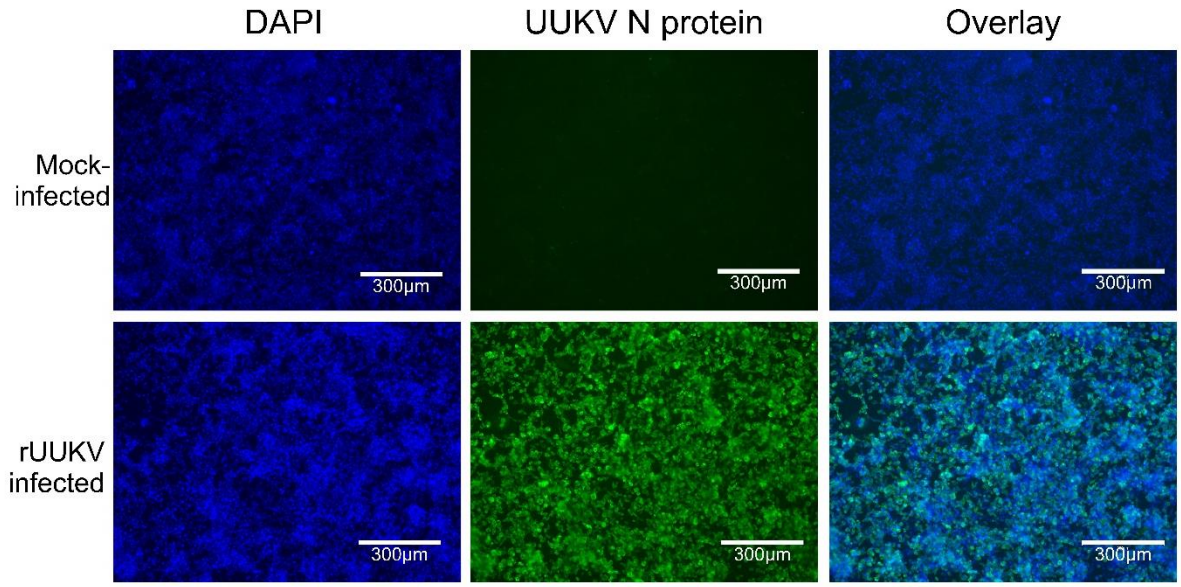

Figure 7.1: Immunofluorescent imaging of ISE6 cell monolayers infected with rUUKV at 9 d p.i. ISE6 cell monolayers were infected with rUUKV at a MOI of 5 FFU/cell or mock infected. At 9 days p.i., ISE6 cell monolayers were fixed, stained with DAPI (blue), and probed for UUKV N protein (green) to qualitatively investigate the percentage infection of the cell monolayers. Cell monolayers were imaged using an EVOS microscope using a 10x lens. Scale bar is equal to 300 µm.

To examine for the potential that UUKV RNA could interact with oligo(dT) capture beads, the RNA sequence of each viral genomic segment was scanned for poly(A) or poly(A)-like sequences which could have bound the oligo(dT) capture beads causing the UUKV M RNA to be captured. Poly(A) or poly(A)-like sequences were defined as a minimum of 5 sequential A nucleotides, with any larger sections being at least 80% A content. Overall, over 100 poly(A)-like sequences were found within the UUKV M segment, while UUKV L has over 400 and UUKV S has just over 50 (Figure 7.2.A).

The irradiated and mock-irradiated samples for mass spectrometry analysis of the infected ISE6 RBPome were prepared in triplicate using the confirmed infection conditions, following the methodology as described in Chapter 6. Small fractions of all inputs and eluates were removed and stored for protein and RNA analysis.

To probe for the presence of vRNA within the input and eluate RNAs of both the infected samples generated in this chapter and the non-infected samples generated in the previous chapter, samples were analysed by RT qPCR, using primers against the UUKV M RNA (Figure 7.2.B). As expected, neither uninfected inputs nor eluates contained UUKV RNA, while all infected inputs were positive for UUKV M RNA (Figure 7.2.B). The eluates of both crosslinked and non-crosslinked infected samples were positive for UUKV M RNA, although the normalised Ct score of the infected eluate samples was lower than that of the respective inputs.

The protein content of the inputs and eluates was analysed by silver staining. No obvious difference in banding pattern was seen within or between the inputs of the crosslinked and non-crosslinked infected triplicates, although this was a subjective observation, as the purposes of the silver stain gel was to determine if proteins were present within the sample. When analysing the eluates, no protein was seen in the mock-exposed (0 mJ/cm^2) samples. In the crosslinked eluates, the banding pattern was similar between the triplicates and distinct from the input banding pattern as seen within the non-infected irradiated triplicates in Figure 6.3. I did not expect to observe substantial differences protein content when comparing infected and mock cells as silver stating only reveal the most prominent RBPs with central housekeeping functions (Garcia-Moreno et al., 2019). An exception to this, however, unlike in the non-infected crosslinked triplicates, a band can be seen at ~25 kDa which likely corresponds to the UUKV N protein (Figure 7.2.C).

Finally, the RNA was also analysed by RT qPCR using primers against the tick cell ribosomal subunit (18S) and ELF1A to calculate the expression of 18s per sample normalised to ELF1A via the $2^{-\Delta\Delta Ct}$ method, to determine the fold-enrichment of mRNA

within the eluates compared to the corresponding inputs. All samples exceeded the minimum mRNA fold enrichment, with all samples showing over 10-fold enrichment (Figure 7.2.D) and therefore all samples were prepared for mass-spectrometric based proteomics by SP3 as described in Section 3.7.13.

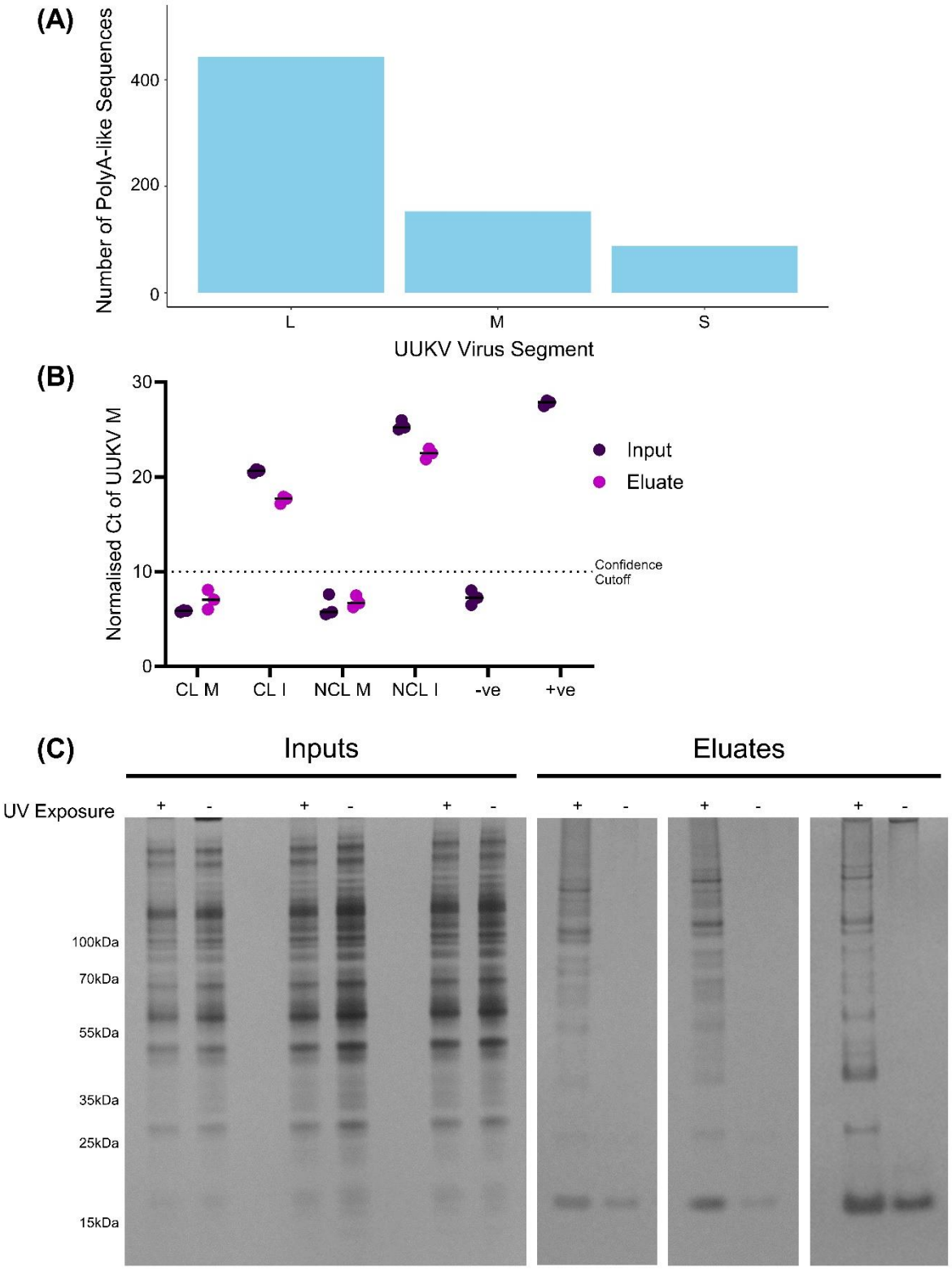
(A)
Number of PolyA-like Sequences
400
200
0
L
M
S
UUKV Virus Segment
(B)
Normalised Ct of UUKV M
30
20
10
0
Input
Eluate
Confidence Cutoff
CL M
CL I
NCL M
NCL I
-ve
+ve
(C)
Inputs
Eluates
UV Exposure
+ - + - + - + - + - + -
100kDa
70kDa
55kDa
35kDa
25kDa
15kDa

(D)

Sample	mRNA fold enrichment	Starting RNA quantity (ng/µl)	Eluted RNA quantity (ng/µl)
CL1	≥ 10	193.5	106.7
CL2	≥ 10	214.2	71.3
CL3	≥ 10	237.8	57.1
NCL 1	≥ 10	227.8	90.2
NCL 2	≥ 10	306.3	119.2
NCL 3	≥ 10	355.4	76.3

Figure 7.2: Preparation of triplicate RNA interactome capture (RIC) samples in the UUKV infected ISE6 cell line and validation for further mass spectrometry analysis. Preparations of 9 d p.i. UUKV infected ISE6 cell monolayers (in triplicate) were exposed to 150mJ/cm^2 or mock irradiated before lysis. Input samples were extracted, and cell lysates were prepared for RNA interactome capture (RIC) using oligo(dT) capture beads. (A) A poly(A) or poly(A) adjacent scan was run on each of the viral segments, with poly(A)/poly(A) like being defined as a minimum of 5 A nucleotides next to each other, with any larger sections being at least 80% A content. (B) RT qPCR analysis was conducted on RNA from input and eluate samples for the non-infected (M) samples described in Chapter 6 and the infected samples (I) in 7.2.A using UUKV M probes. RNA isolated from non-infected ISE6 cells was used as a negative control, and RNA from 12 days p.i. infected ISE6 cells produced from the growth curves in Figure 5.3 was used as positive control. Ct values were normalised by subtracting the Ct of the sample from the Ct limit of the system (Ct = 40), with the confidence cut-off for the presence of UUKV being a normalised Ct of 10 as defined by blank RT qPCR results. (C) Whole cell lysates from either before (input) or after (eluate) RNA capture were separated by SDS PAGE and resolved proteins were visualised using silver staining. (D) RNA quantities in the infected crosslinked (CL) and non-crosslinked (NCL) input and eluate samples were measured via a nanodrop spectrophotometer. RT qPCR was performed against tick cell 18S ribosomal RNA and eukaryotic elongation factor 1-alpha (*ELF1A*; mRNA used as a housekeeping gene). The ΔΔCT method was used to measure the quantity of 18S RNA normalised to *ELF1A* RNA levels, and the mRNA fold enrichment in the eluate compared to the input sample was calculated for each biological sample.

The mass-spectrometry results of the non-infected crosslinked and non-crosslinked samples generated in Chapter 6, and the infected crosslinked and non-crosslinked samples shown in Figure 7.2.A, were carried out in tandem. As the goal of these analyses is to compare the infected RBPome to the mock RBPome to elucidate the differential expression of RBPs that occur during infection, the evaluation of the infected biological triplicates (crosslinked and non-crosslinked) was carried out with the evaluation of the mock-infected samples shown in Figure 6.4 (Figure 7.3).

As seen in the mock-infected samples, the distribution of proteins intensities between the biological triplicates of both the infected crosslinked and infected non-crosslinked conditions showed minimal variation, and the crosslinked samples intensities were far larger than the intensities in the non-crosslinked triplicates. This was also seen within the equivalent non-crosslinked triplicates. When comparing the number of missing values between the different conditions, the crosslinked samples had far fewer missing values than the non-crosslinked samples, and the levels of missing values between the infected and uninfected samples for each crosslinking condition were comparable (Figure 7.3.B). Lastly, PCA was used to examine the variability between samples. As can be seen on the resulting plot, all triplicates from the respective conditions discretely grouped together (Figure 7.3.C). The factor that accounted for the largest proportion of the variability (~85%) was as seen in the mock PCA analysis in the Chapter 6, whether the samples were subjected to UV radiation or not. The factor which accounts for the second largest proportion of variability (~6%) was if the samples were infected with rUUKV or uninfected. From these results it was established data could be used for further analyses to characterise the infected ISE6 RBPome.

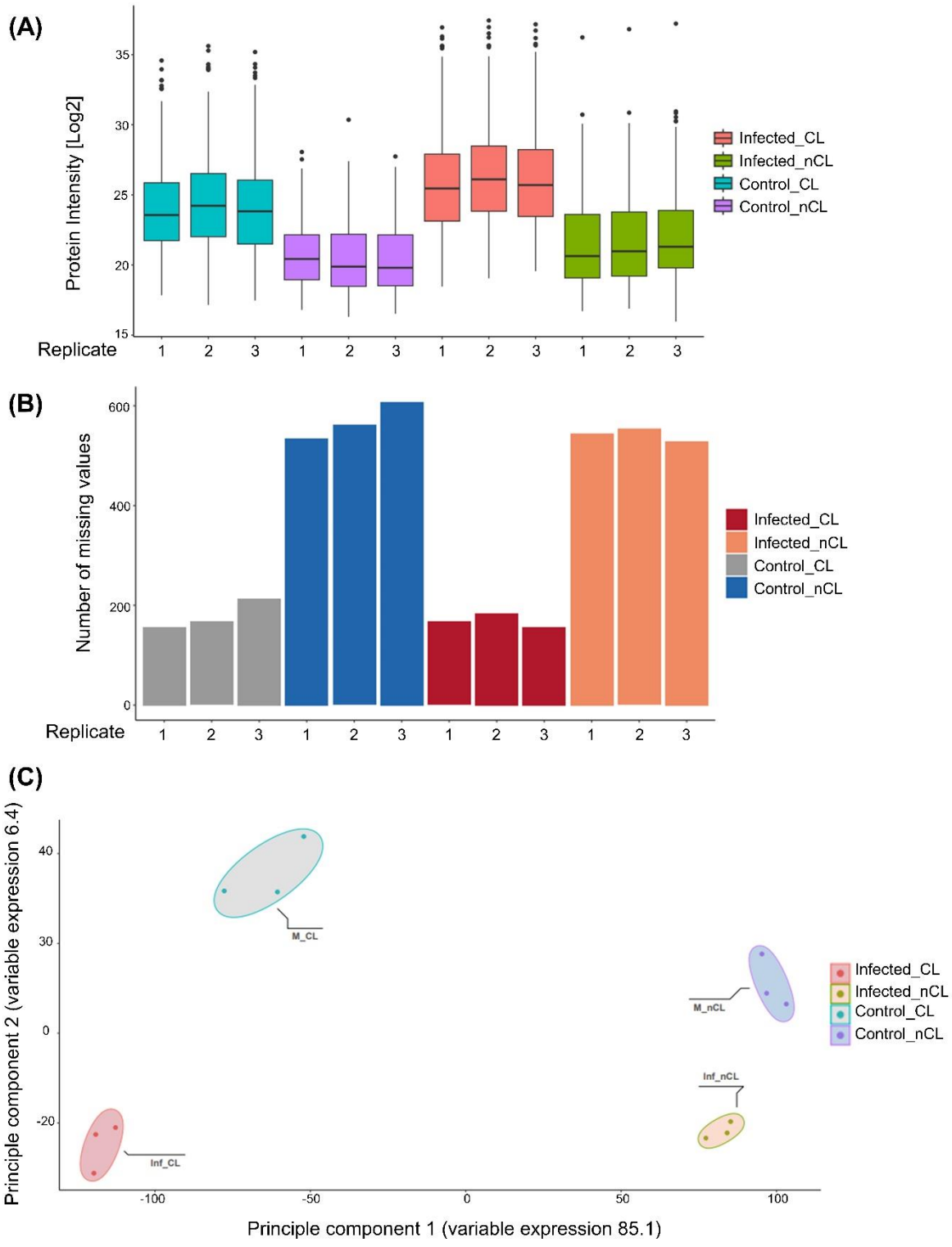

Figure 7.3: Diagnostics of mass spectrometry results from UUKV infected ISE6 RIC biological triplicates. Triplicate UUKV infected ISE6 cell monolayers were exposed to 150mJ/cm^2 UV-irradiation or mock irradiated prior to lysis. Input samples were extracted, and cell lysates were prepared for RNA interactome capture (RIC) using oligo(dT) capture beads. UV-exposed and mock exposed eluates were prepared by utilising a SP3 protocol in preparation for liquid-chromatography mass spectrometry (LC-MS). The mass spectrometry for this experiment was done alongside mass spectrometry of non-infected ISE6 cell cultures also used for RIC assays (previously described in

Chapter 6). Therefore, for diagnostic analysis the samples will be referred to as Infected (Inf) and the data are displayed in addition to the Mock (M) data previously mentioned. The mass-spectrometry outputs were processed through MaxQuant to produce identified peptides with corresponding intensities for each sample. Potential contaminants were subsequently removed. (A) The log2 intensity values for all proteins within the mock crosslinked (M_CL), mock non-crosslinked (M_nCL), infected crosslinked (Inf_CL), and infected non-crosslinked (Inf_nCL) samples were plotted. (B) The number of unidentified proteins and missing values were plotted for the mock non-crosslinked (M_nCL), infected crosslinked (Inf_CL), and infected non-crosslinked (Inf_nCL) samples. (C) Principal component analysis (PCA) was carried out and plotted for the mock non-crosslinked (M_nCL), infected crosslinked (Inf_CL), and infected non-crosslinked (Inf_nCL) samples.

7.3.2 Defining the RBPome of UUKV infected ISE6 cells

Although the crosslinked and non-irradiated samples for both mock and infected samples were deemed suitable for further analysis, before the comparison between the RBPomes of these conditions could be compared, the proteins of the infected RBPome need to be further defined as with the mock samples in Chapter 6. When comparing the fold change of each protein and the associated adj.P.val in the crosslinked samples compared to the non-irradiated samples, of the 572 proteins present, in total 541 proteins were present within the 10% FDR group, and 530 proteins were present within 1% FDR (Figure 7.4.A, 10% and 1% FDR coloured orange and red, respectively). To maintain comparability between the Mock and Infected samples, and due to the difference in number of proteins between the 1% and 10% FDR groupings being less than 2% of the total proteins found, all analysis was done using the 541 proteins of the 10% FDR group. As the aim of this chapter is to focus on the comparison of the mock and infected RBPomes, the ortholog analysis was not conducted on the proteins isolated from the infected samples.

As carried out with the mock RBPome the HI, pI, and percentage intrinsic disorder of the infected RBPome were calculated and compared against the ISE6 whole cell proteome. Similar to the mock, the HI was more negative in the infected cell RBPome compared to the whole cell proteome (Figure 7.4.B). The pI analysis also followed the expected trend of having a broad curve with a peak at a high pI. However, unlike the mock pI curve (Figure 7.5.D), the infected RBPome pI peak occured at a higher pI than the background proteome and the peak of the mock RBPome (Figure 7.4.C). Finally, the percentage intrinsic disorder was compared between the infected RBPome and whole proteome. No significant differences were found in this analysis (Figure 7.4.D). As the mass spectrometry diagnostics and biochemical characteristics for the infected sample matched the expected results and trends seen in the mock sample, the next step was to further analyse the domains present within the 10% FDR infected RBPome, which will be referred to in all further writing as the infected RBPome.

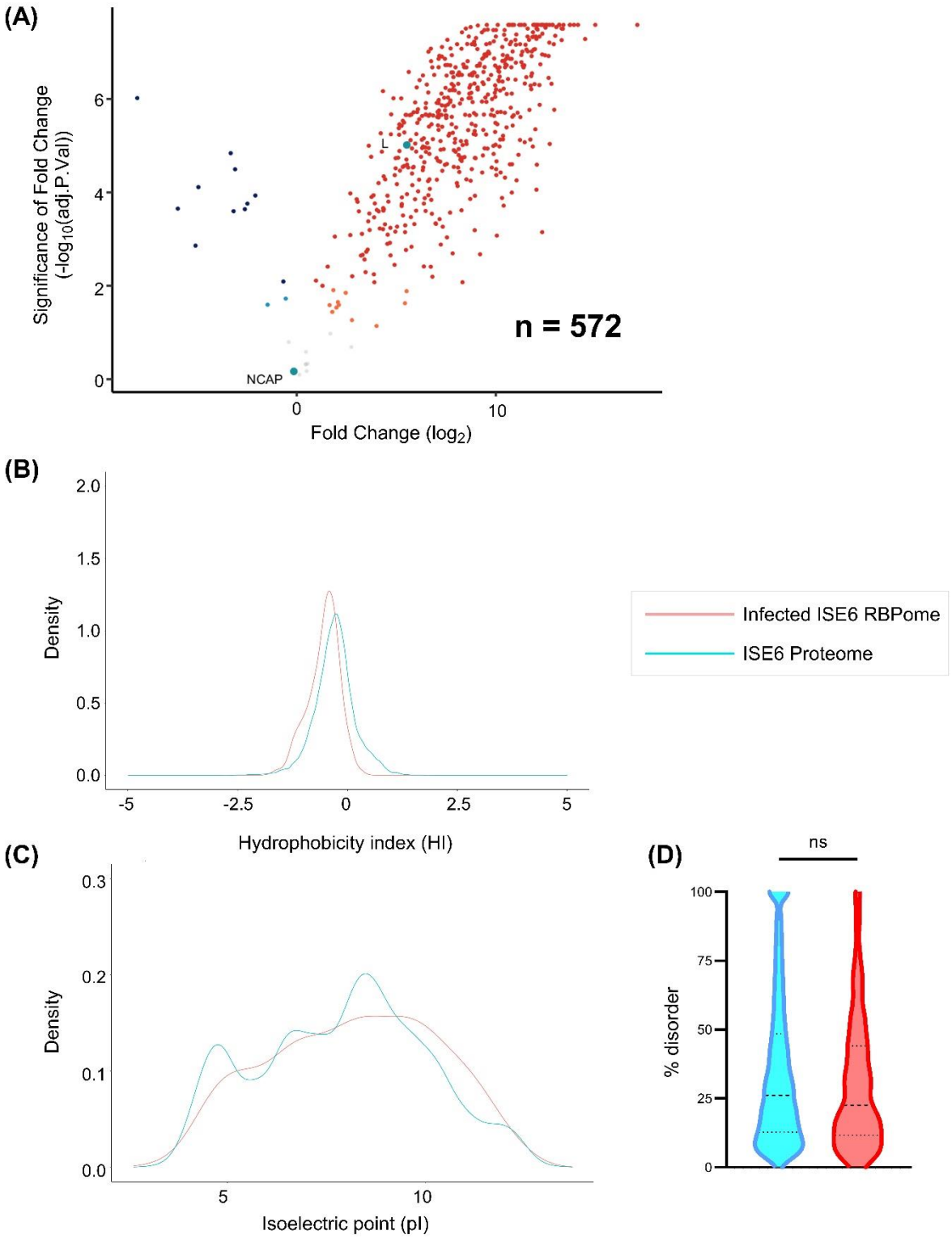

Figure 7.4: Analysis of rUUKV-infected ISE6 cell derived RNA Binding Proteome (RBPome). Analysis of samples prepared for mass spectrometry as described in Figure 7.2. The mass spectrometry for this experiment was done alongside mass spectrometry of UUKV-infected ISE6 cell cultures also used for RIC assays (further described in Chapter 8). Therefore, for this current analysis the samples will be referred to as Infected (I). (A) The fold change of the proteins found in the infected crosslinked samples compared to the infected non-crosslinked (x axis) were plotted against the significance of this fold change (-log10(p value), y axis). For proteins with a positive fold

change, and therefore in higher quantities in crosslinked samples, proteins at a 1-10% false discovery rate ($0.0001 > p > 0.001$) are coloured in orange, and proteins at a 1% false discovery rate or below ($p < 0.0001$) are coloured red. For proteins with a negative fold change, and therefore in higher quantities in non-crosslinked samples, proteins at a 1-10% false discovery rate ($0.0001 > p > 0.001$) are coloured in light blue, and proteins at a 1% false discovery rate or below ($p < 0.0001$) are coloured dark blue. Proteins with a positive fold change at a 10% or below false discovery rate were used in further analysis. Of these proteins that had a ≤10% false discovery rate (further described as 10% FDR proteins), using the provided FASTA files for these proteins from VectorBase (https://VectorBase.org) the hydrophobicity (B), isoelectric points (C), and (D) isoelectric points of the proteins, which were plotted using R and compared against the whole proteome derived from ISE6 cell cultures (whole proteome FASTA files were downloaded from VectorBase). This analysis was done through InterproScan MobiDB, and all proteins where 0% intrinsic disorder or those whose disorder were unable to be calculated were removed. Statistical significance in percentage disorder distribution was analysed using the non-parametric Kolmogorov-Smirnov test. (ns) = non-significant.

Using InterproScan, as described in Section 6.3.3, 88 proteins showed no identifiable domains within their sequence. Of the 453 proteins which did contain identifiable proteins domains, 243 (~54%) of the proteins contain at least one RBD (Figure 7.5.A). The RBD containing and non-RBD containing proteins increased by 13 and 26 proteins, respectively, in the infected RBPome compared to the mock. This was expected as the number of proteins within the infected RBPome was higher than in the mock, however it was interesting that although the protein number increased, the roughly 50-50 split of RBD to non-RBD proteins was maintained. The odds ratio was also very similar to that recorded for the mock-infected samples, although there was a slight reduction (difference in odds ratio >1) of odds within the classical RDBs. Overall, both types of domains were significantly enriched within the infected RBPome (Figure 7.5.B).

When examining the domain types in more detail, the RNA binding motif group was the most enriched, however this not deemed significant within analysis and one-fold less-enriched than in the mock RBPome. The RNA recognition motif (RMM, RDB, and RMP) domain group was the only group that was significant within the infected RBPome and was more enriched within this group than compared to the mock. There was a reduction in the enrichment of Zinc-finger containing family domains in the infected RBPome, and an increase in the RNA recognition 2, KH domain, and RNA recognition motif of the spliceosomal Pr8 domain groups, although for these latter two the odds ratio was ~1 indicating these domains were not enriched when compared to the background (Figure 7.5.C). As seen in the mock RBPome, no non-classical RBDs were enriched within the infected RBPome (Figure 7.5.D).

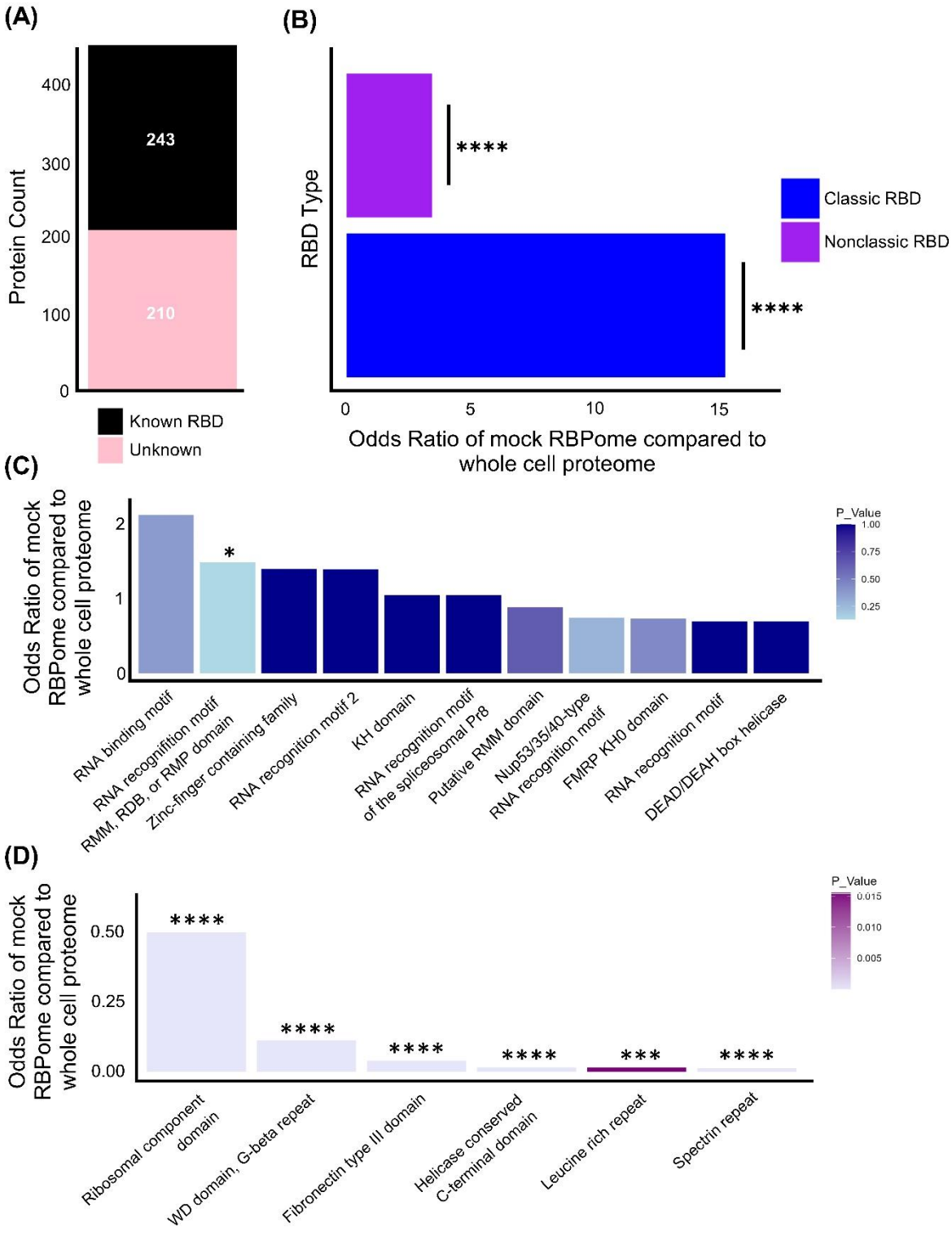

Figure 7.5: Analysis of rUUKV infected ISE6 cell monolayer derived RNA Binding Proteome (RBPome) known RNA binding domains. The FASTA files of the proteins defined in the 10% FDR infected RBPome were analysed using Interpro Scan to determine the protein domains present within the cells. 88 proteins from this group displayed no identifiable domains and were therefore removed from further analysis. (A) Using the established list of known RBDs, which includes both classical and nonclassical RBDs, the proteins were grouped based on if they contained at least one known RBD (known RBD) or contained no known RBDs (unknown). (B) For the Known RBD group from (A), the odds ratio and significance for a protein containing a classical or non-classical domain

compared to the whole proteome proteins containing RBDs were calculated using Fisher's exact test. For proteins containing classical (C) and non-classical (D) domains, odds ratio and significance were calculated using Fisher's exact tests against the whole proteome proteins containing these respective domains. Results with an odds ratio < 0.01 were excluded for plotting. Statistical analysis was carried out using R. Asterisks indicates significance **** = $p < 0.01$, * = $p \leq 0.25$.

Continuing the protein analysis, the proteins which contained no known RBDs were isolated, and the biochemical properties analysed and compared against the whole proteome. As seen within the mock RBPome analysis (Figure 6.7.A), the higher end of the pI distribution collapses when the proteins with known RDBs are not present within the analysis, and this reduction is more prominent than in the mock samples (Figure 7.6.A). When comparing the HI of the infected RBPome proteins with no known RBDs against the whole proteome, as expected, the HI of the no RBD RBPome is still more negative than the whole proteome (Figure 7.6.B). Finally, the percentage intrinsic disorder for each protein within the various samples were plotted (Figure 7.6.C). Although there was no significant difference between the groups, there were noticeable differences between the mock unknown (Figure 6.7.C) and infected unknown protein groups (Figure 7.6.C). The mock protein groups appear to have a larger proportion of proteins with between 5-25% intrinsic protein disorder. However, this may be due to more proteins within the known and unknown groups of the infected RBPome group compared to the mock. This increase is not matched in the number of proteins that produce a % intrinsic disorder score meaning there are more proteins within this sample with a % disorder of 0 (Figure 7.6.C).

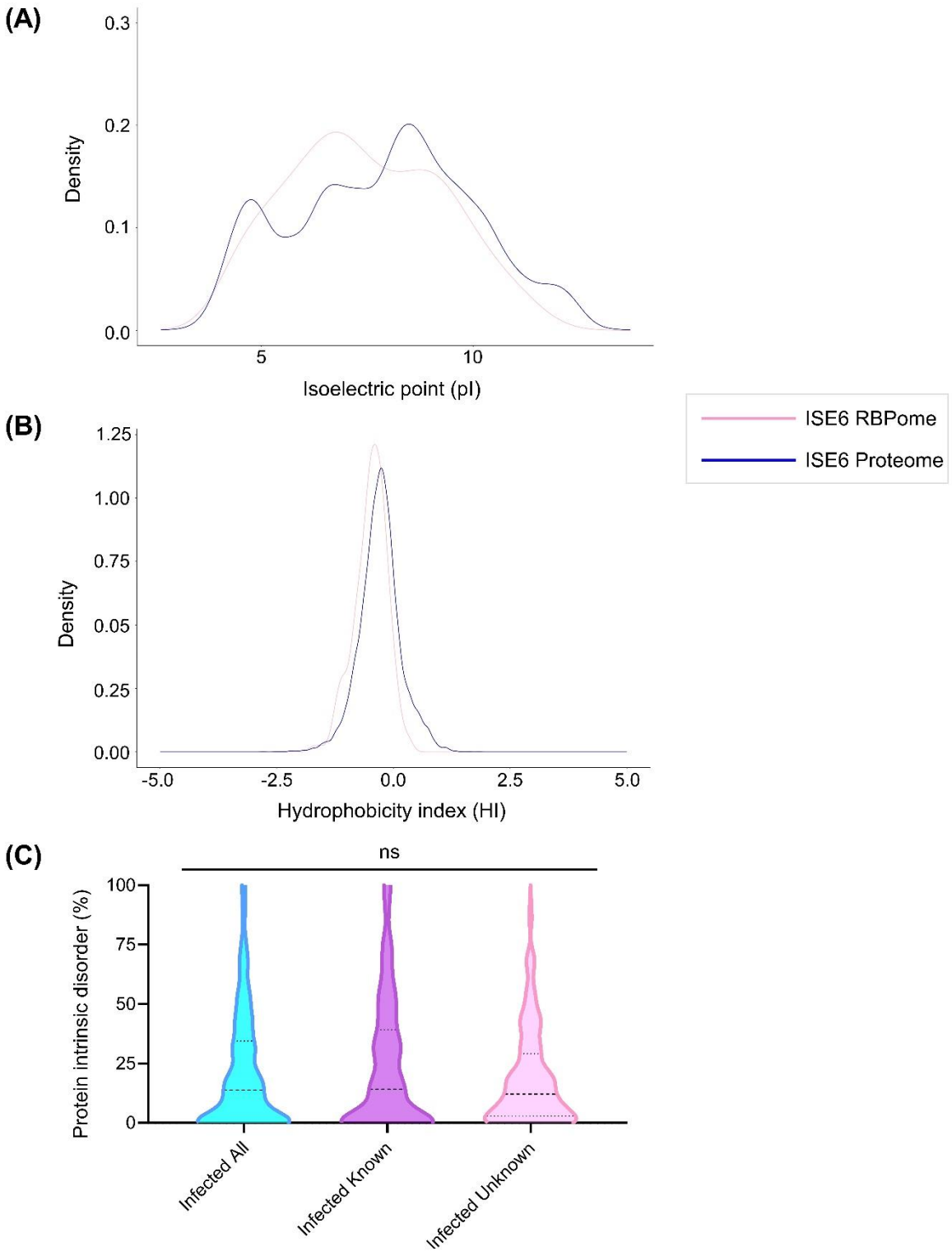

Figure 7.6: Analysis of rUUKV infected ISE6 cell derived RNA Binding Proteome (RBPome) against proteins containing 'non-known' RNA binding domains. Proteins containing 'no known' RBD domains from Figure 7.5.A were analysed to determine their (A) hydrophobicity and (B) isoelectric points. These were plotted using R and compared against the whole proteome derived from ISE6 cell cultures. (C) Protein intrinsic disorder was also calculated using MobiDB, comparing the whole mock RBPome (blue), the mock RBPs with known RBDs (purple), and the mock RBPs with no known RBDs (pink). From the data, 154 out of the 243 proteins with known RBDs and 164

out of 210 proteins with no known RBDs returned % intrinsic disorder scores, and therefore all results where no intrinsic order was returned were given a value of 0. A one-way ANOVA was used to determine statistical significance. (ns) non-significant.

The biochemical properties of the mock RBPome and infected RBPome were further compared against each other as opposed to the ISE6 background. As indicated in the previous analysis of the mock RBPome (Figure 6.5.C) and infected RBPome (Figure 7.4.B), both RBPomes showed very similar HI (Figure 7.7.A). Similarly, when analysing the pIs of the mock RBPome proteins (Figure 6.5.D) and infected RBPome proteins (Figure 7.4.C) there was a similar overall trend, although the peak of the infected proteome was broader and overall higher than that of the mock RBPome (Figure 7.7.B). The percentage intrinsic disorders between the mock RBPome (Figure 6.5.E) and infected RBPome (Figure 7.4.D) were not significantly different (Figure 7.7.C). The proteins within the mock RBPome or infected RBPome were separated by if the protein contained a known RBD or not (as done previously in Figures 6.7 and 7.6, respectively), and the distribution of intrinsic protein disorder were compared. No significant differences in the intrinsic protein disorder were found between these groups (Figure 7.7.D). However, this does not mean that percentage intrinsic disorder was not biologically relevant. Interestingly, though the distribution of intrinsic disorders were very similar within the two groups with known RBDs, when comparing the groups with no known RBDs the mock unknown group showed a higher average percentage intrinsic disorder. This may be due to the infected unknown group containing more proteins which did not return a percentage intrinsic value. The differences between the unknown groups warrants further investigation. Overall, due to the analysis of the mock and infected RBPomes, the analysis can be continued to establish the differentially expressed RBPome.

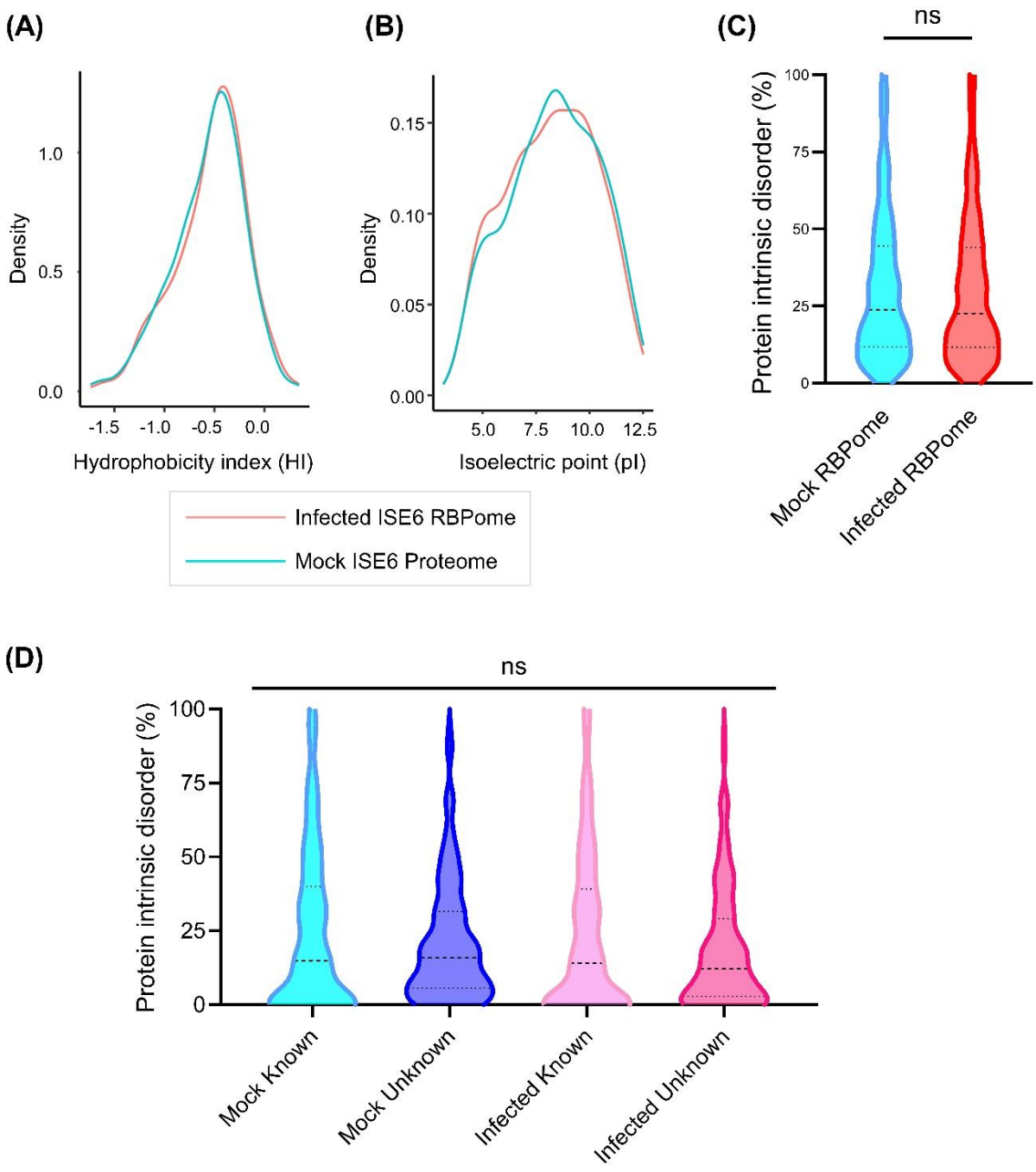

Figure 7.7: Comparison of the biochemical properties of the mock RBPome and infected RBPome of ISE6 cell cultures. Analysis of the biochemical properties of the proteins contained within the mock RBPome and infected RBPome, as defined in Figure 6.5.A and Figure 7.4.A, respectively. The FASTA files for these mock and infected RBPome 10% FDR proteins were used to calculate the (A) hydrophobicity (B) isoelectric points of the proteins, and (C) % intrinsic disorder of the proteins, which were plotted using R and compared against the whole proteome derived from ISE6 cell cultures (whole proteome FASTA files were downloaded from VectorBase). This analysis was done through InterproScan MobiDB, and all proteins where 0% intrinsic disorder or those whose disorder were unable to be calculated were removed. Statistical significance in percentage disorder distribution was analysed using the non-parametric Kolmogorov-Smirnov test. Both mock and

infected groups InterproScan results were previously subdivided based on if the RBPome proteins contained known RBDs as shown in Figure 6.7.C and 7.6.C.

Finally, the biological processes enriched in the infected RBPome were determined through GO enrichment analysis using the tools available in VectorBase with both computed and curated evidence inputted and an assigned p-value cutoff of 0.05. In the mock RBPome (Figure 6.8), 241 biological processes were found to fall within the enrichment criteria, 252 biological processes were found to be enriched within the infected RBPome. The processes with the most significant fold enrichment were also involved in gene expression and mRNA biogenesis, such as cleavage for processing or polyadenylation, processing, and splicing (Figure 7.8.A). The enriched biological processes were then plotted with the fold-enrichment on the x-axis and the -Log2(P.val) on the y-axis (Figure 7.8.B), and to visualise the most the 10 most significant pathways affected these points were labelled on the plot. These pathways were: gene expression, translation, peptide biosynthesis, amide biosynthesis, cellular nitrogen compound metabolism, peptide metabolism, cellular amide metabolism, cellular nitrogen compound biosynthesis, cellular macromolecule biosynthesis, and mRNA metabolic processes. Although most of these pathways reflect the results seen in the mock RBPome, amide biosynthesis is more significantly enriched within the infected RBPome as this was not seen within the top ten pathways in the mock RBPome. Additionally, mRNA metabolic processes were also not highlighted in the mock RBPome top ten, and macromolecule biosynthesis is not seen within the infected RBPome top ten significantly enriched pathways.

In concluding this analysis, it can be confidently stated that the RBPome of rUUKV infected ISE6 cell cultures at 9 d p.i. has been established. This can be compared against the mock RBPome established within Chapter 6 to establish the differential expression of RBPs within ISE6 cells during infection.

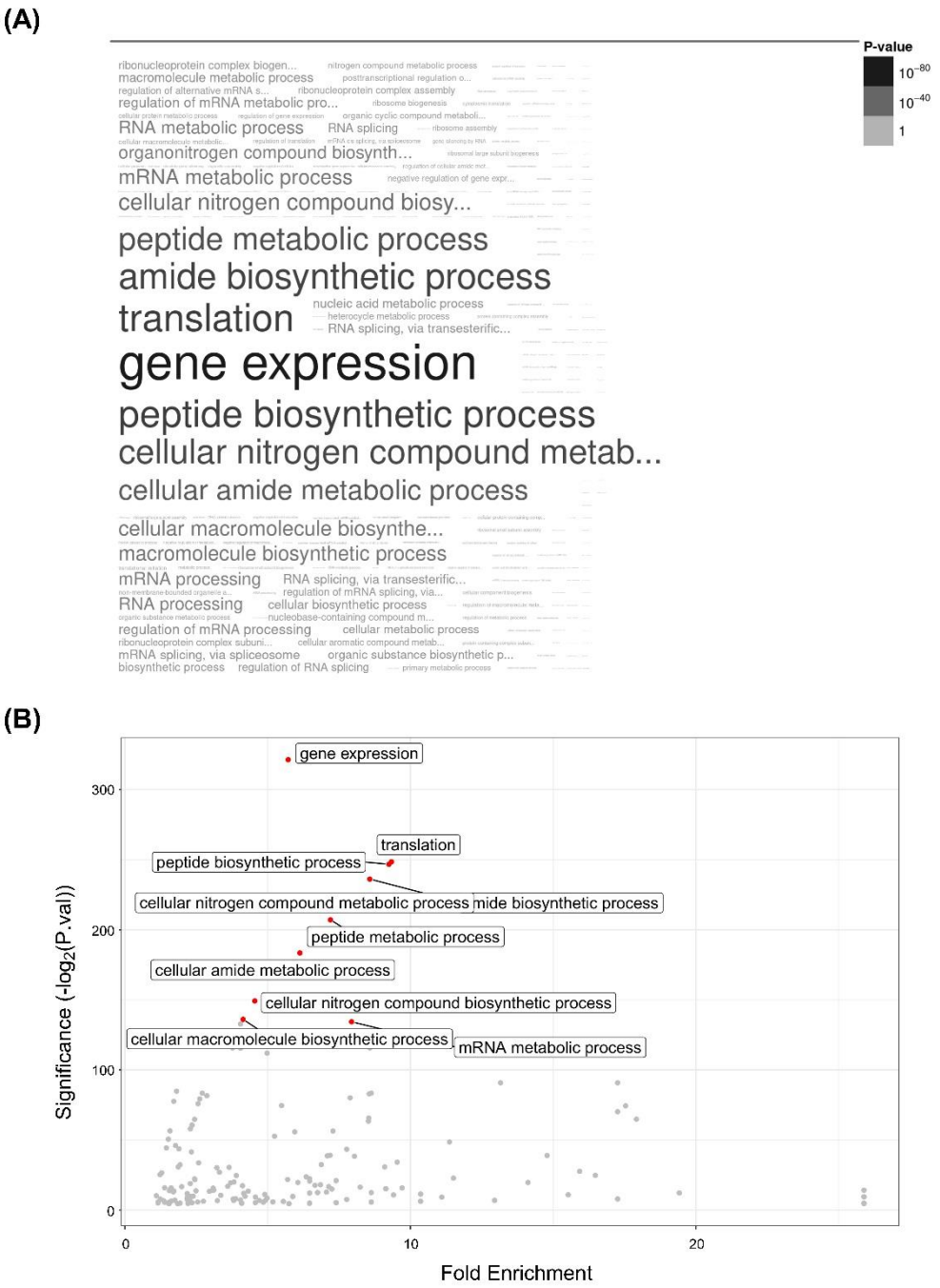

Figure 7.8: Analysis of biological processes enriched in the RBPome of rUUKV infected ISE6 cell culture. The proteins from Figure 7.4 were analysed using the gene ontology (GO) enrichment analysis tools in VectorBase. (A) An analysis of the biological processes with which the RBPome proteins were associated. The word cloud demonstrates the most enriched processes compared to the background ISE6 proteome based on the associated p-value. (B) The biological processes that the identified proteins from (A) were involved in were plotted against the fold enrichment of these processes. Infected RIC samples compared to the background ISE6 proteome are shown on the x-axis and the significance plotted on the y-axis. The top ten most significant pathways are highlighted on the graph.

7.3.3 Comparing the uninfected and UUKV infected RBPomes of ISE6 cells

In order to establish the differential expression of RBPs during rUUKV infection, the mock and infected RBPomes established from the 10% FDR groups of Figure 6.5.A and Figure 7.4.A, respectively, were compared. The fold change (FC) of the proteins within the infected RBPome compared to the mock RBPome was plotted against the -Log10 of the adj.P.val, meaning if the FC was positive the protein was more enriched within the infected RBPome and vice versa (Figure 7.9.A). Proteins with 10% or 1% false discovery rate (FDR) and a fold change of $-1 > FC < 1$ were considered as candidate of high confidence differentially regulated RBPs. Before further defining this differential binding, Inparanoid analysis (E. Persson & Sonnhammer, 2022) was used to determine the number of human orthologs able to be identified within the 10% FDR differentially expressed group. Roughly 70% of the proteins were matched to human orthologs (Figure 7.9.B), which is slightly higher than that of the mock RBPome alone (Figure 6.5.B). As before, when discussing individual genes and proteins, the human ortholog name will be used where it is able to be. At a 10% FDR, 283 RBPs were differentially enriched, with 127 and 156 proteins being downregulated and upregulated, respectively. When focusing only in the 1% FDR differentially regulated RBPs, 45 and 72 proteins were downregulated and upregulated, respectively (Figure 7.9.C). The 10% FDR cut-off differentially regulated RBPs were chosen for further analyses to prevent information loss.

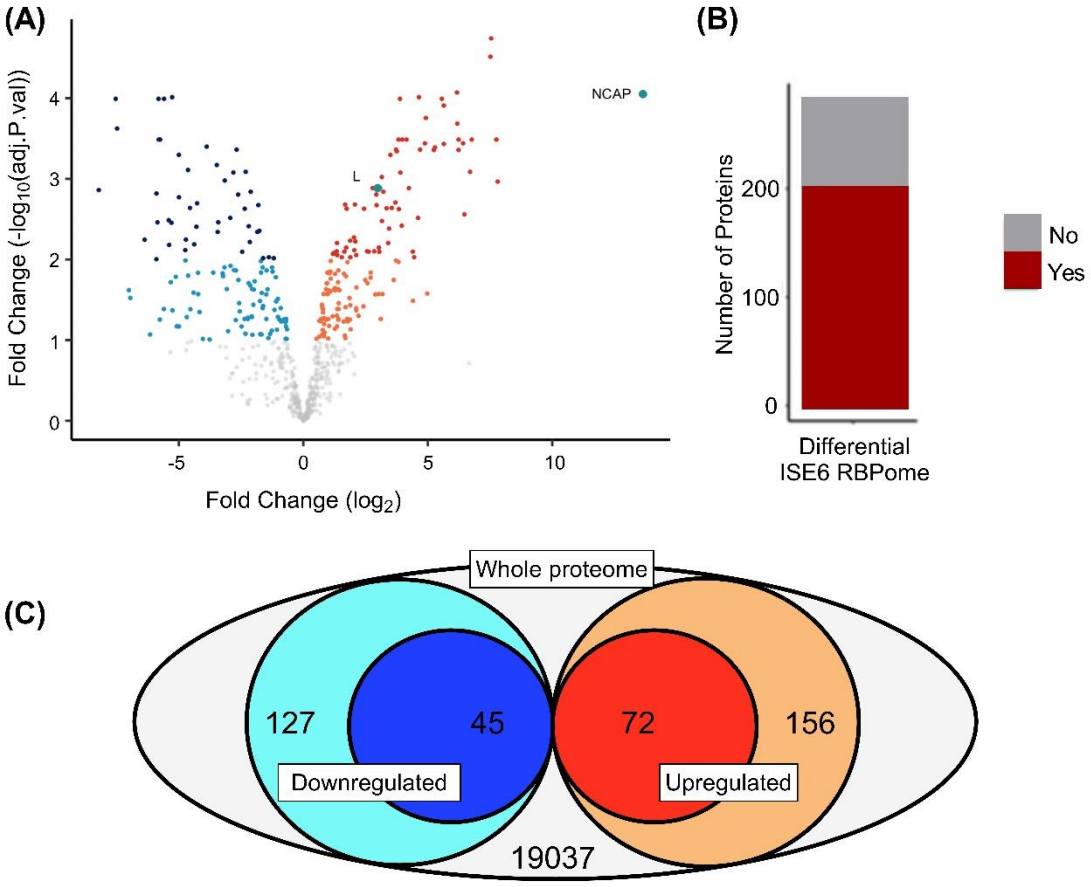

Figure 7.9: Analysis of ISE6 cell derived differential RNA Binding Proteome (RBPome). Analysis of 10% FDR non-infected and 10% FDR infected RBPome from Figure 6.5 and Figure 7.4. The mass spectrometry of the crosslinked and non-crosslinked non-infected (mock) and rUUKV infected ISE6 cells were done in tandem allowing for comparative analysis to be carried out. (A) The fold change of the proteins found in the infected crosslinked samples compared to the mock crosslinked samples (x axis) were plotted against the significance of this fold change (-log10(p value), y axis). For proteins with a positive fold change, and therefore in higher quantities in the infected samples, proteins at a 1-10% false discovery rate ($0.0001 > p > 0.001$) are coloured in orange, and proteins at a 1% false discovery rate or below ($p < 0.0001$) are coloured red. For proteins with a negative fold change, and therefore in higher quantities in non-crosslinked samples, proteins at a 1-10% false discovery rate ($0.0001 > p > 0.001$) are coloured in light blue, and proteins at a 1% false discovery rate or below ($p < 0.0001$) are coloured dark blue. Proteins with a positive fold change at a 10% or below false discovery rate were used in further analysis. (B) Of these proteins that had a ≤10% false discovery rate (further described as 10% FDR proteins), using the provided FASTA files for these proteins from VectorBase (https://VectorBase.org). InParanoid analysis was used to determine the number of proteins which had corresponding human orthologs. (C) Venn diagram comparing the number of proteins identified that were upregulated and downregulated in the RBPome at 1% and 10% FDR in the infected RBPome compared to the mock.

To assess the domains of the virus-regulated RBPs, I employed InterproScan. Of the 283 regulated RBPs, 243 (85%) returned at least one recognised domain using InterproScan. The split of RBPs which contained known RBDs was 49% (Figure 7.10.A), this was slightly lower than the mock and infected RBPomes. When focusing on the types of RBDs within the known RBD group (Figure 7.10.B), the non-classical enrichment maintained a similar level as seen in previous comparisons, however the classical RBD enrichment was lower (odds ratio ~10) (odds ratio ~15). Nevertheless, as expected, both types of domains were significantly enriched. The distribution of Pfam domains was examined in both the known RBD group (Figure 7.10.C) and unknown RBD group (Figure 7.10.D). Interestingly, most of the families enriched in both mock and infected RBPomes were not enriched in the virus regulated RBP set. FMRP KH0 domain was the most significantly enriched domain within the differential RBPome. No non-classical domains were enriched within the differential RBPome. As the pI and HI properties of the mock and infected samples have previously been examined (Figure 7.7), only intrinsic disorder was examined. No significant difference in the distribution of percentage intrinsic disorder between the known RDB compared to unknown domain differential RBPomes (Figure 7.10.E).

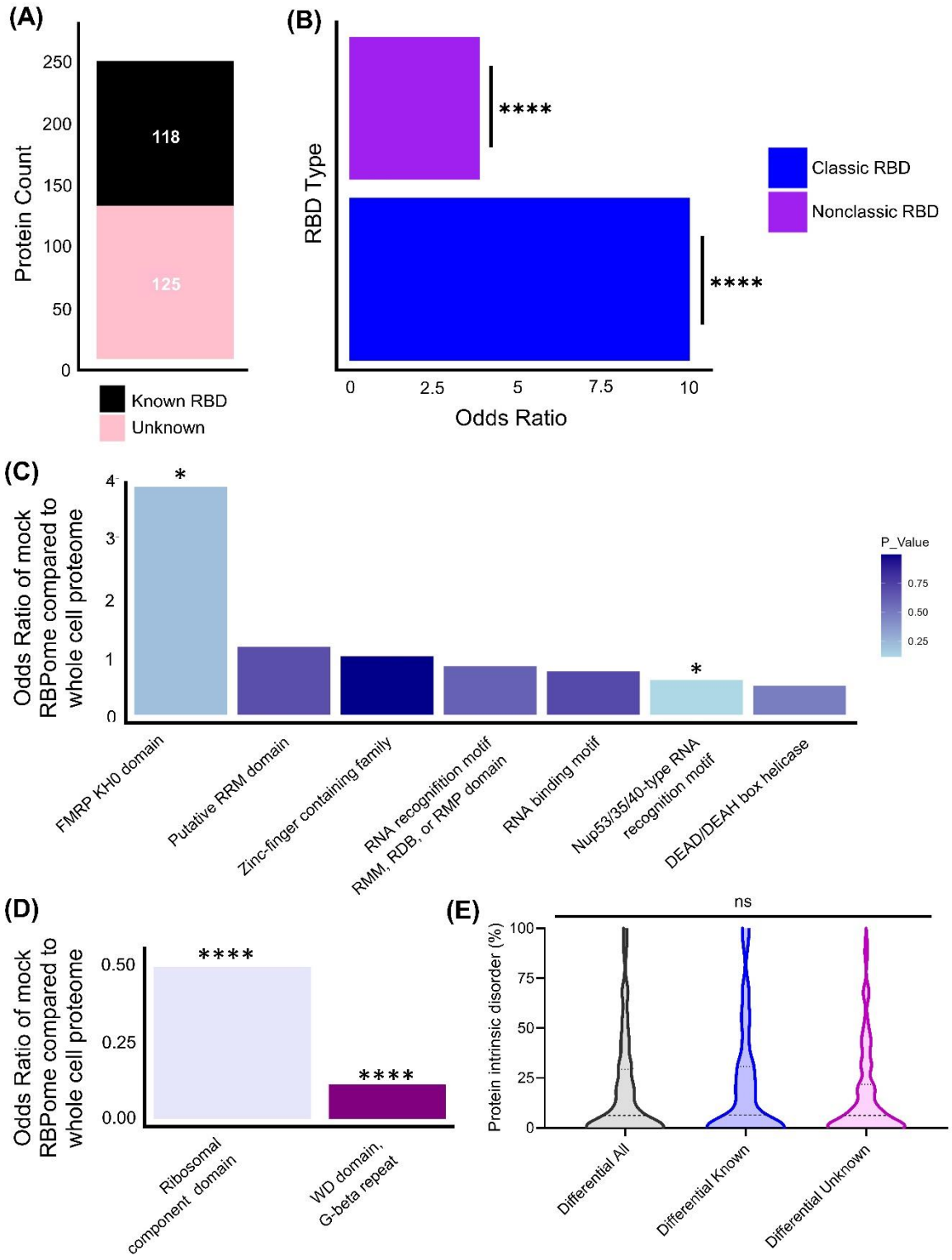

Figure 7.10: Analysis of ISE6 cell derived differential RNA Binding Proteome known RNA binding domains. The FASTA files of the proteins defined in the differential RBPome were analysed using InterproScan to determine the protein domains present within the cells, of which, 40 proteins from this group displayed no identifiable domains and were therefore removed from further analysis. (A) Using the established list of known RBDs, which includes both classical and nonclassical RBDs, the proteins were grouped based on whether they contained at least one known RBD (known RBD) or contained no known RBDs (unknown). (B) For the Known RBD group from

(A), the odds ratio and significance for a protein containing a classical or non-classical domain compared to the whole proteome proteins containing RBDs were calculated using Fisher's exact test. For proteins containing classical (C) and non-classical (D) domains, odds ratio and significance were calculated using Fisher's exact tests against the whole proteome proteins containing these respective domains. Results with an odds ratio < 0.01 were excluded for plotting. Statistical analysis was carried out using R. Asterisks indicates significance **** = $p < 0.01$, * = $p \leq 0.25$. (E) Protein intrinsic disorder was also calculated using MobiDB, comparing the whole differential RBPome (blue), the differential RBPs with known RBDs (red), and the differential RBPs with no known RBDs (pink). From the data, 65 out of the 118 proteins with known RBDs and 80 out of 125 proteins with no known RBDs returned % intrinsic disorder scores, and therefore all results where no percentage intrinsic disorder was returned were given a value of 0. A one-way ANOVA was used to determine statistical significance.

Finally, as the differential RBPome had been established, the upregulated and downregulated proteins were separated and the biological processes that were enriched within these groups, relative to the ISE6 background, were visualised using GO tools in VectorBase (Figure 7.11).

When analysing the 156 upregulated RBPs, 169 pathways were enriched compared to the background. As shown within the word cloud, the most enriched pathway was mRNA metabolic processes, followed by other pathways related in mRNA/RNA processes and metabolic processes (Figure 7.11.A). When examining the infected RBPome without comparing it to the mock RBPome to examine differential expression, the most significantly enriched term was gene expression. Although gene expression was still enriched within the upregulated differential proteins, the upregulated pathways appeared to shift more towards mRNA/RNA processing and biogenesis. This was better visualised when plotting the fold enrichment against the -Log2(P.val) and labelling the top ten most significantly enriched pathways. Whereas in both the mock and infected RBPomes (Figure 6.8.B and Figure 7.7.B, respectively) many of the most significantly enriched pathways were involved in protein synthesis, within the upregulated differential pathways all but one related to gene expression or RNA processing (Figure 7.11.B).

Conversely, when analysing the 127 downregulated proteins, 214 pathways were enriched compared to the background. These pathways include translation, peptide biosynthetic processes, and amide biosynthetic processes (Figure 7.11.C). The top ten most significantly enriched pathways included many previously observed in the mock and infected RBPome, nearly all relating to protein synthesis (Figure 7.11.D). Interestingly, gene expression appeared in both the upregulated and downregulated pathways, and indicating that these may be different genes being regulated within the upregulated and downregulated pathways.

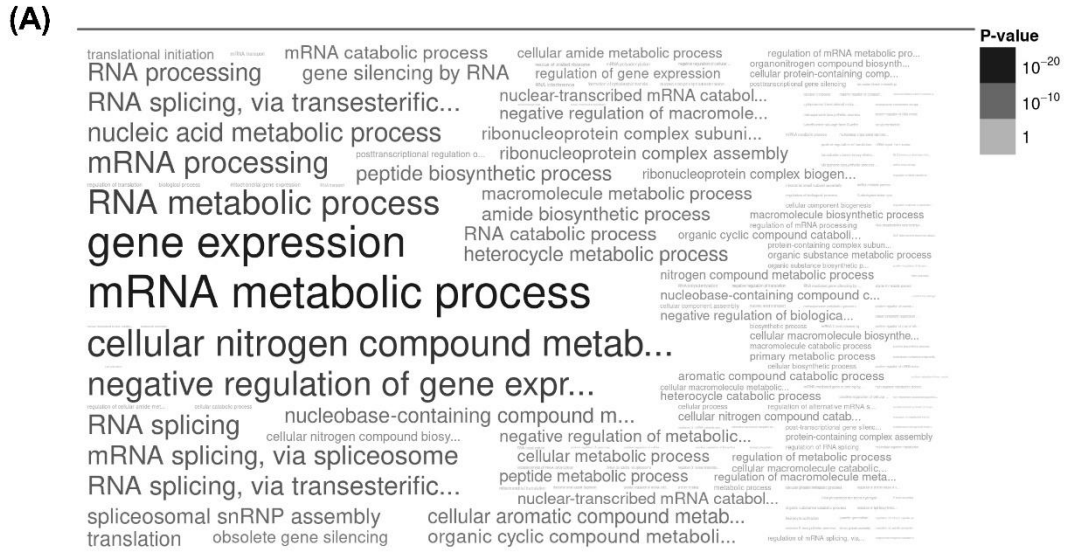
(A)
P-value
10^{-20}
10^{-10}
1
translational initiation
mRNA catabolic process
cellular amide metabolic process
RNA processing
gene silencing by RNA
regulation of gene expression
RNA splicing, via transesterific...
nuclear-transcribed mRNA catabol...
negative regulation of macromole...
nucleic acid metabolic process
ribonucleoprotein complex subuni...
mRNA processing
ribonucleoprotein complex assembly
peptide biosynthetic process
ribonucleoprotein complex biogen...
RNA metabolic process
macromolecule metabolic process
amide biosynthetic process
gene expression
RNA catabolic process
heterocycle metabolic process
mRNA metabolic process
nitrogen compound metabolic process
cellular nitrogen compound metab...
negative regulation of gene expr...
RNA splicing
nucleobase-containing compound m...
mRNA splicing, via spliceosome
negative regulation of metabolic...
cellular metabolic process
RNA splicing, via transesterific...
peptide metabolic process
nuclear-transcribed mRNA catabol...
spliceosomal snRNP assembly
cellular aromatic compound metab...
translation
obsolete gene silencing
organic cyclic compound metaboli...

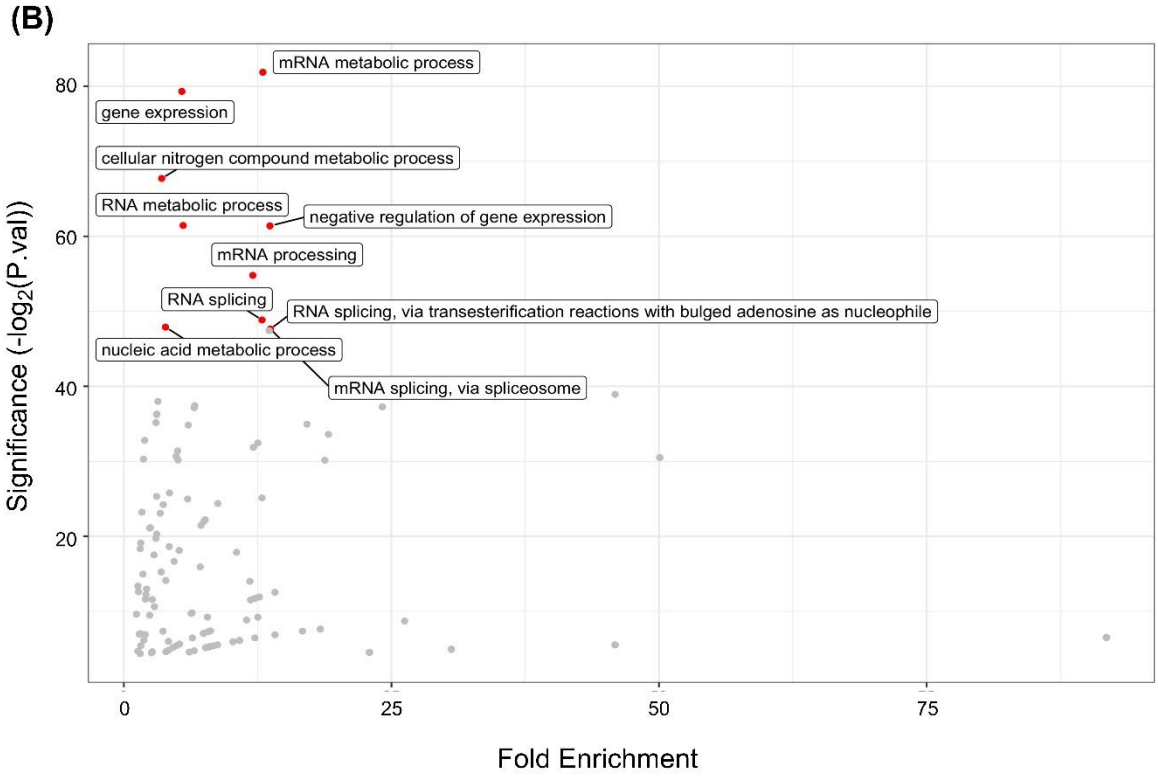
(B)
mRNA metabolic process
gene expression
cellular nitrogen compound metabolic process
RNA metabolic process
negative regulation of gene expression
mRNA processing
RNA splicing
RNA splicing, via transesterification reactions with bulged adenosine as nucleophile
nucleic acid metabolic process
mRNA splicing, via spliceosome
Significance (-log2(P.val))
80
60
40
20
0
25
50
75
Fold Enrichment

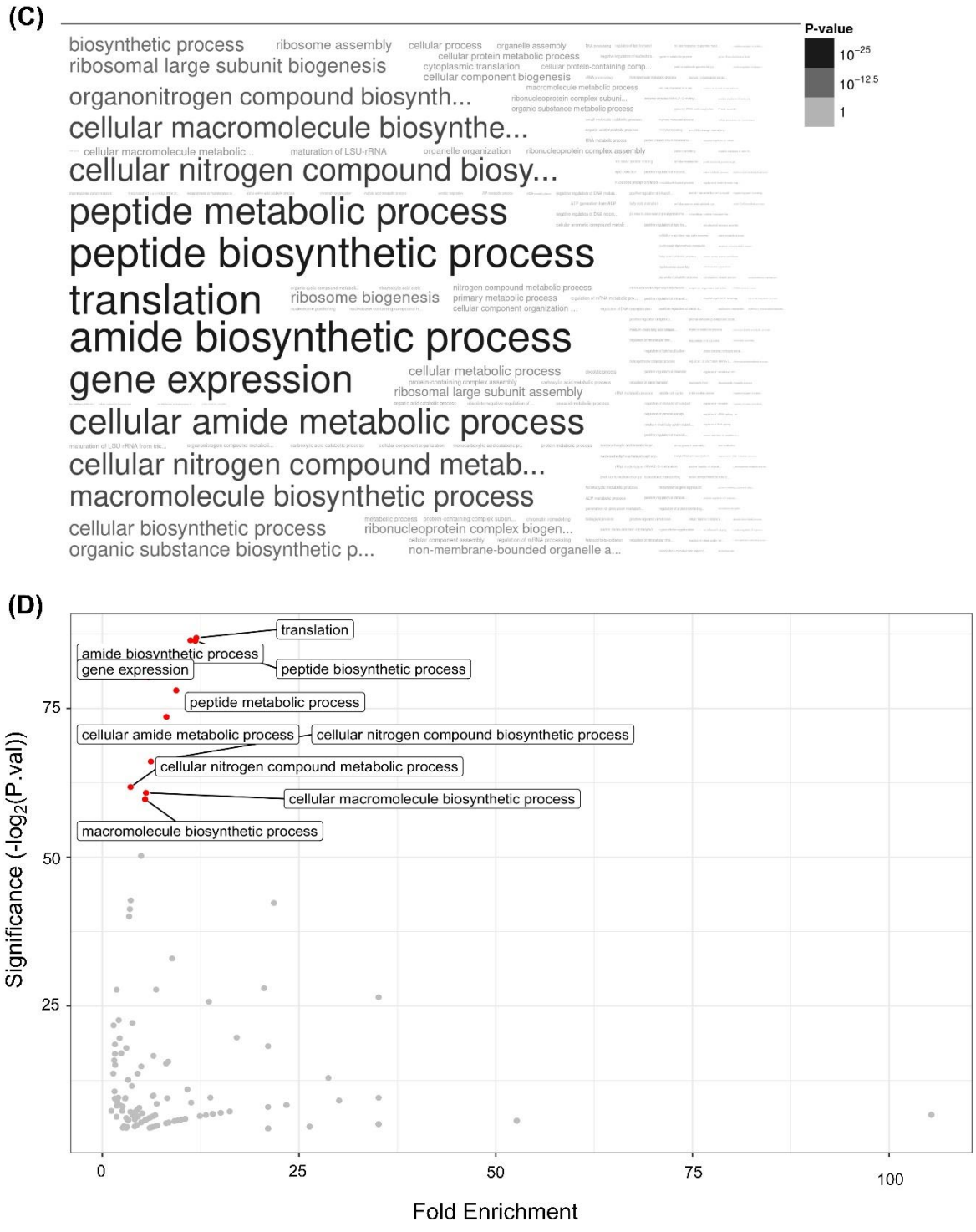

Figure 7.11: Analysis of biological processes enriched in the 10% FDR of the differential ISE6 RBPome. (A) An analysis of the biological processes with which the RBPome proteins contained within the proteins upregulated during infection are associated. The word cloud demonstrates the most enriched processes compared to the background ISE6 proteome based on the associated p-value. (B) The biological processes from (A) were plotted against the fold enrichment. RIC samples compared to the background ISE6 proteome are shown on the x- axis and the significance plotted on the y-axis. The top ten most significant pathways are highlighted on the graph. (C) An analysis of

the biological processes with which the RBPome proteins contained within the proteins downregulated during infection are associated. The word cloud demonstrates the most enriched processes compared to the background ISE6 proteome based on the associated p-value. (D) The biological processes from (C) were plotted against the fold enrichment. RIC samples compared to the background ISE6 proteome are shown on the x- axis and the significance plotted on the y-axis. The top ten most significant pathways are highlighted on the graph.

7.3.4 Selecting targets for downstream experimentation

The analysis of the differential RBPome from Figure 7.9.A was used as a basis for selecting the genes for subsequent knockdown experiments. This differential plot is shown again in Figure 7.12.A, but in this plot the human ortholog labels have been added where possible. Although to this point the 10% FDR was used to define the RBPome groups, for the knockdown gene selection, it was ensured proteins from both 10% FDR and 1% FDR were selected. The proteins contained within the 1% FDR differential RBPome were qualified to be potential knockdown targets (represented by the inner circles of Figure 7.9.C). From this 1% FDR group, the downregulated and upregulated proteins within the top 50% average intensity were isolated in order to ensure that gene knockdowns from this group would target the most abundant proteins to theoretically produce the most apparent results (Figure 7.12.B). From the 10% FDR proteins, where the human homolog was available, a literature search was carried out to determine if these proteins were cited in relation to pro- or anti viral activity as shown in Figure 7.12.C. From this analysis, factoring in the role of the proteins in the enriched pathways, their abundance within the 1% FDR differential RBPome, their significance within the RBPome, and the results of the literature search, the genes selected for knockdown are highlighted in red in Figure 7.12.C. The following genes were selected for further characterisation utilising dsRNA knockdown transfections and subsequent rUUKV infection: *AGO2*, *CUL1*, *EIF3A*, *PABP1*, *PRKRA*, *RBM8A*, *RUXE*, *SND1*, *TOP3B*, *UNKL*, and *XRN1*.

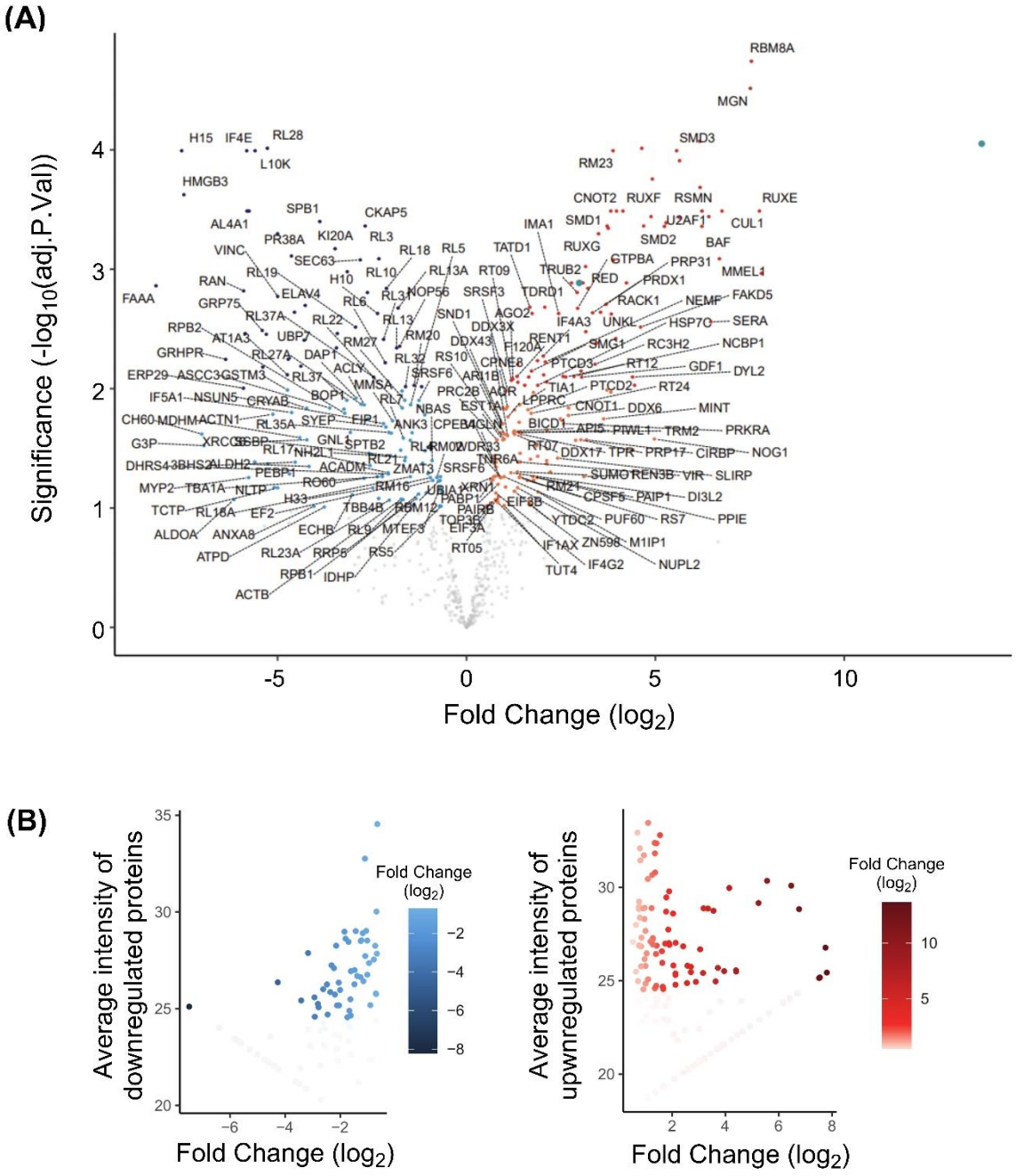
(A)
Significance (-log10(adj.P.Val))
Fold Change (log2)
(B)
Average intensity of downregulated proteins
Fold Change (log2)
Average intensity of upwnregulated proteins
Fold Change (log2)

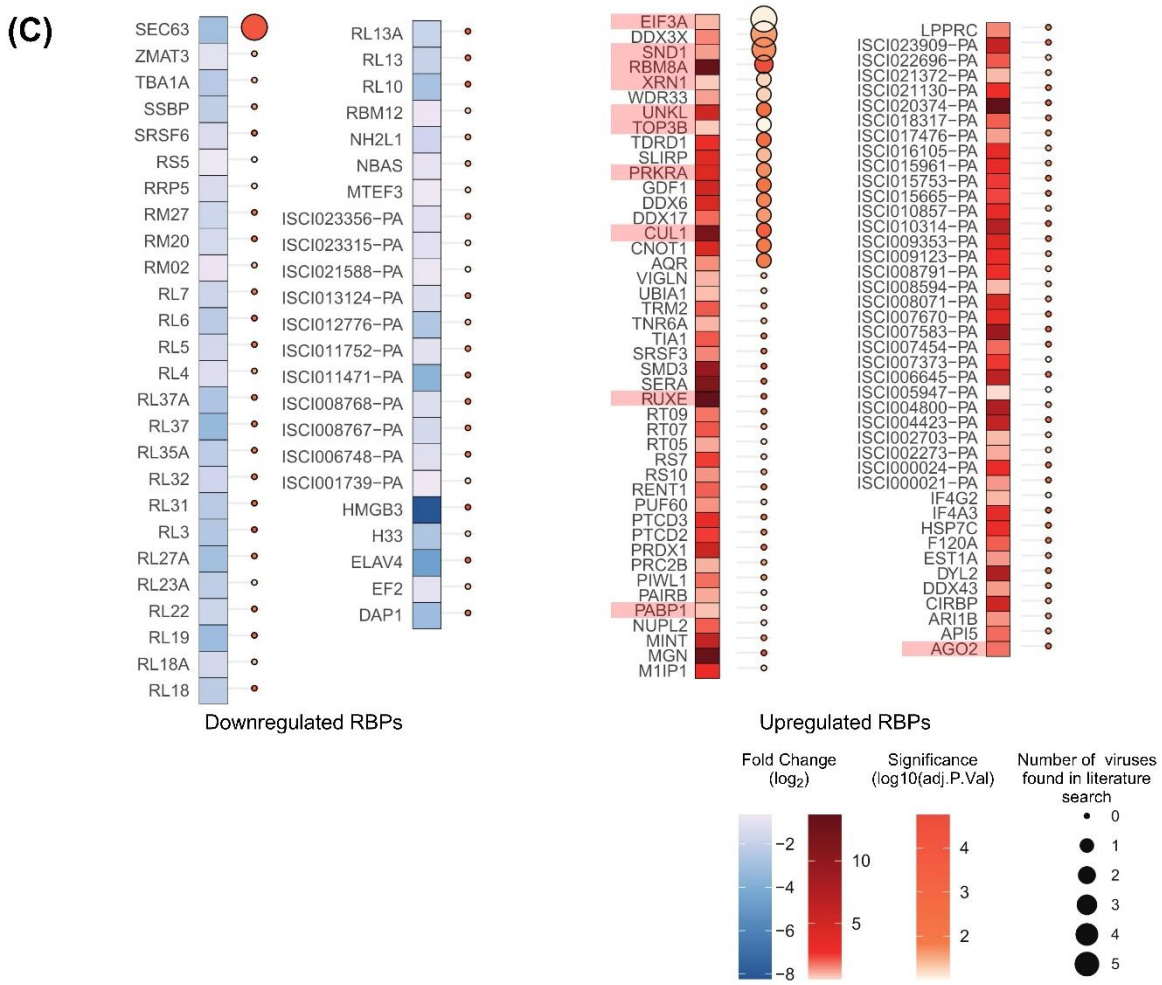

Figure 7.12: Selection of targets for knockdown analysis. (A) Analysis of differential RBPome from Figure 7.9.A with all 10% FDR proteins labelled with human orthologs where possible. (B) To select potential targets for knockdown studies, the 1% FDR proteins within the upper 50% of most abundant (highest intensity) that were at a significantly upregulated (red) and downregulated (blue) fold change were plotted against the -Log10(adj.P.val). (C) The proteins from (B) were screened to determine if the human orthologs were referenced in terms of pro- or anti-viral properties within the literature. The proteins highlighted in the red boxes correspond to the targets selected for dsRNA knockdown.

7.4 Discussion

In order to determine the ISE6 UUKV-infected RBPome and subsequently the proteins that were differentially expressed during infection, the method used to establish the naïve ISE6 RBPome was repeated in UUKV infected ISE6 cell culture. However, before this could be carried out, the infection conditions needed to be confirmed. Although the species from which ISE6 is derived, *I. scapularis*, is very closely related to the vector species for UUKV, *I. ricinus*, and previous growth curve work within this thesis has shown that ISE6 can support UUKV infection (Figure 5.3.A and Figure 5.3.B), RIC requires over 60% of the cells to be in the condition that is to be analysed. In the case of this research, this condition is "infected with UUKV", and therefore from the UUKV ISE6 growth curve data it was determined 9 d p.i. following infection with rUUKV at a MOI of 5 FFU/cell would be a suitable as described in results. To confirm the percentage of infected cells within the monolayer in these conditions, the infected ISE6 cell monolayer was fixed and probed for UUKV N (Figure 7.1). It was important to compare the infected cell monolayers to mock-infected control monolayers as ISE6 cells can auto-fluoresce within the green channel, particularly when cells are under stress. From the differences in fluorescence within the green channel, it was that clear the signal seen within the infected cell monolayers were due to UUKV infection. As seen within the EVOS images, over 95% of the cells showed green fluorescence surrounding the stained nuclei (indicating UUKV infection within the cell), and therefore infection using these conditions ensured that enough starting material would be present for RIC. This represents a potential drawback of this methodology. It would be beneficial in future to expand to earlier infection timepoints to determine if and how the differential RBPome changed during the establishment of infection. However, when infection is first being established there may not be enough material or infected cells to determine the initial RBPome response. Previous studies have shown that some viruses, such as TBEV, are transmitted in under one hour post attachment of the infected tick (Tahir et al., 2020), and therefore it is likely that the cell response does change over time, and so it would be beneficial to attempt to study these earlier timepoints. For the purposes of this research, as this technique had not been attempted previously on UUKV infection in ISE6 cells, ensuring enough material was present to establish confidently an infected RBPome was the priority. In doing this, it was hoped that differential proteins that may play a key role in infection could be identified as a starting point for further investigation and comparison when this methodology was expanded to other conditions within the ISE6 cell line. In line with discussing other conditions, it is arguable whether a MOI of 5 FFU/cell is biologically relevant, as little is known about the range of MOI that is ingested by ticks, or the route of

dissemination of virus into the tick organism post-feeding. As a MOI of 5 FFU/cell caused enough cells to be infected to guarantee effective RIC, it may be beneficial to repeat the methodology at a lower MOI alongside varying the timepoints tested to determine whether the differential RBPome was a dose-dependent response.

As mentioned in the chapter 7.3.1, it is plausible that the UUKV genome contained regions which were capable of interacting with the oligo(dT) capture beads despite the UUKV RNA not being polyadenylated (Elliott & Weber, 2009), allowing them to be isolated during RIC alongside cellular mRNAs. During infection, viral RNA becomes one of the most abundant types of RNA within the cell. I hypothesised that if the oligo(dT) beads were capable of capturing viral RNA (and the vector proteins bound to it), using RIC would be highly informative for elucidating important RBPs during infection. To determine the likelihood of this occurring, the UUKV genomic segments were scanned for poly(A)/poly(A) like sequences. Poly(A)/poly(A)-like sequences were defined as a minimum of 5 A concurrent nucleotides with any sections above 5 concurrent A's being at least 80% A content. All three genomic segments returned over 50 sections of their respective sequences that fit these criteria, meaning it was highly likely RIC methodology I optimised in Chapter 6 would allow the capture viral RNA and development of a more informed model of the infected RBPome.

Once the infected RIC samples were generated, RT qPCR was performed on the inputs and eluates of both infected and non-infected samples to probe for presence of UUKV RNA. As expected, no presence of UUKV M segment RNA was detected within the "mock_infected" samples, but was detected within the "infected" inputs. Most importantly, within the infected samples although the eluate normalised Ct scores were lower than the inputs, which is most likely due to some loss of material during the capture and washing stages, UUKV M RNA was detected within the eluates. This confirmed that UUKV RNA was able to be captured by the oligo(dT) capture beads, and that this technique could be used to determine the landscape of protein-RNA interaction occurring in both viral and cellular RNAs. As the poly(A)-like analysis does not consider the potential formation of secondary RNA structures which may affect affinity to the oligo(dT) capture beads. It would be interesting to repeat the UV-crosslinking and oligo(dT) capture of infected ISE6 cells and calculate the ratio of L:M:S segments within the input and eluate to see if the eluate ratio reflected the number of poly(A)-like sequences within the corresponding segments. Although there were higher levels of RNA within the input samples compared to the mock, which may be due to the presence of infectious material, the decrease of RNA in the eluates was larger than that of the mock samples. This may be due to the UUKV RNA being captured during the RIC 'blocking' vector mRNA binding to the oligo(dT) beads, and then subsequently being

removed during the washing step as these poly(A)-like vRNA sequences are likely to have a weaker affinity to the oligo(dT) capture beads compared to poly(A) mRNA.

When visualising the biological triplicate proteins samples from the RIC of crosslinked and non-crosslinked infected ISE6 cell monolayers via silver staining, there was no difference seen within the inputs. As expected, no proteins (aside from the band representing proteinase K at ~17 kDa) were seen within the non-crosslinked samples. This indicates that UUKV infection does not alter the intracellular environment to where non-crosslinked proteins are pulled down during oligo(dT) capture. From a visual comparison of the banding pattern in the silver stain gels, the eluates not only appeared distinct from that of the inputs, indicating a sub-population of the intracellular proteins were pulled down, but there was an additional band seen at ~25kDa which was not visible within the mock sample silver stains. This band may correspond to the UUKV N protein, further adding to the conclusion that oligo(dT) beads isolated UUKV RNA. Although there is some evidence that UUKV N interacts with mammalian host cell proteins such as GBF1 (Uckeley et al., 2019), to date UUKV N binding to vector mRNA has not been demonstrated. To investigate whether an interaction occurred between cellular RNA and UUKV N, and if so, occurred with specific vector RNA transcripts, UV-crosslinking could be performed before immunoprecipitation using antibodies specific for UUKV N to isolate the N proteins and bound RNA. These could then be analysed by RNA seq.

When finalising the quality of the samples, despite this reduction in eluate RNA, overall, the enrichment of the samples surpassed the minimal threshold. This factor, combined with the silver stains, confirmed that the infected RIC samples were suitable for mass spectrometry, which was then carried out alongside the mass spectrometry of the mock samples in order to minimise the potential variables that may affect the outputs.

Mass-spectrometry is a very sensitive process, and therefore by carrying out the mass-spectrometry runs concurrently on the same apparatus any variability that would be introduced by using different machinery or operator is minimised. However, the MaxQuant output analysis of the infected biological triplicates was still required to undergo diagnostic analysis. This was done by including the infected triplicates data to the previous diagnostics of the non-infected biological triplicates. By doing so, it allows evaluation of not only the quality of the infected crosslinked and non-crosslinked biological triplicates, but to assess if there was evidence of variation between the mock and infected samples. A lack of difference between the mock and infected crosslinked samples would indicate an error upstream of the analysis. These errors could include not enough infected material present during the RIC, or

that minimal/no protein expression and activity changes occurred within the cell. Realistically, this latter hypothesis is not biologically feasible. For the triplicates for each condition (crosslinked and non-crosslinked, mock and infected), several analyses were carried out. These were plotting the Log2 of the protein intensities for each sample to compare the overall distribution of intensities between the samples (Figure 7.3.A), determining the number of missing values when comparing the samples (Figure 7.3.B), and performing a PCA on the data set (Figure 7.3.C). Overall, the results were in line with what was expected. Within the crosslinked samples the intensities of the crosslinked samples were far higher than those in the non-crosslinked. It was unclear whether the infected cell cultures would produce higher intensities in the crosslinked samples, given that viruses can shut off host protein synthesis, hijack cellular machinery to promote viral protein production, and prevent cellular apoptosis and protein degradation, all of which would have an impact on the overall levels of protein (and therefore levels of RBPs) within the cell. Conclusions cannot be drawn as to the cause of the increase seen in the infected triplicates. Conversely, the number of missing values was far smaller in the crosslinked samples compared to the non-crosslinked samples, indicating that the crosslinking caused the isolation of specific RBPs. This increase in intensity of the infected non-crosslinked samples compared to the mock non-infected samples was more expected, as it is likely that abundant 'sticky' viral proteins, such as the UUKV N protein, were also pulled down in a non-specific manner adding to the background of the RIC. Similarly, when analysing the missing values in the data, the minimal variation between and within the triplicates, and the reduced number of missing values in the crosslinked sample compared to the non-crosslinked sample is significant. A large difference between the missing values of the crosslinked infected and non-infected triplicates would potentially indicate a loss of material within the samples during the RIC process, producing samples indistinguishable from background. Although a shift in the RBPome is expected during infection this would not produce a complete abolition of a large proportion of proteins. Similarly, if the missing values of non-crosslinked triplicates was lower/comparable with the crosslinked samples, it would indicate that potential cross-contamination occurred, or the infection affected the capabilities of RIC to isolate only RBPome-related proteins. However, although the overall levels of intensities and missing values were comparable between the equivalent mock and infected samples for crosslinked and non-crosslinked samples, this does not necessarily mean that the specific RBPs within these groups had equivalent levels of intensities in the mock and infected samples, or that the missing values were of the same types of proteins. In this regard, PCA analysis is informative. As two variables were applied to the samples; crosslinking and infection, it is

expected that these would be the main causes of grouping on a PCA plot. If the mock and infected, crosslinked and non-crosslinked samples had similar specific protein intensities and missing values, we would expect to see these groups cluster together, and if this occurred, we could conclude that although the cells were infected there was not enough difference from the mock RBPome or enough material for RIC. When analysing the PCA plot. the biological triplicates discretely grouped together, with the primary factor causing variability being whether the samples were crosslinked, the secondary factor being whether the samples were infected. Given that the purpose of this research was to establish the differential expression of RBPS during UUKV infection within ISE6 which have undergone UV-crosslinking, using the non-crosslinked equivalent samples as a control, this was a significant result as the variable factors of the data were the factors intended for investigation. Therefore, not only did this analysis confirm that the infected crosslinked and non-crosslinked samples were suitable for use in the establishment of the infected ISE6 RBPome, but also in comparison of the mock and infected ISE6 RBPomes.

When looking more in depth at the infected RBPome, it cannot be assumed that the protein makeup, and therefore features such as the biochemical properties and domain types, would be wholly similar to those within the mock RBPome. Although there will be some overlap of protein types due to the lower number of missing values in the crosslinked samples, these missing values may not be the same proteins from the total protein types across the groups, and this is supported by the results of the PCA plot showing clear separation of the biological conditions.

A total of 29 more proteins were found within the infected biological triplicates compared to the mock, and when the 10% FDR criteria was applied to the biological triplicates, 46 more proteins were within the infected RBPome compared to the mock. This is in line with the slightly larger spread of intensities and fewer missing values in the infected crosslinked samples compared to the mock crosslinked samples, as seen within the diagnostic analysis. This is an interesting observation as viruses often try to enact ‘host shut off’ to prevent the infected cells from producing immune proteins which would negatively impact protein types present (Eifan et al., 2013). However, as UUKV has previously been identified as a weak immune antagonist within host cells (Rezelj et al., 2017), and from the growth curve work it is known UUKV infection is not cleared from ISE6 cells, this increase in the number of proteins most likely reflects the production of antiviral RBPs. Interestingly, the UUKV N protein (NCAP) did not appear to be significantly enriched within the crosslinked samples. After examining the intensities related to the NCAP protein, it was determined that the protein was so abundant within both crosslinked and non-crosslinked groups statistically

significant enrichment was unable to be calculated, most likely due to the UUKV N protein being abundant and sticky within the inputs, preventing the UUKV N protein from being removed during RIC. The UUKV L protein was significantly enriched within the crosslinked sample, showing that the specificity of the pulldown was maintained during infection and infection was present within the starting material. Additionally, as we have seen that UUKV M RNA (and therefore potentially the other viral genomic segments) were isolated within the RIC, this may also cause other RBPs which do not necessarily have antiviral activity but can bind the vRNA to be pulled down. When looking at the biochemical properties of the infected RBPome, aside from the expected results of following the trends seen within the mock RBPome, there was one notable difference in that the peak of the pI was higher within the infected RBPome compared to mock. As there were 46 more proteins in the infected RBPome than in the mock RBPome, these proteins may have contributed to the higher pI peak. This may also indicate that the additional proteins within the infected RBPome interact with RNA through specific positively charged domains, however further analysis into the differential RBPome and the structures of these proteins would be needed to determine if this theory was accurate. As seen in the mock RBPome, no significant differences were found in the intrinsic disorder analysis (Figure 7.4.D), however as mentioned in the previous chapter, this does not mean that the intrinsic disorder seen within the infected RBPs has no biological or functional relevance.

The infected RBPome proteins were also analysed via InterproScan, which returned 88 proteins with no identifiable protein domains. Of these proteins, 75 were also within the mock RBPome. Due to most of these proteins being found in both samples, it can be hypothesised that the lack of identifiable domains may be due to the quality of the FASTA files, as their significant presence within the crosslinked groups for both mock and infected indicated that they bind specifically to the RNA. Additionally, despite the increased number of proteins within the infected RBPome compared to the mock RBPome, the ratio of proteins with known RBDs and unknown domains was maintained at roughly 50%, adding to previous evidence of potential conserved methods of RNA interaction in the RBPome relying on both specific RBDs and other mechanisms. Similarly, the odds ratios of domain enrichment were maintained within the infected RBPome compared to the mock RBPome, whereby the classical RBDs were over 3 times more enriched than the non-classical. As there was overlap between the types of proteins within the mock RBPome and infected RBPome, it was unclear what the overall distribution of enriched domain types would be and how comparable the domain types would be between the groups. There were a few differences noted between the mock RBPome and infected RBPome, as described in Chapter

7.3.2. The most interesting of these differences being the reduced enrichment of Zinc-finger containing family domains compared to the other domains within the enriched domain types, indicating that there may be a different level of reliance on domain types when the ISE6 cells are infected. As in the mock RBPome analysis, there are many proteins within the cells that contain classical RBDs, and therefore the odds enrichments may not be significant as the difference between the small RBPome sample size and the whole proteome prevents a more accurate assessment of enrichment. In comparison, there are far fewer non-classical domains within the whole proteome, and therefore significance is able to be determined, although no non-classical domain was upregulated in the infected RBPome. When looking at only the proteins with no known RBDs, the biochemical properties of this group reflected the properties found within the mock equivalent, further supporting the hypothesis that the proteins which contain no known RBDs rely in other features such as intrinsic disorder in order to interact with UUKV.

The biochemical properties of the mock and infected RBPomes were then compared directly to each other. The HI and overall percentage disorder were indistinguishable. As expected from the previous pI curves, the infected RBPome peak was broader and covered a higher pI than the mock RBPome. When splitting the percentage disorder distribution of mock and infected RBPome proteins with known RBDs and unknown domains, the known RDB groups were very similar. In comparison to this, when comparing the mock and infected unknown groups, potentially due to the infected unknown group having more proteins (of which more return no percentage intrinsic disorder), there is a more prominent group of proteins with an intrinsic disorder between 5-25% in the mock group which seems to be reduced in the infected unknown group. This was the opposite of what was expected, as it was hypothesised prior to this that the ISE6 cells may use proteins with intrinsic disorder in an antiviral manner to bind viral genomic segments as these regions may allow greater flexibility and a variety of conformations within the protein to maximise interaction with the viral material. From these data, a new hypothesis is that the proteins containing these intrinsic disordered regions are reduced within the infected cells to prevent viral promotion through allowing greater flexibility within the protein, preventing differentiation between cellular and viral RNA. To confirm this hypothesis, it would be interesting to analyse the structure of the proteins showing intrinsic disorder to see if these features play a role in the proteins RNA binding capabilities and functions.

Unsurprisingly given there were more proteins present within the infected RBPome, 11 more pathways were enriched within the RBPome, although similar to the domain enrichment, there were minimal differences aside from the increase in enrichment of amide biosynthesis

and inclusion of mRNA metabolic processes within the top ten significantly enriched pathways. The enrichment of the mRNA metabolic processes was most likely due to either the virus hijacking the cellular machinery to promote viral replication, transcription, and translation, or the vector cell upregulating the proteins involved in producing antiviral peptides. The latter is arguably more likely, as the increase in enrichment of amide biosynthetic processes may be related to producing antiviral peptides.

However, although elucidating the details of the biochemical properties and domain details of the infected RBPome is interesting, as this has previously been undefined and can in future be used to compare to the infection conditions of other viruses and/or other tick cell lines, this group contains both upregulated and downregulated RBPs during UUKV infection and therefore the amount of information that can be gained upon the differences that occur during infection is limited without further differential comparison to the mock RBPome. When this was carried out, 283 proteins were significantly up- or down- regulated to a 10% FDR, which will be referred to as the differential RBPome. Just over 2/3rds of these proteins had identifiable human orthologs, and therefore these will be used to refer to the proteins involved in the differential RBPome wherever possible. Of these 283 proteins, 127 were significantly downregulated, and 156 were significantly upregulated, within the differential RBPome when the ISE6 cells were infected with UUKV, corresponding to less than 2% of the identified proteome. These percentages fall within the expected range, as when looking at HEK cells as a comparative example, less than 4% of the total proteome are RBPs that have been shown to interact with mRNA, and therefore we would expect a lower percentage than 4% to be differentially expressed in different conditions (Castello et al., 2016). Additionally, these results are similar to the differential transcriptomics of *A. phagocytophilum*, where bacterial infection caused the upregulation of 45 genes and the downregulation of 129 genes (P. Alberdi et al., 2015; P. Alberdi et al., 2016). Although these levels were lower than the number of proteins found within this study, one of the drawbacks to transcriptomic analyses is that less abundant transcripts within the cells are often missed. This differential RBPome is an exciting result, as by using the UV-crosslinking and oligo(dT) method the proteins captured, and therefore those that are differentially expressed, can be considered to reflect the activity within the cells as these proteins were captured when actively interacting with the RNA. This differs from other proteomic techniques, such as whole cell proteomics, whereby a shift in protein quantities may not accurately reflect the changes in activity within the cells. However, the caveat to this method is that because of the nature of the capture method, the analysis is biased towards the RBPome function. Therefore, although the results allow for investigation into the RBPome activity within

infection, this only provides a partial picture of the activity changes within the cell and may miss out on other important pathways such as those involved in the RNAi pathway described in the introduction. When translating this to domains, the only enriched domain, within the differential RBPome was the FMRP KH0 domain. The fragile X mental retardation protein (FMRP)'s function is currently not fully understood, but is known to control different steps of mRNA metabolism in humans through interacting with proteins, mRNA and non-coding RNAs, and in humans when this protein is lacking or mutated it can lead to intellectual neurodiversity such as autism spectrum disorder (ASD) or intellectual disability (D'Annessa, Cicconardi, & Di Marino, 2019). The KH0 of this domain is considered a non-canonical/degenerate KH domain lacking the conserved GxxG motif loop, which appears to destabilise the protein, however the structure of these domains needs to be further investigated before conclusions can be drawn upon the impact in arthropods (Pereira & Lupas, 2018; Santorelli et al., 2022). These results need to be taken with caution, as the size difference between the differential group and the whole proteome may prevent enrichment and significance being accurately assessed, and therefore it was decided not to segment the data further to conduct domain analysis. The other interesting detail of the domain analysis is that, when visualising the spread of percentage intrinsic disorders, in continuing what has previously been seen in the unknown samples, there is a bulge at a percentage intrinsic disorder between 5-25%, although this is less apparent in the differential RBPome, however this may be due to the smaller number of proteins.

Moving on from the domain analysis, the enriched upregulated and downregulated pathways were examined using the tools available in VectorBase. As expected, the upregulated pathways were predominantly involved in mRNA processing (including metabolism and splicing) and gene expression, which signifies the cell moving to an antiviral state, potentially alongside the virus hijacking the machinery of the cell to promote viral replication. A similar result was seen within TBEV infection of IDE8 cell cultures at 6 days p.i., where through transcriptomic and whole cell proteomic analysis, nucleic acid processing was shown to be upregulated (Weisheit et al., 2015). What was particularly interesting from these results was the significant enrichment of cellular nitrogen metabolic processing, as it has been observed in other arthropod species (such as mosquitoes) that triggering of the antiviral response causes the production of reactive nitrogen species, and so this may also be a response within tick cells (Fogaça et al., 2021). Similarly, the downregulated pathways were involved predominantly in peptide and macromolecule metabolism. It can be hypothesised that the gene expression cited in the downregulated pathways is involved in the reduction of these metabolic pathways within the cells. Infected cells often undergo

suppression of translation in order to produce an antiviral state within the cell and prevent viral replication.

From the experimental work and analyses in this chapter and the previous chapter, the differential RBPome at an infection timepoint at 9 d p.i was established, alongside the up- and down-regulated pathways that were enriched during infection. Although these proteins are more likely to signify a change in activity within the cells due to being isolated from actively binding mRNA, at this point the specific roles for each identified protein within the RBPome in terms of UUKV kinetics cannot be confirmed. Just because a protein is upregulated within infection, does not mean it plays a direct role in UUKV infection, as there is a possibility this upregulation is a biproduct of other activity changes within the infected cells. To validate the mass spectrometry data and to provide proof of principle for this work, the next stages of this research were to carry out knockdowns of selected genes to determine if the proteins have a pro- or anti- viral effects on UUKV replication kinetics. Although the following analysis was carried out for both the upregulated and downregulated proteins, only upregulated proteins were selected for targeting to maximise the possibility of seeing an effect on viral kinetics when the protein was removed. The selection process was ensured a breadth of targets, although the criteria may overlap for certain proteins; proteins within the 10% FDR group (EIF3A, SND1, XRN1, TOP3B, PRKRA, and PABP1), proteins within the 10% FDR group that are also within the top 50% most abundant proteins (RBM8A, UNKL, RUXE, CUL1, and AGO2), and proteins where the human ortholog has been cited in the literature in relation to viral kinetics (EIF3A, SND1, RBM8A, XRN1, UNKL, TOP3B, PRKRA, and CUL1). Again, for this latter criterion, just because the human orthologs have pro- or antiviral activity does not guarantee the tick protein will also carry out this activity in the vector cells. Once selected, the next steps were to carry out dsRNA knockdowns. In future, it would be interesting to also target downregulated proteins, to determine if these proteins (even if reduced within the cell) are acting in an antiviral manner, or if by completely removing the protein from the cell acts in a proviral manner.

In conclusion, the previously undefined RBPome of rUUKV infected ISE6 cell cultures was elucidated and used to compare against the mock RBPome previously defined in Chapter 5 to determine the differential expression of RBPs during infection (the differential RBPome). This research is the first example of the RBPome of an infected tick cell line that has been established, and therefore this is the first differential RBPome to be elucidated using this method. The infected and differential RBPome showed many of the expected biochemical properties and indicated that proteins may use intrinsically disordered regions to allow different protein conformations capable of binding RNA where no known RBDs are present.

The next stages of this research will therefore be to carry out dsRNA knockdowns as will be discussed in the next chapter.

Chapter 8 Analysing the effect of RBP knockdown on UUKV infection in ISE6 cell cultures

8.1 Introduction

The methodology of using dsRNA transfection to knock down genes within cell lines and organisms has been employed since the early 2000's (Elbashir et al., 2001; Mocellin & Provenzano, 2004; Montgomery, 2004). The initial study by Elbashir et al., found that when a long dsRNA homologous to the gene that is intended to be silenced is cleaved into siRNAs of 21-22 nucleotides in length, the siRNAs then go on to be taken up by the cell's RISC machinery (previously described in Chapter 7). This then targets the mRNA transcripts of the gene of interest, causing them to be degraded and preventing the production of their corresponding proteins (Au, Portelli, & DeWitte-Orr, 2022; Elbashir et al., 2001; Mocellin & Provenzano, 2004; Schnettler et al., 2014). This technique has been used for knockdown of both the cell's own genes and the genes of viruses introduced into the cells, the latter of which results in the reduction or prevention of viral infection (Au et al., 2022; Mocellin & Provenzano, 2004). There are certain drawbacks and risk factors that must be considered when applying dsRNA silencing. In contrast to producing cell lines or organisms that containing stably transfected DNA plasmids producing the RNA to be cleaved, or mutating/deleting the gene of interest from the genome to produce a stable knockdown, dsRNA knockdowns can be considered transient as over time the introduced dsRNA will be degraded (Chong, Yeap, & Ho, 2021; Mocellin & Provenzano, 2004). In addition, there are several different reagents and established methods for transfecting the dsRNA into target cells, which run the risk of triggering an immune or apoptotic response within the cells, and produce varying degrees of transfection efficiency (Chong et al., 2021; Fiszer-Kierzkowska et al., 2011; Jacobsen, Calvin, & Lobenhofer, 2009; Mocellin & Provenzano, 2004). Beyond just the variables surrounding introducing genetic material into a cell, in both examples of transfecting in a stable plasmid or dsRNA, there is a risk that the sequences utilized have off-target interactions. This occurs if the siRNA is not specific to the sequence of the gene of interest. Therefore, when deciding upon the sequences used for the knockdown, care must be taken to prevent and/or reduce off-target effects which may prevent the accurate analysis of any results generated. Optimisation experiments therefore need to be conducted and validated before any knockdown experiments can commence (Chong et al., 2021; Mocellin & Provenzano, 2004; Montgomery, 2004).

The use of RNA knockdowns and interference has been applied to tick research over the last past twenty years, with the first publication demonstrating the successful application of RNAi gene silencing in ticks being published in 2002 (Aljamali, Sauer, & Essenberg, 2002). The introduction of RNA material was achieved through incubation with or injection of dsRNA, and once internalised by the cells the siRNA production pathway was induced

(Aljamali et al., 2002). Introduction of dsRNA by either incubation or injection has shown that the dsRNA is capable of permeating a variety of organs (past the point of the injection site), such as the synganglia, salivary glands, and midguts (Karim, Kenny, Troiano, & Mather, 2008). In comparison, the first case of chemically induced transfection in ticks, which is the most similar methodology comparatively to the technique used in this work, was done by incubation of the *R. haemaphysaloides* with liposomes containing dsRNA (Y. Zhang et al., 2018). According to Fuente and Kocan, by 2022 over 250 publications have been released describing RNA interference in ticks, examining the impact of protein knockdowns on a variety of topics including cellular molecular pathways, fertility, and pathogen infection (de la Fuente & Kocan, 2022). Although more data is needed to validate this, there is evidence to suggest that dsRNA knockdown can be persistent and even passed on into offspring (de la Fuente & Kocan, 2022; Nijhof et al., 2007). When *R. microplus* females were injected with dsRNA against several tick antigens, downregulated levels of mRNA could be detected in the eggs laid by the injected female, with this downregulation still being present several weeks after as the larvae hatched and developed (Nijhof et al., 2007). Further, work by Barry et al, demonstrated that the length of RNA introduced impacted the efficiency of the knockdown. They demonstrated that dsRNA was overall, a better tool than siRNA for gene knockdowns (Barry et al., 2013). The method adopted in this study used the introduction of dsRNA by magnetofection (magnetic beads and transfection reagent; Oz Biosciences) targeting ten candidate RNA-binding proteins, selected from ISE6 genes present in ISE6 cell culture. I will briefly summarise the genes of interest as defined by Figure 7.12 in Chapter 7 and describe the associated proteins, using the human ortholog counterparts as assigned through Inparanoid analysis. All functions described below are documented within mammalian systems unless specified otherwise, with the ortholog ID mapping obtained from Uniprot. If any information has been attributed to the description of the protein or gene found in ISE6 as detailed by VectorBase, this will be highlighted.

8.1.1 *AGO2*

The human ortholog for the gene and corresponding protein for Argonaute RISC Catalytic Component 2 (AGO2) corresponds to the ISE6 protein coding gene *ISCI013378*, which is labelled as a gene with an unspecified product. There are 4 AGO proteins expressed in humans (AGO1-4), all of which share a large amount of structural similarity. These proteins are largely known for being important components of the RISC complex, aiding in small RNA (smRNA) biogenesis. Of all 4 AGO proteins, in mammals only AGO2 mediates the

endonucleolytic cleavage of their target mRNAs (Bodak, Cirera-Salinas, Luitz, & Ciaudo, 2017; Muller, Fazi, & Ciaudo, 2019; H. Su, Trombly, Chen, & Wang, 2009). Unlike many of the other genes and proteins described this chapter, AGO2 has been characterised and studied within arthropods such as mosquitoes and drosophila as previously described in Chapter 1.1.1.2 and Chapter 7, including highlighting it as a key player in antiviral immunity through its functions in the RNAi pathway. It is a common feature of both DNA and RNA viruses to encode viral suppressors of the RNAi pathway to prevent siRNAs targeting the viral genome, and this suppressive activity can target several different stages of the RNAi pathway including preventing dsRNA cleavage by Dcr-2, binding or degrading the siRNA to prevent it associating with the RISC machinery, or interfering directly with Dcr2 or AGO2 function (Bonning & Saleh, 2021; van Rij et al., 2006). In the mosquito species *Aedes aegypti*, when AGO2 knockout mosquitoes were infected with arboviruses such as DENV2, ZIKV, Mayaro Virus (MAYV) and the bunyavirus RVFV, the instances of organism death were highly increased due to the increased level of infection, vRNA buildup, cell lysis and tissue damage (Dietrich, Jansen, et al., 2017; S. Dong & Dimopoulos, 2023).

8.1.2 *CUL1*

The human ortholog for Cullin 1 (*CUL1*) corresponds to the ISE6 protein coding gene *ISCI013256*, which is labelled as a gene with an unspecified product. In mammalian systems, CUL1 is an essential component of the SKP1-CUL1/CDC53-F box proteins (SCF) ubiquitin E3 ligase complex, which functions to catalyse the ubiquitination of regulatory proteins such as β-catenin and IκB (J. Zheng et al., 2002). Essentially, the protein functions as a scaffold onto which adaptor, substrate receptor, and regulator proteins get loaded, and this complex is then further regulated by post-translational modifications (Mahon, Krogan, Craik, & Pick, 2014). The protein itself is an elongated protein consisting of a long stalk and globular domain (N. Zheng et al., 2002). At the time of writing, there is no confirmed direct CUL1-RNA interaction, although through association with RING proteins, CUL1 works to ubiquitinate DNA-bound proteins and represses nuclear-encoded mitochondrial and splicing-associated genes when co-localised with c-MYC (Sweeney et al., 2020). CUL1 localises in both the nucleus and cytoplasm and has also been shown to interact with hnRNP (complexes of RNA and protein localised within the nucleus) binding proteins (Cano, Rapiteanu, Sebastiaan Winkler, & Lehner, 2015; Hildebrandt et al., 2017; Sweeney et al., 2020). Viral proteins have been shown to interact with and hijack E3 ligase complexes in order to degrade host cell factors that would otherwise be present within the cell and able to act in an anti-viral manner, such as intracellular immune factors (Mahon et al., 2014). CUL1

and associated factors have been shown to be targeted for degradation by Kaposi's sarcoma-associated herpesvirus, myxoma virus, rotavirus, polerovirus, HIV-1, and RVFV to name a few (Mahon et al., 2014). RVFV NSs protein has been shown to target the substrate receptor of CUL1 FBXO3, which causes the degradation of transcription factors leading to a dampening of the up-regulation of intracellular innate immune factors (Kainulainen et al., 2014; Le May et al., 2004).

8.1.3 *EIF3A*

The human ortholog for eukaryotic translation initiation factor 3a (*eIF3a*) corresponds to the ISE6 protein coding gene *ISCI020306*, which is labelled as a gene with an unspecified product. Eukaryotic translation initiation factors (eIFs) play an important part of translational control by exerting effects over the initiation of translation. eIF3 is the largest of the eIF complexes and consists of 13 subunits, including eIF3a, and functions by preventing the reassociation of the 40S ribosome with the 60S ribosome alongside recruiting other eIFs to produce a ternary complex (Gomes-Duarte, Lacerda, Menezes, & Romao, 2018; S. Ma, Dong, Huang, Liu, & Zhang, 2022). The protein is 170 kDa in size and contains three putative domains including proteasome-COP9-initiating factor 3, spectrin, and the C-terminal 10 AA repeat (Pincheira, Chen, & Zhang, 2001). EIF3a has been shown to have RNA interaction capabilities, as it is capable of regulating mRNA translation via binding to the 5'-UTR sequence in the transcript corresponding to the internal ribosome entry site sequence (Gomes-Duarte et al., 2018; Yin et al., 2013). There is also some evidence to suggest this protein can accelerate the translation of mRNAs by interacting with the 3' UTR, however this mechanism has yet to be defined (Z. Dong, Liu, & Zhang, 2020). In the context of viral infection, many viruses interact with eIF3a. When eIF3a was depleted in cells before infection with hepatitis E virus, there was a significant reduction in viral replication and eIF3a was also found in the viral translation/replication factories (Subramani et al., 2018). This is also like the non-structural protein of mammalian orthoreoviruses, which strongly interacts with eIF3a in viral inclusion bodies to recruit and maintain ribosomes for the translation of viral mRNA (Desmet, Anguish, & Parker, 2014). The NS38 proteins from aquareoviruses also associate with eIF3a and it is speculated that these interactions promote viral mRNA translation (J. Zhang et al., 2019). In comparison to this, the foot and mouth disease virus viral protease degrades eIF3a and eIF3b which may contribute to the shutdown of host mRNA translation (Rodriguez Pulido, Serrano, Saiz, & Martinez-Salas, 2007).

8.1.4 *PABP1*

The human ortholog for polyadenylate-binding protein 1 (*PABP1*) corresponds to the ISE6 protein coding gene *ISCI014211*, which is labelled as polyadenylate-binding protein. The specific functions depend on the localisation of the protein, as PABP1 can be located in both the cytoplasm or the nucleus, although for this study we will focus only on the cytoplasmic functions (Nicola K. Gray, Hrabálková, Scanlon, & Smith, 2015). In mammals, PABP1 plays an important role in the initiation of translation by interacting with eIF4, recruiting additional translation factors, and helping to bring the ends of the mRNA into functional proximity creating a 'closed loop' conformation. This conformation increases ribosomal recruitment while also protecting the mRNA from degradation. Other functions include regulating the transcription, polyadenylation, deadenylation, and degradation of mRNA. Outside of this role, PABP1 is involved in the miRNA-mediated repression and nonsense-mediated decay mRNA surveillance pathway. In some instances, these functions such as recruiting transcription factors, are independent of the mRNA containing a poly(A) tail by interacting with AU rich regions on RNA. (M. Brook et al., 2012; Matthew Brook, Smith, & Gray, 2009; Derry, Yanagiya, Martineau, & Sonenberg, 2006; Nicola K. Gray et al., 2015; R. W. Smith, Blee, & Gray, 2014). PABP1 can interact with RNA and proteins via four distinct RRMs, a proline-rich region and a C-terminal domain (M. Brook et al., 2012; Matthew Brook et al., 2009). PABPs as a family are very common targets for viruses, including several viruses that do not have poly-adenylated RNAs, and can be acted upon by the virus in a number of ways, including modifying their stability, complex formation, or cellular localisation (Gao, Tang, Hu, & Zheng, 2022). It has been reported that upon infection, bunyaviruses re-localise PABP1 from the cytoplasm to the nucleus (Burgess et al., 2011). In RVFV infection, the non-structural S (NSs) protein is responsible for the removal of PABP1 from the cytoplasm and transportation into the nucleus. Although this is not required for RVFV replication, by removing PABP1 the translation of viral mRNA is favoured over that of host mRNA causing a more pro-viral intracellular environment and increasing viral translation (Copeland, Altamura, Van Deusen, & Schmaljohn, 2013).

8.1.5 *PRKRA*

The human ortholog for the protein activator of interferon induced protein kinase EIF2AK2 (*PRKRA*) is the gene that encodes for the protein known as protein activator of the interferon-induced protein kinase (PACT), and corresponds to the ISE6 protein coding gene *ISCI023181*, which is labelled as a gene with an unspecified product. Although there is a low level of PACT always expressed within cells, the PRKRA gene becomes activated

during the IFN or cell stress responses, such as upon detection of viral infection. The production of the PACT protein triggers a signalling cascade through activating the protein kinase R (PKR), which goes on to inactivate eIF2α and results in lowered protein production within the cell. There is also evidence to suggest that PACT production can cause cellular apoptosis (R. C. Patel & Sen, 1998; Peters, Hartmann, Qin, & Sen, 2001). Additionally, in humans, PACT can associate with a complex of Dicer, hAgo2, and TAR RNA binding protein (TRBP), and plays a role in the RNA silencing pathway. If PACT is depleted in cells, the accumulation of mature miRNAs and siRNAs leads to an increase in interference and prevents continuation of the cell cycle. This protein has also been shown to be required for cardiovirus-triggered interferon responses in mammalian cells (Y. Lee et al., 2006; M. Miyamoto & Komuro, 2017). PACT contains two dsRNA-binding motifs (Peters, Seachrist, Keri, & Sen, 2009). Viral proteins involved in the PKR cascade prevent the cellular antiviral response by preventing the cells producing anti-viral factors and slowing protein translation within the cells. The VP35 protein of both Ebola and Marburg viruses bind to PACT to prevent PKR activation (Hume & Muhlberger, 2018; Schumann, Gantke, & Muhlberger, 2009). Although there has been some evidence to show that several bunyaviruses, including TOSV and RVFV, target PKR for proteasomal degradation, no conclusive evidence has yet been found that shows PACT was targeted (Cesaro & Michiels, 2021).

8.1.6 *RBM8A*

The human ortholog for RNA-binding protein 8A (RBM8A) corresponds to the ISE6 protein coding gene *ISCI016642*, which is labelled as a gene with an unspecified product. This protein is highly conserved among species and is an important component of the splicing-dependant multiprotein exon junction complex (EJC), alongside the Mago homolog (MAGOH), eIF4a3, and to a lesser degree metastatic lymph node 51 (MLN51) and other auxiliary factors. In some publications, RBM8A is also referred to as Y14, when describing non-mammalian homologs (Asthana et al., 2022; Chuang, Lee, & Tarn, 2015). The EJC associates with newly spliced mRNAs to help guide downstream mRNA biogenesis in an almost imprinting manner post-splicing. RBM8A and the associated complex are also reportedly involved in nonsense-mediated mRNA decay, translational enhancement through bridging the EJC and 48S pre-initiation complex, and mRNA metabolism. The latter of which can also be independent of the EJC complex (Asthana et al., 2022; Chuang et al., 2015; Kataoka et al., 2000; Nott, Le Hir, & Moore, 2004). Although primarily concentrated within the nucleus, some RBM8A is diffused throughout the cytoplasm and is shuttled back and forth (Chuang et al., 2015; Salicioni et al., 2000). This protein contains a single RNA

binding domain (RBD) comprising of two RNP-CS and RNP-2 consensus motifs (Conklin et al., 2000; Salicioni et al., 2000). Although there is a lot of evidence to show that viruses target various components of the EJC, there is not as much evidence to show that viruses target RBM8A specifically (Popp, Cho, & Maquat, 2020). One example is that RBM8A has been shown to target WNV RNA for non-sense mediated decay, however this interaction is disrupted by the capsid protein of the virus by interfering with RBM8A's association to a helper protein – PYM1. This is also seen within DENV (M. Li et al., 2019).

8.1.7 *RUXE*

The human ortholog gene corresponding to the ID *RUXE* produces the protein with the recommended name small nuclear ribonucleoprotein E (SNRPE) corresponds to the ISE6 protein coding gene *ISCI013993*, which is also labelled as producing the small nuclear ribonucleoprotein E protein. The human SNRPE protein is also known as Sm-E, and is one of seven consistent core components of the pre-mRNA processing U-rich small nuclear ribonucleoproteins (U snRNPs) complexes which assemble in a stepwise manner onto single-stranded snRNAs and function to catalyse the excision of introns to produce processed mRNA through both splicing and alternate splicing (Boudreault, Roy, Lemay, & Bisaillon, 2019; Pasternack et al., 2013; Urlaub, Raker, Kostka, & Luhrmann, 2001; Will & Luhrmann, 2011). There are five U snRNPs which function on different types of intron junctions (Will & Luhrmann, 2011). When RNA is absent, the Sm proteins form three stable heteromeric complexes, with the Sm-E/SNRPE protein being complexed to Sm-F and Sm-G. SNRPE contains the SM motif, which is composed of two conserved regions and a non-conserved linker region. Although through cross-linking studies, no specific SNRPE-RNA interaction was elucidated, it is highly likely this protein interacts with RNA, there is evidence to show that the Sm domains recognise short U-rich stretches and that this is conserved throughout eukaryotes (Achsel, Stark, & Luhrmann, 2001; Urlaub et al., 2001). At the time of writing, there is no published evidence to show conclusively the presence of SNRPE within the cytoplasm in mammalian cells. However, in plants the core spliceosomal Sm proteins have been shown to be present in the cytoplasm as part of mRNA complexes, and it is possible to hypothesise that SNRPE may be exported to the cytoplasm either as part of a complex or individually (Hyjek-Skladanowska et al., 2020). Many viruses, including those in the *Herpesviridae*, *Papillomaviridae*, *Flaviviridae*, and *Orthomyxoviridae* modulate alternative splicing for their own benefit, such as to generate alternatively spliced viral mRNA or prevent host snRNA from being spliced (Boudreault et al., 2019; R. Li et al., 2023). There is no evidence at this current time to show that bunyaviral RNA interacts with

the spliceosome complex in order to edit vRNAs, partially given that bunyavirus mRNA synthesis is coupled directly to translation to prevent premature transcription termination, this does not remove the possibility the vRNA interacts with components of the complex for non-splicing purposes (Barr, 2007).

8.1.8 *SND1*

The human ortholog gene corresponding to *SND1* produces the protein staphylococcal nuclease and Tudor domain-containing protein 1 (SND1) and corresponds to the ISE6 protein coding gene *ISCI014289*, which is also labelled as producing the staphylococcal nuclease domain-containing protein. This protein is highly conserved in mammalian systems, and has also been identified in other species such as drosophila (Ying & Chen, 2012). This protein is present in the cytoplasm and is an important component of the RISC complex, and mediates miRNA decay in AGO2-loaded and unloaded miRNAs, with this decay being required for cell cycle progression (Elbarbary et al., 2017; Tsuchiya et al., 2007). Outside of this function, SND1 has shown multiple other biological functions including dsRNA editing, pre-mRNA splicing, and germline piwi-interacting (pi)RNA biogenesis, through interactions with proteins such as Piwi, Ago2, and Myb (Ishizu, Kinoshita, Hirakata, Komatsuzaki, & Siomi, 2019; Selenko et al., 2001; Ying & Chen, 2012; Yoo et al., 2011) SND1 contains four tandem repeats of the staphylococcus nuclease-like (SN) domains, followed by a Tudor domain and a final C-terminal SN domain, which is also why this protein has also been called the Tudor-SN protein. Evidence suggests that the tandem repeats create not only a concave surface for RNA-binding, but also act as a clamp to capture RNA substrates (C. L. Li, Yang, Chen, & Yuan, 2008). In the context of viral infection, there is evidence to suggest that SND1 can function in a pro-viral manner. During SARS-CoV-2 infection, SND1 binds the virus negative sense RNA and promotes further vRNA synthesis through recruiting NSP9, and through modelling the data from Schmidt et al, it is suggested that SND1 has the ability to accumulate on negative sense RNA (Schmidt et al., 2023). SND1 is also required for lytic replication of Kaposi's sarcoma-associated herpesvirus in infected cells, and though infection studies involving this virus it is indicated SND1 may be able to recognise RNA post-transcriptional modifications alongside unmodified RNA (Baquero-Perez et al., 2019). At the time of writing there was no conclusive evidence that SND1-bunyavirus interactions had been established.

8.1.9 *TOP3B*

The human ortholog for the gene and corresponding protein for topoisomerase 3 beta (TOP3B) corresponds to the ISE6 protein coding gene *ISCI010954*, which is labelled as a gene with an unspecified product. The label topoisomerase gives an indication to the protein function, in that it changes the topological state of genetic material through breaking and then reforming genomic nucleic acid strands to unwind supercoils, resolve catenates, and undo knots. Usually for topoisomerases this genetic material is DNA, however, TOP3B is the only known topoisomerase to interact with both DNA and RNA. TOP3B is dispersed within the cytoplasm and contains an RGG box RBD with which it can form cleavage complexes in single-stranded nucleic acids. It is also speculated that TOP3B interacts with other RNA-binding proteins to regulate mRNA translation and may play a role in aiding the stability of mRNAs, thus promoting their translation (Ahmad et al., 2016; Pommier, Nussenzweig, Takeda, & Austin, 2022; S. Su et al., 2022; Yang, Saha, Yang, Neuman, & Pommier, 2022). When examining the effect on replication of single-stranded RNA viruses in humans, whether the protein acts in a pro-viral or anti-viral manner appears to partially be determined by if the viral genomic RNA is positive or negative sense. When testing positive sense ssRNA viruses, TOP3B was required for efficient replication of YFV, ZIKV and DENV2 (Prasanth et al., 2020). Although this suggests that TOP3B may be pro-viral for positive sense RNA viruses, this result was not reflected when Zhang and colleagues tested TOP3B KO mice against murine coronavirus (T. Zhang et al., 2022). In terms of negative sense ssRNA viruses, Prasanth et al. also found that when the negative sense ssRNA viruses Ebola and influenza A virus (IAV) infected cells that had been depleted of TOP3B, replication appeared enhanced compared to parental cell lines (Prasanth et al., 2020). It has been suggested that removal of TOP3B does not affect *Flavivirus* translation or replication, but does impair the production of infectious viral particles, although overall release of virions is unaffected (Diosa-Toro, Prasanth, Bradrick, & Garcia Blanco, 2020). Overall, more research needs to be carried out on the impact of TOP3B on viral infection. From current literature, this protein appears to be pro-viral in the context of positive ssRNA virus infection, and anti-viral in negative ssRNA infection.

8.1.10 *UNKL*

The human ortholog gene corresponding to UNKL produces the protein unk-like zinc finger (UNKL) and corresponds to the ISE6 protein coding gene *ISCI021949*, which is labelled as producing the unkempt protein-putative (fragment). This protein contains a RING finger domain and is homologous to the drosophila unkempt protein (Mohler et al., 1992). The

RING finger domain is a specific type of zinc finger domain structure. Zinc fingers have demonstrated DNA and RNA binding abilities, and many proteins containing RING fingers play a key role in the ubiquitination pathway (Brown, 2005). It is believed UNKL may promote protein ubiquitination through E3 ligase activity via RAC1 regulation, however more experimentation is required to definitively define the role of this protein within cells (Lorès, Visvikis, Luna, Lemichez, & Gacon, 2010). No publications could be found which suggested a link between UNKL and either pro-viral or anti-viral activity.

8.1.11 *XRN1*

The human ortholog for the gene and corresponding protein for 5'-3' exoribonuclease 1 (XRN1) corresponds to the ISE6 protein coding gene *ISCI019569*, which is labelled as a gene with an unspecified product. During the process of mRNA degradation, mRNA has its poly(A) tail shortened by deadenylase complexes, which render the mRNA in a state of limbo where the mRNA can be reactivated by restoring the poly(A) tail via polymerase action, or undergo de-capping via the Dcp1/Dcp2 de-capping complex and further degraded from either terminus (J. Coller & Parker, 2005; J. M. Coller, Tucker, Sheth, Valencia-Sanchez, & Parker, 2001). XRN1, as implied by the name, functions as a ribonuclease to carry out this degradation from the 5' to 3' direction. This activity occurs primarily within the cytoplasm, potentially within specific processing bodies (as has been shown in yeast), although exosome components are found in both the cytoplasm and nucleus (Chang, Xiang, Xiang, Manley, & Tong, 2011; Mullen & Marzluff, 2008; Sheth & Parker, 2003). Within mammalian cells, when investigating the nonsense mediated decay (NMD) pathway it has been shown that NMD factors such as Upf1 interact with the de-capping enzyme Dcp2, 5'-3' exonucleases including XRN1, 3'-5' exonucleases including Rrp4, and de-polyadenylating enzymes in order to rapidly degrade mRNAs from both ends (Lejeune, Li, & Maquat, 2003). Within the last 5 years another function of XRN1 has been established, Blasco-Moreno et al demonstrated that XRN1 promoted translation of a niche group of membrane protein mRNA transcripts by localising the transcripts to the transcription initiation machinery in the endoplasmic reticulum (Blasco-Moreno et al., 2019). Many viruses hijack the mRNA degradation process described above to accelerate host mRNA degradation in what is termed 'host shut off' in order to restrict cellular gene expression and host immune response (Abernathy, Gilbertson, Alla, & Glaunsinger, 2015; Covarrubias et al., 2011; Gaglia, Covarrubias, Wong, & Glaunsinger, 2012). Given that many vRNAs are uncapped, this protein also has some intrinsic antiviral activity which may be another reason for these hijacking mechanisms to evolve (Ng, Kasumba, Fujita, & Luo, 2020; Rowley, Ho,

Bushong, Johnson, & Sawyer, 2016). In more direct viral-XRN1 interactions, XRN1 has been shown to behave as either a pro-viral or an anti-viral factor, depending on the viral infection under study. In the case of IVA infection, XRN1 acts in a pro-viral manner by interacting with NS1 in processing bodies (PBs), whereby when XRN1 is depleted viral replication is impaired (Y. C. Liu et al., 2021). XRN1 also acts as a pro-viral factor during measles virus (MeV) replication, as during infection MeV causes the protein to be relocated to inclusion bodies (IBs) which are the centres of virus replication. XRN1 degrades dsRNA within these IBs to avoid the activation of dsRNA-induced innate immune responses (BenDavid et al., 2022). Comparatively, instead of co-opting XRN1, flaviviruses such as DENV have evolved to contain sequence specific secondary structures within the 3' UTR to stall XRN1 and prevent the degradation of its RNA genome, allowing for the production of small flaviviral RNAs (sfRNA) which are non-coding and have been shown to play a large role in viral pathogenesis (Chapman, Moon, Wilusz, & Kieft, 2014). This stalling technique has also been demonstrated to occur during RVFV infection, and therefore this may be a strategy employed by more species within the *Phenuiviridae* viral family and should be further explored (Charley, Wilusz, & Wilusz, 2018).

8.2 Aims

The aims of the research presented in this chapter were to:

- **Optimise the use of Magnetofectamine O2 (Oz Biosciences) to transfect dsRNA into ISE6 cell cultures.** There are many methods for transfecting genetic material into cell cultures, however previous work performed by Dr Marine Petit (unpublished) demonstrated success in using the Magnetofectamine O2 (Oz Biosciences) transfection kit on *Rhipicephalus microplus* (BME6) cell cultures. This research aims to use this kit to transfect ISE6 cell monolayers with dsRNAs homologous to selected tick genes. However, to do this, an optimal reagent to dsRNA (v:v) ratio must be established to minimise toxicity within transfected cell monolayers. In addition, transfection with a negative control dsRNA corresponding to the ORF of the eGFP which should not interact with ISE6 genes and a positive control dsRNA homologous to UUKV N will be conducted. The dsUUKV N should only impact viral infection and must be carried out to ensure the system is working optimally and that any data can be analysed appropriately.
- **Determine if gene targets selected for dsRNA knockdown impact UUKV replication kinetics.** Once the transfection methodology was optimised in ISE6 monolayers, dsRNA knockdown of the selected genes of interest as defined in Chapter 3 were carried out. As these proteins were highlighted as upregulated during UUKV infection, it is important to investigate whether these proteins have a pro- or anti-viral role within the infected ISE6 cell. By analysing the levels of UUKV M RNA within both the infected-cell and the cell culture supernatant, the accumulation of UUKV N protein within the cells, the viral titre in the cell culture supernatant, and cell viability we can begin to examine the impact of these proteins on UUKV infection biology.

8.3 Results

8.3.1 Knockdown optimisation

To determine the impact of the ratio of dsRNA (µg):transfection reagent (µg/µl) and to select the optimal conditions for transfection, ISE6 cell monolayers were transfected with 1 µg of either double stranded RNA to eGFP (dseGFP) or double stranded RNA targeted towards UUKV N (dsUUKV N) per million cells and either 1 µl, 2 µl, or 3 µl of transfection reagent as indicated in Figure 8.1. At 24 hours post transfection the cell monolayers were infected with rUUKV at a MOI of 5 FFU/cell or mock-infected. At 3 or 6 days p.i., cell culture supernatant was harvested from rUUKV-infected monolayers and viral titre determined via foci forming assays. When performing the analysis, the specific dsRNA transfections at each timepoint were used for comparison. At 3 days p.i., there was no significant difference recorded in the viral titre of either dseGFP or dsUUKV N samples. At 6 days p.i., in the cells treated with the dseGFP RNA there was no significant difference between a ratio of 1:1 and 1:2, however there was a significant increase in virus titre in the 1:3 ratio, where the rUUKV titre was over ten-fold higher (Figure 8.1.A). At 6 days p.i., infected cell monolayers were washed and lysed, whole cellular RNA was extracted, and RT qPCR performed against ISE6 cell 18S ribosomal RNA (18S) and UUKV M RNA. The $2^{-\Delta\Delta CT}$ values of UUKV N were calculated using 18S as the housekeeping gene and were further normalised to the rUUKV-infected sample treated with dseGFP RNA at a ratio of 1:2 (dsRNA:transfection reagent).

For analysis, each of the dsRNA:transfection reagent ratios were compared for each dsRNA, and in addition the results between dseGFP RNA and dsUUKV N RNA were also examined at fixed ratios of dsRNA:transfection reagent. For infections treated with dseGFP RNA a ratio of 1:2 resulted in a significantly lower amount of UUKV M RNA being detected, whereas the 1:3 ratio resulted in a significantly higher quantity of UUKV M RNA being recorded. In contrast, there was no significant difference in UUKV M RNA levels between any of the dsUUKV N ratios. When comparing the UUKV M RNA levels at each ratio between the dseGFP and dsUUKV N, respectively, as expected dseGFP was significantly higher at each ratio (Figure 8.1.B), showing that in the dsUUKV N samples UUKV M RNA replication had been significantly reduced or prevented. From these findings, the ratio of 1:1 was selected. To assess the impact of transfection on cell viability and monolayer health, the samples were imaged using an EVOS microscope before transfection (-1 days), the day of infection (0 days), 3 days p.i., and 6 days p.i. . No significant changes to the morphology of the cells or the health of the monolayer were seen at any timepoint or transfection reagent ratio (Figure 8.1.C). For all further experiments it was decided that a dsRNA:transfection

reagent ratio of 1µg:1µl would be used. Additionally, the harvest timepoints were extended to 9 days p.i. to reflect the mass spectrometry data from the previous chapter.

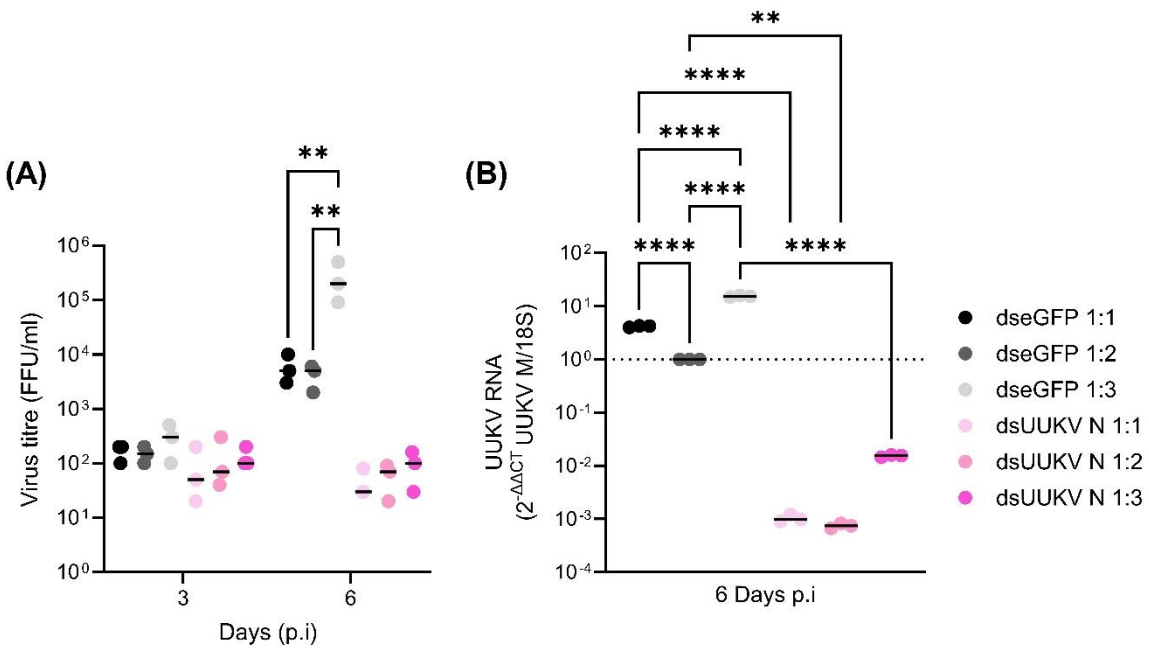
(A)
Virus titre (FFU/ml)
Days (p.i)
3
6
**
**
(B)
UUKV RNA
(2-ΔΔCT UUKV M/18S)
6 Days p.i
**
****
****
****
****
dseGFP 1:1
dseGFP 1:2
dseGFP 1:3
dsUUKV N 1:1
dsUUKV N 1:2
dsUUKV N 1:3

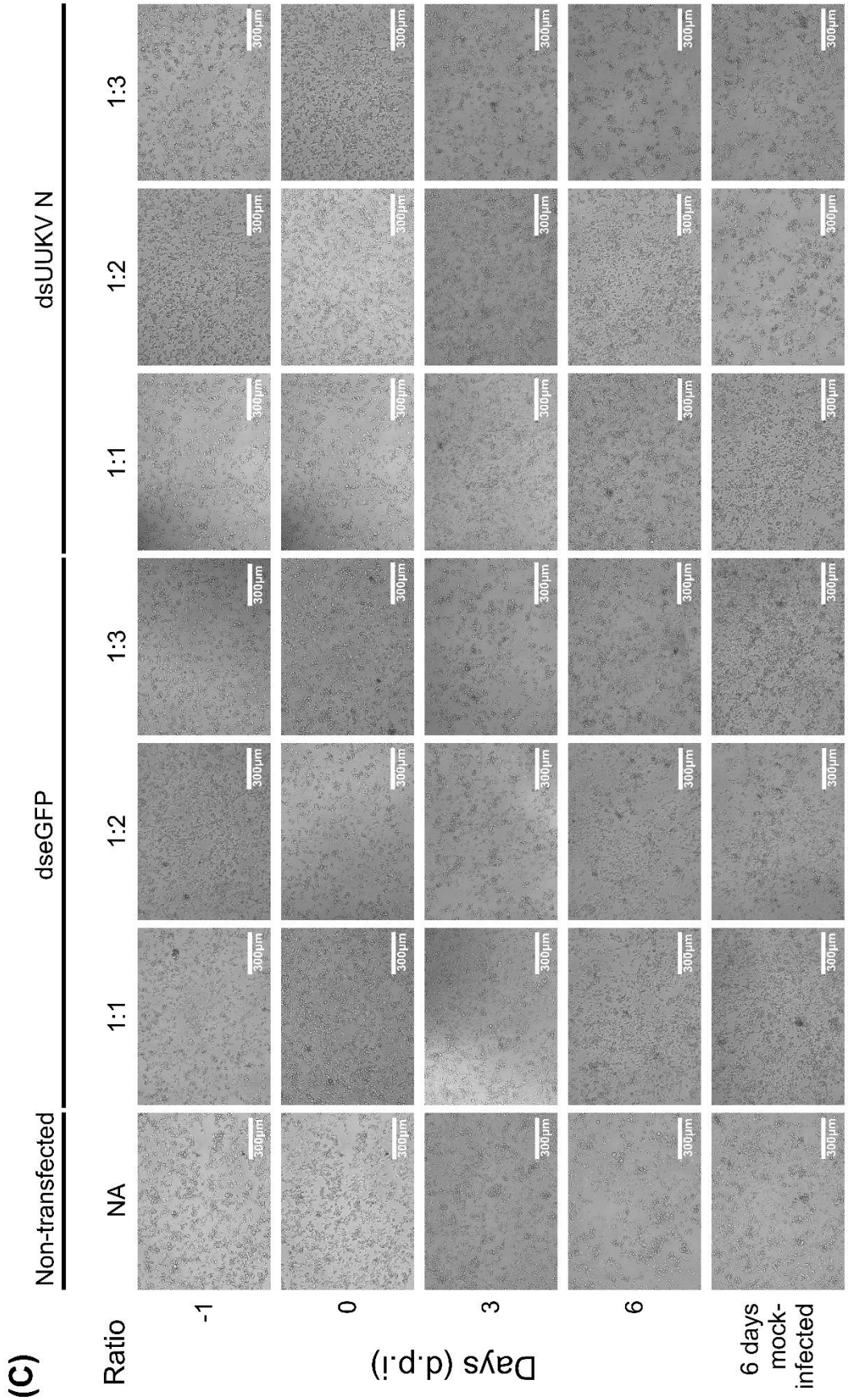

Figure 8.1: Optimisation of double stranded RNA transfection in rUUKV-infected ISE6 cell cultures. ISE6 cells were transfected with 2 µg of dsRNA targeted against eGFP (dseGFP) or UUKV N (dsUUKV N) at the indicated ratio of (µg dsRNA: µl transfection reagent). At 24 hours post

transfection (h.p.t)., cell cultures were infected with rUUKV at a MOI of 5 FFU/cell. (A). Cell culture supernatants were collected at the timepoints indicated and virus titre measured via immunofocus assay (B). At 6 days p.i., cell monolayers were lysed and total cellular RNA was isolated. Extracted RNA was then reverse transcribed and RT qPCR performed to quantify levels of UUKV M RNA and the tick cell ribosomal 18S subunit as a housekeeping control. Quantities of UUKV M were calculated using the $2^{-\Delta\Delta CT}$ method. Statistical significance was measured by ordinary one-way ANOVA with Tukey's multiple comparisons test or an ordinary two-way ANOVA with Tukey's multiple comparisons test. Asterisks indicates significance **** = $p < 0.0001$, *** = $p \leq 0.001$, ** = $p \leq 0.01$, * = $p \leq 0.05$, no label = not significant. C) At timepoints indicated, transfected cell monolayers as described above were imaged using an EVOS microscope.

Double stranded RNA containing the sequence corresponding to the ORF of eGFP (dseGFP) was chosen to be the negative transfection control. To establish the impact of transfection of eGFP dsRNA using the selected transfection reagent ratio (1µg:1µl) upon viral kinetics and to assess its suitability as a negative control for further data analysis. ISE6 cell monolayers were either non-transfected or transfected with dseGFP following the methodology established. At 24 hours post-transfection, the ISE6 cell monolayers were either mock-infected or infected with UUKV at an MOI of 5 FFU/cell. At 3, 6, and 9 days p.i., cell monolayers were washed and lysed, whole cellular RNA was extracted, and RT qPCR performed against 18s and UUKV M. The $2^{-\Delta\Delta CT}$ values of UUKV N using 18s as the housekeeping gene were calculated using rUUKV-infected dseGFP transfected samples at each timepoint to normalise. Virus supernatant was harvested from these infected cell monolayers and viral titre determined via foci forming assays. RNA was also extracted from the cell supernatant and absolute quantitation of the UUKV M RNA using RT qPCR of the supernatant was determined using a standard curve. To analyse the UUKV N protein expression and impact on cell viability, this method was repeated with all gene dsRNA transfection knock downs, alongside the positive and negative control, for each biological replicate were carried out simultaneously (Figures 8.2. B, Figure 8.3. B, Figure 8.5 and Figure 8.7); half of the cells were fixed and stained with DAPI, anti-UUKV N and fluorescent secondary antibody to measure quantity of UUKV N protein in the monolayer, and the other half were lysed and cell viability measured using the CellTiter-Glo® 2.0 Cell Viability Assay (Promega). Therefore, for the UUKV N protein and viability results, it is important to note that the comparison of all further gene knockdowns are against the dseGFP results obtained from the simultaneous gene transfections (Figure 8.2).

When analysing the quantity of UUKV M RNA within the cells, there were no significant differences between the non-transfected and dseGFP-transfected cell monolayers at any timepoint, although variability seems to increase as time progresses (Figure 8.2.A). Cell viability was determined via a luminescence assay, where higher luminescence corresponded to living cells. Comparing viability in infected and non-infected cells for dseGFP and non-transfected samples, a significant decrease in infected samples compared to non-infected was only seen in non-transfected cells at 6 days p.i., and 9 days p.i., (Figure 8.2.B). The infected dseGFP and non-transfected cell monolayers were imaged before cell western blots were carried out Figure 8.3.C. At 6 days and 9 days p.i., there appeared to be slightly more UUKV N protein within cell monolayers. Overall, no major differences in cell monolayer morphology or health were noticeable (Figure 8.2.F). Upon analysing UUKV N protein expression at both 6 and 9 days p.i., fluorescence was significantly lower in non-

transfected compared to dseGFP-transfected wells, when samples were normalised to non-infected controls (Figure 8.2.C). Viral titre was not significantly different between the dseGFP and non-transfected samples at 3- or 6-days p.i. However, at 9 days p.i., there was a small but significant (p value = 0.0357) decrease in virus titre (Figure 8.2.D), and no significant difference was seen in UUKV M copy number within the supernatant at any timepoint (Figure 8.2.E). From these results, it was determined that dseGFP was a suitable negative control for further gene knockdowns.

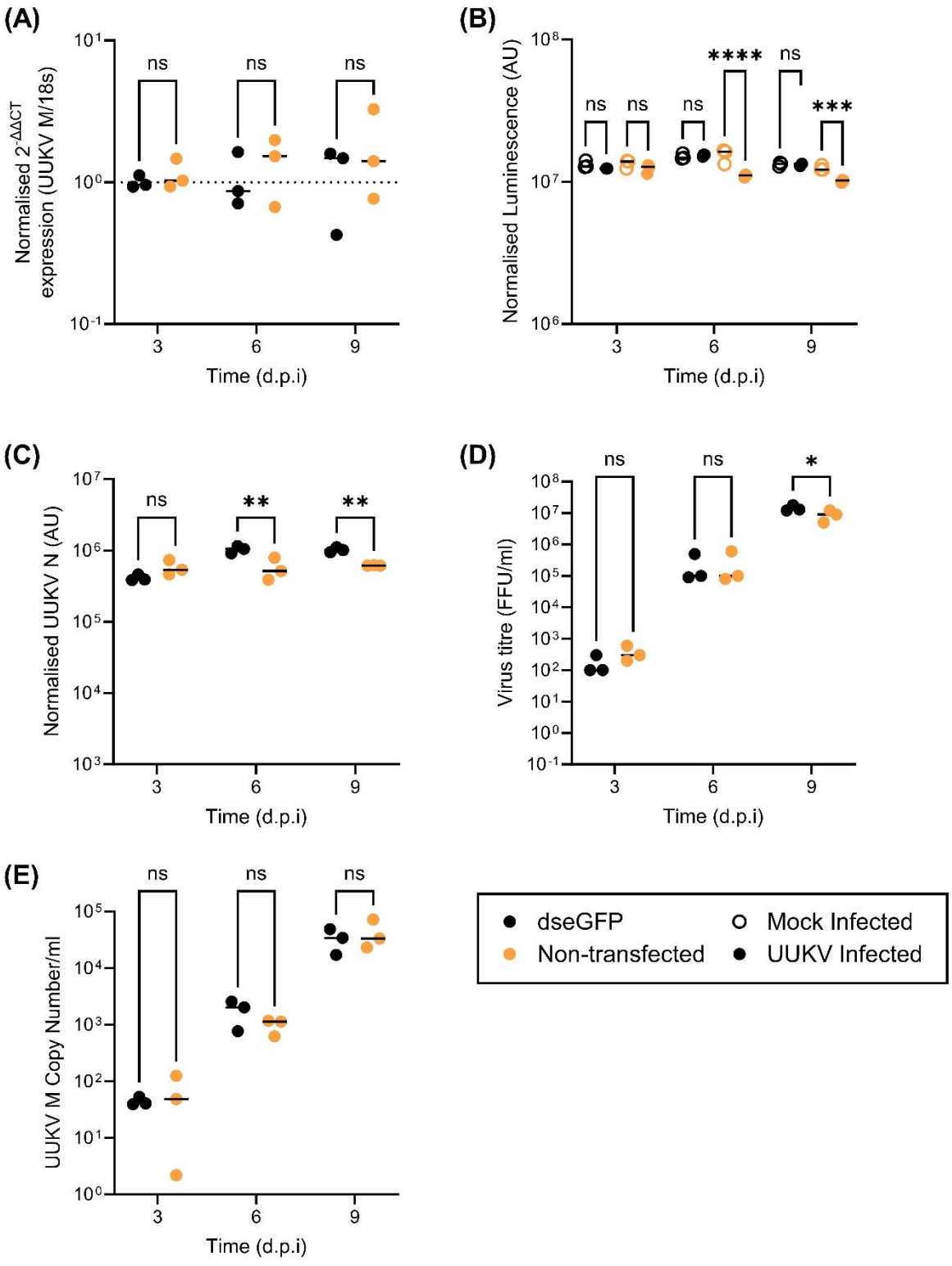
(A)
Normalised 2-ΔΔCT expression (UUKV M/18s)
ns
Time (d.p.i)
(B)
Normalised Luminescence (AU)
****
***
(C)
Normalised UUKV N (AU)
**
(D)
Virus titre (FFU/ml)
*
(E)
UUKV M Copy Number/ml
dseGFP
Non-transfected
Mock Infected
UUKV Infected

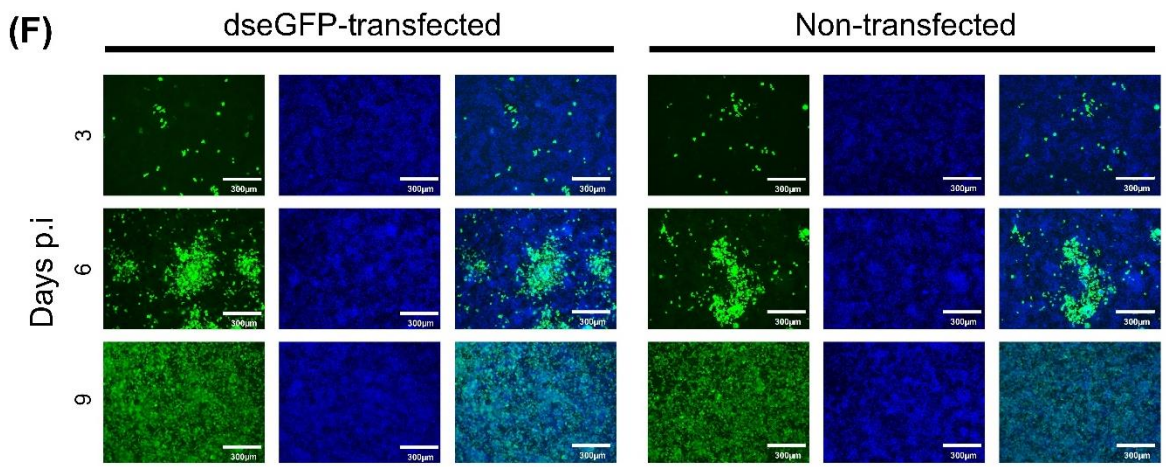

Figure 8.2: Effect of eGFP dsRNA transfection on rUUKV replication in infected ISE6 cells. ISE6 cell monolayers were transfected with 2µg of either eGFP dsRNA (dseGFP) (*black*) or non-transfected (non-transfected) (*orange*). At one day post transfection cell monolayers were infected with rUUKV at 5 FFU/cell. At the timepoints indicated supernatant was harvested and cell monolayers were either fixed using formaldehyde or lysed with TRIzol and RNA extracted. For all RT qPCRs, primers against UUKV M and 18s were used. For western blot and cell viability assays, each gene type knockdown biological replicate was carried out conjointly with all other gene type knockdowns alongside the positive and negative control, and therefore each individual gene knockdown was compared to the same positive and negative control carried out during this method. (A) Cell lysates probed for RNA RT qPCR and $2^{-\Delta\Delta CT}$ analysis allowed for the calculation of the quantity of UUKV M RNA within the cells in comparison to 18S. Samples were normalised against the dseGFP samples. (B) Cell viability was measured using the CellTitre-Glo 2.0 Cell Viability Assay (Promega). Luminescence was measured using a GloMax plate reader. Samples were normalised against blank wells containing only media. Non-infected (*line-only circular symbol*) and infected (*filled circular symbol*) of the same knockdown were compared to each other. (C) Fixed cell monolayers were stained using mouse anti-UUKV N primary antibody with anti-mouse fluorescent antibody (green). Fluorescence intensity was measured using the Odyssey imager and normalised to non-infected cells. (D) Supernatant virus titre was determined using foci-forming assay (E). Supernatant RNA was isolated using TRIzol extraction and UUKV M copy number determined using standard curve RT qPCR and primers against UUKV M. (F) Fixed cell monolayers were stained using DAPI (blue) and mouse anti-UUKV N primary antibody with anti-mouse fluorescent antibody (green). Imaging was carried out using an EVOS microscope. Statistical significance was measured by ordinary two-way ANOVA with Tukey's multiple comparisons test. Asterisks indicates significance **** = $p < 0.0001$, *** = $p \leq 0.001$, ** = $p \leq 0.01$, * = $p \leq 0.05$, ns = not significant.

Double stranded RNA containing the sequence corresponding to the ORF of the UUKV N protein (dsUUKV N) was chosen to be the positive transfection control. In order to establish the efficiency of knockdowns using this positive control, ISE6 cell monolayers were transfected with either dseGFP or dsUUKV N following the methodology established in Figure 8.1. At 24 hours post-transfection, the ISE6 cell monolayers were either mock-infected or infected with UUKV at an MOI of 5 FFU/cell. At 3, 6, and 9 days p.i., cell monolayers and supernatant were harvested and analysed as described in the dseGFP vs non-transfected samples in Figure 8.2 to assess UUKV M RNA levels intracellularly, virus titre, UUKV M supernatant copy number, normalised UUKV N protein, and normalised cell luminescence (Figure 8.3).

Upon analysing the quantity of UUKV M RNA within the cells, there were significant differences between the dseGFP and dsUUKV N-transfected cell monolayers at all timepoints, with UUKV M RNA being at a much lower quantity than in the dsUUKV N-transfected samples compared to the dseGFP samples, with the difference between the transfections increasing over time. This suggests that UUKV M RNA increases within dseGFP samples whereas no/minimal increase occurs in dsUUKV N samples (Figure 8.3.A). When comparing viability in infected and non-infected cells treated with dseGFP or dsUUKV N, there was a significant decrease in viability in infected samples compared to non-infected samples in dsUUKV N treatment at 9 days p.i., (Figure 8.3.B). When analysing UUKV N protein expression, at all timepoints fluorescence was significantly lower in dsUUKV N compared to dseGFP when samples were normalised to non-infected controls. There was a very small increase of signal of UUKV N in the dsUUKV N samples over time, whereas signal increased between 3 and 6 days p.i., but remained consistent between 6 and 9 days p.i., in dseGFP samples (Figure 8.3.C). Viral titre was not significantly different between the two dsRNA groups at 3 days 6 days p.i., although virus titre for dseGFP was higher than dsUUKV N at 6 days p.i. due to the variation between the three biological replicates at 6 days p.i., both being significantly lower than that at day 9. At 9 days p.i., there was a significant (p value < 0.0001) increase in virus titre in dseGFP treated samples compared to the dsUUKV N samples. No increase in virus titre was observed across the timeframe for dsUUKV N, with only one out of three biological replicates producing any plaques (Figure 8.3.D). This lack of increase in viral titre was reflected in the dsRNA UUKV M copy number, which was significantly lower than dseGFP at 9 days p.i. and showed no signs of increasing over the timeframe (Figure 8.3.E). Finally, the infected dseGFP and dsUUKV N cell monolayers were imaged before cell western blots were carried out to

produce Figure 8.4.D. No strong fluorescent green signal and few UUKV infected cells were identifiable at any timepoint (Figure 8.3.F).

From the results of the negative and positive control experiments, we can conclude that dseGFP is a suitable negative control, and that this transfection method achieves a high knockdown efficiency using the dsUUKV N positive control dsRNA.

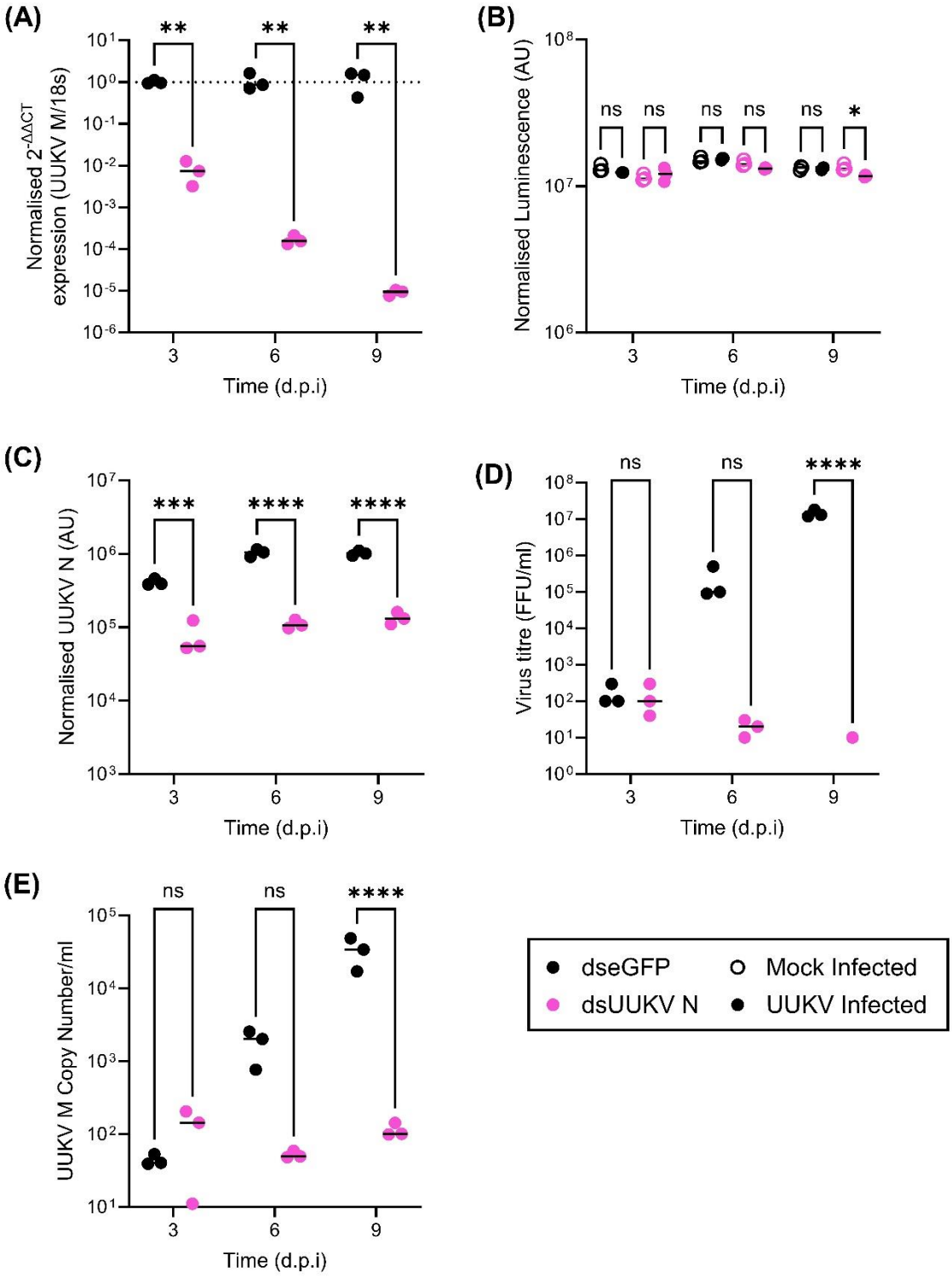
(A)
Normalised 2-ΔΔCT expression (UUKV M/18s)
Time (d.p.i)
(B)
Normalised Luminescence (AU)
Time (d.p.i)
(C)
Normalised UUKV N (AU)
Time (d.p.i)
(D)
Virus titre (FFU/ml)
Time (d.p.i)
(E)
UUKV M Copy Number/ml
Time (d.p.i)
dseGFP
dsUUKV N
Mock Infected
UUKV Infected

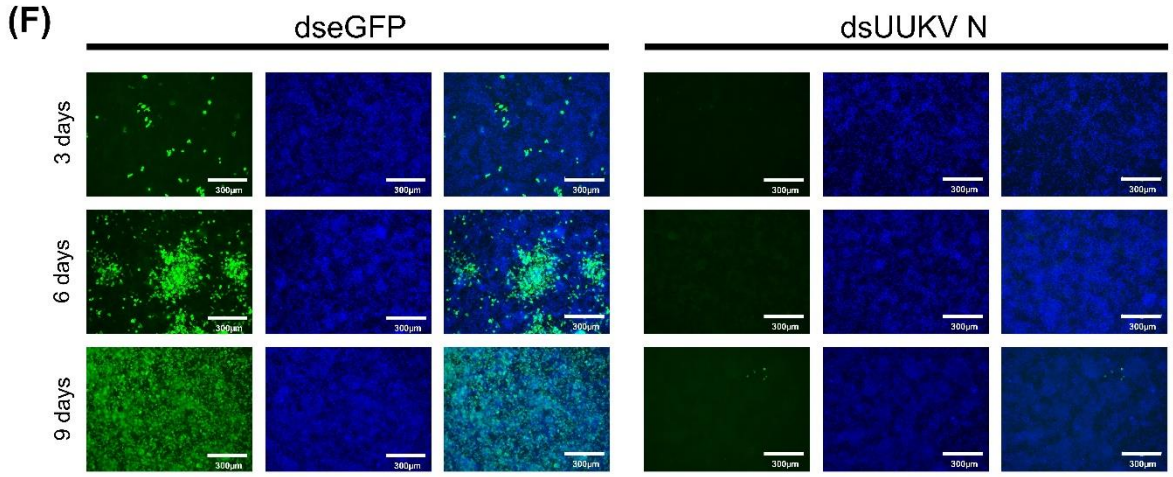

Figure 8.3: Effect of UUKV N dsRNA transfection on rUUKV replication in infected ISE6 cell. ISE6 cell monolayers were transfected with 2µg of either eGFP dsRNA (dseGFP) (*black*) or UUKV N dsRNA (dsUUKV N) (*pink*). At one day post transfection cell monolayers were infected with rUUKV at 5FFU/cell. At timepoints indicated supernatant was harvested and cell monolayers were either fixed using formaldehyde or lysed via TRIzol and RNA extracted. Primers against UUKV M and 18S were used for all RT qPCRs. For western blot and cell viability assays, all knockdowns were compared to the same dseGFP knockdown samples, as corresponding replicates for each knockdown gene were carried out in tandem. (A) Cell lysates probed for RNA RT qPCR and $2^{-\Delta\Delta CT}$ analysis allowed for the calculation of the quantity of UUKV M RNA within the cells in comparison to 18S. Samples were normalised against the dseGFP samples. (B) Cell viability was measured using the CellTitre-Glo 2.0 Cell Viability Assay (Promega). Luminescence was measured using a GloMax plate reader. Samples were normalised against blank wells containing only media. Non-infected (*line-only circular symbol*) and infected (*filled circular symbol*) of the same knockdown were compared to each other. (C) Fixed cell monolayers were stained using mouse anti-UUKV N primary antibody with anti-mouse fluorescent antibody (green). Fluorescence intensity was measured using the Odyssey imager and normalised to non-infected cells. (D) Supernatant virus titre was determined using focus-forming assay. (E). Supernatant RNA was isolated using TRIzol extraction and UUKV M copy number determined using standard curve RT qPCR and primers against UUKV M. (F) Gene knockdowns and infections were repeated and fixed cell monolayers were stained using DAPI (blue) and mouse anti-UUKV N primary antibody with anti-mouse fluorescent antibody (green). Imaging was carried out using an EVOS microscope. Statistical significance was measured by ordinary two-way ANOVA with Tukey's multiple comparisons test. Asterisks indicates significance **** = $p < 0.0001$, *** = $p \leq 0.001$, ** = $p \leq 0.01$, * = $p \leq 0.05$, ns = not significant.

8.3.2 The impact of gene knockdowns on UUKV viral kinetics

For the following experiments, dsRNA homologous to the specified ISE6 genes, as described by their human ortholog names, were transfected into ISE6 cells (dsGene), with dseGFP transfected ISE6 cell monolayers acting as negative control. At 24 hours post-transfection, the ISE6 cell monolayers were either mock-infected or infected with rUUKV at an MOI of 5 FFU/cell. At 3, 6, and 9 days p.i., cell monolayers and supernatant were harvested and analysed to determine if the transcript has been successfully knocked down via RT qPCR, alongside the other analyses as described in the dseGFP vs non-transfected samples in Figure 8.2. As described previously, for each gene I assessed intracellular normalised cell viability, UUKV M RNA levels, normalised UUKV N protein expression, virus titre, and UUKV M RNA copy number in the supernatant. This allows for an assessment of the impact of knocking down these genes on UUKV viral replication. When discussing the impact of these knockdowns the genes will be referred to by their human orthologs.

As previously mentioned, as the method was repeated with all gene knockdown transfections for each biological replicate being carried out simultaneously to analyse UUKV N protein expression and cell viability, it is important to note that the comparison for these analyses is against the same dseGFP results from these simultaneous transfections (Figure 8.5 and Figure 8.7).

The first step of the dsRNA transfection analysis was to determine the efficacy of the knockdown, by isolating the cellular RNA of the gene transfected and dseGFP transfected cell monolayers using TRIzol. This cellular RNA was then analysed using RT qPCR to calculate the normalised level of target gene within the samples. The smaller the level of gene mRNA within the gene knockdown in comparison with the dseGFP, the more effective the knockdown. The dsRNA transfections for *RBM8A* (Figure 8.4.F) and *PABP1* (Figure 8.4.D) showed significant knockdown efficiency of 90% or above at all three timepoints, meaning these cells had 10% or below of the gene mRNA content compared to the dseGFP transfected cell monolayers. If *RBM8A* and *PABP1* impact viral kinetics, it is likely that within these knockdowns a difference will be seen within analyses of the cell monolayers in respect to the UUKV infection,. In comparison, the dsRNA transfections for *AGO2* (Figure 8.4.A) and *EIF3A* (Figure 8.4.C) showed a knockdown efficiency of 70% or above. Although this is not as efficient as the *RBM8A* and *PABP1*, a reduction of gene mRNA to less than 30% of the levels found in the dseGFP transfections was still significant, and this knockdown level was also maintained across all three timepoints. When looking at *TOP3B*

knockdowns (Figure 8.4.I), although the *TOP3B* mRNA level was 20% or less of that found within dseGFP transfected cells, the levels of *TOP3B* mRNA within dseGFP cells were more variable and therefore this knockdown returned a less statistically significant knockdown value than the *RBM8A* and *PABP1* analysis. However, within this work, this knockdown was effective as the knockdown level was maintained across the timepoints. *SND1* (Figure 8.4.H), *RUXE* (Figure 8.4.G), and *UNKL* (Figure 8.4.J) showed an average reduction of 70% or above at 3 and 6 days p.i. However, at 9 days p.i., there was a less significant decrease of the gene knockdown. This was more prominent in the *PRKRA* knockdowns (Figure 8.4.E), where at 3 days p.i. the level of *PRKRA* mRNA was 10% or less of the dseGFP-transfected control. This percentage increased to roughly 50% at day 6 p.i., and at 9 days p.i. there was no significant difference between conditions. This needs to be accounted for in further UUKV kinetics analysis, as any impact seen at 6 and 9 days p.i. may not be due to knockdowns, or this knockdown may have had a detrimental effect on the cell monolayer outside of UUKV infection. Finally, *CUL1* (Figure 8.4.B) and *XRN1* (Figure 8.4.K) knockdowns showed roughly 50% of the mRNA levels found in dseGFP at 3 and 6 days p.i., with *XRN1* mRNA increasing to roughly 60% and *CUL1* mRNA increasing to levels comparable to the dseGFP cell monolayers by 9 days p.i. Like *PRKRA* knockdowns. This reduction in efficiency and potential recovery of gene mRNA levels needs to be factored into further analysis.

All knockdowns showed a minimum of 50% gene reduction by dsRNA transfection in comparison to the dseGFP transfection at 3 days p.i., and this did not continue for all transfections across the timepoint. Therefore, gene dsRNA-mediated knockdowns would be further analysed to determine the effect upon both the cell viability and viral kinetics, given that several knockdowns showed variation and reduction in efficiency. The next step was to assess the impact of the transfection on cell viability, in the context of mock and rUUKV infection. This was to determine if the proteins targeted were key to cellular function, which would impact, but not directly affect viral replication kinetics or virus yield.

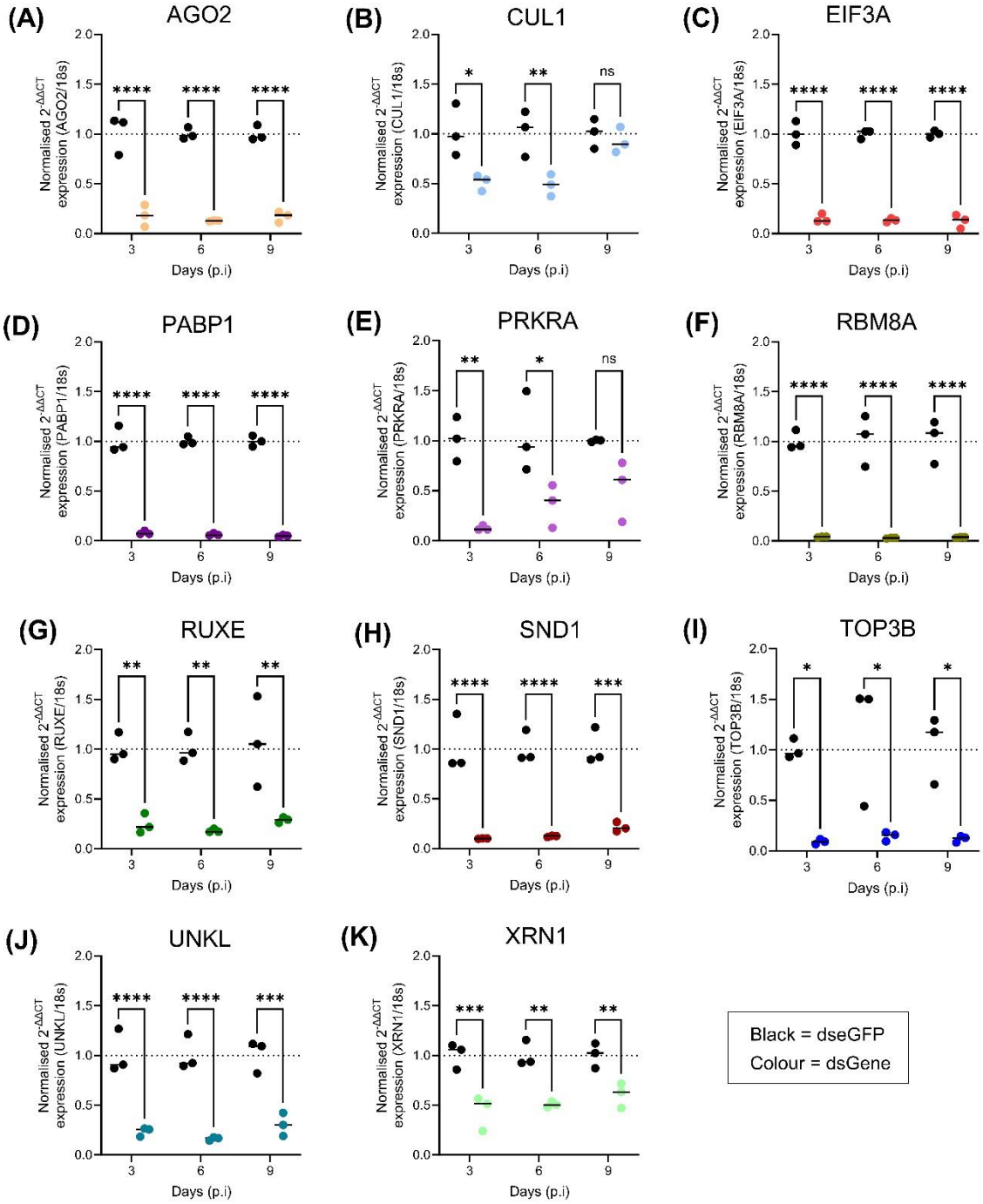

Figure 8.4: Effect of dsRNA transfections on selected gene expression within ISE6 cell culture. ISE6 cell monolayers were transfected with 2µg of dsRNA homologous to either eGFP (dseGFP) or (A) *AGO2* (dsAGO2), (B) *CUL1* (dsCUL1), (C) *EIF3A* (dsEIF3A), (D) *PABP1* (dsPABP1), (E) *PRKRA* (dsPRKRA), (F) *RBM8A* (dsRBM8A), (G) *RUXE* (dsRUXE), (H) *SND1* (dsSND1), (I) *TOP3B* (dsTOP3B), (J) *UNKL* (dsUNKL), or (K) *XRN1* (dsXRN1). At one day post-transfection, cell monolayers were infected with rUUKV at 5 FFU/cell. At timepoints indicated, cell monolayers were lysed with TRIzol and cellular RNA extracted. RT qPCR was performed on the cellular RNA using primers against the respective ISE6 gene and 18S as the 'housekeeping' gene, and the normalised expression of the ISE6 gene calculated using the $2^{-\Delta\Delta Ct}$ method. Statistical significance was measured by ordinary two-way ANOVA with Tukey's multiple comparisons test. Asterisks

indicates significance **** = $p < 0.0001$, *** = $p \leq 0.001$, ** = $p \leq 0.01$, * = $p \leq 0.05$, ns = not significant.

Normalised cell viability was determined using the CellTiter-Glo® 2.0 Cell Viability Assay (Promega), whereby the level of ATP and therefore the luminescent signal produced from the assay reagent is inversely proportional to cell cytotoxicity and mortality. By comparing the dseGFP and gene dsRNA transfection in either mock-infected or infected conditions respectively, at each timepoint, the impact of transfection of the dsRNA of the gene on cell viability can be investigated. The caveat to this is that, as each sample is an individual cell monolayer, there may be some variability in the viability seen within the monolayers. By comparing the luminescence of the mock-infected cell monolayers to the infected cell monolayers for each dsRNA transfection, at each timepoint, the impact of UUKV infection on the cell culture can be analysed.

A common result among the gene transfections, when comparing the mock infected samples to the infected samples, was that by 9 days p.i. there was a significant decrease in luminescence in the infected samples in comparison to the mock-infected controls (Figure 8.5). This was observed most strongly within the knockdown of *PABP1* (Figure 8.5.D). In the case of *AGO2* and *SND1* knockdown, there was also a significant decrease in viability in the rUUKV-infected dsAGO2 (Figure 8.5.A) and dsSND1 (Figure 8.5.H) transfections compared to the mock infected samples at 3 and at 6 days p.i. dsUNKL transfected infected samples had a significant decrease in luminescence compared to the mock-infected control (Figure 8.5.J). The only knockdown where this was not seen, where neither the transfection nor infection appeared to make a significant difference to cell culture viability, was the transfection of dsTOP3B (Figure 8.5.I). Unexpectedly in some knockdowns, the gene dsRNA transfection appeared to increase viability, where the viability of the infected ISE6 gene transfected cell culture was significantly higher than that of the non-infected equivalent cell culture. This was the case for *RBM8A* (Figure 8.5.F) and *EIF3A* (Figure 8.5.C) at all timepoints, *SND1* at 3 and 6 days p.i., and *UNKL* at 6 and 9 days p.i., although at the later timepoints the infected gene dsRNA transfected cell cultures had a significantly lower viability than their non-infected counterparts. Interestingly, at 6 days p.i. the mock-infected dsXRN1 transfected cell cultures had significantly lower viability than the infected and the dseGFP transfected counterparts (Figure 8.5.K). No significant differences in viability were observed between the mock and infected dseGFP transfected samples.

Once the viability had been assessed, the next stage of analysis was to determine the impact of gene knockdowns on the levels of intracellular UUKV M RNA.

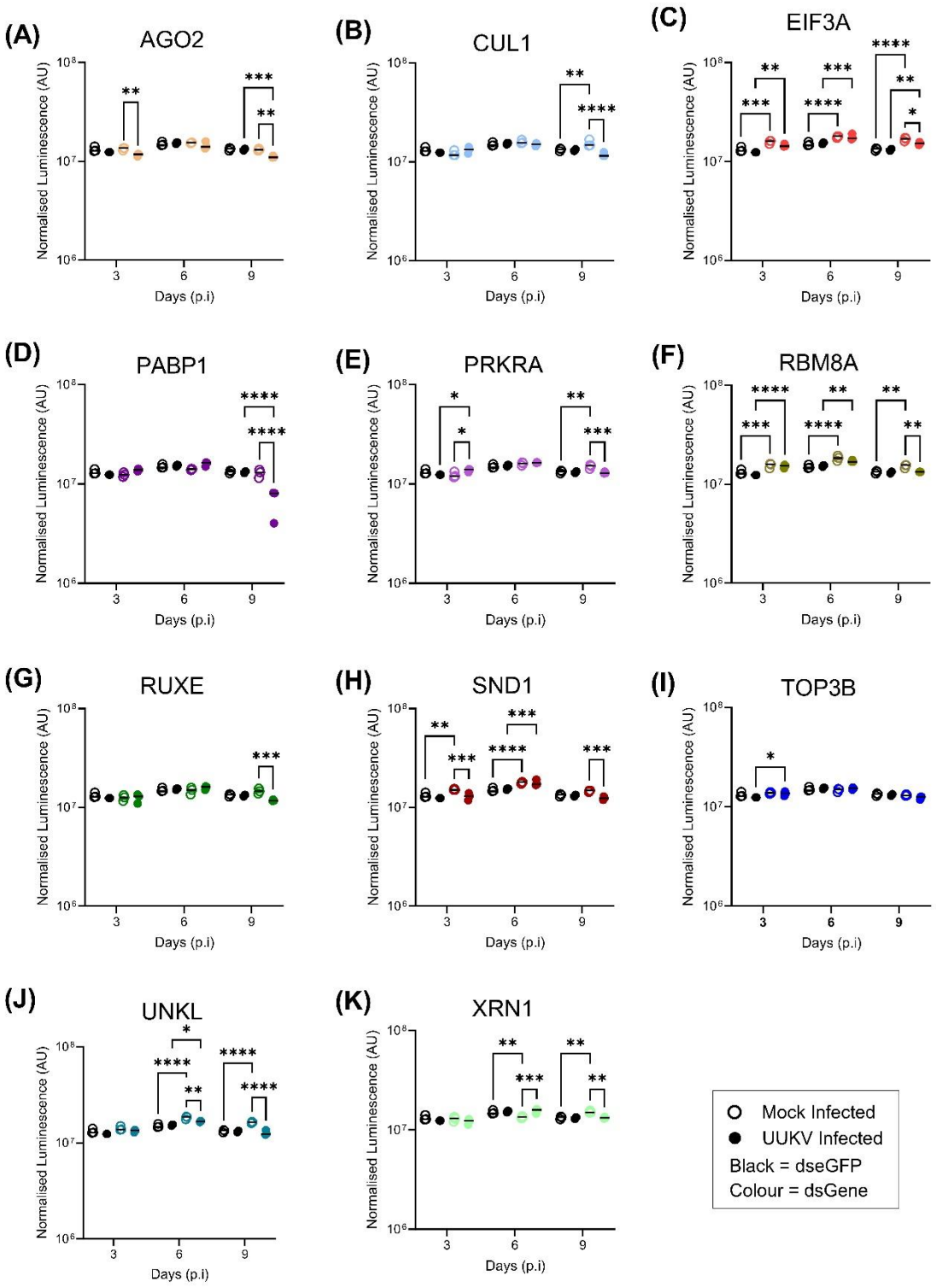

Figure 8.5: Effect of dsRNA transfections on the viability within ISE6 cells culture. ISE6 cell monolayers were transfected with 2µg of dsRNA homologous to either eGFP (dseGFP) or; (A) *AGO2* (dsAGO2), (B) *CUL1* (dsCUL1), (C) *EIF3A* (dsEIF3A), (D) *PABP1* (dsPABP1), (E) *PRKRA* (dsPRKRA), (F) *RBM8A* (dsRBM8A), (G) *RUXE* (dsRUXE), (H) *SND1* (dsSND1), (I) *TOP3B* (dsTOP3B), (J) *UNKL* (dsUNKL), or (K) *XRN1* (dsXRN1). At one day post-transfection, cell monolayers were mock-infected or infected with rUUKV at 5 FFU/cell. At timepoints indicated, cell monolayers were washed with PBS before cell viability was analysed using CellTitre-Glo 2.0 Cell

Viability Assay kit (Promega). Luminescence was measured using a GloMax plate reader. Samples were normalised against blank wells containing only media. Mock and infected samples for each type of dsRNA transfections were compared at each timepoint, and the dseGFP and ISE6 gene dsRNA transfections at each timepoint, for mock and infected respectively, were also compared. Statistical significance was measured by ordinary two-way ANOVA with Tukey's multiple comparisons test. Asterisks indicates significance **** = $p < 0.0001$, *** = $p \leq 0.001$, ** = $p \leq 0.01$, * = $p \leq 0.05$, no label = not significant.

To determine the effect of the gene knockdown on the intracellular levels of UUKV M RNA, the cellular RNA was isolated and was then processed using RT qPCR with primers against UUKV M RNA and 18S as the housekeeping gene to calculate the normalised fold change in expression level of UUKV M RNA within the samples. The expression of UUKV M RNA was normalised to the dseGFP samples at each respective timepoint, meaning that if the normalised UUKV M expression was higher within the target gene dsRNA transfection compared to the dseGFP transfections it can be inferred that the level of replication and/or transcription was increased. The UUKV M RNA primers targeted the positive strand, otherwise known as the cRNA of the UUKV genome, they will also detect the sub genomic mRNA encoding the viral glycoproteins. Therefore an increase in the UUKV M RNA indicated an increase in the number of cDNA transcripts, however, there is a feedback loop in that the more replication that occurs producing more negative strands (vRNA), the more these strands can be used to produce cRNA causing a 'knock-on' impact on transcript numbers. It cannot be concluded whether this increase is due to just an increase in the rate of transcription, a result of an increase in the rate of replication increase, or both.

Aside from *TOP3B*, where no differences were seen between the dseGFP and dsTOP3B transfections at any timepoint (Figure 8.6.I), all gene knockdowns at either 3 days or both 3 and 6 days p.i. showed a significant impact on the levels of UUKV M RNA. Interestingly, at 9 days p.i., no ISE6 gene transfections resulted in UUKV M RNA levels that were significantly different from the dseGFP transfections, and for the knockdown of *PABP1* it appeared that the level of UUKV M RNA reduced to less than 1% of the level in dseGFP (although due to the previous timepoint differences being over 10 times more than the dseGFP transfection, this fell within the non-significant range) (Figure 8.6.D). *PABP1* was also the only transfection where a higher level of UUKV M RNA was seen at 6 days p.i. as compared to 3 days p.i. For the *EIF3A* (Figure 8.6.C), *PRKRA* (Figure 8.6.E), *RBM8A* (Figure 8.6.F), *RUXE* (Figure 8.6.G), *SND1* (Figure 8.6.H), and *XRN1* (Figure 8.6.K) knock downs, the level of UUKV M RNA was significantly higher in the gene transfections compared to the dseGFP transfections at 3 and 6 days p.i., although comparing the level at 3 days p.i. to the level at 6 days p.i. a decrease was noted in the later timepoints. Of these knockdowns, the reduction in *PRKRA* resulted in an initial increase in UUKV M RNA level up to 10 times that of the dseGFP, whereas the other gene knockdowns showed a higher initial UUKV M RNA level increase of up to roughly 70 times. In comparison, *CUL1* (Figure 8.6.B) and *UNKL* (Figure8.6.J) only showed a significant increase in UUKV M RNA at 3 days p.i.

The next stage of this analysis was then to use parallel cell culture transfections to produce the cell viability data in Figure 8.5 to determine the impact of gene transfection on the production of the UUKV N protein.

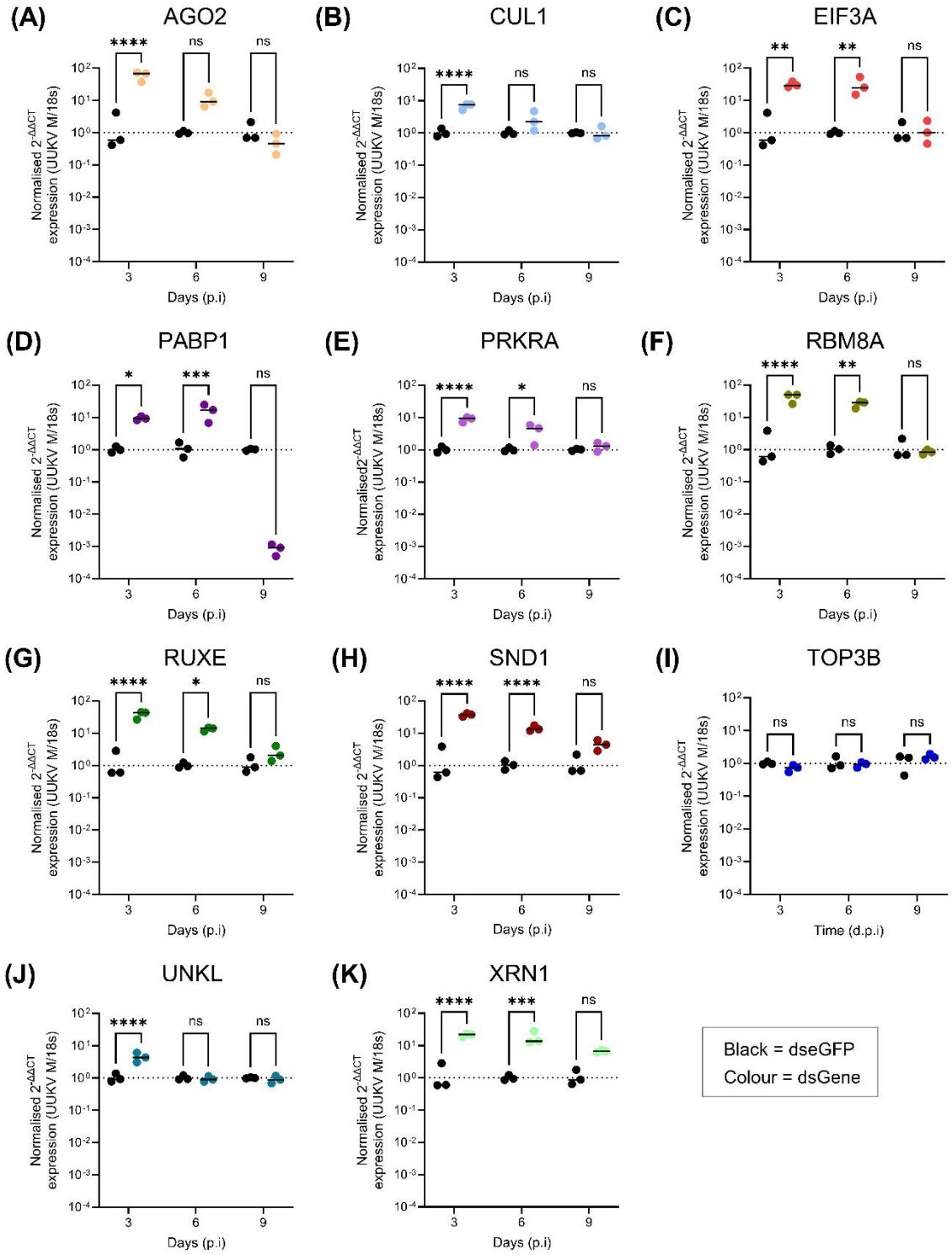

Figure 8.6: Effect of dsRNA transfections on the expression of UUKV M RNA levels within UUKV infected ISE6 cell culture. ISE6 cell monolayers were transfected with 2µg of dsRNA homologous to either eGFP (dseGFP) or (A) *AGO2* (dsAGO2), (B) *CUL1* (dsCUL1), (C) *EIF3A* (dsEIF3A), (D) *PABP1* (dsPABP1), (E) *PRKRA* (dsPRKRA), (F) *RBM8A* (dsRBM8A), (G) *RUXE* (dsRUXE), (H) *SND1* (dsSND1), (I) *TOP3B* (dsTOP3B), (J) *UNKL* (dsUNKL), or (K) *XRN1* (dsXRN1), where *black symbols* represent dseGFP data and *coloured symbols* represent dsGene data. At one day post-transfection, cell monolayers were infected with rUUKV at 5 FFU/cell. At timepoints indicated, cell monolayers were lysed via TRIzol and cellular RNA extracted. RT qPCR

was performed on the cellular RNA using primers against UUKV M RNA, and 18S as the 'housekeeping' gene. The normalised expression of UUKV M RNA was calculated using the $2^{-\Delta\Delta Ct}$ method. Statistical significance was measured by ordinary two-way ANOVA with Tukey's multiple comparisons test. Asterisks indicates significance **** = $p < 0.0001$, *** = $p \leq 0.001$, ** = $p \leq 0.01$, * = $p \leq 0.05$, ns = not significant.

Expression of UUKV N protein within infected cells was analysed by probing the fixed cell monolayers with an anti-UUKV N antibody, followed by visualisation using an anti-mouse IgG fluorescent green antibody. The fluorescence intensity of each dsRNA transfected and infected cell monolayer was then normalised to the equivalent dsRNA treated and non-infected sample to remove background autofluorescence.

There was no significant difference between the gene and dseGFP transfections at 3 days p.i. for any gene, and only *XRN1* showed no significant difference between levels of N protein at any timepoint (Figure 8.7.K). For the *AGO2* (Figure 8.7.A), *PABP1* (Figure 8.7.D), and *RUXE* (Figure 8.7.G) transfections, the normalised intensities showed significantly less N protein at 6 and 9 days p.i. in the dsRNA transfection samples compared to the dseGFP transfection samples, where it appeared that there was little to no increase of protein within the dsRNA transfection samples across the time course. In comparison, *PRKRA* (Figure 8.7.E), *RBM8A* (Figure 8.7.F), *SND1* (Figure 8.7.H), *TOP3B* (Figure 8.7.I), and *UNKL* (Figure 8.7.J) only showed significantly less N protein at 6 days p.i., but these levels appear to catch up by 9 days p.i. and become comparable to dseGFP samples. Finally, *EIF3A* (Figure 8.7.C) was the only knockdown where there was a significant decrease in N protein at 9 days p.i. only.

These results were interesting, as from the previous data (Figure 8.6) most of the transfections resulted in an increase in the number of UUKV M RNA copies (and therefore presumably an increase in the number of all virus transcripts) at the 3 days p.i. timepoint. Therefore, it was expected that this would have a positive effect on the production of UUKV N protein, however from these results it seems the inverse occurs.

Next to explore the impact on infectious virus production, focus forming assays were performed on cell culture supernatant samples collected at each time point.

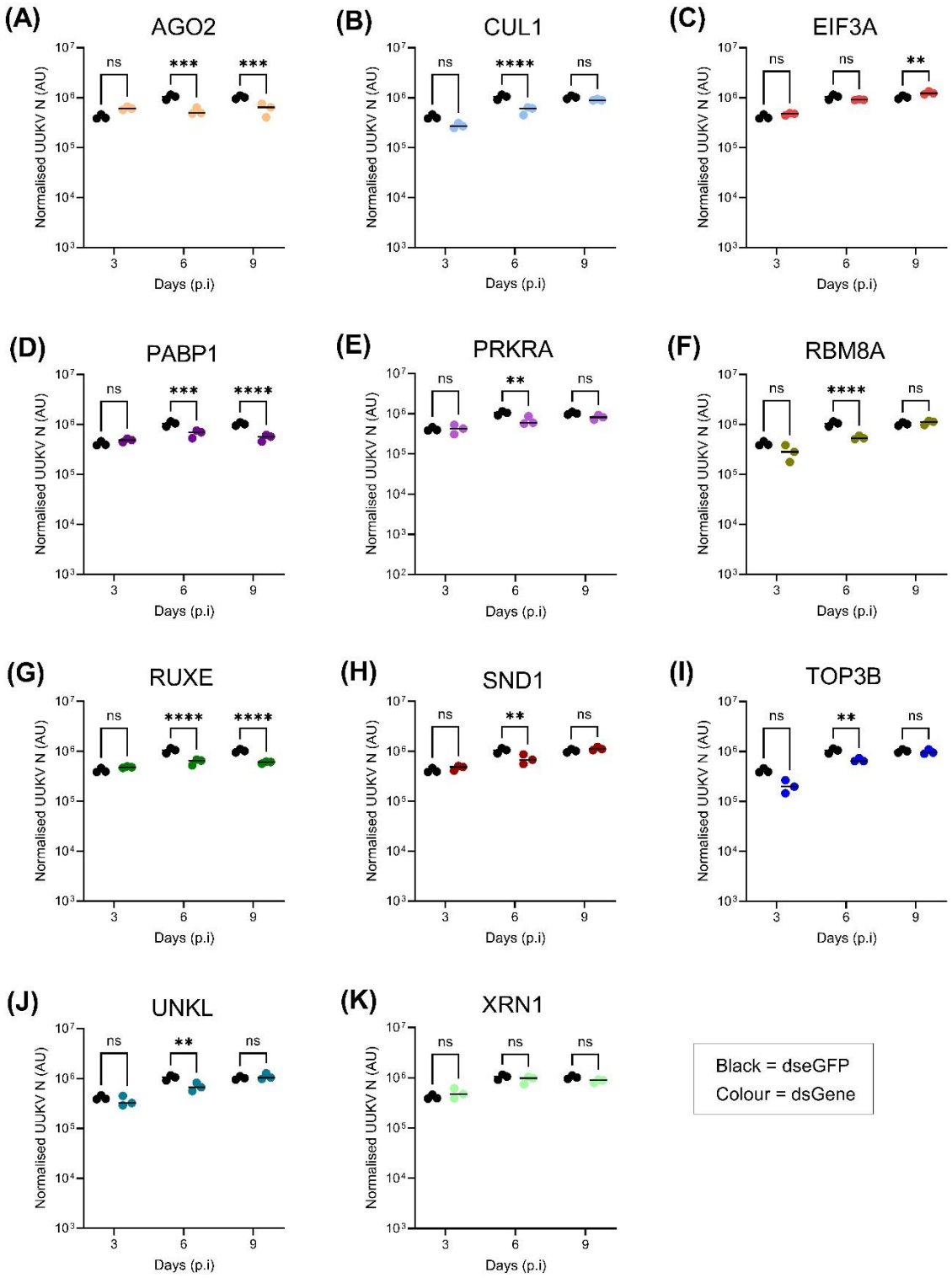

Figure 8.7: Effect of dsRNA transfections on the UUKV N protein expression within UUKV infected ISE6 cell culture. ISE6 cell monolayers were transfected with 2µg of dsRNA homologous to either eGFP (dseGFP) or (A) *AGO2* (dsAGO2), (B) *CUL1* (dsCUL1), (C) *EIF3A* (dsEIF3A), (D) *PABP1* (dsPABP1), (E) *PRKRA* (dsPRKRA), (F) *RBM8A* (dsRBM8A), (G) *RUXE* (dsRUXE), (H) *SND1* (dsSND1), (I) *TOP3B* (dsTOP3B), (J) *UNKL* (dsUNKL), or (K) *XRN1* (dsXRN1), where *black symbols* represent dseGFP data and *coloured symbols* represent dsGene data. At one day post-transfection, cell monolayers were mock-infected or infected with rUUKV at 5 FFU/cell. At

timepoints indicated, cell monolayers were fixed using formaldehyde. Cell monolayers were then probed using mouse anti-UUKV primary antibody and anti-mouse fluorescent antibody. Fluorescence intensity was measured using the Odyssey imager and normalised to non-infected cells. Statistical significance was measured by ordinary two-way ANOVA with Tukey's multiple comparisons test. Asterisks indicates significance **** = $p < 0.0001$, *** = $p \leq 0.001$, ** = $p \leq 0.01$, * = $p \leq 0.05$, ns = not significant.

The viral titre of the cell supernatants was then analysed via focus forming assay. The supernatants of the non-infected cell monolayers for all transfections were also analysed to confirm transfection did not impact the focus-forming assay methodology, and as expected no foci were visible, therefore these data were not plotted.

Overall and unexpectedly, most dsRNA knockdown transfections showed an exponential increase in virus titre over the time course, as observed in dseGFP transfected samples. No significant differences were seen at 3 or 6 days p.i. for any dsRNA knockdown when compared to the dseGFP transfection. This lack of difference between the dsRNA transfection and dseGFP transfection samples extended to 9 days p.i. for *UNKL* (Figure 8.8.J) and *XRN1* (Figure 8.8.K). For all other knockdowns, there was a decrease in titre at 9 days p.i. compared to controls. In *CUL1* (Figure 8.8.B), *PABP1* (Figure 8.8.D), *PRKRA* (Figure 8.8.E), and *TOP3B* (Figure 8.8.I) this decrease in titre was tenfold or less that on the dseGFP biological triplicates. In *EIF3A* (Figure 8.8.C), *RBM8A* (Figure 8.8.F), *RUXE* (Figure 8.8.G), and *SND1* (Figure 8.8.H) knockdown samples this significant decrease in titre at 9 days p.i. was larger than tenfold. In particular, the results of *EIF3A* showed a large amount of variability at 9 days p.i., and unlike all other knockdowns the *RBM8A* titre at 9 days p.i. appeared to have not increased from the 6 days p.i. titre indicating a complete prevention of infective viral production.

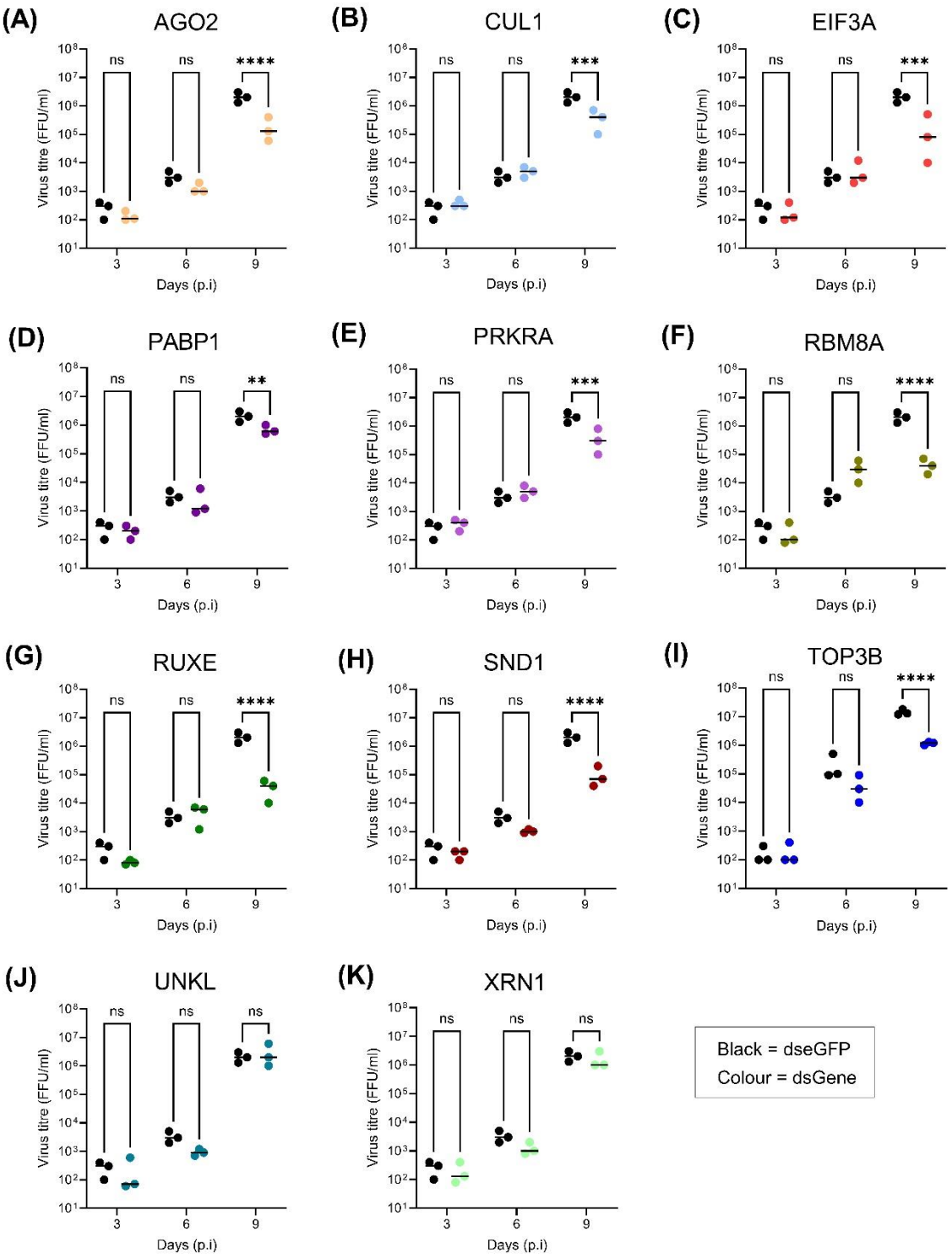

Figure 8.8: Effect of dsRNA transfections on UUKV supernatant titre within UUKV infected ISE6 cell cultures. ISE6 cell monolayers were transfected with 2µg of dsRNA homologous to either eGFP (dseGFP) or (A) *AGO2* (dsAGO2), (B) *CUL1* (dsCUL1), (C) *EIF3A* (dsEIF3A), (D) *PABP1* (dsPABP1), (E) *PRKRA* (dsPRKRA), (F) *RBM8A* (dsRBM8A), (G) *RUXE* (dsRUXE), (H) *SND1* (dsSND1), (I) *TOP3B* (dsTOP3B), (J) *UNKL* (dsUNKL), or (K) *XRN1* (dsXRN1), where *black symbols* represent dseGFP data and *coloured symbols* represent dsGene data. At one day post-transfection, cell monolayers were infected with rUUKV at 5 FFU/cell. At timepoints indicated, cell supernatant was harvested, and titre determined using foci-forming assay. Statistical significance was

measured by ordinary two-way ANOVA with Tukey's multiple comparisons test. Asterisks indicates significance **** = $p < 0.0001$, *** = $p \leq 0.001$, ** = $p \leq 0.01$, * = $p \leq 0.05$, ns = not significant.

Although the titre of the supernatant was elucidated, it was also important to determine the copy number of UUKV M RNA within the supernatant, as discrepancies between the titre and copy number indicates an impact on the production of infectious particles. To calculate this copy number, RNA within the supernatant (that was also used to calculate viral titres in Figure 8.8) was isolated using TRIzol extraction. RT qPCR was then performed on the RNA samples using primers against UUKV M RNA. Consecutive dilutions of UUKV M standard DNA were included within the RT qPCR analysis to provide a standard curve with which the copy number of UUKV M within each sample could be enumerated as described in Methods (representative standard curve results shown in Appendices [Figure 10.2]).

Only TOP3B knockdown demonstrated no significant difference between the copy number of the dsRNA transfections and dseGFP transfections at any timepoint (Figure 8.9.I). All other gene knockdowns had no significant difference between the dsRNA gene transfections and dseGFP controls until 9 days p.i., where there was a significant decrease in copy number compared to dseGFP. When relating this back to the viral titre, the estimates of copy number within *AGO2* (Figure 8.9.A), *CUL1* (Figure 8.9.B), *EIF3A* (Figure 8.9.C), *PABP1* (Figure 8.9.D), *PRKRA* (Figure 8.9.E), *RBM8A* (Figure 8.9.F), *RUXE* (Figure 8.9.G), and *SND1* (Figure 8.9.H) all followed the same trend as their respective viral titre results. Although both *UNKL* and *XRN1* showed no significant difference in titre at any timepoint (Figure 8.8.J and Figure 8.8.K), the copy number at 9 days p.i. was significantly lower in both dsRNA transfections (Figure 8.9.J and Figure 8.9.K, respectively). Finally, despite the titre of *TOP3B* transfections being significantly lower at 9 days p.i., no significant difference was noted within the UUKV M RNA copy number at any timepoint compared to the dseGFP transfections (Figure 8.9.I). From these analyses, it was concluded that dsRNA can be transfected into ISE6 cell cultures at high levels of efficiency. In addition, these dsRNA transfections using nucleotide sequences homologous to the genes identified from the mass spectrometry are effective in impacting viral kinetics of UUKV infection of ISE6.

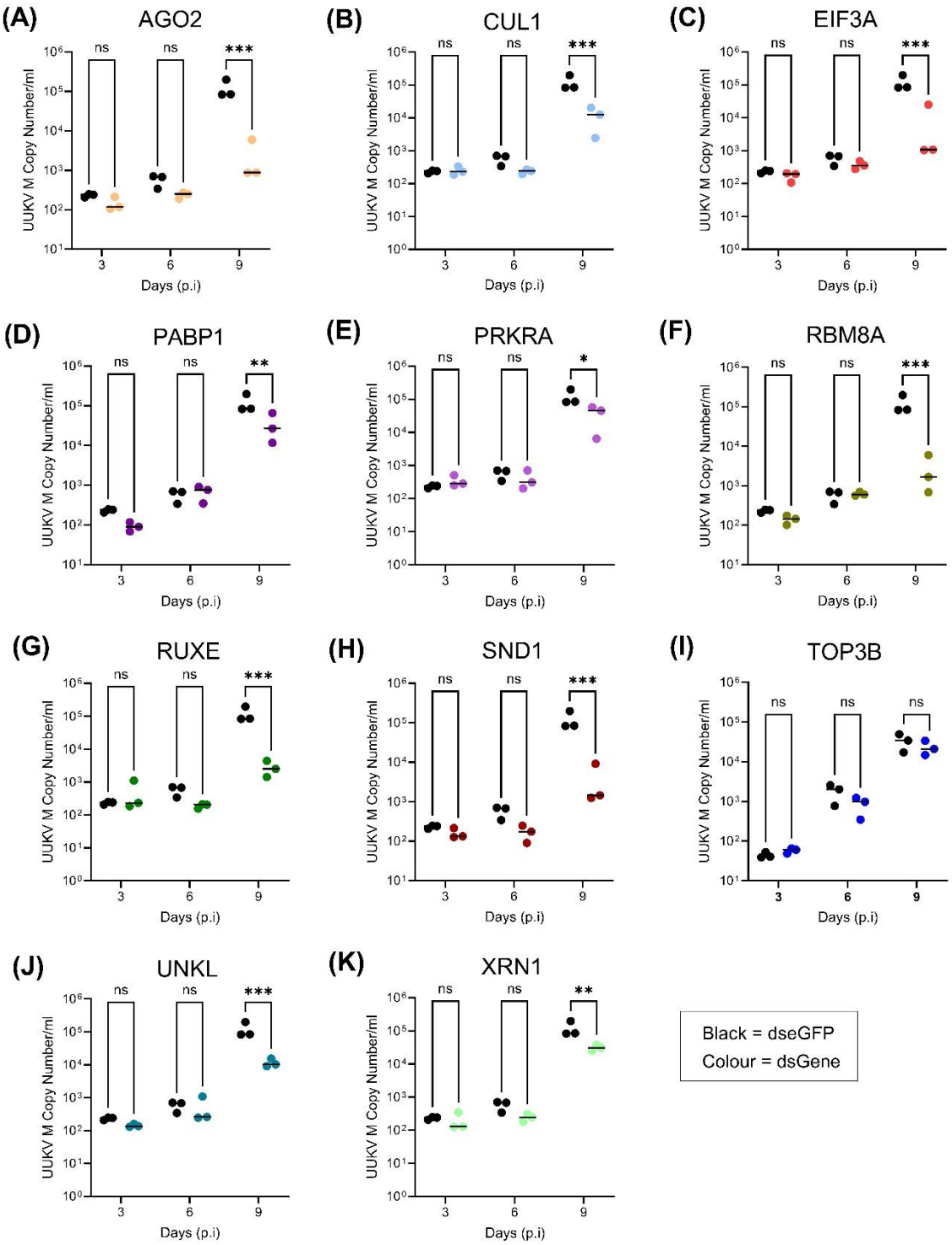

Figure 8.9: Effect of dsRNA transfections on the UUKV M RNA copy number within the supernatant of UUKV infected ISE6 cell cultures. ISE6 cell monolayers were transfected with 2µg of dsRNA homologous to either eGFP (dseGFP) or (A) *AGO2* (dsAGO2), (B) *CUL1* (dsCUL1), (C) *EIF3A* (dsEIF3A), (D) *PABP1* (dsPABP1), (E) *PRKRA* (dsPRKRA), (F) *RBM8A* (dsRBM8A), (G) *RUXE* (dsRUXE), (H) *SND1* (dsSND1), (I) *TOP3B* (dsTOP3B), (J) *UNKL* (dsUNKL), or (K) *XRN1* (dsXRN1), where *black symbols* represent dseGFP data and *coloured symbols* represent dsGene data. At one day post-transfection, cell monolayers were infected with rUUKV at 5 FFU/cell. At timepoints indicated, cell supernatants were harvested and RNA extracted using TRIzol. RT qPCR

was performed on the supernatant RNA using primers targeting UUKV M RNA. The copy number of UUKV M RNA was calculated and statistical significance measured by ordinary two-way ANOVA with Tukey's multiple comparisons test. Asterisks indicates significance **** = $p < 0.0001$, *** = $p \leq 0.001$, ** = $p \leq 0.01$, * = $p \leq 0.05$, ns = not significant.

8.4 Discussion

Preliminary knockdowns using positive and negative dsRNA controls were carried out to optimise the ratio of transfection reagent to dsRNA (µl:µg) . Previous research carried out through the work of Dr Marine Petit (unpublished) indicated that a high volume of transfection reagent can accelerate viral titre production/produce higher virus titres. Therefore, the results presented here are in line with previous observations made by Dr Petit, at the higher dsRNA to transfection reagent ratio of 1:3 (µg:µl), a small increase in viral titre at 3 days p.i., and a significant increase at 6 days p.i., was found for the negative control dseGFP knockdowns. To a lesser extent, this was also seen in the positive control dsUUKV knockdown (Figure 8.1). This indicates that a higher quantity of transfection reagent may induce a pro-viral environment within the cells in a mechanism not yet defined, and confirmed this ratio would not be suitable for the knockdown studies within this research, as the aim was to assess the effect of gene knockdown in 'normal' cell conditions. In contrast to this, when comparing the 1:1 and 1:2 ratios, although there was no significant difference in titres between the ratios at either timepoint, there was a significant difference between the levels of mRNA within the cell (Figure 8.1). This effect was very apparent in the dseGFP transfections but was also seen to a much lesser degree within the dsUUKV N transfection. This was expected as the dsUUKV N transfection should obliterate viral N protein production, and therefore prevent signs of UUKV replication. It is interesting that even when this appeared to be the case, at the highest ratio the viral replication in dsUUKV N transfections viral replication showed signs of recovery, further indicating higher levels of transfection reagent promote viral replication. It is unclear why increasing the transfection reagent ratio from 1:1 to 1:2 (µl:µl) slightly decreased the intracellular UUKV M RNA quantity whilst increasing the supernatant titre. It may be possible that increasing the transfection reagent quantity acted to enhance replication and packaging, but at the 1:2 ratio the rate of packaging and viral output prevents accumulation of viral RNAs within the cell. As more research is conducted into the anti-viral and stress response of ticks, it would be beneficial to determine the regulatory pathways triggered through this transfection methodology at different reagent ratios. For the purposes of this research, it was decided that a ratio of 1:1 would be used to further examine the knockdown controls before carrying out the gene knockdowns. This ratio was decided as this did not produce a difference in titre, reduced the volume of transfection reagent to which the ISE6 cells were exposed, and allowed for conservation of materials. In addition, given that the mass-spectrometry data which allowed target selection used material isolated at 9 days p.i., the time frame of the

experiments was extended to 3, 6 days p.i., or 9 days p.i., in order to examine the impact of the knockdowns on the establishment of the exponential phase of infection.

Once the reagent:dsRNA ratio was established, the impact of transfecting the negative control eGFP dsRNA was further examined. This experiment revealed that transfection of dseGFP significantly increased the amount of UUKV N protein produced despite there being no effect on UUKV M RNA production, meaning that transfection potentially accelerated the ability of the cells to translate proteins. There was also a significant decrease in cell viability in infected but non-transfected cells at 6 days p.i., and 9 days p.i., which may be an alternative reason as to why the normalised UUKV N (AU) signal was lower at 6 days p.i., and 9 days p.i. in non-transfected cells. There was also a small but significant decrease in viral titre at 9 days p.i., however it remains to be shown if this was due to the increased cell death (Figure 8.3). It is unclear why transfection impacted cell viability. Overall, it was confirmed that dseGFP would be a suitable negative control as although transfection may have made the cells more sensitive to infection, from the EVOS images (Figure 8.2), titre and RT qPCR analysis the overall cell morphology and health was not severely affected by transfection of dseGFP.

The efficiency of the knockdown methodology was then tested using the positive control of dsUUKV N dsRNA. By using UUKV N specific dsRNA, which does not target ISE6 genes, the efficiency of the transfection and dsRNA induced silencing can be assessed by whether the cells are able to establish a UUKV infection. From the results in Figure 8.4, there was no UUKV replication taking place within the cells. As we were infecting with an MOI of 5 FFU/cell, it is possible that all, or most cells, were exposed to UUKV infection. Combining the data with the microscopy observations in Figure 8.4.F, there were no visible clusters of infected cells, which are a sign of an established infection (an example of which is seen in the dseGFP equivalents), the results indicate a high level of transfection efficiency and therefore moving forward with the ISE6 gene dsRNA transfections it is highly likely that the majority of cells received the dsRNA used.

However, although the transfection indicated that most, if not all, cells would have had dsRNA deposited into them, this did not guarantee that the dsRNA would knock down the gene mRNA effectively. The dsRNA was designed to be homologous to the respective gene, and therefore should be used by the RNAi machinery as described in the introduction of Chapter 8 to degrade the mRNA of each gene within the cell and prevent protein production. These dsRNA segments were designed in NCBI using the ISE6 proteome as a background to prevent off target interactions, but due to the quality of the ISE6 genome and proteome

there is still a potential that the dsRNA would knockdown non-desired mRNA or was not able to degrade the desired mRNA sufficiently to impact protein expression.

Most transcripts were effectively knocked down, and therefore any effects seen upon the viral kinetics were likely due to the removal of the mRNA from the cell cultures. The results of *CUL1*, *PRKRA*, and *XRN1* need to be interpreted more cautiously, particularly at the later timepoints, as the level of mRNA for these genes was only knocked down to 50% of the levels seen in their dseGFP counterparts. Initially it was hypothesised that this lesser knockdown efficiency, and in the case of *CUL1* and *PRKRA* 'recovery' of gene mRNA levels, may be due to the protein removal being lethal meaning only cells which were not transfected efficiently survived. This may have been a contributing factor, as there was a reduction in cell viability at 9 days p.i.. However, this loss of viability was also seen within other knockdowns where no loss of transfection efficiency was seen, and at 6 days p.i. the *XRN1* knockdown showed a higher level of viability. Published data suggests that knocking down *CUL1* or *PRKRA* does not impact cell viability (Neault et al., 2021; Z. Q. Ren et al., 2020). Previous knockdown studies have suggested that removing *CUL1* in human cell lines causes a decrease in cell adhesion (Z. Q. Ren et al., 2020), but this decrease in adhesion was not also seen within the ISE6 cell culture as there was no decrease in dsCUL1 viability (infected and mock) compared to dseGFP transfected controls, meaning there was no substantial loss of cells before viability was assessed. This indicates that the function of these proteins may not be fully comparable between mammalian and ISE6 cell lines, and therefore hypotheses based on the homologous proteins needs to be interpreted with caution. Similar to *CUL1*, there is no established link between *XRN1* knockdown and cell lethality, however this is within the context of non-infected cells. In an interferon-activated (viral-infected) state A549 XRN1-KO (knockout) cells show increased cell death, which may reflect the viability data at 9 days p.i. (Zou et al., 2023). For *CUL1*, this protein was in the upper 50% for protein abundance within the mass spectrometry samples, and so there may have been a large amount of mRNA transcripts within the ISE6 cells. This abundance of *CUL1* has previously been seen in studies comparing the intracellular expression of the cullin genes (*CUL1-7*), where it was found *CUL1* and *CUL4B* were the most highly transcribed cullin genes in primary human tissues (Sweeney et al., 2020). When knockdown occurs, the cell is therefore not capable of degrading a large enough proportion of these abundant transcripts. However, in this cullin gene study, Sweeny et al. were able to knockdown *CUL1* efficiently. While it was not confirmed that the levels of *CUL1* mRNA transcript in primary human tissue and ISE6 cell culture were equal, this study indicated that this abundance may not be the reason for the lack of knockdown efficiency (Sweeney et al., 2020).

As the dsRNA is degraded to siRNA by the cellular machinery, the cleaved sections of RNA may not be specific or able to bind strongly enough to the CUL1, PRKRA and XRN1 mRNA to cause it to be degraded. This hypothesis is supported as PRKRA and XRN1 have also been successfully knocked down in mammalian cell cultures using dsRNA knockdown (M. Miyamoto & Komuro, 2017). An alternative hypothesis is that the knockdown is effective, however the removal of the transcripts triggers an upregulation response which counters the initial degradation. This would also account for the increase in mRNA of PRKRA and CUL1 over time, yet there is no confirmed evidence of this within the literature. The current hypothesis is that it is most likely that both the dsRNA sequences are insufficient for full knockdown efficiency and the cells activate feedback mechanisms. However, more investigation would need to be undertaken in order to confirm this hypothesis and elucidate what degree of impact both factors have.

Examining the other gene knockdowns, the overall viability data was in line with what has been seen previous in other studies. This is with the exception of RUXE and UNKL where no previous knockdown data were found and XRN1 where inhibition was achieved through exposure of cells to adenosine 3', 5'-bisphosphate and therefore direct links between protein inhibition and viability cannot be drawn (Y. C. Liu et al., 2021). It was expected that dsAGO2 transfection would not significantly affect cell mortality, as in other arthropod cell cultures (such as the mosquito cell line AF525) stably transfected AGO2 knockout cell lines have been developed (Scherer et al., 2021). There was a decrease in viability at 3 days p.i. which recovered by day 6 p.i., but as previously mentioned in chapter 1.1.1.2, the ISE6 genome contains five homologous AGO genes, and therefore as AGO2 is removed by day 6 another may be able to be substituted in its place (Baxter et al., 2017; Fogaça et al., 2021). In the EIF3A knockdowns, even at 9 d p.i., the higher level of viability in the dsEIF3A transfected cells was somewhat unexpected. Prior experiments where EIF3A was knocked down in hamster cells showed that the knockdown caused cell cycle arrest, and if this occurred within the ISE6 culture this may have prevented cells from moving through the cell cycle and undergoing apoptosis, although in hamster cells apoptosis was actually increased during knockdown (Zheng, Wang, Hong, Liu, & Jiang, 2021). PABP1 and RBM8A knockdown experiments were in line with EIF3A. PABP1 may have less of an increase in viability at earlier timepoints and a more severe drop in viability by 9 days post transfection as this protein has additional functions in relation to transcription and translation as compared to EIF3A. Finally, although the impact on cell cycle has not been investigated, viability was assessed at 3 days p.i. for SND1 knockdowns in A549 cells and these studies

also demonstrated an impact on cell viability following SND1 depletion (Schmidt et al., 2023).

Overall, it is hypothesised that the reduction in viability at 9 days p.i. is predominantly due to cellular exhaustion from viral infection. From the viability data, the knockdown prevents the normal cellular homeostasis that occurs in the dseGFP transfected cells. This subsequently has a knock-on impact on viral titre, as the increased cell mortality decreases the number of cells actively producing virus, thereby reducing the titre by 9 d p.i., and increased amounts of cellular debris in the supernatant may hypothetically decrease the viral titre. The cellular exhaustion may not occur until the later timepoint as ISE6 cells have a slower replication time compared to other arthropod cell lines (which can be seen through the increased number of times cells need to be split per week as described in Section 4.1), taking roughly 4-5 days to divide (Kurtti et al., 2008), meaning there may be a delay in seeing the impact of depleting the protein within the cells. In addition to this, many of the knockdown studies involving these proteins are in relation to cancer research in cell cultures which replicate far faster than ISE6 cells, meaning the effects of the protein knockdown are likely to be seen at an earlier timepoint within these cell cultures.

It would be beneficial in future, when more molecular tools are available against tick cells, to use antibodies against these proteins in a method such as western blotting or immunofluorescence to examine the effect of the knockdowns on the respective proteins and to revisit these results as more structural and functional information is gained about these proteins. This would allow for more certainty on the effectiveness on the knockdowns and would potentially allow for visualisation of colocalization of vRNA or proteins with the ISE6 cellular protein. The impact these proteins have on UUKV infection within ISE6 cells can still be hypothesised by analysing the impact of the knockdowns on UUKV viral kinetics and using the information available on the protein orthologs, a schematic of which is shown in Figure 8.10. It could not be determined if the knockdowns impacted viral titre, as was not possible to discern whether cellular exhaustion occured before the impact on viral kinetics or directly extended to decreasing infectious virus production. The exception to this was TOP3B, which showed no signs on reduced viability.

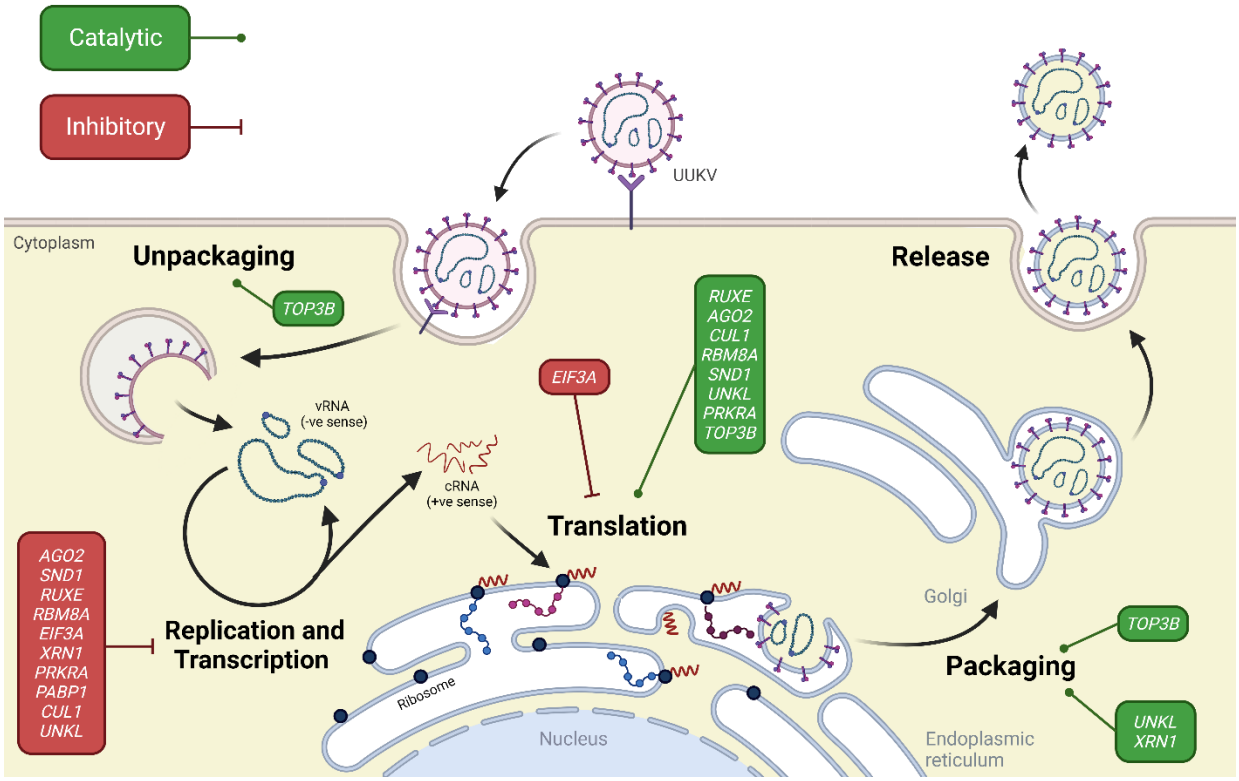

Figure 8.10: Schematic of simplified UUKV lifecycle within the vector cell showing where selected gene targets are proposed to act. The results from the dsRNA transfections (Figure 8.7-8.9) were analysed and the catalytic (green) and inhibitory (red) genes were added at where the hypothesised interaction with the UUKV replication process occurs within the ISE6 cells. Where more than one gene affected the same stage of the viral replication cycle, the genes were listed with those causing the largest effect at the top moving to the smallest at the bottom. This ranking was based on the significant increase (for catalytic effects) or decrease (for inhibitory effects) when comparing the gene knockdown to the dseGFP knockdown.

The stages of viral replication were segmented to analyse the impact of the dsRNA transfection on ISE6 cellular genes; uncoating, replication and transcription, translation, and packaging. Replication and transcription, although separate processes, are grouped together within this analysis due to the inability to differentiate whether the increase in UUKV M RNA was due to an increase in the rate of transcription of the sub genomic Gn/Gc mRNA or viral antigenome, a product of an increase in the rate of replication increase, or both, as previously mentioned.

Uncoating

The results from the dsRNA knockdown of TOP3B indicated that this protein was important for uncoating and/or packaging, as although there was an impact on viral protein production, the largest impact TOP3B knockdown caused was the drop in titre at 9 days post-infection.

However, this decrease was not reflected within the copy number of UUKV M RNA in the supernatant, indicating that although the same level of RNA was being released from the cells not all the viral particles that were released were infectious. This was an exciting result, as previous research has shown TOP3B knockout impairs the production of infectious flavivirus particles, although overall release of virions is unaffected, and this is in line with the results from this study (Diosa-Toro et al., 2020). The suggested mechanism for this is that TOP3B aids in changing the conformation of the UUKV RNA to promote replication, transcription and/or translation. It is unclear if TOP3B is packaged into viral particles, however if this is the case it may be used to unwrap the UUKV RNA from the viral nucleocapsid to promote initial viral infection. It would be interesting to analyse the protein makeup of UUKV viral particles to determine if TOP3B is present within the virions which would support this hypothesis. In addition, it would be useful to perform infection assays, using viral particles produced from TOP3B silenced UUKV infected cell cultures, on cell cultures where TOP3B is either over expressed or under expressed. If a difference in viral titre was seen between these two cell cultures this would also support the hypothesis that TOP3B was used by UUKV to aid in unpacking the virus and establishing early infection.

Replication and Transcription

When looking at replication and transcription, as there is an increase in UUKV M RNA detected present in the total cell RNA from all gene knockdown experiments apart from TOP3B, these genes may work in an inhibitory manner to limit the rate of production of vRNA (although from the dseGFP results it appeared that the UUKV RNA reached a plateau level at by day 9 p.i.). This could, potentially, prevent triggering of a large intracellular antiviral response, (as is indicated when these genes are knocked down) exhausting the cellular resources through diverting protein factors to viral replication/transcription, and/or triggering apoptosis. However, although they all appear to cause this outcome of increased UUKV M RNA at earlier timepoints, this does not mean that this is achieved through similar mechanisms. There are several mechanisms by which these genes may impact UUKV replication kinetics, either directly, through interacting with the UUKV RNA (e.g. through binding the RNA and promoting replication/transcription or promoting degradation), or indirectly, by impacting cellular factors that would influence UUKV replication (e.g. through upregulating proviral factors or downregulating antiviral factors), or a mixture of both by interacting directly with UUKV RNA or additional cellular factors. Overall, it is hypothesised that AGO2 and RBM8A impact UUKV kinetics directly, whereas CUL1, PABP1, PRKRA, RUXE, SND1, XRN1 impact UUKV kinetics indirectly, and EIF3A and UNKL may act by a combination of both direct and indirect methods. It would be useful in

future to knock down other factors in the pathways within which these proteins are involved, or to carry out inhibition using alternative means (such as enzymatic inhibitors) to see if similar results are obtained. Proteins directly impacting replication and transcription kinetics:

- **AGO2**: This is an antiviral protein that is upregulated during infection and is a key component the RNAi pathway RISC complex. As previously mentioned, infection with arboviruses such as DENV2, ZIKV, MAYV and the bunyavirus RVFV causes an increase in mosquito death when AGO2 is knocked out (Dietrich, Jansen, et al., 2017; S. Dong & Dimopoulos, 2023; Schnettler et al., 2014). Within the AGO2 knockdown results, it can therefore be hypothesised that by removing this protein the antiviral response within the cells is hindered, although as mentioned previously, this may recover over time if the cell is able to upregulate the other AGO proteins within the genome. This allows UUKV RNA replication and transcription to become significantly upregulated, which can be seen as AGO2 knockouts produce the highest increase in normalised expression at 3 days post infection.
- **RBM8A**: RBM8A has dual functions within the cell. The protein plays a role in the exon junction complex (EJC) by associating with newly spliced mRNA and aiding in guiding the newly spliced mRNA to ribosomes for translation (Ishigaki et al., 2013). However, as UUKV RNA does not undergo splicing (this does not mean that the EJC does not interact with the vRNA), it is more likely that it is the second role of RBM8A within the nonsense mediated decay pathway that has the greater influence on viral kinetics. This was seen within WNV and DENV infection, where the vRNA was targeted for degradation (M. Li et al., 2019). Therefore, when this protein was knocked down within the cell, UUKV M replication and transcription was upregulated in an exponential manner as the RNA segments were not removed by the nonsense mediated decay pathway.
- **XRN1**: XRN1 has degradation capabilities for non-poly(A) mRNAs, such as vRNA or poly(A)-stripped cellular mRNA, and when analysing RVFV-XRN1 interactions there was evidence to suggest that XRN1 directly degraded the vRNA and therefore RVFV had evolved measures to counter this (Chapman et al., 2014). XRN1 can also be hijacked by the virus, not only to prevent this degradation of vRNA, but also to target vector mRNA for degradation to prevent antiviral factors being produced in a pro-viral manner. Accordingly, it is not likely this occurs. This is presumed due to the knockdowns producing increased UUKV M RNA expression, indicating this

protein is antiviral, and when XRN1 is present within the cell it targets UUKV RNA for degradation.

Proteins indirectly impacting replication and transcription kinetics:

- **CUL1**: CUL1 is known to be targeted by RVFV NSs protein in order to degrade transcription factors that would aid in mounting the innate immune response (Kainulainen et al., 2014; Le May et al., 2004), including potentially the upregulation of other gene factors analysed in these knockdowns such as AGO2. By knocking down this protein the immune response is dampened, allowing the virus to increase the rate of both transcription and translation, but not to the levels seen within the gene knockdowns this protein affects (e.g. the AGO2 knockdown) as the knockdown was not as efficient and seemed to recover by 9 days post transfection.
- **PABP1**: Similar to CUL1, RVFV NSs also targets PABP1 for degradation or nuclear re-localisation in order to create an intracellular environment that favours viral replication and translation by inhibiting the miRNA-mediated repression and nonsense-mediated decay mRNA surveillance pathway and preventing vector mRNAs from being translated (M. Brook et al., 2012; Copeland et al., 2013). Although it cannot be determined if UUKV interacts with or inhibits PABP1, by knocking this protein down a similar effect is seen, in that a favourable intracellular environment is produced for the increased replication and translation of UUKV.
- **PRKRA**: PRKRA has not previously been shown to be directly targeted by viruses, however the IFN activated signalling pathway (the PKR) in which this protein is involved acts to shut down translation, induce apoptosis, and upregulate the antiviral RNA silencing pathway within the cell (R. C. Patel & Sen, 1998; Peters et al., 2001; Peters et al., 2009). As described for PABP1, it is not known if UUKV interacts with or inhibits PRKRA to prevent transcriptional shut off and antiviral activity, but by knocking down this protein, a favourable intracellular environment is produced for the increased replication and translation of UUKV.
- **RUXE**: As mentioned in the introduction, there is no evidence that bunyavirus RNA interacts with RUXE individually or as part of the spliceosome complex, as bunyavirus cRNA synthesis is coupled directly to translation and does not contain introns (Barr, 2007). Therefore, it is more plausible that during knockdown of the RUXE protein the pre-mRNA processing U snRNP complexes are disrupted and therefore cellular splicing and alternative splicing are impeded, and pre-mRNAs are unable to be translated, preventing antiviral factors being produced.

- **SND1**: Alongside RUXE, there is also no evidence that SND1 interacts with bunyavirus RNA. SND1 is an important component in mediating miRNA decay in the RISC complex. It is hypothesised that, when this protein is knocked down, RNAi turnover is reduced and therefore the RISC complex is unable to uptake new miRNA generated from the UUKV infection. This in turn prevents the UUKV RNA being degraded within the cell by this complex.

Proteins directly and indirectly impacting replication and transcription kinetics:

- **EIF3A**: EIF3A as a translation initiation factor, in terms of viral activity, is usually considered to work in either a proviral manner by being recruited by the virus to upregulate viral transcription, or antiviral manner and is therefore degraded by the virus in a 'host cell shut off' mechanism to prevent antiviral components being transcribed (Desmet et al., 2014; Rodriguez Pulido et al., 2007; Subramani et al., 2018; J. Zhang et al., 2019). From the results of this thesis, it is hypothesized that if the protein is recruited to the viral genetic material, it is in a transcription limiting capacity, and/or that EIF3A acts in an antiviral manner within the cell to upregulate production of antiviral factors similar to the suggested mechanism of CUL1.
- **UNKL**: As the function of UNKLs is still mostly undefined, it is unclear whether this protein has direct interactions with the UUKV RNA, although these zinc-fingers domains do have the ability to interact with vRNA. In addition, this protein may be involved with the ubiquitination pathway, and therefore could actively degrade viral proteins or prevent the degradation of antiviral factors (Brown, 2005; Lorès et al., 2010).

Translation

EIF3A is the only gene which appears to be antiviral, as at 9 days p.i. the quantity of UUKV N was significantly higher than the dseGFP transfected cells. Although this may be a consequence of having an increased level of UUKV RNA within the cells, as EIF3A is an elongation factor this may be specific to promoting cellular mRNAs, and therefore when knocked down there are more resources available to translate the viral transcripts. Conversely, although AGO2, CUL1, PRKRA, RBM8A, RUXE, SND1, and UNKL are inhibitory to replication and/or transcription, these proteins alongside TOP3B appear to be proviral when looking at the impact on translation, as for at least one timepoint in each knockdown shows a significant reduction in UUKV N protein accumulation. This initially was an unexpected result, as it was theorised that if the UUKV M RNA increased this would then cause the level of transcription to increase. For the factors which affect vector mRNA processing, such as RBM8A, RUXE, and SND1, removing these proteins may impede pre-

mRNA processing (e.g. splicing) or may produce incorrect transcripts that induce ribosomal stalling, preventing viral proteins from being transcribed (Hsu & Hertel, 2009). In the knockdowns where the proteins play a role within the antiviral response, such as AGO2, PRKRA, and SND1, the removal of these proteins may cause the cells to overcompensate or activate additional feedback loops which carry out host protein shut off (Hoang, Neault, Pelin, & Alain, 2020; Stern-Ginossar, Thompson, Mathews, & Mohr, 2019). For CUL1, which does not fit in either of these two categories, as this protein acts as a key component and scaffold for the ubiquitin E3 ligase complex, once this protein is removed this may cause the complex proteins to become dysregulated and increase the ubiquitination of UUKV N protein (J. Zheng et al., 2002). Finally, TOP3B is indicated in both packaging and unpackaging/uncoating, due to its function as a topoisomerase, which will be expanded upon below. However, as topoisomerases are capable of changing the topology of RNA and have been implicated in mRNA stability, this protein may be used to ensure that UUKV RNA is stable and in the correct secondary structure to be translated. Overall, as the effects on the UUKV N protein do not appear consistent across the timepoints, it indicates that these responses may be indirect consequences rather than due to the specific gene knockdown. For example, the increased level of UUKV RNA may trigger additional cellular pathways which decrease translation. It would be interesting in future to repeat these knockdowns and quantify the levels of expression for non-viral vector proteins to analyse if this decrease in protein is targeted only to UUKV N which would imply a specific mechanism, or applicable to cellular proteins across the board which would indicate an impact on general cellular translation shutoff.

Packaging

Unexpectedly, both UNKL and XRN1 produced similar results where although there was no significant difference in virus titre there was a significantly lower UUKV M RNA copy number within the supernatant. This indicated that either the dseGFP transfections produce a subset of viral particles which are non-infectious that are not produced when UNKL and XRN1 are knocked down, or the viral particles produced from UNKL and XRN1 knockdowns do not contain all the genomic segments but still produce a high enough titre that this lack of all three segments in each virion is compensated by multiple virions infecting the same cell. Currently there is no mechanistic hypothesis to explain these results. However, further experimentation by visualising the structure of the virion particles using electron microscopy or examining the density of the viral particles to determine if all three segments are present within most virions would add evidence to determine if this hypothesis is correct.

As mentioned in the uncoating section, TOP3B may be required to change the topology of the UUKV RNA to efficiently establish infection. Either in addition or instead of this, TOP3B may be required to help ensure the UUKV RNA is in the correct secondary structure for effective packaging to produce infectious viral particles. It would be useful to carry out a knockdown of TOP3B once UUKV infection has been established in ISE6 cells, as if a drop in titre is seen that is significant compared to dseGFP and no drop in supernatant copy number occurs this adds evidence to the hypothesis that TOP3B acts to package UUKV RNA.

In conclusion, this research has optimised the knockdown of gene targets within ISE6 cell cultures using novel dsRNA transfections methodologies and applied this technique to show a proof of principle that several of the proteins highlighted from the differential RBPome experiments (Chapter 7) impact UUKV infection. Although due to the level of understanding around these proteins it cannot be confirmed at this time that the suggested mechanisms are correct, it has been shown these proteins impact UUKV replication. This work provides grounding for further investigation and direction to elucidate the factors important for establishing UUKV infection in ISE6 cells. Further analysis around these proteins can be expanded into other timepoints and to different levels of dsRNA in order to determine if there is a dose dependant response. The long-term goal of this work will be to evaluate the mechanisms of these proteins, and how they interact within the cellular landscape to allow for perpetual and persistent infection of UUKV without causing distress to the vector.

Chapter 9 Final Conclusions and Future Perspectives.

This project can be divided into two primary aims: determination of the 'block' in replication of UUKV in mosquito cells and elucidating the factors within ISE6 cells that impact viral replication within vector derived cell lines.

Before investigating the block in UUKV replication in mosquito cells, it was important to confirm previous findings within the literature, in that tick borne bunyaviruses do not replicate within non-tick arthropods such as mosquitoes. Through conducting growth curve experiments, I was able to demonstrate that UUKV was unable to complete replication within mosquito cell lines derived from *Aedes aegypti*, and that this was independent of the RNAi response within the mosquito cells, indicating that the block occurred early within the replication cycle. An additional interesting result from this work was that deleting the NSs protein appeared to prevent effective UUKV replication within ISE6 cells, which was relevant to the second aim of this project and provides avenues for further investigation as described below. The results within the mosquito cell lines were useful in determining which stage of viral replication to investigate further, particularly as previously no published experiments had attempted to visualize whether UUKV virus could bind to or penetrate mosquito cells. By dying the UUKV viral particles with a fluorescent glycoprotein dye, and to visualize binding under different conditions within AF5 cells in comparison to cells where binding was known to occur (ISE6 and BSR cells), I was able to demonstrate that UUKV was able to bind AF5 cells but showed no evidence of internalization following the binding process (Chapter 5). This is the demonstration of a tick-borne bunyavirus being capable of binding arthropod cells not derived from tick species with high affinity. As it is currently unknown what receptors are employed by UUKV and other bunyaviruses to bind tick cells, it will be important to elucidate how these viruses access tick cells before we are able to compare these binding factors with those found on mosquito cells. It may be the case that as the virus is able to bind, but unable to be internalized, the mosquito cells may have receptors that bind UUKV but lack a co-receptor required to trigger internalization, or the receptor that binds UUKV is unable to induce the conformational change required to trigger internalization. This glycoprotein dye protocol could be used to visualize where the viral particles are bound on the cell before performing cryogenic electron microscopy. It may then be possible to visualize the structures with which UUKV interacts within each cell type and visualise if a conformational change is induced. In addition, isolating these membrane factors through immunoprecipitation and analysing them by mass spectrometry will allow for characterization of these cell surface proteins. Once identified, mutational analysis and recombinant assays would allow for further characterization of these factors. In the long term, identifying these factors may allow for the identification of therapeutic targets and

production of transgenic ticks with mutated receptors that are less susceptible to bunyavirus infection. This would be particularly useful if it was then compared with the factors on the mosquito cell surface that are unable to cause internalization, which may allow for a new method of disease control within the wild vector population (Chapter 5). Additionally, the identification of the factors that permit internalisation of bunyaviruses within the vector species is critical to surveillance of arthropod-borne diseases given bunyaviruses have shown reassortment capabilities and mosquito and tick-borne bunyaviruses circulate within the same geographical areas. Until these factors are identified we are unable to fully assess the likelihood of reassortment, or the potential disease impact such reassortments could cause. A plausible first step to identifying both the factors responsible for internalisation and the potential outcomes of reassortment is through the use of minigenome systems, which can be utilised to assess the ability of tick-borne virus genomic segments to replicate within a mosquito cell (and vice versa) through bypassing internalisation into the cell. This methodology has already been successfully employed in investigating reassortment between UUKV, HRTV, and SFTSV (Rezelj et al., 2019). In addition, VLP systems can be employed to 'mix and match' the viral protein composition of virions, and therefore by substituting in different proteins from mosquito-borne viruses into UUKV virions. By using these VLPs to infect mosquito cells, it can be determined what components would be required to allow the virus to overcome the block to entry in mosquito cells, and once this has been identified further studies can be carried out to determine the likelihood of this recombination event occurring in nature.

When elucidating the factors within ISE6 cell cultures that impact viral replication within the vector, there were several hurdles that needed to be overcome before the differential expression of RBPs during infection could be examined. The biggest of these hurdles was the lack of information available on the genomes of ticks and tick cells. Although RIC utilising UV crosslinking and oligo(dT) capture beads has been carried out within cell cultures derived from various other species, this is the first example of this technique being applied to and optimised in tick cell cultures. Through this method, I was able to establish the first tick cell line RBPome, which can be used in future as a comparative measure not only for ISE6 cell cultures in other conditions (such as infection with different viruses, collections at different timepoints, or variation in inoculum MOIs), but for different tick species (either cell lines or whole organisms) (Chapter 6). By building a better understanding of the baseline intracellular RBPome environment, further study will be able to ascertain the importance of different RBPs under different environmental conditions, which can then be mapped into the whole organism. As ISE6 is currently the most well characterised tick cell

line available, the data generated for the cellular RBPome may also be used to inform on other less well-characterised tick cell lines. However, although ortholog analysis allowed the structure and mechanisms of roughly 2/3rds of these proteins to be predicted, this data set would benefit from further definition and mapping of the ISE6 proteome and genome. At the time of writing these data sets are still considered to be in draft form. Further proteomic analysis would allow for improved homology and protein structure/mechanism studies, and with the proteins presented in this study these may be used for more targeted investigations.

From these techniques, I was also able to produce and characterise the first ISE6 RBPome in virus infected cells, and by comparing this data set to that of the mock RBPome, elucidated the RBPs that were differentially expressed during UUKV infection (Chapter 7). These data show similarities with differential infection data seen through previous transcriptomic and whole cell proteomic studies within several tick cell lines and furthers our understanding of the RBPs that may play an important role in the establishment of persistent tick-borne virus infection. This differential RBPome also provides a useful starting point, not only for downstream validation of the mass spectrometry results using dsRNA transfection, but for future work in identifying if these proteins are significant in vector-viral interactions across different tick species, virus species, and timepoints, as currently we can only assess the significance of these proteins in the ISE6 cell line at 9 days post-infection. To expand this work, it would be useful to repeat this methodology at different timepoints, both earlier (for example 1 day, 3 days, and 6 days) and once persistence was established (for example over 2 weeks post-infection) to investigate the dynamic changes of RBP expression over the course of infection. It is most likely that different RBPs play important roles at different timepoints when establishing persistent infection after virus exposure within the vector. Therefore, to fully elucidate the role of each RBP in establishing infection, a picture needs to be built of how expression changes over time.

Currently, the availability of antibodies and other molecular probes against tick proteins is severely limited, with none being available for tick specific RBPs. Prior to the establishment of the differential RBPome, it was unclear which RBPs may play an active role in infection. These elucidated RBPs can now provide a guide for developing molecular tools for further investigation within ticks. By using the significantly differentiated proteins as a starting list, for example, to produce recombinant protein to raise antibodies, a molecular toolkit can and should be developed. This toolkit would progress our knowledge within the area of vector-virus interactions by allowing more in-depth structural studies (e.g. through x-ray crystallography), interaction studies (e.g. through immunoprecipitation), and intracellular localisation studies (e.g. confocal microscopy probing both the viral and tick proteins). These

tools could also potentially have other uses such as homology studies, cell line characterisation studies, and pathogen studies outside of vector-virus interactions (Chapter 7).

Finally, to validate experimentally the differential RBPs established in Chapter 7 in an *in vitro* model, I carried out transfections utilising dsRNA homologous to the RBPs in question in ISE6 cell cultures, to knock down the respective protein. This method of transfection has been developed in recent years, and in the context of tick cell lines has previously been used successfully in the BME6 tick cell line by Dr Petit. The results from this study confirm this transfection method is efficient in multiple cell lines and will be a useful tool for future experiments given the minimal impact to cell viability. However, if this technique is to be used on tick cell lines it would be beneficial to carry out transcriptomic and proteomic studies to confirm the effects of the transfection protocol on the cell lines in question, as they do appear to have a small impact on viral kinetics. Additionally, as the ISE6 genome is not fully defined, there was a risk that the gene targeting would not be specific enough, or that off-target effects may occur. Therefore, if antibodies are raised against the proteins in question as described in the previous paragraph, it would be beneficial to repeat these studies whilst in tandem probing for the proteins via western blot in order to confirm specific protein reduction was achieved. Despite this, from the data produced in Chapter 8, I am confident that successful and specific gene knockdown was achieved. From these data I have confirmed that the proteins in question all have a role in the replication of UUKV, validating the results produced in Chapter 7. In particular, an exciting result was seen with TOP3B, as the proposed function within this study matches the role proposed by recently published data from mammalian infection models. The data generated require further validation to build a functional model for each of the identified RBPs, as this is the first time the importance of RBPs has been examined through this methodology and RIC information gathered in tick cells. When combined with the large gaps in information about the ISE6 proteome and intracellular environment, it is prudent to further validate my findings. Predictive modelling, structural analysis, overexpression studies and competitive inhibitor assays would allow for further validation of the hypothesised functions presented in Chapter 8. In the long term, it would be interesting to carry out this protocol on identified homologs/orthologs within other arthropod systems. By repeating these assays within other cell lines derived from other tick species, one will be able to determine if there are shared mechanisms or pathways in viral interaction and establishing persistence that have evolved across disparate tick species. This could then be expanded to determining if this response is specific to UUKV or if the same viral kinetics are seen across infections with different viral species. By repeating these assays

on non-tick arthropods, such as mosquitoes, the similarities between the RBPome responses can be determined and key or core RBPs can be identified for arthropods. By defining the differences and similarities between the RBPome responses of different arthropods, one is able to better understand the progression of viral infection and identify key therapeutic targets or predict recombination events (Chapter 8).

To conclude, the work carried out within this PhD has contributed to our understanding of how vector tropism is achieved with the tick-borne bunyavirus, UUKV. It has presented not only the first established tick cell-line derived RBPome but additionally highlighted the differential RBPs which play an active role in UUKV infection. Through transfection experiments *in vitro*, these differential RBPs have been validated experimentally and provide the first insights into the potential roles of RBPs during establishing infection. Overall, it is hoped that this work will be carried on, being used in future as a starting point to develop much needed molecular tools for studying tick borne viruses, and a key part of the foundation from which our understanding of the intracellular interactions between ticks and tick-borne viruses can continue to grow.

Chapter 10 Appendices

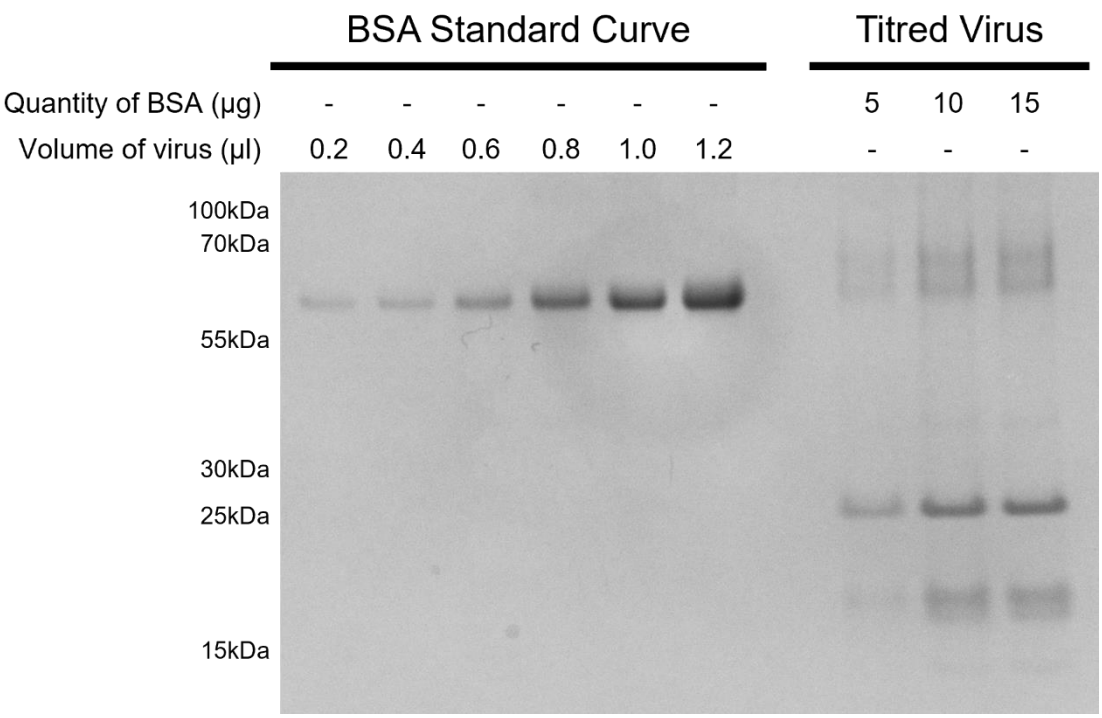

Figure 10.1: Example of band visualisation for quantification of UUKV glycoproteins. Serial dilutions of BSA (BSA standard curve) alongside serial dilutions of UUKV (titred virus) were prepared for gel electrophoresis and visualised using Coomassie blue staining.

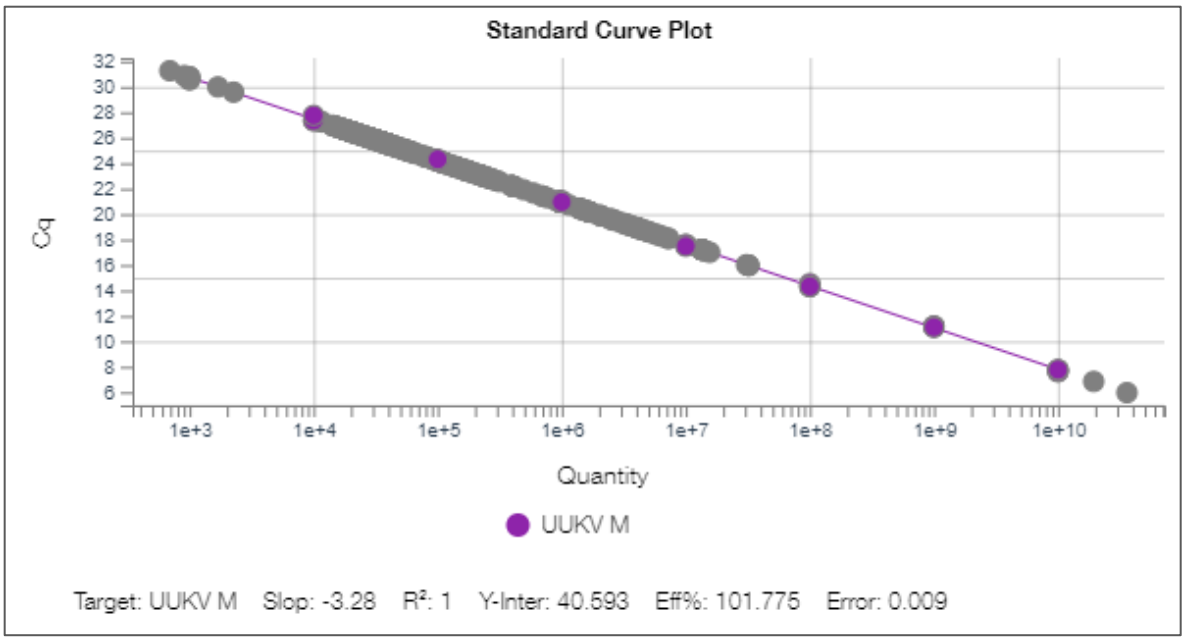

Figure 10.2: Representative standard curve of RT qPCR for UUKV M for copy number calculations. Serial dilutions of UUKV M standard DNA were analysed via RT qPCR. The quantity in ng vs Ct score was plotted to allow for the production of a standard curve from which UUKV M copy numbers can be calculated.

Chapter 11 List of References

Abernathy, E., Gilbertson, S., Alla, R., & Glaunsinger, B. (2015). Viral Nucleases Induce an mRNA Degradation-Transcription Feedback Loop in Mammalian Cells. *Cell Host Microbe, 18*(2), 243-253. doi:10.1016/j.chom.2015.06.019

Abudurexiti, A., Adkins, S., Alioto, D., Alkhovsky, S. V., Avsic-Zupanc, T., Ballinger, M. J., . . . Kuhn, J. H. (2019). Taxonomy of the order Bunyavirales: update 2019. *Arch Virol, 164*(7), 1949-1965. doi:10.1007/s00705-019-04253-6

Achsel, T., Stark, H., & Luhrmann, R. (2001). The Sm domain is an ancient RNA-binding motif with oligo(U) specificity. *Proc Natl Acad Sci U S A, 98*(7), 3685-3689. doi:10.1073/pnas.071033998

Ahmad, M., Xue, Y., Lee, S. K., Martindale, J. L., Shen, W., Li, W., . . . Wang, W. (2016). RNA topoisomerase is prevalent in all domains of life and associates with polyribosomes in animals. *Nucleic Acids Res, 44*(13), 6335-6349. doi:10.1093/nar/gkw508

Alberdi, M. P., Nijhof, A. M., Jongejan, F., & Bell-Sakyi, L. (2012). Tick cell culture isolation and growth of Rickettsia raoultii from Dutch Dermacentor reticulatus ticks. *Ticks Tick Borne Dis, 3*(5-6), 349-354. doi:10.1016/j.ttbdis.2012.10.020

Alberdi, P., Ayllon, N., Cabezas-Cruz, A., Bell-Sakyi, L., Zweygarth, E., Stuen, S., & de la Fuente, J. (2015). Infection of Ixodes spp. tick cells with different Anaplasma phagocytophilum isolates induces the inhibition of apoptotic cell death. *Ticks Tick Borne Dis, 6*(6), 758-767. doi:10.1016/j.ttbdis.2015.07.001

Alberdi, P., Mansfield, K. L., Manzano-Roman, R., Cook, C., Ayllon, N., Villar, M., . . . de la Fuente, J. (2016). Tissue-Specific Signatures in the Transcriptional Response to Anaplasma phagocytophilum Infection of Ixodes scapularis and Ixodes ricinus Tick Cell Lines. *Front Cell Infect Microbiol, 6*, 20. doi:10.3389/fcimb.2016.00020

Albornoz, A., Hoffmann, A. B., Lozach, P. Y., & Tischler, N. D. (2016). Early Bunyavirus-Host Cell Interactions. *Viruses, 8*(5). doi:10.3390/v8050143

Aliyari, R., & Ding, S. W. (2009). RNA-based viral immunity initiated by the Dicer family of host immune receptors. *Immunol Rev, 227*(1), 176-188. doi:10.1111/j.1600-065X.2008.00722.x

Aljamali, M. N., Sauer, J. R., & Essenberg, R. C. (2002). RNA interference: applicability in tick research. *Exp Appl Acarol, 28*(1-4), 89-96. doi:10.1023/a:1025346131903

Aljofan, M., Saubern, S., Meyer, A. G., Marsh, G., Meers, J., & Mungall, B. A. (2009). Characteristics of Nipah virus and Hendra virus replication in different cell lines and their suitability for antiviral screening. *Virus Res, 142*(1-2), 92-99. doi:10.1016/j.virusres.2009.01.014

Amos, B., Aurrecoechea, C., Barba, M., Barreto, A., Basenko, E. Y., Bazant, W., . . . Zheng, J. (2022). VEuPathDB: the eukaryotic pathogen, vector and host bioinformatics resource center. *Nucleic Acids Res, 50*(D1), D898-D911. doi:10.1093/nar/gkab929

Andersson, A. M., Melin, L., Bean, A., & Pettersson, R. F. (1997). A retention signal necessary and sufficient for Golgi localization maps to the cytoplasmic tail of a Bunyaviridae (Uukuniemi virus) membrane glycoprotein. *J Virol, 71*(6), 4717-4727. doi:10.1128/JVI.71.6.4717-4727.1997

Anywaine, Z., Lule, S. A., Hansen, C., Warimwe, G., & Elliott, A. (2022). Clinical manifestations of Rift Valley fever in humans: Systematic review and meta-analysis. *PLoS Negl Trop Dis, 16*(3), e0010233. doi:10.1371/journal.pntd.0010233

Armstrong, P. M., Ehrlich, H. Y., Magalhaes, T., Miller, M. R., Conway, P. J., Bransfield, A., . . . Brackney, D. E. (2020). Successive blood meals enhance virus dissemination within mosquitoes and increase transmission potential. *Nat Microbiol, 5*(2), 239-247. doi:10.1038/s41564-019-0619-y

Artigas-Jeronimo, S., Alberdi, P., Villar Rayo, M., Cabezas-Cruz, A., Prados, P. J. E., Mateos-Hernandez, L., & de la Fuente, J. (2019). Anaplasma phagocytophilum modifies tick cell microRNA expression and upregulates isc-mir-79 to facilitate infection by targeting the Roundabout protein 2 pathway. *Sci Rep, 9*(1), 9073. doi:10.1038/s41598-019-45658-2

Asgari, S. (2014). Role of microRNAs in arbovirus/vector interactions. *Viruses, 6*(9), 3514-3534. doi:10.3390/v6093514

Aslam, S., Latif, M. S., Daud, M., Rahman, Z. U., Tabassum, B., Riaz, M. S., . . . Husnain, T. (2016). Crimean-Congo hemorrhagic fever: Risk factors and control measures for the infection abatement. *Biomed Rep, 4*(1), 15-20. doi:10.3892/br.2015.545

Asthana, S., Martin, H., Rupkey, J., Patel, S., Yoon, J., Keegan, A., & Mao, Y. (2022). The Physiological Roles of the Exon Junction Complex in Development and Diseases. *Cells, 11*(7). doi:10.3390/cells11071192

Atim, S. A., Niebel, M., Ashraf, S., Vudriko, P., Odongo, S., Balinandi, S., . . . Thomson, E. C. (2023). Prevalence of Crimean-Congo haemorrhagic fever in livestock following a confirmed human case in Lyantonde district, Uganda. *Parasit Vectors, 16*(1), 7. doi:10.1186/s13071-022-05588-x

Au, S. K. W., Portelli, I. V., & DeWitte-Orr, S. J. (2022). Using long, sequence-specific dsRNA to knockdown inducible protein expression and virus production via an RNAi-like mechanism. *Fish Shellfish Immunol, 131*, 945-957. doi:10.1016/j.fsi.2022.10.061

Bach-Pages, M., Homma, F., Kourelis, J., Kaschani, F., Mohammed, S., Kaiser, M., . . . Preston, G. (2020). Discovering the RNA-Binding Proteome of Plant Leaves with an Improved RNA Interactome Capture Method. *Biomolecules, 10*(4). doi:10.3390/biom10040661

Backes, S., Langlois, R. A., Schmid, S., Varble, A., Shim, J. V., Sachs, D., & tenOever, B. R. (2014). The Mammalian response to virus infection is independent of small RNA silencing. *Cell Rep, 8*(1), 114-125. doi:10.1016/j.celrep.2014.05.038

Ballinger, M. J., & Taylor, D. J. (2019). Evolutionary persistence of insect bunyavirus infection despite host acquisition and expression of the viral nucleoprotein gene. *Virus Evol, 5*(2), vez017. doi:10.1093/ve/vez017

Baltz, A. G., Munschauer, M., Schwanhausser, B., Vasile, A., Murakawa, Y., Schueler, M., . . . Landthaler, M. (2012). The mRNA-bound proteome and its global occupancy profile on protein-coding transcripts. *Mol Cell, 46*(5), 674-690. doi:10.1016/j.molcel.2012.05.021

Bang, M. S., Kim, C. M., Kim, D. M., & Yun, N. R. (2022). Effective Drugs Against Severe Fever With Thrombocytopenia Syndrome Virus in an in vitro Model. *Front Med (Lausanne), 9*, 839215. doi:10.3389/fmed.2022.839215

Baquero-Perez, B., Antanaviciute, A., Yonchev, I. D., Carr, I. M., Wilson, S. A., & Whitehouse, A. (2019). The Tudor SND1 protein is an m(6)A RNA reader essential for replication of Kaposi's sarcoma-associated herpesvirus. *Elife, 8*. doi:10.7554/eLife.47261

Barr, J. N. (2007). Bunyavirus mRNA synthesis is coupled to translation to prevent premature transcription termination. *RNA, 13*(5), 731-736. doi:10.1261/rna.436607

Barry, G., Alberdi, P., Schnettler, E., Weisheit, S., Kohl, A., Fazakerley, J. K., & Bell-Sakyi, L. (2013). Gene silencing in tick cell lines using small interfering or long double-stranded RNA. *Exp Appl Acarol, 59*(3), 319-338. doi:10.1007/s10493-012-9598-x

Baudin, M., Jumaa, A. M., Jomma, H. J. E., Karsany, M. S., Bucht, G., Naslund, J., . . . Mohamed, N. (2016). Association of Rift Valley fever virus infection with miscarriage in Sudanese women: a cross-sectional study. *Lancet Glob Health, 4*(11), e864-e871. doi:10.1016/S2214-109X(16)30176-0

Baxter, R. H., Contet, A., & Krueger, K. (2017). Arthropod Innate Immune Systems and Vector-Borne Diseases. *Biochemistry, 56*(7), 907-918. doi:10.1021/acs.biochem.6b00870

Beckmann, B. M., Horos, R., Fischer, B., Castello, A., Eichelbaum, K., Alleaume, A. M., . . . Hentze, M. W. (2015). The RNA-binding proteomes from yeast to man harbour conserved enigmRBPs. *Nat Commun, 6*, 10127. doi:10.1038/ncomms10127

Bell-Sakyi, L. (2004). Ehrlichia ruminantium grows in cell lines from four ixodid tick genera. *J Comp Pathol, 130*(4), 285-293. doi:10.1016/j.jcpa.2003.12.002

Bell-Sakyi, L., Kohl, A., Bente, D. A., & Fazakerley, J. K. (2012). Tick cell lines for study of Crimean-Congo hemorrhagic fever virus and other arboviruses. *Vector Borne Zoonotic Dis, 12*(9), 769-781. doi:10.1089/vbz.2011.0766

Bell-Sakyi, L., Zweygarth, E., Blouin, E. F., Gould, E. A., & Jongejan, F. (2007). Tick cell lines: tools for tick and tick-borne disease research. *Trends Parasitol, 23*(9), 450-457. doi:10.1016/j.pt.2007.07.009

BenDavid, E., Pfaller, C. K., Pan, Y., Samuel, C. E., & Ma, D. (2022). Host 5'-3' Exoribonuclease XRN1 Acts as a Proviral Factor for Measles Virus Replication by Downregulating the dsRNA-Activated Kinase PKR. *J Virol, 96*(22), e0131922. doi:10.1128/jvi.01319-22

Berlanga, J. J., Ventoso, I., Harding, H. P., Deng, J., Ron, D., Sonenberg, N., . . . de Haro, C. (2006). Antiviral effect of the mammalian translation initiation factor 2alpha kinase GCN2 against RNA viruses. *EMBO J, 25*(8), 1730-1740. doi:10.1038/sj.emboj.7601073

Bermudez-Mendez, E., Bronsvoort, K. F., Zwart, M. P., van de Water, S., Cardenas-Rey, I., Vloet, R. P. M., . . . Wichgers Schreur, P. J. (2022). Incomplete bunyavirus particles can

cooperatively support virus infection and spread. *PLoS Biol, 20*(11), e3001870. doi:10.1371/journal.pbio.3001870

Bermudez-Mendez, E., Katrukha, E. A., Spruit, C. M., Kortekaas, J., & Wichgers Schreur, P. J. (2021). Visualizing the ribonucleoprotein content of single bunyavirus virions reveals more efficient genome packaging in the arthropod host. *Commun Biol, 4*(1), 345. doi:10.1038/s42003-021-01821-y

Bermudez, Y., Hatfield, D., & Muller, M. (2023). A Balancing Act: The Viral-Host Battle over RBPs. *Preprints*. doi:10.20944/preprints202312.1320.v1

Bernard, C., Holzmuller, P., Bah, M. T., Bastien, M., Combes, B., Jori, F., . . . Vial, L. (2022). Systematic Review on Crimean-Congo Hemorrhagic Fever Enzootic Cycle and Factors Favoring Virus Transmission: Special Focus on France, an Apparently Free-Disease Area in Europe. *Front Vet Sci, 9*, 932304. doi:10.3389/fvets.2022.932304

Berry, G. E., & Tse, L. V. (2017). Virus Binding and Internalization Assay for Adeno-associated Virus. *Bio Protoc, 7*(2). doi:10.21769/BioProtoc.2110

Bertrand, M. R., & Wilson, M. L. (1996). Microclimate-dependent survival of unfed adult Ixodes scapularis (Acari:Ixodidae) in nature: life cycle and study design implications. *J Med Entomol, 33*(4), 619-627. doi:10.1093/jmedent/33.4.619

Billecocq, A., Spiegel, M., Vialat, P., Kohl, A., Weber, F., Bouloy, M., & Haller, O. (2004). NSs protein of Rift Valley fever virus blocks interferon production by inhibiting host gene transcription. *J Virol, 78*(18), 9798-9806. doi:10.1128/JVI.78.18.9798-9806.2004

Binarova, P., & Tuszynski, J. (2019). Tubulin: Structure, Functions and Roles in Disease. *Cells, 8*(10). doi:10.3390/cells8101294

Bird, B. H., Ksiazek, T. G., Nichol, S. T., & Maclachlan, N. J. (2009). Rift Valley fever virus. *J Am Vet Med Assoc, 234*(7), 883-893. doi:10.2460/javma.234.7.883

Bitto, D., Halldorsson, S., Caputo, A., & Huiskonen, J. T. (2016). Low pH and Anionic Lipid-dependent Fusion of Uukuniemi Phlebovirus to Liposomes. *J Biol Chem, 291*(12), 6412-6422. doi:10.1074/jbc.M115.691113

Blair, C. D. (2011). Mosquito RNAi is the major innate immune pathway controlling arbovirus infection and transmission. *Future Microbiol, 6*(3), 265-277. doi:10.2217/fmb.11.11

Blair, C. D., & Olson, K. E. (2015). The role of RNA interference (RNAi) in arbovirus-vector interactions. *Viruses, 7*(2), 820-843. doi:10.3390/v7020820

Blakqori, G., Delhaye, S., Habjan, M., Blair, C. D., Sanchez-Vargas, I., Olson, K. E., . . . Weber, F. (2007). La Crosse bunyavirus nonstructural protein NSs serves to suppress the type I interferon system of mammalian hosts. *J Virol, 81*(10), 4991-4999. doi:10.1128/JVI.01933-06

Blasco-Moreno, B., de Campos-Mata, L., Bottcher, R., Garcia-Martinez, J., Jungfleisch, J., Nedialkova, D. D., . . . Diez, J. (2019). The exonuclease Xrn1 activates transcription and translation of mRNAs encoding membrane proteins. *Nat Commun, 10*(1), 1298. doi:10.1038/s41467-019-09199-6

Blitvich, B. J., Beaty, B. J., Blair, C. D., Brault, A. C., Dobler, G., Drebot, M. A., . . . Weaver, S. C. (2018). Bunyavirus Taxonomy: Limitations and Misconceptions Associated with the Current ICTV Criteria Used for Species Demarcation. *Am J Trop Med Hyg, 99*(1), 11-16. doi:10.4269/ajtmh.18-0038

Bodak, M., Cirera-Salinas, D., Luitz, J., & Ciaudo, C. (2017). The Role of RNA Interference in Stem Cell Biology: Beyond the Mutant Phenotypes. *J Mol Biol, 429*(10), 1532-1543. doi:10.1016/j.jmb.2017.01.014

Bonning, B. C., & Saleh, M. C. (2021). The Interplay Between Viruses and RNAi Pathways in Insects. *Annu Rev Entomol, 66*, 61-79. doi:10.1146/annurev-ento-033020-090410

Borucki, M. K., Chandler, L. J., Parker, B. M., Blair, C. D., & Beaty, B. J. (1999). Bunyavirus superinfection and segment reassortment in transovarially infected mosquitoes. *J Gen Virol, 80 (Pt 12)*, 3173-3179. doi:10.1099/0022-1317-80-12-3173

Boshra, H. (2022). An Overview of the Infectious Cycle of Bunyaviruses. *Viruses, 14*(10). doi:10.3390/v14102139

Boucas, J., Fritz, C., Schmitt, A., Riabinska, A., Thelen, L., Peifer, M., . . . Reinhardt, H. C. (2015). Label-Free Protein-RNA Interactome Analysis Identifies Khsrp Signaling Downstream of the p38/Mk2 Kinase Complex as a Critical Modulator of Cell Cycle Progression. *PLoS One, 10*(5), e0125745. doi:10.1371/journal.pone.0125745

Boudreault, S., Roy, P., Lemay, G., & Bisaillon, M. (2019). Viral modulation of cellular RNA alternative splicing: A new key player in virus-host interactions? *Wiley Interdiscip Rev RNA, 10*(5), e1543. doi:10.1002/wrna.1543

Brackney, D. E., Beane, J. E., & Ebel, G. D. (2009). RNAi targeting of West Nile virus in mosquito midguts promotes virus diversification. *PLoS Pathog, 5*(7), e1000502. doi:10.1371/journal.ppat.1000502

Brackney, D. E., LaReau, J. C., & Smith, R. C. (2021). Frequency matters: How successive feeding episodes by blood-feeding insect vectors influences disease transmission. *PLoS Pathog, 17*(6), e1009590. doi:10.1371/journal.ppat.1009590

Brackney, D. E., Scott, J. C., Sagawa, F., Woodward, J. E., Miller, N. A., Schilkey, F. D., . . . Ebel, G. D. (2010). C6/36 Aedes albopictus cells have a dysfunctional antiviral RNA interference response. *PLoS Negl Trop Dis, 4*(10), e856. doi:10.1371/journal.pntd.0000856

Brennan, B., Li, P., Zhang, S., Li, A., Liang, M., Li, D., & Elliott, R. M. (2015). Reverse genetics system for severe fever with thrombocytopenia syndrome virus. *J Virol, 89*(6), 3026-3037. doi:10.1128/JVI.03432-14

Briese, T., Calisher, C. H., & Higgs, S. (2013). Viruses of the family Bunyaviridae: Are all available isolates reassortants? *Virology, 446*(1-2), 207-216. doi:10.1016/j.virol.2013.07.030

Brimacombe, R., Stiege, W., Kyriatsoulis, A., & Maly, P. (1988). Intra-RNA and RNA-protein cross-linking techniques in Escherichia coli ribosomes. *Methods Enzymol, 164*, 287-309. doi:10.1016/s0076-6879(88)64050-x

Brook, M., McCracken, L., Reddington, J. P., Lu, Z. L., Morrice, N. A., & Gray, N. K. (2012). The multifunctional poly(A)-binding protein (PABP) 1 is subject to extensive dynamic post-translational modification, which molecular modelling suggests plays an important role in co-ordinating its activities. *Biochem J, 441*(3), 803-812. doi:10.1042/BJ20111474

Brook, M., Smith, J. W. S., & Gray, N. K. (2009). The DAZL and PABP families: RNA-binding proteins with interrelated roles in translational control in oocytes. *Reproduction, 137*(4), 595-617. doi:10.1530/rep-08-0524

Brown, R. S. (2005). Zinc finger proteins: getting a grip on RNA. *Current Opinion in Structural Biology, 15*(1), 94-98. doi:10.1016/j.sbi.2005.01.006

Brugier, A., Hafirrassou, M. L., Pourcelot, M., Baldaccini, M., Kril, V., Couture, L., . . . Amara, A. (2022). RACK1 Associates with RNA-Binding Proteins Vigilin and SERBP1 to Facilitate Dengue Virus Replication. *J Virol, 96*(7), e0196221. doi:10.1128/jvi.01962-21

Bryden, S. R., Dunlop, J. I., Clarke, A. T., Fares, M., Pingen, M., Wu, Y., . . . Brennan, B. (2022). Exploration of immunological responses underpinning severe fever with thrombocytopenia syndrome virus infection reveals IL-6 as a therapeutic target in an immunocompromised mouse model. *PNAS Nexus, 1*(1), pgac024. doi:10.1093/pnasnexus/pgac024

Buchholz, U. J., Finke, S., & Conzelmann, K. K. (1999). Generation of bovine respiratory syncytial virus (BRSV) from cDNA: BRSV NS2 is not essential for virus replication in tissue culture, and the human RSV leader region acts as a functional BRSV genome promoter. *J Virol, 73*(1), 251-259. doi:10.1128/JVI.73.1.251-259.1999

Budasha, N. H., Gonzalez, J. P., Sebhatu, T. T., & Arnold, E. (2018). Rift Valley fever seroprevalence and abortion frequency among livestock of Kisoro district, South Western Uganda (2016): a prerequisite for zoonotic infection. *BMC Vet Res, 14*(1), 271. doi:10.1186/s12917-018-1596-8

Bugrysheva, J., Dobrikova, E. Y., Godfrey, H. P., Sartakova, M. L., & Cabello, F. C. (2002). Modulation of Borrelia burgdorferi stringent response and gene expression during extracellular growth with tick cells. *Infect Immun, 70*(6), 3061-3067. doi:10.1128/IAI.70.6.3061-3067.2002

Burgess, H. M., Richardson, W. A., Anderson, R. C., Salaun, C., Graham, S. V., & Gray, N. K. (2011). Nuclear relocalisation of cytoplasmic poly(A)-binding proteins PABP1 and PABP4 in response to UV irradiation reveals mRNA-dependent export of metazoan PABPs. *J Cell Sci, 124*(Pt 19), 3344-3355. doi:10.1242/jcs.087692

Burkard, C., Bloyet, L. M., Wicht, O., van Kuppeveld, F. J., Rottier, P. J., de Haan, C. A., & Bosch, B. J. (2014). Dissecting virus entry: replication-independent analysis of virus binding, internalization, and penetration using minimal complementation of beta-galactosidase. *PLoS One, 9*(7), e101762. doi:10.1371/journal.pone.0101762

Burrell, C. J., Howard, C. R., & Murphy, F. A. (2017). Bunyaviruses. In *Fenner and White's Medical Virology* (pp. 407-424).

Calabretta, S., & Richard, S. (2015). Emerging Roles of Disordered Sequences in RNA-Binding Proteins. *Trends Biochem Sci, 40*(11), 662-672. doi:10.1016/j.tibs.2015.08.012

Calisher, C. H., & Goodpasture, H. C. (1975). Human infection with Bhanja virus. *Am J Trop Med Hyg, 24*(6 Pt 1), 1040-1042. doi:10.4269/ajtmh.1975.24.1040

Cano, F., Rapiteanu, R., Sebastiaan Winkler, G., & Lehner, P. J. (2015). A non-proteolytic role for ubiquitin in deadenylation of MHC-I mRNA by the RNA-binding E3-ligase MEX-3C. *Nat Commun, 6*, 8670. doi:10.1038/ncomms9670

Capelli-Peixoto, J., Carvalho, D. D., Johnson, W. C., Scoles, G. A., Fogaca, A. C., Daffre, S., & Ueti, M. W. (2017). The transcription factor Relish controls Anaplasma marginale infection in the bovine tick Rhipicephalus microplus. *Dev Comp Immunol, 74*, 32-39. doi:10.1016/j.dci.2017.04.005

Carrera-Faja, L., Cardells, J., Pailler-Garcia, L., Lizana, V., Alfaro-Deval, G., Espunyes, J., . . . Cabezon, O. (2022). Evidence of Prolonged Crimean-Congo Hemorrhagic Fever Virus Endemicity by Retrospective Serosurvey, Eastern Spain. *Emerg Infect Dis, 28*(5), 1031-1034. doi:10.3201/eid2805.212335

Castello, A., Fischer, B., Eichelbaum, K., Horos, R., Beckmann, B. M., Strein, C., . . . Hentze, M. W. (2012). Insights into RNA biology from an atlas of mammalian mRNA-binding proteins. *Cell, 149*(6), 1393-1406. doi:10.1016/j.cell.2012.04.031

Castello, A., Fischer, B., Frese, C. K., Horos, R., Alleaume, A. M., Foehr, S., . . . Hentze, M. W. (2016). Comprehensive Identification of RNA-Binding Domains in Human Cells. *Mol Cell, 63*(4), 696-710. doi:10.1016/j.molcel.2016.06.029

Castello, A., Frese, C. K., Fischer, B., Jarvelin, A. I., Horos, R., Alleaume, A. M., . . . Hentze, M. W. (2017). Identification of RNA-binding domains of RNA-binding proteins in cultured cells on a system-wide scale with RBDmap. *Nat Protoc, 12*(12), 2447-2464. doi:10.1038/nprot.2017.106

Castello, A., Horos, R., Strein, C., Fischer, B., Eichelbaum, K., Steinmetz, L. M., . . . Hentze, M. W. (2013). System-wide identification of RNA-binding proteins by interactome capture. *Nat Protoc, 8*(3), 491-500. doi:10.1038/nprot.2013.020

Caudron-Herger, M., Jansen, R. E., Wassmer, E., & Diederichs, S. (2021). RBP2GO: a comprehensive pan-species database on RNA-binding proteins, their interactions and functions. *Nucleic Acids Res, 49*(D1), D425-D436. doi:10.1093/nar/gkaa1040

Caudron-Herger, M., Rusin, S. F., Adamo, M. E., Seiler, J., Schmid, V. K., Barreau, E., . . . Diederichs, S. (2019). R-DeeP: Proteome-wide and Quantitative Identification of RNA-Dependent Proteins by Density Gradient Ultracentrifugation. *Mol Cell, 75*(1), 184-199 e110. doi:10.1016/j.molcel.2019.04.018

Cesaro, T., & Michiels, T. (2021). Inhibition of PKR by Viruses. *Front Microbiol, 12*, 757238. doi:10.3389/fmicb.2021.757238

Cevik, M. A., Erbay, A., Bodur, H., Gulderen, E., Bastug, A., Kubar, A., & Akinci, E. (2008). Clinical and laboratory features of Crimean-Congo hemorrhagic fever: predictors of fatality. *Int J Infect Dis, 12*(4), 374-379. doi:10.1016/j.ijid.2007.09.010

Chang, J. H., Xiang, S., Xiang, K., Manley, J. L., & Tong, L. (2011). Structural and biochemical studies of the 5'-->3' exoribonuclease Xrn1. *Nat Struct Mol Biol, 18*(3), 270-276. doi:10.1038/nsmb.1984

Chapman, E. G., Moon, S. L., Wilusz, J., & Kieft, J. S. (2014). RNA structures that resist degradation by Xrn1 produce a pathogenic Dengue virus RNA. *Elife, 3*, e01892. doi:10.7554/eLife.01892

Charles, R. A., Bermudez, S., Banovic, P., Alvarez, D. O., Diaz-Sanchez, A. A., Corona-Gonzalez, B., . . . Cabezas-Cruz, A. (2021). Ticks and Tick-Borne Diseases in Central America and the Caribbean: A One Health Perspective. *Pathogens, 10*(10). doi:10.3390/pathogens10101273

Charley, P. A., Wilusz, C. J., & Wilusz, J. (2018). Identification of phlebovirus and arenavirus RNA sequences that stall and repress the exoribonuclease XRN1. *J Biol Chem, 293*(1), 285-295. doi:10.1074/jbc.M117.805796

Charrel, R. N., Attoui, H., Butenko, A. M., Clegg, J. C., Deubel, V., Frolova, T. V., . . . de Lamballerie, X. (2004). Tick-borne virus diseases of human interest in Europe. *Clin Microbiol Infect, 10*(12), 1040-1055. doi:10.1111/j.1469-0691.2004.01022.x

Chen, B., Sweeny, A. R., Wu, V. Y., Christofferson, R. C., Ebel, G., Fagre, A. C., . . . Carlson, C. J. (2023). Exploring the Mosquito-Arbovirus Network: A Survey of Vector Competence Experiments. *Am J Trop Med Hyg, 108*(5), 987-994. doi:10.4269/ajtmh.22-0511

Chen, S., Xu, M., Wu, X., Bai, Y., Shi, J., Zhou, M., . . . Shen, S. (2022). A new luciferase immunoprecipitation system assay provided serological evidence for missed diagnosis of severe fever with thrombocytopenia syndrome. *Virol Sin, 37*(1), 107-114. doi:10.1016/j.virs.2022.01.018

Chen, Y., & Varani, G. (2005). Protein families and RNA recognition. *FEBS J, 272*(9), 2088-2097. doi:10.1111/j.1742-4658.2005.04650.x

Chevalier, V., Pépin, M., Plée, L., & Lancelot, R. (2010). Rift Valley fever - a threat for Europe? *Eurosurveillance, 15*(10). doi:10.2807/ese.15.10.19506-en

Chong, Z. X., Yeap, S. K., & Ho, W. Y. (2021). Transfection types, methods and strategies: a technical review. *PeerJ, 9*, e11165. doi:10.7717/peerj.11165

Choudhury, N. R., Heikel, G., Trubitsyna, M., Kubik, P., Nowak, J. S., Webb, S., . . . Michlewski, G. (2017). RNA-binding activity of TRIM25 is mediated by its PRY/SPRY domain and is required for ubiquitination. *BMC Biol, 15*(1), 105. doi:10.1186/s12915-017-0444-9

Chuang, T. W., Lee, K. M., & Tarn, W. Y. (2015). Function and pathological implications of exon junction complex factor Y14. *Biomolecules, 5*(2), 343-355. doi:10.3390/biom5020343

Cléry, A., & Allain, F. H.-T. (2013). From Structure to Function of RNA Binding Domains. *Madame Curie Bioscience Database*.

Coller, J., & Parker, R. (2005). General translational repression by activators of mRNA decapping. *Cell, 122*(6), 875-886. doi:10.1016/j.cell.2005.07.012

Coller, J. M., Tucker, M., Sheth, U., Valencia-Sanchez, M. A., & Parker, R. O. Y. (2001). The DEAD box helicase, Dhh1p, functions in mRNA decapping and interacts with both the decapping and deadenylase complexes. *RNA, 7*(12), 1717-1727. doi:10.1017/s135583820101994x

Conklin, D. C., Rixon, M. W., Kuestner, R. E., Maurer, M. F., Whitmore, T. E., & Millar, R. P. (2000). Cloning and gene expression of a novel human ribonucleoprotein. *Biochim Biophys Acta, 1492*(2-3), 465-469. doi:10.1016/s0167-4781(00)00090-7

Conrad, T., Albrecht, A. S., de Melo Costa, V. R., Sauer, S., Meierhofer, D., & Orom, U. A. (2016). Serial interactome capture of the human cell nucleus. *Nat Commun, 7*, 11212. doi:10.1038/ncomms11212

Cooper, S. (2003). Reappraisal of serum starvation, the restriction point, G0, and G1 phase arrest points. *FASEB J, 17*(3), 333-340. doi:10.1096/fj.02-0352rev

Copeland, A. M., Altamura, L. A., Van Deusen, N. M., & Schmaljohn, C. S. (2013). Nuclear relocalization of polyadenylate binding protein during rift valley fever virus infection involves expression of the NSs gene. *J Virol, 87*(21), 11659-11669. doi:10.1128/JVI.01434-13

Corley, M., Burns, M. C., & Yeo, G. W. (2020). How RNA-Binding Proteins Interact with RNA: Molecules and Mechanisms. *Mol Cell, 78*(1), 9-29. doi:10.1016/j.molcel.2020.03.011

Coutinho-Abreu, I. V., Riffell, J. A., & Akbari, O. S. (2022). Human attractive cues and mosquito host-seeking behavior. *Trends Parasitol, 38*(3), 246-264. doi:10.1016/j.pt.2021.09.012

Covarrubias, S., Gaglia, M. M., Kumar, G. R., Wong, W., Jackson, A. O., & Glaunsinger, B. A. (2011). Coordinated destruction of cellular messages in translation complexes by the gammaherpesvirus host shutoff factor and the mammalian exonuclease Xrn1. *PLoS Pathog, 7*(10), e1002339. doi:10.1371/journal.ppat.1002339

Cox, J., & Mann, M. (2008). MaxQuant enables high peptide identification rates, individualized p.p.b.-range mass accuracies and proteome-wide protein quantification. *Nat Biotechnol, 26*(12), 1367-1372. doi:10.1038/nbt.1511

Cozzarolo, C.-S., Glaizot, O., Christe, P., & Pigeault, R. (2020). Enhanced Attraction of Arthropod Vectors to Infected Vertebrates: A Review of Empirical Evidence. *Frontiers in Ecology and Evolution, 8*. doi:10.3389/fevo.2020.568140

Crabtree, M. B., Kent Crockett, R. J., Bird, B. H., Nichol, S. T., Erickson, B. R., Biggerstaff, B. J., . . . Miller, B. R. (2012). Infection and transmission of Rift Valley fever viruses lacking the NSs and/or NSm genes in mosquitoes: potential role for NSm in mosquito infection. *PLoS Negl Trop Dis, 6*(5), e1639. doi:10.1371/journal.pntd.0001639

Cramaro, W. J., Hunewald, O. E., Bell-Sakyi, L., & Muller, C. P. (2017). Genome scaffolding and annotation for the pathogen vector Ixodes ricinus by ultra-long single molecule sequencing. *Parasit Vectors, 10*(1), 71. doi:10.1186/s13071-017-2008-9

Cramaro, W. J., Revets, D., Hunewald, O. E., Sinner, R., Reye, A. L., & Muller, C. P. (2015). Integration of Ixodes ricinus genome sequencing with transcriptome and proteome annotation of the naive midgut. *BMC Genomics, 16*, 871. doi:10.1186/s12864-015-1981-7

Crispin, M., Harvey, D. J., Bitto, D., Halldorsson, S., Bonomelli, C., Edgeworth, M., . . . Bowden, T. A. (2014). Uukuniemi Phlebovirus assembly and secretion leave a functional imprint on the virion glycome. *J Virol, 88*(17), 10244-10251. doi:10.1128/JVI.01662-14

Croce, A. C., & Scolari, F. (2022). Autofluorescent Biomolecules in Diptera: From Structure to Metabolism and Behavior. *Molecules, 27*(14). doi:10.3390/molecules27144458

D'Annessa, I., Cicconardi, F., & Di Marino, D. (2019). Handling FMRP and its molecular partners: Structural insights into Fragile X Syndrome. *Prog Biophys Mol Biol, 141*, 3-14. doi:10.1016/j.pbiomolbio.2018.07.001

da Costa, C. F., da Silva, A. V., do Nascimento, V. A., de Souza, V. C., Monteiro, D., Terrazas, W. C. M., . . . Naveca, F. G. (2018). Evidence of vertical transmission of Zika virus in field-collected eggs of Aedes aegypti in the Brazilian Amazon. *PLoS Negl Trop Dis, 12*(7), e0006594. doi:10.1371/journal.pntd.0006594

Dantas-Torres, F. (2015). Climate change, biodiversity, ticks and tick-borne diseases: The butterfly effect. *Int J Parasitol Parasites Wildl, 4*(3), 452-461. doi:10.1016/j.ijppaw.2015.07.001

Daubney, R., Hudson, J. R., & Garnham, P. C. (1931). Enzootic hepatitis or rift valley fever. An undescribed virus disease of sheep cattle and man from east africa. *The Journal of Pathology and Bacteriology, 34*(4), 545-579. doi:10.1002/path.1700340418

de la Calle-Prieto, F., Martin-Quiros, A., Trigo, E., Mora-Rillo, M., Arsuaga, M., Diaz-Menendez, M., & Arribas, J. R. (2018). Therapeutic management of Crimean-Congo haemorrhagic fever. *Enferm Infecc Microbiol Clin (Engl Ed), 36*(8), 517-522. doi:10.1016/j.eimc.2017.04.007

de la Fuente, J., & Kocan, K. M. (2022). The Impact of RNA Interference in Tick Research. *Pathogens, 11*(8). doi:10.3390/pathogens11080827

De, S., Kingan, S. B., Kitsou, C., Portik, D. M., Foor, S. D., Frederick, J. C., . . . Pal, U. (2023). A high-quality Ixodes scapularis genome advances tick science. *Nat Genet, 55*(2), 301-311. doi:10.1038/s41588-022-01275-w

Derry, M. C., Yanagiya, A., Martineau, Y., & Sonenberg, N. (2006). Regulation of poly(A)-binding protein through PABP-interacting proteins. *Cold Spring Harb Symp Quant Biol, 71*, 537-543. doi:10.1101/sqb.2006.71.061

Desmet, E. A., Anguish, L. J., & Parker, J. S. (2014). Virus-mediated compartmentalization of the host translational machinery. *mBio, 5*(5), e01463-01414. doi:10.1128/mBio.01463-14

Despic, V., Dejung, M., Gu, M., Krishnan, J., Zhang, J., Herzel, L., . . . Neugebauer, K. M. (2017). Dynamic RNA–protein interactions underlie the zebrafish maternal-to-zygotic transition. *Genome Research, 27*(7), 1184-1194. doi:10.1101/gr.215954.116

Diaz-Martin, V., Manzano-Roman, R., Valero, L., Oleaga, A., Encinas-Grandes, A., & Perez-Sanchez, R. (2013). An insight into the proteome of the saliva of the argasid tick Ornithodoros moubata reveals important differences in saliva protein composition between the sexes. *J Proteomics, 80*, 216-235. doi:10.1016/j.jprot.2013.01.015

Dietrich, I., Jansen, S., Fall, G., Lorenzen, S., Rudolf, M., Huber, K., . . . Becker, S. C. (2017). RNA Interference Restricts Rift Valley Fever Virus in Multiple Insect Systems. *mSphere, 2*(3). doi:10.1128/mSphere.00090-17

Dietrich, I., Shi, X., McFarlane, M., Watson, M., Blomstrom, A. L., Skelton, J. K., . . . Schnettler, E. (2017). The Antiviral RNAi Response in Vector and Non-vector Cells against Orthobunyaviruses. *PLoS Negl Trop Dis, 11*(1), e0005272. doi:10.1371/journal.pntd.0005272

Diosa-Toro, M., Prasanth, K. R., Bradrick, S. S., & Garcia Blanco, M. A. (2020). Role of RNA-binding proteins during the late stages of Flavivirus replication cycle. *Virol J, 17*(1), 60. doi:10.1186/s12985-020-01329-7

Dong, S., & Dimopoulos, G. (2023). Aedes aegypti Argonaute 2 controls arbovirus infection and host mortality. *Nat Commun, 14*(1), 5773. doi:10.1038/s41467-023-41370-y

Dong, Z., Liu, J., & Zhang, J. T. (2020). Translational regulation of Chk1 expression by eIF3a via interaction with the RNA-binding protein HuR. *Biochem J, 477*(10), 1939-1950. doi:10.1042/BCJ20200025

Du, G., Wang, X., Luo, M., Xu, W., Zhou, T., Wang, M., . . . Wu, X. (2020). mRBPome capture identifies the RNA-binding protein TRIM71, an essential regulator of spermatogonial differentiation. *Development, 147*(8). doi:10.1242/dev.184655

Dunham-Ems, S. M., Caimano, M. J., Pal, U., Wolgemuth, C. W., Eggers, C. H., Balic, A., & Radolf, J. D. (2009). Live imaging reveals a biphasic mode of dissemination of Borrelia burgdorferi within ticks. *J Clin Invest, 119*(12), 3652-3665. doi:10.1172/JCI39401

Dutuze, M. F., Nzayirambaho, M., Mores, C. N., & Christofferson, R. C. (2018). A Review of Bunyamwera, Batai, and Ngari Viruses: Understudied Orthobunyaviruses With Potential One Health Implications. *Front Vet Sci, 5*, 69. doi:10.3389/fvets.2018.00069

E. Vibeke Thrane, P. E. S. (2009). Persistent Versus Transient Map Kinase (Erk) Activation in the Proliferation of Lung Epithelial Type 2 Cells. *Experimental Lung Research, 27*(4), 387-400. doi:10.1080/01902140118484

Eifan, S., Schnettler, E., Dietrich, I., Kohl, A., & Blomstrom, A. L. (2013). Non-structural proteins of arthropod-borne bunyaviruses: roles and functions. *Viruses, 5*(10), 2447-2468. doi:10.3390/v5102447

Eisen, L., & Eisen, R. J. (2023). Changes in the geographic distribution of the blacklegged tick, Ixodes scapularis, in the United States. *Ticks Tick Borne Dis, 14*(6), 102233. doi:10.1016/j.ttbdis.2023.102233

Eisen, R. J., & Eisen, L. (2018). The Blacklegged Tick, Ixodes scapularis: An Increasing Public Health Concern. *Trends Parasitol, 34*(4), 295-309. doi:10.1016/j.pt.2017.12.006

Elbarbary, R. A., Miyoshi, K., Myers, J. R., Du, P., Ashton, J. M., Tian, B., & Maquat, L. E. (2017). Tudor-SN-mediated endonucleolytic decay of human cell microRNAs promotes G(1)/S phase transition. *Science, 356*(6340), 859-862. doi:10.1126/science.aai9372

Elbashir, S. M., Harborth, J., Lendeckel, W., Yalcin, A., Weber, K., & Tuschl, T. (2001). Duplexes of 21-nucleotide RNAs mediate RNA interference in cultured mammalian cells. *Nature, 411*(6836), 494-498. doi:10.1038/35078107

Eley, S. M., & Nuttall, P. A. (1984). Isolation of an English uukuvirus (family Bunyaviridae). *Journal of Hygiene, 93*(2), 313 - 316. doi:10.1017/S0022172400064846

Elhachimi, L., Valcarcel, F., Olmeda, A. S., Elasatey, S., Khattat, S. E., Daminet, S., . . . Duchateau, L. (2021). Rearing of Hyalomma marginatum (Acarina: Ixodidae) under laboratory conditions in Morocco. *Exp Appl Acarol, 84*(4), 785-794. doi:10.1007/s10493-021-00641-3

Elliott, R. M. (2009). Bunyaviruses and climate change. *Clin Microbiol Infect, 15*(6), 510-517. doi:10.1111/j.1469-0691.2009.02849.x

Elliott, R. M., Blakqori, G., van Knippenberg, I. C., Koudriakova, E., Li, P., McLees, A., . . . Szemiel, A. M. (2013). Establishment of a reverse genetics system for Schmallenberg virus, a newly emerged orthobunyavirus in Europe. *J Gen Virol, 94*(Pt 4), 851-859. doi:10.1099/vir.0.049981-0

Elliott, R. M., & Brennan, B. (2014). Emerging phleboviruses. *Curr Opin Virol, 5*(100), 50-57. doi:10.1016/j.coviro.2014.01.011

Elliott, R. M., Dunn, E., Simons, J. F., & Pettersson, R. F. (1992). Nucleotide sequence and coding strategy of the Uukuniemi virus L RNA segment. *J Gen Virol, 73 (Pt 7)*, 1745-1752. doi:10.1099/0022-1317-73-7-1745

Elliott, R. M., & Weber, F. (2009). Bunyaviruses and the type I interferon system. *Viruses, 1*(3), 1003-1021. doi:10.3390/v1031003

Elveborg, S., Monteil, V. M., & Mirazimi, A. (2022). Methods of Inactivation of Highly Pathogenic Viruses for Molecular, Serology or Vaccine Development Purposes. *Pathogens, 11*(2). doi:10.3390/pathogens11020271

Engdahl, C., Näslund, J., Lindgren, L., Ahlm, C., & Bucht, G. (2012). The Rift Valley Fever virus protein NSm and putative cellular protein interactions. *Virology Journal, 9*(1). doi:10.1186/1743-422x-9-139

Fabian, M. R., Sonenberg, N., & Filipowicz, W. (2010). Regulation of mRNA translation and stability by microRNAs. *Annu Rev Biochem, 79*, 351-379. doi:10.1146/annurev-biochem-060308-103103

Fanelli, A., & Buonavoglia, D. (2021). Risk of Crimean Congo haemorrhagic fever virus (CCHFV) introduction and spread in CCHF-free countries in southern and Western Europe: A semi-quantitative risk assessment. *One Health, 13*, 100290. doi:10.1016/j.onehlt.2021.100290

Fanelli, A., Tizzani, P., & Buonavoglia, D. (2022). Crimean-Congo Haemorrhagic Fever (CCHF) in animals: Global characterization and evolution from 2006 to 2019. *Transbound Emerg Dis, 69*(3), 1556-1567. doi:10.1111/tbed.14120

Fares, M., & Brennan, B. (2022). Virus-host interactions during tick-borne bunyavirus infection. *Current Opinion in Virology, 57*. doi:10.1016/j.coviro.2022.101278

Fatica, A., & Tollervey, D. (2002). Making ribosomes. *Curr Opin Cell Biol, 14*(3), 313-318. doi:10.1016/s0955-0674(02)00336-8

Feng, K., Deng, F., Hu, Z., Wang, H., & Ning, Y. J. (2019). Heartland virus antagonizes type I and III interferon antiviral signaling by inhibiting phosphorylation and nuclear translocation of STAT2 and STAT1. *J Biol Chem, 294*(24), 9503-9517. doi:10.1074/jbc.RA118.006563

Feng, K., Zhang, H., Jiang, Z., Zhou, M., Min, Y. Q., Deng, F., . . . Ning, Y. J. (2023). SFTS bunyavirus NSs protein sequestrates mTOR into inclusion bodies and deregulates mTOR-ULK1 signaling, provoking pro-viral autophagy. *J Med Virol, 95*(1), e28371. doi:10.1002/jmv.28371

Ferron, F., Weber, F., de la Torre, J. C., & Reguera, J. (2017). Transcription and replication mechanisms of Bunyaviridae and Arenaviridae L proteins. *Virus Res, 234*, 118-134. doi:10.1016/j.virusres.2017.01.018

Fielden, L. J., & Lighton, J. R. B. (1996). Effects of Water Stress and Relative Humidity on Ventilation in the Tick Dermacentor andersoni (Acari: Ixodidae). *Physiological Zoology, 69*(3), 599-617. doi:10.1086/physzool.69.3.30164218

Fiszer-Kierzkowska, A., Vydra, N., Wysocka-Wycisk, A., Kronekova, Z., Jarzab, M., Lisowska, K. M., & Krawczyk, Z. (2011). Liposome-based DNA carriers may induce cellular stress response and change gene expression pattern in transfected cells. *BMC Mol Biol, 12*, 27. doi:10.1186/1471-2199-12-27

Flick, K., Katz, A., Overby, A., Feldmann, H., Pettersson, R. F., & Flick, R. (2004). Functional analysis of the noncoding regions of the Uukuniemi virus (Bunyaviridae) RNA segments. *J Virol, 78*(21), 11726-11738. doi:10.1128/JVI.78.21.11726-11738.2004

Flick, R., & Pettersson, R. F. (2001). Reverse genetics system for Uukuniemi virus (Bunyaviridae): RNA polymerase I-catalyzed expression of chimeric viral RNAs. *J Virol, 75*(4), 1643-1655. doi:10.1128/JVI.75.4.1643-1655.2001

Fogaça, A. C., Sousa, G., Pavanelo, D. B., Esteves, E., Martins, L. A., Urbanová, V., . . . Daffre, S. (2021). Tick Immune System: What Is Known, the Interconnections, the Gaps, and the Challenges. *Frontiers in Immunology, 12*. doi:10.3389/fimmu.2021.628054

Fontana, J., Lopez-Montero, N., Elliott, R. M., Fernandez, J. J., & Risco, C. (2008). The unique architecture of Bunyamwera virus factories around the Golgi complex. *Cell Microbiol, 10*(10), 2012-2028. doi:10.1111/j.1462-5822.2008.01184.x

Fontenille, D., Traore-Lamizana, M., Diallo, M., Thonnon, J., Digoutte, J. P., & Zeller, H. G. (1998). New vectors of Rift Valley fever in West Africa. *Emerg Infect Diseases, 4*(2). doi:10.3201/eid0402.980218

Franz, A. W., Kantor, A. M., Passarelli, A. L., & Clem, R. J. (2015). Tissue Barriers to Arbovirus Infection in Mosquitoes. *Viruses, 7*(7), 3741-3767. doi:10.3390/v7072795

Freitas, N., Enguehard, M., Denolly, S., Levy, C., Neveu, G., Lerolle, S., . . . Cosset, F. L. (2020). The interplays between Crimean-Congo hemorrhagic fever virus (CCHFV) M segment-encoded accessory proteins and structural proteins promote virus assembly and infectivity. *PLoS Pathog, 16*(9), e1008850. doi:10.1371/journal.ppat.1008850

Fukunaga, R., & Zamore, P. D. (2012). Loquacious, a Dicer Partner Protein, Functions in Both the MicroRNA and siRNA Pathways. In *Eukaryotic RNases and their Partners in RNA Degradation and Biogenesis, Part B* (pp. 37-68).

Gaglia, M. M., Covarrubias, S., Wong, W., & Glaunsinger, B. A. (2012). A common strategy for host RNA degradation by divergent viruses. *J Virol, 86*(17), 9527-9530. doi:10.1128/JVI.01230-12

Gahmberg, N., Kuismanen, E., Keranen, S., & Pettersson, R. F. (1986). Uukuniemi virus glycoproteins accumulate in and cause morphological changes of the Golgi complex in the absence of virus maturation. *J Virol, 57*(3), 899-906. doi:10.1128/JVI.57.3.899-906.1986

Ganaie, S. S., Leung, D. W., Hartman, A. L., & Amarasinghe, G. K. (2023). Host entry factors of Rift Valley Fever Virus infection. *Adv Virus Res, 117*, 121-136. doi:10.1016/bs.aivir.2023.09.001

Gao, J., Tang, Y. D., Hu, W., & Zheng, C. (2022). When Poly(A) Binding Proteins Meet Viral Infections, Including SARS-CoV-2. *J Virol, 96*(7), e0013622. doi:10.1128/jvi.00136-22

Garcia-Moreno, M., Jarvelin, A. I., & Castello, A. (2018). Unconventional RNA-binding proteins step into the virus-host battlefront. *Wiley Interdiscip Rev RNA, 9*(6), e1498. doi:10.1002/wrna.1498

Garcia-Moreno, M., Noerenberg, M., Ni, S., Jarvelin, A. I., Gonzalez-Almela, E., Lenz, C. E., . . . Castello, A. (2019). System-wide Profiling of RNA-Binding Proteins Uncovers Key Regulators of Virus Infection. *Mol Cell, 74*(1), 196-211 e111. doi:10.1016/j.molcel.2019.01.017

Garcia, S., Billecocq, A., Crance, J. M., Munderloh, U., Garin, D., & Bouloy, M. (2005). Nairovirus RNA sequences expressed by a Semliki Forest virus replicon induce RNA interference in tick cells. *J Virol, 79*(14), 8942-8947. doi:10.1128/JVI.79.14.8942-8947.2005

Garcia, S., Billecocq, A., Crance, J. M., Prins, M., Garin, D., & Bouloy, M. (2006). Viral suppressors of RNA interference impair RNA silencing induced by a Semliki Forest virus replicon in tick cells. *J Gen Virol, 87*(Pt 7), 1985-1989. doi:10.1099/vir.0.81827-0

Garry, C. E., & Garry, R. F. (2004). Proteomics computational analyses suggest that the carboxyl terminal glycoproteins of Bunyaviruses are class II viral fusion protein (beta-penetrenes). *Theor Biol Med Model, 1*, 10. doi:10.1186/1742-4682-1-10

Gauliard, N., Billecocq, A., Flick, R., & Bouloy, M. (2006). Rift Valley fever virus noncoding regions of L, M and S segments regulate RNA synthesis. *Virology, 351*(1), 170-179. doi:10.1016/j.virol.2006.03.018

Gerrard, S. R., Li, L., Barrett, A. D., & Nichol, S. T. (2004). Ngari virus is a Bunyamwera virus reassortant that can be associated with large outbreaks of hemorrhagic fever in Africa. *J Virol, 78*(16), 8922-8926. doi:10.1128/JVI.78.16.8922-8926.2004

Giorgi, C., Accardi, L., Nicoletti, L., Gro, M. C., Takehara, K., Hilditch, C., . . . Bishop, D. H. (1991). Sequences and coding strategies of the S RNAs of Toscana and Rift Valley fever viruses compared to those of Punta Toro, Sicilian Sandfly fever, and Uukuniemi viruses. *Virology, 180*(2), 738-753. doi:10.1016/0042-6822(91)90087-r

Girardi, E., Pfeffer, S., Baumert, T. F., & Majzoub, K. (2021). Roadblocks and fast tracks: How RNA binding proteins affect the viral RNA journey in the cell. *Semin Cell Dev Biol, 111*, 86-100. doi:10.1016/j.semcdb.2020.08.006

Gligić, A., Stamatović, L., Stojanović, R., Obradović, M., & Bosković, R. (1977). The first isolation of the Crimean hemorraghic fever virus in Yugoslavia. [Prva izolacija virusa krimske hemoragicne groznice u Jugoslaviji.]. *Vojnosanit Pregl, 34*(5), 318-321.

Glisovic, T., Bachorik, J. L., Yong, J., & Dreyfuss, G. (2008). RNA-binding proteins and post-transcriptional gene regulation. *FEBS Lett, 582*(14), 1977-1986. doi:10.1016/j.febslet.2008.03.004

Godsey, M. S., Savage, H. M., Burkhalter, K. L., Bosco-Lauth, A. M., & Delorey, M. J. (2016). Transmission of Heartland Virus (Bunyaviridae: Phlebovirus) by Experimentally Infected Amblyomma americanum (Acari: Ixodidae). *J Med Entomol, 53*(5), 1226-1233. doi:10.1093/jme/tjw080

Gomes-Duarte, A., Lacerda, R., Menezes, J., & Romao, L. (2018). eIF3: a factor for human health and disease. *RNA Biol, 15*(1), 26-34. doi:10.1080/15476286.2017.1391437

Gondard, M., Michelet, L., Nisavanh, A., Devillers, E., Delannoy, S., Fach, P., . . . Moutailler, S. (2018). Prevalence of tick-borne viruses in Ixodes ricinus assessed by high-throughput real-time PCR. *Pathog Dis, 76*(8). doi:10.1093/femspd/fty083

Gray, J., Kahl, O., & Zintl, A. (2021). What do we still need to know about Ixodes ricinus? *Ticks Tick Borne Dis, 12*(3), 101682. doi:10.1016/j.ttbdis.2021.101682

Gray, J. S., Kahl, O., Lane, R. S., Levin, M. L., & Tsao, J. I. (2016). Diapause in ticks of the medically important Ixodes ricinus species complex. *Ticks Tick Borne Dis, 7*(5), 992-1003. doi:10.1016/j.ttbdis.2016.05.006

Gray, Nicola K., Hrabálková, L., Scanlon, J. P., & Smith, Richard W. P. (2015). Poly(A)-binding proteins and mRNA localization: who rules the roost? *Biochemical Society Transactions, 43*(6), 1277-1284. doi:10.1042/bst20150171

Greenberg, J. R. (1979). Ultraviolet light-induced crosslinking of mRNA to proteins. *Nucleic Acids Res, 6*(2), 715-732. doi:10.1093/nar/6.2.715

Grossi-Soyster, E. N., & LaBeaud, A. D. (2020). Rift Valley Fever: Important Considerations for Risk Mitigation and Future Outbreaks. *Trop Med Infect Dis, 5*(2). doi:10.3390/tropicalmed5020089

Grubaugh, N. D., Ruckert, C., Armstrong, P. M., Bransfield, A., Anderson, J. F., Ebel, G. D., & Brackney, D. E. (2016). Transmission bottlenecks and RNAi collectively influence tick-borne flavivirus evolution. *Virus Evol, 2*(2), vew033. doi:10.1093/ve/vew033

Guglielmone, A. A., Nava, S., & Robbins, R. G. (2023). Geographic distribution of the hard ticks (Acari: Ixodida: Ixodidae) of the world by countries and territories. *Zootaxa, 5251*(1), 1-274. doi:10.11646/zootaxa.5251.1.1

Gulia-Nuss, M., Nuss, A. B., Meyer, J. M., Sonenshine, D. E., Roe, R. M., Waterhouse, R. M., . . . Hill, C. A. (2016). Genomic insights into the Ixodes scapularis tick vector of Lyme disease. *Nat Commun, 7*, 10507. doi:10.1038/ncomms10507

Hacker, D., Raju, R., & Kolakofsky, D. (1989). La Crosse virus nucleocapsid protein controls its own synthesis in mosquito cells by encapsidating its mRNA. *J Virol, 63*(12), 5166-5174. doi:10.1128/JVI.63.12.5166-5174.1989

Hadi, I., & Adventini, M. (2015). *Fecundity, Oviposition and Egg Incubation Period of Female Rhipicephalus Sanguineus Latreille (Acari: Ixodidae) Ticks*.

Halldorsson, S., Li, S., Li, M., Harlos, K., Bowden, T. A., & Huiskonen, J. T. (2018). Shielding and activation of a viral membrane fusion protein. *Nat Commun, 9*(1), 349. doi:10.1038/s41467-017-02789-2

Hart, T. J., Kohl, A., & Elliott, R. M. (2009). Role of the NSs protein in the zoonotic capacity of Orthobunyaviruses. *Zoonoses Public Health, 56*(6-7), 285-296. doi:10.1111/j.1863-2378.2008.01166.x

Hartman, A. L., & Myler, P. J. (2023). Bunyavirales: Scientific Gaps and Prototype Pathogens for a Large and Diverse Group of Zoonotic Viruses. *J Infect Dis, 228*(Suppl 6), S376-S389. doi:10.1093/infdis/jiac338

Hawman, D. W., & Feldmann, H. (2023). Crimean–Congo haemorrhagic fever virus. *Nature Reviews Microbiology, 21*(7), 463-477. doi:10.1038/s41579-023-00871-9

Heath, W. R., & Carbone, F. R. (2013). The skin-resident and migratory immune system in steady state and memory: innate lymphocytes, dendritic cells and T cells. *Nat Immunol, 14*(10), 978-985. doi:10.1038/ni.2680

Heitmann, A., Gusmag, F., Rathjens, M. G., Maurer, M., Frankze, K., Schicht, S., . . . Becker, S. C. (2021). Mammals Preferred: Reassortment of Batai and Bunyamwera orthobunyavirus Occurs in Mammalian but Not Insect Cells. *Viruses, 13*(9). doi:10.3390/v13091702

Hentze, M. W., Castello, A., Schwarzl, T., & Preiss, T. (2018). A brave new world of RNA-binding proteins. *Nat Rev Mol Cell Biol, 19*(5), 327-341. doi:10.1038/nrm.2017.130

Hermance, M. E., & Thangamani, S. (2015). Tick Saliva Enhances Powassan Virus Transmission to the Host, Influencing Its Dissemination and the Course of Disease. *J Virol, 89*(15), 7852-7860. doi:10.1128/JVI.01056-15

Hermance, M. E., Widen, S. G., Wood, T. G., & Thangamani, S. (2019). Ixodes scapularis salivary gland microRNAs are differentially expressed during Powassan virus transmission. *Sci Rep, 9*(1), 13110. doi:10.1038/s41598-019-49572-5

Hernandez, E. P., Kusakisako, K., Talactac, M. R., Galay, R. L., Yoshii, K., & Tanaka, T. (2018). Induction of intracellular ferritin expression in embryo-derived Ixodes scapularis cell line (ISE6). *Sci Rep, 8*(1), 16566. doi:10.1038/s41598-018-34860-3

Hewlett, M. J., Pettersson, R. F., & Baltimore, D. (1977). Circular forms of Uukuniemi virion RNA: an electron microscopic study. *J Virol, 21*(3), 1085-1093. doi:10.1128/JVI.21.3.1085-1093.1977

Hildebrandt, A., Alanis-Lobato, G., Voigt, A., Zarnack, K., Andrade-Navarro, M. A., Beli, P., & Konig, J. (2017). Interaction profiling of RNA-binding ubiquitin ligases reveals a link between posttranscriptional regulation and the ubiquitin system. *Sci Rep, 7*(1), 16582. doi:10.1038/s41598-017-16695-6

Hoang, H. D., Neault, S., Pelin, A., & Alain, T. (2020). Emerging translation strategies during virus–host interaction. *WIREs RNA, 12*(1). doi:10.1002/wrna.1619

Hodge, K., Have, S. T., Hutton, L., & Lamond, A. I. (2013). Cleaning up the masses: exclusion lists to reduce contamination with HPLC-MS/MS. *J Proteomics, 88*, 92-103. doi:10.1016/j.jprot.2013.02.023

Hoffmann, A. B., Mazelier, M., Leger, P., & Lozach, P. Y. (2018). Deciphering Virus Entry with Fluorescently Labeled Viral Particles. *Methods Mol Biol, 1836*, 159-183. doi:10.1007/978-1-4939-8678-1_8

Hoffmann, B., Scheuch, M., Hoper, D., Jungblut, R., Holsteg, M., Schirrmeier, H., . . . Beer, M. (2012). Novel orthobunyavirus in Cattle, Europe, 2011. *Emerg Infect Dis, 18*(3), 469-472. doi:10.3201/eid1803.111905

Hofmann, H., & Pohlmann, S. (2011). DC-SIGN: access portal for sweet viral killers. *Cell Host Microbe, 10*(1), 5-7. doi:10.1016/j.chom.2011.07.003

Holding, M., Dowall, S. D., Medlock, J. M., Carter, D. P., Pullan, S. T., Lewis, J., . . . Hewson, R. (2020). Tick-Borne Encephalitis Virus, United Kingdom. *Emerging Infectious Diseases, 26*(1), 90-96. doi:10.3201/eid2601.191085

Hopkins, K. C., McLane, L. M., Maqbool, T., Panda, D., Gordesky-Gold, B., & Cherry, S. (2013). A genome-wide RNAi screen reveals that mRNA decapping restricts bunyaviral replication by limiting the pools of Dcp2-accessible targets for cap-snatching. *Genes Dev, 27*(13), 1511-1525. doi:10.1101/gad.215384.113

Hornak, K. E., Lanchy, J. M., & Lodmell, J. S. (2016). RNA Encapsidation and Packaging in the Phleboviruses. *Viruses, 8*(7). doi:10.3390/v8070194

Horne, K. M., & Vanlandingham, D. L. (2014). Bunyavirus-vector interactions. *Viruses, 6*(11), 4373-4397. doi:10.3390/v6114373

Hsu, S. N., & Hertel, K. J. (2009). Spliceosomes walk the line: splicing errors and their impact on cellular function. *RNA Biol, 6*(5), 526-530. doi:10.4161/rna.6.5.9860

Hu, Y. Y., Zhuang, L., Liu, K., Sun, Y., Dai, K., Zhang, X. A., . . . Liu, W. (2020). Role of three tick species in the maintenance and transmission of Severe Fever with Thrombocytopenia Syndrome Virus. *PLoS Negl Trop Dis, 14*(6), e0008368. doi:10.1371/journal.pntd.0008368

Hubalek, Z. (1987). Geographic distribution of Bhanja virus. *Folia Parasitol (Praha), 34*(1), 77-86. Retrieved from https://www.ncbi.nlm.nih.gov/pubmed/3108117

Hubálek, Z. (1987). Experimental pathogenicity of Bhanja virus. *Zentralblatt für Bakteriologie, Mikrobiologie und Hygiene. Series A: Medical Microbiology, Infectious Diseases, Virology, Parasitology, 266*(1), 284-291. doi:https://doi.org/10.1016/S0176-6724(87)80042-1

Hubalek, Z., Mittermayer, T., Halouzka, J., & Cerny, V. (1988). Isolation of "exotic" Bhanja virus (Bunyaviridae) from ticks in the temperate zone. *Arch Virol, 101*(3-4), 191-197. doi:10.1007/BF01311000

Hughes, C. S., Moggridge, S., Muller, T., Sorensen, P. H., Morin, G. B., & Krijgsveld, J. (2019). Single-pot, solid-phase-enhanced sample preparation for proteomics experiments. *Nat Protoc, 14*(1), 68-85. doi:10.1038/s41596-018-0082-x

Hume, A., & Muhlberger, E. (2018). Marburg Virus Viral Protein 35 Inhibits Protein Kinase R Activation in a Cell Type-Specific Manner. *J Infect Dis, 218*(suppl_5), S403-S408. doi:10.1093/infdis/jiy473

Hussain, M., Walker, T., O'Neill, S. L., & Asgari, S. (2013). Blood meal induced microRNA regulates development and immune associated genes in the Dengue mosquito vector, Aedes aegypti. *Insect Biochem Mol Biol, 43*(2), 146-152. doi:10.1016/j.ibmb.2012.11.005

Hyjek-Skladanowska, M., Bajczyk, M., Golebiewski, M., Nuc, P., Kolowerzo-Lubnau, A., Jarmolowski, A., & Smolinski, D. J. (2020). Core spliceosomal Sm proteins as constituents of cytoplasmic mRNPs in plants. *Plant J, 103*(3), 1155-1173. doi:10.1111/tpj.14792

Ikegami, T., Narayanan, K., Won, S., Kamitani, W., Peters, C. J., & Makino, S. (2009). Rift Valley fever virus NSs protein promotes post-transcriptional downregulation of protein kinase PKR and inhibits eIF2alpha phosphorylation. *PLoS Pathog, 5*(2), e1000287. doi:10.1371/journal.ppat.1000287

Iselin, L., Palmalux, N., Kamel, W., Simmonds, P., Mohammed, S., & Castello, A. (2022). Uncovering viral RNA-host cell interactions on a proteome-wide scale. *Trends Biochem Sci, 47*(1), 23-38. doi:10.1016/j.tibs.2021.08.002

Ishigaki, Y., Nakamura, Y., Tatsuno, T., Hashimoto, M., Shimasaki, T., Iwabuchi, K., & Tomosugi, N. (2013). Depletion of RNA-binding protein RBM8A (Y14) causes cell cycle deficiency and apoptosis in human cells. *Exp Biol Med (Maywood), 238*(8), 889-897. doi:10.1177/1535370213494646

Ishizu, H., Kinoshita, T., Hirakata, S., Komatsuzaki, C., & Siomi, M. C. (2019). Distinct and Collaborative Functions of Yb and Armitage in Transposon-Targeting piRNA Biogenesis. *Cell Rep, 27*(6), 1822-1835 e1828. doi:10.1016/j.celrep.2019.04.029

Jacobsen, L., Calvin, S., & Lobenhofer, E. (2009). Transcriptional effects of transfection: the potential for misinterpretation of gene expression data generated from transiently transfected cells. *Biotechniques, 47*(1), 617-624. doi:10.2144/000113132

Jacobson, D. R., & Saleh, O. A. (2017). Counting the ions surrounding nucleic acids. *Nucleic Acids Res, 45*(4), 1596-1605. doi:10.1093/nar/gkw1305

Jaenson, T. G., Jaenson, D. G., Eisen, L., Petersson, E., & Lindgren, E. (2012). Changes in the geographical distribution and abundance of the tick Ixodes ricinus during the past 30 years in Sweden. *Parasit Vectors, 5*, 8. doi:10.1186/1756-3305-5-8

James H. Oliver, J., Ellen M. Dotson. (1993). Hormonal Control of Molting and Reproduction in Ticks. *Amer. Zool., 33*(3), 384-396.

Jaronczyk, K., Carmichael, J. B., & Hobman, T. C. (2005). Exploring the functions of RNA interference pathway proteins: some functions are more RISCy than others? *Biochem J, 387*(Pt 3), 561-571. doi:10.1042/BJ20041822

Jayabalan, A. K., Adivarahan, S., Koppula, A., Abraham, R., Batish, M., Zenklusen, D., . . . Leung, A. K. L. (2021). Stress granule formation, disassembly, and composition are regulated by alphavirus ADP-ribosylhydrolase activity. *Proc Natl Acad Sci U S A, 118*(6). doi:10.1073/pnas.2021719118

Jayabalan, A. K., Griffin, D. E., & Leung, A. K. L. (2023). Pro-Viral and Anti-Viral Roles of the RNA-Binding Protein G3BP1. *Viruses, 15*(2). doi:10.3390/v15020449

Jenkin, D., Wright, D., Folegatti, P. M., Platt, A., Poulton, I., Lawrie, A., . . . Warimwe, G. M. (2023). Safety and immunogenicity of a ChAdOx1 vaccine against Rift Valley fever in UK adults: an open-label, non-randomised, first-in-human phase 1 clinical trial. *Lancet Infect Dis, 23*(8), 956-964. doi:10.1016/S1473-3099(23)00068-3

Jia, N., Wang, J., Shi, W., Du, L., Sun, Y., Zhan, W., . . . Cao, W. C. (2020). Large-Scale Comparative Analyses of Tick Genomes Elucidate Their Genetic Diversity and Vector Capacities. *Cell, 182*(5), 1328-1340 e1313. doi:10.1016/j.cell.2020.07.023

Johnson, K. N., Zeddam, J. L., & Ball, L. A. (2000). Characterization and construction of functional cDNA clones of Pariacoto virus, the first Alphanodavirus isolated outside Australasia. *J Virol, 74*(11), 5123-5132. doi:10.1128/jvi.74.11.5123-5132.2000

Johnstone-Robertson, S. P., Diuk-Wasser, M. A., & Davis, S. A. (2020). Incorporating tick feeding behaviour into R(0) for tick-borne pathogens. *Theor Popul Biol, 131*, 25-37. doi:10.1016/j.tpb.2019.10.004

Kading, R. C. C., Mary B. Bird, Brian H. Nichol, Stuart T. Erickson, Bobbie Rae. Horiuchi, Kalanthe. Biggerstaff, Brad J. Miller, Barry R. (2014). Deletion of the NSm virulence gene of Rift Valley fever virus inhibits virus replication in and dissemination from the midgut of Aedes aegypti mosquitoes. *PLoS Negl Trop Dis, 8*(2). doi:10.1371/journal.pntd.0002670

Kahl, O., & Gray, J. S. (2023). The biology of Ixodes ricinus with emphasis on its ecology. *Ticks Tick Borne Dis, 14*(2), 102114. doi:10.1016/j.ttbdis.2022.102114

Kahlon, S. S., Peters, C. J., Leduc, J., Muchiri, E. M., Muiruri, S., Njenga, M. K., . . . King, C. H. (2010). Severe Rift Valley fever may present with a characteristic clinical syndrome. *Am J Trop Med Hyg, 82*(3), 371-375. doi:10.4269/ajtmh.2010.09-0669

Kainulainen, M., Habjan, M., Hubel, P., Busch, L., Lau, S., Colinge, J., . . . Weber, F. (2014). Virulence factor NSs of rift valley fever virus recruits the F-box protein FBXO3 to degrade subunit p62 of general transcription factor TFIIH. *J Virol, 88*(6), 3464-3473. doi:10.1128/JVI.02914-13

Kalveram, B., Lihoradova, O., & Ikegami, T. (2011). NSs protein of rift valley fever virus promotes posttranslational downregulation of the TFIIH subunit p62. *J Virol, 85*(13), 6234-6243. doi:10.1128/JVI.02255-10

Kamel, W., Noerenberg, M., Cerikan, B., Chen, H., Jarvelin, A. I., Kammoun, M., . . . Castello, A. (2021). Global analysis of protein-RNA interactions in SARS-CoV-2-infected cells reveals key regulators of infection. *Mol Cell, 81*(13), 2851-2867 e2857. doi:10.1016/j.molcel.2021.05.023

Karim, S., Kenny, B., Troiano, E., & Mather, T. N. (2008). RNAi-mediated gene silencing in tick synganglia: a proof of concept study. *BMC Biotechnol, 8*, 30. doi:10.1186/1472-6750-8-30

Kataoka, N., Yong, J., Kim, V. N., Velazquez, F., Perkinson, R. A., Wang, F., & Dreyfuss, G. (2000). Pre-mRNA splicing imprints mRNA in the nucleus with a novel RNA-binding protein that persists in the cytoplasm. *Mol Cell, 6*(3), 673-682. doi:10.1016/s1097-2765(00)00065-4

Katz, A., Freiberg, A. N., Backstrom, V., Schulz, A. R., Mateos, A., Holm, L., . . . Plyusnin, A. (2010). Oligomerization of Uukuniemi virus nucleocapsid protein. *Virol J, 7*, 187. doi:10.1186/1743-422X-7-187

Kazimirova, M., Thangamani, S., Bartikova, P., Hermance, M., Holikova, V., Stibraniova, I., & Nuttall, P. A. (2017). Tick-Borne Viruses and Biological Processes at the Tick-Host-Virus Interface. *Front Cell Infect Microbiol, 7*, 339. doi:10.3389/fcimb.2017.00339

Kevely, A., Pranclova, V., Slavikova, M., Haviernik, J., Honig, V., Novakova, E., . . . Koci, J. (2022). Fitness of mCherry Reporter Tick-Borne Encephalitis Virus in Tick Experimental Models. *Viruses, 14*(12). doi:10.3390/v14122673

Kielian, M. (2006). Class II virus membrane fusion proteins. *Virology, 344*(1), 38-47. doi:10.1016/j.virol.2005.09.036

Kilchert, C., Kecman, T., Priest, E., Hester, S., Aydin, E., Kus, K., . . . Vasiljeva, L. (2020). System-wide analyses of the fission yeast poly(A)(+) RNA interactome reveal insights into organization and function of RNA-protein complexes. *Genome Res, 30*(7), 1012-1026. doi:10.1101/gr.257006.119

Kim, J. Y., Jeon, K., Hong, J. J., Park, S. I., Cho, H., Park, H. J., . . . Nam, J. H. (2023). Heterologous vaccination utilizing viral vector and protein platforms confers complete protection against SFTSV. *Sci Rep, 13*(1), 8189. doi:10.1038/s41598-023-35328-9

Kim, J. Y., Jeon, K., Park, S. I., Bang, Y. J., Park, H. J., Kwak, H. W., . . . Nam, J. H. (2023). mRNA vaccine encoding Gn provides protection against severe fever with thrombocytopenia syndrome virus in mice. *NPJ Vaccines, 8*(1), 167. doi:10.1038/s41541-023-00771-2

Kim, K. H., Yi, J., Kim, G., Choi, S. J., Jun, K. I., Kim, N. H., . . . Oh, M. D. (2013). Severe fever with thrombocytopenia syndrome, South Korea, 2012. *Emerg Infect Dis, 19*(11), 1892-1894. doi:10.3201/eid1911.130792

Kim, Y., Jang, G., Lee, D., Kim, N., Seon, J. W., Kim, Y. H., & Lee, C. (2022). Trypsin enhances SARS-CoV-2 infection by facilitating viral entry. *Arch Virol, 167*(2), 441-458. doi:10.1007/s00705-021-05343-0

Kitagawa, Y., Sakai, M., Shimojima, M., Saijo, M., Itoh, M., & Gotoh, B. (2018). Nonstructural protein of severe fever with thrombocytopenia syndrome phlebovirus targets STAT2 and not STAT1 to inhibit type I interferon-stimulated JAK-STAT signaling. *Microbes and Infection, 20*(6), 360-368. doi:10.1016/j.micinf.2018.05.007

Kitandwe, P. K., McKay, P. F., Kaleebu, P., & Shattock, R. J. (2022). An Overview of Rift Valley Fever Vaccine Development Strategies. *Vaccines (Basel), 10*(11). doi:10.3390/vaccines10111794

Klenk, H. D., Rott, R., Orlich, M., & Blodorn, J. (1975). Activation of influenza A viruses by trypsin treatment. *Virology, 68*(2), 426-439. doi:10.1016/0042-6822(75)90284-6

Kocan, K. M., de la Fuente, J., & Coburn, L. A. (2015). Insights into the development of Ixodes scapularis: a resource for research on a medically important tick species. *Parasit Vectors, 8*, 592. doi:10.1186/s13071-015-1185-7

Koch, H. G., & Tuck, M. D. (1986). Molting and Survival of the Brown Dog Tick (Acari: Ixodidae) under Different Temperatures and Humidities1. *Annals of the Entomological Society of America, 79*(1), 11-14. doi:10.1093/aesa/79.1.11

Koch, J., Xin, Q., Tischler, N. D., & Lozach, P. Y. (2021). Entry of Phenuiviruses into Mammalian Host Cells. *Viruses, 13*(2). doi:10.3390/v13020299

Kohl, A., Clayton, R. F., Weber, F., Bridgen, A., Randall, R. E., & Elliott, R. M. (2003). Bunyamwera virus nonstructural protein NSs counteracts interferon regulatory factor 3-mediated induction of early cell death. *J Virol, 77*(14), 7999-8008. doi:10.1128/jvi.77.14.7999-8008.2003

Kotsarenko, K., Vechtova, P., Lieskovska, J., Fussy, Z., Cabral-de-Mello, D. C., Rego, R. O. M., . . . Grubhoffer, L. (2020). Karyotype changes in long-term cultured tick cell lines. *Sci Rep, 10*(1), 13443. doi:10.1038/s41598-020-70330-5

Kreher, F., Tamietti, C., Gommet, C., Guillemot, L., Ermonval, M., Failloux, A. B., . . . Flamand, M. (2014). The Rift Valley fever accessory proteins NSm and P78/NSm-GN are distinct determinants of virus propagation in vertebrate and invertebrate hosts. *Emerg Microbes Infect, 3*(10), e71. doi:10.1038/emi.2014.71

Kuehnert, P. A., Stefan, C. P., Badger, C. V., & Ricks, K. M. (2021). Crimean-Congo Hemorrhagic Fever Virus (CCHFV): A Silent but Widespread Threat. *Curr Trop Med Rep, 8*(2), 141-147. doi:10.1007/s40475-021-00235-4

Kuhn, J. H., Adkins, S., Alkhovsky, S. V., Avsic-Zupanc, T., Ayllon, M. A., Bahl, J., . . . Okland, A. L. (2022). 2022 taxonomic update of phylum Negarnaviricota (Riboviria: Orthornavirae), including the large orders Bunyavirales and Mononegavirales. *Arch Virol, 167*(12), 2857-2906. doi:10.1007/s00705-022-05546-z

Kumar, R., Khandelwal, N., Thachamvally, R., Tripathi, B. N., Barua, S., Kashyap, S. K., . . . Kumar, N. (2018). Role of MAPK/MNK1 signaling in virus replication. *Virus Res, 253*, 48-61. doi:10.1016/j.virusres.2018.05.028

Kurscheid, S., Lew-Tabor, A. E., Rodriguez Valle, M., Bruyeres, A. G., Doogan, V. J., Munderloh, U. G., . . . Bellgard, M. I. (2009). Evidence of a tick RNAi pathway by comparative genomics and reverse genetics screen of targets with known loss-of-function phenotypes in Drosophila. *BMC Mol Biol, 10*, 26. doi:10.1186/1471-2199-10-26

Kurtti, T. J., Mattila, J. T., Herron, M. J., Felsheim, R. F., Baldridge, G. D., Burkhardt, N. Y., . . . Munderloh, U. G. (2008). Transgene expression and silencing in a tick cell line: A model system for functional tick genomics. *Insect Biochem Mol Biol, 38*(10), 963-968. doi:10.1016/j.ibmb.2008.07.008

Kurtti, T. J., Munderloh, U. G., Andreadis, T. G., Magnarelli, L. A., & Mather, T. N. (1996). Tick cell culture isolation of an intracellular prokaryote from the tick Ixodes scapularis. *J Invertebr Pathol, 67*(3), 318-321. doi:10.1006/jipa.1996.0050

Kwon, S. C., Yi, H., Eichelbaum, K., Fohr, S., Fischer, B., You, K. T., . . . Kim, V. N. (2013). The RNA-binding protein repertoire of embryonic stem cells. *Nat Struct Mol Biol, 20*(9), 1122-1130. doi:10.1038/nsmb.2638

Lauterbach, R., Wells, K., O'Hara, R. B., Kalko, E. K., & Renner, S. C. (2013). Variable strength of forest stand attributes and weather conditions on the questing activity of Ixodes ricinus ticks over years in managed forests. *PLoS One, 8*(1), e55365. doi:10.1371/journal.pone.0055365

Lawrie, C. H., Uzcategui, N. Y., Armesto, M., Bell-Sakyi, L., & Gould, E. A. (2004). Susceptibility of mosquito and tick cell lines to infection with various flaviviruses. *Med Vet Entomol, 18*(3), 268-274. doi:10.1111/j.0269-283X.2004.00505.x

Le May, N., & Bouloy, M. (2012). Antiviral escape strategies developed by bunyaviruses pathogenic for humans. *Front Biosci (Schol Ed), 4*(3), 1065-1077. doi:10.2741/s318

Le May, N., Dubaele, S., Proietti De Santis, L., Billecocq, A., Bouloy, M., & Egly, J. M. (2004). TFIIH transcription factor, a target for the Rift Valley hemorrhagic fever virus. *Cell, 116*(4), 541-550. doi:10.1016/s0092-8674(04)00132-1

Le May, N., Mansuroglu, Z., Leger, P., Josse, T., Blot, G., Billecocq, A., . . . Bouloy, M. (2008). A SAP30 complex inhibits IFN-beta expression in Rift Valley fever virus infected cells. *PLoS Pathog, 4*(1), e13. doi:10.1371/journal.ppat.0040013

Lee, J. K., & Shin, O. S. (2021). Nonstructural Protein of Severe Fever with Thrombocytopenia Syndrome Phlebovirus Inhibits TBK1 to Evade Interferon-Mediated Response. *J Microbiol Biotechnol, 31*(2), 226-232. doi:10.4014/jmb.2008.08048

Lee, Y., Hur, I., Park, S. Y., Kim, Y. K., Suh, M. R., & Kim, V. N. (2006). The role of PACT in the RNA silencing pathway. *EMBO J, 25*(3), 522-532. doi:10.1038/sj.emboj.7600942

Lefteri, D. A., Bryden, S. R., Pingen, M., Terry, S., McCafferty, A., Beswick, E. F., . . . McKimmie, C. S. (2022). Mosquito saliva enhances virus infection through sialokinin-dependent vascular leakage. *Proc Natl Acad Sci U S A, 119*(24), e2114309119. doi:10.1073/pnas.2114309119

Leger, E., Vourc'h, G., Vial, L., Chevillon, C., & McCoy, K. D. (2013). Changing distributions of ticks: causes and consequences. *Exp Appl Acarol, 59*(1-2), 219-244. doi:10.1007/s10493-012-9615-0

Léger, P., Lara, E., Jagla, B., Sismeiro, O., Mansuroglu, Z., Coppee, J. Y., . . . Bouloy, M. (2013). Dicer-2- and Piwi-mediated RNA interference in Rift Valley fever virus-infected mosquito cells. *J Virol, 87*(3), 1631-1648. doi:10.1128/JVI.02795-12

Léger, P., & Lozach, P.-Y. (2015). Bunyaviruses: from transmission by arthropods to virus entry into the mammalian host first-target cells. *Future Virology, 10*(7), 859-881. doi:10.2217/fvl.15.52

Lejeune, F., Li, X., & Maquat, L. E. (2003). Nonsense-mediated mRNA decay in mammalian cells involves decapping, deadenylating, and exonucleolytic activities. *Mol Cell, 12*(3), 675-687. doi:10.1016/s1097-2765(03)00349-6

Leontieva, O. V., & Blagosklonny, M. V. (2014). Gerosuppression in confluent cells. *Aging (Albany NY), 6*(12), 1010-1018. doi:10.18632/aging.100714

Lerolle, S., Freitas, N., Cosset, F. L., & Legros, V. (2021). Host Cell Restriction Factors of Bunyaviruses and Viral Countermeasures. *Viruses, 13*(5). doi:10.3390/v13050784

Leventhal, S. S., Wilson, D., Feldmann, H., & Hawman, D. W. (2021). A Look into Bunyavirales Genomes: Functions of Non-Structural (NS) Proteins. *Viruses, 13*(2). doi:10.3390/v13020314

Li, C. L., Yang, W. Z., Chen, Y. P., & Yuan, H. S. (2008). Structural and functional insights into human Tudor-SN, a key component linking RNA interference and editing. *Nucleic Acids Res, 36*(11), 3579-3589. doi:10.1093/nar/gkn236

Li, J. C., Zhao, J., Li, H., Fang, L. Q., & Liu, W. (2022). Epidemiology, clinical characteristics, and treatment of severe fever with thrombocytopenia syndrome. *Infect Med (Beijing), 1*(1), 40-49. doi:10.1016/j.imj.2021.10.001

Li, M., Johnson, J. R., Truong, B., Kim, G., Weinbren, N., Dittmar, M., . . . Ramage, H. (2019). Identification of antiviral roles for the exon-junction complex and nonsense-mediated decay in flaviviral infection. *Nat Microbiol, 4*(6), 985-995. doi:10.1038/s41564-019-0375-z

Li, R., Gao, S., Chen, H., Zhang, X., Yang, X., Zhao, J., & Wang, Z. (2023). Virus usurps alternative splicing to clear the decks for infection. *Virol J, 20*(1), 131. doi:10.1186/s12985-023-02098-9

Li, Y., Li, S., Li, R., Xu, J., Jin, P., Chen, L., & Ma, F. (2017). Genome-wide miRNA screening reveals miR-310 family members negatively regulate the immune response in Drosophila melanogaster via co-targeting Drosomycin. *Dev Comp Immunol, 68*, 34-45. doi:10.1016/j.dci.2016.11.014

Liepelt, A., Naarmann-de Vries, I. S., Simons, N., Eichelbaum, K., Fohr, S., Archer, S. K., . . . Ostareck-Lederer, A. (2016). Identification of RNA-binding Proteins in Macrophages by Interactome Capture. *Mol Cell Proteomics, 15*(8), 2699-2714. doi:10.1074/mcp.M115.056564

Linder, P., & Jankowsky, E. (2011). From unwinding to clamping - the DEAD box RNA helicase family. *Nat Rev Mol Cell Biol, 12*(8), 505-516. doi:10.1038/nrm3154

Linthicum, K. J., Davies, F. G., Kairo, A., & Bailey, C. L. (1985). Rift Valley fever virus (family Bunyaviridae, genus Phlebovirus). Isolations from Diptera collected during an inter-epizootic period in Kenya. *J Hyg (Lond), 95*(1), 197-209. doi:10.1017/s0022172400062434

Liu, L., Dai, J., Zhao, Y. O., Narasimhan, S., Yang, Y., Zhang, L., & Fikrig, E. (2012). Ixodes scapularis JAK-STAT pathway regulates tick antimicrobial peptides, thereby controlling the agent of human granulocytic anaplasmosis. *J Infect Dis, 206*(8), 1233-1241. doi:10.1093/infdis/jis484

Liu, Q., He, B., Huang, S. Y., Wei, F., & Zhu, X. Q. (2014). Severe fever with thrombocytopenia syndrome, an emerging tick-borne zoonosis. *Lancet Infect Dis, 14*(8), 763-772. doi:10.1016/S1473-3099(14)70718-2

Liu, Y. C., Mok, B. W., Wang, P., Kuo, R. L., Chen, H., & Shih, S. R. (2021). Cellular 5'-3' mRNA Exoribonuclease XRN1 Inhibits Interferon Beta Activation and Facilitates Influenza A Virus Replication. *mBio, 12*(4), e0094521. doi:10.1128/mBio.00945-21

Lopez, N., Muller, R., Prehaud, C., & Bouloy, M. (1995). The L protein of Rift Valley fever virus can rescue viral ribonucleoproteins and transcribe synthetic genome-like RNA molecules. *J Virol, 69*(7), 3972-3979. doi:10.1128/JVI.69.7.3972-3979.1995

Lorès, P., Visvikis, O., Luna, R., Lemichez, E., & Gacon, G. (2010). The SWI/SNF protein BAF60b is ubiquitinated through a signalling process involving Rac GTPase and the RING finger protein Unkempt. *The FEBS Journal, 277*(6), 1453-1464. doi:10.1111/j.1742-4658.2010.07575.x

Lozach, P. Y., Kuhbacher, A., Meier, R., Mancini, R., Bitto, D., Bouloy, M., & Helenius, A. (2011). DC-SIGN as a receptor for phleboviruses. *Cell Host Microbe, 10*(1), 75-88. doi:10.1016/j.chom.2011.06.007

Lozach, P. Y., Mancini, R., Bitto, D., Meier, R., Oestereich, L., Overby, A. K., . . . Helenius, A. (2010). Entry of bunyaviruses into mammalian cells. *Cell Host Microbe, 7*(6), 488-499. doi:10.1016/j.chom.2010.05.007

Lunde, B. M., Moore, C., & Varani, G. (2007). RNA-binding proteins: modular design for efficient function. *Nat Rev Mol Cell Biol, 8*(6), 479-490. doi:10.1038/nrm2178

Lvov, D. (1979). Natural foci of arboviruses, related with the birds in USSR. *Lvov DK, Ilyichev VD, eds. Migration of the birds and transduction of contagium*, 37-101.

Lvov, D. K., Shchelkanov, M. Y., Alkhovsky, S. V., & Deryabin, P. G. (2015). Single-Stranded RNA Viruses. In *Zoonotic Viruses in Northern Eurasia* (pp. 135-392).

Ly, H. J., & Ikegami, T. (2016). Rift Valley fever virus NSs protein functions and the similarity to other bunyavirus NSs proteins. *Virol J, 13*, 118. doi:10.1186/s12985-016-0573-8

Ma, S., Dong, Z., Huang, Y., Liu, J. Y., & Zhang, J. T. (2022). eIF3a regulation of mTOR signaling and translational control via HuR in cellular response to DNA damage. *Oncogene, 41*(17), 2431-2443. doi:10.1038/s41388-022-02262-5

Ma, W., Tang, C., & Lai, L. (2005). Specificity of trypsin and chymotrypsin: loop-motion-controlled dynamic correlation as a determinant. *Biophys J, 89*(2), 1183-1193. doi:10.1529/biophysj.104.057158

MacLachlan, N. J., & Dubovi, E. J. (2017). Bunyaviridae. In *Fenner's Veterinary Virology* (pp. 411-424).

Macpherson, I., & Stoker, M. (1962). Polyoma transformation of hamster cell clones--an investigation of genetic factors affecting cell competence. *Virology, 16*, 147-151. doi:10.1016/0042-6822(62)90290-8

Madani, T. A., Al-Mazrou, Y. Y., Al-Jeffri, M. H., Mishkhas, A. A., Al-Rabeah, A. M., Turkistani, A. M., . . . Shobokshi, O. (2003). Rift Valley fever epidemic in Saudi Arabia: epidemiological, clinical, and laboratory characteristics. *Clin Infect Dis, 37*(8), 1084-1092. doi:10.1086/378747

Maes, P., Adkins, S., Alkhovsky, S. V., Avsic-Zupanc, T., Ballinger, M. J., Bente, D. A., . . . Kuhn, J. H. (2019). Taxonomy of the order Bunyavirales: second update 2018. *Arch Virol, 164*(3), 927-941. doi:10.1007/s00705-018-04127-3

Maes, P., Alkhovsky, S. V., Bao, Y., Beer, M., Birkhead, M., Briese, T., . . . Kuhn, J. H. (2018). Taxonomy of the family Arenaviridae and the order Bunyavirales: update 2018. *Arch Virol, 163*(8), 2295-2310. doi:10.1007/s00705-018-3843-5

Magyar, N., Kis, Z., Barabás, É., Nagy, A., Henczkó, J., Damjanova, I., . . . Pályi, B. (2021). New geographical area on the map of Crimean-Congo hemorrhagic fever virus: First serological evidence in the Hungarian population. *Ticks and Tick-borne Diseases, 12*(1). doi:10.1016/j.ttbdis.2020.101555

Mahon, C., Krogan, N. J., Craik, C. S., & Pick, E. (2014). Cullin E3 ligases and their rewiring by viral factors. *Biomolecules, 4*(4), 897-930. doi:10.3390/biom4040897

Malet, H., Williams, H. M., Cusack, S., & Rosenthal, M. (2023). The mechanism of genome replication and transcription in bunyaviruses. *PLoS Pathog, 19*(1), e1011060. doi:10.1371/journal.ppat.1011060

Marondedze, C., Thomas, L., Serrano, N. L., Lilley, K. S., & Gehring, C. (2016). The RNA-binding protein repertoire of Arabidopsis thaliana. *Sci Rep, 6*, 29766. doi:10.1038/srep29766

Massung, R. F., Levin, M. L., Munderloh, U. G., Silverman, D. J., Lynch, M. J., Gaywee, J. K., & Kurtti, T. J. (2007). Isolation and propagation of the Ap-Variant 1 strain of Anaplasma phagocytophilum in a tick cell line. *J Clin Microbiol, 45*(7), 2138-2143. doi:10.1128/JCM.00478-07

Mateos-Hernandez, L., Pipova, N., Allain, E., Henry, C., Rouxel, C., Lagree, A. C., . . . Simo, L. (2021). Enlisting the Ixodes scapularis Embryonic ISE6 Cell Line to Investigate the Neuronal Basis of Tick-Pathogen Interactions. *Pathogens, 10*(1). doi:10.3390/pathogens10010070

Matera, A. G., Terns, R. M., & Terns, M. P. (2007). Non-coding RNAs: lessons from the small nuclear and small nucleolar RNAs. *Nat Rev Mol Cell Biol, 8*(3), 209-220. doi:10.1038/nrm2124

Matia-Gonzalez, A. M., Jabre, I., & Gerber, A. P. (2021). Biochemical approach for isolation of polyadenylated RNAs with bound proteins from yeast. *STAR Protoc, 2*(4), 100929. doi:10.1016/j.xpro.2021.100929

Matsuno, K., Kajihara, M., Nakao, R., Nao, N., Mori-Kajihara, A., Muramatsu, M., . . . Ebihara, H. (2018). The Unique Phylogenetic Position of a Novel Tick-Borne Phlebovirus Ensures an Ixodid Origin of the Genus Phlebovirus. *mSphere, 3*(3). doi:10.1128/mSphere.00239-18

Matsuno, K., Weisend, C., Kajihara, M., Matysiak, C., Williamson, B. N., Simuunza, M., . . . Ebihara, H. (2015). Comprehensive molecular detection of tick-borne phleboviruses leads to the retrospective identification of taxonomically unassigned bunyaviruses and the discovery of a novel member of the genus phlebovirus. *J Virol, 89*(1), 594-604. doi:10.1128/JVI.02704-14

Mazelier, M., Rouxel, R. N., Zumstein, M., Mancini, R., Bell-Sakyi, L., & Lozach, P. Y. (2016). Uukuniemi Virus as a Tick-Borne Virus Model. *J Virol, 90*(15), 6784-6798. doi:10.1128/JVI.00095-16

McMullan, L. K., Folk, S. M., Kelly, A. J., MacNeil, A., Goldsmith, C. S., Metcalfe, M. G., . . . Nichol, S. T. (2012). A new phlebovirus associated with severe febrile illness in Missouri. *N Engl J Med, 367*(9), 834-841. doi:10.1056/NEJMoa1203378

McNally, K. L., Mitzel, D. N., Anderson, J. M., Ribeiro, J. M., Valenzuela, J. G., Myers, T. G., . . . Bloom, M. E. (2012). Differential salivary gland transcript expression profile in Ixodes scapularis nymphs upon feeding or flavivirus infection. *Ticks Tick Borne Dis, 3*(1), 18-26. doi:10.1016/j.ttbdis.2011.09.003

Medlock, J. M., & Leach, S. A. (2015). Effect of climate change on vector-borne disease risk in the UK. *Lancet Infect Dis, 15*(6), 721-730. doi:10.1016/S1473-3099(15)70091-5

Meier, R., Franceschini, A., Horvath, P., Tetard, M., Mancini, R., von Mering, C., . . . Lozach, P. Y. (2014). Genome-wide small interfering RNA screens reveal VAMP3 as a novel host factor required for Uukuniemi virus late penetration. *J Virol, 88*(15), 8565-8578. doi:10.1128/JVI.00388-14

Mekata, H., Umeki, K., Yamada, K., Umekita, K., & Okabayashi, T. (2023). Nosocomial Severe Fever with Thrombocytopenia Syndrome in Companion Animals, Japan, 2022. *Emerg Infect Dis, 29*(3), 614-617. doi:10.3201/eid2903.220720

Messina, J. P., Pigott, D. M., Golding, N., Duda, K. A., Brownstein, J. S., Weiss, D. J., . . . Hay, S. I. (2015). The global distribution of Crimean-Congo hemorrhagic fever. *Trans R Soc Trop Med Hyg, 109*(8), 503-513. doi:10.1093/trstmh/trv050

Meyer, J. M., Kurtti, T. J., Van Zee, J. P., & Hill, C. A. (2010). Genome organization of major tandem repeats in the hard tick, Ixodes scapularis. *Chromosome Res, 18*(3), 357-370. doi:10.1007/s10577-010-9120-4

Migne, C. V., Honig, V., Bonnet, S. I., Palus, M., Rakotobe, S., Galon, C., . . . Moutailler, S. (2022). Evaluation of two artificial infection methods of live ticks as tools for studying interactions between tick-borne viruses and their tick vectors. *Sci Rep, 12*(1), 491. doi:10.1038/s41598-021-04498-9

Miller, J. R., Koren, S., Dilley, K. A., Harkins, D. M., Stockwell, T. B., Shabman, R. S., & Sutton, G. G. (2018). A draft genome sequence for the Ixodes scapularis cell line, ISE6. *F1000Res, 7*, 297. doi:10.12688/f1000research.13635.1

Min, Y. Q., Ning, Y. J., Wang, H., & Deng, F. (2020). A RIG-I-like receptor directs antiviral responses to a bunyavirus and is antagonized by virus-induced blockade of TRIM25-mediated ubiquitination. *J Biol Chem, 295*(28), 9691-9711. doi:10.1074/jbc.RA120.013973

Miyamoto, M., & Komuro, A. (2017). PACT is required for MDA5-mediated immunoresponses triggered by Cardiovirus infection via interaction with LGP2. *Biochem Biophys Res Commun, 494*(1-2), 227-233. doi:10.1016/j.bbrc.2017.10.048

Miyamoto, S., Ito, T., Terada, S., Eguchi, T., Furubeppu, H., Kawamura, H., . . . Kakihana, Y. (2019). Fulminant myocarditis associated with severe fever with thrombocytopenia syndrome: a case report. *BMC Infect Dis, 19*(1), 266. doi:10.1186/s12879-019-3904-8

Mocellin, S., & Provenzano, M. (2004). RNA interference: learning gene knock-down from cell physiology. *J Transl Med, 2*(1), 39. doi:10.1186/1479-5876-2-39

Mohler, J., Weiss, N., Murli, S., Mohammadi, S., Vani, K., Vasilakis, G., . . . English, J. (1992). The embryonically active gene, unkempt, of Drosophila encodes a Cys3His finger protein. *Genetics, 131*(2), 377-388. doi:10.1093/genetics/131.2.377

Montgomery, M. K. (2004). The use of double-stranded RNA to knock down specific gene activity. *Methods Mol Biol, 260*, 129-144. doi:10.1385/1-59259-755-6:129

Moutailler, S., Krida G Fau - Madec, Y., Madec Y Fau - Bouloy, M., Bouloy M Fau - Failloux, A.-B., & Failloux, A. B. Replication of Clone 13, a naturally attenuated avirulent isolate of Rift Valley fever virus, in Aedes and Culex mosquitoes. (1557-7759 (Electronic)).

Moutailler, S., Roche, B., Thiberge, J. M., Caro, V., Rougeon, F., & Failloux, A. B. (2011). Host alternation is necessary to maintain the genome stability of rift valley fever virus. *PLoS Negl Trop Dis, 5*(5), e1156. doi:10.1371/journal.pntd.0001156

Moy, Ryan H., Cole, Brian S., Yasunaga, A., Gold, B., Shankarling, G., Varble, A., . . . Cherry, S. (2014). Stem-Loop Recognition by DDX17 Facilitates miRNA Processing and Antiviral Defense. *Cell, 158*(4), 764-777. doi:10.1016/j.cell.2014.06.023

Mullen, T. E., & Marzluff, W. F. (2008). Degradation of histone mRNA requires oligouridylation followed by decapping and simultaneous degradation of the mRNA both 5' to 3' and 3' to 5'. *Genes Dev, 22*(1), 50-65. doi:10.1101/gad.1622708

Muller, M., Fazi, F., & Ciaudo, C. (2019). Argonaute Proteins: From Structure to Function in Development and Pathological Cell Fate Determination. *Front Cell Dev Biol, 7*, 360. doi:10.3389/fcell.2019.00360

Munderloh, U. G., Liu, Y., Wang, M., Chen, C., & Kurtti, T. J. (1994). Establishment, Maintenance and Description of Cell Lines from the Tick Ixodes scapularis. *The Journal of Parasitology, 80*(4). doi:10.2307/3283188

Murithi, R. M., Munyua, P., Ithondeka, P. M., Macharia, J. M., Hightower, A., Luman, E. T., . . . Njenga, M. K. (2011). Rift Valley fever in Kenya: history of epizootics and identification of vulnerable districts. *Epidemiol Infect, 139*(3), 372-380. doi:10.1017/S0950268810001020

Nava, S. (2009). An overview of systematics and evolution of ticks. *Frontiers in Bioscience, Volume*(14). doi:10.2741/3418

Neault, N., O'Reilly, S., Baig, A. T., Plaza-Diaz, J., Azimi, M., Farooq, F., . . . MacKenzie, A. (2021). High-throughput kinome-RNAi screen identifies protein kinase R activator (PACT) as a novel genetic modifier of CUG foci integrity in myotonic dystrophy type 1 (DM1). *PLoS One, 16*(9), e0256276. doi:10.1371/journal.pone.0256276

Nelson, C. R., Mrozowich, T., Park, S. M., D'Souza, S., Henrickson, A., Vigar, J. R. J., . . . Patel, T. R. (2020). Human DDX17 Unwinds Rift Valley Fever Virus Non-Coding RNAs. *Int J Mol Sci, 22*(1). doi:10.3390/ijms22010054

Ng, C. S., Kasumba, D. M., Fujita, T., & Luo, H. (2020). Spatio-temporal characterization of the antiviral activity of the XRN1-DCP1/2 aggregation against cytoplasmic RNA viruses to prevent cell death. *Cell Death Differ, 27*(8), 2363-2382. doi:10.1038/s41418-020-0509-0

Nicoletti, L. (2014). Rift Valley Fever and Other Phleboviruses (Bunyaviridae)☆. In *Reference Module in Biomedical Sciences*.

Nijhof, A. M., Taoufik, A., de la Fuente, J., Kocan, K. M., de Vries, E., & Jongejan, F. (2007). Gene silencing of the tick protective antigens, Bm86, Bm91 and subolesin, in the one-host tick Boophilus microplus by RNA interference. *Int J Parasitol, 37*(6), 653-662. doi:10.1016/j.ijpara.2006.11.005

Ning, Y. J., Feng, K., Min, Y. Q., Cao, W. C., Wang, M., Deng, F., . . . Wang, H. (2015). Disruption of type I interferon signaling by the nonstructural protein of severe fever with thrombocytopenia syndrome virus via the hijacking of STAT2 and STAT1 into inclusion bodies. *J Virol, 89*(8), 4227-4236. doi:10.1128/JVI.00154-15

Niu, G., Li, J., Liang, M., Jiang, X., Jiang, M., Yin, H., . . . Li, D. (2013). Severe fever with thrombocytopenia syndrome virus among domesticated animals, China. *Emerg Infect Dis, 19*(5), 756-763. doi:10.3201/eid1905.120245

Nott, A., Le Hir, H., & Moore, M. J. (2004). Splicing enhances translation in mammalian cells: an additional function of the exon junction complex. *Genes Dev, 18*(2), 210-222. doi:10.1101/gad.1163204

Nuttall, P. A. (2023). Tick saliva and its role in pathogen transmission. *Wien Klin Wochenschr, 135*(7-8), 165-176. doi:10.1007/s00508-019-1500-y

Nuttall, P. A., Carey, D., Reid, H. W., & Harrap, K. A. (1981). Orbiviruses and bunyaviruses from a seabird colony in Scotland. *J Gen Virol, 57*(1), 127-137. doi:10.1099/0022-1317-57-1-127

Nuttall, P. A., Jones, L. D., Labuda, M., & Kaufman, W. R. (1994). Adaptations of arboviruses to ticks. *J Med Entomol, 31*(1), 1-9. doi:10.1093/jmedent/31.1.1

Obbard, D. J., Gordon, K. H., Buck, A. H., & Jiggins, F. M. (2009). The evolution of RNAi as a defence against viruses and transposable elements. *Philos Trans R Soc Lond B Biol Sci, 364*(1513), 99-115. doi:10.1098/rstb.2008.0168

Oliver, J. D., Chavez, A. S., Felsheim, R. F., Kurtti, T. J., & Munderloh, U. G. (2015). An Ixodes scapularis cell line with a predominantly neuron-like phenotype. *Exp Appl Acarol, 66*(3), 427-442. doi:10.1007/s10493-015-9908-1

Olschewski, S., Cusack, S., & Rosenthal, M. (2020). The Cap-Snatching Mechanism of Bunyaviruses. *Trends Microbiol, 28*(4), 293-303. doi:10.1016/j.tim.2019.12.006

Oluwayelu, D., Adebiyi, A., & Tomori, O. (2018). Endemic and emerging arboviral diseases of livestock in Nigeria: a review. *Parasit Vectors, 11*(1), 337. doi:10.1186/s13071-018-2911-8

Ottoz, D. S. M., & Berchowitz, L. E. (2020). The role of disorder in RNA binding affinity and specificity. *Open Biol, 10*(12), 200328. doi:10.1098/rsob.200328

Överby, A. K., Pettersson, R. F., Grunewald, K., & Huiskonen, J. T. (2008). Insights into bunyavirus architecture from electron cryotomography of Uukuniemi virus. *Proc Natl Acad Sci U S A, 105*(7), 2375-2379. doi:10.1073/pnas.0708738105

Överby, A. K., Pettersson, R. F., & Neve, E. P. (2007). The glycoprotein cytoplasmic tail of Uukuniemi virus (Bunyaviridae) interacts with ribonucleoproteins and is critical for genome packaging. *J Virol, 81*(7), 3198-3205. doi:10.1128/JVI.02655-06

Överby, A. K., Popov, V., Neve, E. P., & Pettersson, R. F. (2006). Generation and analysis of infectious virus-like particles of uukuniemi virus (bunyaviridae): a useful system for studying bunyaviral packaging and budding. *J Virol, 80*(21), 10428-10435. doi:10.1128/JVI.01362-06

Överby, A. K., Popov, V. L., Pettersson, R. F., & Neve, E. P. (2007). The cytoplasmic tails of Uukuniemi Virus (Bunyaviridae) G(N) and G(C) glycoproteins are important for intracellular targeting and the budding of virus-like particles. *J Virol, 81*(20), 11381-11391. doi:10.1128/JVI.00767-07

Oymans, J., Wichgers Schreur, P. J., van Keulen, L., Kant, J., & Kortekaas, J. (2020). Rift Valley fever virus targets the maternal-foetal interface in ovine and human placentas. *PLoS Negl Trop Dis, 14*(1), e0007898. doi:10.1371/journal.pntd.0007898

Palmer, M. J., Bantle, J. A., Guo, X., & Fargo, W. S. (1994). Genome size and organization in the ixodid tick Amblyomma americanum (L.). *Insect Mol Biol, 3*(1), 57-62. doi:10.1111/j.1365-2583.1994.tb00151.x

Palmer, W. J., & Jiggins, F. M. (2015). Comparative Genomics Reveals the Origins and Diversity of Arthropod Immune Systems. *Mol Biol Evol, 32*(8), 2111-2129. doi:10.1093/molbev/msv093

Papa, A., Kontana, A., Tsioka, K., Chaligiannis, I., & Sotiraki, S. (2016). Novel phleboviruses detected in ticks, Greece. *Ticks Tick Borne Dis, 7*(5), 690-693. doi:10.1016/j.ttbdis.2016.02.017

Papa, A., Zelená, H., Papadopoulou, E., & Mrázek, J. (2018). Uukuniemi virus, Czech Republic. *Ticks and Tick-borne Diseases, 9*(5), 1129-1132.

Paradkar, P. N., Duchemin, J. B., Voysey, R., & Walker, P. J. (2014). Dicer-2-dependent activation of Culex Vago occurs via the TRAF-Rel2 signaling pathway. *PLoS Negl Trop Dis, 8*(4), e2823. doi:10.1371/journal.pntd.0002823

Paradkar, P. N., Trinidad, L., Voysey, R., Duchemin, J. B., & Walker, P. J. (2012). Secreted Vago restricts West Nile virus infection in Culex mosquito cells by activating the Jak-STAT pathway. *Proc Natl Acad Sci U S A, 109*(46), 18915-18920. doi:10.1073/pnas.1205231109

Park, S. Y., Kwon, J. S., Kim, J. Y., Kim, S. M., Jang, Y. R., Kim, M. C., . . . Kim, S. H. (2018). Severe fever with thrombocytopenia syndrome-associated encephalopathy/encephalitis. *Clin Microbiol Infect, 24*(4), 432 e431-432 e434. doi:10.1016/j.cmi.2017.09.002

Pasternack, S. M., Refke, M., Paknia, E., Hennies, H. C., Franz, T., Schafer, N., . . . Betz, R. C. (2013). Mutations in SNRPE, which encodes a core protein of the spliceosome, cause autosomal-dominant hypotrichosis simplex. *Am J Hum Genet, 92*(1), 81-87. doi:10.1016/j.ajhg.2012.10.022

Patel, A. A., Dalal, Y. D., Parikh, A., Gandhi, R., & Shah, A. (2023). Crimean-Congo Hemorrhagic Fever: An Emerging Viral Infection in India, Revisited and Lessons Learned. *Cureus, 15*(8), e43315. doi:10.7759/cureus.43315

Patel, R. C., & Sen, G. C. (1998). PACT, a protein activator of the interferon-induced protein kinase, PKR. *EMBO J, 17*(15), 4379-4390. doi:10.1093/emboj/17.15.4379

Pavlov, P., Rosický, B., Hubálek, Z., Daniel, M., Bárdos, V., Minár, J., & Juricová, Z. (1978). Isolation of Bhanja virus from ticks of the genus Haemaphysalis in southeast Bulgaria and presence of antibodies in pastured sheep. *Folia Parasitol (Praha), 25*(1), 67-73.

Pena, N., Zhang, W., Watkins, C., Halucha, M., Alshammary, H., Hernandez, M. M., . . . Pan, T. (2022). Profiling Selective Packaging of Host RNA and Viral RNA Modification in SARS-CoV-2 Viral Preparations. *Front Cell Dev Biol, 10*, 768356. doi:10.3389/fcell.2022.768356

Pepin, M., Bouloy, M., Bird, B. H., Kemp, A., & Paweska, J. (2010). Rift Valley fever virus(Bunyaviridae: Phlebovirus): an update on pathogenesis, molecular epidemiology, vectors, diagnostics and prevention. *Vet Res, 41*(6), 61. doi:10.1051/vetres/2010033

Perea, W., & Greenbaum, N. L. (2020). Label-free horizontal EMSA for analysis of protein-RNA interactions. *Anal Biochem, 599*, 113736. doi:10.1016/j.ab.2020.113736

Pereira, J., & Lupas, A. N. (2018). The ancestral KH peptide at the root of a domain family with three different folds. *Bioinformatics, 34*(23), 3961-3965. doi:10.1093/bioinformatics/bty480

Perez-Perri, J. I., Noerenberg, M., Kamel, W., Lenz, C. E., Mohammed, S., Hentze, M. W., & Castello, A. (2021). Global analysis of RNA-binding protein dynamics by comparative and enhanced RNA interactome capture. *Nat Protoc, 16*(1), 27-60. doi:10.1038/s41596-020-00404-1

Persson, E., & Sonnhammer, E. L. L. (2022). InParanoid-DIAMOND: faster orthology analysis with the InParanoid algorithm. *Bioinformatics, 38*(10), 2918-2919. doi:10.1093/bioinformatics/btac194

Persson, R., & Pettersson, R. F. (1991). Formation and intracellular transport of a heterodimeric viral spike protein complex. *J Cell Biol, 112*(2), 257-266. doi:10.1083/jcb.112.2.257

Perveen, N., Muhammad, K., Muzaffar, S. B., Zaheer, T., Munawar, N., Gajic, B., . . . Willingham, A. L. (2023). Host-pathogen interaction in arthropod vectors: Lessons from viral infections. *Front Immunol, 14*, 1061899. doi:10.3389/fimmu.2023.1061899

Peters, G. A., Hartmann, R., Qin, J., & Sen, G. C. (2001). Modular structure of PACT: distinct domains for binding and activating PKR. *Mol Cell Biol, 21*(6), 1908-1920. doi:10.1128/MCB.21.6.1908-1920.2001

Peters, G. A., Seachrist, D. D., Keri, R. A., & Sen, G. C. (2009). The double-stranded RNA-binding protein, PACT, is required for postnatal anterior pituitary proliferation. *Proc Natl Acad Sci U S A, 106*(26), 10696-10701. doi:10.1073/pnas.0900735106

Pettersson, R., & Kaariainen, L. (1973). The ribonucleic acids of Uukuniemi virus, a noncubical tick-borne arbovirus. *Virology, 56*(2), 608-619. doi:10.1016/0042-6822(73)90062-7

Pettersson, R., Kaariainen, L., von Bonsdorff, C. H., & Oker-Blom, N. (1971). Structural components of Uukuniemi virus, a noncubical tick-borne arbovirus. *Virology, 46*(3), 721-729. doi:10.1016/0042-6822(71)90074-2

Pettersson, R. F., Hewlett, M. J., Baltimore, D., & Coffin, J. M. (1977). The genome of Uukuniemi virus consists of three unique RNA segments. *Cell, 11*(1), 51-63. doi:10.1016/0092-8674(77)90316-6

Pettersson, R. F., & von Bonsdorff, C. H. (1975). Ribonucleoproteins of Uukuniemi virus are circular. *J Virol, 15*(2), 386-392. doi:10.1128/JVI.15.2.386-392.1975

Pincheira, R., Chen, Q., & Zhang, J. T. (2001). Identification of a 170-kDa protein over-expressed in lung cancers. *Br J Cancer, 84*(11), 1520-1527. doi:10.1054/bjoc.2001.1828

Pingen, M., Bryden, S. R., Pondeville, E., Schnettler, E., Kohl, A., Merits, A., . . . McKimmie, C. S. (2016). Host Inflammatory Response to Mosquito Bites Enhances the Severity of Arbovirus Infection. *Immunity, 44*(6), 1455-1469. doi:10.1016/j.immuni.2016.06.002

Plassmeyer, M. L., Soldan, S. S., Stachelek, K. M., Martin-Garcia, J., & Gonzalez-Scarano, F. (2005). California serogroup Gc (G1) glycoprotein is the principal determinant of pH-dependent cell fusion and entry. *Virology, 338*(1), 121-132. doi:10.1016/j.virol.2005.04.026

Plyusnin, A. (2012). Bunyaviridae. In *Virus Taxonomy* (pp. 725-741): Elsevier.

Poldy, J. (2020). Volatile Cues Influence Host-Choice in Arthropod Pests. *Animals (Basel), 10*(11). doi:10.3390/ani10111984

Pommier, Y., Nussenzweig, A., Takeda, S., & Austin, C. (2022). Human topoisomerases and their roles in genome stability and organization. *Nat Rev Mol Cell Biol, 23*(6), 407-427. doi:10.1038/s41580-022-00452-3

Popp, M. W., Cho, H., & Maquat, L. E. (2020). Viral subversion of nonsense-mediated mRNA decay. *RNA, 26*(11), 1509-1518. doi:10.1261/rna.076687.120

Prasanth, K. R., Hirano, M., Fagg, W. S., McAnarney, E. T., Shan, C., Xie, X., . . . Garcia-Blanco, M. A. (2020). Topoisomerase III-ss is required for efficient replication of positive-sense RNA viruses. *bioRxiv*. doi:10.1101/2020.03.24.005900

Punda, V., Beus, I., Calisher, C., & Vesenjak-Hirjan, J. (1980). Laboratory infections with Bhanja virus. *Zentralblatt fur Bakteriologie*, 297-301.

Rahlenbeck, S., Fingerle, V., & Doggett, S. (2016). Prevention of tick-borne diseases: an overview. *Br J Gen Pract, 66*(650), 492-494. doi:10.3399/bjgp16X687013

Ranjan, T., Ranjan Kumar, R., Ansar, M., Kumar, J., Mohanty, A., Kumari, A., . . . Ahmad, M. F. (2023). The curious case of genome packaging and assembly in RNA viruses infecting plants. *Front Genet, 14*, 1198647. doi:10.3389/fgene.2023.1198647

Ranki, M., & Pettersson, R. F. (1975). Uukuniemi virus contains an RNA polymerase. *J Virol, 16*(6), 1420-1425. doi:10.1128/JVI.16.6.1420-1425.1975

Reichel, M., Liao, Y., Rettel, M., Ragan, C., Evers, M., Alleaume, A. M., . . . Millar, A. A. (2016). In Planta Determination of the mRNA-Binding Proteome of Arabidopsis Etiolated Seedlings. *Plant Cell, 28*(10), 2435-2452. doi:10.1105/tpc.16.00562

Ren, F., Shen, S., Wang, Q., Wei, G., Huang, C., Wang, H., . . . Deng, F. (2021). Recent Advances in Bunyavirus Reverse Genetics Research: Systems Development, Applications, and Future Perspectives. *Front Microbiol, 12*, 771934. doi:10.3389/fmicb.2021.771934

Ren, Z. Q., Yan, W. J., Zhang, X. Z., Zhang, P. B., Zhang, C., & Chen, S. K. (2020). CUL1 Knockdown Attenuates the Adhesion, Invasion, and Migration of Triple-Negative Breast Cancer Cells via Inhibition of Epithelial-Mesenchymal Transition. *Pathol Oncol Res, 26*(2), 1153-1163. doi:10.1007/s12253-019-00681-6

Resck, M. E. B., Padilha, K. P., Cupolillo, A. P., Talyuli, O. A. C., Ferreira-de-Brito, A., Lourenco-de-Oliveira, R., . . . Bruno, R. V. (2020). Unlike Zika, Chikungunya virus interferes in the viability of Aedes aegypti eggs, regardless of females' age. *Sci Rep, 10*(1), 13642. doi:10.1038/s41598-020-70367-6

Rezelj, V. V., Li, P., Chaudhary, V., Elliott, R. M., Jin, D. Y., & Brennan, B. (2017). Differential Antagonism of Human Innate Immune Responses by Tick-Borne Phlebovirus Nonstructural Proteins. *mSphere, 2*(3). doi:10.1128/mSphere.00234-17

Rezelj, V. V., Mottram, T. J., Hughes, J., Elliott, R. M., Kohl, A., & Brennan, B. (2019). M Segment-Based Minigenomes and Virus-Like Particle Assays as an Approach To Assess the Potential of Tick-Borne Phlebovirus Genome Reassortment. *J Virol, 93*(6). doi:10.1128/JVI.02068-18

Rezelj, V. V., Overby, A. K., & Elliott, R. M. (2015). Generation of mutant Uukuniemi viruses lacking the nonstructural protein NSs by reverse genetics indicates that NSs is a weak interferon antagonist. *J Virol, 89*(9), 4849-4856. doi:10.1128/JVI.03511-14

Ribeiro, J. M., Alarcon-Chaidez, F., Francischetti, I. M., Mans, B. J., Mather, T. N., Valenzuela, J. G., & Wikel, S. K. (2006). An annotated catalog of salivary gland transcripts from Ixodes scapularis ticks. *Insect Biochem Mol Biol, 36*(2), 111-129. doi:10.1016/j.ibmb.2005.11.005

Richter, D., Matuschka, F. R., Spielman, A., & Mahadevan, L. (2013). How ticks get under your skin: insertion mechanics of the feeding apparatus of Ixodes ricinus ticks. *Proc Biol Sci, 280*(1773), 20131758. doi:10.1098/rspb.2013.1758

Rieder, M., Brzozka, K., Pfaller, C. K., Cox, J. H., Stitz, L., & Conzelmann, K. K. (2011). Genetic dissection of interferon-antagonistic functions of rabies virus phosphoprotein: inhibition of interferon regulatory factor 3 activation is important for pathogenicity. *J Virol, 85*(2), 842-852. doi:10.1128/JVI.01427-10

Riley, D. G., Joseph, S. V., Srinivasan, R., & Diffie, S. (2011). Thrips Vectors of Tospoviruses. *Journal of Integrated Pest Management, 2*(1), I1-I10. doi:10.1603/ipm10020

Rochlin, I., & Toledo, A. (2020). Emerging tick-borne pathogens of public health importance: a mini-review. *J Med Microbiol, 69*(6), 781-791. doi:10.1099/jmm.0.001206

Rodriguez Pulido, M., Serrano, P., Saiz, M., & Martinez-Salas, E. (2007). Foot-and-mouth disease virus infection induces proteolytic cleavage of PTB, eIF3a,b, and PABP RNA-binding proteins. *Virology, 364*(2), 466-474. doi:10.1016/j.virol.2007.03.013

Rolin, A. I., Berrang-Ford, L., & Kulkarni, M. A. (2013). The risk of Rift Valley fever virus introduction and establishment in the United States and European Union. *Emerg Microbes Infect, 2*(12), e81. doi:10.1038/emi.2013.81

Romano, D., Stefanini, C., Canale, A., & Benelli, G. (2018). Artificial blood feeders for mosquito and ticks-Where from, where to? *Acta Trop, 183*, 43-56. doi:10.1016/j.actatropica.2018.04.009

Ronnholm, R. (1992). Localization to the Golgi complex of Uukuniemi virus glycoproteins G1 and G2 expressed from cloned cDNAs. *J Virol, 66*(7), 4525-4531. doi:10.1128/JVI.66.7.4525-4531.1992

Ronnholm, R., & Pettersson, R. F. (1987). Complete nucleotide sequence of the M RNA segment of Uukuniemi virus encoding the membrane glycoproteins G1 and G2. *Virology, 160*(1), 191-202. doi:10.1016/0042-6822(87)90060-2

Rosa, R. D., Capelli-Peixoto, J., Mesquita, R. D., Kalil, S. P., Pohl, P. C., Braz, G. R., . . . Daffre, S. (2016). Exploring the immune signalling pathway-related genes of the cattle tick Rhipicephalus microplus: From molecular characterization to transcriptional profile upon microbial challenge. *Dev Comp Immunol, 59*, 1-14. doi:10.1016/j.dci.2015.12.018

Rosche, K. L., Sidak-Loftis, L. C., Hurtado, J., Fisk, E. A., & Shaw, D. K. (2020). Arthropods Under Pressure: Stress Responses and Immunity at the Pathogen-Vector Interface. *Front Immunol, 11*, 629777. doi:10.3389/fimmu.2020.629777

Rossmann, M. G., & Rao, V. B. (2012). *Viral Molecular Machines*: Springer New York.

Rossmann, M. G. a. R., V.B. (2012). *Viral Molecular Machines* (V. B. R. Michael G. Rossmann Ed. 1 ed.): Springer New York, NY.

Rowley, P. A., Ho, B., Bushong, S., Johnson, A., & Sawyer, S. L. (2016). XRN1 Is a Species-Specific Virus Restriction Factor in Yeasts. *PLoS Pathog, 12*(10), e1005890. doi:10.1371/journal.ppat.1005890

Saikku, P., & Brummer-Korvenkontio, M. (1973). Arboviruses in Finland II. Isolation and Characterization of Uukuniemi Virus, A Virus Assoiated with Ticks and Birds. *The American Journal of Tropical Medicine and Hygine, 22*(3), 390-399. doi:10.4269/ajtmh.1973.22.390

Salicioni, A. M., Xi, M., Vanderveer, L. A., Balsara, B., Testa, J. R., Dunbrack, R. L., Jr., & Godwin, A. K. (2000). Identification and structural analysis of human RBM8A and RBM8B: two highly conserved RNA-binding motif proteins that interact with OVCA1, a candidate tumor suppressor. *Genomics, 69*(1), 54-62. doi:10.1006/geno.2000.6315

Sanchez-Vargas, I., Olson, K. E., & Black, W. C. t. (2021). The Genetic Basis for Salivary Gland Barriers to Arboviral Transmission. *Insects, 12*(1). doi:10.3390/insects12010073

Santorelli, D., Troilo, F., Fata, F., Angelucci, F., Demitri, N., Giardina, G., . . . Travaglini-Allocatelli, C. (2022). Folding Mechanism and Aggregation Propensity of the KH0 Domain of FMRP and Its R138Q Pathological Variant. *Int J Mol Sci, 23*(20). doi:10.3390/ijms232012178

Sato, M., Maeda, N., Yoshida, H., Urade, M., & Saito, S. (1977). Plaque formation of herpes virus hominis type 2 and rubella virus in variants isolated from the colonies of BHK21/WI-2 cells formed in soft agar. *Arch Virol, 53*(3), 269-273. doi:10.1007/BF01314672

Sato, M., Tanaka, H., Yamada, T., & Yamamoto, N. (1977). Persistent infection of BHK21/WI-2 cells with rubella virus and characterization of rubella variants. *Arch Virol, 54*(4), 333-343. doi:10.1007/BF01314778

Saunders, J. E., Gilbride, C., Dowall, S., Morris, S., Ulaszewska, M., Spencer, A. J., . . . Lambe, T. (2023). Adenoviral vectored vaccination protects against Crimean-Congo Haemorrhagic Fever disease in a lethal challenge model. *EBioMedicine, 90*, 104523. doi:10.1016/j.ebiom.2023.104523

Scallan, M. F., & Elliott, R. M. (1992). Defective RNAs in mosquito cells persistently infected with Bunyamwera virus. *J Gen Virol, 73 (Pt 1)*, 53-60. doi:10.1099/0022-1317-73-1-53

Scherer, C., Knowles, J., Sreenu, V. B., Fredericks, A. C., Fuss, J., Maringer, K., . . . Schnettler, E. (2021). An Aedes aegypti-Derived Ago2 Knockout Cell Line to Investigate Arbovirus Infections. *Viruses, 13*(6). doi:10.3390/v13061066

Schmidt, N., Ganskih, S., Wei, Y., Gabel, A., Zielinski, S., Keshishian, H., . . . Munschauer, M. (2023). SND1 binds SARS-CoV-2 negative-sense RNA and promotes viral RNA synthesis through NSP9. *Cell, 186*(22), 4834-4850 e4823. doi:10.1016/j.cell.2023.09.002

Schneider, C. A., Rasband, W. S., & Eliceiri, K. W. (2012). NIH Image to ImageJ: 25 years of image analysis. *Nat Methods, 9*(7), 671-675. doi:10.1038/nmeth.2089

Schnettler, E., Tykalova, H., Watson, M., Sharma, M., Sterken, M. G., Obbard, D. J., . . . Kohl, A. (2014). Induction and suppression of tick cell antiviral RNAi responses by tick-borne flaviviruses. *Nucleic Acids Res, 42*(14), 9436-9446. doi:10.1093/nar/gku657

Scholte, F. E., Tas, A., Albulescu, I. C., Zusinaite, E., Merits, A., Snijder, E. J., & van Hemert, M. J. (2015). Stress granule components G3BP1 and G3BP2 play a proviral role early in Chikungunya virus replication. *J Virol, 89*(8), 4457-4469. doi:10.1128/JVI.03612-14

Schotthoefer, A. M., & Frost, H. M. (2015). Ecology and Epidemiology of Lyme Borreliosis. *Clin Lab Med, 35*(4), 723-743. doi:10.1016/j.cll.2015.08.003

Schumann, M., Gantke, T., & Muhlberger, E. (2009). Ebola virus VP35 antagonizes PKR activity through its C-terminal interferon inhibitory domain. *J Virol, 83*(17), 8993-8997. doi:10.1128/JVI.00523-09

Scolari, F., Girella, A., & Croce, A. C. (2022). Imaging and spectral analysis of autofluorescence patterns in larval head structures of mosquito vectors. *Eur J Histochem, 66*(4). doi:10.4081/ejh.2022.3462

Scott, T. W., Amerasinghe, P. H., Morrison, A. C., Lorenz, L. H., Clark, G. G., Strickman, D., . . . Edman, J. D. (2000). Longitudinal studies of Aedes aegypti (Diptera: Culicidae) in Thailand

and Puerto Rico: blood feeding frequency. *J Med Entomol, 37*(1), 89-101. doi:10.1603/0022-2585-37.1.89

Scott, T. W., & Takken, W. (2012). Feeding strategies of anthropophilic mosquitoes result in increased risk of pathogen transmission. *Trends Parasitol, 28*(3), 114-121. doi:10.1016/j.pt.2012.01.001

Selenko, P., Sprangers, R., Stier, G., Buhler, D., Fischer, U., & Sattler, M. (2001). SMN tudor domain structure and its interaction with the Sm proteins. *Nat Struct Biol, 8*(1), 27-31. doi:10.1038/83014

Seo, J. W., Kim, D., Yun, N., & Kim, D. M. (2021). Clinical Update of Severe Fever with Thrombocytopenia Syndrome. *Viruses, 13*(7). doi:10.3390/v13071213

Shah Kv Fau - Work, T. H., & Work, T. H. (1969). Bhanja virus: a new arbovirus from ticks Haemaphysalis intermedia Warburton and Nuttall, 1909, in Orissa, India. (0971-5916 (Print)).

Sheehan, G., Garvey, A., Croke, M., & Kavanagh, K. (2018). Innate humoral immune defences in mammals and insects: The same, with differences ? *Virulence, 9*(1), 1625-1639. doi:10.1080/21505594.2018.1526531

Shepherd, A. J., Leman, P. A., & Swanepoel, R. (1989). Viremia and antibody response of small African and laboratory animals to Crimean-Congo hemorrhagic fever virus infection. *Am J Trop Med Hyg, 40*(5), 541-547. doi:10.4269/ajtmh.1989.40.541

Sheth, U., & Parker, R. (2003). Decapping and decay of messenger RNA occur in cytoplasmic processing bodies. *Science, 300*(5620), 805-808. doi:10.1126/science.1082320

Shi, J., Hu, Z., Deng, F., & Shen, S. (2018). Tick-Borne Viruses. *Virol Sin, 33*(1), 21-43. doi:10.1007/s12250-018-0019-0

Shivaprasad, S., Weng, K. F., Ooi, Y. S., Belk, J., Carette, J. E., Flynn, R., & Sarnow, P. (2022). Loquacious modulates flaviviral RNA replication in mosquito cells. *PLoS Pathog, 18*(4), e1010163. doi:10.1371/journal.ppat.1010163

Shtanko, O., Nikitina, R. A., Altuntas, C. Z., Chepurnov, A. A., & Davey, R. A. (2014). Crimean-Congo hemorrhagic fever virus entry into host cells occurs through the multivesicular body and requires ESCRT regulators. *PLoS Pathog, 10*(9), e1004390. doi:10.1371/journal.ppat.1004390

Sidak-Loftis, L. C., Rosche, K. L., Pence, N., Ujczo, J. K., Hurtado, J., Fisk, E. A., . . . Shaw, D. K. (2022). The Unfolded-Protein Response Triggers the Arthropod Immune Deficiency Pathway. *mBio, 13*(4), e0070322. doi:10.1128/mbio.00703-22

Sikutova, S., Hornok, S., Hubalek, Z., Dolezalkova, I., Juricova, Z., & Rudolf, I. (2009). Serological survey of domestic animals for tick-borne encephalitis and Bhanja viruses in northeastern Hungary. *Vet Microbiol, 135*(3-4), 267-271. doi:10.1016/j.vetmic.2008.09.082

Sim, S., Jupatanakul, N., & Dimopoulos, G. (2014). Mosquito immunity against arboviruses. *Viruses, 6*(11), 4479-4504. doi:10.3390/v6114479

Simo, L., Kazimirova, M., Richardson, J., & Bonnet, S. I. (2017). The Essential Role of Tick Salivary Glands and Saliva in Tick Feeding and Pathogen Transmission. *Front Cell Infect Microbiol, 7*, 281. doi:10.3389/fcimb.2017.00281

Simons, J. F., Hellman, U., & Pettersson, R. F. (1990). Uukuniemi virus S RNA segment: ambisense coding strategy, packaging of complementary strands into virions, and homology to members of the genus Phlebovirus. *J Virol, 64*(1), 247-255. doi:10.1128/JVI.64.1.247-255.1990

Simser, J. A., Macaluso, K. R., Mulenga, A., & Azad, A. F. (2004). Immune-responsive lysozymes from hemocytes of the American dog tick, Dermacentor variabilis and an embryonic cell line of the Rocky Mountain wood tick, D. andersoni. *Insect Biochem Mol Biol, 34*(12), 1235-1246. doi:10.1016/j.ibmb.2004.07.003

Singh, G., Pratt, G., Yeo, G. W., & Moore, M. J. (2015). The Clothes Make the mRNA: Past and Present Trends in mRNP Fashion. *Annu Rev Biochem, 84*, 325-354. doi:10.1146/annurev-biochem-080111-092106

Slater, A., Nair, N., Suett, R., Mac Donnchadha, R., Bamford, C., Jasim, S., . . . Hutchinson, E. (2022). Visualising Viruses. *J Gen Virol, 103*(1). doi:10.1099/jgv.0.001730

Slonchak, A., Hugo, L. E., Freney, M. E., Hall-Mendelin, S., Amarilla, A. A., Torres, F. J., . . . Khromykh, A. A. (2020). Zika virus noncoding RNA suppresses apoptosis and is required for virus transmission by mosquitoes. *Nat Commun, 11*(1), 2205. doi:10.1038/s41467-020-16086-y

Smith, A. A., & Pal, U. (2014). Immunity-related genes in Ixodes scapularis--perspectives from genome information. *Front Cell Infect Microbiol, 4*, 116. doi:10.3389/fcimb.2014.00116

Smith, R. W., Blee, T. K., & Gray, N. K. (2014). Poly(A)-binding proteins are required for diverse biological processes in metazoans. *Biochem Soc Trans, 42*(4), 1229-1237. doi:10.1042/BST20140111

Sorvillo, T. E., Rodriguez, S. E., Hudson, P., Carey, M., Rodriguez, L. L., Spiropoulou, C. F., . . . Bente, D. A. (2020). Towards a Sustainable One Health Approach to Crimean-Congo Hemorrhagic Fever Prevention: Focus Areas and Gaps in Knowledge. *Trop Med Infect Dis, 5*(3). doi:10.3390/tropicalmed5030113

Spengler, J. R., Bergeron, E., & Rollin, P. E. (2016). Seroepidemiological Studies of Crimean-Congo Hemorrhagic Fever Virus in Domestic and Wild Animals. *PLoS Negl Trop Dis, 10*(1), e0004210. doi:10.1371/journal.pntd.0004210

Spiegel, M., Plegge, T., & Pohlmann, S. (2016). The Role of Phlebovirus Glycoproteins in Viral Entry, Assembly and Release. *Viruses, 8*(7). doi:10.3390/v8070202

Stenum, T. S., Kumar, A. D., Sandbaumhuter, F. A., Kjellin, J., Jerlstrom-Hultqvist, J., Andren, P. E., . . . Holmqvist, E. (2023). RNA interactome capture in Escherichia coli globally identifies RNA-binding proteins. *Nucleic Acids Res, 51*(9), 4572-4587. doi:10.1093/nar/gkad216

Stern-Ginossar, N., Thompson, S. R., Mathews, M. B., & Mohr, I. (2019). Translational Control in Virus-Infected Cells. *Cold Spring Harb Perspect Biol, 11*(3). doi:10.1101/cshperspect.a033001

Su, H., Trombly, M. I., Chen, J., & Wang, X. (2009). Essential and overlapping functions for mammalian Argonautes in microRNA silencing. *Genes Dev, 23*(3), 304-317. doi:10.1101/gad.1749809

Su, S., Xue, Y., Sharov, A., Zhang, Y., Lee, S. K., Martindale, J. L., . . . Wang, W. (2022). A dual-activity topoisomerase complex regulates mRNA translation and turnover. *Nucleic Acids Res, 50*(12), 7013-7033. doi:10.1093/nar/gkac538

Subramani, C., Nair, V. P., Anang, S., Mandal, S. D., Pareek, M., Kaushik, N., . . . Surjit, M. (2018). Host-Virus Protein Interaction Network Reveals the Involvement of Multiple Host Processes in the Life Cycle of Hepatitis E Virus. *mSystems, 3*(1). doi:10.1128/mSystems.00135-17

Sun, P., Nie, K., Zhu, Y., Liu, Y., Wu, P., Liu, Z., . . . Cheng, G. (2020). A mosquito salivary protein promotes flavivirus transmission by activation of autophagy. *Nat Commun, 11*(1), 260. doi:10.1038/s41467-019-14115-z

Süss, J., Klaus, C., Gerstengarbe, F. W., & Werner, P. C. (2008). What Makes Ticks Tick? Climate Change, Ticks, and Tick-Borne Diseases. *Journal of Travel Medicine, 15*(1), 39-45. doi:10.1111/j.1708-8305.2007.00176.x

Sutejo, R., Yeo, D. S., Myaing, M. Z., Hui, C., Xia, J., Ko, D., . . . Sugrue, R. J. (2012). Activation of type I and III interferon signalling pathways occurs in lung epithelial cells infected with low pathogenic avian influenza viruses. *PLoS One, 7*(3), e33732. doi:10.1371/journal.pone.0033732

Swanepoel, R., Gill, D. E., Shepherd, A. J., Leman, P. A., Mynhardt, J. H., & Harvey, S. (1989). The clinical pathology of Crimean-Congo hemorrhagic fever. *Rev Infect Dis, 11 Suppl 4*, S794-800. doi:10.1093/clinids/11.supplement_4.s794

Swanepoel, R., & Paweska, J. T. (2011). Rift Valley Fever. In *Oxford Textbook of Zoonoses: Biology, Clinical Practice, and Public Health Control (2 edn)* (pp. 423-431).

Sweeney, M. A., Iakova, P., Maneix, L., Shih, F. Y., Cho, H. E., Sahin, E., & Catic, A. (2020). The ubiquitin ligase Cullin-1 associates with chromatin and regulates transcription of specific c-MYC target genes. *Sci Rep, 10*(1), 13942. doi:10.1038/s41598-020-70610-0

Sysoev, V. O., Fischer, B., Frese, C. K., Gupta, I., Krijgsveld, J., Hentze, M. W., . . . Ephrussi, A. (2016). Global changes of the RNA-bound proteome during the maternal-to-zygotic transition in Drosophila. *Nat Commun, 7*, 12128. doi:10.1038/ncomms12128

Szemiel, A. M., Failloux, A. B., & Elliott, R. M. (2012). Role of Bunyamwera Orthobunyavirus NSs protein in infection of mosquito cells. *PLoS Negl Trop Dis, 6*(9), e1823. doi:10.1371/journal.pntd.0001823

Tahir, D., Meyer, L., Fourie, J., Jongejan, F., Mather, T., Choumet, V., . . . Varloud, M. (2020). Interrupted Blood Feeding in Ticks: Causes and Consequences. *Microorganisms, 8*(6). doi:10.3390/microorganisms8060910

Takahashi, T., Maeda, K., Suzuki, T., Ishido, A., Shigeoka, T., Tominaga, T., . . . Saijo, M. (2014). The first identification and retrospective study of Severe Fever with Thrombocytopenia Syndrome in Japan. *J Infect Dis, 209*(6), 816-827. doi:10.1093/infdis/jit603

Thorpe, C. J., Wang, X. R., Munderloh, U. G., & Kurtti, T. J. (2021). Tick Cell Culture Analysis of Growth Dynamics and Cellular Tropism of Rickettsia buchneri, an Endosymbiont of the Blacklegged Tick, Ixodes scapularis. *Insects, 12*(11). doi:10.3390/insects12110968

Tilston-Lunel, N. L., Acrani, G. O., Randall, R. E., & Elliott, R. M. (2015). Generation of Recombinant Oropouche Viruses Lacking the Nonstructural Protein NSm or NSs. *J Virol, 90*(5), 2616-2627. doi:10.1128/JVI.02849-15

Tong, C., Javelle, E., Grard, G., Dia, A., Lacrosse, C., Fourie, T., . . . Pommier de Santi, V. (2019). Tracking Rift Valley fever: From Mali to Europe and other countries, 2016. *Euro Surveill, 24*(8). doi:10.2807/1560-7917.ES.2019.24.8.1800213

Trajkovic, K., Valdez, C., Ysselstein, D., & Krainc, D. (2019). Fluctuations in cell density alter protein markers of multiple cellular compartments, confounding experimental outcomes. *PLoS One, 14*(2), e0211727. doi:10.1371/journal.pone.0211727

Tsuchiya, N., Ochiai, M., Nakashima, K., Ubagai, T., Sugimura, T., & Nakagama, H. (2007). SND1, a component of RNA-induced silencing complex, is up-regulated in human colon cancers and implicated in early stage colon carcinogenesis. *Cancer Res, 67*(19), 9568-9576. doi:10.1158/0008-5472.CAN-06-2707

Tyanova, S., Temu, T., Sinitcyn, P., Carlson, A., Hein, M. Y., Geiger, T., . . . Cox, J. (2016). The Perseus computational platform for comprehensive analysis of (prote)omics data. *Nat Methods, 13*(9), 731-740. doi:10.1038/nmeth.3901

Uckeley, Z. M., Mazelier, M., Lüchtenborg, C., Winter, S., Schad, P., Chlanda, P., . . . Lozach, P. (2022). The glycolipid GlcCer is recruited into the viral envelope to promote phenuivirus binding to host cells. *bioRxiv*. doi:10.1101/2022.08.07.502911

Uckeley, Z. M., Moeller, R., Kuhn, L. I., Nilsson, E., Robens, C., Lasswitz, L., . . . Gerold, G. (2019). Quantitative Proteomics of Uukuniemi Virus-host Cell Interactions Reveals GBF1 as Proviral Host Factor for Phleboviruses. *Mol Cell Proteomics, 18*(12), 2401-2417. doi:10.1074/mcp.RA119.001631

Ullmann, A. J., Lima, C. M., Guerrero, F. D., Piesman, J., & Black, W. C. t. (2005). Genome size and organization in the blacklegged tick, Ixodes scapularis and the Southern cattle tick, Boophilus microplus. *Insect Mol Biol, 14*(2), 217-222. doi:10.1111/j.1365-2583.2005.00551.x

Urlaub, H., Raker, V. A., Kostka, S., & Luhrmann, R. (2001). Sm protein-Sm site RNA interactions within the inner ring of the spliceosomal snRNP core structure. *EMBO J, 20*(1-2), 187-196. doi:10.1093/emboj/20.1.187

van Knippenberg, I., Fragkoudis, R., & Elliott, R. M. (2013). The transient nature of Bunyamwera orthobunyavirus NSs protein expression: effects of increased stability of NSs protein on virus replication. *PLoS One, 8*(5), e64137. doi:10.1371/journal.pone.0064137

van Oort, B. E. H., Hovelsrud, G. K., Risvoll, C., Mohr, C. W., & Jore, S. (2020). A Mini-Review of Ixodes Ticks Climate Sensitive Infection Dispersion Risk in the Nordic Region. *Int J Environ Res Public Health, 17*(15). doi:10.3390/ijerph17155387

van Rij, R. P., Saleh, M. C., Berry, B., Foo, C., Houk, A., Antoniewski, C., & Andino, R. (2006). The RNA silencing endonuclease Argonaute 2 mediates specific antiviral immunity in Drosophila melanogaster. *Genes Dev, 20*(21), 2985-2995. doi:10.1101/gad.1482006

Vancova, M., Bily, T., Simo, L., Tous, J., Horodysky, P., Ruzek, D., . . . Nebesarova, J. (2020). Three-dimensional reconstruction of the feeding apparatus of the tick Ixodes ricinus (Acari: Ixodidae): a new insight into the mechanism of blood-feeding. *Sci Rep, 10*(1), 165. doi:10.1038/s41598-019-56811-2

Varjak, M., Maringer, K., Watson, M., Sreenu, V. B., Fredericks, A. C., Pondeville, E., . . . Schnettler, E. (2017). Aedes aegypti Piwi4 Is a Noncanonical PIWI Protein Involved in Antiviral Responses. *mSphere, 2*(3). doi:10.1128/mSphere.00144-17

Veijola, J., & Pettersson, R. F. (1999). Transient association of calnexin and calreticulin with newly synthesized G1 and G2 glycoproteins of uukuniemi virus (family Bunyaviridae). *J Virol, 73*(7), 6123-6127. doi:10.1128/JVI.73.7.6123-6127.1999

Verani, P., Balducci, M., Lopes, M. C., & Sacca, G. (1970). Isolation of Bhanja virus from Haemaphysalis ticks in Italy. *Am J Trop Med Hyg, 19*(1), 103-105. doi:10.4269/ajtmh.1970.19.103

Verhulst, N. O., Boulanger, N., & Spitzen, J. (2018). Impact of Skin Microbiome on Attractiveness to Arthropod Vectors and Pathogen Transmission. In *Skin and Arthropod Vectors* (pp. 55-81).

Vesenjak-Hirjan, J., Calisher, C., Beus, I., & Marton, E. (1980). First natural clinical human Bhanja virus infection. *Zentralblatt fur Bakteriologie, 9*, 297-301.

Vesenjak-Hirjan, J., Calisher, C. H., Brudnjak, Z., Tovornik, D., Skrtic, N., & Lazuick, J. S. (1977). Isolation of Bhanja virus from ticks in Yugoslavia. *Am J Trop Med Hyg, 26*(5 Pt 1), 1003-1008. doi:10.4269/ajtmh.1977.26.1003

Vilibic-Cavlek, T., Stevanovic, V., Krcmar, S., Savic, V., Kovac, S., Bogdanic, M., . . . Barbic, L. (2023). Detection of Bhanja Bandavirus in Patients with Neuroinvasive Disease of Unknown Etiology in Croatia. *Microorganisms, 11*(9). doi:10.3390/microorganisms11092155

Visser, I., Koenraadt, C. J. M., Koopmans, M. P. G., & Rockx, B. (2023). The significance of mosquito saliva in arbovirus transmission and pathogenesis in the vertebrate host. *One Health, 16*, 100506. doi:10.1016/j.onehlt.2023.100506

Wahl, M. C., Will, C. L., & Luhrmann, R. (2009). The spliceosome: design principles of a dynamic RNP machine. *Cell, 136*(4), 701-718. doi:10.1016/j.cell.2009.02.009

Walter, C. T., & Barr, J. N. (2011). Recent advances in the molecular and cellular biology of bunyaviruses. *J Gen Virol, 92*(Pt 11), 2467-2484. doi:10.1099/vir.0.035105-0

Wang, J., Selleck, P., Yu, M., Ha, W., Rootes, C., Gales, R., . . . Wang, L. F. (2014). Novel phlebovirus with zoonotic potential isolated from ticks, Australia. *Emerg Infect Dis, 20*(6), 1040-1043. doi:10.3201/eid2006.140003

Wang, S., Li, J., Niu, G., Wang, X., Ding, S., Jiang, X., . . . Li, D. (2015). SFTS virus in ticks in an endemic area of China. *Am J Trop Med Hyg, 92*(4), 684-689. doi:10.4269/ajtmh.14-0008

Watson, S. F., Knol, L. I., Witteveldt, J., & Macias, S. (2019). Crosstalk Between Mammalian Antiviral Pathways. *Noncoding RNA, 5*(1). doi:10.3390/ncrna5010029

Weber, F., Bridgen, A., Fazakerley, J. K., Streitenfeld, H., Kessler, N., Randall, R. E., & Elliott, R. M. (2002). Bunyamwera bunyavirus nonstructural protein NSs counteracts the induction of alpha/beta interferon. *J Virol, 76*(16), 7949-7955. doi:10.1128/jvi.76.16.7949-7955.2002

Weisheit, S., Villar, M., Tykalova, H., Popara, M., Loecherbach, J., Watson, M., . . . Bell-Sakyi, L. (2015). Ixodes scapularis and Ixodes ricinus tick cell lines respond to infection with tick-borne encephalitis virus: transcriptomic and proteomic analysis. *Parasit Vectors, 8*, 599. doi:10.1186/s13071-015-1210-x

Welch, S. R., Scholte, F. E. M., Spengler, J. R., Ritter, J. M., Coleman-McCray, J. D., Harmon, J. R., . . . Bergeron, E. (2020). The Crimean-Congo Hemorrhagic Fever Virus NSm Protein is Dispensable for Growth In Vitro and Disease in Ifnar(-/-) Mice. *Microorganisms, 8*(5). doi:10.3390/microorganisms8050775

Wessels, H. H., Imami, K., Baltz, A. G., Kolinski, M., Beldovskaya, A., Selbach, M., . . . Landthaler, M. (2016). The mRNA-bound proteome of the early fly embryo. *Genome Res, 26*(7), 1000-1009. doi:10.1101/gr.200386.115

Wichgers Schreur, P. J., & Kortekaas, J. (2016). Single-Molecule FISH Reveals Non-selective Packaging of Rift Valley Fever Virus Genome Segments. *PLoS Pathog, 12*(8), e1005800. doi:10.1371/journal.ppat.1005800

Wichgers Schreur, P. J., Oreshkova, N., Moormann, R. J., & Kortekaas, J. (2014). Creation of Rift Valley fever viruses with four-segmented genomes reveals flexibility in bunyavirus genome packaging. *J Virol, 88*(18), 10883-10893. doi:10.1128/JVI.00961-14

Wild, T. F., & Brown, F. (1967). Nature of the inactivating action of trypsin on foot-and-mouth disease virus. *J Gen Virol, 1*(2), 247-250. doi:10.1099/0022-1317-1-2-247

Will, C. L., & Luhrmann, R. (2011). Spliceosome structure and function. *Cold Spring Harb Perspect Biol, 3*(7). doi:10.1101/cshperspect.a003707

Won, S., Ikegami, T., Peters, C. J., & Makino, S. (2007). NSm protein of Rift Valley fever virus suppresses virus-induced apoptosis. *J Virol, 81*(24), 13335-13345. doi:10.1128/JVI.01238-07

Wróblewska-Mularczykowa, Z., Sadowski, W., & Żukowski, K. (1970). Isolation of arbovirus strains of Uukuniemi type in Poland. *Folia Parasitologica, 17*(4), 375-378.

Xi, Z., Ramirez, J. L., & Dimopoulos, G. (2008). The Aedes aegypti toll pathway controls dengue virus infection. *PLoS Pathog, 4*(7), e1000098. doi:10.1371/journal.ppat.1000098

Xia, J., Chen, X., Xu, F., Wang, Y., Shi, Y., Li, Y., . . . Zhang, P. (2015). Dengue virus infection induces formation of G3BP1 granules in human lung epithelial cells. *Arch Virol, 160*(12), 2991-2999. doi:10.1007/s00705-015-2578-9

Xiong, S., Zhang, W., Li, M., Xiong, Y., Li, M., Wang, H., . . . Zheng, X. (2016). A simple and practical score model for predicting the mortality of severe fever with thrombocytopenia syndrome patients. *Medicine (Baltimore), 95*(52), e5708. doi:10.1097/MD.0000000000005708

Xu, L., Li, X., Gao, X., Liu, S., Pang, Z., & Wang, Z. (2022). Viral suppression of type I interferon signaling by NSs of DBV, SFSV and UUKV via NSs-mediated RIG-I degradation. *Biosafety and Health, 4*(4), 244-252. doi:10.1016/j.bsheal.2022.05.004

Yang, X., Saha, S., Yang, W., Neuman, K. C., & Pommier, Y. (2022). Structural and biochemical basis for DNA and RNA catalysis by human Topoisomerase 3beta. *Nat Commun, 13*(1), 4656. doi:10.1038/s41467-022-32221-3

Ye, J., Coulouris, G., Zaretskaya, I., Cutcutache, I., Rozen, S., & Madden, T. L. (2012). Primer-BLAST: a tool to design target-specific primers for polymerase chain reaction. *BMC Bioinformatics, 13*, 134. doi:10.1186/1471-2105-13-134

Yeh, S. C., Diosa-Toro, M., Tan, W. L., Rachenne, F., Hain, A., Yeo, C. P. X., . . . Pompon, J. (2022). Characterization of dengue virus 3'UTR RNA binding proteins in mosquitoes reveals that AeStaufen reduces subgenomic flaviviral RNA in saliva. *PLoS Pathog, 18*(9), e1010427. doi:10.1371/journal.ppat.1010427

Yin, J. Y., Dong, Z. Z., Liu, R. Y., Chen, J., Liu, Z. Q., & Zhang, J. T. (2013). Translational regulation of RPA2 via internal ribosomal entry site and by eIF3a. *Carcinogenesis, 34*(6), 1224-1231. doi:10.1093/carcin/bgt052

Ying, M., & Chen, D. (2012). Tudor domain-containing proteins of Drosophila melanogaster. *Dev Growth Differ, 54*(1), 32-43. doi:10.1111/j.1440-169x.2011.01308.x

Yoo, B. K., Santhekadur, P. K., Gredler, R., Chen, D., Emdad, L., Bhutia, S., . . . Sarkar, D. (2011). Increased RNA-induced silencing complex (RISC) activity contributes to hepatocellular carcinoma. *Hepatology, 53*(5), 1538-1548. doi:10.1002/hep.24216

Yoshikawa, T. (2021). Vaccine Development for Severe Fever with Thrombocytopenia Syndrome. *Viruses, 13*(4). doi:10.3390/v13040627

Yu, X. J., Liang, M. F., Zhang, S. Y., Liu, Y., Li, J. D., Sun, Y. L., . . . Li, D. X. (2011). Fever with thrombocytopenia associated with a novel bunyavirus in China. *N Engl J Med, 364*(16), 1523-1532. doi:10.1056/NEJMoa1010095

Zeller, H. G., Cornet, J. P., & Camicas, J. L. (1994). Experimental transmission of Crimean-Congo hemorrhagic fever virus by west African wild ground-feeding birds to Hyalomma marginatum rufipes ticks. *Am J Trop Med Hyg, 50*(6), 676-681. doi:10.4269/ajtmh.1994.50.676

Zhang, J., Guo, H., Zhang, F., Chen, Q., Chang, M., & Fang, Q. (2019). NS38 is required for aquareovirus replication via interaction with viral core proteins and host eIF3A. *Virology, 529*, 216-225. doi:10.1016/j.virol.2019.01.029

Zhang, T., Su, S., Altouma, V., Zhu, X., Xue, Y., Shen, W., . . . Wang, W. (2022). Topoisomerase 3b is dispensable for replication of a positive-sense RNA virus--murine coronavirus. *Antiviral Res, 208*, 105451. doi:10.1016/j.antiviral.2022.105451

Zhang, X., Smits, A. H., van Tilburg, G. B., Ovaa, H., Huber, W., & Vermeulen, M. (2018). Proteome-wide identification of ubiquitin interactions using UbIA-MS. *Nat Protoc, 13*(3), 530-550. doi:10.1038/nprot.2017.147

Zhang, Y., Cui, J., Zhou, Y., Cao, J., Gong, H., Zhang, H., & Zhou, J. (2018). Liposome mediated double-stranded RNA delivery to silence ribosomal protein P0 in the tick Rhipicephalus haemaphysaloides. *Ticks Tick Borne Dis, 9*(3), 638-644. doi:10.1016/j.ttbdis.2018.01.015

Zhang, Y., Huang, Y., & Xu, Y. (2022). Antiviral Treatment Options for Severe Fever with Thrombocytopenia Syndrome Infections. *Infect Dis Ther, 11*(5), 1805-1819. doi:10.1007/s40121-022-00693-x

Zhang, Z., Boonen, K., Ferrari, P., Schoofs, L., Janssens, E., van Noort, V., . . . Geuten, K. (2016). UV crosslinked mRNA-binding proteins captured from leaf mesophyll protoplasts. *Plant Methods, 12*, 42. doi:10.1186/s13007-016-0142-6

Zhao, B., Katuwawala, A., Oldfield, C. J., Hu, G., Wu, Z., Uversky, V. N., & Kurgan, L. (2021). Intrinsic Disorder in Human RNA-Binding Proteins. *J Mol Biol, 433*(21), 167229. doi:10.1016/j.jmb.2021.167229

Zheng, J., Yang, X., Harrell, J. M., Ryzhikov, S., Shim, E. H., Lykke-Andersen, K., . . . Zhang, H. (2002). CAND1 binds to unneddylated CUL1 and regulates the formation of SCF ubiquitin E3 ligase complex. *Mol Cell, 10*(6), 1519-1526. doi:10.1016/s1097-2765(02)00784-0

Zheng, N., Schulman, B. A., Song, L., Miller, J. J., Jeffrey, P. D., Wang, P., . . . Pavletich, N. P. (2002). Structure of the Cul1-Rbx1-Skp1-F boxSkp2 SCF ubiquitin ligase complex. *Nature, 416*(6882), 703-709. doi:10.1038/416703a

Zheng, X., Wang, S., Hong, S., Liu, J., & Jiang, C. (2021). Knockdown of eIF3a attenuated cell growth in K1 human thyroid cancer cells. *Genes & Genomics, 43*(4), 379-388. doi:10.1007/s13258-021-01048-5

Zhuang, L., Sun, Y., Cui, X. M., Tang, F., Hu, J. G., Wang, L. Y., . . . Cao, W. C. (2018). Transmission of Severe Fever with Thrombocytopenia Syndrome Virus by Haemaphysalis longicornis Ticks, China. *Emerg Infect Dis, 24*(5), 868-871. doi:10.3201/eid2405.151435

Zou, T., Zhou, M., Gupta, A., Zhuang, P., Fishbein, A. R., Wei, H. Y., . . . Meyerson, M. (2023). XRN1 deletion induces PKR-dependent cell lethality in interferon-activated cancer cells. *bioRxiv*. doi:10.1101/2023.08.01.551488